UNIVERSITY OF SOUTHAMPTON

FACULTY OF SCIENCE

OCEANOGRAPHY

MAGNETOSTRATIGRAPHY OF US PALEOGENE DEPOSITIONAL SEQUENCES: IMPLICATIONS FOR DATING SEA LEVEL CHANGES

by

Guy Rhodes

A thesis submitted for the degree of
Doctor of Philosophy

Department of Oceanography
The University
Southampton

June 1995

Acknowledgements

I am grateful to Tom Gibson for providing access to the United States Geological Survey core facility at Reston, Virginia and for his expertise which was invaluable during fieldwork in the US and in discussions as the project progressed.

Chris King and Jason Ali must also be thanked for their contribution to fieldwork in Alabama and Virginia with particular mention to Chris and his tireless logging of outcrop sections in *watermocassin* territory.

My supervisor Ernie Hailwood has been an enormous help and inspiration throughout both my undergraduate studies and during the course of this research. His willingness to allow me to take six months out from my PhD studies to work for the UN in Mozambique significantly helped my financial status and enabled me to complete the last phase of my PhD with refreshed enthusiasm.

Further thanks are also given to the following members of the Oceanography and Geology Departments: Fung Ding, Paul Riddy and Liam Grant for assisting me during my periods of computer delinquency; Kevin Padley for his technical support, Bob Jones for providing help during sample preparation, Barbara Cressy for overlooking Scanning Electron Microscope work and especially Paul Montgomery for his humour during our gruelling hours in the laboratory.

I express my thanks to the Natural Environmental Research Council who funded this research project including two extended field trips to the United States.

Special mention however must go to Adele Rackley who has been of great support to me from my early days at University.

UNIVERSITY OF SOUTHAMPTON

ABSTRACT

FACULTY OF SCIENCE

OCEANOGRAPHY

Doctor of Philosophy

Magnetostratigraphy of Paleogene sequences from the US Atlantic margins: Implications for dating sea level changes

by Guy Rhodes

Results of a detailed magnetostratigraphic investigation of late Paleocene and early Eocene sediments from the US Atlantic and Gulf Coastal Plains are presented. In Virginia and Maryland, stratigraphic units from the Aquia, Marlboro Clay and Nanjemoy Formations were examined in outcrop and from core material which spanned calcareous nannofossil zones NP6 to NP13. In Alabama and Georgia sampling extended across the Nanafalia, Tuscahoma, Hatchetigbee and Tallahatta Formations (NP8 to NP14).

In sediments from the US Atlantic Coast a record of normal polarity magnetochrons C26n, C25n, C24n and C23n were identified. On the Gulf Coastal Plain records of magnetochrons C25n, C23n, C22n, and C21n were also recognised. Calcareous nannofossil data were used to correlate the polarity reversal sequence observed with that of the geomagnetic polarity timescale.

The palaeomagnetic results of this study are incorporated into a chronostratigraphic framework based on magnetostratigraphy, where the record of polarity reversal boundaries is linked across the Atlantic to those previously identified in similar-aged sequences in NW Europe. The correlation of polarity boundaries enables a high resolution comparison of depositional cycles between continental margins on both sides of the North Atlantic. The implications for dating and testing sea level cycles using this magnetostratigraphic framework are explored.

Finally, high quality palaeomagnetic data obtained from this study have been used to refine the North American palaeomagnetic pole position for the early Paleogene.

Contents

Section C

List of Abbreviations

AC	Aquia Creek locality
AF	Alternating field
Ala	Alabama
$\alpha 95$	95% confidence angular limit of Fisher statistics
BB	Bull's Bluff locality
BK	Bennett's Creek locality
BL	Bell's Landing locality
BR	Bear Creek locality
BU	Butler locality
BX	Bell's Crossing locality
CA	Campbell locality
CD	Camden locality
CR	Camden radio mast locality
CRM	Chemical Remanent Magnetisation
DDRM	Depositional DRM
Dec or D	Declination
DRM	Detrital Remanent Magnetisation
DSDP	Deep sea drilling project
F	Geomagnetic field vector
FB	Fairview Beach locality
FG	Fort Gaines locality
Ga	Georgia
GPTS	Geomagnetic Polarity Timescale
HB	Hatchetigbee Bluff locality
Inc or I	Inclination
IRM	Isothermal remanent magnetisation
k	Precision parameter of Fisher statistics
KC	Kolomokei Creek locality
L	Latitude
LS	Little Stave Creek locality
LP	Lower Peach Tree locality

Ma	Million years before present (1965 reference)
MAD	Maximum angle of deviation
mA/m	Milliampere per metre
MC	McCrea Creek locality
Md	Maryland
MD	Multi-domain
MM	Matheson Mine locality
MMTP	*Magnetic Measurements* thermal demagnetiser
MORB	Mid-ocean ridge basalts
mT	Millitesla
MW	Midway locality
My	Million years
N	Geomagnetic north pole
n	Magnetic pole
NP	Nannoplankton
NRM	Natural Remanent Magnetisation
OG	Oak Grove core
PDRM	Post Detrital Remanent Magnetisation
PT	Peach Tree locality
PC	Pope's Creek locality
Rc	Regression coefficient for straight line fit
RC	Roaring Creek locality
SC	Scott's Peak locality
SD	Single-domain
SEP	Magnetic vector stable end point
SQUID	Super conducting quantum interference device
TL	Tuscahoma Landing locality
TR	Tinker's Ravine locality
TRM	Thermal Remanent Magnetisation
TS	Tunnel Springs locality
US	United States
Va	Virginia
VGP	Virtual geomagnetic pole
YC	Yacht Club locality

List of figures

List of plates

List of tables

Chapter 1 Introduction

Most stratigraphic classification schemes, to some extent, use sea level variations as a basis for subdividing the geological past. Stratigraphic boundaries are commonly based on unconformities or changes in paleontological properties or other physical characteristics of rock types, which are often related to fluctuation in water depth.

In the past twenty years the concept of sedimentary units being defined by changes in sea level has seen considerable development. Peter Vail and colleagues at Exxon Production Research have used seismic reflection profiles to define sedimentary cycles in shallow water shelf environments. Transgressions and regressions of the palaeocoastline over the continents are identified in such settings by depositional packages whose limits are defined by regional surfaces of erosion and nondeposition that act as reflectors in the seismic record.

Vail et al (1977) suggested that many of these sequence boundaries are of the same age in different parts of the world and therefore are due primarily to the global process of eustasy. Based on this assumption, the Exxon team have developed a series of four cycle charts that depict the chronology of such sea level fluctuations in the Cenozoic, Cretaceous, Jurassic and Triassic, covering the eustatic history of the last 250 million years (Haq et al, 1987).

Figure 1-1 shows the Cenozoic chart of global sea level changes which have been chronicled alongside magneto-, chrono- and the biostratigraphy available for this interval. The depositional sequences are organised into an hierarchy of units, each bounded by unconformities. The first order cycles have a duration of between 100 and 400 m.y., the second order cycles approximately 10 to 50 m.y. and the third order cycles around 1 to 3 m.y. Further subdivisions of sequences are represented by *systems tracts* which are defined by stacking patterns of relatively conformable successions of genetically related beds known as parasequences (Wagoner, 1988). The corresponding sea level fluctuations are determined by the relative change of coastal onlap of sediments. Forty three third order cycles have been recognised for the Cenozoic period alone. Additional sequence stratigraphic concepts, methodology

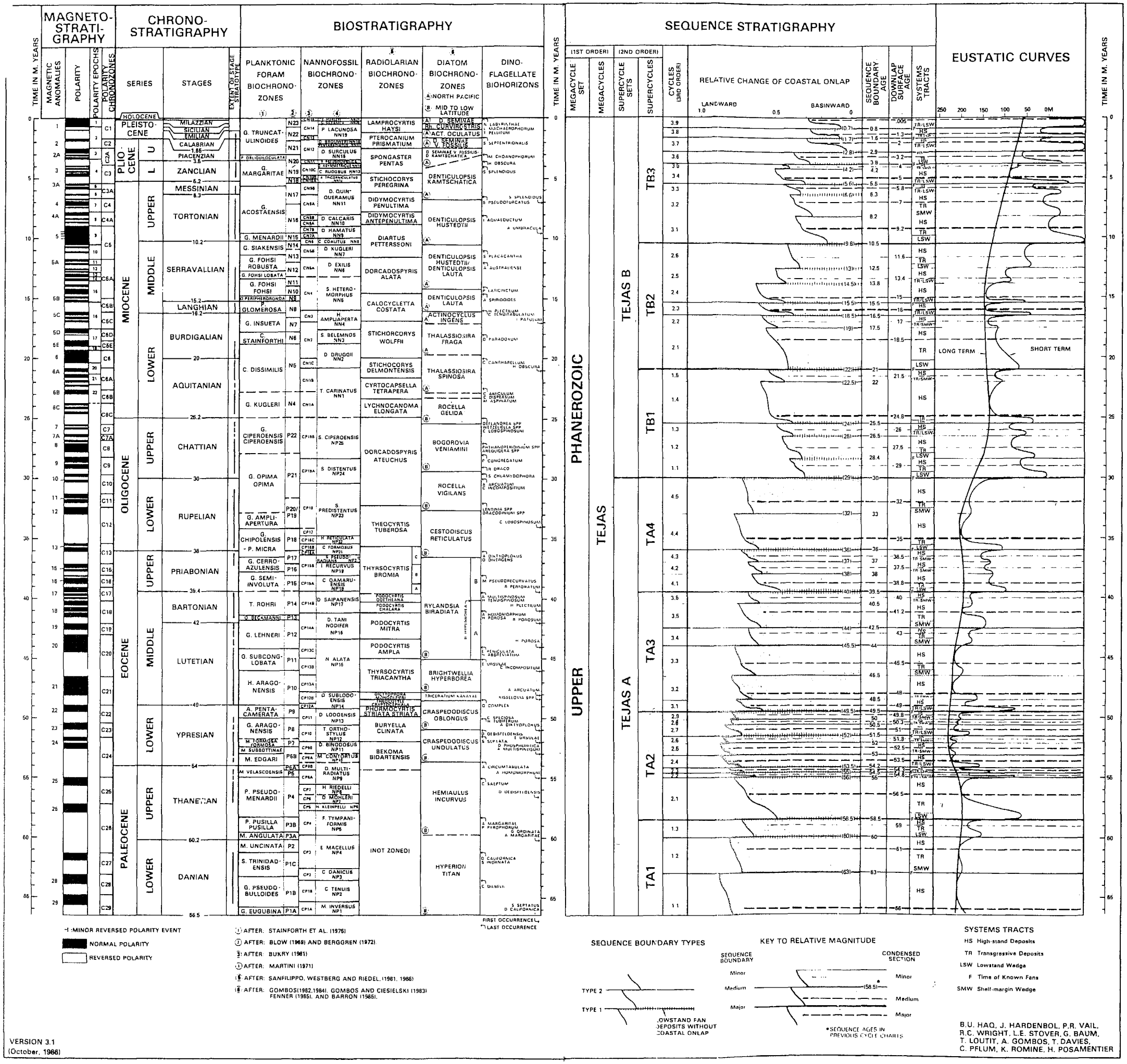

Figure 1-1 *Cenozoic chronostratigraphy and cycles of sea level change (from Haq et al, 1987).*

chronostratigraphical basis of the charts are explained in a comprehensive set of papers by Vail, Mitchum and others (ed. Payton, 1977).

There has been much debate over the accuracy of the proposed eustatic curve since it was first published in 1977, particularly over the magnitude of the sea level fluctuations, the global bias of the data and, most importantly, the validity of 3rd order cycle correlation. Consequently, the Vail curve has undergone some minor adjustments in an effort to address some of the criticisms (Haq et al, 1987; Kerr, 1987). However, some fundamental problems with the model still remain.

The mechanism responsible for generating first order cycles has a time-scale which is probably linked to the amalgamation and dispersion of continents. In a similar way, second order cycles can be adequately explained by the changing shape of the oceans as a result of variations in mid-ocean ridge volumes. However, it is the mechanism to explain third order cycles which generates most debate. Glacial - eustatics could provide an acceptable explanation for such fluctuations, yet Vail/Haq curves span great periods of geological time where there is little evidence of climatic regimes that might provide such a control (Sloss, 1988). Alternatively, intraplate stresses have been suggested by Cloetingh (1988) as a possible cause for rapid cycles, though this idea has gained little support. The lack of an adequate mechanism to fully explain high frequency sea level fluctuations has lead to a general reluctance to accept sea-level changes as the prime explanation for Vail curves.

Furthermore, the magnitude of sea level fluctuations proposed from the curve remains questionable, due primarily to the fact that water depth at a given locality is a relative phenomenon and the global signature of eustatic sea level trends will be further complicated and offset by local or regional tectonic influences and clastic sediment supply (or carbonate sediment production - see Kendall and Lerche, 1988). Thus, lack of adequate corrections for local and regional subsidence are major limiting factors in the estimation of the magnitudes of sea level changes; indeed, there is debate whether the effects of tectonic processes can be isolated from the eustatic record at all (e.g. Bond, 1978; Watts, 1982 and Christie-Blick et al, 1988, 1990).

The validity of third order cycle correlation also continues to be a contentious issue since

the global correlation of any particular event is dependant on the resolution of the age calibration techniques used. Third order cycle duration is often close to, or finer than the biostratigraphical resolution that is used to fix them in the chart and therefore the basic premise of a suite of globally correlatable third order eustatic cycles remains to be proven (Miall, 1992). The debate is further fuelled by the failure of Exxon to release information from which the curves were derived.

The critical test of the Exxon chart therefore is to demonstrate that successions of cycles of precisely the same age do indeed exist in many tectonically independent basins around the world. In order to achieve this, with the precision that Exxon lay claim, a method of correlation with greater age resolution than used at present must be adopted. When combined with biostratigraphic data, magnetostratigraphy can be used as such a tool, to increase the resolution of timescales (see Chapter 2 of this report).

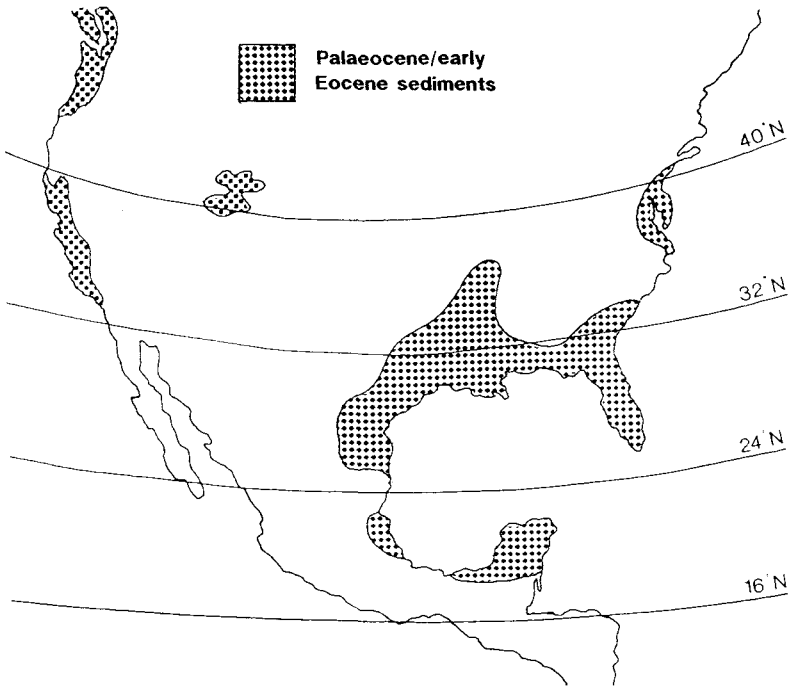

Figure 1-2 *Outcropping Paleocene and early Eocene sediments in the USA (from Schuchert, 1955).*

The choice of depositional setting for an investigation into the effects of eustatic changes in sea level on sediment deposition is critical. Firstly, in order to minimise the influence

of local tectonics, which may complicate the eustatic signature, a passive margin location is a prerequisite to the study. Secondly, the ability to recognise sequences on this type of margin is equally important and therefore the ideal palaeoenvironment is on the mid to outer shelf where sea level changes of several tens of metres are well recorded. Clearly, in deeper water environments the change in water depth may not have such a significant effect on the sedimentation; and closer towards the margin, in shallower water, the erosional potential of such fluctuations may restrict the completeness of the sedimentary record.

The palaeomagnetism group at Southampton University has, to date, done extensive work on the Thanetian and Ypresian (late Paleocene and early Eocene) sequences of NW Europe (e.g. Townsend and Hailwood 1985; Ali, 1989; Ali et al, 1993) and have developed a chronostratigraphic framework based on magnetostratigraphy for this period of time.

The main objective of the present research project is to improve the stratigraphic resolution for the late Paleocene and early Eocene sequences of the United States Gulf and Atlantic Coastal Plains (Fig. 1-2) through a comprehensive magnetostratigraphic investigation of these sequences. In addition, the implications for using a global magnetostratigraphic framework as a means of correlating sequences between continental margins either side of the Atlantic and thus providing a rigid test for the Vail/Haq curve are explored.

The chapters within *Section A* of this thesis outline the fundamental concepts of magnetostratigraphy, the field sampling and laboratory procedures used during the present research and the stratigraphic subdivisions and timescales adopted. The following *Sections B* and *C* present the magnetostratigraphic results for the U.S. Atlantic and Gulf Coastal Plains respectively. In *Section D*, the magnetostratigraphy of sediments from North America and NW Europe are correlated and corresponding sedimentary sequences are compared across the Atlantic. Finally a palaeomagnetic pole is presented for the early Tertiary of North America.

SECTION A

Magnetostratigraphic and palaeomagnetic concepts.
Sampling and laboratory procedures.
Stratigraphic subdivisions and timescales adopted.

Chapter 2 Palaeomagnetism and Magnetostratigraphy

2.1 The Earth's magnetic field

The internally originating part of the earth's magnetic field is thought to be generated by a 'self-exciting dynamo effect' whereby convective cells of conductive material move within the outer core (Hailwood, 1989). The simplest model, which can describe 80% of the geomagnetic field, is a uniformly magnetised sphere with a dipole axis aligned parallel to the Earth's axis of rotation, originally postulated by Gilbert (1600). This is known as the axial geocentric dipole model (Fig. 2-1). The remaining 20% of the field is made up of a weaker non-dipole component which is less stable.

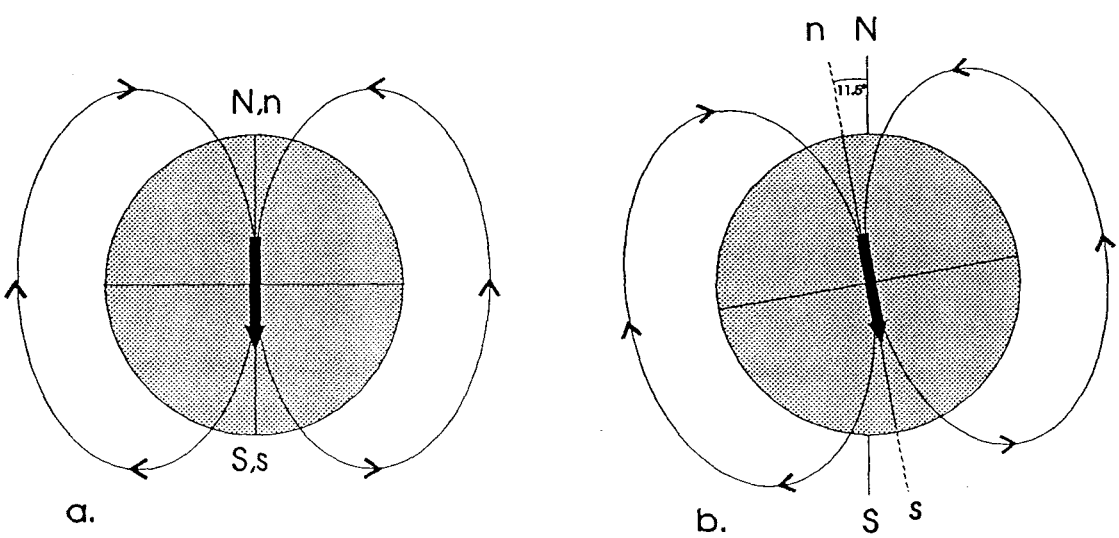

Figure 2-1 *Models of the Earth's magnetic field. (a) Geocentric dipole model (b) Inclined geocentric dipole model. Representation of Earth's geographic poles are 'N' (north) and 'S' (south); geomagnetic poles are indicated by 'n' (north) and 's' (south).*

The orientation of the best fitting dipole varies with time, but when averaged over a period of 10^4 to 10^5 years it is believed to coincide with the axis of rotation as illustrated in figure 2-1a (e.g. Opdyke and Henry, 1969). At present, the best fitting dipole axis is inclined at about 11.5° to the geographic axis (Fig. 2-1b).

The direction and strength of the Earth's field can be expressed by three magnetic elements: the intensity (F), inclination (I) and declination (D) (Fig. 2-2). The directional properties of the field at any given point can be demonatrated using a free swinging compass, where the deviation from geographical north is the declination and the inclined angle the needle makes with the horizontal is the magnetic dip or inclination. In the northern hemisphere the north-seeking end of a magnetised needle will generally be down dipping (referred to as positive inclination) and over most of the southern hemisphere the north-seeking end of the needle will point upwards (negative inclination).

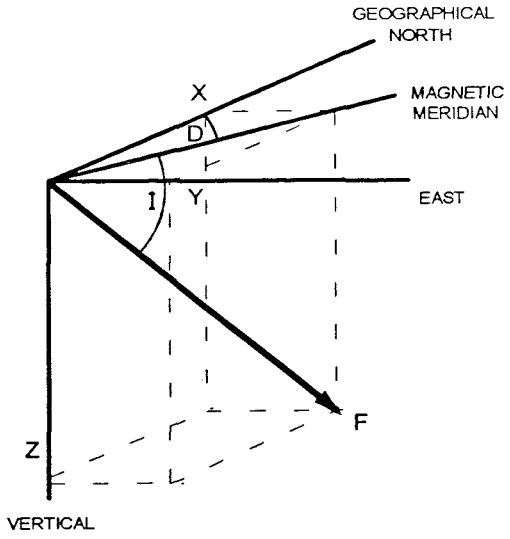

Figure 2-2 *Directional components of the geocentric field vector, F. Inclination (I) and declination (D).*

In the axial geocentric dipole model, the inclination of the magnetic field is related to the latitude (L) of the site by the equation:

$$\tan I = 2\tan L$$

The fluctuations of the dipole orientation, within a limit of about 20°, around the Earth's rotational axis and over timescales of approximately 10^2 to 10^3 years are known as *secular variations*. Information on secular variation is derived partly from direct observation and partly from palaeomagnetism (Irving, 1964). In the latter case the secular changes show themselves as the dispersion of directions observed at different time levels in the rock unit. The pattern in lake sediments is rather complex, showing that secular variations have no obvious long-term cyclic patterns (Tarling, 1983).

Over a greater timescale, however, more profound changes in the Earth's magnetic field occur which, from a stratigraphical point of view, have a greater geological significance.

2.2 Reversal of the Earth's magnetic field

Over timescales of 10^4 - 10^7 years the Earth's magnetic field alternates between normal and reverse polarities. A normal polarity period describes the geomagnetic field in its present state (Fig. 2-3a) where the magnetic pole(n) lies close to the geographic north pole (N). A reverse polarity describes the opposite state where the magnetic north pole lies close to the geographic south pole (Fig. 2-3b). During a polarity inversion the direction of the geomagnetic field swings through about 180°.

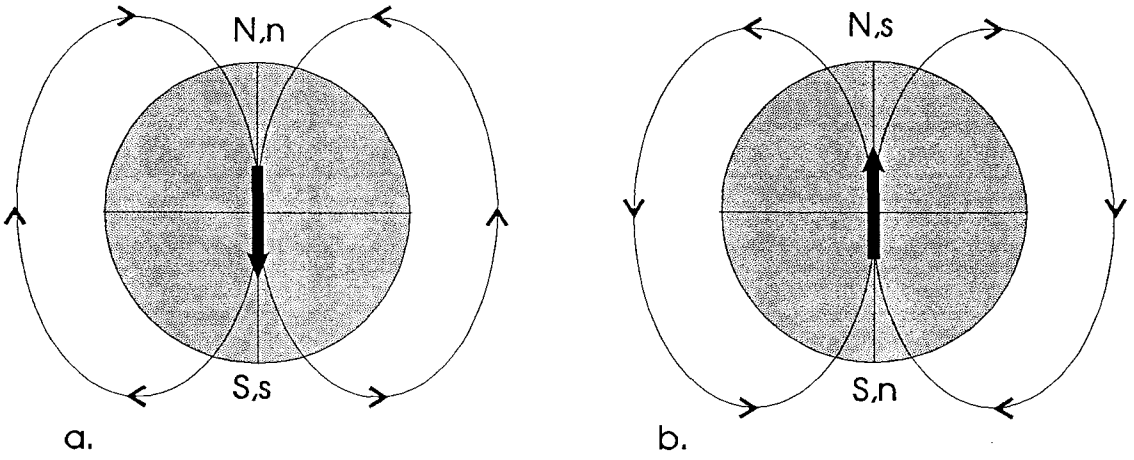

Figure 2-3 *Dipole model of the Earth's magnetic field in (a) a normal polarity and (b) a reverse polarity state (from Hailwood, 1989).*

Brunhes (1906) and Matuyama (1929) were two of the first workers to identify reversals in the geomagnetic field. Since then, some studies have succeeded in identifying a record of the geomagnetic field during the polarity transition itself (e.g. Koci, 1985; Dodson et al 1978). During a reversal, it appears that the intensity of the field decreases for several thousand years while the field direction is maintained (Fig. 2-4). The magnetic vector then usually executes several swings of magnitude before moving along an irregular path to the opposite polarity state, the intensity remaining reduced and rising

to its normal value later (Dodson et al, 1978). Transitions from one polarity state to another vary in duration from 10^3 - 10^4 years (Clement et al, 1982).

In addition to polarity changes, the Earth's magnetic field has often departed for brief periods from its usual near-axial configuration without establishing a reversed direction.

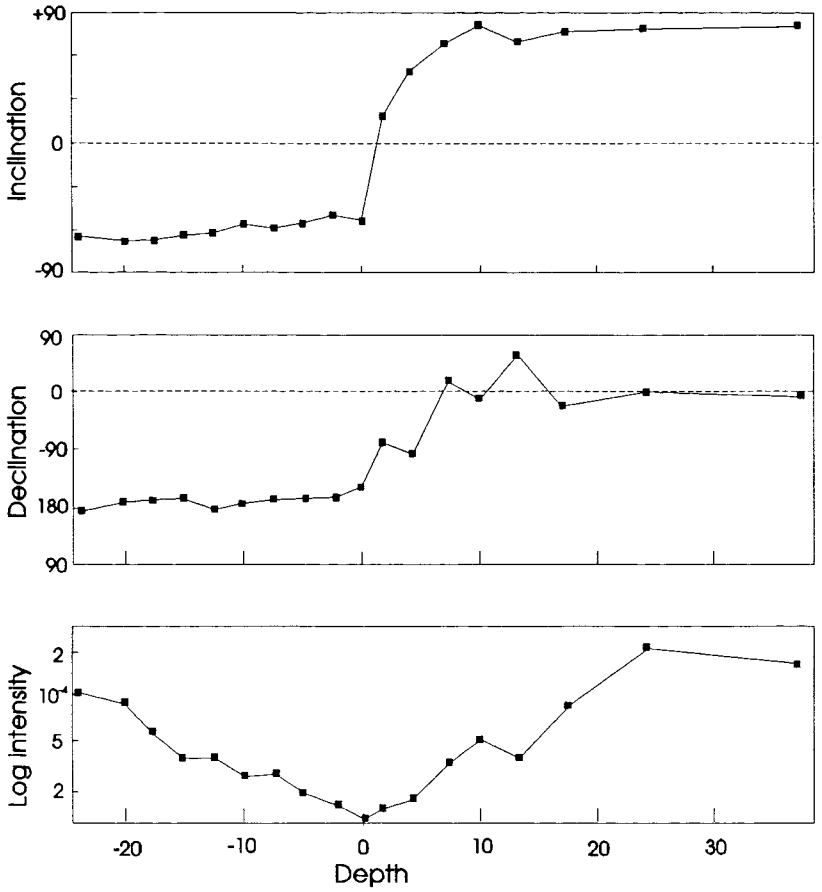

Figure 2-4 *Intensity, declination and inclination changes of the geomagnetic field during a polarity reversal; recorded in the Tatoosh intrusion, USA (from Dobson et al, 1978).*

This type of behavior (which describes a movement of the virtual geomagnetic pole that is >40°away from the geographic pole) is known as a 'geomagnetic excursion' (Jacobs, 1984). It is possible that excursions represent aborted reversals.

2.3 Magnetostratigraphy and the Geomagnetic Polarity Timescale (GPTS)

2.3.1 Geomagnetic polarity timescale (GPTS)

In order to obtain a calibrated record of the sequence of geomagnetic reversals over time (known as a GPTS) it is necessary to define the standard pattern of worldwide polarity reversals and then to derive a numerical age for each successive polarity reversal. The pattern of geomagnetic field reversals may be resolved from marine magnetic anomalies resulting from the magnetic stratigraphy of horizontally accreted oceanic crust away from mid-ocean ridge axes (Fig. 2-5) and from the magnetic stratigraphy of vertically accreted sequences of sedimentary and volcanic rocks (Lowrie and Alverez, 1981). Additional information from sea-floor spreading rates, biostratigraphical calibration techniques, isotopic evidence and other independant means can then be used to date and fine-tune the reversal sequence.

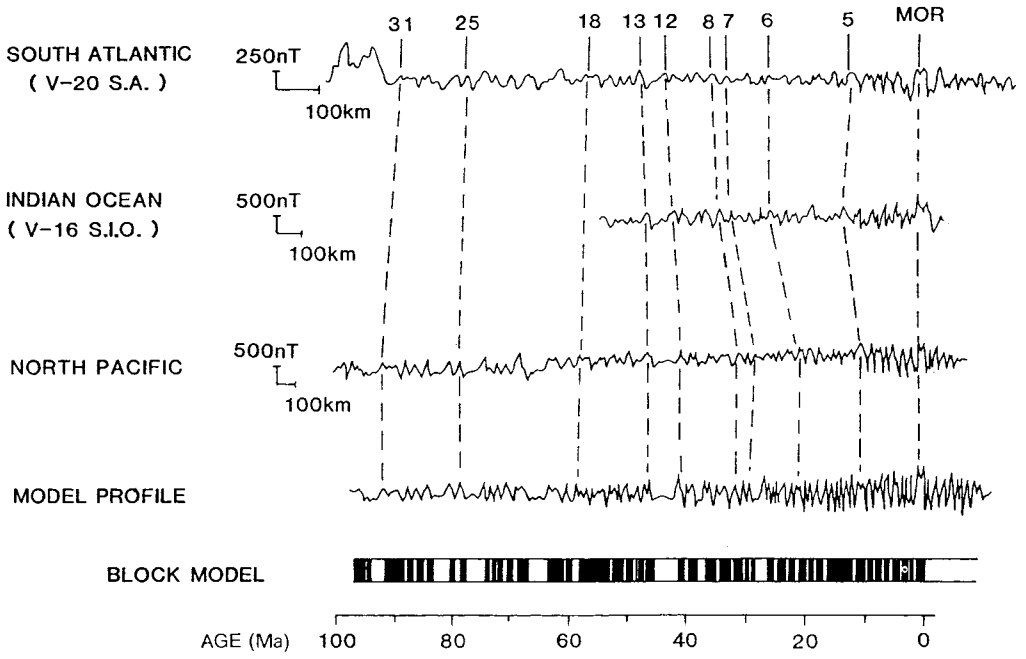

Figure 2-5 *Profiles from the South Atlantic, South Indian Ocean and North Pacific linked by numbered anomalies and aligned against a block model. Black bars represent normal polarity, white reverse polarity (from Hailwood, 1989).*

Heirtzler et al (1968) used the symmetry of the magnetic anomalies across the South Atlantic Ridge to propose the first geomagnetic polarity timescale for the Late Cretaceous to Recent (Fig. 2-6). The timescale was based on the assumption of a constant sea-floor spreading rate (estimated at 1.9cm/year) derived from the isotopic age for the Gauss-Gilbert chron boundary. The broad success of the original timescale can be gauged by the fact that, although parts of the reversal sequence have been subsequently revised, the original relative spacings of the reversals have remained fairly constant between the various timescales that have been proposed since.

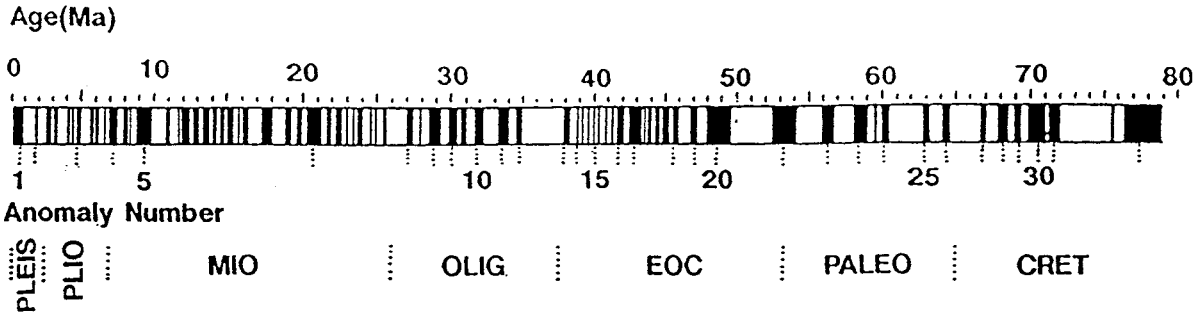

Figure 2-6 *Tertiary and late Cretaceous geomagnetic polarity timescale (from Heirtzler et al, 1968).*

The more recent timescales have improved the resolution of the GPTS by utilising higher resolution profile data, incorporating a number of different spreading rates into the basin model, using stacked profiles from a number of ridges systems, calibrating more isotopic markers into the scale and making full use of biostratigraphic correlations.

However, the construction of a universally accepted GPTS remains to be done and differences of several million years sometimes exist between numerical ages assigned to the same magnetic chron boundary on different versions of the GPTS currently used.

Nomenclature

Geomagnetic polarity has been assigned a basic subdivision, the 'polarity chron' which describes an interval of time composing of either a period of predominently one polarity (e.g Chron C21r and Chron C22n, Fig. 2-7) or a period of two opposite polarities (e.g. C22 and C21, Fig. 2-7). These have a duration of approximately 10^5-10^6 years. Shorter

polarity intervals within the chrons (e.g. C24n.1, Fig. 2-7), having durations of approximately 10^4-10^5 years, are known as 'polarity subchrons'. The terms chron and subchron were officially adopted to replace the former units of 'epoch' and 'event' used prior to 1979. Where longer periods of predominently one polarity occur in the geological record (such as the mid Cretaceous long normal polarity interval) the term 'polarity superchron' is used.

The terms above refer to the subdivisions of *time* based on geomagnetic polarity. Further terms, recommended for describing corresponding *chronostrigraphical* and *lithostratigraphical* intervals are summarised by Hailwood, 1989:

Approximate duration of polarity interval	Revised chronological term recommended by IUGS (Anan 1979)	Equivalent chronostratigraphic term	Equivalent lithostratigraphic term
10^4-10^5 years	Sub-chron	Sub-chronozone	Sub-zone
10^5-10^6 years	Chron	Chronozone	Zone (=Magnetozone)
10^6-10^7 years	Superchron	Superchronozone	Superzone

Table 2-1 *Magnetostratigraphic nomenclature* (from Hailwood, 1989)

2.3.2 Magnetostratigraphy

Due to the relatively short duration of geomagnetic field transitions (on a geological scale) they provide markers that can be regarded as instantaneous events. Furthermore, since the polarity boundaries appear to occur sychronously worldwide (recorded within a wide range of igneous and sedimentary rocks) they provide important sets of time-correlative datum planes which can play an important role in global geological correlations (Hailwood, 1989).

The magnetic intensities of most rocks and sediments are weak but measureable. In most cases the intensity and direction of the magnetic component acquired at or close to the

time of formation of the rock can be determined. If a number of rock samples are analysed in a sequence, a record of any field reversals occuring during deposition of that sequence may be identified. Although direct correlations of distinctive inversion patterns may be possible in some instances, it is usually neccesary to first locate the sequence into its rough position on the standard GPTS using some independant control such as biostratigraphy. In practise therefore, magnetostratigraphy becomes an extension of conventional biostratigraphic and isotopic techniques by refining further the approximate correlation of the specific reversal horizons and enabling a numerical age to be assigned to these points, therefore significantly increasing the dating resolution.

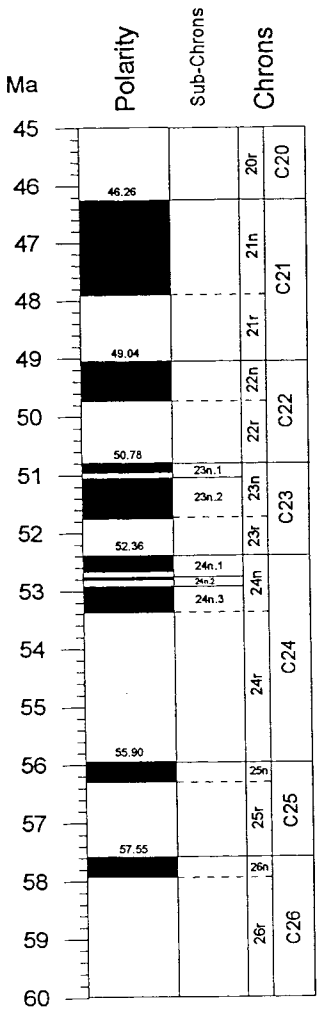

Figure 2-7 *Sub-divisions of the geomagnetic polarity timescale. Example from early Tertiary (after Cande and Kent, 1992). Chron boundary ages (indicated within the polarity column) are taken from Hardenbol, 1994.*

2.4 Minerals and Rock magnetism

In order to stratigraphically interpret the magnetic properties of rocks and sediments reliably, it is necessary to understand the types of minerals that contribute to a rock's magnetisation and the mechanisms by which they align their magnetic moments parallel to the geomagnetic field.

2.4.1 Processes of magnetisation

The mechanisms of magnetic remanence acquisition that are of most significance in this present study are *detrital, post-detrital* and *chemical remanent magnetisation. Thermal remanent magnetisation* does not play a significant role in the magnetisation of material in the sedimentary shelf environments but is included below because of its general applications to GPTS constructions and possible contribution to sediment magnetisation in certain circumstances.

Depositional and post-depositional remanent magnetization (DRM and PDRM)

Depositional remanent magnetisation (DRM) is acquired by a sediment as magnetic grains (acting as free swinging magnets) fall through the water column aligning themselves with the geomagnetic field. Post depositional remanent magnetisation (PDRM) occurs after the grains have settled on the bottom and the rotation of such grains parallel to the local field occurs in the water-filled interstitial waters prior to lithification.

Laboratory experiments indicate that the recorded magnetisation may, in some cases, be subject to a number of errors. This is particularly applicable to the inclination which can show significant departures from the ambient field (for example: Anson and Kodama, 1987; Arason and Levi, 1990; Deamer and Kodama, 1990). The mechanisms that control the inclination error have been posulated by a number of authors; these include the sediment's clay content which may interact with the magnetic particles (Deamer and Kodama, 1990), the effects of the gravitational couple and the hydrodynamic shear due to the bottom currents on grain orientation.

In the laboratory, errors as high as 25° have been recorded (King, 1955; Rees, 1961) although in the natural environment errors are normally considerably less and often can be demonstrated to be totally absent. The effects of Brownian motion of the interstitial water particles on the finer grained magnetic particles may help realign them in the ambient field (Irving and Major, 1964) with bioturbation possibly assisting this process (Kent, 1973). The true age of the remanence in PDRM will therefore be slightly younger than the time of deposition of the sediments. The duration of the lag will differ between sedimentary depositional environments but estimates of several days (Barton et al, 1980) to hundreds of years (Lowrie and Heller, 1982) have been made. When cementation finally occurs, however, the magnetic grains are locked into place.

Chemical remanent magnetisation (CRM)

During the processes of lithification and diagenesis of sediments and also the weathering of all rock types, various chemical changes can take place which may affect the record of magnetic components present in a rock.

Following nucleation, the magnetic minerals are extremely small and have short relaxation times. As they grow and increase in volume they reach a particular size, known as the *blocking volume* where the relaxation time rapidly increases and the magnetism becomes fixed.

The importance of CRM in the partial or total destruction of the primary magnetism in a sediment is crucial when interpreting palaeomagnetic data. Oxidation of titanomagnetites to titanohematites for instance, are common occurrences in some post depositional settings. The CRM of hematite for example, may record the ambient geomagnetic field at some time after deposition; a good example being where the upper part of a homogeneous unit is weathered and possesses spurious magnetic directions.

Thermal remanent magnetisation (TRM)

During the formation of igneous rocks, various minerals including magnetic iron oxides, crystalize from molten material as it cools. At the *Curie point* (temperatures of about 575°C and 675°C for magnetite and hematite) the iron oxide crystals acquire a

magnetisation which is aligned with the local geomagnetic field. Below this point, at a lower temperature called the *blocking temperature,* the stability of the acquired magnetisation rapidly increases; upon more cooling, it increases further and effectively becomes fixed, thus recording the direction of the geomagnetic field present at the time of formation within the rock.

During a subsequent episode of heating an additional component of magnetisation may be acquired which mimics the geomagnetic field at the time of reheating. This component will be carried by any grains which have a blocking temperature up to the maximum reheating temperature and providing the Curie point of the magnetic constituents is not reached, the initial magnetization will be retained in those grains that have a blocking temperature between the reheated temperature and the Curie point. The superposition of a TRM on other magnetic minerals that have been aligned in the Earth's field by different mechanisms (outlined below) will also apply. For instance, in response to the deep burial of sediments and the baking effects of rocks which are in the vicinity of igneous intrusions or affected by regional heating events.

Viscous remanent magnetisation (VRM)

When a rock is subjected to a weak magnetic field over a very long time it can acquire a viscous remanent magnetisation (VRM). Within such a field the magnetic moments of grains that have short relaxation times will slowly become aligned with the ambient field and therefore the VRM often parallels the recent field direction. In sediments where a high proportion of low coercivity grains exist, the *natural remanent magnetism* (NRM) will be dominated by a VRM.

2.4.2 Magnetic minerals and their origins

The sediments sampled in this study ranged from coarse sands to fine clays, calcareous to siliceous material, lithified to unconsolidated units and were formed in palaeo-environments that were outer shelf through inner shelf, deltaic to non-marine. The diversity of lithological units and the varying degree of weathered and fresh material suggests that a wide range of magnetic mineral types are potentially present.

Outlined below are magnetic minerals which, to a greater or lesser extent, may contribute to the magnetism of the sedimentary rocks analysed.

Titanomagnetite series

The titanomagnetites have a cubic (spinel) structure and form a solid-solution series with magnetite and ulvospinel (Fe_2TiO_4) as end-members. Of the end-members, only magnetite is magnetic at room temperature (Tarling, 1983).

Magnetite (Fe_3O_4)

Magnetite has the strongest magnetic properties of any common crustal mineral. The magnetic properties are strongly dependent on grain size, where maximum coercivity occurs in single-domain (SD) sized grains. It seems probable that the stable NRM, which is of principal concern in palaeomagnetism, is carried by multi-domain (MD) or single-domain grains (Stacy, 1963).

The main sources of magnetite in sedimentary rocks are thought to be the weathering of continental igneous rocks (e.g. Morgan and Smith, 1981), submarine weathering of mid-ocean ridge basalts (MORB) (Smith, 1979) or in-situ precipitation of SD magnetite by magnetotactic bacteria (Frankel et al, 1979).

The geological setting for sediment deposition on the US Gulf and Atlantic Coastal Plains in the Paleogene suggests that the most likely source of magnetite is from the Appalachian mountain belt to the north and west and from biogenic sources such as magnetotactic bacteria which are found in most marine, brackish and freshwater environments. Primary remanence on continental shelves and margin basins however is unlikely to have a MORB source.

Maghemite (γFe_3O_4)

Low-temperature ($<200°C$) oxidation of magnetite, such as during subaerial and subaqueous weathering, will often produce maghemite which is a mineral with the composition of hematite but the cubic structure of magnetite (Tarling, 1983). The

contribution of the CRM to the magnetisation of the rock and the effect on isolating a primary component (representative of the Earth's field at the time of deposition) will depend on the relative proportion of maghemite formed and the field direction at the time of formation.

The ilmenohematite series

The ilmenohematites form a solid-solution series with hematite (Fe_20_3) and ilmenite ($FeTiO_3$) as end members. Ilmenite is antiferromagnetic but behaves paramagnetically at room temperature. The series has a rhombohedral (corundum) structure.

Hematite (γFe_2O_3)

Hematite has a spontaneous magnetisation of the order of 0.4-0.5Am^2kg^{-1} which is considerably less than that of magnetite (92Am2kg-1); however it is an extremely common constituent of sedimentary rocks where its specific magnetic properties are strongly dependent on grain size, composition and crystal lattice impurities.

The origin of hematite may be from the direct erosion of hematite from continental rocks or from magnetite that has oxidised during the processes of erosion, transportation and deposition. It can also form by alteration of iron hydroxides and carbonates.

Iron Hydroxides

Goethite (α-FeOOH)

Goethite is antiferromagnetic and therefore the most important of the iron hydroxides; it is in addition a polymorph to which the other iron hydroxide phases eventually revert (Henshaw and Merril, 1980). It can form diagenetically from pyrite (Turner, 1975) and is seen as yellow and brown phases in weathered rocks and soils (Piper, 1987). The exact timing of goethite formation in sediments is usually difficult to determine since it is a product of oxidation and weathering.

Iron sulphides

Pyrrhotite (Fe_7S_8)

Iron sulphides are common minerals in sediments which have been associated with organic material. Pyrite (FeS_2) is a good example though at room temperature it is paramagnetic and does not contribute to the magnetism of sediments. Pyrrhotite however, has a relatively high saturation magnetisation with typical values of 6.3×10^{-4} Am^2kg^{-1} along its c axis (Schwarz, 1974) and can in some instances play a role in sediment magnetism.

Iron is a common component of many other minerals which are common in sediments. Although these minerals do not contribute to the magnetism of the sediments directly, they are an important source for magnetic minerals such as hematite, if broken down by weathering or other diagenetic processes (Tarling, 1983).

Chapter 3 Sampling procedures and analytical techniques

3.1 Sampling and laboratory preparation of material

Preliminary investigations identified low magnetic intensities for the majority of Paleocene and Eocene sediments on the US Gulf and Atlantic coasts (field work undertaken in October, 1991). In order to improve the signal to noise ratio for available instrumentation, large samples (typically 1000cm^3) were collected at each site (Plate 3-1) during the successive field work (April, 1992). These were sub-divided and trimmed in the laboratory into cylindrical specimens with volumes in the range 100-250cm^3. Great care had to be taken whilst sampling, transporting and subsampling samples, particularly those from unconsolidated and friable units which accounted for the majority of the samples analysed.

Plate 3-1 *Orientated field sample*

Samples were taken at approximately 0.5 - 2m intervals, depending on the outcrop. At each site, the outcrop was dug back using a regular garden spade until fresh material

became exposed. All weathered material was trimmed from the sample (seen in plate 3-1 as the brown altered layer on the surface of the ourcrop) thereby minimising the effects of recent magnetic overprints and increasing the chance of isolating the primary component of magnetisation.

A horizontal orientation surface was created using a trowel (confirmed using a spirit level) and the direction of true north was marked by parallel lines and an arrow on the sample. Careful excavation yielded a block which was then trimmed and wrapped in cling film to retain its moisture and provide support for the more friable lithologies. Typically 1 to 5 samples were taken from each level in an outcrop.

Mechanised sampling methods such as rock drills and disc cutters were not used due to the soft nature of the majority of sediments encountered in this study. The small number of lithified units and calareous nodules removed from outcrop were crudely sampled using a hammer on protruding strata and samples were then cut to size in the laboratory using a diamond studded circular saw.

The Paleocene and Eocene sediments on the Gulf and Atlantic seaboard have only shallow regional dips which are minimal on a local scale. For polarity reversal stratigraphy, small errors of a few degrees can be tolerated and therefore no tilt corrections have been applied to field samples during this study.

3.2 Palaeomagnetic measurement

Sediment samples were measured by means of a cryogenic magnetometer and subjected to demagnetisation by either thermal or alternating field (A.F.) techniques. The magnetic susceptibility of all samples was measured and selected samples were then subjected to isothermal remanent magnetisation (IRM) acquisition investigations.

3.2.1 Cryogenic magnetometers

Cryogenic magnetometers are capable of high levels of sensitivity; they utilise superconducting pick-up coils and *super-conducting quantum interference device* (SQUID) sensors which respond to extremely weak magnetic moments. Measurement response times of SQUID electronics are also extremely quick which is a significant advantage over other types of magnetometers when making multiple measurements of weak samples (Hailwood, 1989). Thus, in magnetostratigraphical investigations which commonly involve measurement of a large number of samples with varying magnetic intensities, the cryogenic magnetometer has clear advantages over other less sensitive instruments. Two types of cryogenic magnetometer were used to measure the remanent magnetism of the samples during this present study: the CCL and the 2-G instruments.

CCL cryogenic magnetometer

During the initial stages of research the CCL magnetometer was used for measurement of pilot samples although when it became clear that larger sample volumes and the faster measurement time was required the 2-G magnetometer was used exclusively.

Plate 3-2 shows the exterior of the CCL magnetometer unit. It consists of a shielded A.F. demagnetiser, a CCL cryogenic magnetometer and a vertical sample control motor which manoeuvres the sample from above.

The samples are suspended in a mylar holder and controlled by a stepper motor which moves the samples vertically between the demagnetiser and measurement coils, physically rotating the sample through 90° in the horizontal plane of the demagnetisation coils and the sensor region. Sensor coil geometry and dimensions limit sample size to

a maximum of 3.5cm diameter and 3cm in height (volume 29cm^3). Unconsolidated sedments were measured in cubic plastic specimen boxes with internal volumes of 15.8cm^3. Calibration is carried out using a calibration sample which has a known stable permanent magnetic moment.

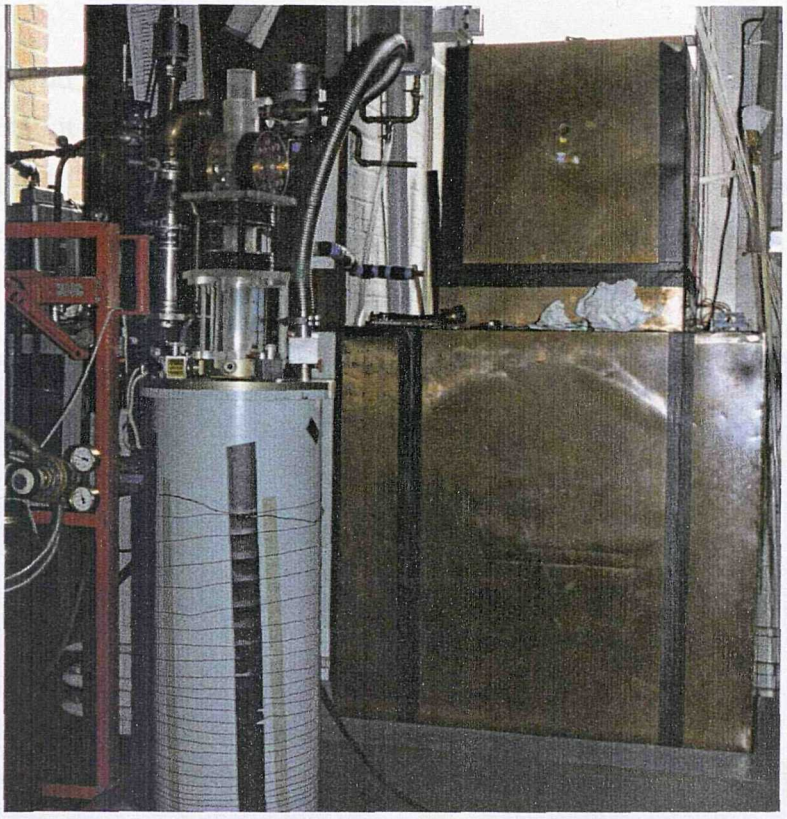

Plate 3-2 *The CCL cryogenic magnetometer in the palaeomagnetic laboratory.*

A paper sample holder has been adapted to further reduce the magnetic moment of the holder, thereby increasing the overall sensitivity of the magnetometer and enabling accurate measurements of samples with intensities as low as 0.003mA/m to be achieved (Montgomery, 1994).

2-G Enterprises whole core cryogenic magnetometer

The whole-core magnetometer was designed to enable cored material to be passed through the magnetometer intact. The system is fully automated for A.F. demagnetisation analysis, incorporating a 1.5m fibreglass sample holder which passes

through an on-line demagnetiser and '3-axis' cryogenic magnetometer (Plate 3-3). Options for discrete sample or whole-core measurement mode are available on the microcomputer which controls the magnetometer system. During this investigation, the discrete sample mode was used (except during experiments on holder intensity and magnetic interaction between samples).

The pick-up coils and SQUID sensors simultaneously measure the three components of magnetisation without the need to rotate the sample. The A.F. demagnetisation coils, due to their close proximity and there interaction potential however, demagnetise each perpendicular axis separately. Samples were typically demagnetised in fields up to 40mT.

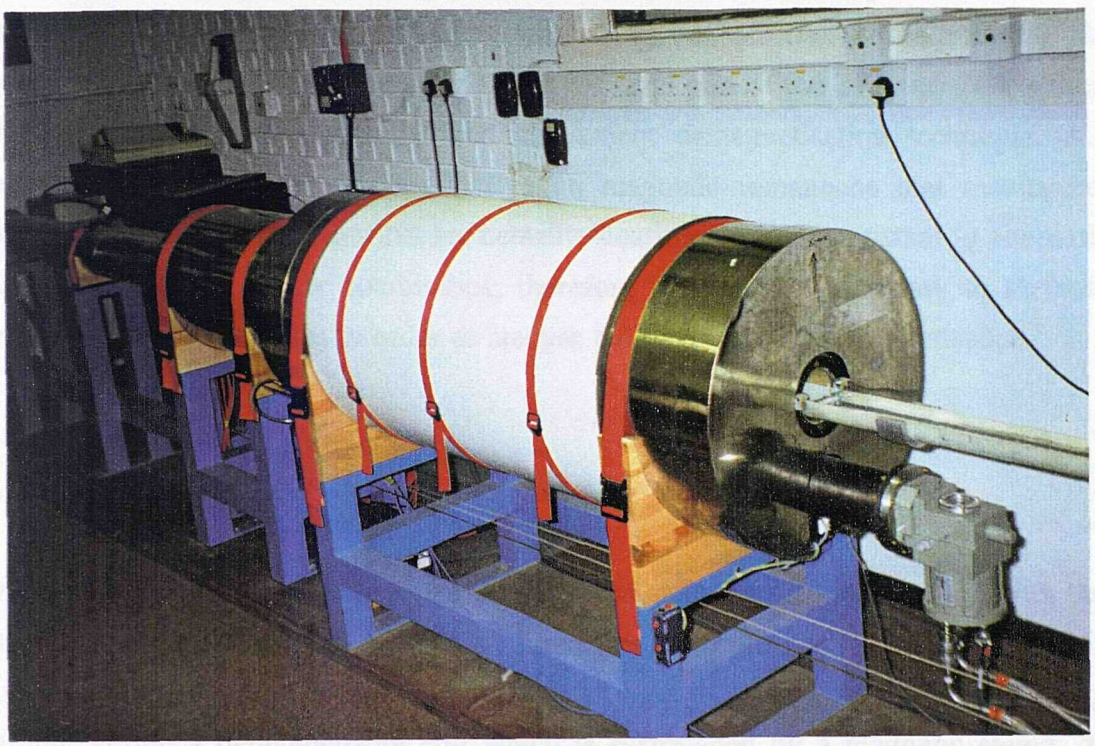

Plate 3-3 *2-G whole-core cryogenic magnetometer.*

Detailed comparison of sample measurement between the CCL and 2-G magnetometers indicate that the two instruments show general agreement between magnetic direction and intensity determinations. Typical directional differences of 1-2° exist; the magnetic intensity determinations on the CCL however, are on average 8% lower than those measured on the 2-G magnetometer (Ting, 1991).

3.3 Progressive demagnetisation

Most rocks and sediments have a number of different components of magnetisation which are retained in different populations of magnetic grains. These components have usually been acquired at different times during the rocks history and since they commonly have different stabilities, it is possible to progressively destroy each component in turn. The component of magnetisation with highest stability will generally be that which was acquired at or close to the time of deposition of the sediment. For magnetostratigraphic investigations therefore, it will be this primary component that is of most significance.

Two methods of progressive demagnetisation were used in this study. At least one sub-sample at each stratigraphic height was demagnetised by the *alternating field demagnetisation (A.F.)* method which is an intergral part of the 2-G and CCL systems and therefore a relatively quick and convenient demagnetisation technique. A.F. demagnetisation is particularly effective on magnetic remanence that results from titanomagnetites but sediments that are hematite-bearing are often resistant to alternating fields due to their higher coercivities; therefore it is usually necessary to *thermally demagnetis*e such samples in order to analyse the components of magnetisation.

3.3.1 Alternating field demagnetisation

During the A.F. demagnetisation of a sample, equal numbers of grains are left with their magnetic moments pointing in opposite directions along the axis of the demagnetising coil which results in no net magnetism from these grains. This is achieved by placing a sample within a demagnetising coil which is surrounded by a magnetic shield, and subjecting it to a decaying alternating field which has been ramped up to a predetermined maximum value. If this process is carried out sequentially along the 3 orthogonal axes of the sample, the magnetisation of grains with coercivities less than or equal to the applied field will be effectively randomised. By progressively increasing the applied field in 5mT increments it is possible to reveal different components of magnetisation.

3.3.2 Thermal demagnetisation

Components of magnetisation can also be isolated by heating a sample to successively higher temperatures. The induced thermal fluctuations will progressively randomize the magnetisation of grains which have a *blocking temperature* less than or equal to the applied temperature. The heating of samples takes place in a non-magnetic oven (Plate 3-4) where they are cooled back to room temperature in a magnetic field-free space. Any viscous components of magnetisation that may have been acquired during the transfer of the specimen between instruments can be removed by routinely applying an alternating field of 5 mT to the specimen prior to measurement.

Plate 3-4 *Magnetic Measurements thermal demagnetiser (MMTD)*

Samples were usually heated in 50°C or 33°C increments until either a demagnetisation stable end point was reached or until there was a mineralogical change (see susceptibility section 3.6). The behaviour of samples of similar composition can be investigated by using a small number of pilot specimens and then the temperature increments of the remaining samples can be adjusted accordingly.

Ideally, as the Curie or phase transition temperatures of the magnetic components are approached, the increments are reduced in order to clearly identify the higher blocking temperature components.

Thermal demagnetisation of sediments has two main disadvantages over the A.F. technique: firstly, it can be extremely time consuming considering only 5-6 large volume samples may be heated at any one time and secondly the process is destructive.

Where samples of a particular type responded well to A.F. demagnetisation, thermal demagnetisation was carried out on samples at larger stratigraphic intervals in order to confirm the polarity determined by the A.F. technique. Where there was some doubt about the polarity that was interpreted from A.F. demagnetisation, a combination of both techniques on subsamples at each stratigraphic site was adopted.

3.4 Representation of demagnetisation data

3.4.1 Graphical illustration of demagnetisation data

The behavioural characteristics of samples during demagnetisation are illustrated graphically by *stereographic projections* (Fig. 3-1a) and *vector end-point (VEP)* diagrams (Fig. 3-1b). On the former projection, the components of magnetisation are displayed on a stereo net where the declination scale runs clockwise from 0-360° around the perimeter of the net and the inclination scales from ±90° at the centre of the net to zero at the perimeter (open or closed circles represent negative or positive inclination values respectively). Normalised intensity variations during progressive demagnetisation are displayed on an accompanying plot.

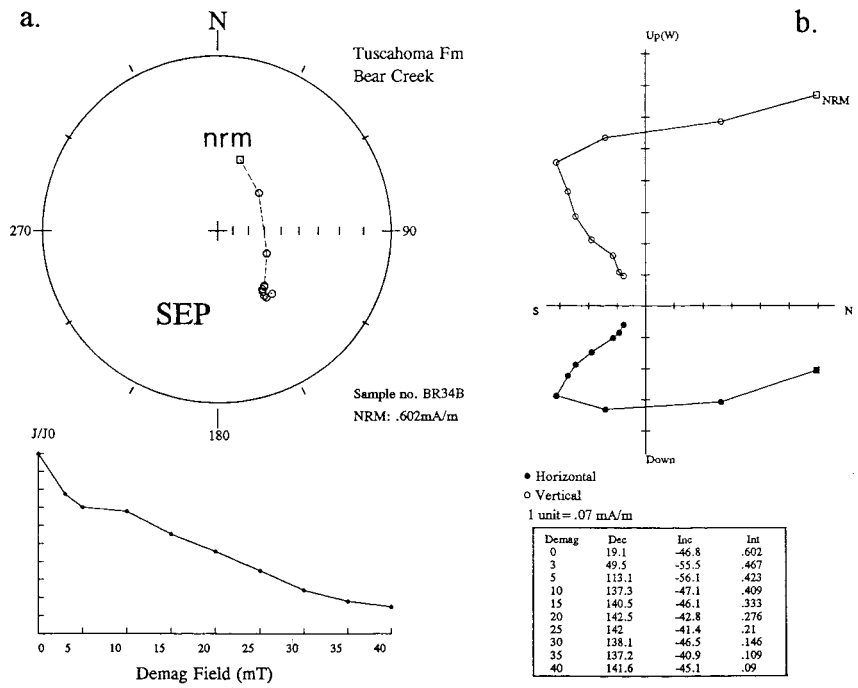

Demag	Dec	Inc	Int
0	19.1	-46.8	.602
3	49.5	-55.5	.467
5	113.1	-56.1	.423
10	137.3	-47.1	.409
15	140.5	-46.1	.333
20	142.5	-42.8	.276
25	142	-41.4	.21
30	138.1	-46.5	.146
35	137.2	-40.9	.109
40	141.6	-45.1	.09

Figure 3-1 **a.** *Stereographic projection* **b.** *Vector end-point plot*

The second type of graph, the vector end-point plot, combines both the magnetisation vector and the intensity at each demagnetisation step on one plot, where the vector is projected onto a horizontal and a vertical plane aligned either N-S or W-E. If successive points, representing demagnetisation steps, lie on a straight line then a single component

of magnetisation is being removed and the gradient of that line indicates the direction of the component. Figure 3-1b for example illustrates two straight lines and thus two components have been identified. When a straight line is directed through the origin then only a single component remains; this is represented on the stereographic projection by a group of closely spaced points known as a *stable end-point (SEP).*

The precise determination of a SEP may not be possible for a variety of reasons; however, for polarity determinations it is often possible to infer the hemisphere in which a SEP is probably located by the trend of the points on a stereographic net and in rare situations identify a confident SEP by the intersection of such trending points from a number of subsamples from the same stratigraphic horizon (for example, Townsend and Hailwood, 1985).

3.4.2 Statistical parameters

α95 (Fisher,1953) The statistical parameter α95 has been used in this study to decribe the confidence of repeatibility of multiple measurements (see section 3.5.3) and the grouping of points around a SEP. The α95 represents the radius of a cone of confidence about the observed mean direction within which there is a 95% probability of the true mean lying (Hailwood, 1989). α95 values $< 10°$ are considered acceptable in this study.

Regression coefficient, Rc The Rc is used to describe straight line fits on the vector end-point plot whereby points from the demagnetisation path are projected onto both the horizontal and vertical plane and the line of best least-squares fit is applied to both these projections. The Rc is therefore given as two index figures ranging from 0-1.0 where the maximum value of 1.0 results from points that lie on an exact straight line. Values of ≥ 0.9 in both projections are considered acceptable for describing straight lines in this study. Regression coefficients however, have now been largely superceded by the *maximum angle of deviation (MAD).*

Maximum angle of deviation, MAD *Principal Component Analysis (PCA)* is a technique used to find and estimate the directions of lines and planes of best least-squares fit along the demagnetisation path of a palaeomagnetic specimen (Kirchvink, 1980). The MAD provides a precision index based on the geometry of the data set where the smaller

the value, the greater the degree of precision of points along a straight line. Values $< 10°$ are considered acceptible in this study.

A combination of $\alpha 95$ and MAD statistics have been applied to the vast majority of demagnetisation data from samples under investigation here. Regression coefficients were used only for the analysis of demagnetisation data from the Oak Grove core, investigated at the beginning of this study.

3.4.3 Classification of demagnetisation data

Sample behaviour during demagnetisation and the quality of data defining that behaviour varied enormously between the samples analysed. In one extreme, fresh clays usually yielded a good quality data set with reliable determination of the primary component; in the other extreme, friable sands generally provided poor data which did not identify a component of characteristic magnetisation. In order to provide an objective assessment of the behavioural characteristics during demagnetisation, *reliability categories* have been adopted (Hailwood, *pers. com.*). Demagnetisation plots can be broadly classified as either:

*Stable end point (SEP) - **S*** *Trending - **T*** *Erratic - **E***

The quality of the data which falls into the first and second broad categories is further ranked from 1-3.

S1 Highest quality data where a well-defined stable end point (SEP) is reached. The SEPs are clearly identified as closely spaced points on the stereographic plot and on the vector end-point plot, several of the last steps of demagnetisation define a line which is directed through the origin. There is no doubt about the polarity assignment (for example: figures 3-2 and 3-3).

S2 Intermediate quality data where polarity assignment is regarded as reliable. The SEP is reasonably well defined by a grouping of points on the stereographic projection (MAD or $\alpha 95$ typically < 10) but the intensity does not always systematically decrease between subsequent demagnetisation steps. The vector plot therefore does not exhibit points that fall on an extensive straight line

through the origin (for example: figures 3-3 and 3-5).

S3 Poor quality data. Directions often become erratic and intensities do not always decrease but there is some degree of grouping on the stereogram (for example: figures 3-6 and 3-7).

* In some cases well-defined SEPs appeared to be located in the 'wrong' hemisphere of the stereogram. For instance, a SEP with positive inclination but with a southerly declination. Samples that show this type of behaviour are difficult to explain magnetostratigraphically and are identified in the summary data sheets by the symbol 'A', for anomalous. A sample that may have been labelled incorrectly or that had become unintentionally inverted during sub-sampling or measurement may explain this phenomenon. Usually, however, sister samples from the same horizon will highlight a measurement error.

T1 Highest quality directional trend data. Trend is relatively long, well-defined and usually reaches the hemisphere of polarity assignment. No doubt about reliability of polarity assignment (for example: figures 3-8 and 3-9).

T2 Intermediate quality directional trend data. Defineable trend evident but may not reach the hemisphere of polarity assignment. No doubt about polarity assignment (for example: figures 3-10 and 3-11).

T3 Poor quality data. Probable trend present but it is poorly defined and destination of the trending points may not be obvious. Some doubt about polarity assignment (for example: figure 3-12).

E Erratic behaviour where no polarity assignment is possible (for example: 3-13).

The final polarity assigned to a specific site in an outcrop or core is determined from the demagnetisation behaviour of all the sub-samples that have been analysed at that particular site.

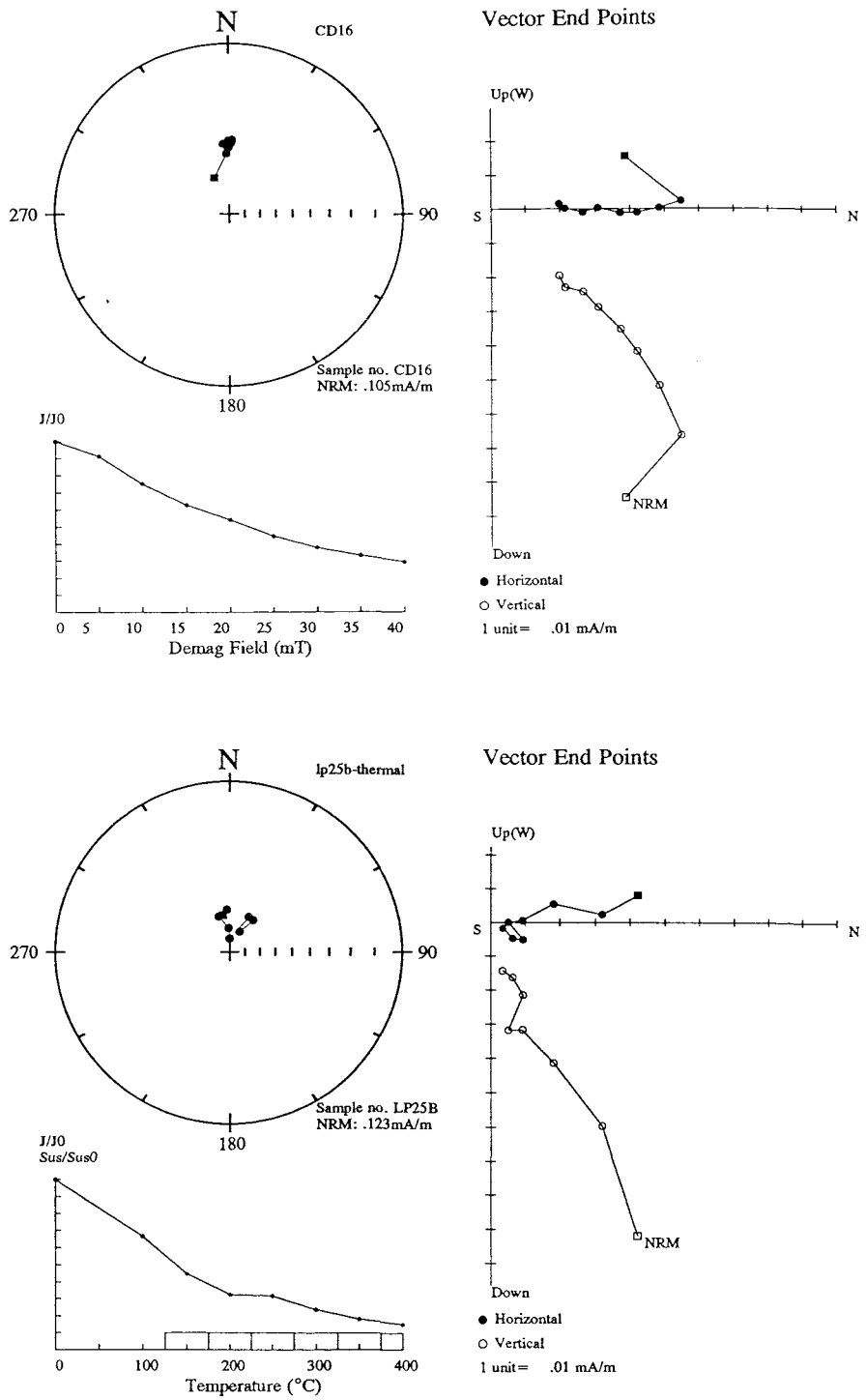

Figure 3-2 *Examples of S1 normal polarity* demagnetisation plots. **Top.** A.F. *demagnetisation.* **Bottom.** *thermal demagnetisation. For explanation of symbols used, refer to Section 3.4.1*

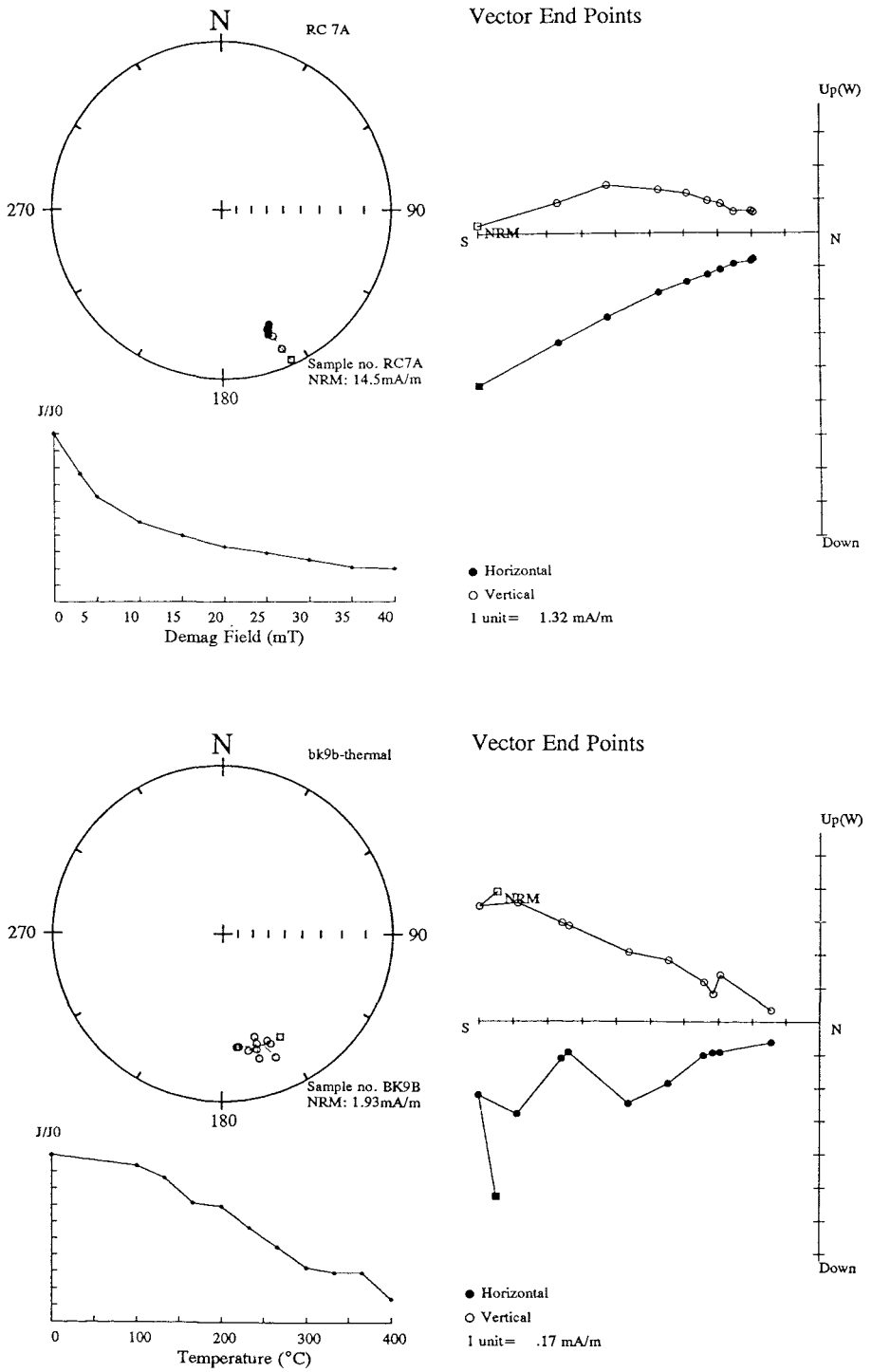

Figure 3-3 Examples of S1 reverse polarity demagnetisation plots. **Top.** A.F. demagnetisation. **Bottom.** thermal demagnetisation. For explanation of symbols used, refer to Section 3.4.1.

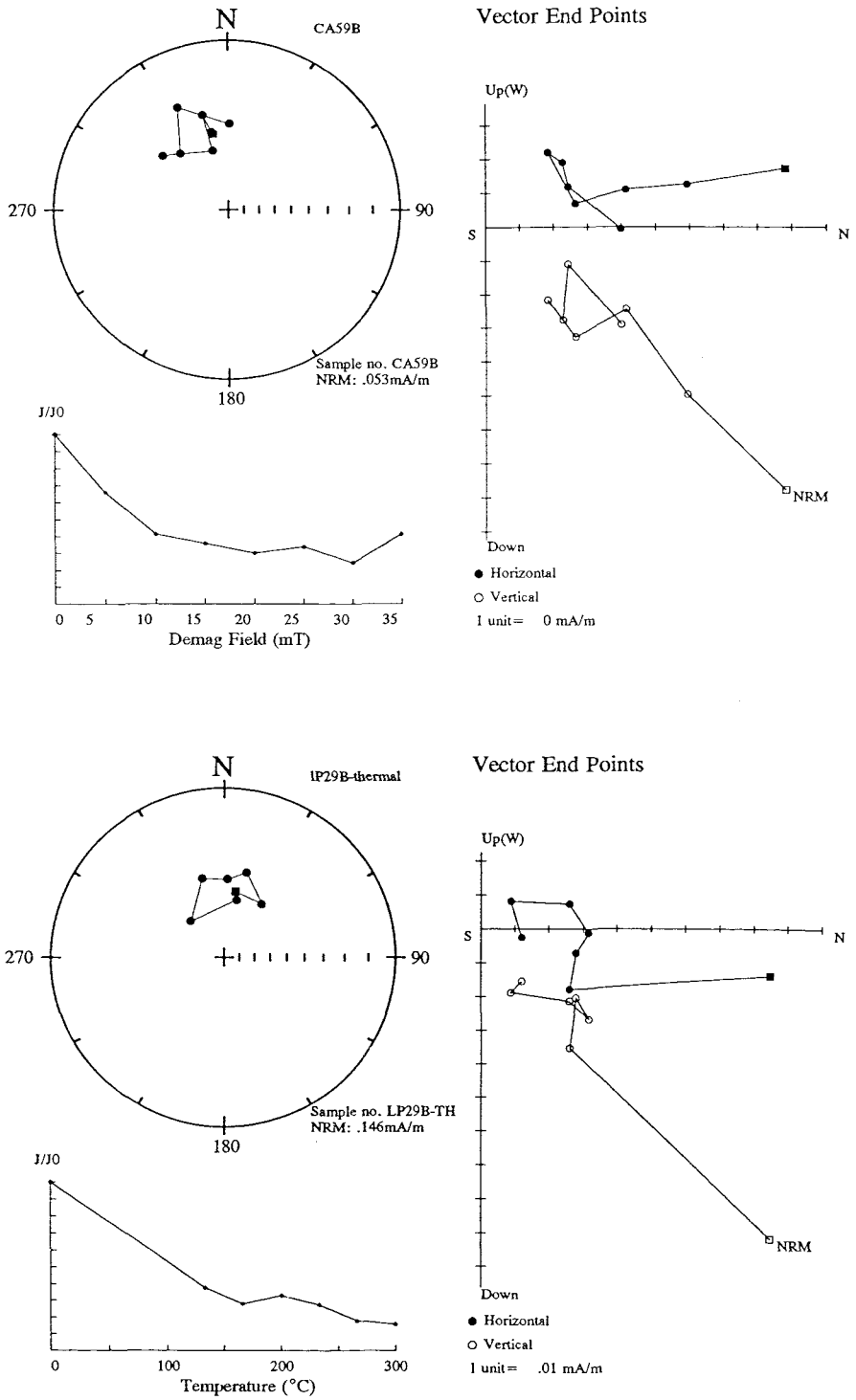

Figure 3-4 *Examples of S2 normal polarity demagnetisation plots.* ***Top.*** *A.F.demagnetisation.* ***Bottom.*** *thermal demagnetisation. For explanation of symbols used, refer to Section 3.4.1.*

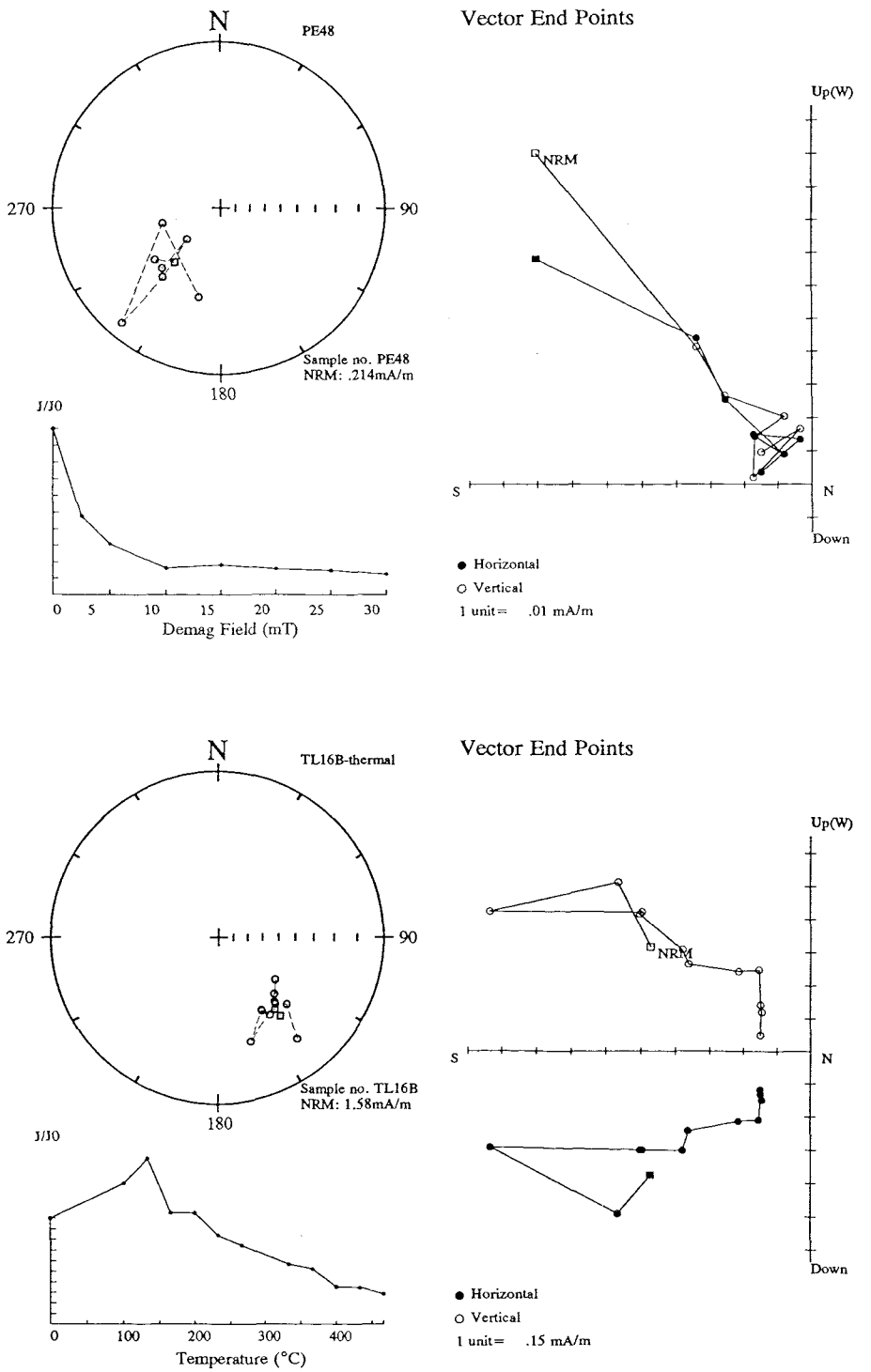

Figure 3-5 *Examples of S2 reverse polarity demagnetisation plots. **Top** A.F.demagnetisation. **Bottom.** thermal demagnetisation. For explanation of symbols used, refer to Section 3.4.1.*

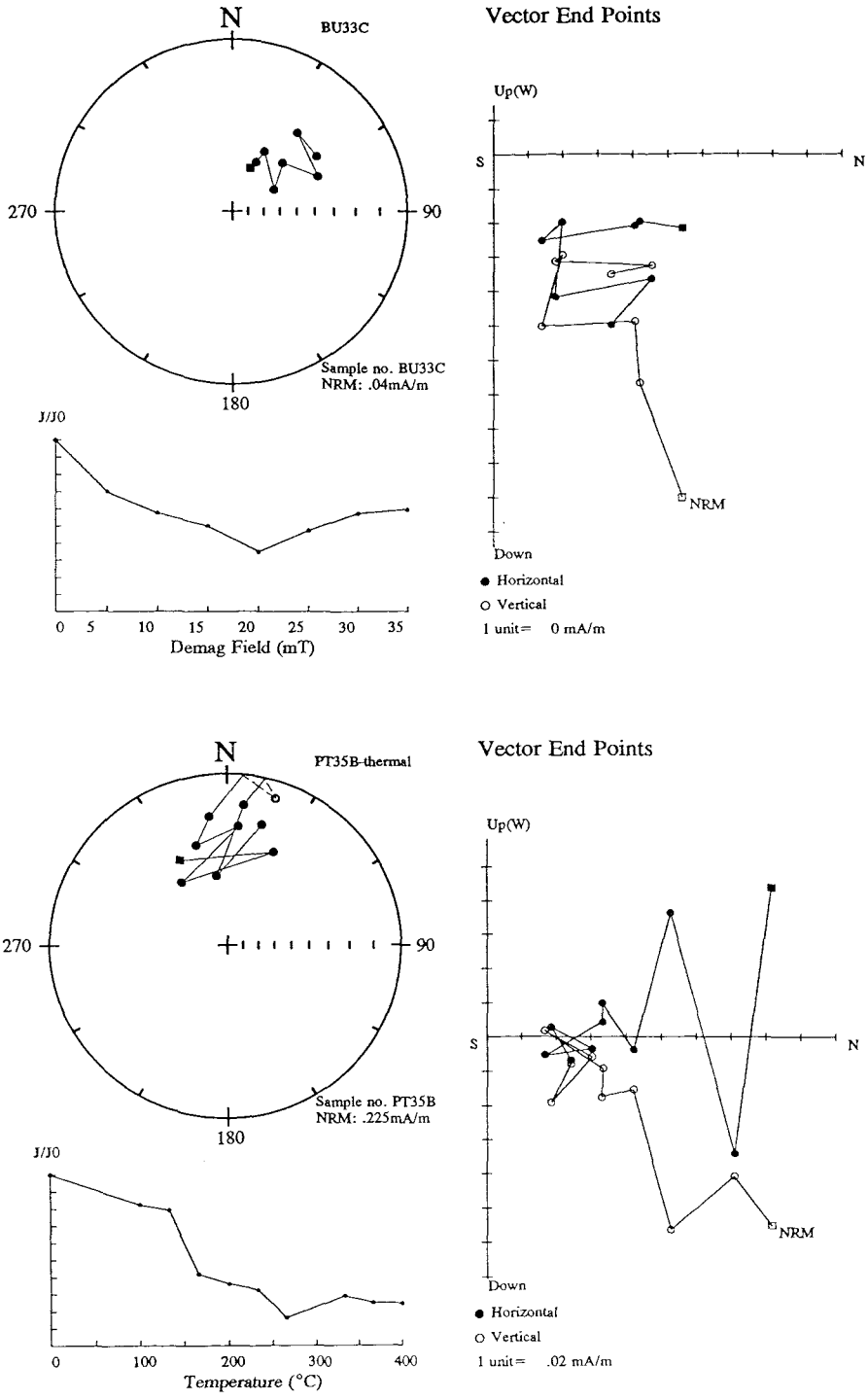

Figure 3-6 *Examples of S3 normal polarity demagnetisation plots.* ***Top*** *.A.F. demagnetisation.* ***Bottom.*** *thermal demagnetisation. For explanation of symbols used, refer to Section 3.4.1.*

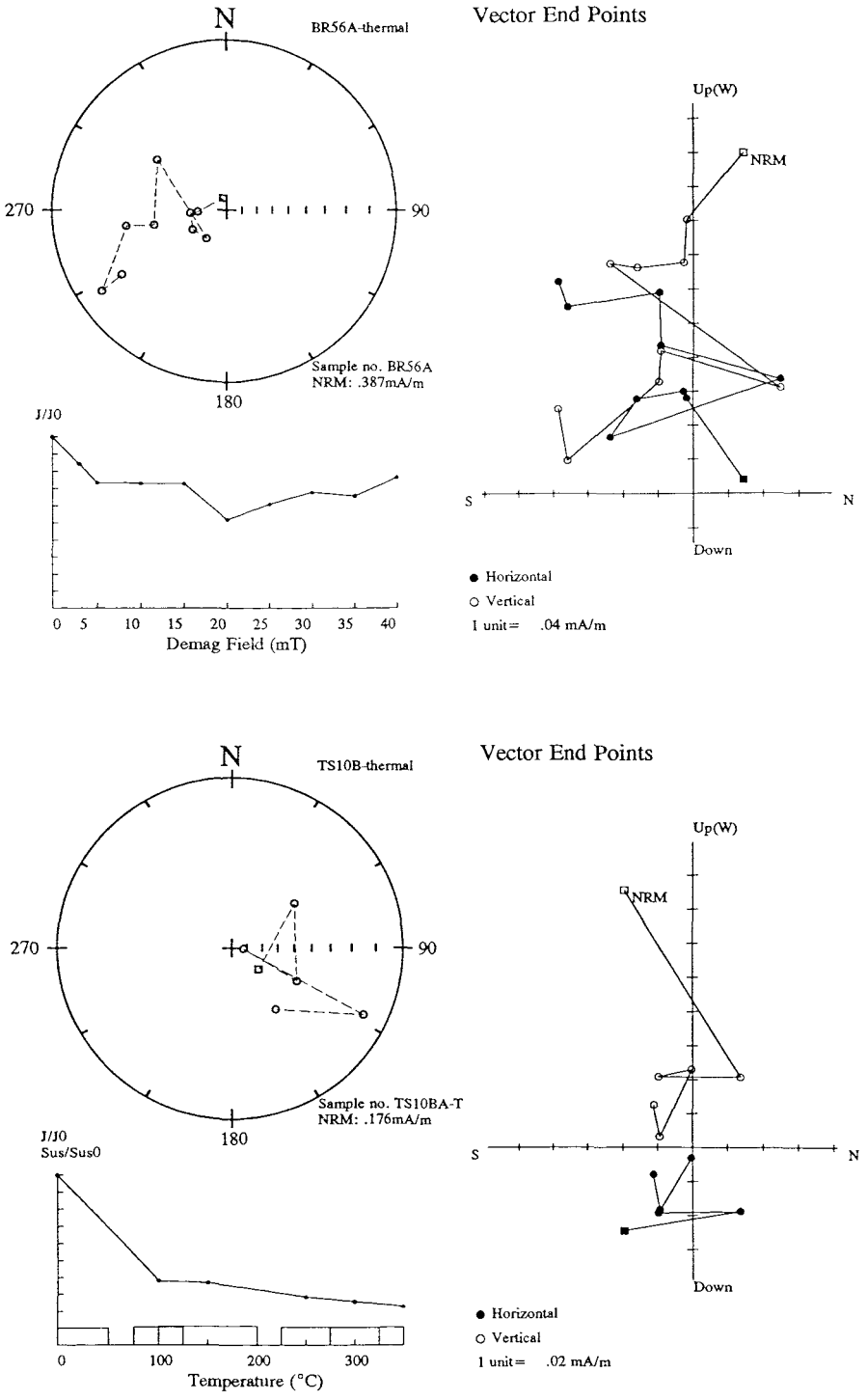

Figure 3-7 *Examples of S3 reverse polarity demagnetisation plots* ***Top.*** *A.F. demagnetisation.* ***Bottom.*** *thermal demagnetisation. For explanation of symbols used, refer to Section 3.4.1.*

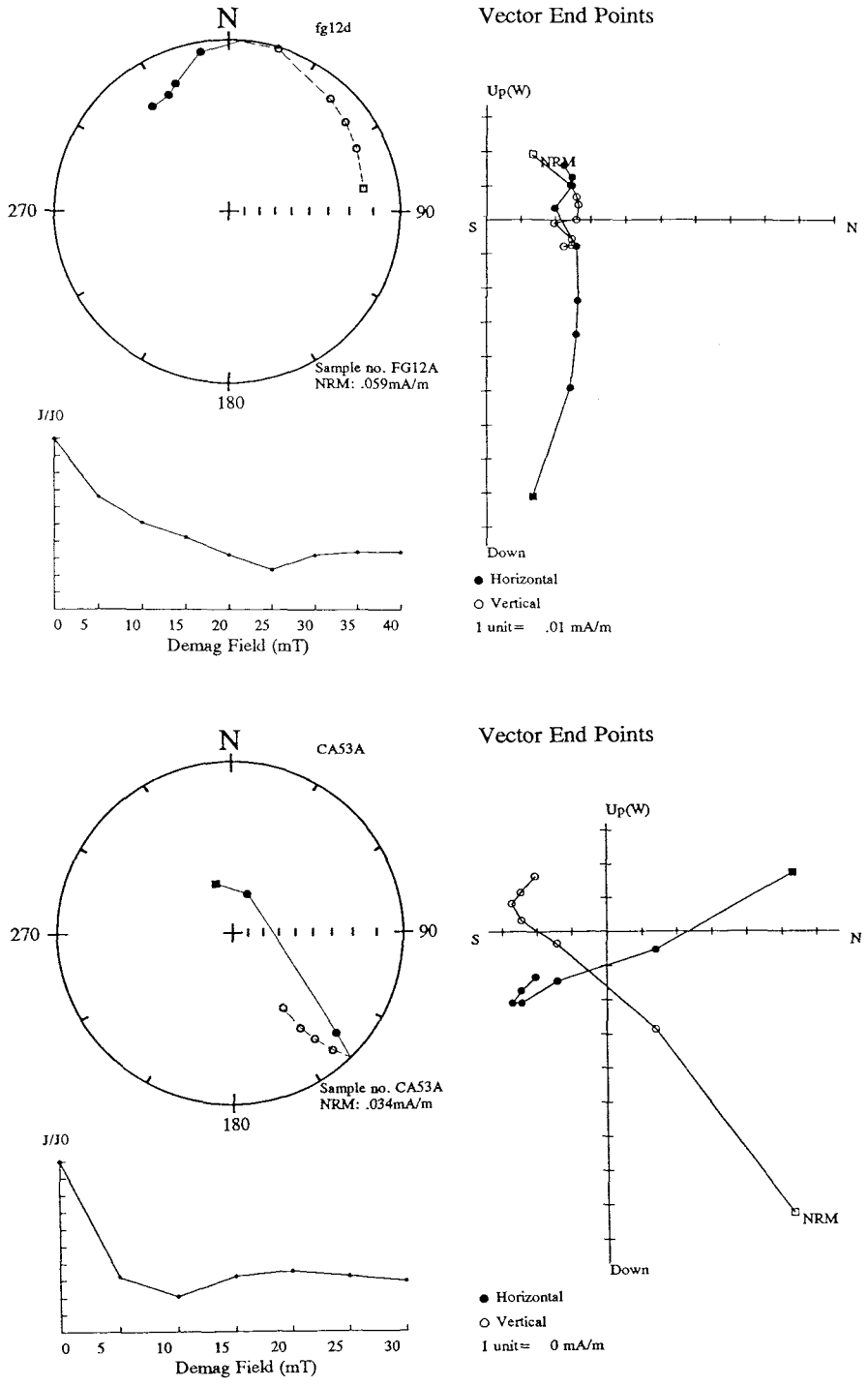

Figure 3-8 *Examples of Tl demagnetisation plots.* ***Top.*** *normal polarity trend - A.F. demagnetisation.* ***Bottom.*** *reverse polarity trend - A.F. demagnetisation. For explanation of symbols used, refer to Section 3.4.1.*

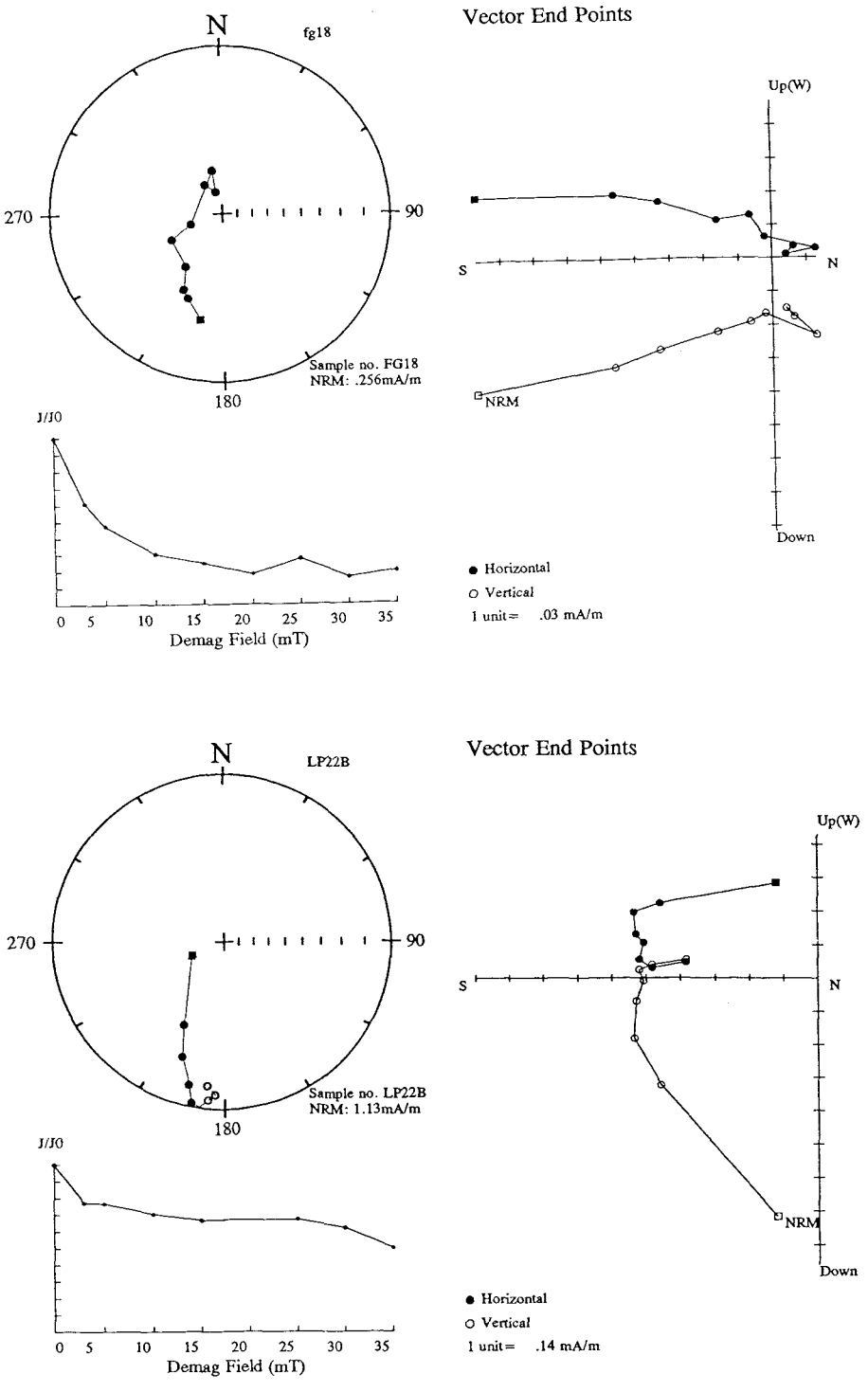

Figure 3-9 *Examples of T1 demagnetisation plots.* ***Top.*** *normal polarity trend - A.F. demagnetisation.* ***Bottom.*** *reverse polarity trend - A.F. demagnetisation. For explanation of symbols used, refer to Section 3.4.1.*

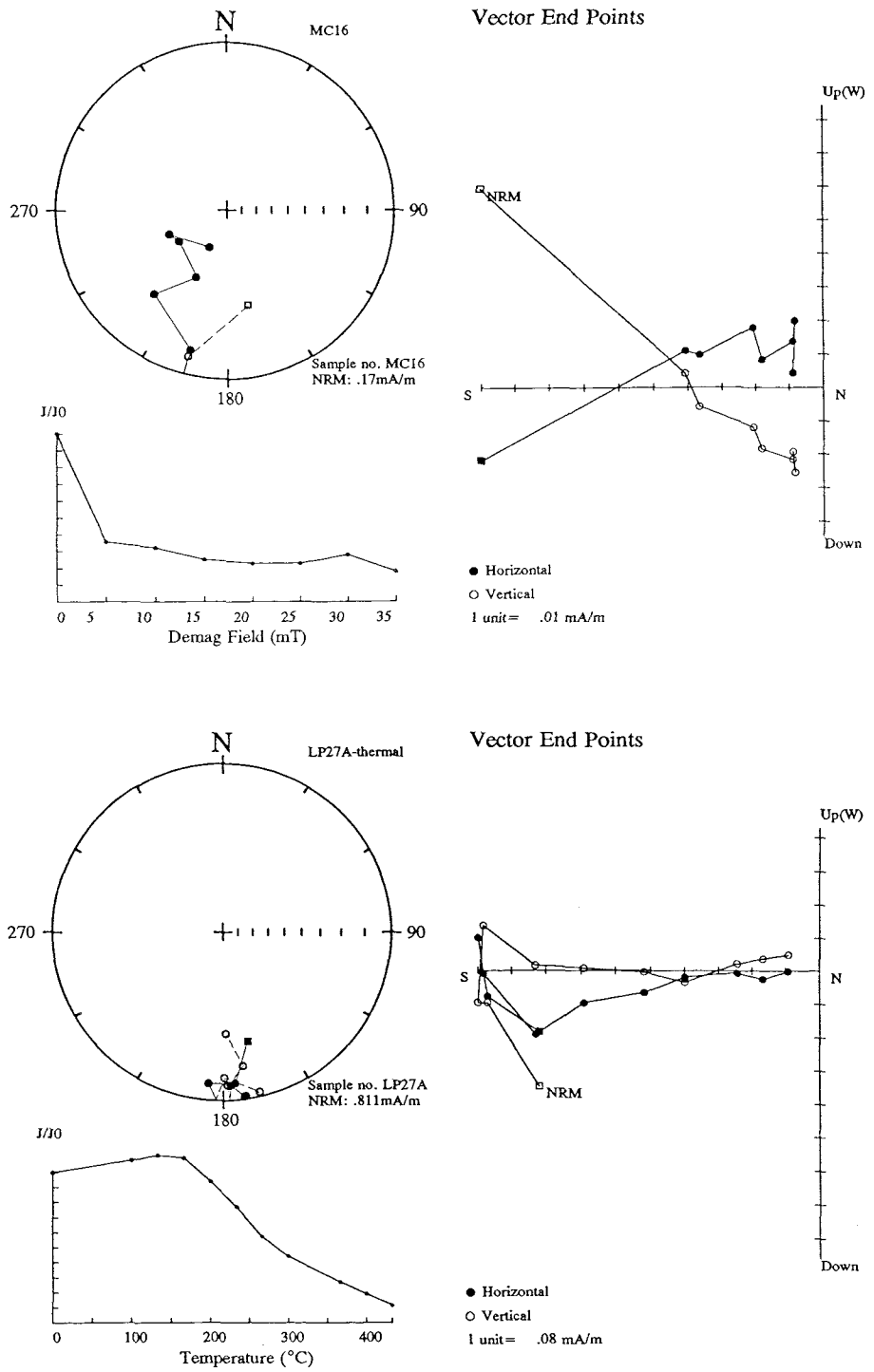

Figure 3-10 *Examples of T2 demagnetisation plots. **Top.** normal polarity trend - A.F. demagnetisation. **Bottom.** reverse polarity trend - thermal demagnetisation. For explanation of symbols used, refer to Section 3.4.1.*

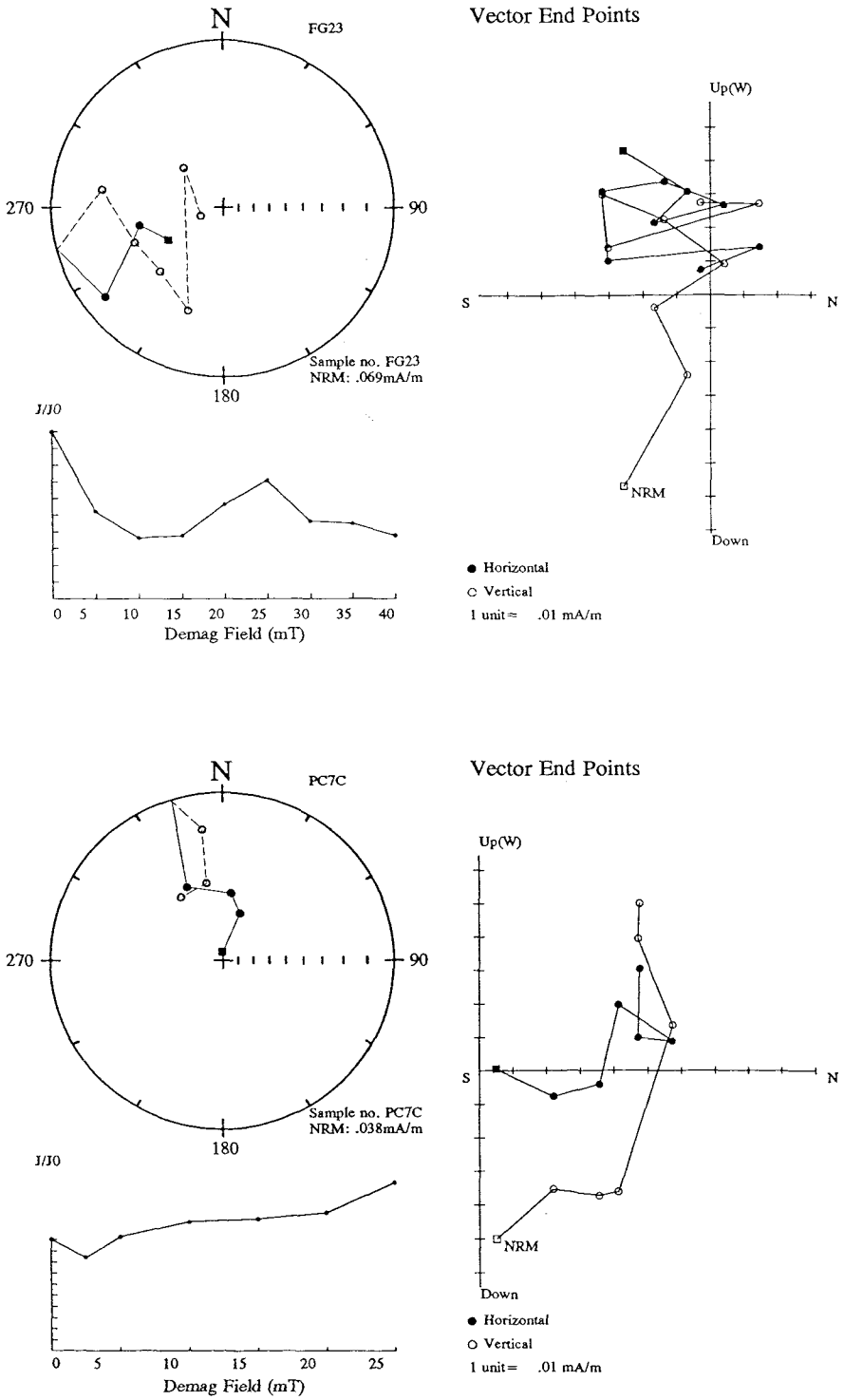

Figure 3-11 *Examples of T2 A.F. demagnetisation showing reverse polarity trends. For explanation of symbols used, refer to Section 3.4.1.*

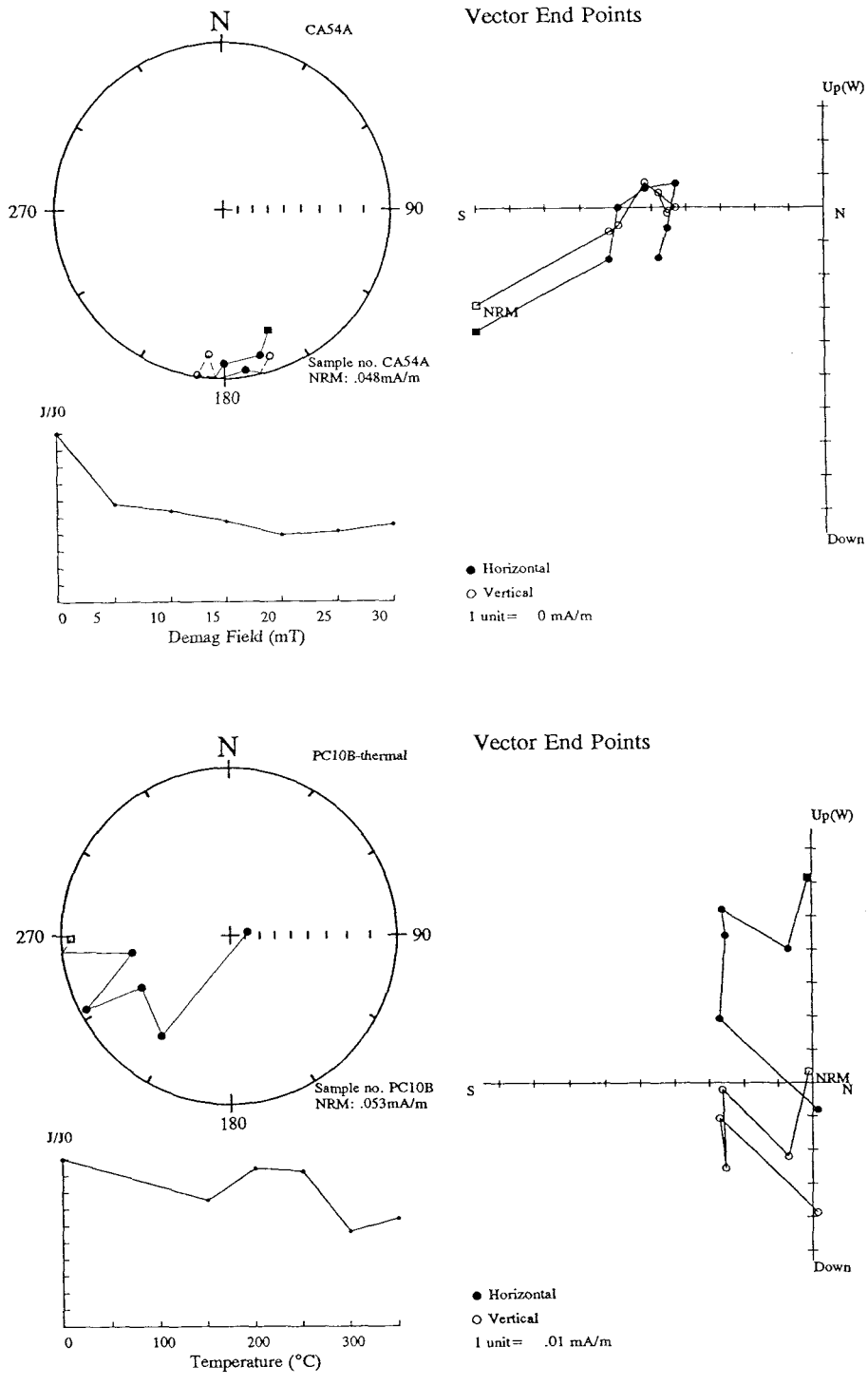

Figure 3-12 *Examples of T3 demagnetisation plots.* ***Top.*** *trend to reverse? - A.F. demagnetisation.* ***Bottom.*** *debatable polarity trend to normal? - thermal demagnetisation.For explanation of symbols used, refer to Section 3.4.1.*

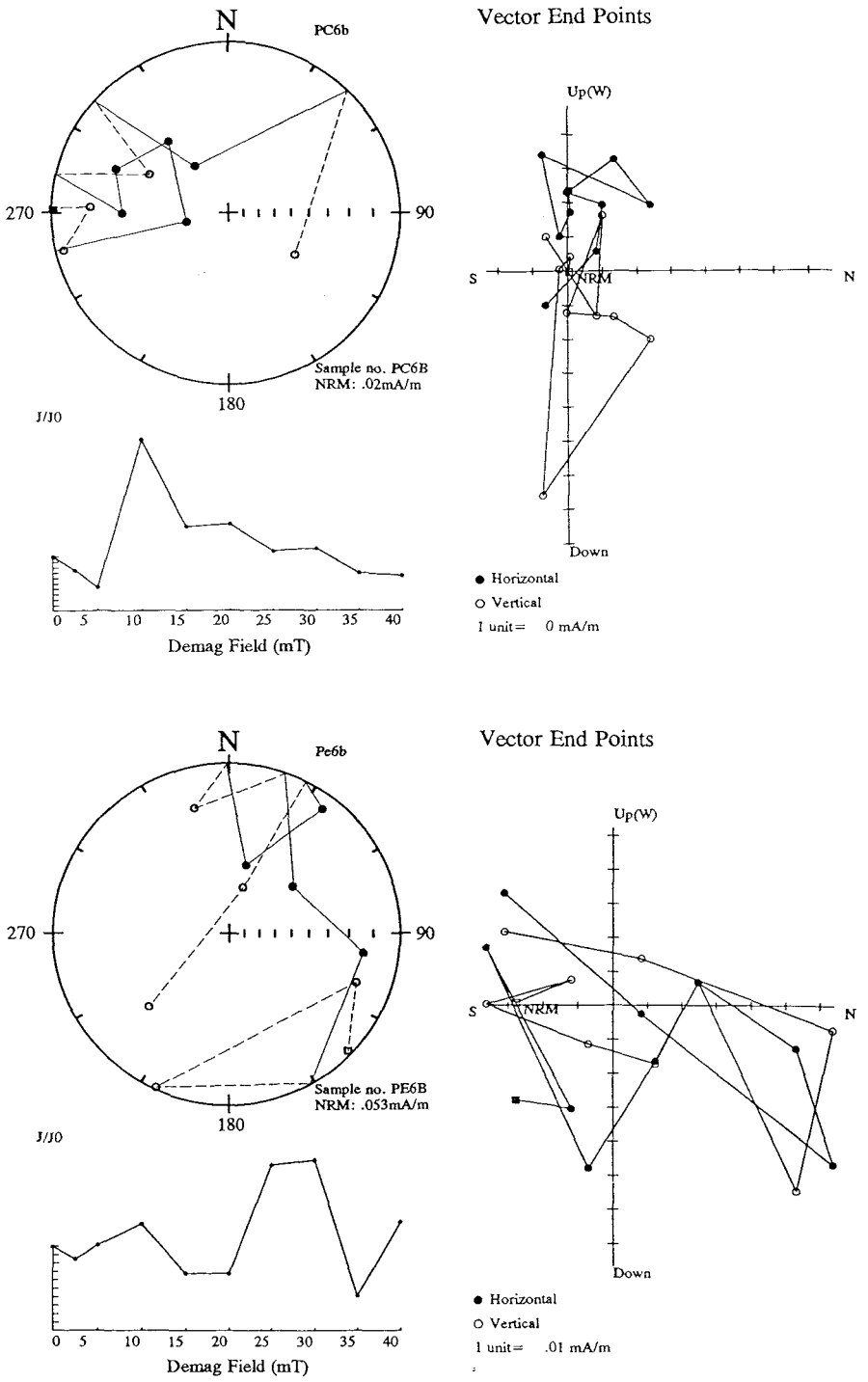

Figure 3-13 *Examples of E-type (erratic) demagnetisation plots from which no reliable polarity determination is possible. For explanation of symbols used, refer to Section 3.4.1.*

3.5 Optimising the measurement reliability of weak magnetic sample

The magnetic intensity and demagnetisation characteristics of samples analysed during this investigation varied enormously. However, with the exception of the Tuscahoma Formation in Alabama the remaining 7 formations that were sampled included certain lithologies which exhibited extremely low magnetic intensities. In order to optimise definition of the magnetic signature of these samples and enable the best polarity determinations to be achieved from their demagnetisation behaviour, the following procedures were used:

- During the magnetometer setup procedure the 'empty holder' option was utilised to subtract the effect of the holder from subsequent measurements (section 3.5.1).

- Large volume samples were measured in order to increase the magnetic moment of the specimen (section 3.5.2)

- Multiple measurements were taken at each demagnetisation step (section 3.5.3).

- The spacing of samples on the holder tray was adjusted according to sample intensities (section 3.5.4).

In addition to these main procedures:

- The holder tray was wiped with a clean cloth soaked in alcohol prior to measurement, thus removing dust and other contaminants.

- Samples were secured in position using non-magnetic 'magic' tape.

- The holder tray was weighted at one end to reduce the amount of rotation which often occurred during measurement.

- Friable samples were wrapped in cling-film to ensure that the holder tray was not contaminated .

3.5.1 Subtraction of the holder magnetism

Figure 3-14 shows a typical plot of the demagnetisation behaviour of the clean 2-G empty holder, at a given point. The plot indicates the relative stability of the magnetic properties of the holder, since the direction and intensity of the magnetic component remains fairly constant throughout the demagnetisation process ($\alpha 95 = 8°$).

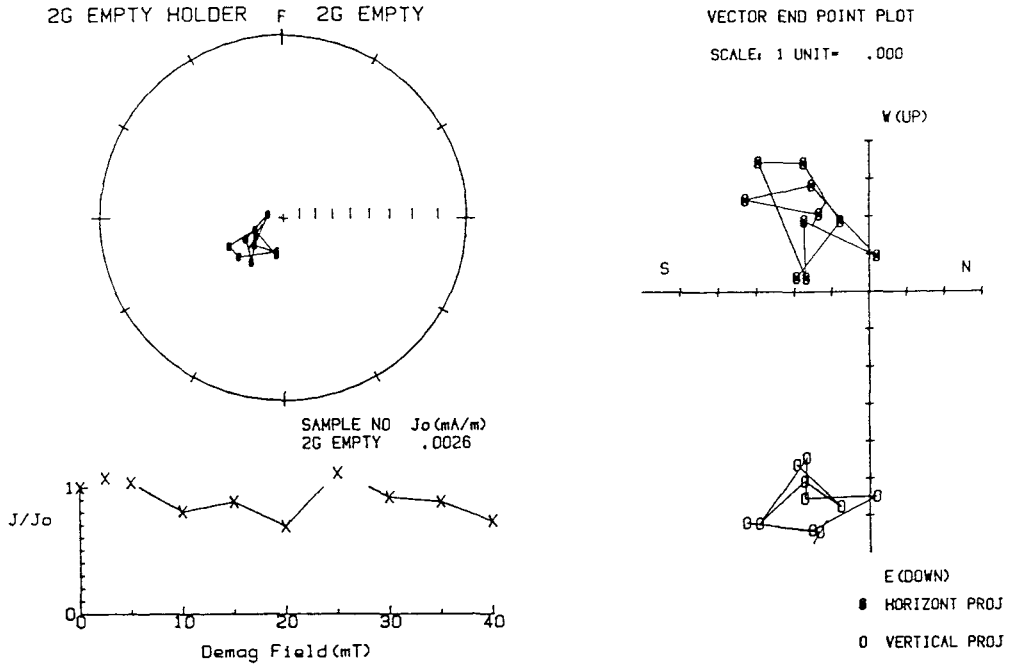

Figure 3-14 *Plot of empty holder measured on the 2-G magnetometer*

The setup procedure on the 2-G magnetometer allows the removal of this holder component from the measured value for each sample. Figure 3-15 illustrates the comparison of the holder behaviour for the mylar and paper holders of the CCL magnetometer and the 2-G system at 3 locations on the sample tray. In addition, it also shows that the setup procedure for the 2-G magnetometer successfully removes the magnetic moment of the holder to a level which compares favourably with that value which exists for the paper holder in the CCL instrument.

In order to confirm that the holder magnetisation has been successfully removed during the setup operation of the 2-G magnetometer it was standard practice to rerun the sample holder and obtain a printout of the background noise levels prior to

measurement.

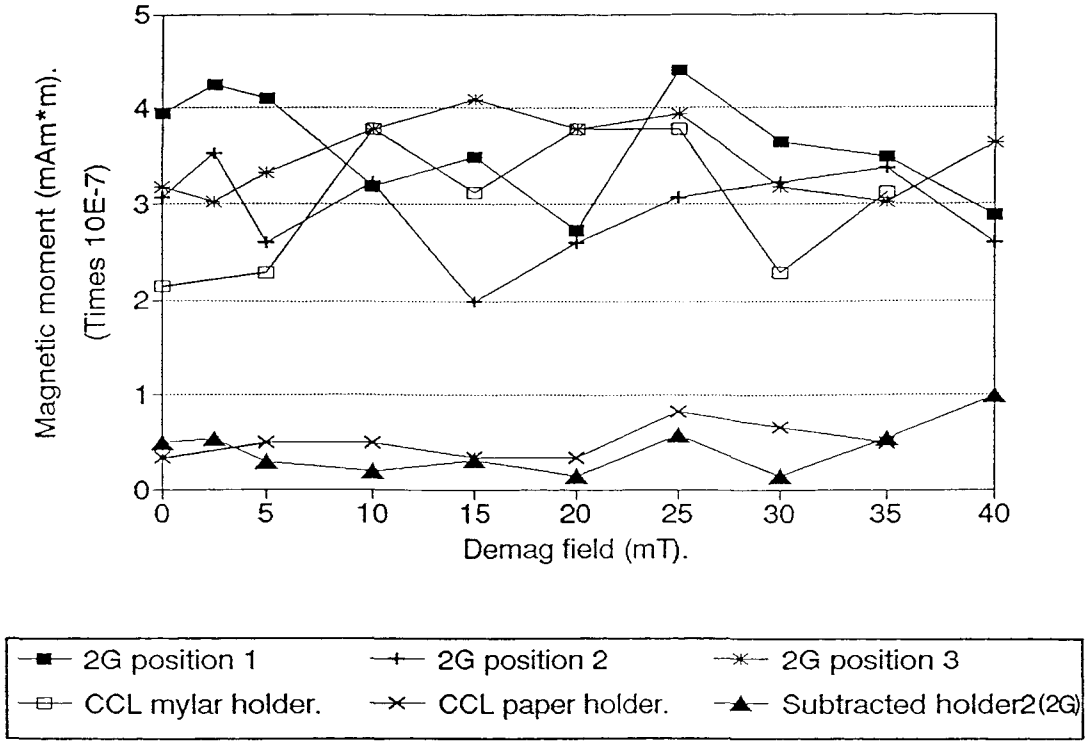

Figure 3-15 *Comparison of empty holder magnetic moments*

3.5.2 Sample volume

When measuring very weakly magnetised material it is vital to maximise the sample's magnetic moment by increasing the sample volume to a limit which is determined by the size of the sensor region within the magnetometer.

Experiments conducted on the 2-G magnetometer identified a 7.5cm optimum length for discrete samples (F.Ting, pers. comm.); this maximizes the amount of sample material in the effective sensor region of the measurement coils (Hailwood et al, 1992). Further limitation on optimum volume is controlled by the 7cm internal diameter of the magnetometer, although a maximum of 6cm is recommended for safe clearance within the instument. Hence an 'ideal' volume is 212cm^3.

Samples within this study had a typical volume of 150cm^3 although where samples exhibited relatively high intensities (well above the holder intensity throughout the demagnetisation process) the sample volumes could be reduced without any detrimental effects (for example, Tuscahoma clays). This was particularly applicable during thermal demagnetisation when many more samples could be heated at each step, significantly reducing measurement time.

3.5.3 Repeat measurements

At each demagnetisation step a minimum of three repeat measurements were carried out in order to identify any spurious values of declination and inclination.

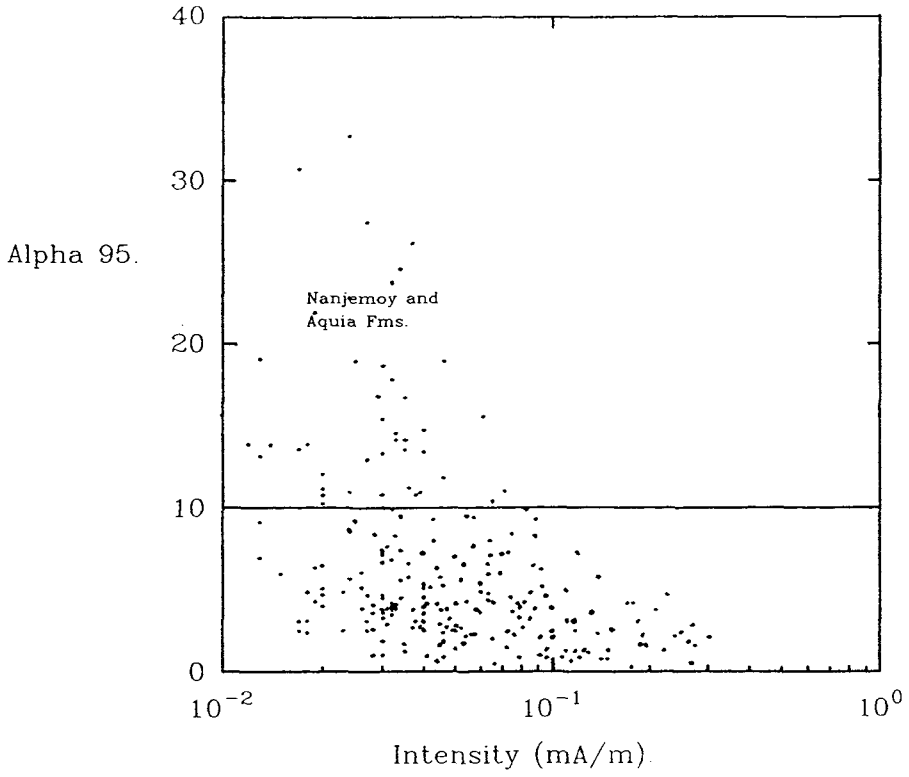

Figure 3-16 *α95 values for triple measurements plotted as a function of magnetic intensity of core material from Oak Grove.*

Figure 3-16 illustrates how the α95 values for triplicate measurements generally increase as the intensity falls. By increasing the number of repeat measurements, however, it is possible to improve the reliability of values for even weaker material. Experiments with

chalk conducted by Paul Montgomery (pers. comm.) suggested that specimens with intensities as low as 0.0015mA/m could be confidently measured on the 2-G magnetometer.

The repeatability of measurements of weak material however, is not only a function of the intensity value but also related to the stability of the magnetisation of the sediment which is determined by the minerology and relative grain coercivity. Therefore different types of lithologies, as well as material showing various degrees of weathering exhibited different repeatability characteristics. It is not possible therefore, to identify a single cut-off intensity value below which all samples can be rejected for possessing unacceptably high $\alpha 95$ values. In addition to a sample's behaviour however, the sensitivity of the magnetometer can vary from day to day.

3.5.4 Sample position on magnetometer holder tray

- When executing the Y-axis demagnetisation component the sample boat protrudes through the open end of the magnetometer shield into the laboratory geomagnetic field by about 85cm (Ting, 1991). Therefore, when the magnetometer was used to measure discrete samples in this study they were usually placed within the protected portion of the sample tray thus avoiding the strong magnetic field gradient at the open end of the magnetometer shield.

- The precise position of discrete samples on the holder tray of the 2-G system is important for the accurate measurement of both the intensity and inclination of magnetisation (declinations were largely unaffected by shifts of up to 2cm away from the point of measurement). Discrepancies of $\pm 10°$ in inclination and a 20% decrease in intensity occured 2cm from the point of measurement (Hailwood et al, 1992).

- It is important to consider the spacing of discrete samples on the sample tray to ensure that there is no interference between specimens during measurement; this is particularly important in this study when the types of lithologies sampled had very different magnetic characteristics. For instance, a weak sample in close proximity to a relatively strong one may be completely or partially 'swamped' by the influence of the stronger material. Clearly the interaction of sample spectra will be a function of sample

intensity, size and distance between successive specimens and it is therefore difficult to assign a standard 'safe' distance to minimise interactions.

Samples with intensities of 1.0 mA/m, placed 10cm apart exhibit considerable overlapping spectra. When the spacing is increased to 20cm the individual spectra of each sample can then be resolved (Hailwood et al, 1992). In this present study, the strongest samples measured had typical intensities of the order of 1.0 mA/m and therefore a sample spacing of 20cm was usually adopted. During routine measurement a quick method of ensuring that spectra separation existed could be achieved by incorporating hypothetical samples between those that were actually being measured. In other words, the sample measurement frequency controlled by the software was doubled (Fig. 3.1).

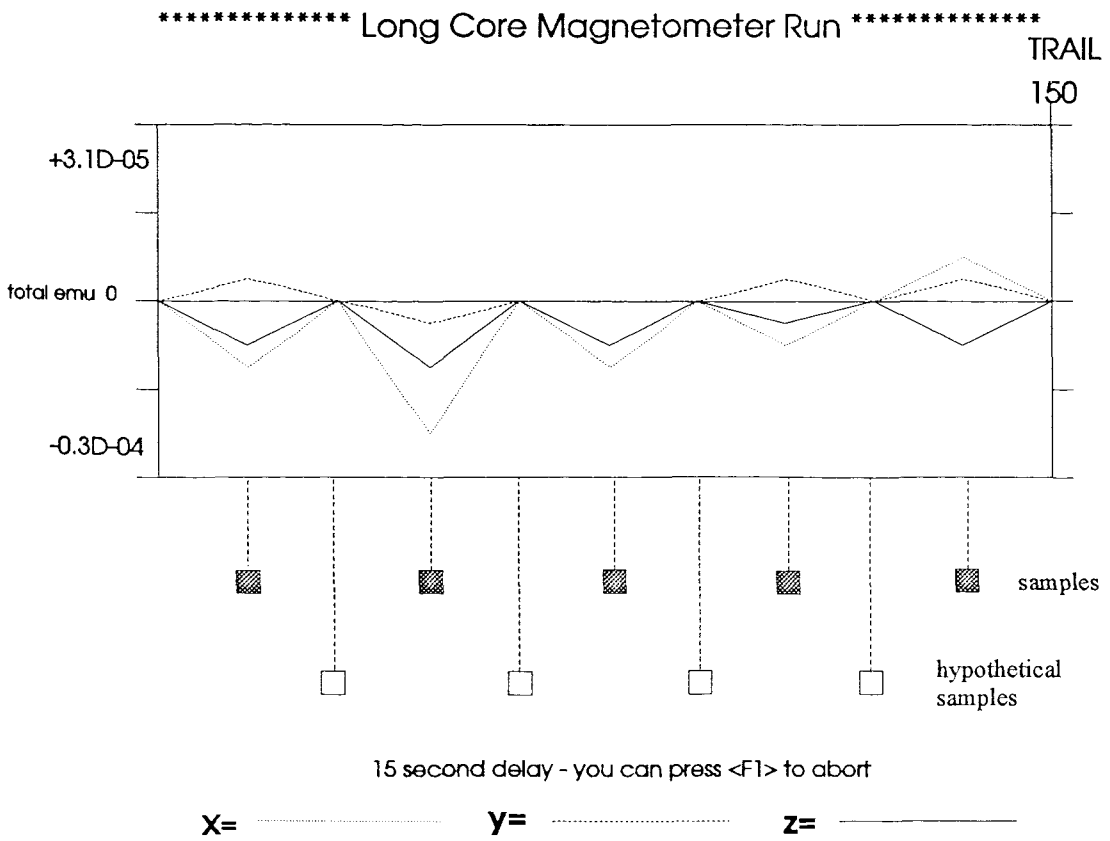

Figure 3-17 *Reproduction of a 2-G printout showing the measurement of 5 samples with hypothetical samples between.*

In this instance, not only are the interactions between sample spectra monitored but any significant spurious fluctuations in background noise level can be immediately identified by jumps in the baseline. This was extremely important when measuring very weak samples, to ensure that the background noise was not approaching the intensity of the sample under measurement.

- Where samples possessed relatively high magnetic intensities (>1mA/m) the volumes of the specimens were reduced. In these cases the samples were elevated in the holder boat of the 2-G magnetometer in order to be centrally placed in the sensor region of the measurement coils. This was achieved by placing the sample on a microscope slide taped across the sample holder.

3.6 Susceptibility

Magnetic susceptibility describes the extent to which a substance is attracted to, or repelled by a magnetic field (Robinson, 1992). It can be measured by the variation in the strength of the field (positive or negative) when a sample is moved in that field. The magnitude of such a variation is a function of the concentration and composition (mineralogy and grain size/shape) of the magnetic material contained within the sample and includes moderately magnetisable paramagnetic substances which may be compounds accommodating Fe^{2+}, Fe^{3+} or Mn^{2+} as well as the strongly magnetisable ferromagnetic minerals.

The susceptibility of discrete samples with relatively large volumes was measured by a susceptibility loop designed primarily for whole-core magnetic susceptibility measurement (Plate 3-6).

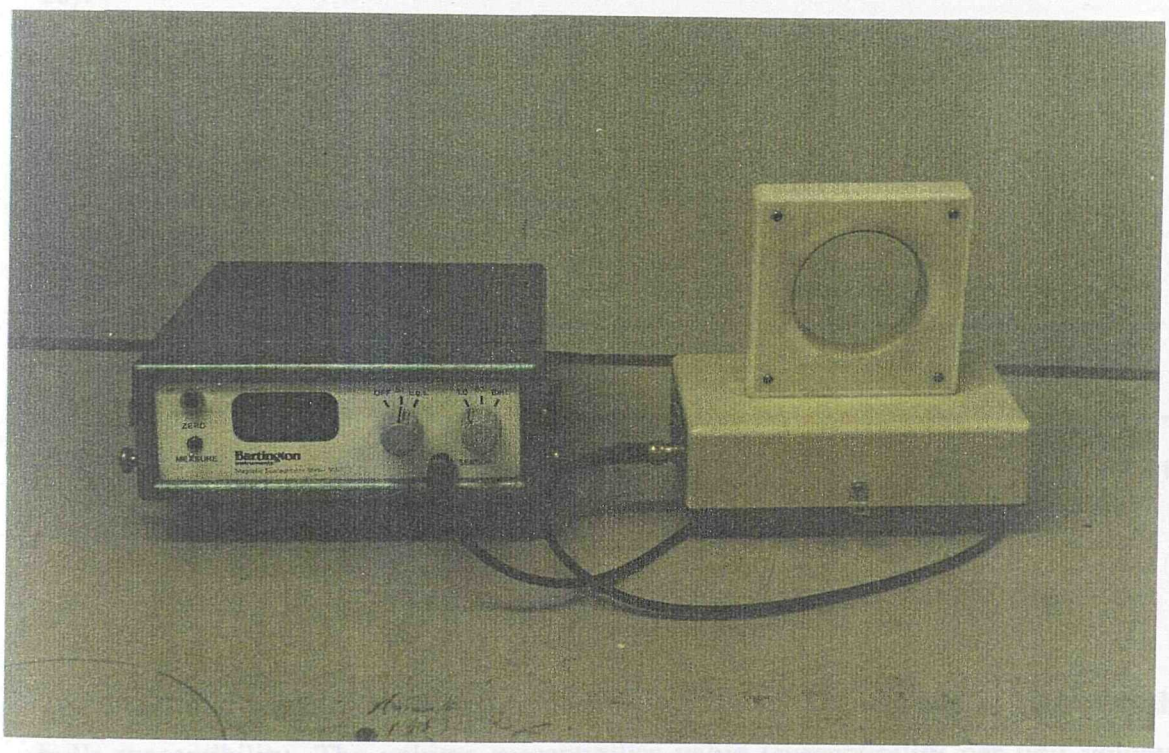

Plate 3-6 *Bartington Instrument's MS system.*

A magnetic field is created by passing an alternating frequency current through a coil that forms the loop (80mm internal diameter). When the sample is inserted into the

loop a sharply tuned oscillator circuit detects the change in the frequency of the alternating current waveform which in turn is directly proportional to the magnetic susceptibility of the sample (Robinson, 1992). The instrument drift was monitored by zeroing the system with an empty loop prior to measurement then remeasuring it after the sample has been removed. Assuming uniform drift, the corrected susceptibilty value could then be determined although in the majority of cases the drift factor over several seconds was minimal. Measurements were repeated three times and the average taken.

Due to the varying sizes of samples from core and outcrops, the Bartington loop had to be calibrated in order to identify the sensor range and the optimum sample length for measurement. A calibration sample was measured at the centre of the loop and moved at 10mm intervals out of the sensor's range. The resulting plot showed a maximum value in the middle of the sensor and then a rapid decrease in magnitude away from the central region until at a distance of approximately 70mm the deflection was negligable (Fig. 3-18).

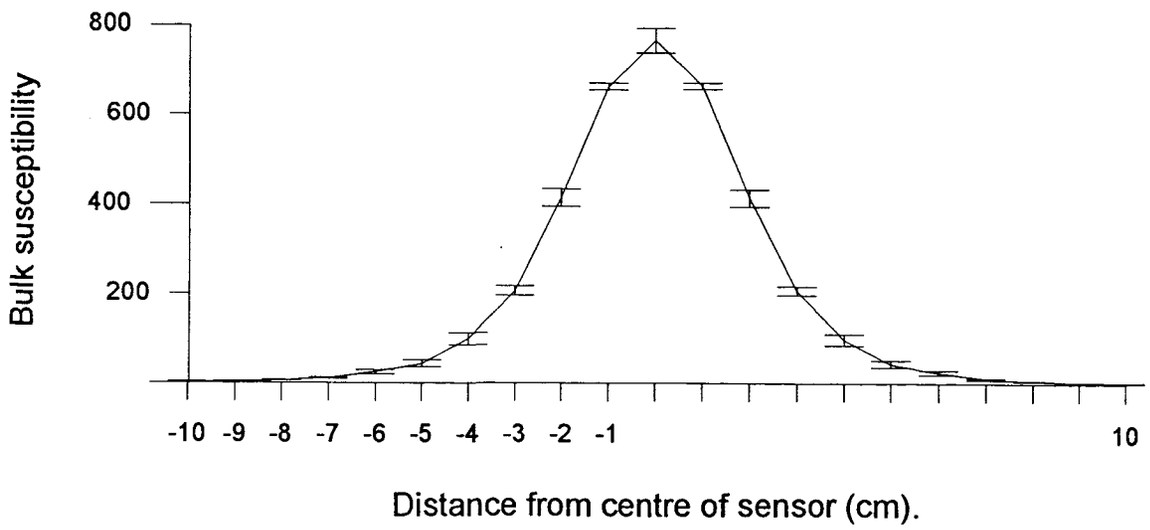

Figure 3-18 *Calibration curve of the Bartington susceptibility loop.*

The measured value of susceptibility has dimensionless SI units and is known as the bulk susceptibility. The volume susceptibility value (susceptibility per unit volume) used in the majority of this study is obtained by dividing the bulk susceptibility by the volume of the sample, in m^3. The susceptibility is then standardized and values between sections and cores (which may have had different sample volumes) can be properly correlated.

The susceptibility measurements were used for 2 purposes:

1. As a direct stratigraphic tool whereby susceptibility measurements were plotted against height in section and from which susceptibility fluctuations, particularly susceptibility peaks could be correlated between sections and cores.

2. As a control on mineralogical phase transitions that may occur during thermal demagnetisation.

The technique of thermal demagnetisation suffers from the disadvantage that heating a sample may lead to undesirable mineralogical phase transitions (Hailwood, 1989). Table 3-1 lists a number of minerals and their alteration products which will affect the magnetic remanence of a sample at certain temperature thresholds.

Initial mineral	**Alteration product**	**Temperature (°C)**
Siderite	Magnetite	>200
Lepidocrocite	Maghematite	220-270
Goethite	Hematite	200-400
Maghemite	Hematite	350-450
Pyrite	Magnetite	350-500
Magnetite	Hematite	>500
Hematite	Magnetite	>550

Table 3-1 *Thermochemical reactions involving magnetic minerals (from Tarling,1983)*

The temperature range and reaction depend critically on the grain sizes and shapes, the presence of impurities (especially water), the atmosphere, rate of heating and so on. They are thus only indicative and poorly defined for natural minerals (Eustance, 1981).

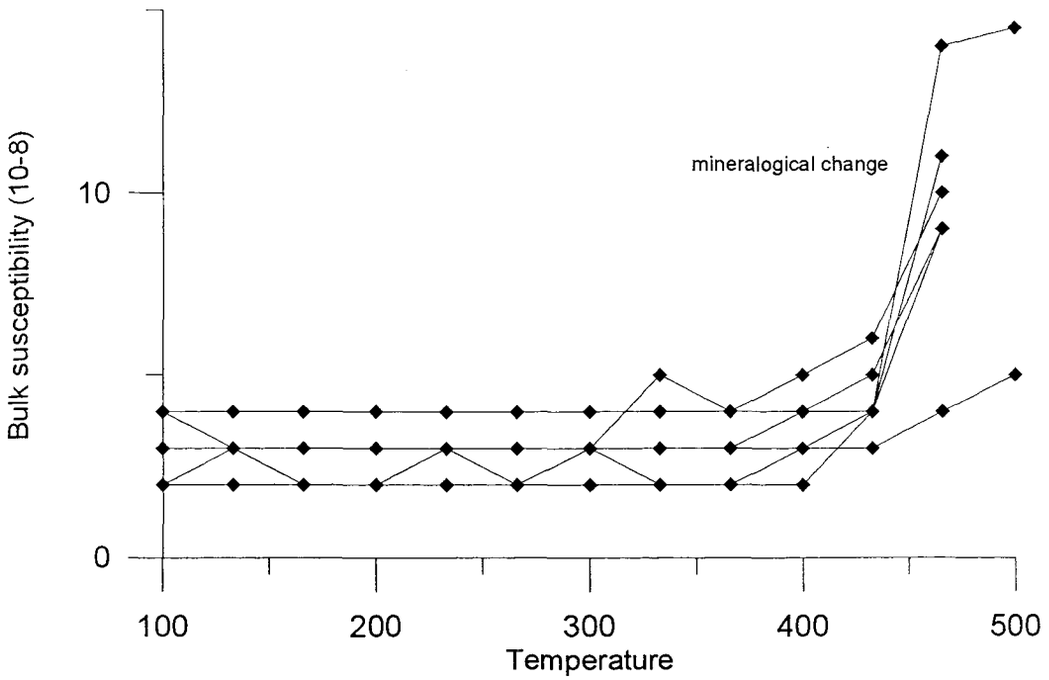

Figure 3-19 *Variations in bulk susceptibility of 5 samples from the Tuscahoma formation during thermal demagnetisation.*

The monitoring of the susceptibility change during progressive temperature steps is a convenient method of identifying these transitions. For example, figure 3-19 illustrates a sudden increase in susceptibility between 433°C-466°C which identifies a consistent mineralogical phase transition occurring in 5 samples from the Tuscahoma Formation in Alabama.

3.7 Isothermal remanent magnetism (IRM)

In order to help establish the origin of the magnetic components and identify possible overprints it is essential to have some standard mineralogical tests. The most reliable studies on the minerals that contribute to a sediment's magnetism and their relationship to one another involve methods such as optical analysis of thin sections, electron probe investigations and transmission and scanning electron microscopy on magnetic separates. Unfortunately, due to the time consuming nature of these techniques and the vast number of samples normally investigated during magnetostratigraphic studies they cannot be used as routine techniques.

The ferromagnetic minerals most common in sediments, however, are magnetite and hematite and since the saturation magnetisation of magnetite is 100 times greater than hematite the response curves of isothermal remanent magnetisation (IRM) gives a good indication of the oxidation state of iron. The technique has the clear advantage in being cheap and quick.

The IRM curves were determined by placing specimens in progressively higher direct fields (supplied by a Molspin pulse magnetiser) up to a maximum of 0.86 Tesla (T) and then plotting the applied field against the normalised intensity that was acquired at each step.

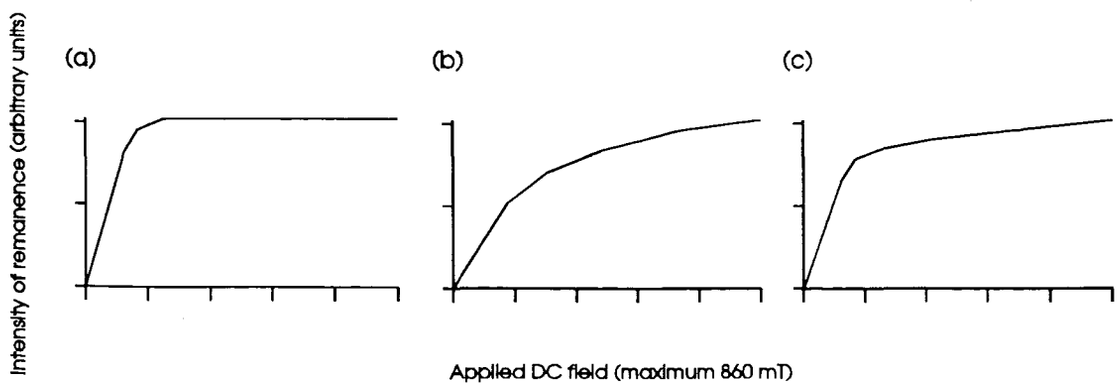

Figure 3-20 *Examples of IRM acquisition curves.* ***a.*** *early saturation of magnetite* ***b.*** *unsaturated hematite* ***c.*** *both minerals present.*

Figure 3-20a shows a sample where the magnetic moment reaches a maximum constant value within the applied field of 0.86T. IRM response curves that saturate in this way are interpreted as containing magnetite. For hematite samples, saturation will not occur within the range of fields applied, and the IRM acquired therefore continues to increase with increases in the direct field (Fig. 3-20b). A curve that demonstrates an initial sharp rate of saturation but which fails to totally saturate before 0.86T probably represents a sample which contains both magnetite and hematite, though magnetite will normally dominate the curve even when only present as a few percentage of the total (Tarling, 1983) (Fig. 3-20c).

A simple but useful method of categorising IRM acquisition curves was adopted by Ali, 1989. He introduced an IRM ratio index whereby the IRM values at 0.3T are divided by those at 0.86T; IRM ratios below 0.9 suggest a hematite content and those above 0.9 magnetite.

3.8 Reliability of magnetostratigraphy

In this study, the lack of igneous intrusions and any significant dip of sedimentary strata ruled out the use of standard tests that are often applied to palaeomagnetic results (e.g. fold and baked contact tests). Consequently, the existence of magnetic components that completely 'overprint' the primary component of magnetisation may not always be readily identified. The reliability of polarity determination therefore is acertained from:

1. The consistency between subsamples at the same stratigraphic level above the sampling datum.

2. The correlation between samples demagnetised by thermal and A.F. techniques.

3. The correlation of sections that are assumed to be of similar ages (and their relationship to the GPTS).

4. IRM interpretations and the quality of demagnetisation behaviour.

5. The anticlockwise deflection of SEPs on a stereographic projection away from north by approximately 10° as predicted from magnetic poles calculated for this interval of time on the North American continent (Besse and Courtillot, 1991).

Chapter 4 Early Tertiary timescales and stratigraphic background

4.1 Stratigraphic subdivisions

The Tertiary Sub-Erathem includes the Paleogene and Neogene Systems (Fig. 4-1). The Paleogene System is further divided into the Paleocene, Eocene and Oligocene Series and the Neogene into the Miocene and Pliocene Series.

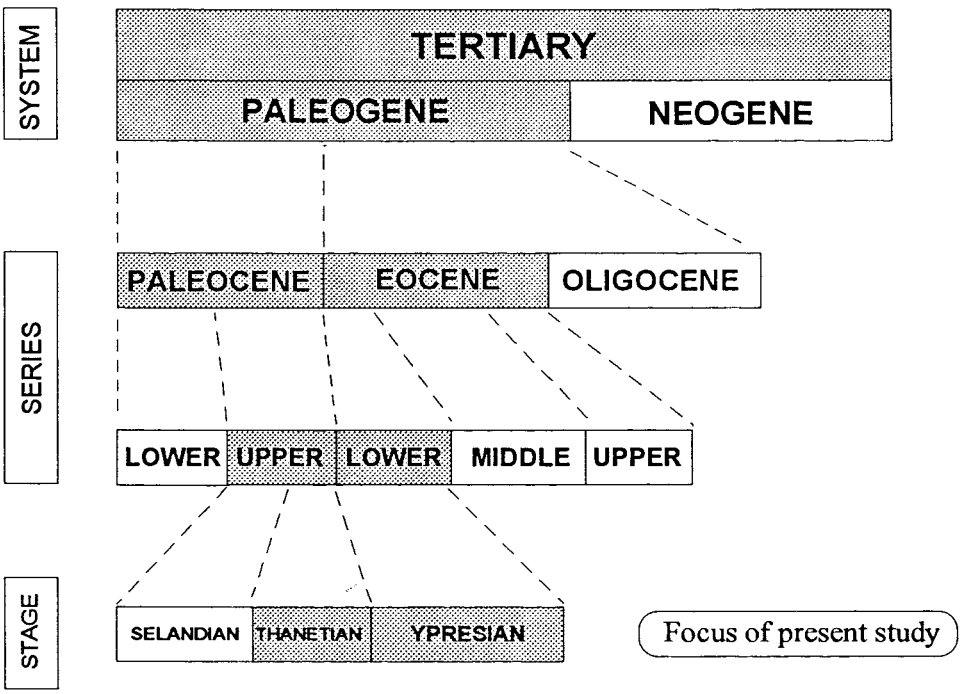

Figure 4-1 *Focus of present study (n.b. geochronological nomenclature substitutes System, Series and Stages with Period, Epoch and Age and upper and lower with late and early).*

The present study is directed at sediments from the upper Paleocene and lower Eocene Thanetian and Ypresian Stages. Various authors have used different schemes for subdividing the Paleocene (Berggren, 1994); in some literature, for instance, the Thanetian Stage is not recognised (Berggren, 1985) but here the Selandian/Thanetian boundary is taken as being at the base of Chron C26n (Berggren, 1994).

4.2 Biostratigraphic zonation schemes

In order to calibrate a sequence of magnetic reversals, it is usually necessary to first position the sequence into its rough position on the standard GPTS using some independent control such as biostratigraphy.

A variety of microfossil zonation schemes have been developed, based on the first or last appearance datum (FAD or LAD) of particular species. Providing the initial environment was suitable for the species and that the microfossils are preserved, each scheme provides an alternative method for subdividing a geological succession. The schemes, however, are continually being improved and significant revisions emphasise the potential errors that may be involved when using such schemes for dating and correlating.

Calcareous nannofossils and foraminifera (planktonic and benthic) are the two fossil groups that are most commonly used for worldwide Paleogene biostratigraphic correlations. Many of the Paleocene and Eocene units in the U.S. however also contain other fossil groups including molluscs (e.g. Govoni, 1991), dinoflagellates (e.g. Edwards et al, 1984), spores and pollen (e.g. Frederiksen et al, 1982), ostracods (Hazel, 1968) and vertebrate remains (e.g. Weems, 1984, 1988) which can be important tools in otherwise barren strata.

Calcareous nannofossils

There are two commonly used calcareous nannofossil zonations, that of Martini (1971,1986) which is based primarily upon studies of hemipelagic sediments and the zonation of Bukry (1973, 1978; Okada and Bukry, 1980) which is based primarily upon studies of samples collected by the Deep Sea Drilling Project. The zonation of Martini (1971) has proved to be more useful in the sediments under investigation in the present study because the diagnostic species in this zonation are prevalent in the study area. Figure 4-3 shows the placement of Martini's nannoplankton (NP) Zones relative to Berggren's planktonic foraminifera zones.

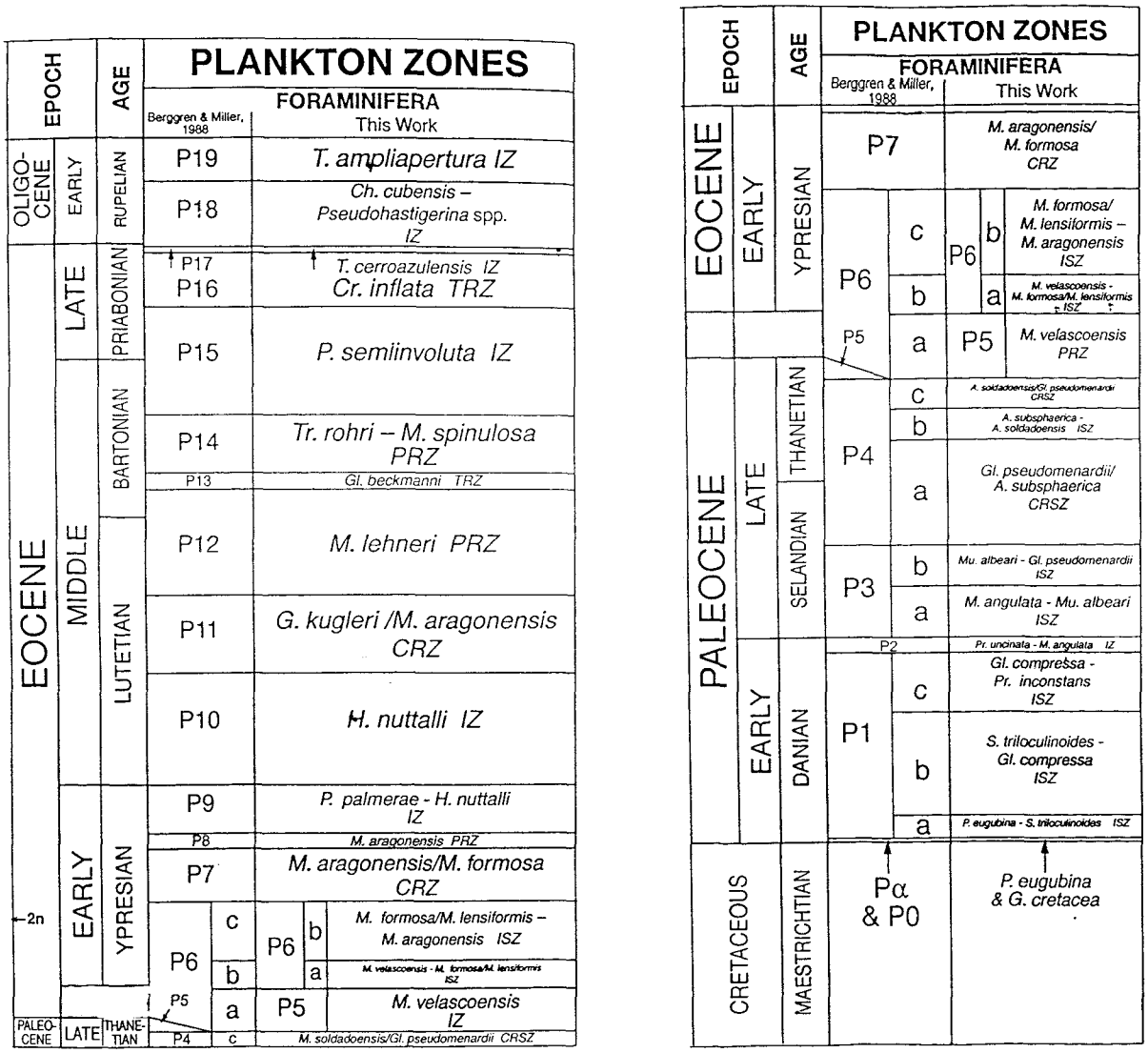

Figure 4-2 *Planktonic foraminifera zones for the Paleocene and Eocene (Berggren, 1994).*

Foraminifers

Planktonic foraminifers are less common than calcareous nannofossils but are sufficiently diverse in some Gulf Coast and Atlantic Coastal stratigraphic units to allow placement within a specific zone (for example: Mancini and Tew, 1991). The Paleogene planktonic foraminiferal zonation utilized in this study was first established by Bolli (1957, 1966) and later modified by Stainforth et al (1975) then Berggren (1988,1994) (Fig. 4-2). This zonation has been used widely as an accepted biostratigraphic standard for warm water areas of the world, including the Gulf and Atlantic Coastal Plains during the Paleogene. In addition to planktonic species some benthonic foraminifera with the US Gulf and Atlantic regions have ranges restricted to parts of the upper Paleocene and lower Eocene which may prove useful for correlation within similar inner-neritic depositional environments elsewhere (Bybell and Gibson, 1991).

4.3 Geochronology

The most favoured Cenozoic geochronologies are those based on magneto-biostratigraphic studies integrated with isolated radiometric dates. Properly calibrated biostratigraphic zones have the potential for correlations on time scales of about 0.5 m.y. (Berggren et al, 1985). However, direct calibration to magnetostratigraphy has the potential for significantly improving correlations (e.g. Berggren et al, 1985; Miller et al, 1985a) further increasing the resolution to within 0.25m.y. or better for some intervals.

Stratigraphic and magnetostratigraphic dates and correlations are standardised throughout this study. Figure 4-3 illustrates the period of time under investigation (45-60Ma), chronicled alongside the standard GPTS (Kent et al, 1994) and the biostratigraphic framework of nannofossil zones (Martini, 1971; 1986) and planktonic foraminifera (Berggren, 1994). The rough positioning of supercycles TA 1-3 and the third order subdivisions (Haq et al, 1987) have been included on the right of the chart.

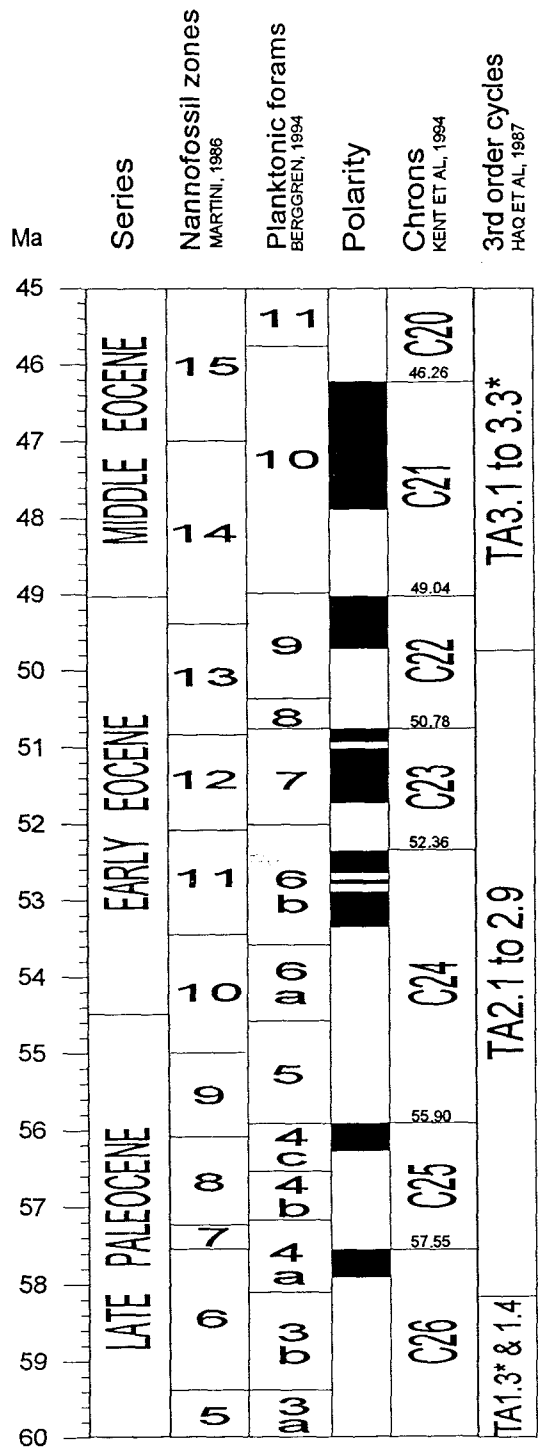

Figure 4-3 *Chronostratigraphy adopted for this project* (based on Hardenbol, 1994).

SECTION B

Magnetostratigraphy of sediments from the US Atlantic Coastal Plain

Chapter 5 Early Tertiary deposits of the U.S. Atlantic Coastal Plain

5.1 Regional setting

The western limit of the US Atlantic Coastal Plain (Fig. 5-1) marks the inner margin of the preserved onlap of Cretaceous and Cenozoic sedimentary rocks of the Atlantic Coastal Plain Province onto the Precambrian and early Paleozoic crystalline rocks and

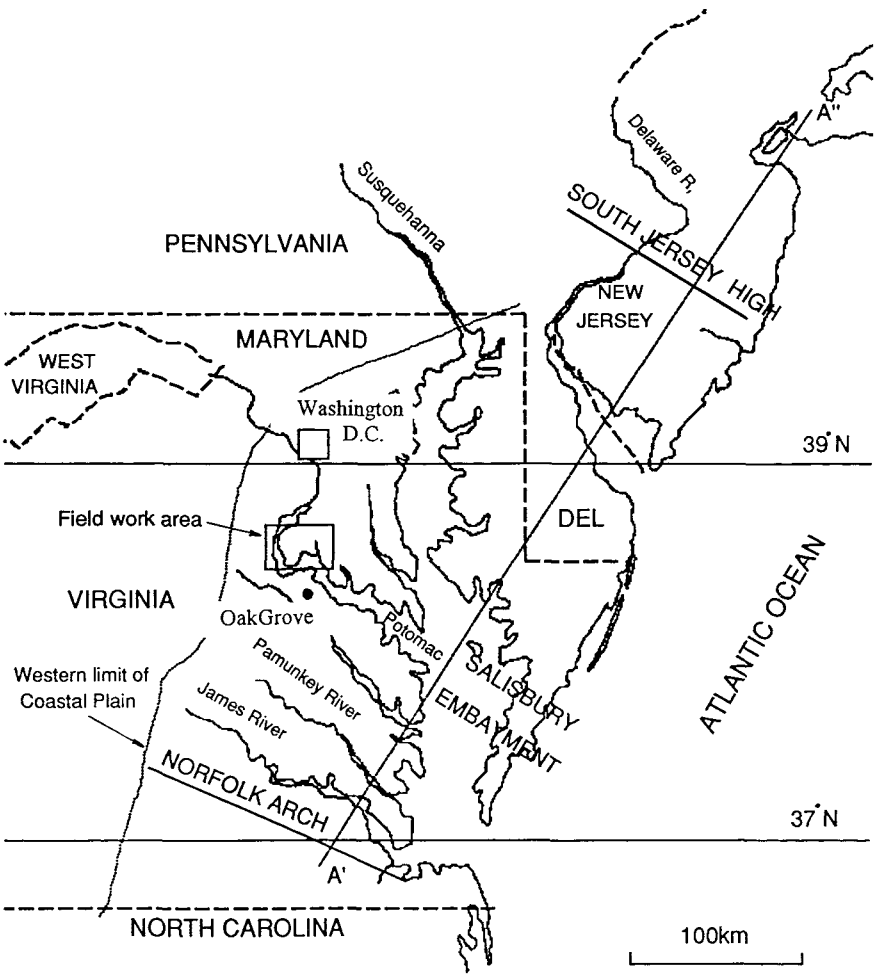

Figure 5-1 *Map of U.S. Eastern Seaboard. Line A'A'' refers to the section in figure 5-2.*

early Mesozoic sedimentary rocks of the Piedmont Province that lie at the exposed edge of the continental craton (Gibson, 1991). Sedimentary deposits of Paleocene and Eocene

age outcrop near the inner (western) margin of the Atlantic Coastal Plain from New Jersey to Georgia. In the Potomac River Valley in Maryland and Virginia, these deposits are exposed to the south of Washington D.C.

The Atlantic Coastal Plain of the U.S. consists of a series of embayments and structural highs which are controlled by the underlying Triassic basement rift system (Hansen, 1978). In the Chesapeake Bay region the basement complex forms the Salisbury Embayment (also known as the Chesapeake-Delaware Basin) (Richards, 1948) which is bounded by the South Jersey High to the north and the Norfolk Arch to the south (Figs. 5-1 and 5-2).

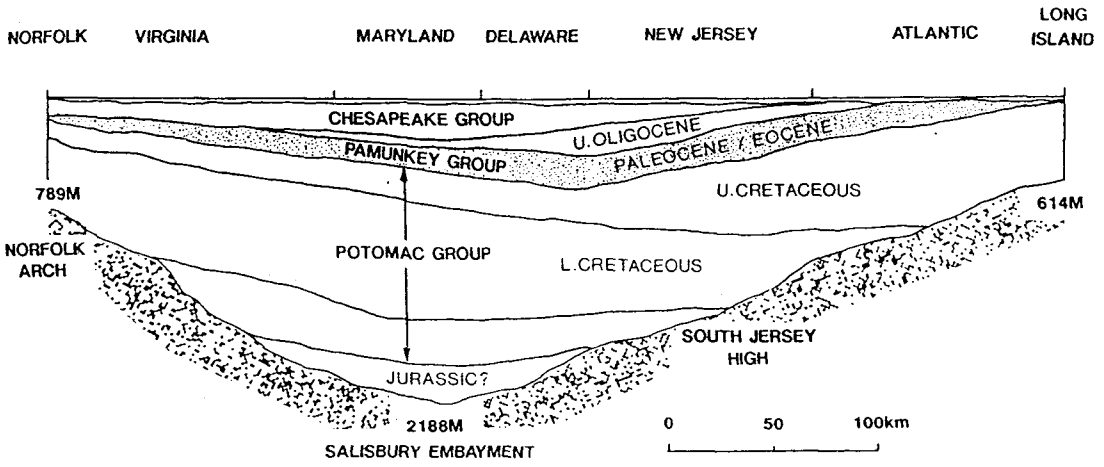

Figure 5-2 *Cross-section (A'A'' Fig. 5-1) from Norfolk to Fire Island (from Olsson et al, 1988). Vertical scale exaggerated.*

Sedimentation within the embayment was controlled, to an extent, by these tectonic features and their relative movements. The early Tertiary sequence, for instance, is thickest on the flanks of the South Jersey High and thins into the Chesapeake-Delaware Basin eventually pinching out against the Norfolk Arch (Fig. 5-2).

5.2 Stratigraphy of the Potomac River Valley Paleocene and Eocene

The late Paleocene and early Eocene units in Virginia and Maryland are found within the Pamunkey Group (Fig. 5-2). In the Potomac River Valley this group is subdivided into four units; the Brightseat Formation (lower Paleocene), Aquia Formation (upper Paleocene), Marlboro Clay (upper Paleocene) and Nanjemoy Formation (lower Eocene). Additional units of the Piney Point Formation and Chickenhoming Formation (upper Eocene) are seen in the subsurface. Figure 5-3 illustrates the upper Paleocene and lower Eocene formations investigated in this present study.

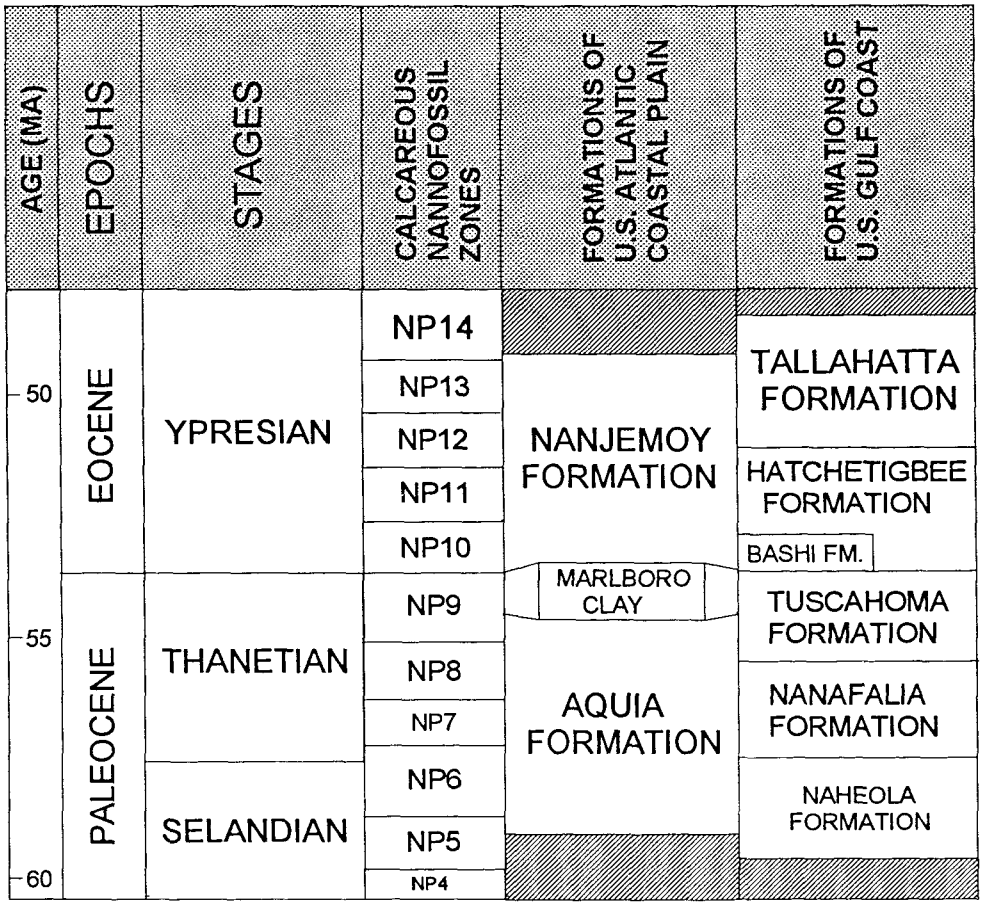

Figure 5-3 *Correlation chart of late Paleocene and early Eocene strata from the U.S. Atlantic and Gulf Coastal Plains.*

Sedimentation during this period occurred in a relatively stable inner to middle shelf environment (Gibson et al, 1980) in which distinctive sediments were deposited which

differ from the overlying fine grained siliceous Chesapeake Group and the underlying arkosic Potomac Group. The Pamunkey Group form a series of predominantly unconsolidated argillaceous sands, glauconitic sands and clays which dip gently to the east. The Marlboro Clay Formation interrupts the relatively homogeneous massive greensand sequence with an abrupt mineralogical shift to a kaolinite dominated clay.

The total thickness of the outcropping sediments in the Potomac River Valley is about 60m which provides a less complete sedimentary record than that preserved in New Jersey or in the Gulf Coastal Plain. Three formations within the 60m of strata represent all calcareous nannofossil zones between NP5 and NP13. The percentage of authigenic glauconite in the Pamunkey Group often reaches as high as 70 percent (Glaser, 1971) which suggests a low sedimentation rate throughout much of the interval. Gibson and Bybell (1991) have recorded thin glauconitic, quartz sand beds with thicknesses of 0.5-2m, or less, which represent entire calcareous nannofossil zones.

Gibson (in press) has identified 6 sea level cycles in the lower Eocene based upon *tau* values of nannofossils which are calculated from the number of benthic species x planktonic percentage (Gibson, 1988) and where *tau* values are considered to increase with increasing water depth (Fig. 5-4). The thickness of the units in the Central Atlantic Coastal Plain suggests that the sequences have been susceptible to erosion which has resulted in the removal of partial or complete cycles. This is particularly evident when comparing cycles to the thicker Gulf Coastal plain sequences and therefore Gibson (in press) considers that many cycles only represent portions of the transgressive-regressive episodes.

Biostratigraphy

Eocene Markers

LAD **Chiasmolithus bidens / solitus* - top of Zone NP 16

FAD *Daktylethra punctulata* - Zone NP 15

LAD **#Discoaster sublodoensis* - base of NP 14

LAD **Tribrachiatus orthostylus* - top of Zone NP 12

FAD *Helicosphaera lophota* - near topf NP 12; marker for NP 12/13 boundary

LAD *Ellipsolithus macellus* - near the top of Zone NP 12
FAD *Helicosphaera seminulum* - mid Zone NP 12
FAD **#Discoaster lodoensis* - base of Zone NP 12
FAD *Chiphragmalithus calathus* - in Zone NP 11
LAD **#Tribrachiatus contortus* - top of Zone NP 10
LAD *Discoaster multiradiatus* - near top of Zone NP 10
LAD *Tribrachiatus bramlettei* - near top of NP 10
FAD *Tribrachiatus orthostylus* - upper part of Zone NP 10
FAD *#Discoaster diastypus* - mid Zone NP 10
FAD *#Tribrachiatus contortus* - mid Zone NP 10
LAD *Placozygus sigmoides* - lower Zone NP 10
LAD *Fasciculithus spp.* - lower Zone NP 10
LAD *Hornibrookina sp.* - lower Zone NP 10
FAD **Tribrachiatus bramlettei* - base Zone NP 10

Paleocene Markers

FAD *Transversopontis pulcher* - uppermost Zone NP 9
LAD *Scapholithus apertus* - upper Zone NP 9
LAD *Biantholithus astralis* - upper Zone NP 9
FAD *Toweius occultatus* - in Zone NP 9
FAD *Toweius callosus* - in Zone NP 9
FAD *Lophodolithus nascens* - upper Zone NP 9
FAD *#Campylosphaera eodela / dela* - mid Zone NP 9
FAD **#Discoaster multiradiatus* - base of Zone NP 9
FAD **Heliolithus riedelii* - base of NP 8
FAD *#Discoaster mohleri* - base of Bukry's CP6; approximately Martini's NP7
FAD **#Heliolithus kleinpellii* - base of Zone Np 6

* indicates a species used to define a horizon in the zonation of Martini (1971)
\# indicates a species used to define a horizon in the zonation of Bukry (1973, 1978)

Table 4-1 *Calcareous nannofossil horizons used to date the Paleocene and Eocene sediments from Maryland and Virginia (Bybell and Gibson, 1991).*

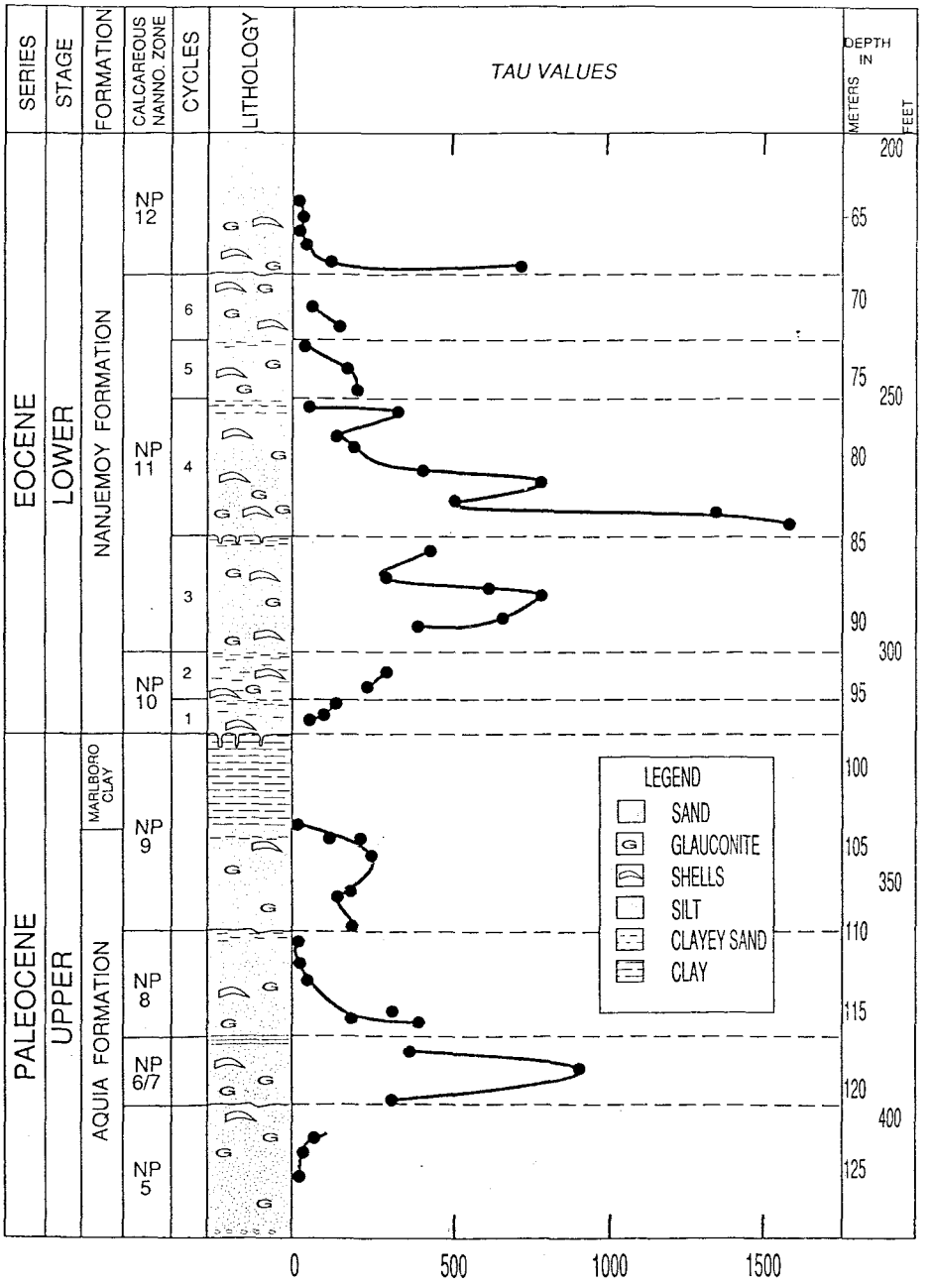

Figure 5-4 *Depositional cycles identified by tau values in the upper Paleocene and lower Eocene of Maryland and Virginia.*

5.2.1 Aquia Formation

The upper Paleocene Aquia Formation is a friable unit of massively bedded glauconitic sand. Foraminiferal assemblages (Nogan, 1964; Gibson, unpubl. data) and sedimentary characteristics (Beauchamp, 1984) suggest an inner-neritic depositional environment, representing a general upward shoaling in the basin (Olsson et al, 1988). Abundant shell material, particularly robust bivalves and the mollusc *Turritella mortoni* are found throughout the Aquia Formation, often concentrated into lenses (Plate 5-1).

Plate 5-1 *Common fauna of the Aquia Formation.*

The Aquia Formation has an approximate thickness of 25m in the type area at Aquia Creek but thickens to 50m 60km to the east at the Solomon's Island corehole location. In the south it disappears against the Norfolk Arch. The lowermost Aquia strata are placed in the upper part of nannofossil zone NP5 (early late Paleocene). Zones NP6, NP7, NP8 and NP9 (late Paleocene) are also present in the remainder of the formation (Bybell and Gibson, 1991).

Clark and Martin (1901) originally divided the Aquia Formation into two members; the lower Piscataway Member of poorly sorted clayey sand and the upper Paspotansa Member of better sorted glauconitic sands. The lower Aquia, as revised by Ward (1985), bears a relatively low diversity dinoflagellate flora dominated by the *Glasphrocysta exuberans* complex (Edwards et al, 1984). The upper Aquia is marked by an influx of species including *Kallosphaeridium brevibarbatum*. The Aquia/Marlboro contact in outcrop and the subsurface generally has a disconformable relationship, although transitional interbedded laminae within the Oak Grove Core indicate a conformable contact at this location.

The Aquia Formation (upper NP5-NP9) correlates with the Naheola (NP5/6), Nanafalia (NP6/7/8) and the Tuscahoma Formation (NP9) in Alabama (Fig 5-3).

5.2.2 Marlboro Clay

The Marlboro Clay Formation is a light grey to reddish brown clay whose origins have been the cause of much debate. It has been described variously as a lagoonal, estuarine and marginal marine deposit, although Gibson (pers.comm.) now identifies the Marlboro Clay as an inner to middle shelf deposit. The bulk of the formation is typically 50 percent kaolinite and 40 percent illite (Reinhardt et al, 1980). It is a thin but widespread unit, ranging in thickness from 0.1m to a maximum of 10m in the subsurface (Glaser, 1971) and is bounded above and below by disconformities, although a conformable transition occurs in the Oak Grove Core.

In outcrop sections large burrows are seen, extending up to 0.5m downwards from the upper Marlboro contact. The more sandy lithology of the Nanjemoy Formation fills these burrows in both straight and open spiral fashions (Reinhardt et al, 1980). Below the burrows, the Marlboro Clay is massively bedded, although laminations of silt and clay occur periodically. Calcareous nannofossils occur in these thin laminae in some borehole localities and these place the Marlboro Clay Formation in the upper NP9 nannofossil zone, although some Marlboro sections in down basin coreholes are zone NP 10 in age (Gibson, pers.comm.). Various authors suggest that the Paleocene - Eocene boundary occurs within this formation but along the Potomac River sections and in the Oak Grove core Gibson and Bybell (1991) place the Marlboro Clay entirely in the upper Paleocene, based on calcareous nannofossil data. Berggren et al (1985) put the Paleocene - Eocene contact at the NP9-NP10 junction. In this case, the contact probably lies at the base of the Nanjemoy

Formation and not within the Marlboro Clay itself. The Marlboro Clay correlates with the upper part of the Tuscahoma Formation in Alabama on the Gulf Coast.

5.2.3 Nanjemoy Formation

After the Marlboro Clay Formation had been deposited there was a return to a shelly glauconitic clayey sand, similar in some respects to that of the Aquia Formation lithology. Mollusc shells are found throughout most of the formation but are not as abundant as in the Aquia. The Nanjemoy Formation has been divided into two members: a more clayey lower member, the Potapaco and a sandier upper member, the Woodstock (Clark and Martin, 1901; Ward, 1985). Early Eocene in age, the formation thickens northwards from the James River to a thickness of approximately 75m in the subsurface in Maryland (Olsson et al, 1988). It is best exposed in bluffs along the Potomac River where the formational strike is north-south with a dip to the east of about 2-3m per kilometre. The top of the Nanjemoy is a major erosional surface and is overlain by the middle Eocene Piney Point Formation, Miocene deposits or by Plio-Pleistocene sands and gravels.

The first appearance datum (FAD) of *Tribrachiatus bramlettei* marks the base of NP10 and thus the Paleocene - Eocene boundary according to Berggren (1985). Progressively younger sediments span the NP10, NP11, NP12, and NP13 zones, though different exposures exhibit differing amounts of this interval. Local variations in the degree of stripping has been attributed in part to faulting (Mixon and Powars, 1984). Planktonic foraminiferal assemblages in the Nanjemoy are scarce and have low diversity. The few diagnostic forms that are found agree with the calcareous nannofossil zonation.

The depositional environment for the majority of the Nanjemoy Formation is inner neritic although the strata of NP11 age in the Oak Grove Core, Putney Mill and Solomon's Island coreholes suggest a deeper water setting, reaching a middle neritic environment in the Solomon's Island Corehole (Gibson, 1991). The Nanjemoy Formation correlates with the Bashi and Hatchetigbee formations (NP10-NP11) and the lower Tallahatta Formation (NP12-NP14) in the Gulf Coastal Plain.

Chapter 6 Atlantic Coastal Plain fieldwork and palaeomagnetic results

6.1 Sampling coverage

The late Paleocene and early Eocene sediments sampled in this region lie exposed along the banks of the Potomac River and its tributaries. The low lying topography limits section height from about 2m of fresh material exposed at Bull's Bluff to 12m at Tinker's Creek (Fig. 6-1). Total coverage of field and core material spanned the majority of the calcareous nannofossil zones NP6-NP13 with a short break at the base of NP12.

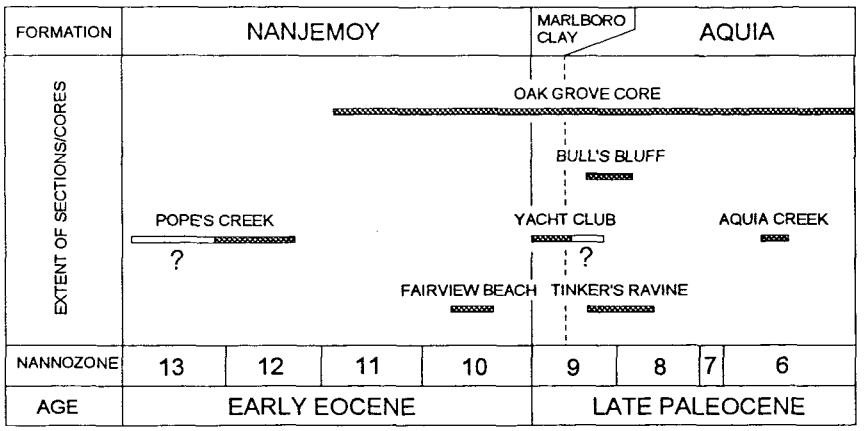

SECTION	CODE	FORMATION	NO. OF SITES	APPROX. SECTION THICKNESS (m)
TINKER'S RAVINE	TC	AQUIA	8	12
BULL'S BLUFF	BB	AQUIA	7	2
YACHT	YC	AQUIA/MARLBORO	11	3
FAIRVIEW BEACH	FB	AQUIA	3	2
AQUIA CREEK	AC	AQUIA	2	3
POPE'S CREEK	PC	NANJEMOY	13	10
OAK GROVE CORE	OG	NANJ/MARL/AQUIA	49	55

Figure 6-1 *Field section and core coverage in Virginia and Maryland. Question marks indicate where the biostratigraphic extent of the section is unknown.*

Six field sections and one core were sampled in the Virginia and Maryland region of the Atlantic Coast. The field site at Aquia Creek (the type section for the Aquia Formation) was sampled during preliminary studies (Nov 1991) but due to the very high shell content and its sandy nature the section was not sampled on the May 1992 field trip.

6.2 Oak Grove Core

The Oak Grove Corehole located near Oak Grove, Virginia (Fig. 5-1) penetrated Miocene, Eocene, Paleocene and the lower Cretaceous sediments of the Potomac group. It is a 6" (15.2cm) split core which has been stored at the United States Geological Survey (U.S.G.S) in Reston, Virginia since its recovery in 1975 (Plate 6-1). The Paleocene and Eocene section represents 77.4m of core extending from 60.8m to 138.4m; the Aquia Formation covers the interval 103m-138.4m, the Marlboro Clay 98.2m-103.6m and the Nanjemoy Formation 60.8m-98.2m.

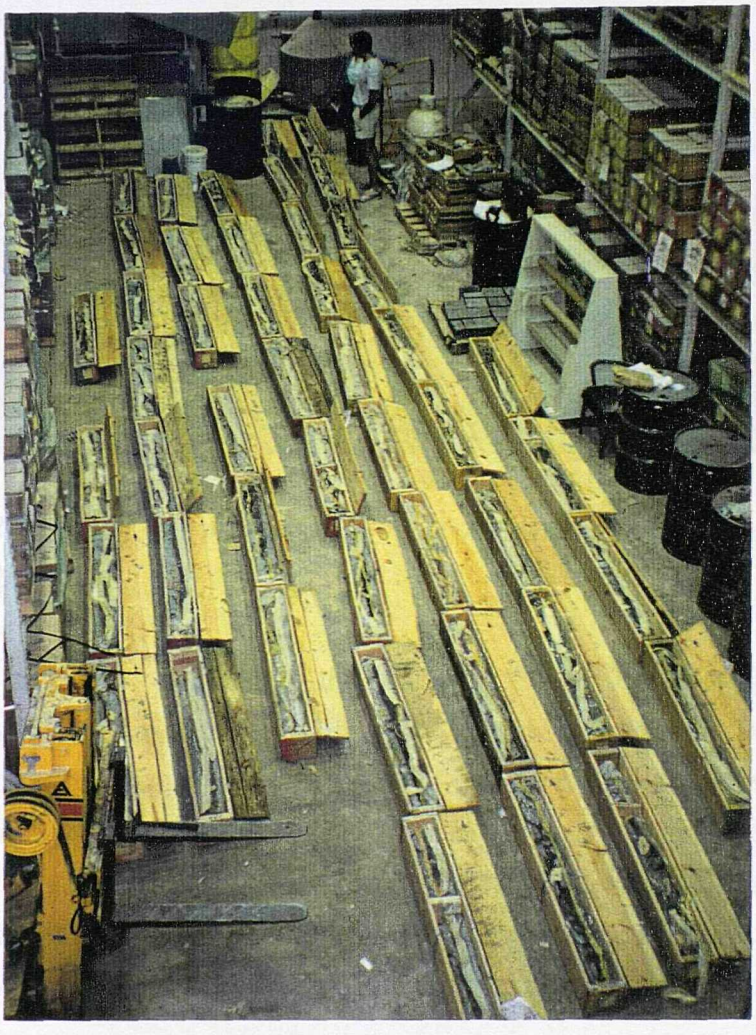

Plate 6-1 *60m of Oak Grove Core spanning the Nanjemoy, Marlboro and Aquia Formations (stored at Reston, Virginia).*

6.2.1 Sampling Procedures

The condition of the core severely restricted sampling. The top 9.5m and the bottom 15.8m of the Pumunkey Group could not be sampled due to the deterioration of the core (Plate 6-2).

Plate 6-2 *Nanjemoy Formation showing poor condition of the core in some intervals.*

Samples were therefore restricted to the range 70.5m-122.6m and even within this interval friable sands increased the sampling interval to an average of 1.06m. The depth of the sample downcore measured to the centre of the sample, to the nearest 0.01m. All specimens except for the consolidated Marlboro Clays were sprayed with aerosol mounting glue. This bound loose surface grains and helped preserve the samples during handling and transportation. Great care was taken to minimize sample loss during sub-sampling but unfortunately a small number of samples were lost due to their extremely friable nature.

Figure 6-2 shows the labelling scheme for Oak Grove core specimens. The maximum number of sub-samples at a given site was 4: [A(I); A(II); B(I); B(II)], 15% of the sites

had this number, 78% had 2-3 samples and 7% had only one sample. Each piece of sediment was trimmed to volumes typically 150-200cm^3 which falls within the optimum range for use in the 2-G magnetometer (see section 3.5.2).

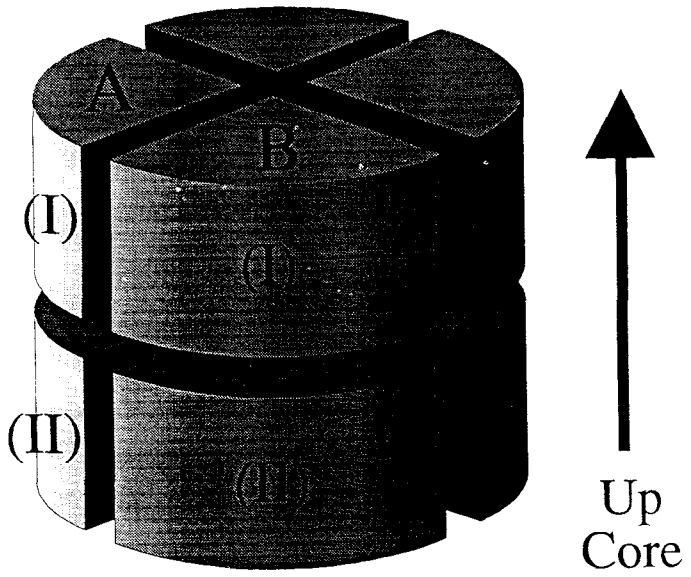

Figure 6-2 *Schematic representation of core showing sub-sampling.*

6.2.2 Palaeomagnetic analysis

Access to the Oak Grove Core had been granted by the U.S. Geological Survey on condition that the samples were returned intact. Specimens were therefore normally only demagnetised by the non-destructive alternating field method; the few samples thermally demagnetised however, did exhibit a polarity that generally showed agreement with the A.F. results (for example OG14 and OG48 in appendix 1).

Natural Remanent Magnetism (NRM) measurements

The average NRM intensity was calculated from subsamples at a given site and plotted against their depth in the core (Fig. 6-3). The majority of the specimens from the Aquia

and Nanjemoy Formations had relatively low intensity values (0.01-0.2mA/m) whilst those from the Marlboro Clay Formation had relatively high intensities in comparison (10-40mA/m).

The formation boundaries are sharply defined by the intensity fluctuations. The disconformable contact at the Marlboro Clay/Nanjemoy boundary (depth 98.2m) is marked by a dramatic increase in NRM intensities of 2 orders of magnitude. The base of the Marlboro Clay (103.6m) is also evident but due to the gradational relationship between the formations and the overall higher magnetic intensities in the Aquia (compared to the Nanjemoy) the change in lithologies is not so pronounced as the upper contact.

Bulk susceptibility

The bulk susceptibility measurements show a downcore fluctuation in values which broadly follows the NRM intensity pattern. A peak in susceptibility is observed across the Marlboro Clay samples with generally lower values in the Nanjemoy and Aquia Formations above and below. The magnitude of susceptibility depends on the composition and total amount of ferromagnetic and paramagnetic material within a sample (and the geomagnetic field intensity at the time of deposition) while the NRM intensity values are controlled by the ferromagnetic components of magnetisation; under many circumstances these two parameters will show a sympathetic relationship but where samples have high amounts of paramagnetic material or where components of magnetisation are oppositely aligned, the parameters will differ from a simple relationship. Some differences are seen within the Oak Grove Core, particularly in the Nanjemoy Formation.

Susceptibility fluctuations can also be used as an important lithological logging tool for correlating between different cores and outcrop sections of a similar age. In the Tertiary sediments studied here however, correlations other than those defining formation boundaries were difficult to determine; this was probably due to the irregular sampling intervals between sections and core as well as possible localised weathering and effects of storage.

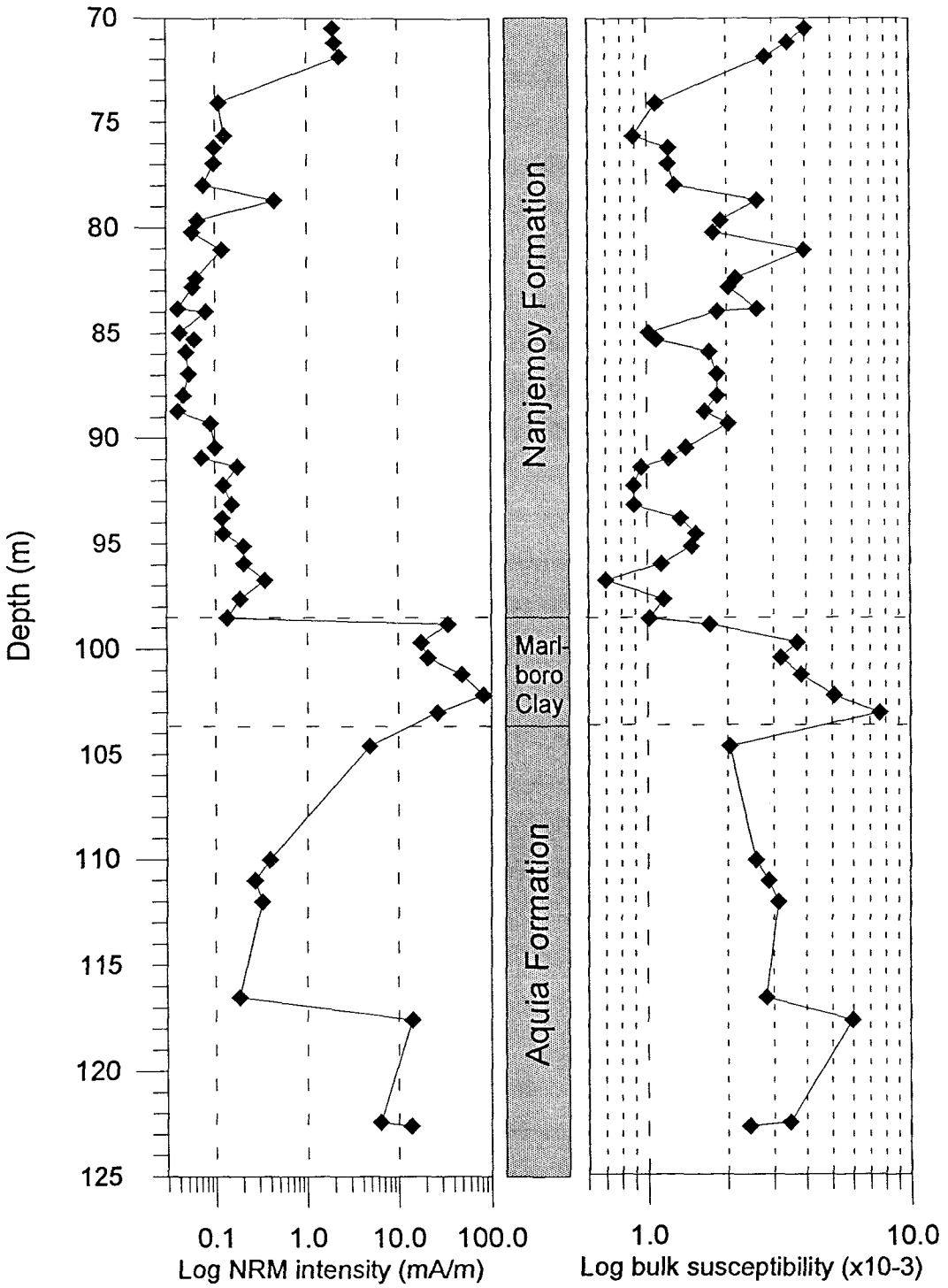

Figure 6-3 *Average NRM intensity and Bulk Susceptibility values for samples from the Oak Grove Core.*

Isothermal Remanent Magnetism (IRM)

A selection of 16 IRM curves for samples form Oak Grove Core illustrated in figure 6-4. The majority of samples indicate a combination of magnetite and hematite due to the initial sharp saturation rate, followed by an interval in which the magnetic minerals do not reach total saturation.

IRM analysis of samples from the upper part of the core suggests a largely hematite dominated magnetic fraction (Fig. 6-4a). The average IRM ratio for the top 3 samples is 0.78 and the normalised IRM values continue to increase with progressive increases in the applied field. In addition, thermal and A.F. demagnetisation of sample OG48 (depth 71.2m) illustrate an extremely stable magnetisation as temperatures up to 500°C and A.F. fields of 40mT have little effect on the sample's intensity. Samples from the Nanjemoy Formation, below a depth of 72m, however, can be identified by the faster saturation of the magnetic material and hence the increased IRM ratio to an average of 0.9 (Fig. 6-4b). This 20m interval of glauconitic sand and clay provides almost identical IRM plots, which in each case indicate a magnetite dominated sediment.

The 5m of Marlboro Clay is magnetically homogeneous. The IRM plots have identical ratios and very similar maximum IRM values (Fig. 6-4c). The sharp initial increase in the isothermal magnetisation at low applied fields is characteristic of magnetite but since the samples fail to saturate even at high fields (0.86T) a hematite component may be present. The extremely high intensities and maximum IRM values of the Marlboro Clay are also indicative of magnetite.

The remaining Aquia Formation, to a depth of 122.4m, produces further magnetite dominated plots, although a sample at 104.6m (OG8) contains a significantly greater proportion of hematite (Fig. 6-4d).

a

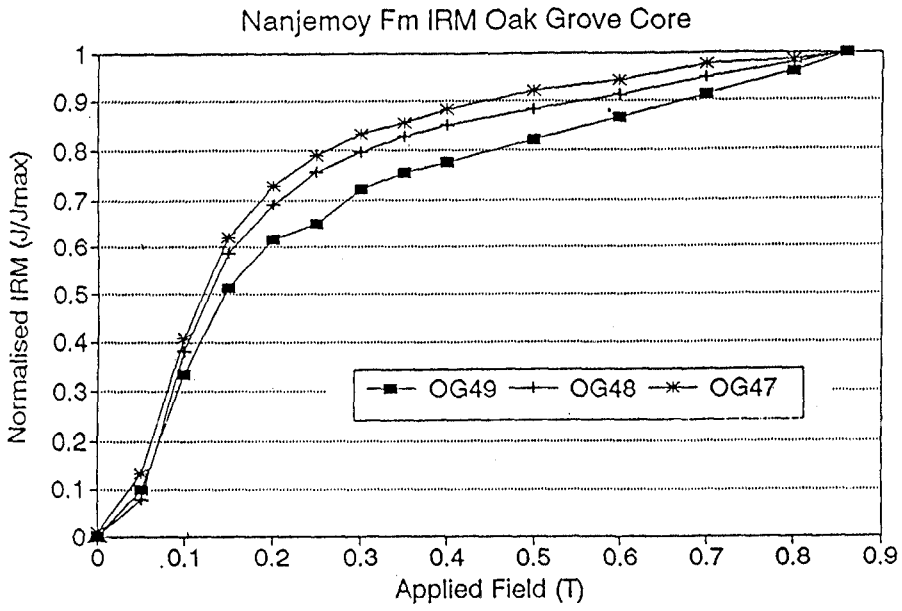

Sample no.	OG49	OG48	OG47
Max. IRM Value	754	959.8	645
IRM Ratio	0.72	0.8	0.83
Depth (m)	70.49	71.2	71.88

b

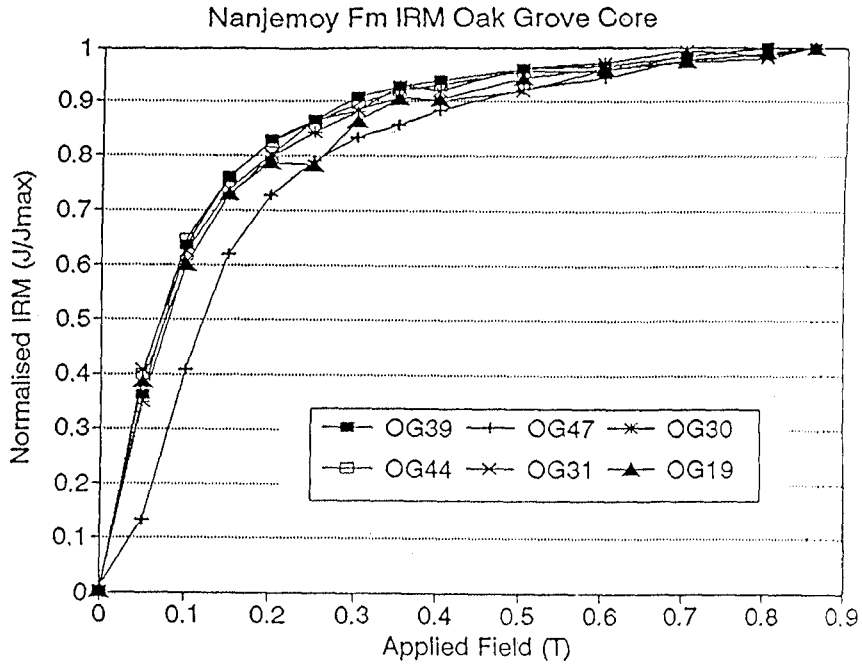

Sample no.	OG47	OG44	OG39	OG31	OG30	OG19
Max. IRM Value	645	33.2	27	42.5	33.7	54.5
IRM Ratio	0.83	0.9	0.91	0.89	0.88	0.87
Depth (m)	71.9	76.2	80.2	85.8	86.9	95.1

Figure 6-4 *IRM acquisition curves for the Nanjemoy Formation. a. uppermost part of core b. 72-96m.*

c

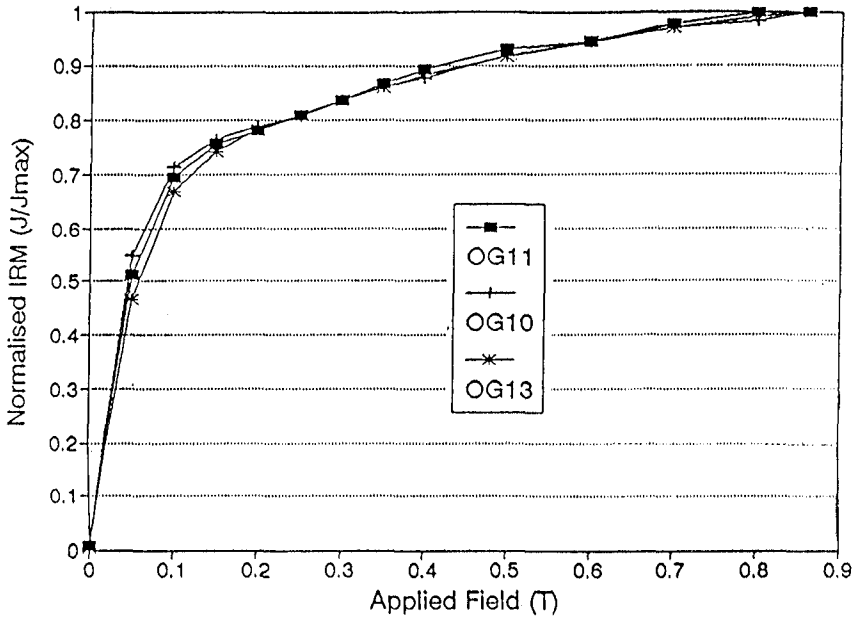

Sample no.	OG13	OG11	OG10
Max. IRM Value	5880	6497	5880
IRM Ratio	0.84	0.84	0.84
Depth (m) down core	99.7	101.2	102.2

d

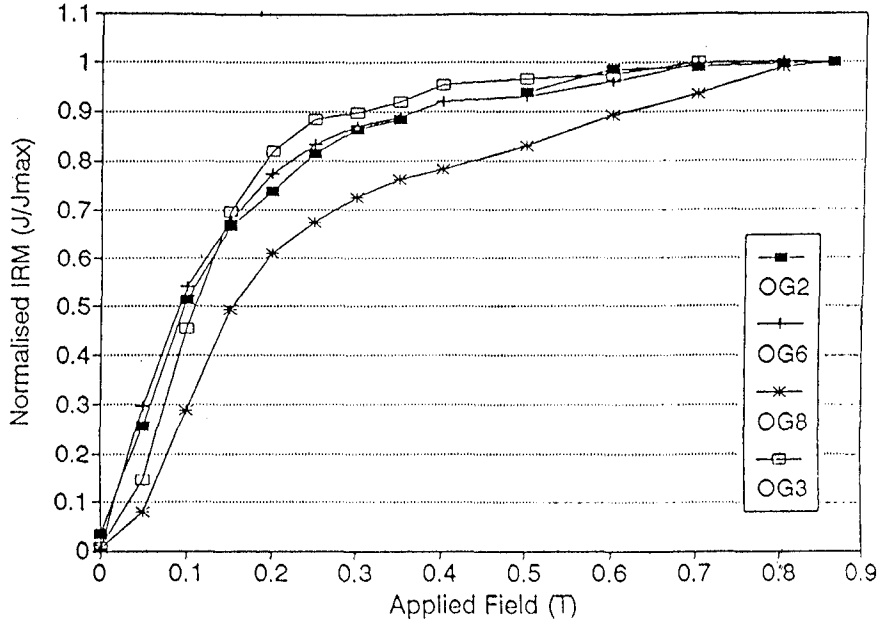

Sample no.	OG8	OG6	OG3	OG2
Max. IRM Value	921.8	155.5	603.7	183.3
IRM Ratio	0.73	0.87	0.9	0.86
Depth (m) Down core	104.6	111	117.6	122.4

Figure 6-4 - continued. *IRM acquisition curves for c) the Marlboro Clay and d) the Aquia Formation.*

Scanning Electron Microscope (SEM) and Electron Probe Analysis of Marlboro Clay

Scanning electron microscopy and electron probe analysis studies were directed at the Marlboro Clay in an attempt to explain the difference in intensity and demagnetisation characteristics between core and outcrop material. Unfortunately the polished slide containing the field section sample was polished too thin and its failure to conduct restricted its analysis considerably.

The core material contained a back scatter of high atomic number fragments, ranging in size from 0.1μm - 2μm. In addition, a small number of clusters of sub-micron crystals occurred.

Iron containing grains analysed with the electron probe fell into 3 main categories:

1. Iron /Oxygen + background signal of clay matrix (Figs 6-5a and b)

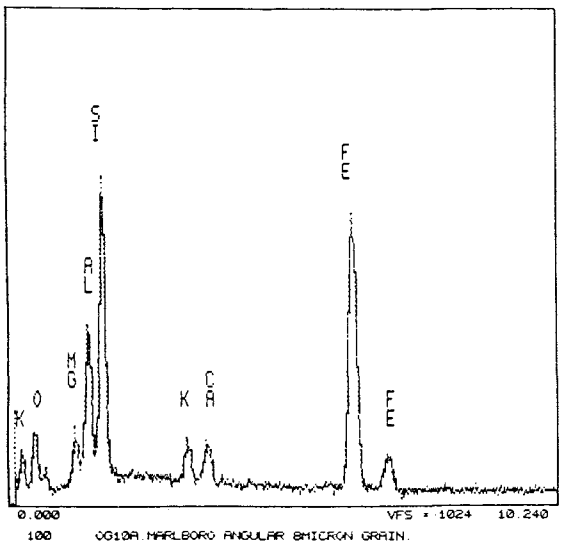

Figure 6-5a *Electron probe analysis of an angular 8μm grain from the Marlboro Clay.*

Figures 6-5a and b are examples of two iron containing grains. The peaks of elements other than iron (potassium, magnesium, aluminium and silicon) are typical clay mineral constituents and represent the background signal of the clay matrix in which the iron

oxide grain is located. Numerous grains of similar dimensions and content where scattered across the slide under analysis. An IRM acquisition curve and demagnetisation plot for this same sample (OG10) are illustrated in figures 6-4c and 6-8b respectively.

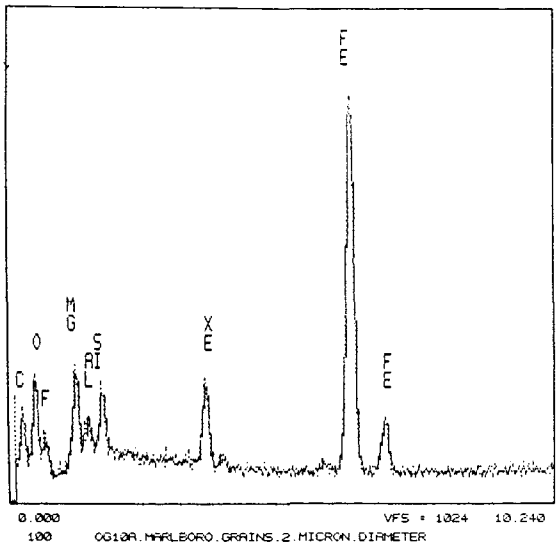

Figure 6-5b *Analysis of a 2μm grain from the Marlboro Clay.*

2. Iron / Titanium / Oxygen + background clay matrix (Fig. 6-6).

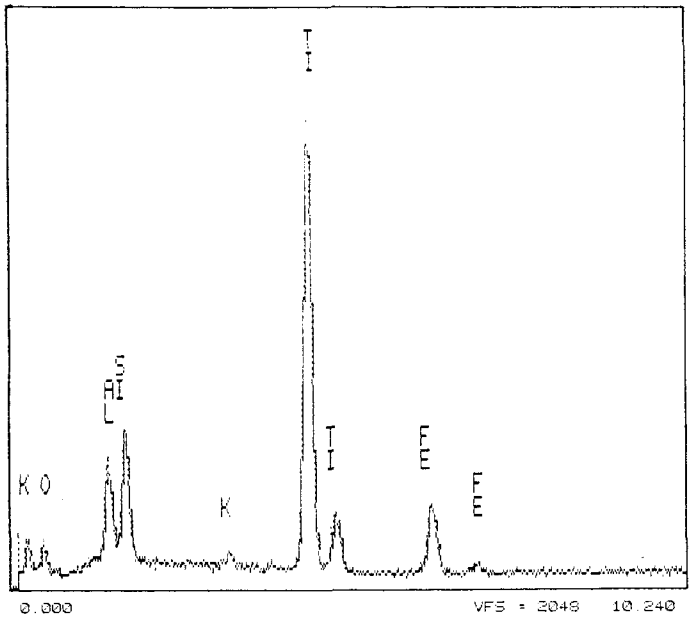

Figure 6-6 *Electron probe analysis of a high atomic number particle in the Marlboro Clay of the Oak Grove core.*

Other atomic number particles that were observed on the back scatter mode of the SEM revealed a composition of iron, titanium and oxygen (Fig. 6-6). The remaining peaks of potassium, silicon and aluminium are indicative of the clay matrix.

3. Iron / Sulphur

Plate 6-3 illustrates an example of a frambule arrangement of particles but in which the particles appear to be joined in one or two chains.

Plate 6-3 *Spherical cluster of submicron particles within the Marlboro Clay Formation of the Oak Grove core.*

Electron probe analysis of this particular cluster was not carried out due to failure of the instrument. Similar spherical clusters but with no evidence of chain linkage analysed at a later date, revealed an elemental content of entirely iron and sulphur (Fig. 6-7).

Beaded chains of magnetic particles usually suggest a biogenic origin. However the probable composition and size range of these particles (0.6-0.7 microns) are not indicative of the single domain magnetite normally associated with biogenic material.

The elemental composition of iron and sulphur seen here probably represent a grain of either pyrite (non-magnetic) or pyrrhotite (ferromagnetic). During thermal demagnetisation, phase transitions of these sulphur minerals usually occur at around 300-350°C; however no mineralogical change is evident during the heating of Marlboro Clay samples up to 600°C. This suggests that these frambules are either non-magnetic or represent such a small fraction of the measurable magnetisation of a sample, that their overall magnetic contribution to the sample is minimal.

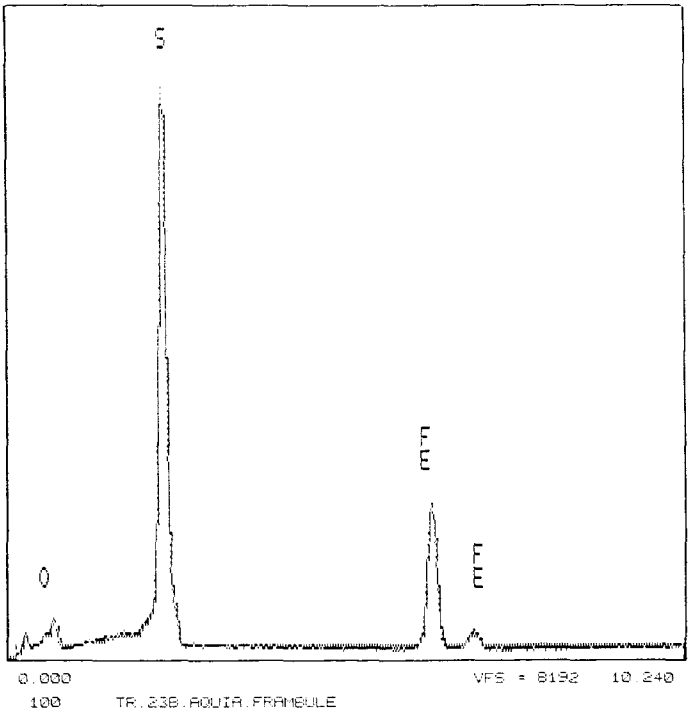

Figure 6-7 *Electron probe analysis of spherical cluster of submicron particles*

Electron probe analysis has limited applications for determining magnetic mineralogy since it only supplies information about the elements present under the electron probe; it gives no indication of the proportions of each element. In the case of iron and oxygen, for instance, it is not possible to differentiate between magnetite and hematite. Further information on magnetic minerals in a sample requires either optical work under a polarised light microscope or separation of the magnetic fraction and subsequent X-ray analysis.

6.2.3 Magnetostratigraphy

Since no declination control exists for the Oak Grove Core, polarity determination is based on inclination values alone.

After A.F. demagnetisation up to a maximum of 40mT 35% of the samples produced stereographic and vector end plots which have been classified as a stable end point (SEP) category (Fig. 6-8); the remaining specimens exhibited "trends" (Fig. 6-9) or erratic behaviour, where 20% of sites gave spurious plots from which no polarity could be reliably obtained or where sub-samples provided mixed polarities that could not be satisfactorily interpreted (see appendix 1).

The stable end points and reliable trend polarities have been used to construct the magnetostratigraphy for the Oak Grove Core (Fig. 6-10). Specimens showing trending characteristics have been used to further control the vertical extent of a given polarity interval but under no circumstances have magnetozones been defined using "trend" data alone. Samples with trending demagnetisation behaviour are distinguished from SEPs on this plot by being assigned a nominal $\pm 90^{\circ}$ inclination value. This magnetostratigraphy is correlated with the GPTS for an interval defined by the nannofossil zonation of the core (Gibson, pers. comm.).

Normal interval in NP 11

The top 2.5m of the core is dominated by high coercivity grains and therefore the sample intensities only decrease to approximately 80% of their initial NRM values during A.F. demagnetisation to 40mT and thermal demagnetisation up to 600°C. The extremely stable components of magnetisation identified within this zone were normal polarity except for one sample which showed a stable reverse polarity with a steep negative inclination. The normal polarity interval continues for another 3m in which samples exhibit complicated plots of trending and erratic demagnetisation behaviour but from which a predominantly normal polarity can be interpreted.

At 76.9m a reverse interval of 3m is observed before the polarity reverts to a normal,

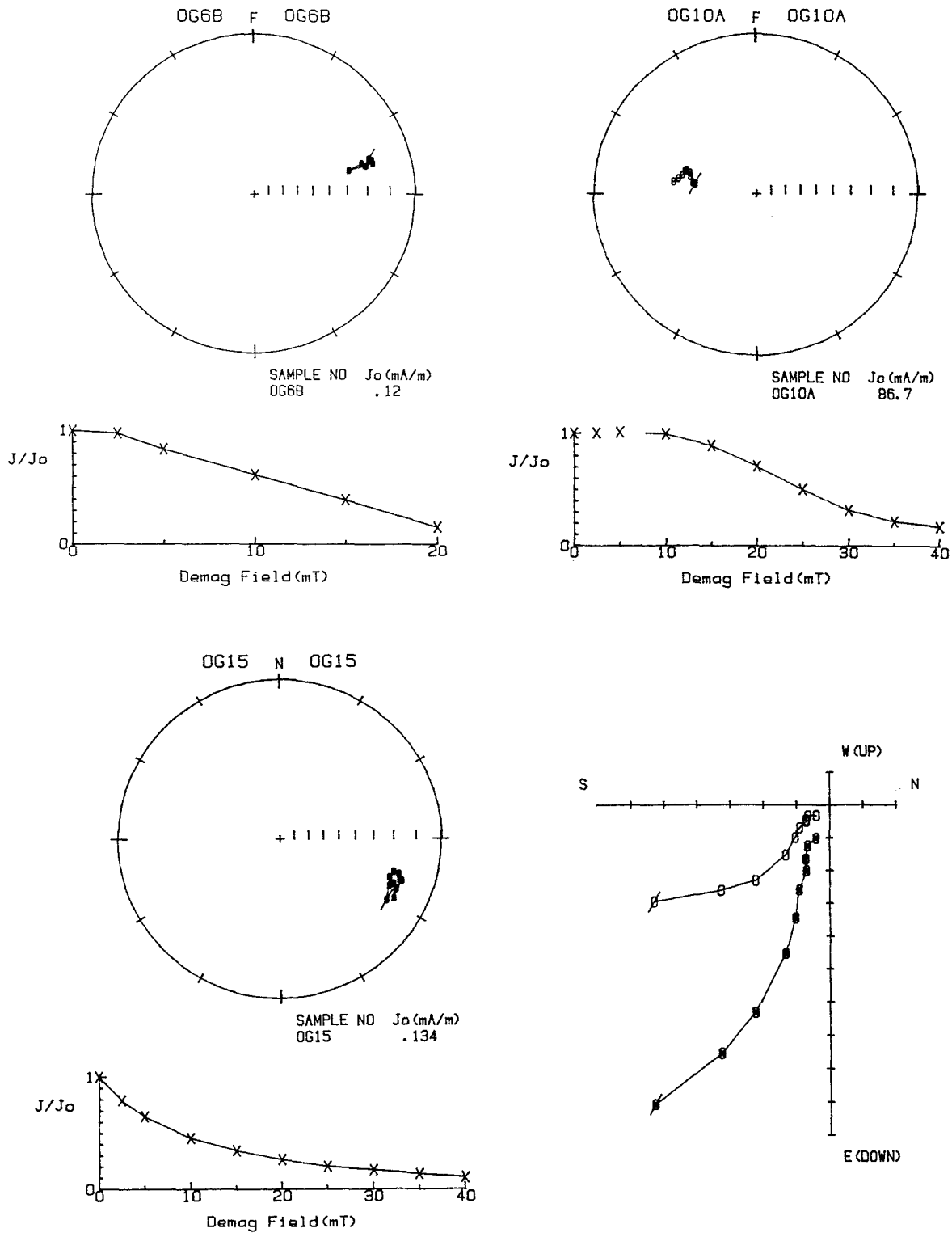

Figure 6-8 *Examples of SEPs from the Oak Grove Core a) Aquia Fm b) Marlboro Clay c) Nanjemoy Fm.*

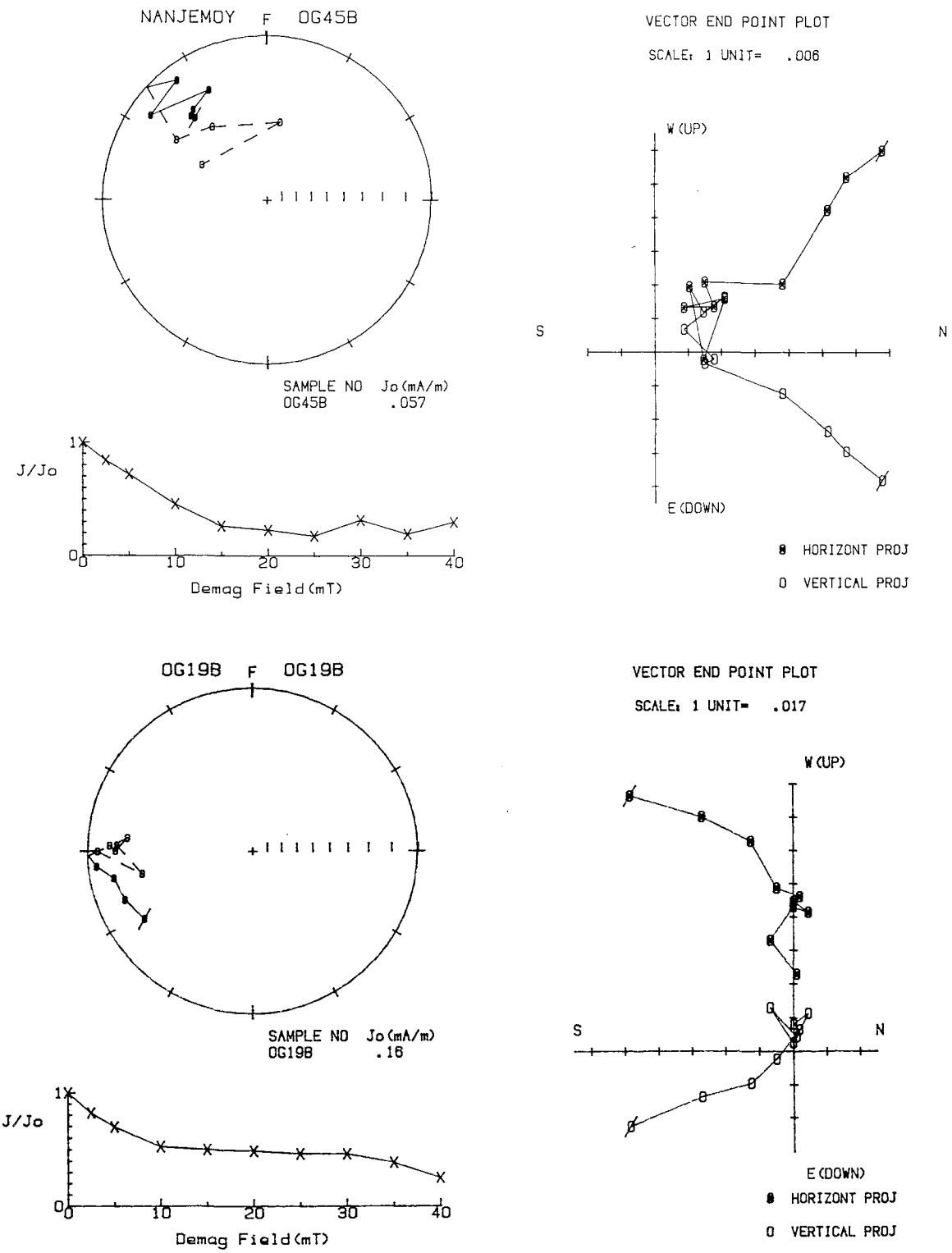

Figure 6-9 *Examples of trending palaeomagnetic behaviour from the Oak Grove Core.*

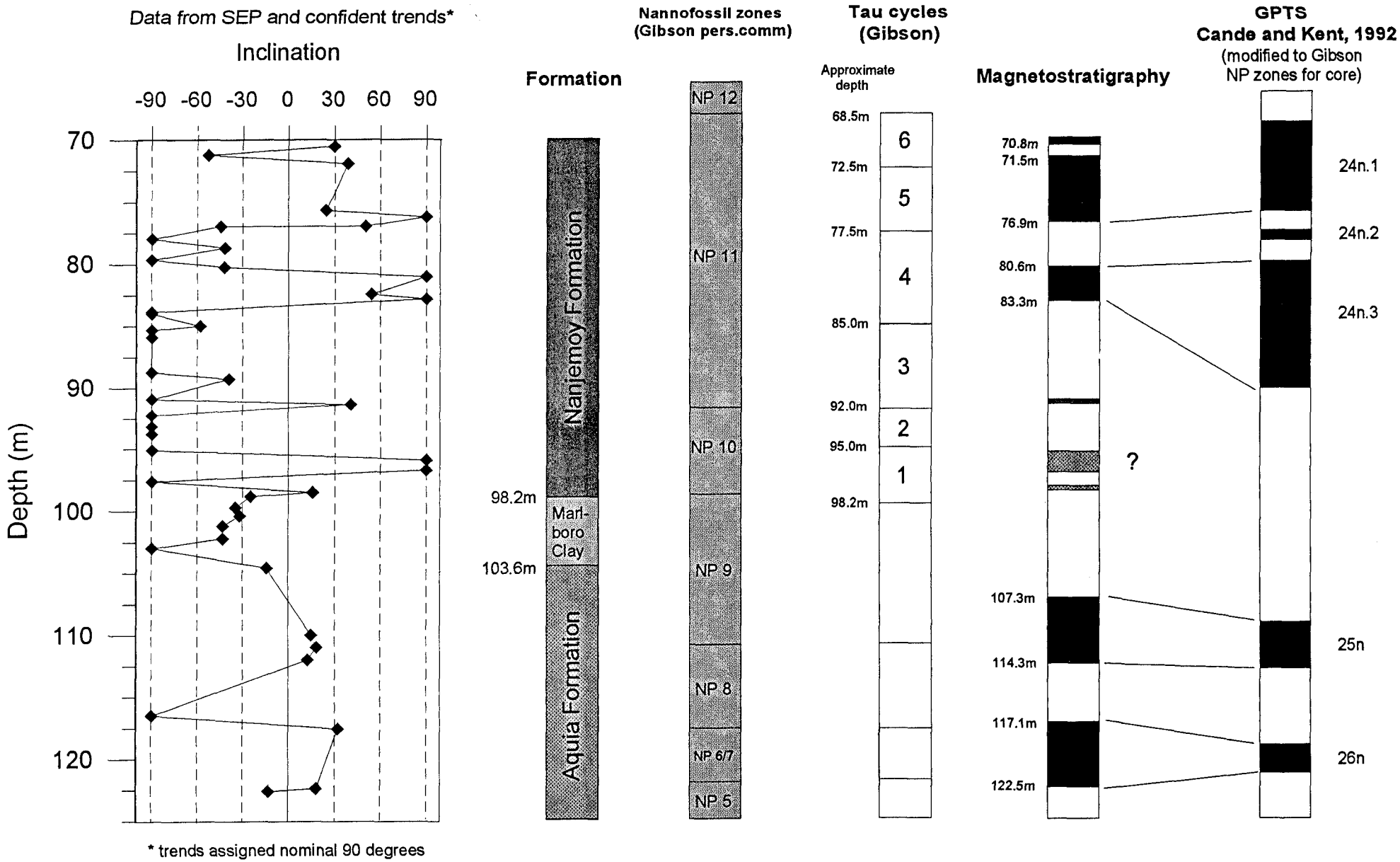

Figure 6-10 *Summary of the magnetostratigraphy of the Oak Grove Core.*

at a depth between 80.6m until 83.3m. This entire upper zone of mostly normal polarity contains nannofossils of NP11 in age and therefore corresponds with Chron C24n of the Geomagnetic Polarity Timescale. The underlying 6.8m represents a clearly defined reverse polarity interval, probably Chron C24r.

Anomalous normal polarities in NP10 of the Nanjemoy Formation

Within NP10 four reliable samples are identified as normal polarity in an interval which is expected to be exclusively reverse. These specimens emphasise the problems encountered when trying to reliably identify magnetic overprints particularly when dealing with horizontal strata, without thermal demagnetisation backup and working on samples with no declination control.

The anomalous normal zone located here at the base of the Nanjemoy Formation is considered an overprint based on two criteria. Firstly it is not consistent with the reverse polarity zone found in outcrop material of similar age at Fairview Beach and secondly the samples come from within a sandy interval directly above the impermeable Marlboro Clay. In this regime it is most probable that subterranean water would either flow along or accumulate at this formation boundary thus increasing the potential for alteration of minerals and the subsequent loss of the primary remanence. One sample shows a trend to reverse which may represent the only surviving relic of the primary component within this anomalous normal interval.

Marlboro Clay reverse polarity zone

The Marlboro Clay in the Oak Grove Core is confined to the upper NP9 nannofossil zone which corresponds to the lower portion of Chron C24r. The palaeomagnetic samples analysed within this interval of the core yield reliable reverse polarity SEP plots which are consistent with the polarity expected.

Aquia Formation polarity zonation

Below the Marlboro Clay, the Aquia Formation is extremely friable and therefore the sampling interval was decreased over intervals of poor core condition. Three sections of

core restricted sampling over approximately 5m, reducing the overall average sampling interval for the Aquia Formation to 2.4m. Polarity intervals which are preserved over short sections of core will therefore remain undetected between such samples and resolution of reversal boundaries are considerably reduced. This uncertainty is particularly evident below the upper Aquia contact. A return to a normal polarity occurs here but it can only be positioned between 1.6m to 7.0m below the Marlboro Clay Formation. The lower boundary of this normal interval also has poor resolution, being confined between opposite polarity samples 4.5m apart.

The vertical extent of the zone is therefore unknown but the 3 sites which define it span the NP9/NP8 nannofossil boundary, suggesting that the normal polarity observed corresponds to Chron C25n.

Chron C25r at the base of NP8, seems to be identified by sub-samples at a site located within a 5.6m interval of otherwise unsampled core. Below this, normal polarity samples have been tentatively identified in NP6/7 before another return to a reverse polarity occurs. Demagnetisation plots, however, over this normal zone show a stable magnetisation whose intensity only falls 20% using both A.F. and thermal demagnetisation procedures. If this does in fact represent a primary magnetisation, a linkage to Chron C26n would be expected.

The Oak Grove Core has a latitude of 38.5° and assuming the North American continent has remained more or less at a similar latitude since the Paleocene, an inclination of $\pm 58°$ would be expected. In practice inclination values of SEPs are consistently low; the best quality SEP demagnetisation behaviour of the Marlboro Clay for instance, gives inclinations of -42° to -43°. A shallowing of inclination of this magnitude is not uncommon (for example, Anson and Kodama, 1987; Deamer and Kodama, 1990; Arason and Levi, 1990) however some of the SEPs from the Aquia and Nanjemoy record even shallower inclinations which are difficult to explain.

6.3 Field sections on the Potomac River

Six sections were sampled on two independent field trips to the Potomac River area of Maryland and Virginia. The stratigraphic extent of these sections are shown in figure 6-1 and their geographic locations are illustrated below (Fig. 6-11).

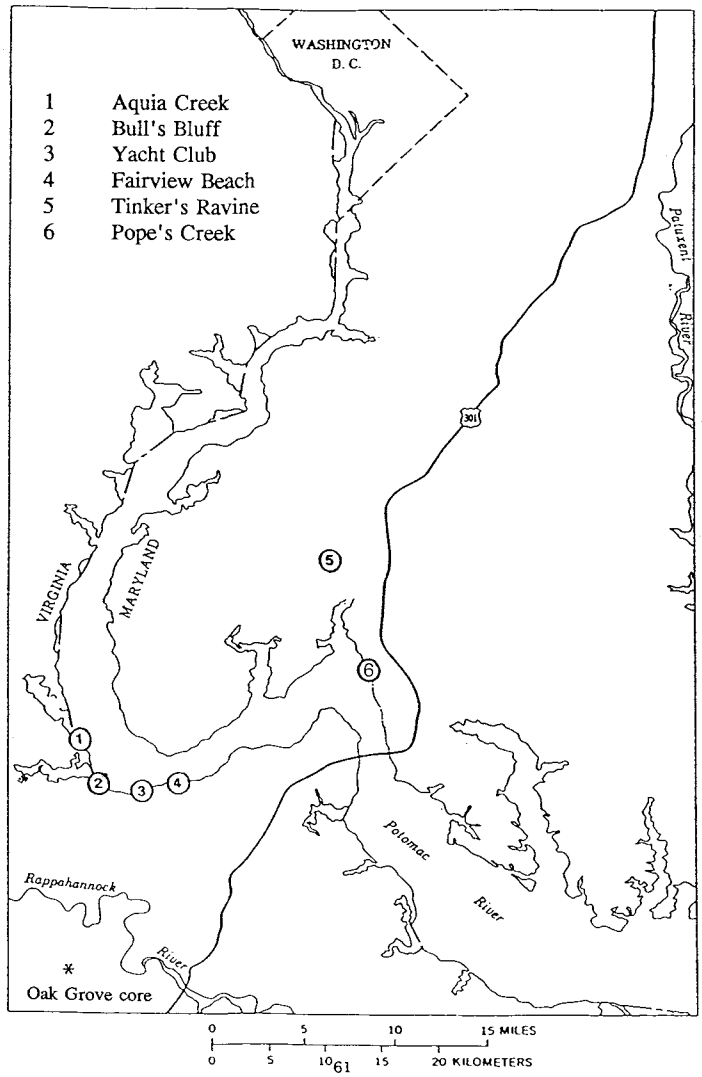

Figure 6-11 *Geographic location of field sections visited along the Potomac River.*

6.3.1 Pope's Creek locality

Location - Northeast bank of the Potomac River 2.9km upstream from the mouth of Pope's Creek, Charles County, Maryland, Mathias Point 7 1/2 minute quadrangle.

Approximately 10m of Nanjemoy Formation are exposed at the Popes Creek location (Plate 6-4). The section spans part of the nannofossil zone NP12, possibly extending upwards into NP13 although the exact biostratigraphy is unknown; it is overlain by Miocene sediments of the Calvert Formation and appears oxidised towards the top.

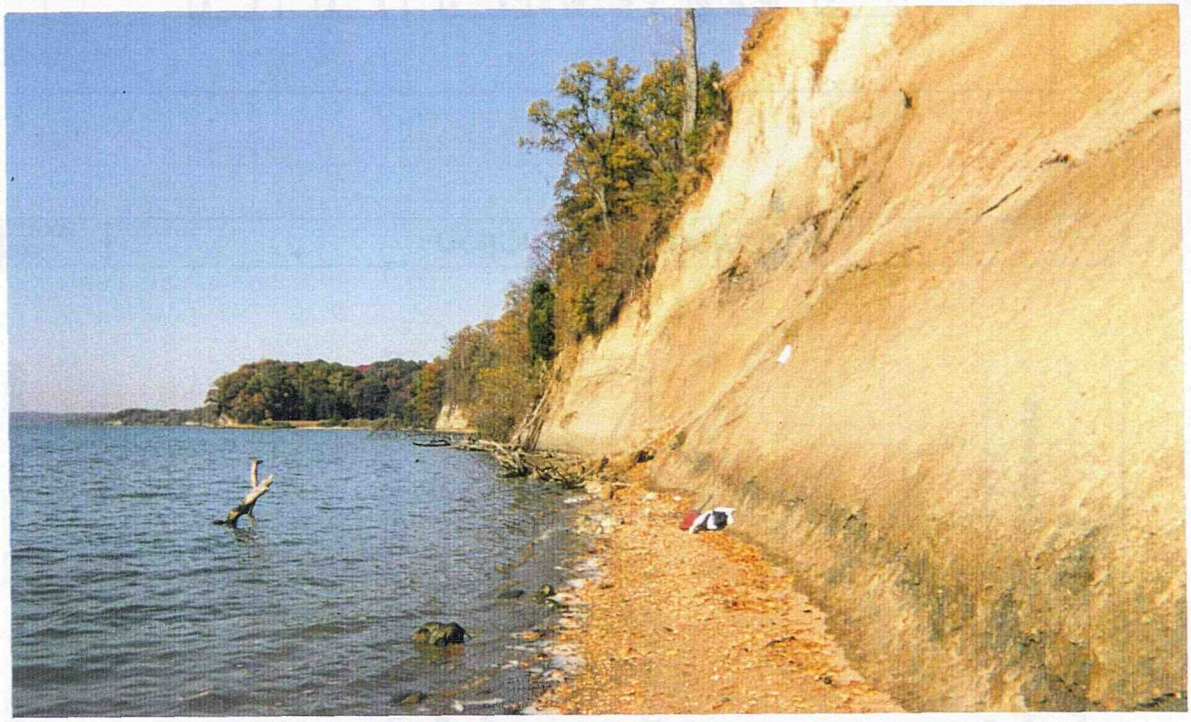

Plate 6-4 *Pope's Creek Section.*

The sediments exposed are predominantly olive-grey sand, bioturbated with abundant glauconite in the lower section. Scattered molluscs and concentrations of fine silts and clay horizons occur at intervals although towards the top of the section the shells appear as moulds. Other characteristics of this Nanjemoy outcrop are a burrowed surface at about 1m above beach level and an intermittent calcareous band at about 5m (Fig. 6-12).

Polarity analysis

Thirteen stratigraphic sites were sampled from the outcrop, each yielding between 2 and 6 specimens for analysis (appendix 2). Thermal and A.F. demagnetisation techniques and IRM analysis was then carried out at each of the sites (Fig. 6-13).

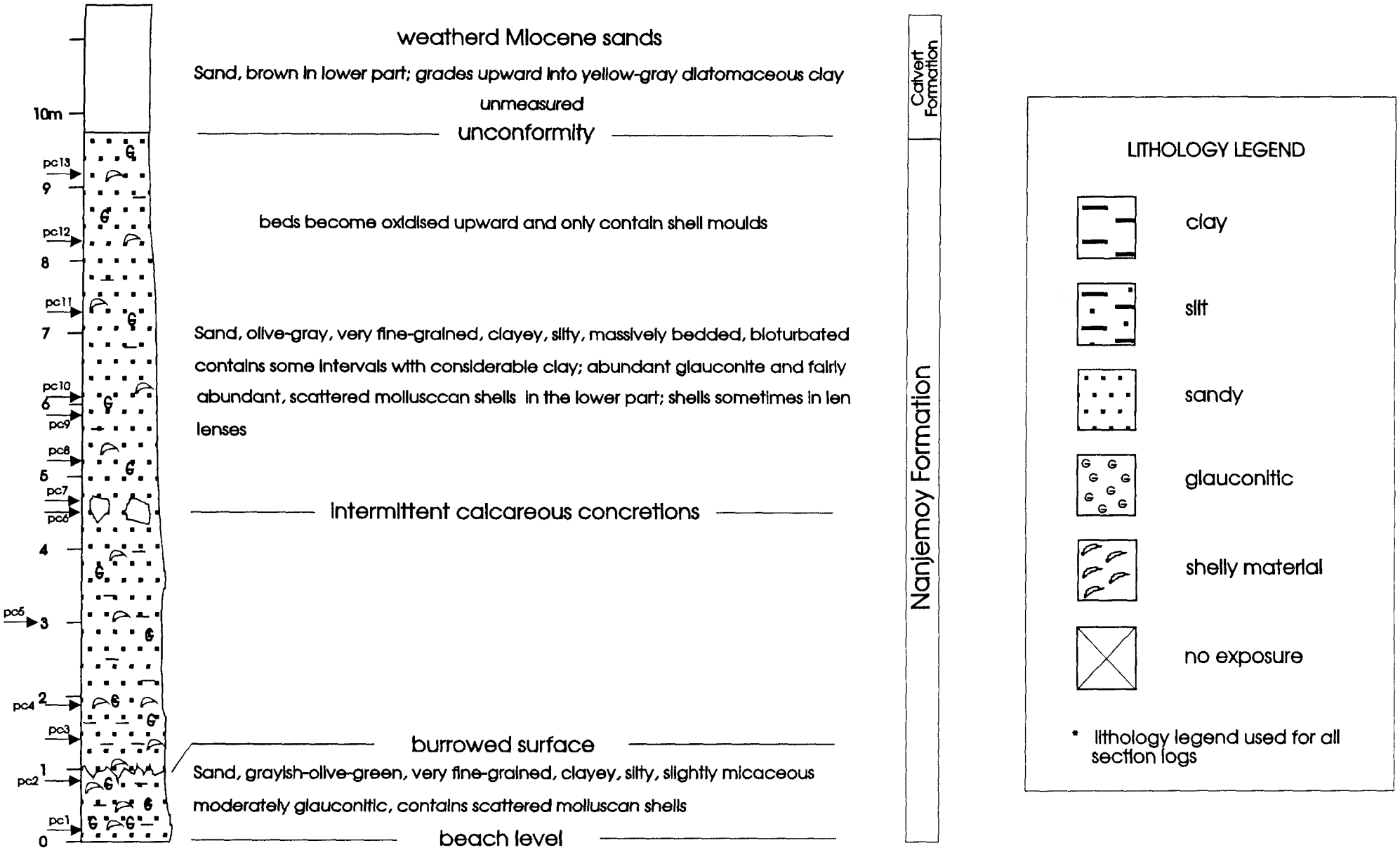

Figure 6-12 *Stratigraphic log and sample sites for the Pope's Creek locality.*

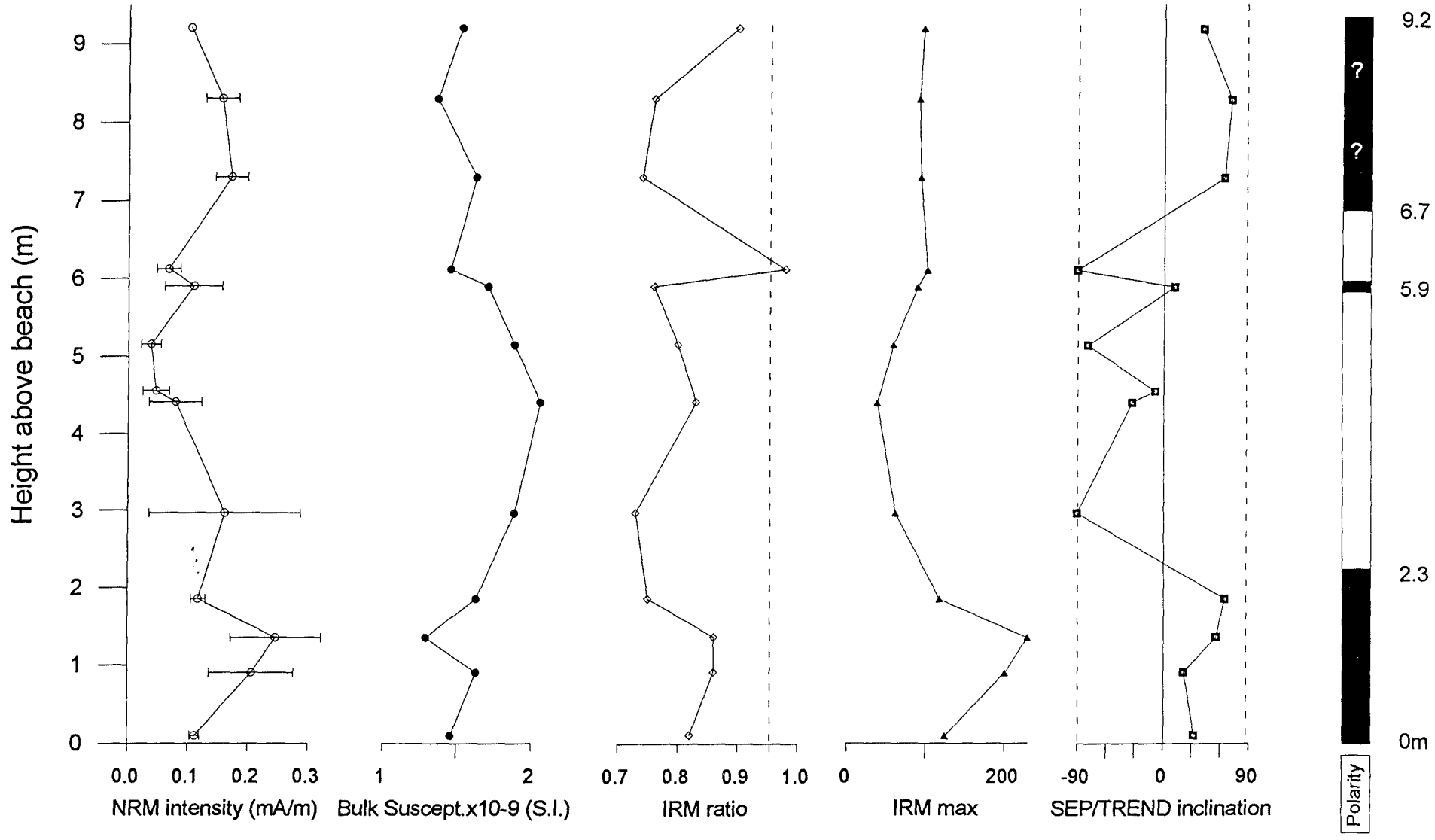

Figure 6-13 *Magnetic parameters of the Pope's Creek section (NRM, susceptibility, IRM ratio, maximum IRM and the average inclination values of SEP and trends at each site summarized in a polarity reversal sequence).*

The A.F. demagnetisation behaviour of samples in most cases exhibited noisy characteristics. Typically, as intensity decreases during progressive demagnetisation steps, the declination and inclination values fluctuate considerably but remain essentially in a particular area on the stereographic plot (Fig. 6-14). Good agreement generally exists between the polarity determination of subsamples from the same stratigraphic height from both thermal and A.F. demagnetisation.

Thirteen subsamples corresponding to 4 sites up to 1.85m from beach level gave consistent normal polarities, 2 other subsamples suggested possible trends to reverse and 4 subsamples produced well grouped positive inclination values in the southern hemisphere of the stereographic projection from which no polarity could be determined.

A reversal of polarity occurs between samples at 1.85m and 2.96m above which 4.3m of sediments have a stable reverse polarity component, seen as good trends in 72% of the subsamples (Fig. 6-15). The remaining samples within this reversed polarity zone gave shallow normal inclination plots or wildly erratic behaviour and trends from which no polarity can be inferred.

The remainder of the section, above 6.7m to the last sample height of 9.21m, reverted to a probable normal polarity where a combination of very erratic plots and mixed polarity subsamples made interpretation difficult. The sediments here at the top of the section appeared weathered and shelly material evident further down the outcrop was now reduced to moulds. It is therefore possible that this predominantly normal interval may actually represent an overprint.

Isothermal remanent acquisition

During IRM acquisition work sediment from each site was transferred into plastic sample holders of internal volume $8cm^3$. Each sample was magnetised by a direct field up to a maximum of 0.86T and measured on the 2-G magnetometer.

Figure 6-16 illustrates the IRM curve for one specimen at each stratigraphic level sampled at Pope's Creek. The general shape of the curves are indicative of the magnetic minerals present in the samples; minor variations probably represent errors introduced

during delays in measurement or possibly by movement of unconsolidated sand and silts within the sample holder during the transfer from the pulse magnetiser to the 2-G magnetometer.

The early saturation seen in some samples (PC1, 2, 3, 7, 10 and 13) has been attributed to a magnetite component and possibly influenced by other magnetic minerals such as pyrrhotite whose presence may be suggested by susceptibility jumps during thermal demagnetisation between 250° and 350°C (though pyrite or goethite could also be responsible). At other sites the samples do not reach saturation at applied fields of 0.3-0.4T and therefore a component of hematite is probably present.

No obvious pattern exists between what is considered hematite-dominated material and that which is assumed to be predominantly magnetite. The differing magnetic mineralogies are not confined to exclusive polarity zones. Both hematite-type curves and magnetite-type curves are found in both normal and reverse intervals suggesting that differential oxidation up the section is not a clear factor controlling the polarities. PC 10 for instance, is a magnetite containing sample (IRM ratio 0.98) found in the middle of a reverse polarity interval containing largely hematite-dominated sediments. PC 10 together with the samples above and below it, yield reverse polarities irrespective of the dominant magnetic carrying mineral.

The magnetostratigraphy of the Pope's Creek section

The samples analysed at Pope's Creek though often erratic, show a normal polarity interval interrupted by an approximate 4m reverse polarity zone. If further biostratigraphical investigations reveal that this section is confined entirely within the top of NP 12 then the section is probably confined to Chron C23n which includes a short period of reverse polarity (Cande and Kent, 1991). Alternatively, if it proves to span nannofossil zones NP12 and NP 13 then the normal polarity at the base of the outcrop is Chron C23n and the reversal boundary observed at approximately 2m above the beach will represent the junction between Chron C23n and Chron C22r. The normal polarity zone at the top of the section may then indicate the overprint suggested by some of the samples. If this is the case, the secondary magnetisation may be an artifact of the weathering observed below the Miocene unconformity at the top of this location.

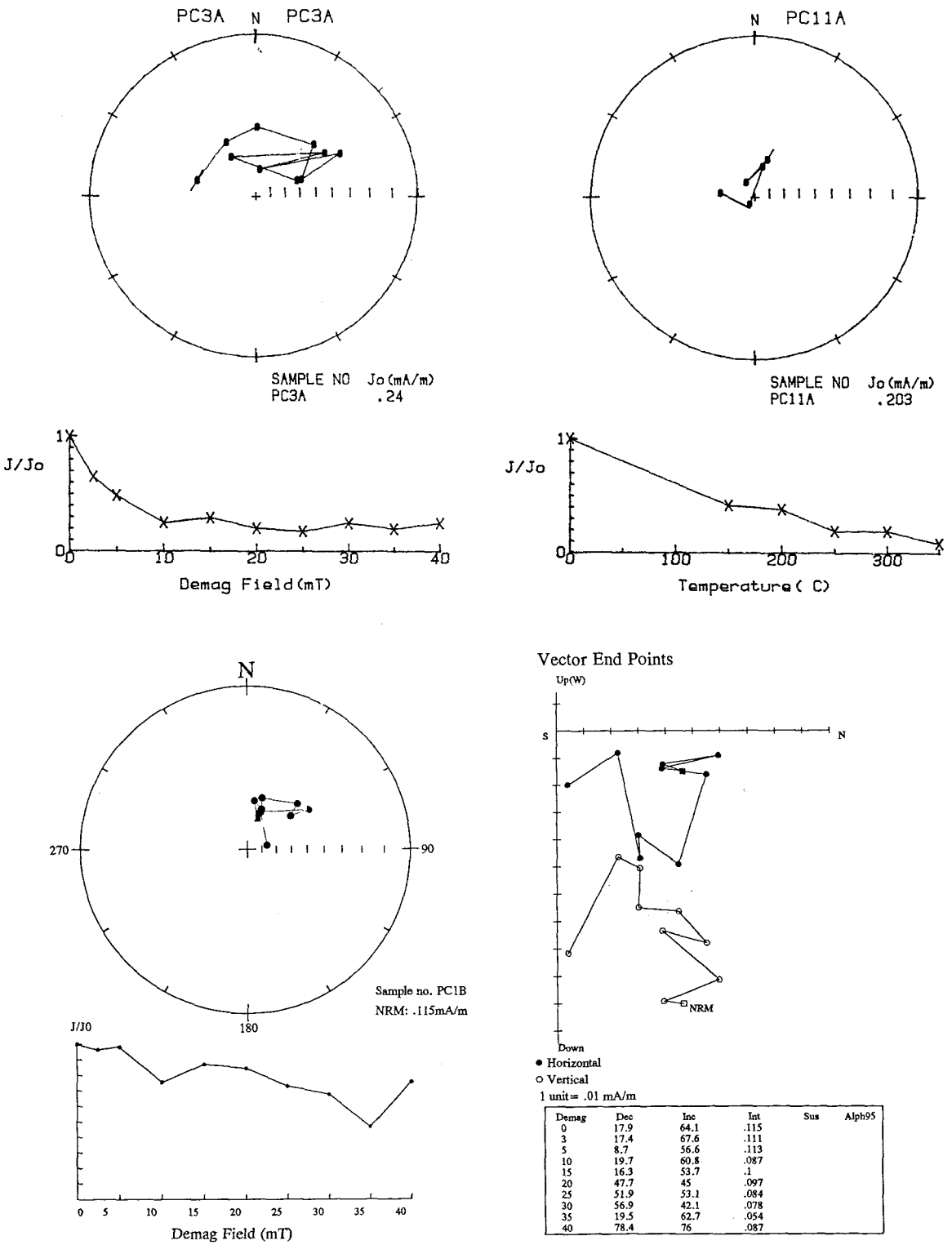

Demag	Dec	Inc	Int	Sus	Alph95
0	17.9	64.1	.115		
3	17.4	67.6	.111		
5	8.7	56.6	.113		
10	19.7	60.8	.087		
15	16.3	53.7	.1		
20	47.7	45	.097		
25	51.9	53.1	.084		
30	56.9	42.1	.078		
35	19.5	62.7	.054		
40	78.4	76	.087		

Figure 6-14 *Examples of poor quality normal polarity samples at Pope's Creek.*

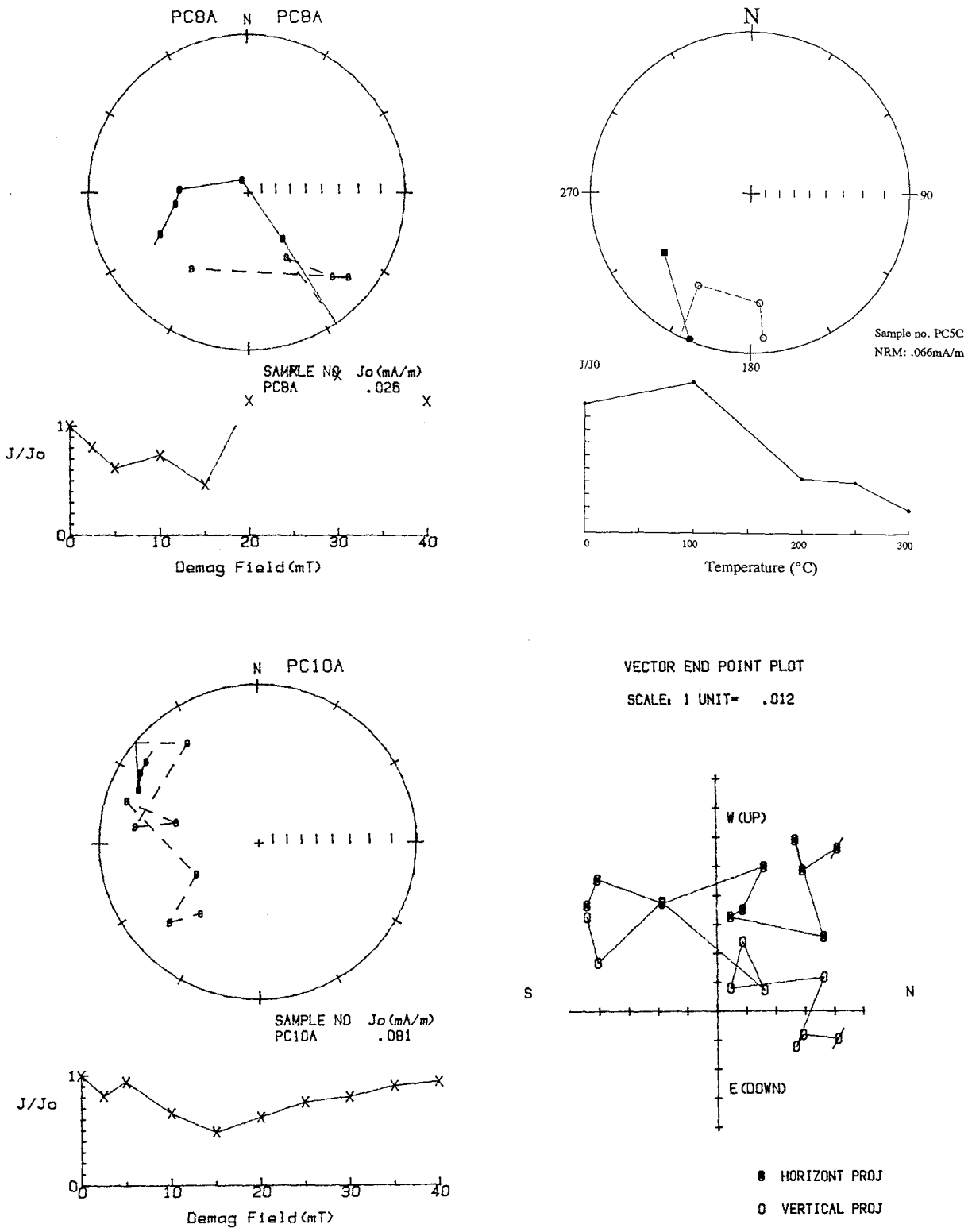

Figure 6-15 *Examples of poor quality reverse polarity samples at Pope's Creek.*

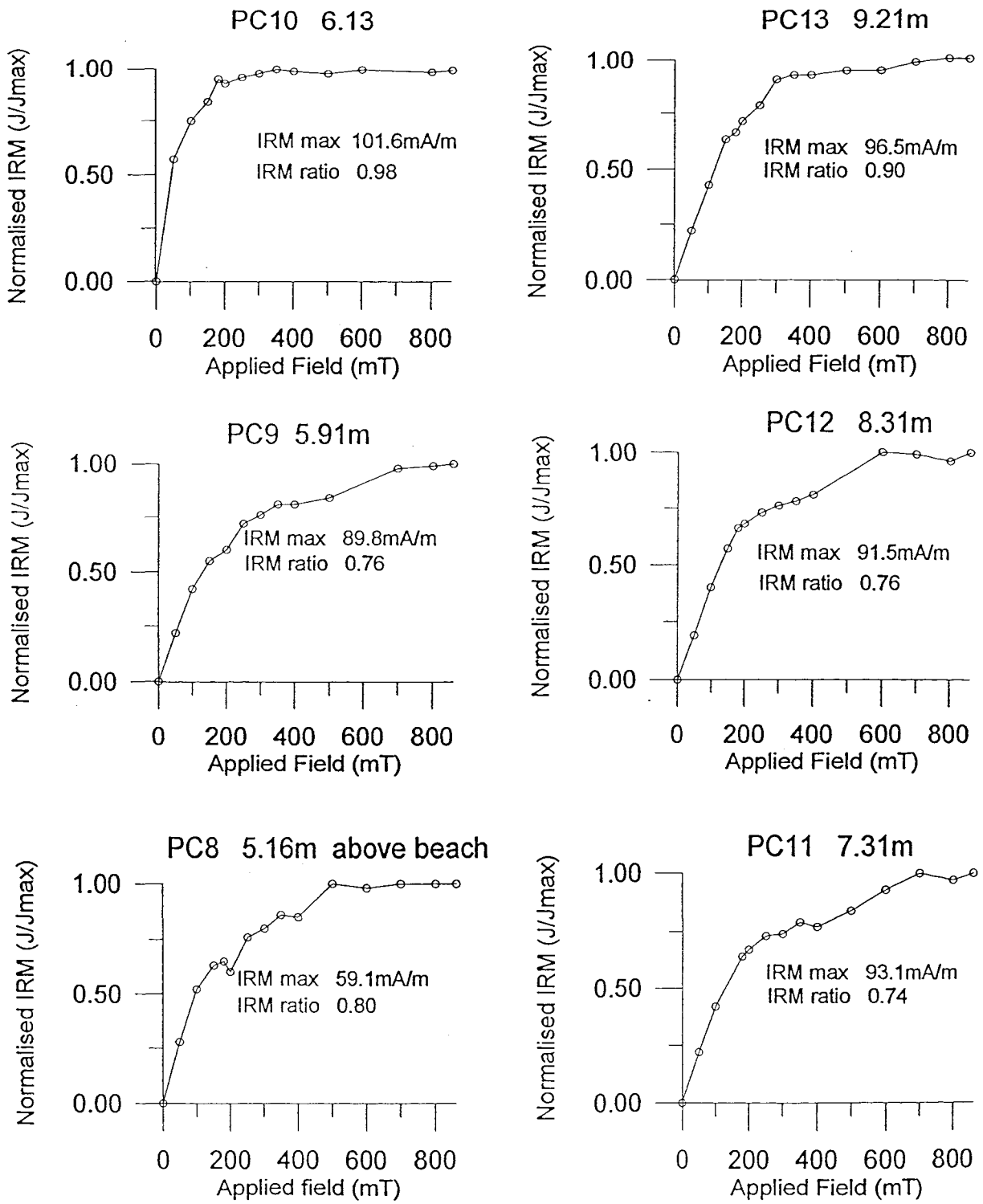

Figure 6-16 *IRM curves for samples at Pope's Creek.*

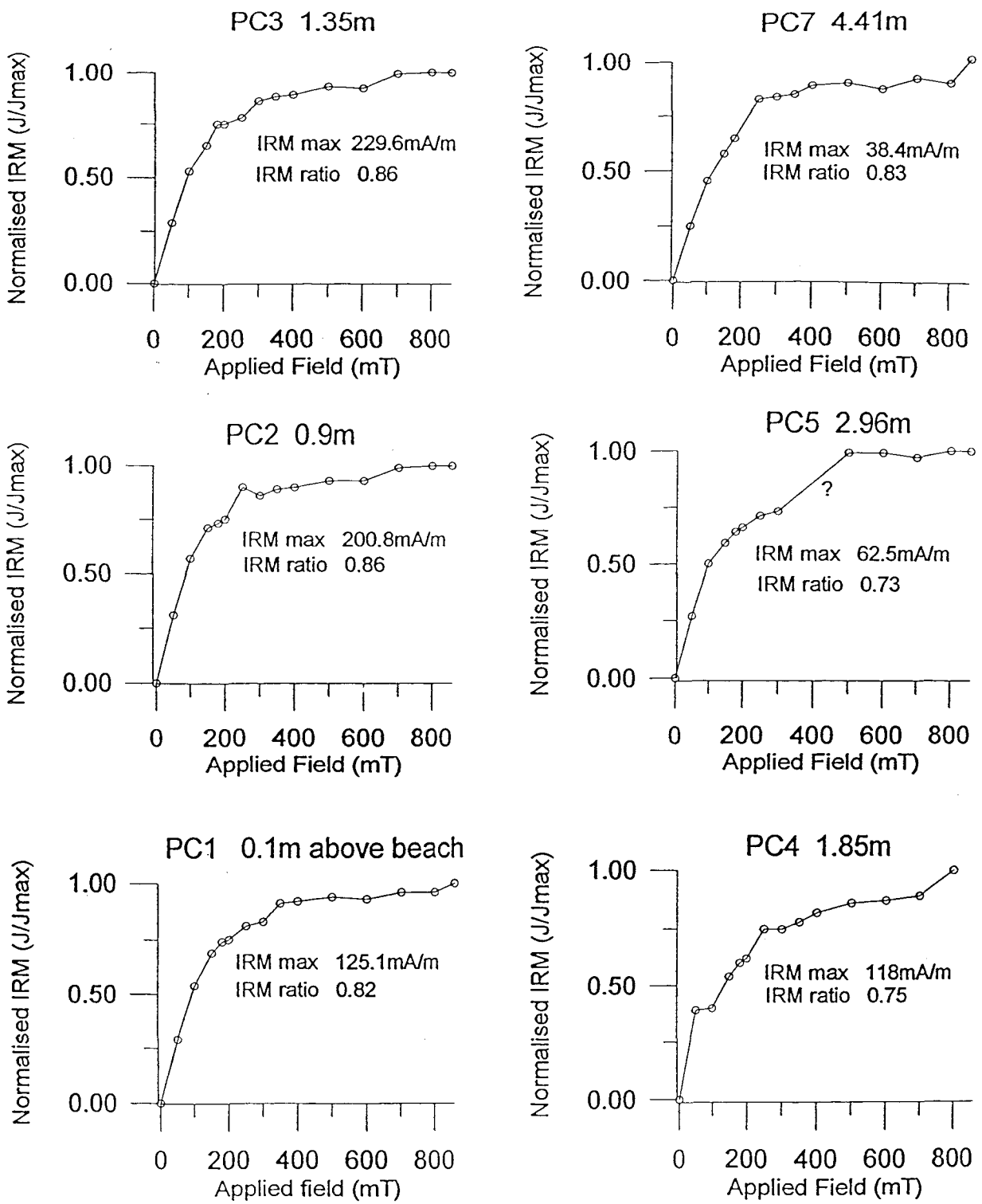

Figure 6-16 - continued *IRM curves for samples at Pope's Creek.*

6.3.2 Yacht Club locality

Location - South bank of the Potomac River, 1.1km down river from Fairview Beach wharf, King George County, Virginia, King George 7 1/2 minute quadrangle.

Plate 6-5 *Yacht Club exposure on the Potomac River.*

The Aquia, Marlboro and Nanjemoy Formations outcrop at this 5m section. The massively bedded glauconitic sand of the Nanjemoy Formation is weathered and has a burrowed contact at its lower junction with the Marlboro Clay (Plate 6-5 and Fig. 6-17). Burrows extend up to 0.5m into the Marlboro Clay, which is exposed as a fresh grey massively bedded clay with a thickness of approximately 2m.

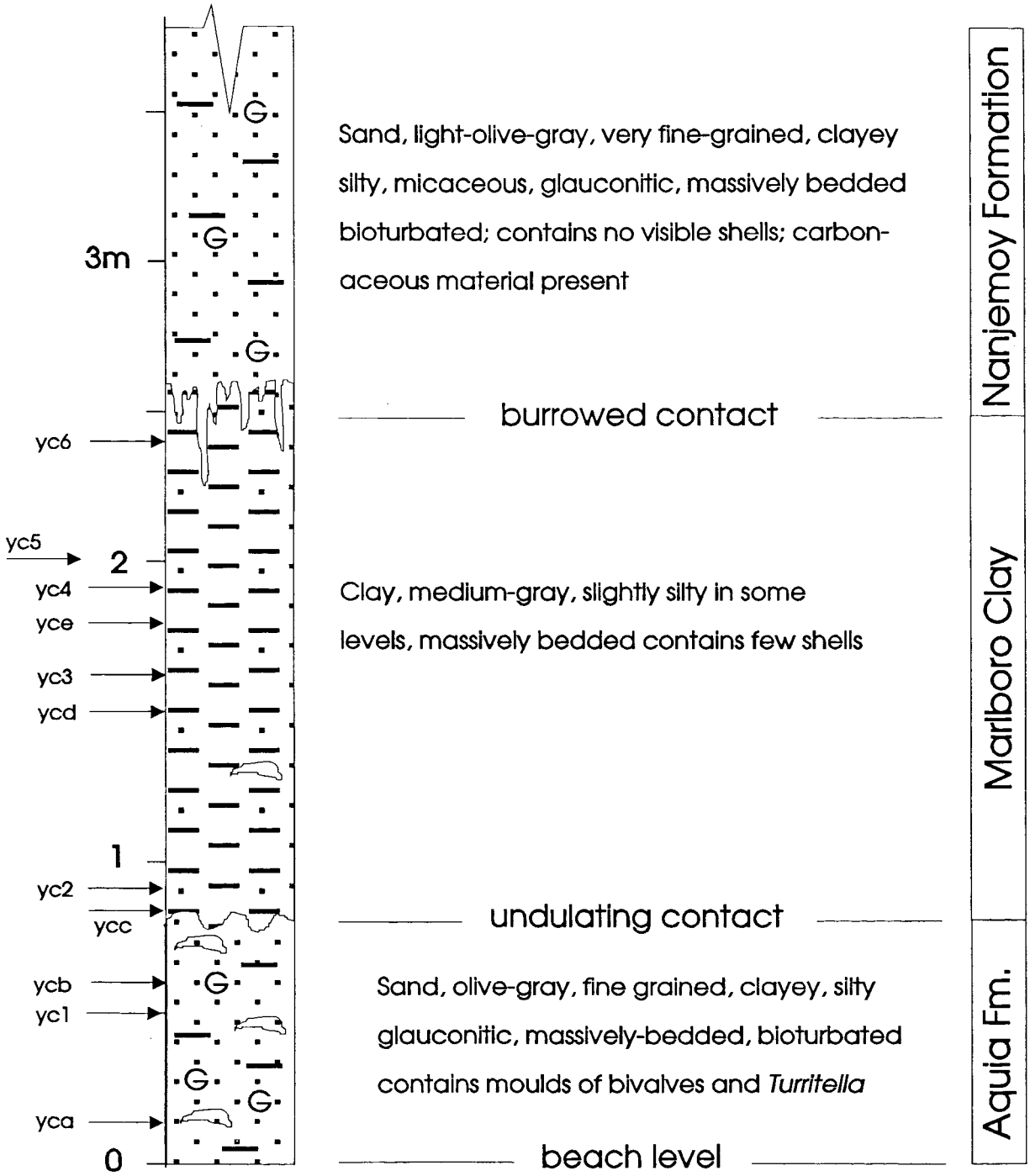

Figure 6-17 *Stratigraphic log and sample sites at the Yacht Club locality.*

Rare ghosts of the gastropod *Turritella* were observed during June 1992 which up to now have been undocumented. The Marlboro Clay at this locality has an age which has been determined by biostratigraphy to be within the uppermost part of NP 9 (Gibson, pers. comm.).

An undulating contact separates the Marlboro Clay from the underlying fine glauconitic sand of the Aquia Formation (which contrasts with the two units above in that it has abundant moulds of bivalves and *Turritella).*

Polarity Analysis

Sampling was restricted to 11 sites over a stratigraphic interval of 2.2m. The lower 5 sites sampled the top of the Aquia Formation and the remaining 6 sites were located within the 2m of exposed Marlboro Clay. The sampling interval averaged 0.2m with samples being further subdivided into 1-4 subsamples.

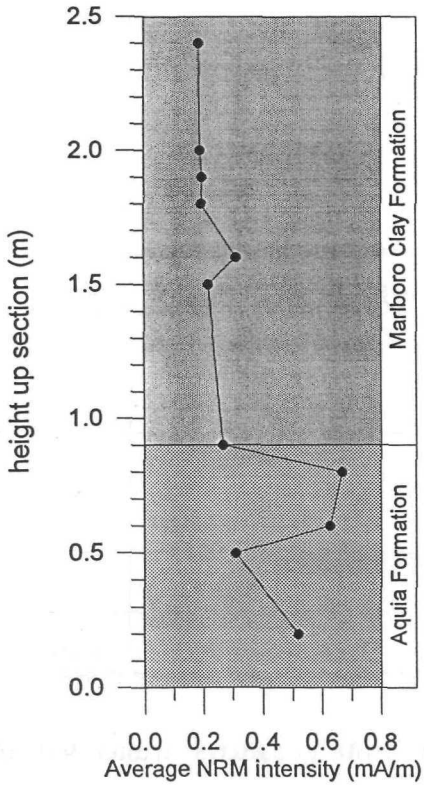

Figure 6-18 *Average NRM intensities of samples at the Yacht Club locality.*

The NRM intensities ranged from 0.31 to 0.67mA/m in the Aquia Formation and 0.185 to 0.266mA/m in the Marlboro Clay, showing a marked change across the boundary of the formations (Fig. 6-18). IRM acquisition curves from one sample at each site show early saturation of the magnetic minerals suggesting a magnetite dominated magnetic component (Fig. 6-19). Thermal demagnetisation of samples from the Marlboro Clay show a steady drop in intensity to a minimum at 350°C at which point sample intensities approach the sensitivity limit of the magnetometer. Within this temperature range there is little evidence of mineralogical phase transitions (Figs. 6-20b and 6-21b).

Marlboro Clay reverse polarity zone

The Marlboro Clay outcropping at the Yacht Club locality shows considerable differences in magnetic properties to that of the Marlboro Clay from the Oak Grove core located approximately 20km to the south (Fig. 6-11). Intensity values for instance are two orders of magnitude lower in outcrop material and NRM intensities increase rather than decrease across the Aquia Formation / Marlboro Clay boundary (compare for example Fig. 6-3 and Fig. 6-18). These magnetic and other contrasting properties are summarised in Table 6-1.

Marlboro Clay	**Yacht Club locality**	**Oak Grove Core**
Thickness	2m	5.5m
Average intensity	0.12mA/m	20mA/m
Colour	blue	pink
Peak IRM	100	5000
IRM Ratio	0.83-0.9	0.7-0.9
Unconformable boundaries	upper and lower	upper (lower is gradational)

Table 6-1 *Contrasting characteristics of Marlboro Clay core and outcrop material.*

The sets of samples from both the Marlboro Clay outcrop and core material are confirmed as upper NP9 and therefore should possess similar primary components of

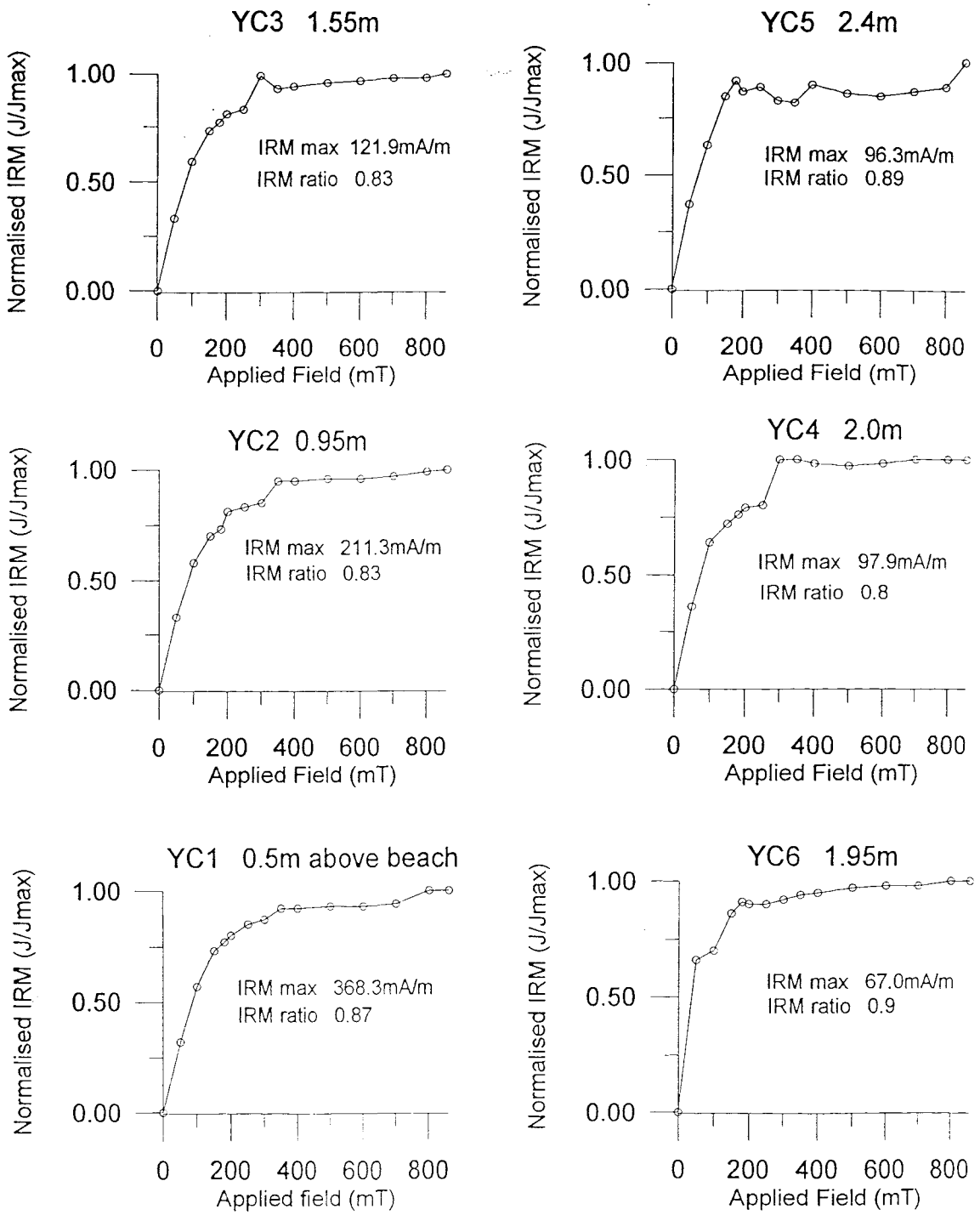

Figure 6-19 *IRM acquisition curves for sediments at 6 sites at the Yacht Club locality.*

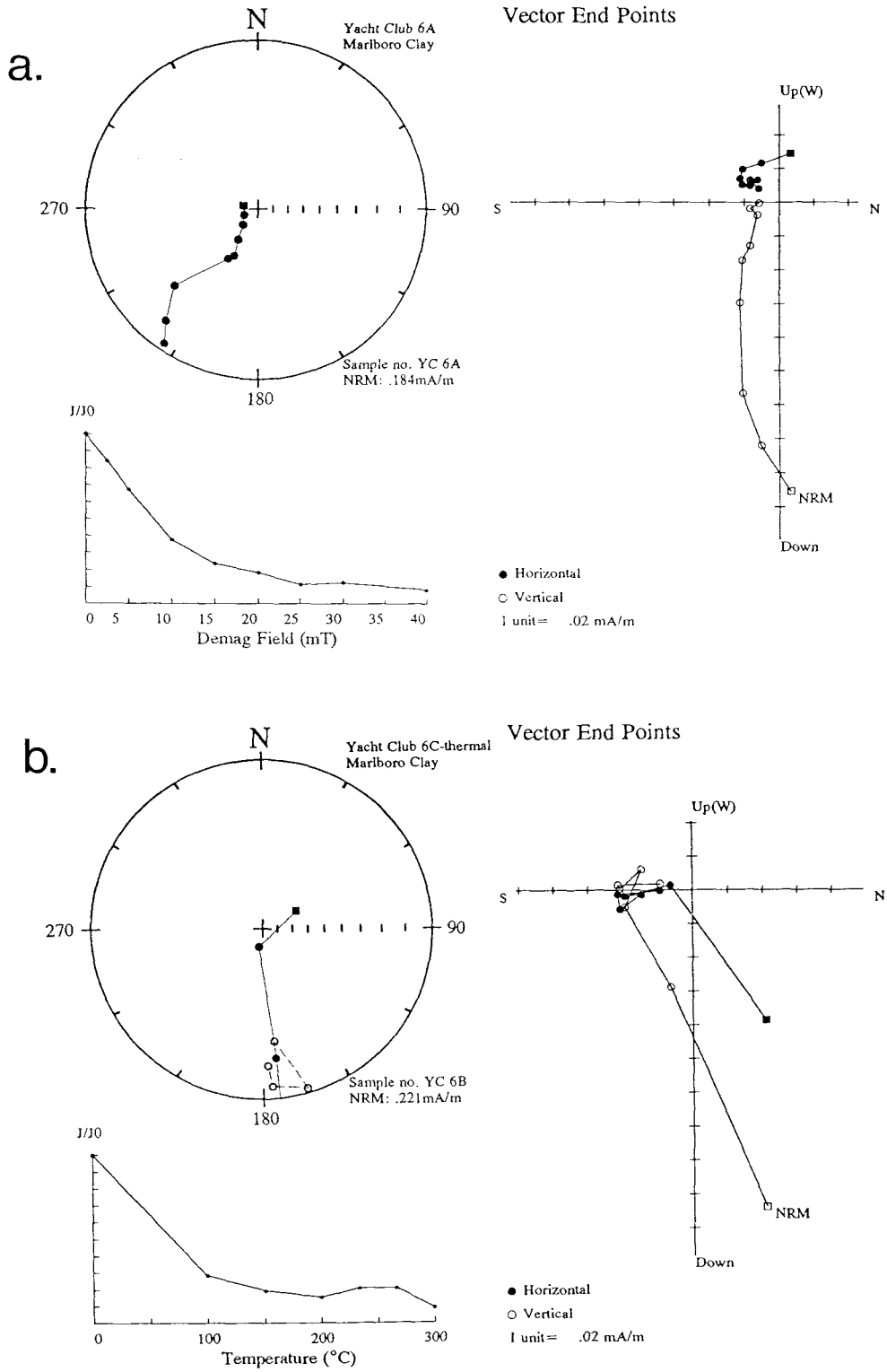

Figure 6-20 *Reverse polarity trends from a site within the Marlboro Clay at the Yacht Club locality. a. A.F. demagnetisation b. Thermal demagnetisation.*

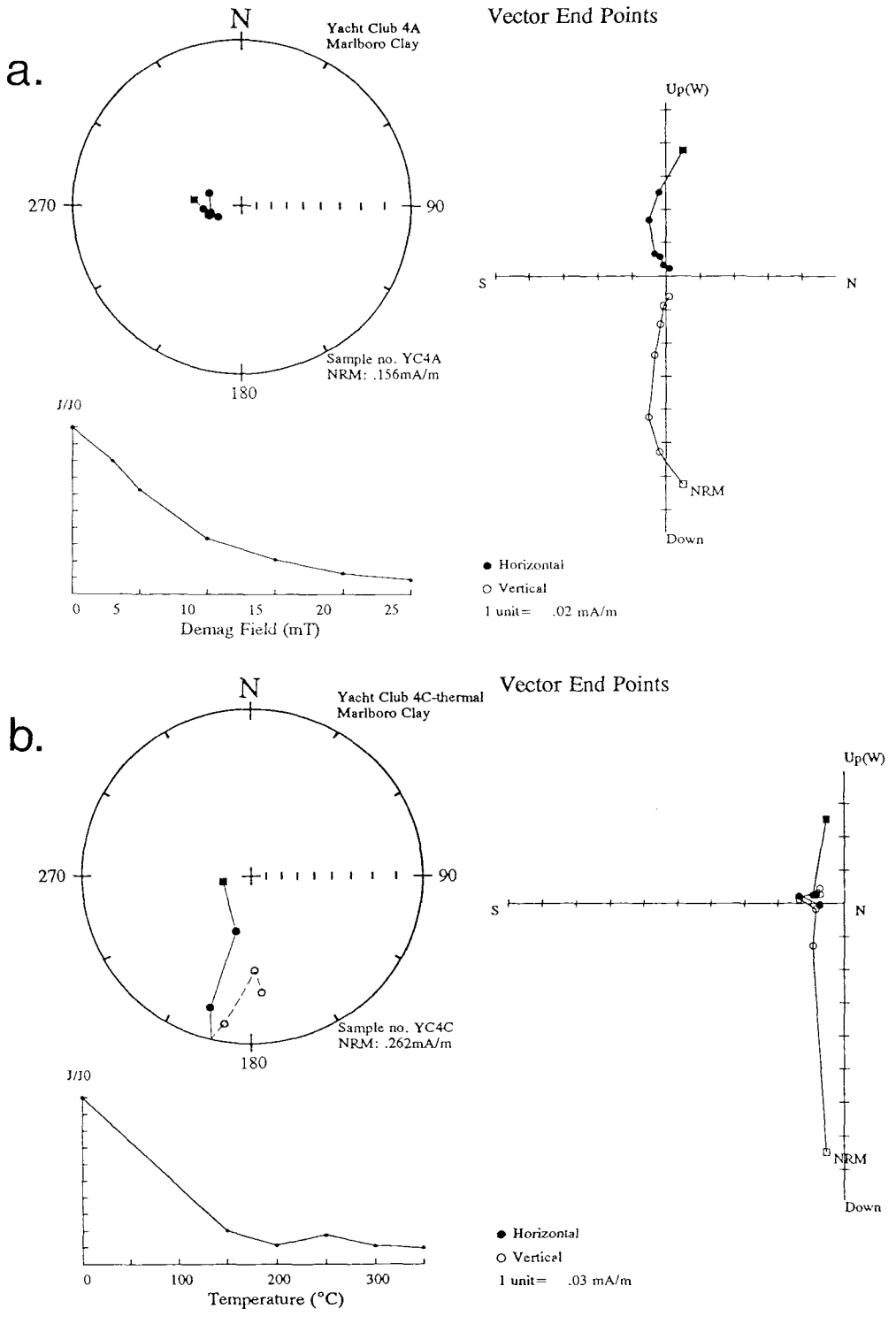

Figure 6-21 *Demagnetisation behaviour of samples from the same site within the Marlboro Clay at the Yacht Club locality. a. A.F. demagnetisation b. Thermal demagnetisation.*

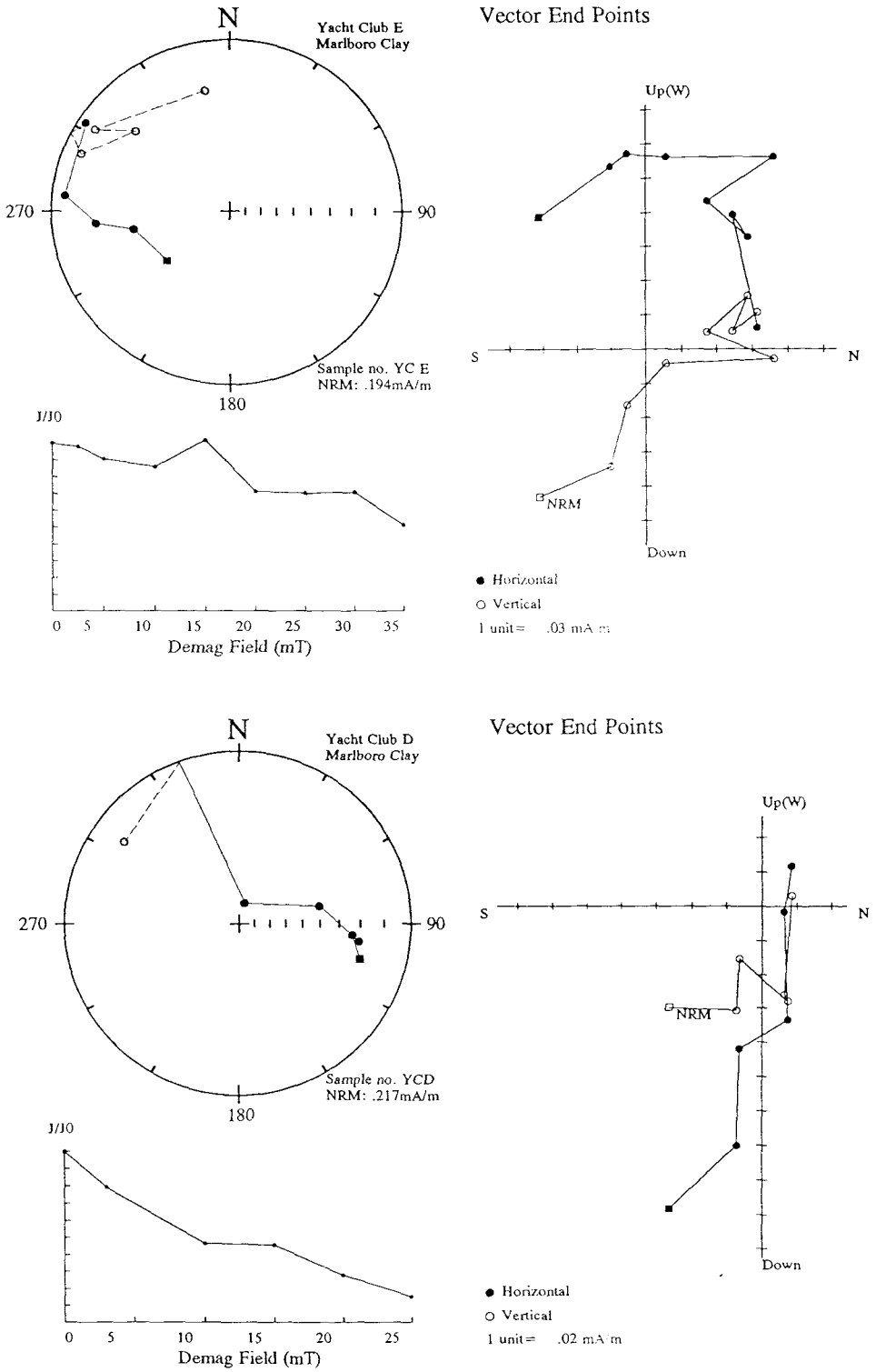

Figure 6-22 *Marlboro Clay samples from the Yacht Club locality showing possible trends to a reverse polarity after A.F. demagnetisation.*

magnetisation if they are preserved. The demagnetisation behaviour of Marlboro Clay in outcrop however does not exhibit the clear reverse polarity components observed in core material (Fig. 6-7). Infact there are no samples that show reverse polarity SEPs, only trends to reverse which exhibit varying degrees of reliability (appendix 3).

The A.F demagnetisation plots generally show fewer distinct trends to a reverse polarity than thermally demagnetised sub-samples from the same stratigraphic site. For instance, at site 6 the A.F. demagnetised sample (Fig. 6-20a) does not show a trend that is of sufficient length to reveal a negative component although one is inferred. The thermally demagnetised sample however (Fig. 6-20b) illustrates a more complete trend to a reverse polarity. In a more extreme case, figure 6-21 shows an A.F. plot indicating an apparent SEP with steep positive inclination; the corresponding thermally demagnetised sample however exhibits a clear trend to a reverse polarity. Further sites in the Marlboro Clay suggest a possible high coercivity component with negative inclination (Fig. 6-22).

If the spurious plots are ignored, 80% of the remaining samples exhibit trends to a reverse polarity. The Marlboro Clay section at the Yacht Club locality has therefore been assigned a reverse polarity throughout, although the quality of data suggests that the reliable primary component showing a clear reverse polarity interval seen in the Marlboro Clay of the Oak Grove core (and expected of upper NP9 material) has been obscured and in some cases destroyed by subsequent overprints of magnetisation at this location.

Aquia Formation mixed polarity zone

Below the Marlboro Clay, 0.7m of sandy sediment from the Aquia Formation exhibited mixed polarity plots. Samples were extremely friable and most disintegrated during sub-sampling. From A.F. demagnetisation alone a predominently normal polarity zone is suggested; however the lack of thermal demagnetisation carried out due to the difficulties in sub-dividing samples puts the existence of this normal zone in question.

Magnetostratigraphy of the Yacht Club section

Polarity determination of material from this outcrop has proved difficult. This is primarily due to the lack of SEPs, the frequent existence of short questionable trends and inconsistency of sub-samples at some sites.

The upper Aquia and Marlboro Clay Formations are positioned within the upper NP9 nannofossil zone which should correlate with Chron C24r. It is not possible to determine a reliable magnetostratigraphy for this section. However, based on trending data alone the Marlboro Clay samples are assigned to a reverse polarity zone which overlies a mixed polarity interval at the top of the Aquia. This tentative magnetostratigraphy is indicated in the summary diagram in section 6.9 of this chapter.

6.3.3 Tinker's Ravine locality

Location - Stream draining into Port Tobacco, Charles County.

At this location, the Aquia Formation is exposed over approximately 12m, of which only a 5m section is suitable for palaeomagnetic sampling (Fig. 6-23). This interval consists of glauconitic sands with varying amounts of silt and clay interspersed with fossiliferous beds.

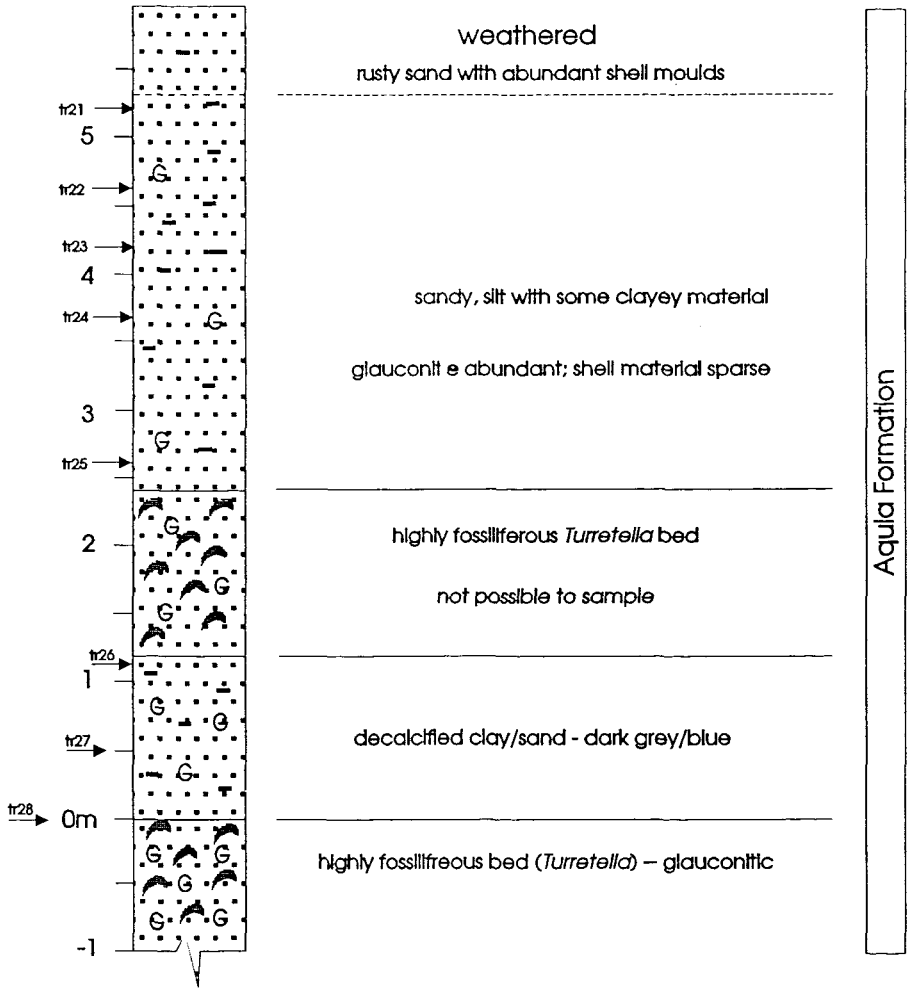

Figure 6-23 *Stratigraphic log and sample positions at Tinker's Ravine.*

A sharp contact exists between an overlying unfossiliferous glauconitic sand and a *Turretella* bed; this was used as a datum from which sample heights are given. At least the upper 10m of the section is NP9 (Gibson, pers. comm.).

Large block samples were taken at an average interval of 0.88m over 6m of the upper part of the section. These were divided into 3 subsamples and demagnetised using A.F. and thermal demagnetisation procedures. The mean NRM intensities for the section was 0.453 ± 0.24mA/m (Fig. 6-27) with relatively good consistency between subsamples measured from the same level.

Isothermal remanent magnetic investigations at each site in the section suggest a magnetite-dominated magnetic fraction (Fig. 6-24). The average IRM ratio is 0.86 with samples showing total saturation by 0.4 T, except for TR26, sampled at 0.5m above the shell bed datum, which saturates at 0.6 T. There is no evidence, based on IRM acquisition, for a hematite component of magnetism.

SEM and electron probe analysis

A polished slide of material sampled from the Tinker's Ravine (TR23) was carbon coated to enhance conductivity and observed under a scanning electron microscope. An electron probe was then used to analyse the elemental composition of the high atomic number particles seen on the SEM back scatter mode.

Plate 6-6 *SEM image of an Fe/S containing particle within a fibrous elongate clast.*

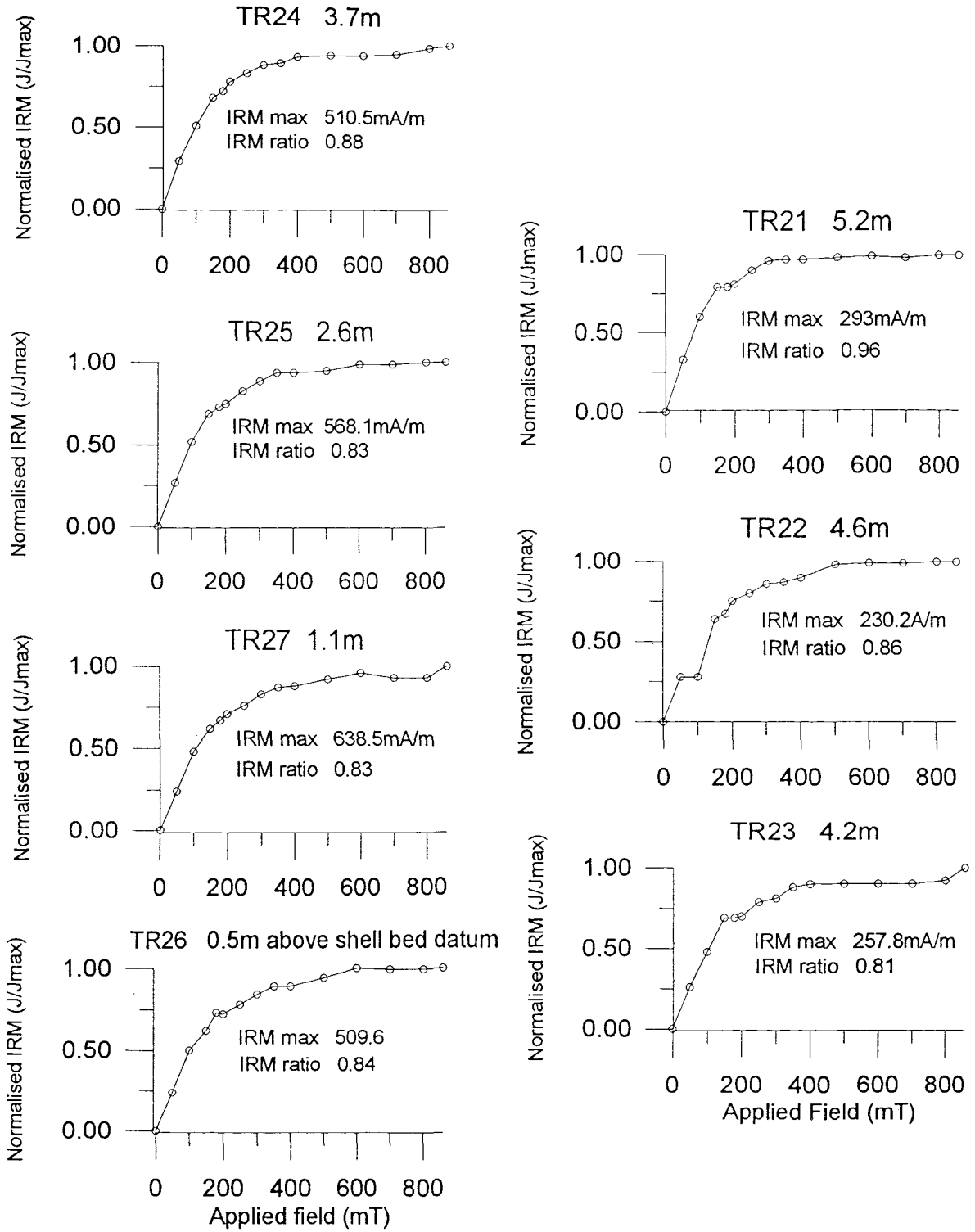

Figure 6-24 *IRM acquisition curves for 7 sites at Tinker's Ravine*

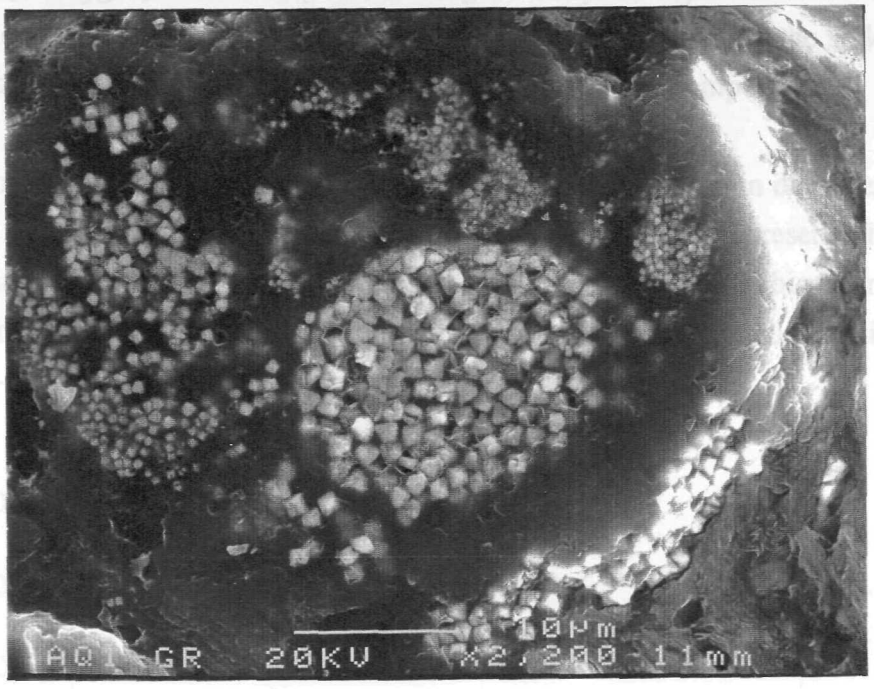

Plate 6-7 *SEM image of a sulphur/iron frambule from the Aquia Formation at Tinker's Ravine.*

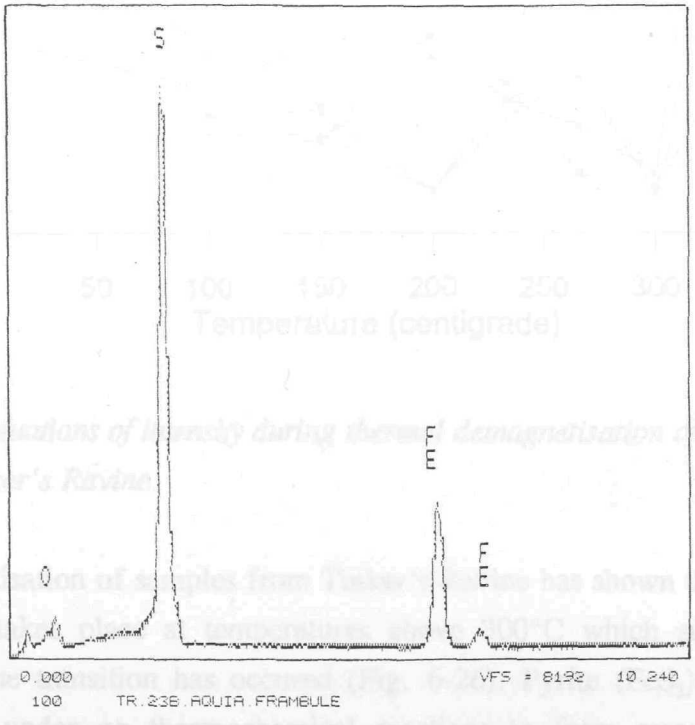

Figure 6-25 *Electron probe analysis of the grain clusters in Plate 6-7.*

The grains providing the highest degree of back scatter had a composition of either zircon/silica (+ oxygen) or iron/sulphur, although subsequent experiments have shown that iron oxides produce less back scatter and were probably missed on the slide. Plate 6-6 and Plate 6-7 illustrate the grains with an iron and sulphur composition.

Plate 6-6 shows a number of angular crystals, approximately 2-5μm in diameter which have grown within a fibrous elongate particle. Plate 6-6 however, represents the more typical arrangement of iron and sulphur containing grains where cubic or rhombic crystals form clusters of varying sizes. Each frambule however, contains similar size crystals 0.3-1.5μm suggesting that they are of a similar age.

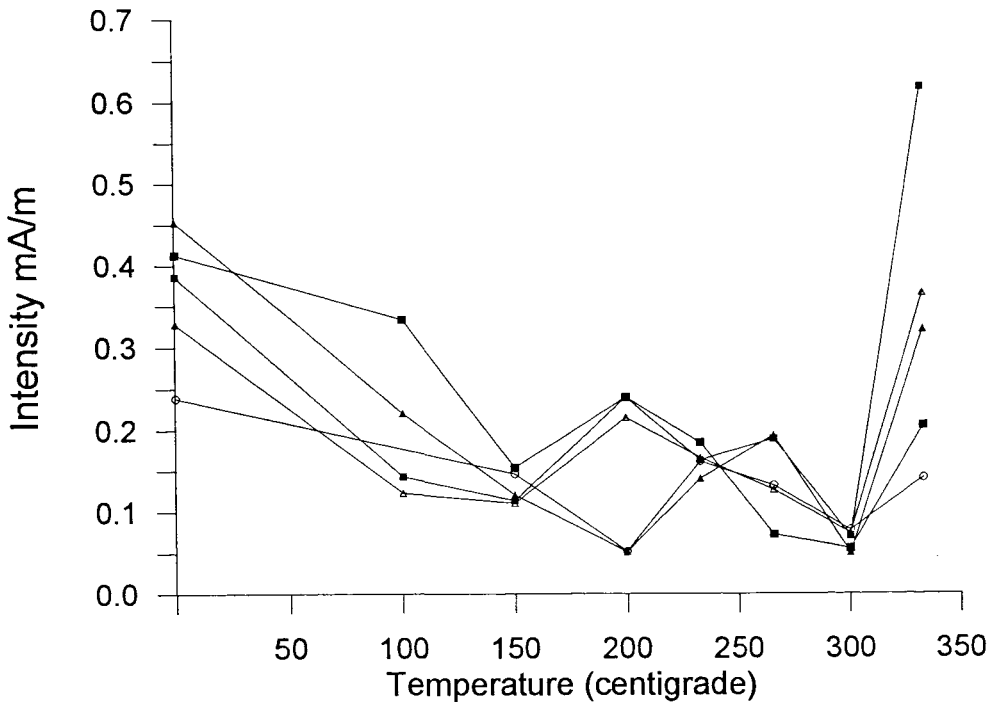

Figure 6-26 *Fluctuations of intensity during thermal demagnetisation of samples from Tinker's Ravine.*

Thermal demagnetisation of samples from Tinker's Ravine has shown that a dramatic rise of intensity takes place at temperatures above 300°C which suggests that a mineralogical phase transition has occured (Fig. 6-26). Pyrite (FeS_2) or pyrrhotite (Fe_7O_8) typically under go thermochemical reactions to form magnetite at such

temperatures. The presence of pyrite or pyrrhotite here would explain the intensity jump observed during thermal demagnetisation above 300°C and also agree with a mineral composition of iron and sulphur seen under the SEM. Pyrite particularly is also commonly known in sediments associated with fossilized organic matter.

If pyrrhotite is present and carries a magnetic overprint however, it can create complications when considering polarity determinations, since it has a relatively rapid saturation magnetisation which influences the shape of IRM acquisition curves in a similar way to magnetite. It can also exist in a number of mineralogical forms whose palaeomagnetic influence is far from understood.

Polarity analysis

The A.F demagnetisation of 8 sites at Tinker's Ravine indicate a reverse polarity zone of at least 2.5m thickness in an otherwise normal interval.

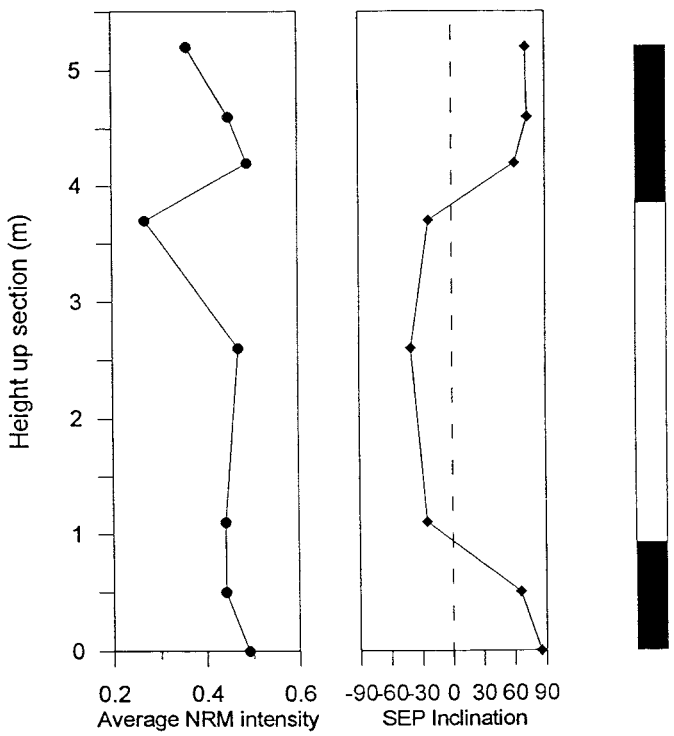

Figure 6-27 *Average NRM intensities and SEP inclination values at each site plotted against their stratigraphic height and aligned with a polarity sequence.*

The majority of samples demagnetised by the A.F. technique show normal polarities that can be categorised as SEPs (Fig. 6-29). Thermal demagnetisation confirms the normal polarity at most sites but the quality of data is significantly reduced (Fig. 6-31, upper). At a height of 1.1m to 3.7m above the shell bed datum, a clear reverse polarity is interpreted which is consistent between demagnetisation behaviour of A.F. and thermally treated samples (Figs. 6-30 and 6-31, lower). A stereographic summary plot of all SEP directional data is shown in figure 6-28.

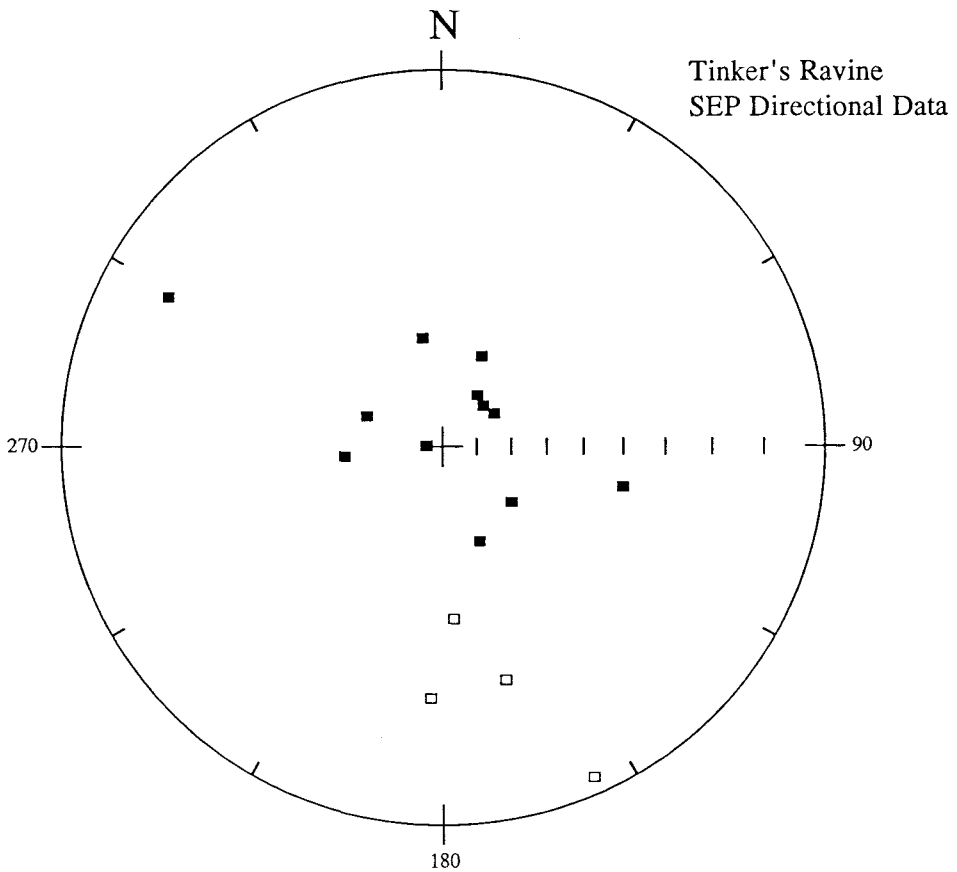

Figure 6-28 *Stereographic projection of all SEP data for Tinker's Ravine*

Magnetostratigraphy of the Tinker's Ravine section

Assuming that the stable magnetic components identified here represent true primary components then placing the polarity sequence at Tinker's Ravine within the Geomagnetic Polarity Timescale is problematic.

The biostratigraphy for Tinker's Ravine indicates a nannofossil NP9 zonation which would infer that the normal polarities determined for much of Tinker's Ravine correspond to Chron C25n. In this case the reverse zone, within the centre of the section, suggests a reverse polarity interval during Chron C25n.

In New Jersey upper NP9 is exposed, resting on NP8. It appears that no lower zone NP9 is present. However, lack of upper zone NP9 biostratigraphic markers in the Maryland and Virginia area suggest that lower NP9 may be found here (Gibson, pers. comm.). If lower NP9 is absent then the whole of Tinker's Ravine would be expected to fall within Chron C24r. The presence of good quality normal polarity samples at several sites, however, is good evidence of a lower NP9 age for the section at Tinker's Ravine (see section 6.9).

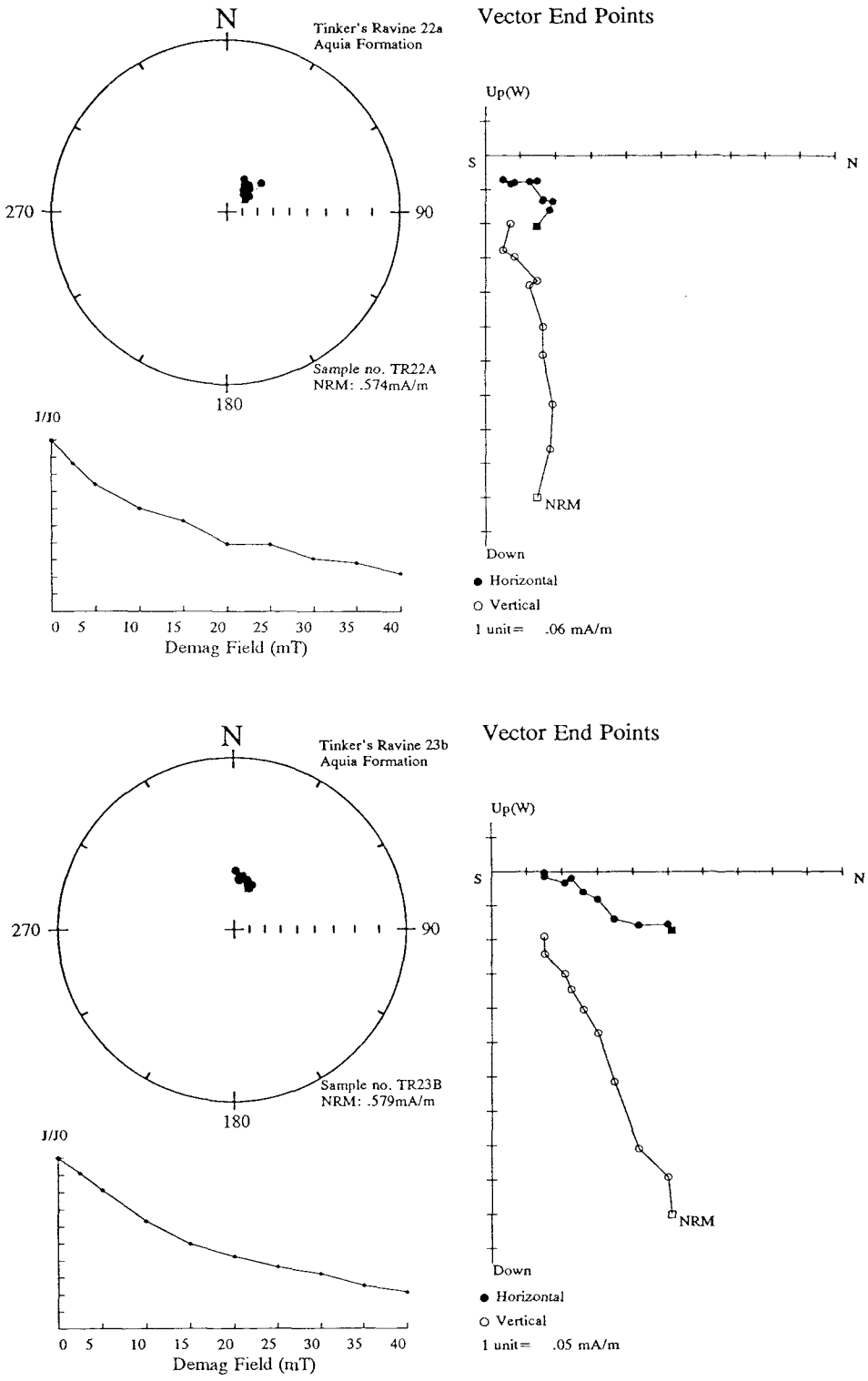

Figure 6-29 *A.F. demagnetisation behaviour of normal polarity SEP from Tinker's Ravine.*

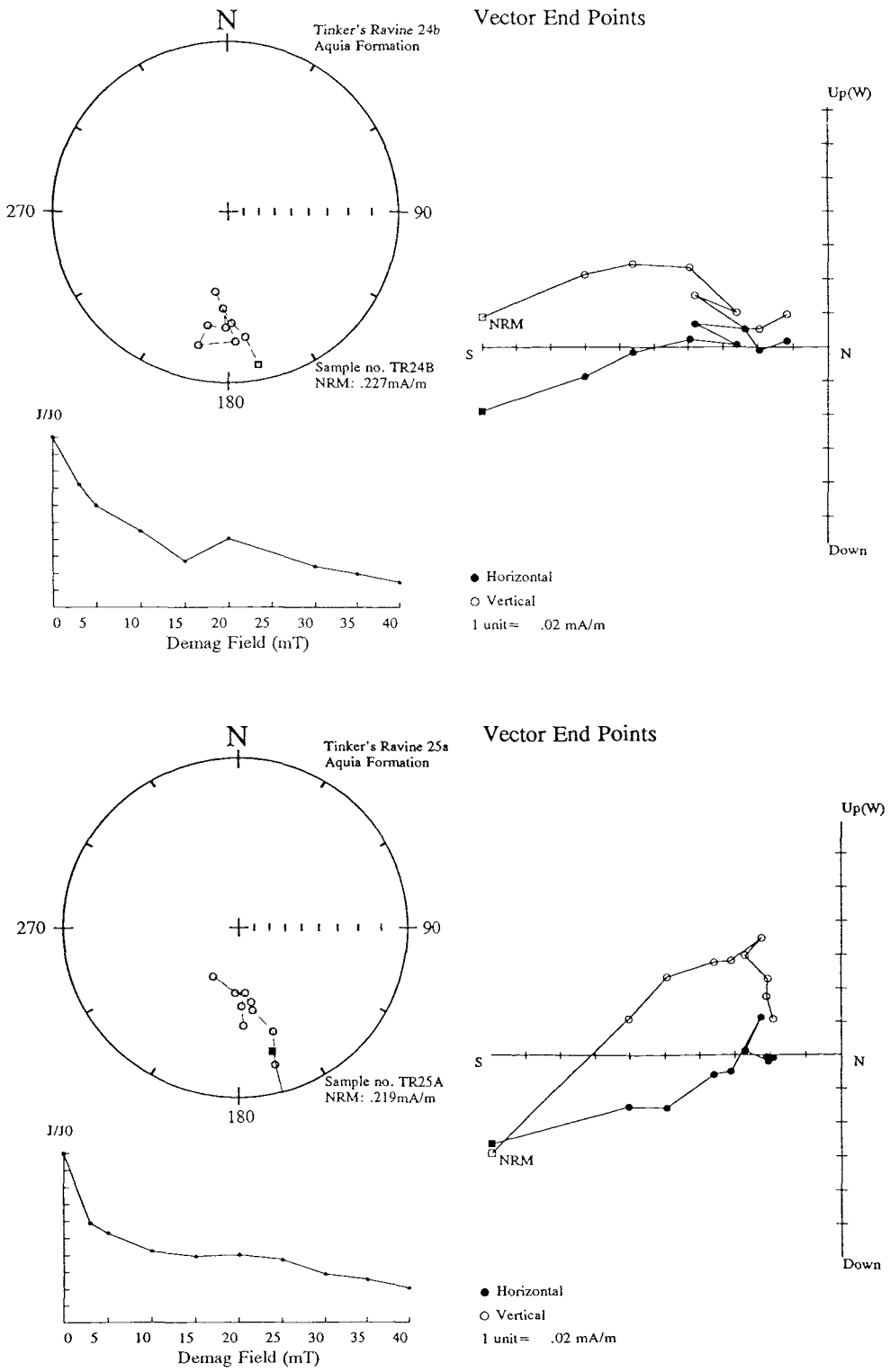

Figure 6-30 *A.F. demagnetisation behaviour of reverse polarity SEP from Tinker's Ravine.*

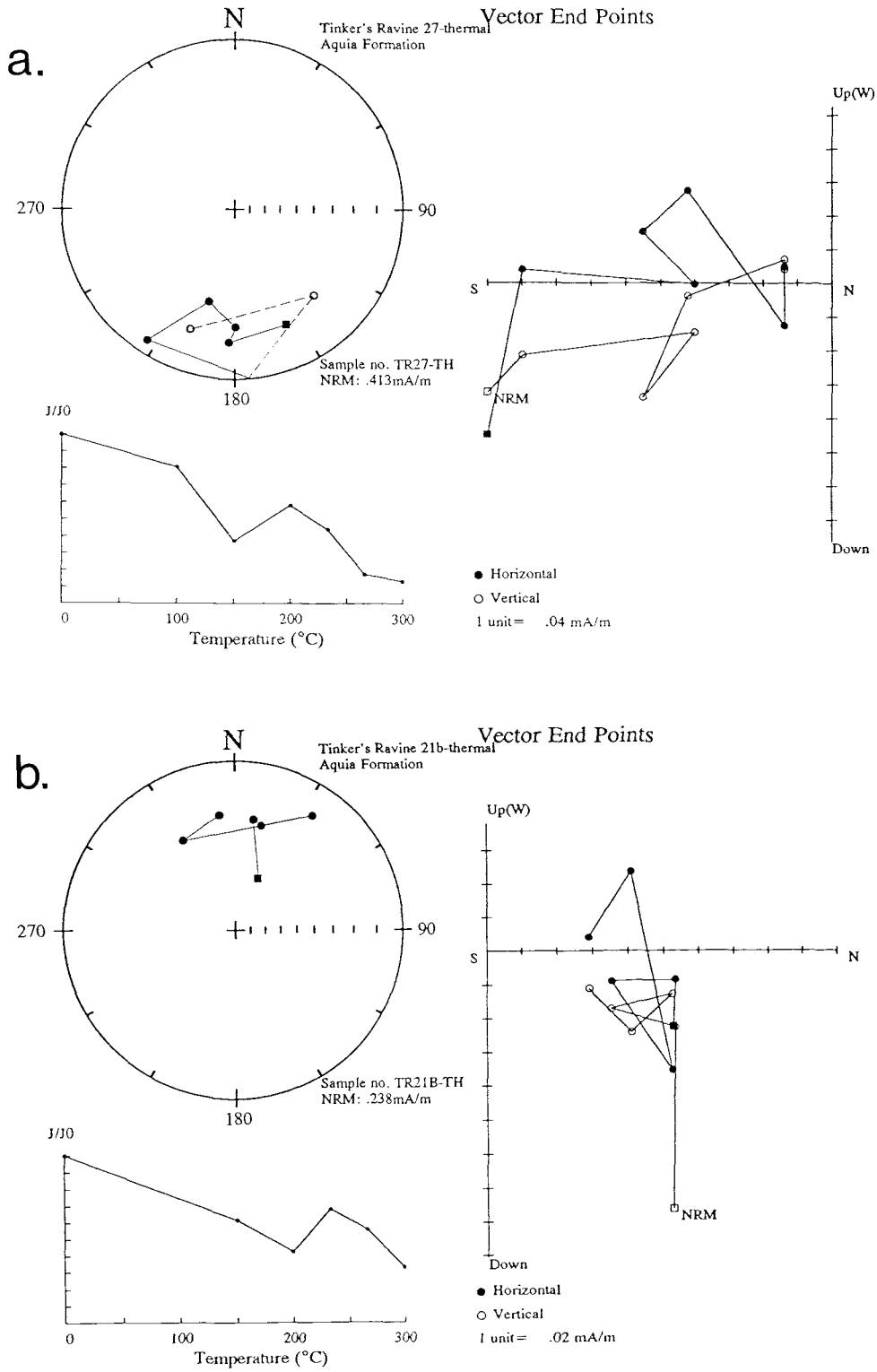

Figure 6-31 *Thermal demagnetised samples from Tinker's Ravine. a. reverse polarity b. normal polarity.*

6.3.4 Bulls Bluff (Potomac Creek) locality

Location - South bank of Potomac Creek just to the west off Bulls Bluff, King George County, Virginia, Passapatanzy 7 1/2 minute quadrangle.

A short 2m section of fresh upper Aquia sediments at Bull's Bluff contains an undulating contact 0.5m above beach level that separates a lower, highly fossiliferous glauconitic sand (containing the NP8/NP9 boundary) from a less fossiliferous sand above. Below this contact the abundance of mollusca shells, corals and vertebrates severely limits palaeomagnetic sampling.

The IRM acquisition curves for 3 sites show an average IRM ratio of 0.9 which indicates an early saturation and hence the section is probably magnetite-dominated (Fig. 6-32).

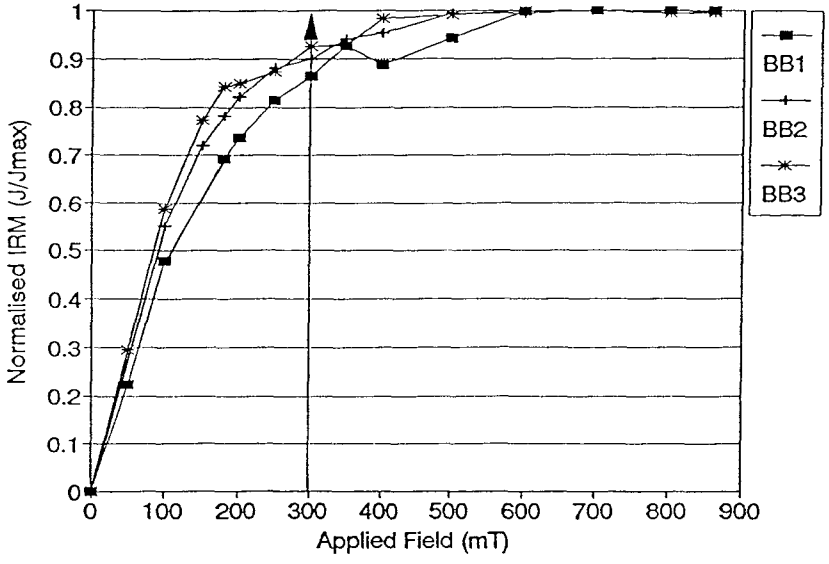

Figure 6-32 *IRM Acquisition curves for the three sites at Bull's Bluff.*

Polarity analysis

A.F. and thermal demagnetisation of 7 sites from a 1.3m section yielded a relatively consistent component of magnetisation (Figs. 6-33 and 6-34). This component has a steep positive inclination and a southerly declination.

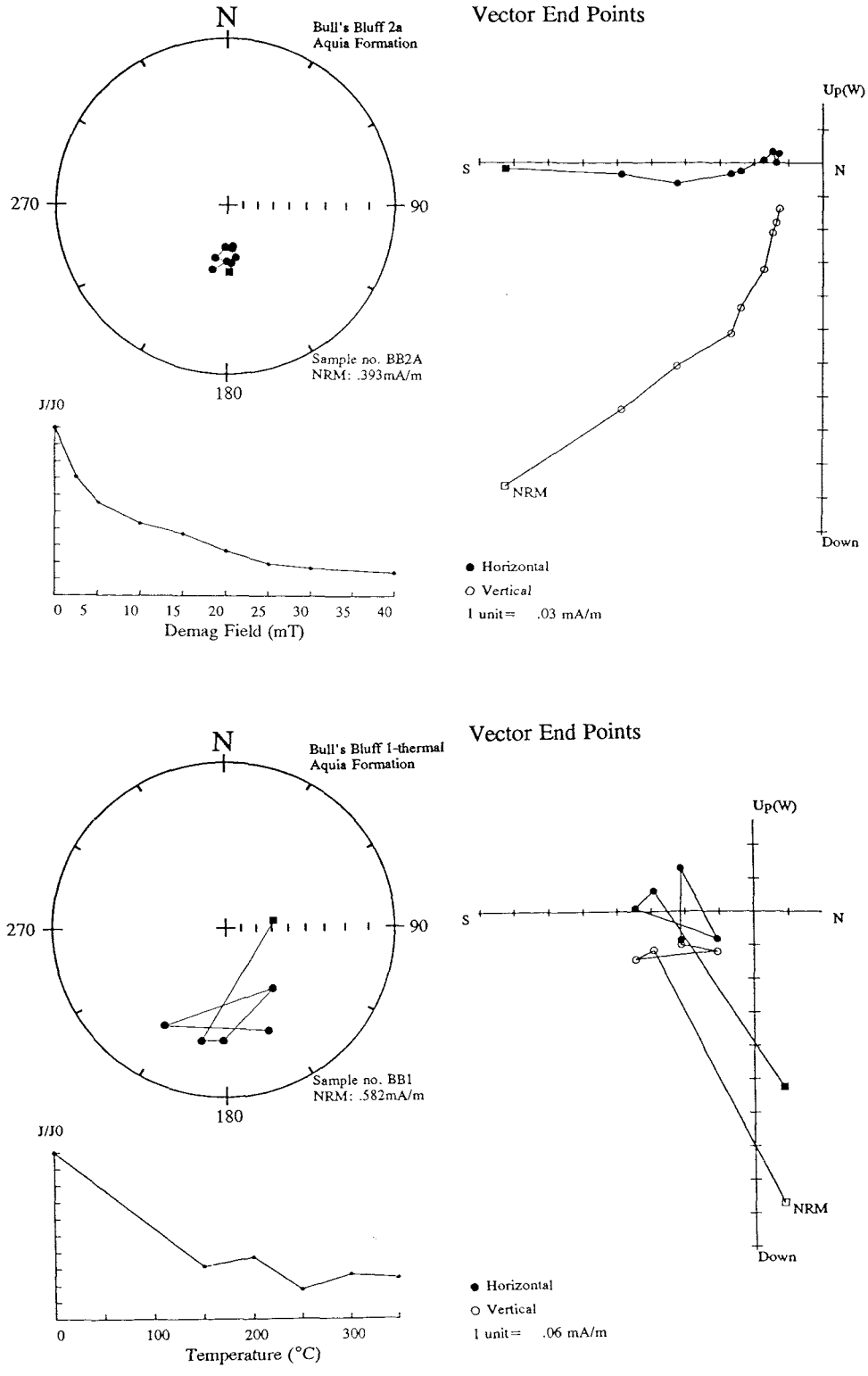

Figure 6-33 *Examples of the demagnetisation behaviour at Bull's Bluff.*

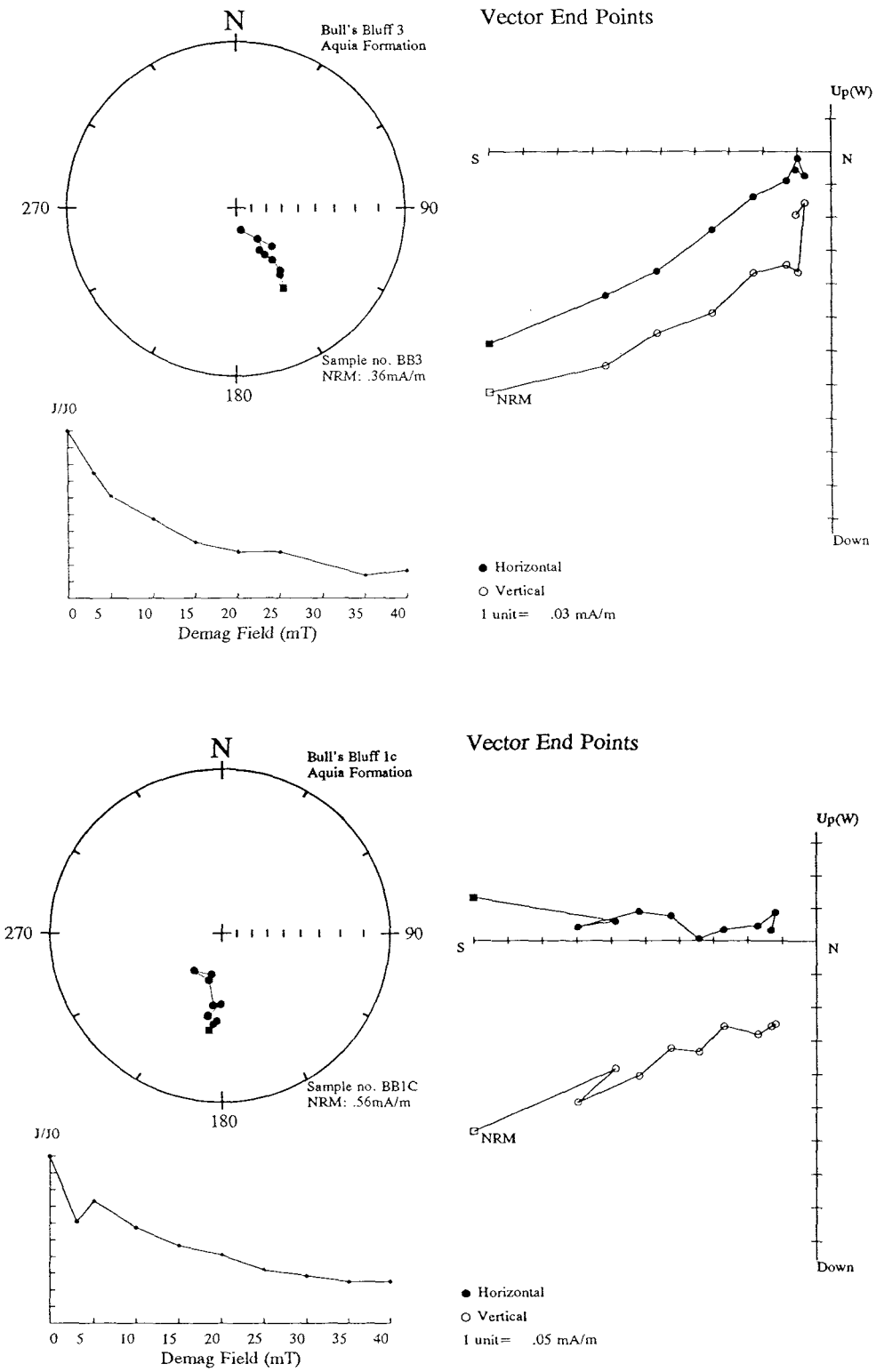

Figure 6-33 - continued *Examples of the demagnetisation behaviour at Bull's Bluff.*

Magnetostratigraphy of Bull's Bluff section

If lower NP9 is present at Bull's Bluff, the interval sampled at the nannofossil junction between NP8 and NP9 should contain C25n. Intervals of what is assumed to be the same age material at Tinker's Ravine and in the Aquia Formation of the Oak Grove Core exhibit a normal polarity which is considered to be C25n. The consistency of data, good NRM intensities and a magnetic fraction that is thought to be dominantly magnetite, lead to the possibility that the original blocks removed from the outcrop had an orientation error of 180°.

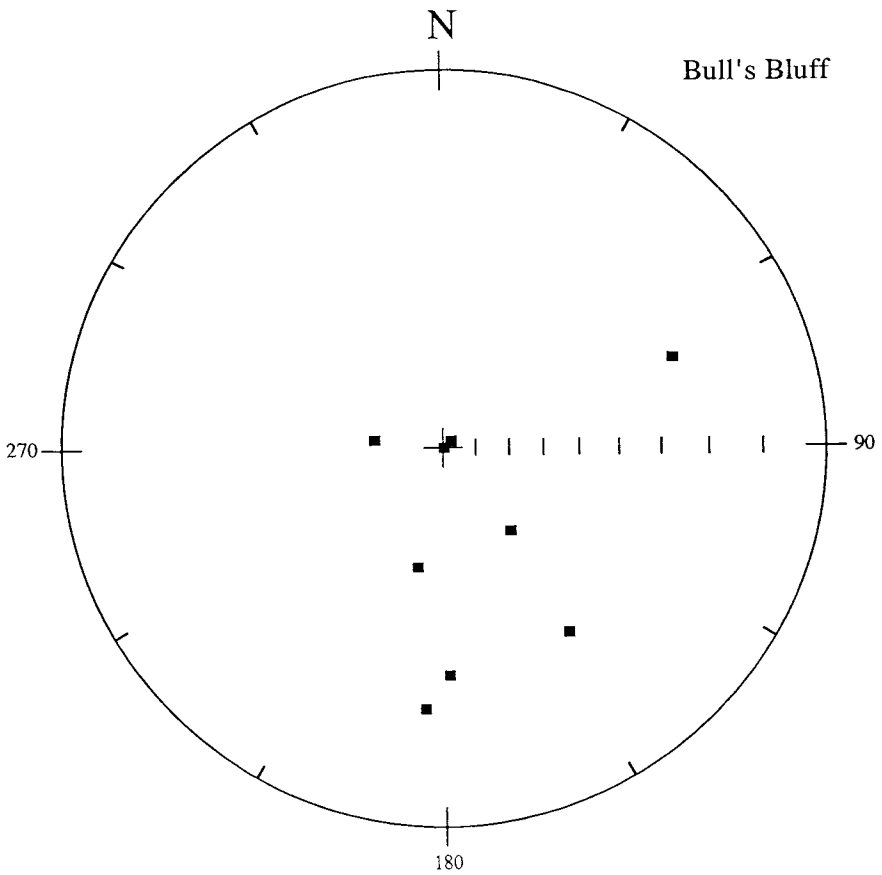

Figure 6-34 *Stereographic projection plot of SEP data from Bull's Bluff.*

6.3.5 Fairview Beach locality

Situated on the south bank of the Potomac River, 2.1km downriver from the Fairview Beach Wharf, King George County, Virginia. King George 7.5 minute quadrangle. Stop 5 (Gibson,1991).

Pleistocene conglomerates unconformably overlie the Nanjemoy Formation at this location. The Nanjemoy exposes as a fine grained silty sand with scattered shells and shell fragments; calcareous boulders occur at a height of 0.5m from the beach, above which the lithologies become weathered with only trace fossils evident. The Pleistocene contact lies at approximately 5m.

Polarity analysis

Three sample sites were taken during preliminary investigations (1991); one at 0.2m above the beach, one at 0.3m beneath beach level and a further site was dug to 1m below the beach. Samples were taken in $15cm^3$ plastic sample holders and A.F demagnetised to 35mT. The Fairview Beach section however, was not accessible during a subsequent field trip and therefore polarity determination is based on these initial samples (Fig. 6-35).

The demagnetisation behaviour of the samples produce spurious trends in which there is a clear movement towards a reverse polarity however the sense of the trend is wrong since it should take the shortest route along the great circle to the end-point.

A nannofossil NP10 zonation has been determined for this section which would place the samples within Chron C24r. The short interval sampled here at Fairview Beach corresponds to the material within the Nanjemoy Formation of the Oak Grove core which exhibited several anomalous normal polarity samples. Unfortunately the quality of palaeomagnetic data here is such that a confident polarity determination cannot be made for this section.

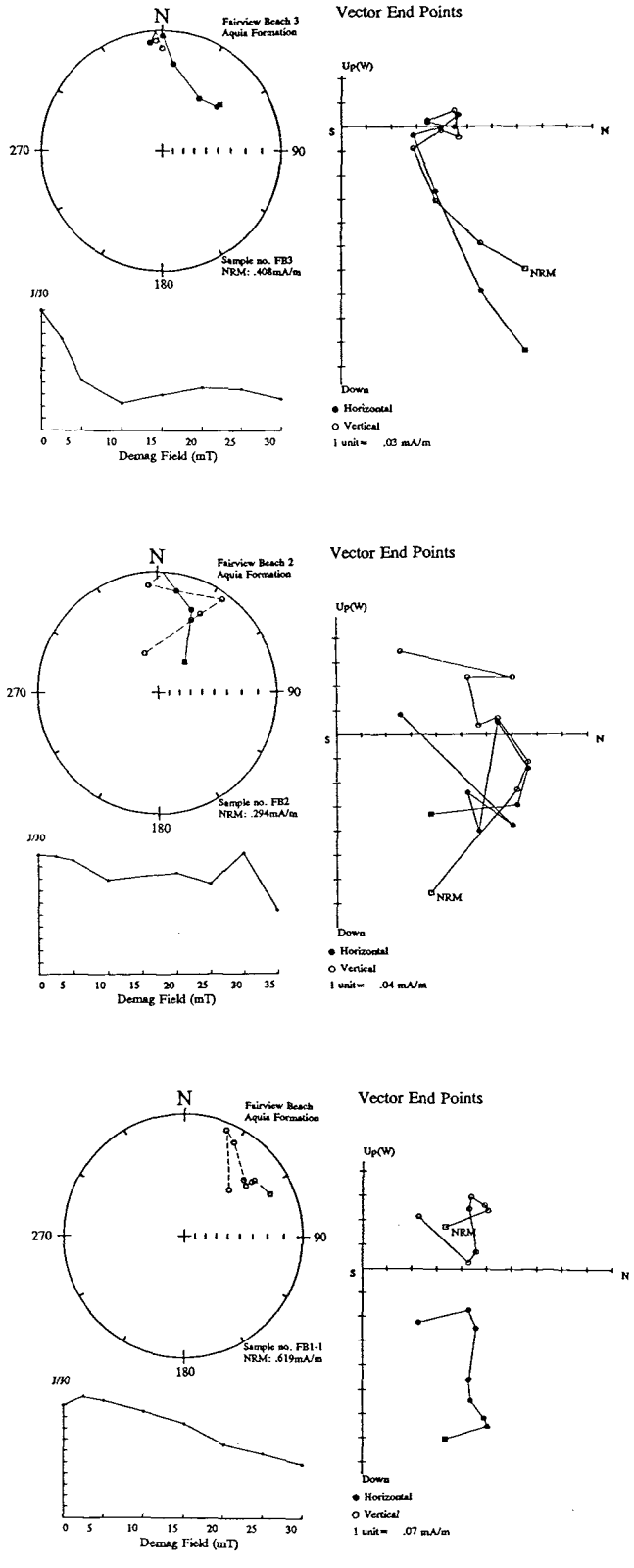

Figure 6-35 *Demagnetisation plots for the 3 sites at Fairview Beach.*

6.3.6 Aquia Creek locality

Located on the SW bank of the Potomac River, 2km SE of Youbedamn Landing at the mouth of Aquia Creek, Stafford County, Virginia. Passapatanzy 7.5 minute quadrangle.

This is the type locality of the Aquia Formation. Approximately 3m of fresh glauconitic sand with abundant mollusc and oyster debris corresponding to nannofossil zone NP6, outcrop above beach level. A consolidated sand at 3m limits the extent of fresh outcrop; above this bed the section is severely weathered and mostly unexposed.

The abundance of shell material limited palaeomagnetic sampling. Samples from this location produced spurious and erratic demagnetisation plots from which no confident polarity determination was possible.

6.9 Summary of the magnetostratigraphy determined for the Oak Grove core and outcrop sections along the Potomac River.

The shallow dipping Tertiary strata and the low lying topography of the region, limit the extent of outcrop exposures on the U.S. Atlantic Seaboard. The lithologies are largely unconsolidated and coarse-grained sediments which are difficult to sample and transport and whose nature also leaves them particularly vulnerable to remagnetisation. The magnetic instability and weak magnetic intensities observed in many of the samples is emphasised by the lack of stable end point demagnetisation behaviour and the common occurrence of noisy erratic characteristics.

Approximately 15% of samples exhibited mixed polarity determinations for subsamples from the same site, erratic orientation of declination and inclination or stable positive inclination values with southerly declinations that could not be satisfactorily explained. Confidence that many of the remaining samples preserve a genuine primary magnetic component has been increased by polarity consistency between subsamples, agreement between results from both thermal and A.F.demagnetisation procedures and correlation with other sections of the same age and the GPTS. Figure 6-36 illustrates the general agreement between the GPTS, the Oak Grove core and the six outcrop sections. Within the interval of time defined by the biostratigraphy, each of the normal polarity chrons of the GPTS has been recognised in the sediments sampled. The reliability of these correlations are gauged by the quality and quantity of specimens defining each zone. The reliability of each of the magnetozones identified in this study is critically summarised below:

Chron C26n

Defined by 2 sites and 4 sub-samples from the Oak Grove core. All specimens consistently show high quality SEPs but with low inclination and without declination control (Fig. 6-10).

Chron C25n - defined by 3 independent sources:

Core material 3 sites and 5 sub-samples exhibiting good quality SEPs but with

low inclination and without declination control (Fig. 6-10).

Tinker's Ravine — 5 sites and 11 sub-samples have normal polarity SEPs at this location (Fig. 6-28).

Bull's Bluff — 7 sites and 14 sub-samples predominantly show high quality SEPs but with a southerly declination (Fig. 6-33). An orientation error is suspected.

There has been some debate about the existence of sediments of lower NP9 age in this region; however the recognition of Chron C25n within the NP9 interval here confirms that at least some material of this age is present.

Chron C24n

Defined by 9 sites and 15 sub-samples from the Oak Grove core which yield reliable trends and SEPs but have no declination control. Evidence of sub-Chron C24n.2. (Fig. 6-10).

Chron C23n

Defined by 7 sites and 19 sub-samples primarily showing good quality SEPs and trends to a normal polarity (Figs. 6-13 and 6-14). Some questions remain on the exact positioning of Pope's Creek in the nannofossil zones NP12/NP13.

The Oak Grove core and all outcrop sections that have been sampled (excluding Pope's Creek) have reliable biostratigraphic control.

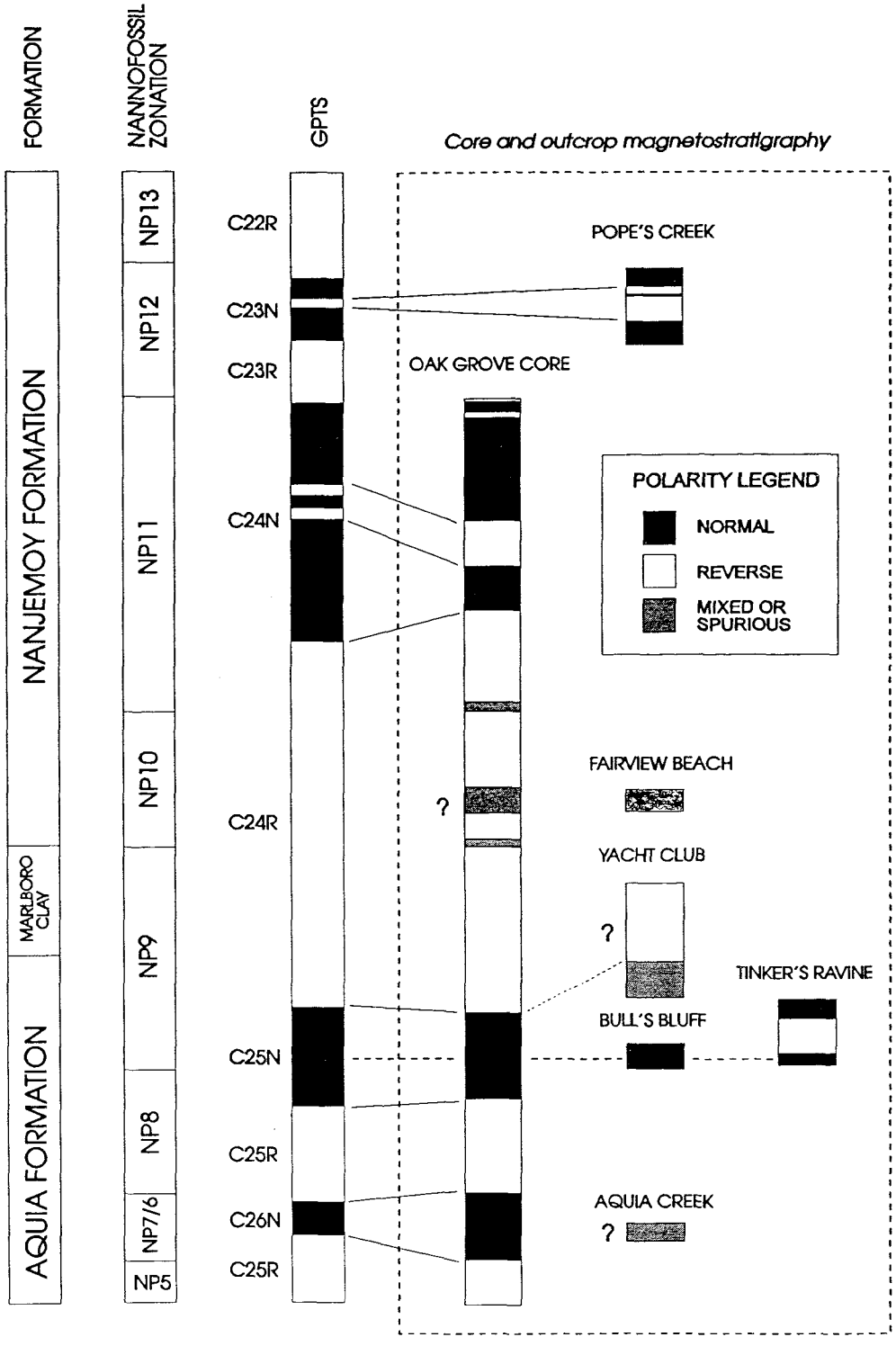

Figure 6-36 *Summary of the Virginia and Maryland Magnetostratigraphy.*

SECTION C

Magnetostratigraphy of sediments from the US Gulf Coastal Plain

Chapter 7 Early Tertiary deposits of the U.S. Gulf Coast (Alabama)

7.1 Regional setting

The Paleogene strata of the eastern Gulf Coastal Plain generally dip seaward, reflecting the infilling of the subsiding depositional basin on the passive southern margin of the North American Continent.

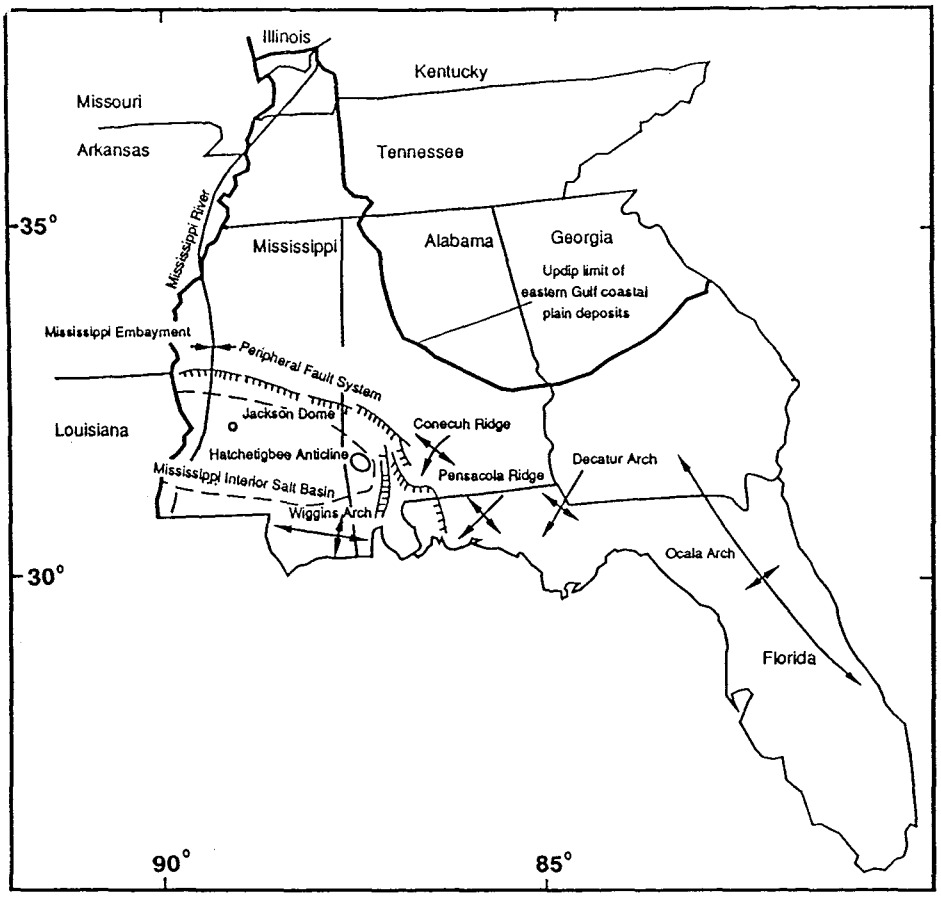

Figure 7-1 *Map of the eastern Gulf Coastal Plain area illustrating major structural features (from: Mancini and Tew, 1991).*

West to east across the eastern Gulf states the general depositional conditions of the strata alter from deltaic and marginal marine in Mississippi to a carbonate dominated

facies in eastern Alabama, Georgia and Florida. These lithologies intertongue across south-western Alabama with a regional dip of strata of less than 7m/km or $<0.5°$ (Toulmin, 1977).

Structural development of south western Alabama was controlled by movement of the Jurassic Louann Salt at depth (Mancini and Tew, 1991). Displacements of up to 15m in Eocene strata along the regional peripheral fault trend have taken place, together with uplift of Eocene and Oligocene strata around the Hatchetigbee anticline, a major salt dome feature (Fig. 7-1).

The Paleogene of the eastern Gulf Coastal Plain consists of about 762m of non-marine, marginal marine and marine clastic and carbonate sediments (Mancini and Tew, 1991). The general lithologies across Alabama, however, are similar although a considerable increase in thickness of most of the units occurs from east to west across the state (much of which is probably associated with deltaic deposition and probably deeper water deposits in some of the depositional cycles in western Alabama).

7.2 Paleogene stratigraphy of Alabama

Figure 7-2 illustrates the Paleocene and Eocene stratigraphy of Alabama. The formation equivalents in the Maryland and Virginia area of the Atlantic Coast are shown in figure 5-3. The late Paleocene and early Eocene exposures sampled during fieldwork extend from nannofossil zone NP6 at the base of the Wilcox Group to NP14, possibly NP15 within the Claiborne Group.

The Wilcox Group consists of the Nanafalia, Tuscahoma, Bashi and Hatchetigbee Formations and the lower Claiborne Group consists of the Tallahatta. This interval from Nanafalia to top of the Tallahatta Formation is bounded above by the Lisbon Formation and below by the Porter Creek and Clayton Formations of the Midway Group.

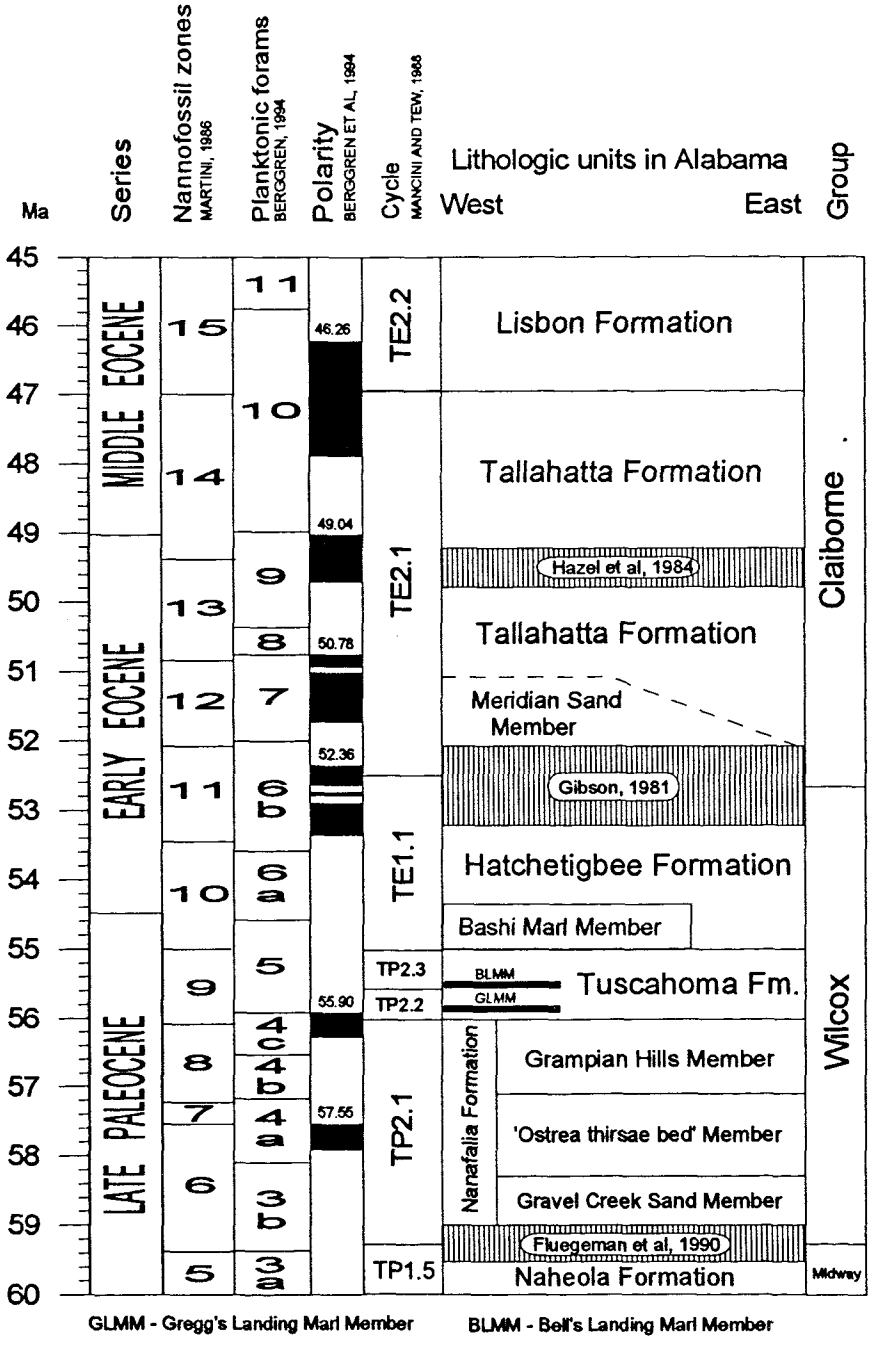

Figure 7-2 *Chronostratigraphic framework for the late Paleocene to middle Eocene strata of Alabama (adapted from Mancini, 1991).*

7.2.1 Nanafalia Formation

The Nanafalia Formation was named by Smith (1983) after exposures at Nanafalia Landing on the Tombigbee River. It is up to 70m thick in SW Alabama and is divided into 3 members: the Lower Gravel Creek sand member, "*Ostrea thirsae* beds" and the Grampian Hills member which can be traced across the state, although facies changes occur up and down dip. At the type locality along Gravel Creek, Wilcox County the Lower Gravel Creek sand member is a white to yellow, cross-bedded, medium to coarse grained sand with abundant mica. It is a non-marine sand which thickens progressively northward until it makes up the entire Nanafalia Formation (Siesser, 1983). The middle member, the *Ostrea thirsae* beds, are fossiliferous, usually massively bedded, glauconitic sand and silts. The characteristic Nanafalia macrofossil *Odontogryphaea thirsae* is abundant within this member. These beds thin from a maximum thickness of 20m in western Alabama to about 7m on the Alabama/Georgia border (Toulmin, 1977). The overlying Grampian Hills member consists of glauconitic sand and clay which are thickest in central Alabama (up to 35m) but which thins to the east to about 9m and to the west to 6m. Both the *Ostrea thirsae* beds and the Grampian Hills Member pinch out to the north (Cushing et al, 1964).

The Nanafalia Formation overlies the Clayton Formation with marked disconformity in eastern Alabama and is also disconformable where it rests on the Naheola elsewhere in Alabama (Toulmin, 1977). Gibson et al (1982) estimated the time represented by the hiatus in western Alabama as equivalent to NP6. However, Mancini (1984) suggests that the hiatus may lie within the *Morozovella pusilla* Interval Zone which indicates a shorter interval of time than that proposed by Gibson (1982). In eastern Alabama and western Georgia a more pronounced hiatus in the Paleocene section is apparent where it is calculated as being up to 3.4 m.y. (Fluegeman et al, 1990). Various biostratigraphic workers (for example: Bybell, 1980; Gibson et al, 1982; Mancini, 1981 and Seisser, 1983) have judged the Nanafalia Formation to range from nannoplankton zones NP6-NP9 where the Ostrea thirsae beds have been assigned to NP7 and NP8 and the Grampian Hills to NP8 and NP9 zones. No calcareous microfossils have been reported from the Gravel Creek Sand Member (Mancini and Tew, 1991).

The Salt Moutain limestone outcrops as a hard coral bearing recrystallized limestone near

Jackson. The exposures are about 30m thick (Fisher, 1961) but the lateral extent is limited due to the contol of the Jackson Fault. Toulmin (1940) considered the Salt Mountain limestone to be an offshore facies correlative to the *O. thirsae* beds of the Nanafalia. Twenty two species of calcareous nannoplankton described by Wind (1974) confirm this by assigning the limestone to the *Discoaster gemmeus* zone of Hay et al (1967) which is equivalent to NP7.

7.2.2 Tuscahoma Formation

The Tuscahoma Formation is the thickest formation in the Wilcox Group, reaching about 160m in the OSM No.2 Wahalak corehole in Choctaw County (Mancini, 1981) although it thins to 46m in southeastern Alabama (Toulmin and LaMoreaux, 1963). The Tuscahoma conformably overlies the Nanafalia Formation and typically consists of a thick sequence of interbedded very fine grained sand, silt and clay, often abundant in shells and glauconite with prominent incursions of marine marl units in an otherwise largely non-marine interval.

Two of these marl beds have been formally identified in western Alabama: the Greggs Landing Marl member is a fossiliferous calcareous, glauconitic fine grained sand and marl of about 1.8m thickness, occurring near the middle of the formation (LaMoreaux and Toulmin, 1959) and the Bells Landing Marl member reaches 2.7m, higher up. The Greggs Landing and Bells Landing Marl members have been assigned to planktonic foraminiferal zone P5 which lies within nannofossil zone NP9 (Mancini, 1984). The Marls contain a diversified fauna dominated by *Ostrea*, *Venericardia* and *Turritella* (Toulmin, 1977). Two other unnamed marls below the Bells Landing Marl have been observed in several sections. Lignite seams are commonly found in the upper part of the formation in western Alabama; these lignite beds are probably characteristic of more updip areas (Gibson et al, 1982) since a downdip corehole near Monroeville did not encounter lignite seams (Gibson, unpublished data).

The Tuscahoma Formation extends from Georgia across Alabama into Mississippi but the Greggs and Bells Landing Marl Members are distinguishable only in western Alabama (Fig. 7-2).

7.2.3 Bashi Marl Member and Hatchetigbee Formation

The Hatchetigbee Formation conformably overlies the Tuscahoma Sands and is about 75m thick throughout SW Alabama. It was divided into the lower Bashi Marl Member and an upper 'unnamed' member by Toulmin et al (1951) although Gibson (1982) considers the Bashi as an independant formation which is a time equivalent of the Hatchetigbee.

The Hatchetigbee Formation is characterised by several lithologies including massively bedded, well-sorted, very fine grained quartz sand; cross bedded fine sand; and interlaminated sequences of very fine sand, silt and clay with carbonaceous debris (Gibson et al, 1982). In general, the cross bedded sands are dominant in the east of the state and interlaminated sequences more common in the west. Samples of both Bashi and Hatchetigbee lithologies investigated (for example; Bybell, 1980; Gibson, 1982; Mancini, 1981 and Siesser, 1983) contain calcareous nannofossils of earliest Eocene age representing zones NP9/NP10; NP11 is not reported as being present which indicates a significant hiatus at the top of the Hatchetigbee (Gibson, 1981).

Shelly glauconitic sand and clayey silt of the Bashi Marl Member in the more southward or downdip regions interfingers with the Hatchetigbee Formation in the northern or updip sections. Three tongues of Bashi, representing marine incursions, are observed across the state except in updip regions of eastern Alabama where the Bashi disappears and Hatchetigbee lithologies dominate (Gibson, 1982).

7.2.4 Tallahatta Formation

In Alabama, the siliceous claystones and siltstones of the Tallahatta Formation are commonly seen as prominent strata which form steep rugged outcrops. In the earlier literature (for example, Smith et al, 1894) these siliceous sediments were called buhrstones because of their hardness and resistence to erosion. Beneath the buhrstone, the Meridian Sand Member of the Tallahatta Formation exists. This unit is extensive in Alabama and Mississippi and normally consists of pale-coloured, cross bedded fine to coarse-grained sand which commonly contains quartz granules and clay clasts (Bybell and Gibson, 1985). The Meridian Sand Member is a clear marker in outcrop, reaching

a maximum thickness of approximately 70m (Childress, 1973) in western Alabama but which pinches out eastwards and is either absent in some outcrops or observed as infill within undulating channels cut into the top of the Hatchetigbee Formation (Bybell and Gibson, 1985).

The basal Tallahatta beds in eastern Alabama are considered the lateral time equivalent of the Meridian Sand Member in western Alabama (Fig. 7-2). Siliceous beds are also thinner in the east with more of the sections composed of quartzose sand and glauconite where further west siliceous clay and siltstone dominate the lower and middle part of the Tallahatta Formation with shelly glauconitic sand becoming more common towards the top. The overall Tallahatta Formation diminishes in thickness from 43m-61m near Little Stave Creek (Toulmin, 1944) to 34m at Columbia on the Chattahoochee River (Bybell and Gibson, 1985).

A prominent erosional surface is present between the Hatchetigbee and the basal Meridian Sand Member of the Tallahatta (Gibson, 1980). This hiatus had a duration which was initially calculated by Gibson as being about 2.6 m.y. However, subsequent investigations of the formation boundaries over a wide area in Alabama have since updated this value to approximately 1 m.y. (Bybell and Gibson, 1985).

Extensive biostratigraphic investigations of 8 outcrop sections and 5 coreholes by Bybell and Gibson have revealed that nannofossil zones NP12, NP13 and NP14 are present in the formation although intervals barren of calcareous nannofossils are frequently present in sections across the state. NP15 may also be present at the very top of the Little Stave Creek section.

Several erosional surfaces are observed within the Tallahatta Formation, some of which correspond to calcareous nannofossil boundaries. In addition to the considerable hiatus at the base of the formation for instance, an erosional surface has been noted by Bybell and Gibson (1985) at the NP12/NP13 zonal contact and a further significant break in sedimentation has been proposed as being present at the NP13/NP14 boundary by Hazel et al (1984) - a hiatus of 1.4 m.y. being postulated although the extent of this is questionable.

7.3 Sequence stratigraphy

Cyclic global changes in eustatic sea level and coastal onlap (progressive landward encroachment of coastal deposits) have been recognised in the Gulf Coast area by Baum (1986). Baum reported 19 global unconformities, which he used to subdivide the Paleogene of Alabama into 18 depositional sequences. The sequence stratigraphy below is based on the scheme of Baum (1986) but modified by Mancini and Tew (1991).

The following sequence desciptions are taken from Mancini and Tew (1991) and refer to figure 7-3:

The TP2.1 sequence consists of a basal Type 1 unconformity, lowstand incised valley fill deposits (Gravel Creek marine barrier to marginal marine, cross-bedded, fine- to medium-grained sands), transgressive and condensed section deposits ('Ostrea thirsae' marine shelf marls and glauconitic sands), and highstand regressive deposits (Grampian Hills and lower Tuscahoma marine and marginal marine silts, clays and marls). The incised valley fill deposits have a discontinuous distribution throughout southwestern Alabama and where present, the strata are of variable thickness up to 12.2m thick in Choctaw County and up to 15.2m thick in Wilcox County.

The TP2.2 sequence includes a basal Type 1 unconformity, lowstand deposits (Tuscahoma marine-shelf to marginal marine cross-bedded fine- to medium-grained sands), transgressive and condensed section deposits (Gregg's Landing marine-shelf marls and glauconitic sands) and highstand regressive deposits (middle Tuscahoma marine and marginal marine sands, silts and clays). The lowstand shelf deposits have a discontinuous distribution throughout southwestern Alabama.

The TP2.3 sequence consists of a basal Type 2 unconformity, transgressive and condensed section deposits (Bell's Landing marine-shelf marls and glauconitic sands), and highstand regressive deposits (upper Tuscahoma marginal marine sands, silts, clays and lignite beds). The TP2.3 sequence has an upper Type 1 unconformity (Baum, 1986).

The TE1.1 sequence includes the basal Type 1 unconformity, transgressive and condensed section deposits (Bashi marine-shelf marls and glauconitic sands), and highstand regressive deposits (Hatchetigbee marginal marine sands, silts and clays).

The TE2.1 sequence consists of a basal Type 1 unconformity, lowstand shelf deposits (Meridian marine-shelf fine- to medium-grained sands), transgressive deposits (Basic City marine-shelf marls and glauconitic sands), condensed section deposits (Basic City marine-shelf clays and silts), and highstand regressive deposits (Basic City marine and marginal marine clays and Neshoba marine and marginal marine sands). This sequence is represented by the Tallahatta Formation in southwestern Alabama.

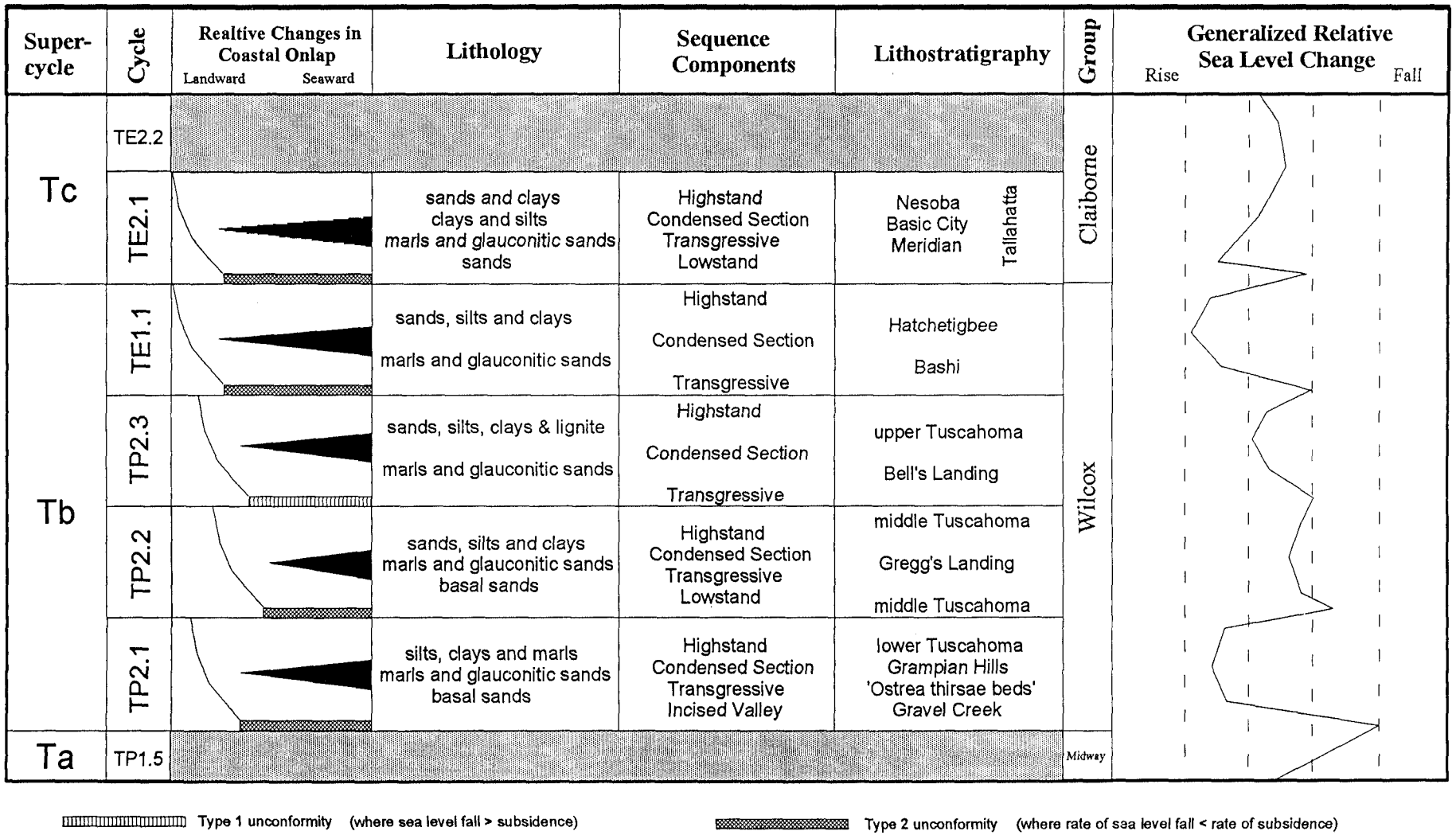

Figure 7-3 *Sequence stratigraphy of late Paleocene and early Eocene strata in southwestern and south-central Alabama (from: Mancini and Tew, 1991).*

7.4 Sampling Coverage

Eighteen outcrop sections and one core were sampled during field work in May and June, 1992. The location of the outcrops are shown in figures 7-4 and 7-5. In addition, previous work by the palaeomagnetic group at Southampton University identified tentative magnetozones at some localities and where possible useful information from this study was integrated into the present study.

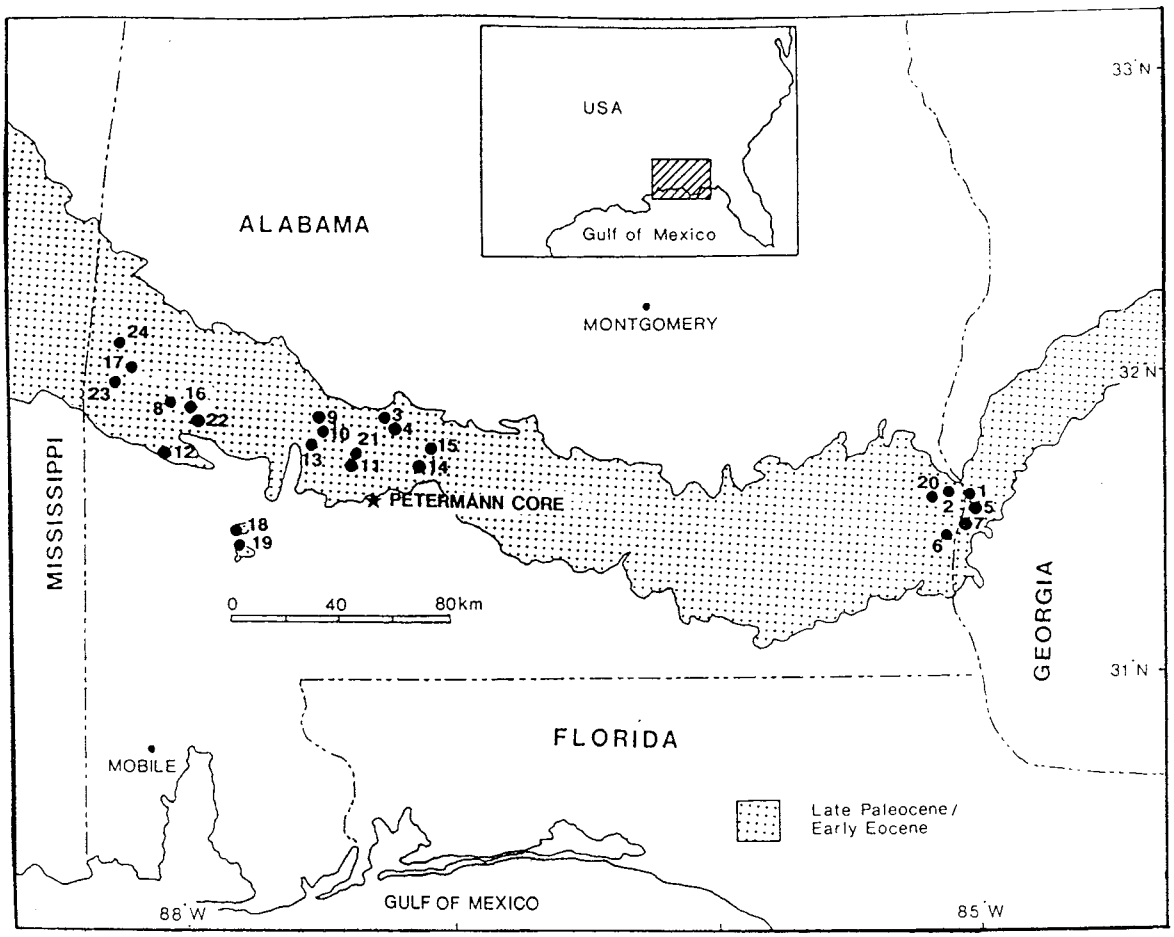

Figure 7-4 *Location of field sections visited in Alabama. Locality names are listed in table 7-1 along side the corresponding reference number.*

Lithologies were generally more finer grained than corresponding Atlantic Coastal sediments and therefore field sampling and the transportation of material was considerably easier.

Alabama 6/1992

Section	Ref. no,	Section Code	Formation
Fort Gaines *	1	FG	Nanafalia
McCrea Creek *	2	MC	Nanafalia
Camden *	3	CD	Nanafalia
CD Radio Station	4	CR	Nanafalia
Roaring Creek	5	RC	Tuscahoma
Bennett's Creek *	6	BK	Tuscahoma
Kolomokei Creek	7	KC	Tuscahoma
Tuscahoma Lg	8	TL	Tuscahoma
Bear Creek	9	BR	Tuscahoma
Peach Tree *	10	LP	Tuscahoma
Bell's Crossing	11	BX	Hatchetigbee
Hatch. Bluff	12	HB	Hatchetigbee
Lower Peach Tree *	13	PT	Hatchetigbee
Tunnel Springs	14	TS	Hatch / Talla
Midway *	15	MW	Hatch / Talla
Cambell (HW69) *	16	CA	Hatch / Talla
Butler *	17	BU	Hatch / Talla
Little Stave Creek *	18	LS	Tallahatta

* sampled 1990 & 92

Additional Sites 4/90

Salt Mountain	19	SC	Nanafalia
Mathieson Mine	20	MM	Tuscahoma
Bell's Landing	21	BL	Tuscahoma
Bashi Creek	22	BC	Bashi
Hobson's Studio	23	XZ	Hatchetigbee
Scott's Peak	24	SM	Hatchetigbee

Table 7-1 *Locality names, section codes and formations exposed at outcrops in Alabama. Reference numbers refer to figure 7-4.*

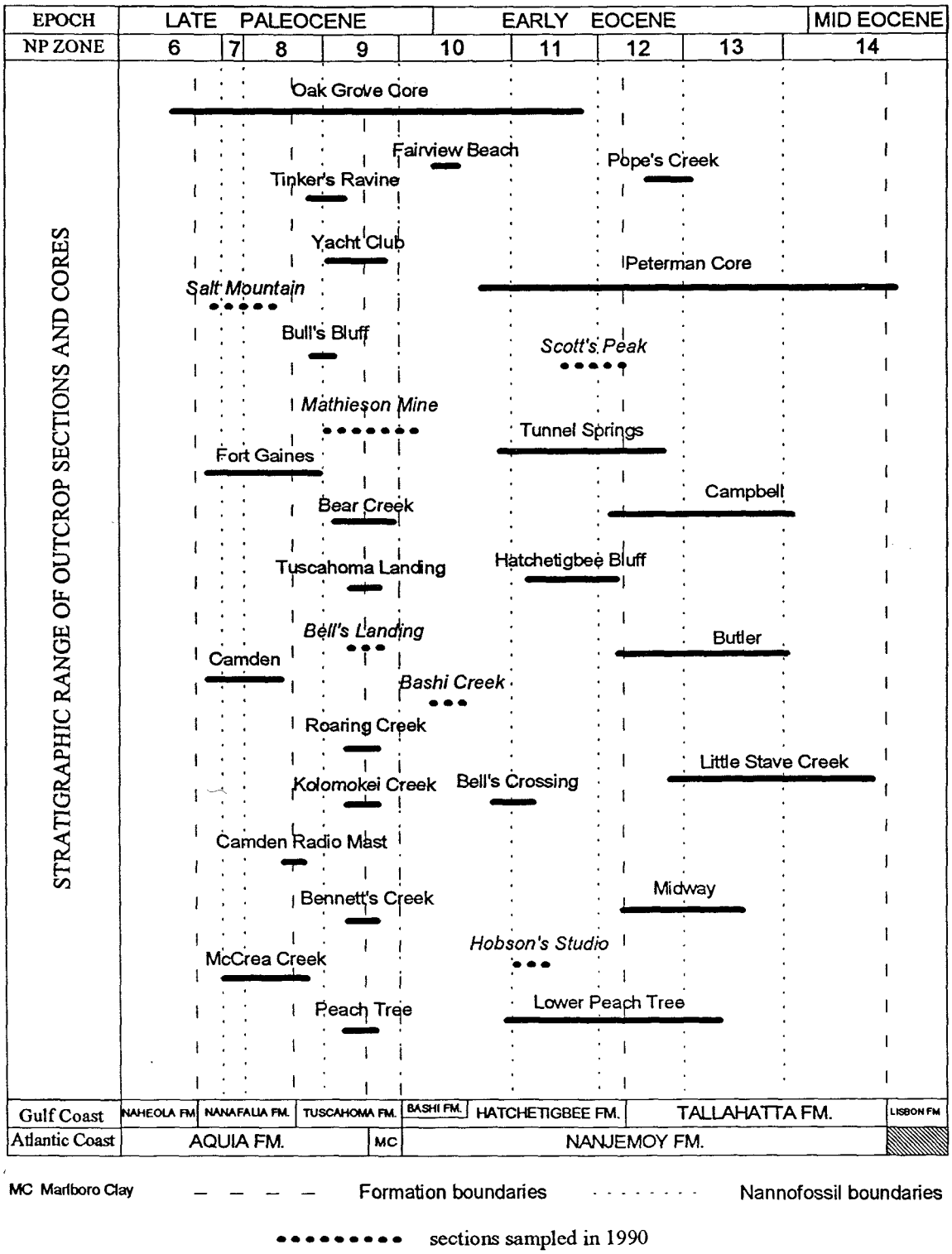

Figure 7-5 *Approximate stratigraphic range of field sections and cores sampled from the Gulf and Atlantic Coasts.*

Chapter 8 Magnetostratigraphy of late Paleocene outcrops in Alabama

8.1 Nanafalia outcrops

8.1.1 Fort Gaines locality

Location: Across river from Franklin Landing, immediately south of Highway 10 bridge to Fort Gaines, Clay County, Georgia.

The Fort Gaines Paleocene section is exposed along the banks of the Chattahoochee River, close to the Georgia/Alabama state boundary (Fig. 7-4). The burrowed contact at the base of the Nanafalia Formation and the fossiliferous limestone of the Clayton Formation is clearly visible at the bottom of this section where sand of the thin Gravel Creek Sand Member fills solution pits in the limestone (Toulmin and LaMoreaux, 1963)(Plate 8-1).

The upper contact of the Nanafalia Formation is measured at approximately 10m up the section above which the weathered clay and sand of the lower Tuscahoma Formation are exposed. The section was traced laterally under the nearby bridge where sampling was continued to a height of approximately 16m (Fig. 8-1). The average dip of strata is 3m per kilometre to the south (0.2°).

The Lowermost shelly beds of the Nanafalia are dominated by *Odontogryphaea thirsae* together with lesser numbers of *Ostrea sinuosa*. Beds here are considered to represent a very shallow, inner neritic, rather than a restricted marine environment because of relatively high benthic foraminiferal diversity (17 species) and almost one percent planktonic formainifers (Reinhardt and Gibson, 1980). Higher in the section however, fluctuations to restricted-marine environments are indicated by a marked increase in clay content, a decrease in benthic foraminiferal species and a general absence of planktonic specimens.

The Fort Gaines section spans the whole of the Nanafalia Formation although the thickness is considerably less than seen in sections and cores to the west.

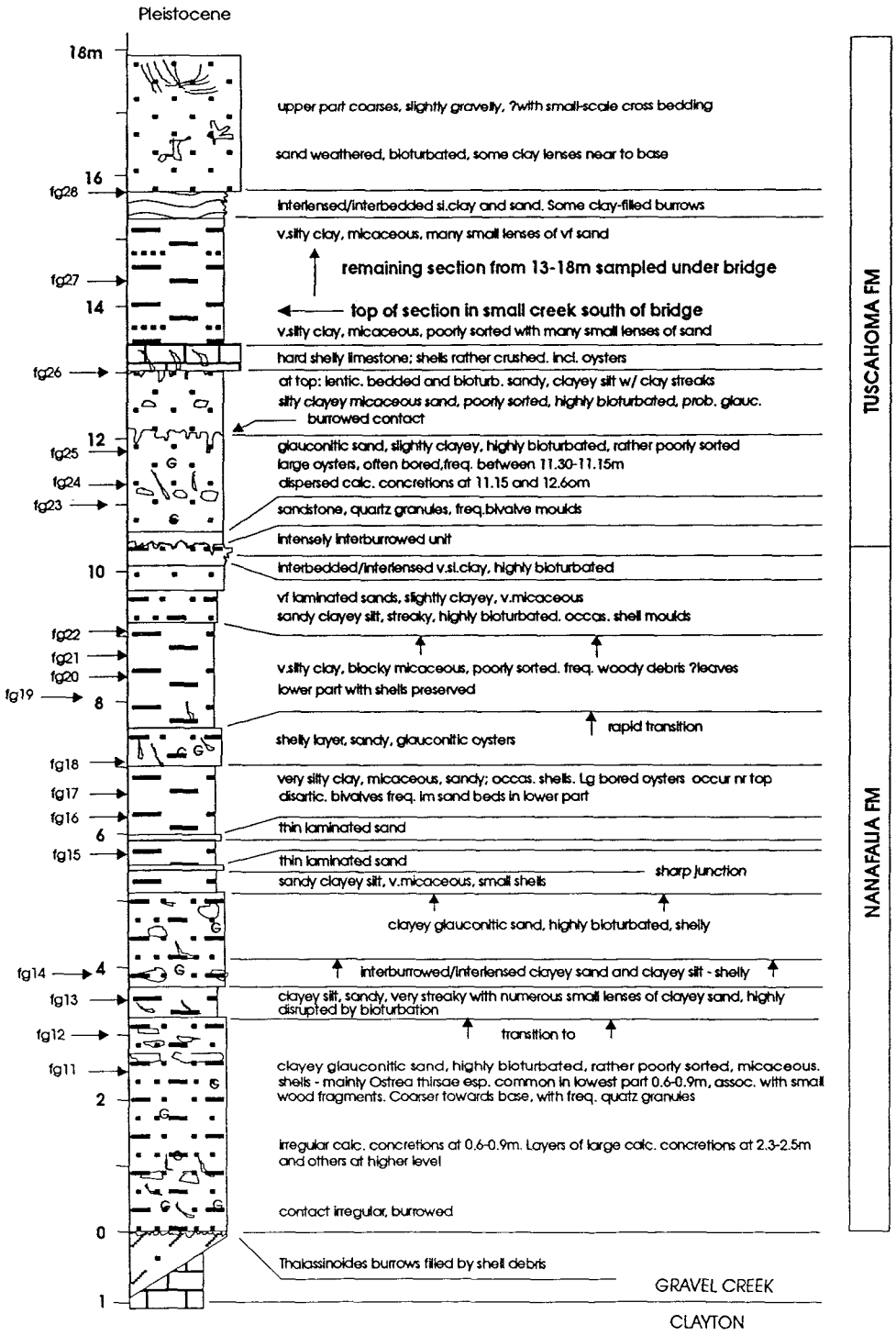

Figure 8-1 *Section log at Fort Gaines and position of sample sites.*

Sampling

Large block samples were removed from eighteen sites with an average sampling interval of approximately 1m. The blocks were subsequently split into 1-6 sub-samples and demagnetised by both thermal and A.F. methods (Appendix 6). Two samples (fg11 and fg14) were taken from calcareous nodules.

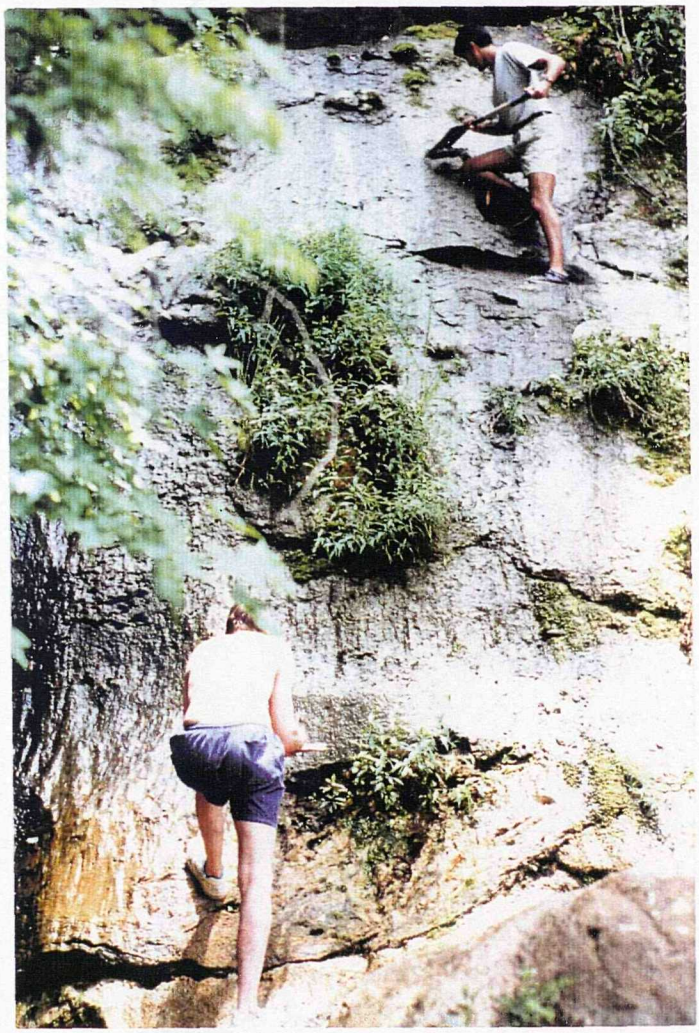

Plate 8-1 *Base of the Fort Gaines outcrop section.*

IRM investigations were carried out on 3 horizons of differing lithologies; each yielding saturation curves that were characteristic of magnetite rather than hematite (Fig. 8-2).

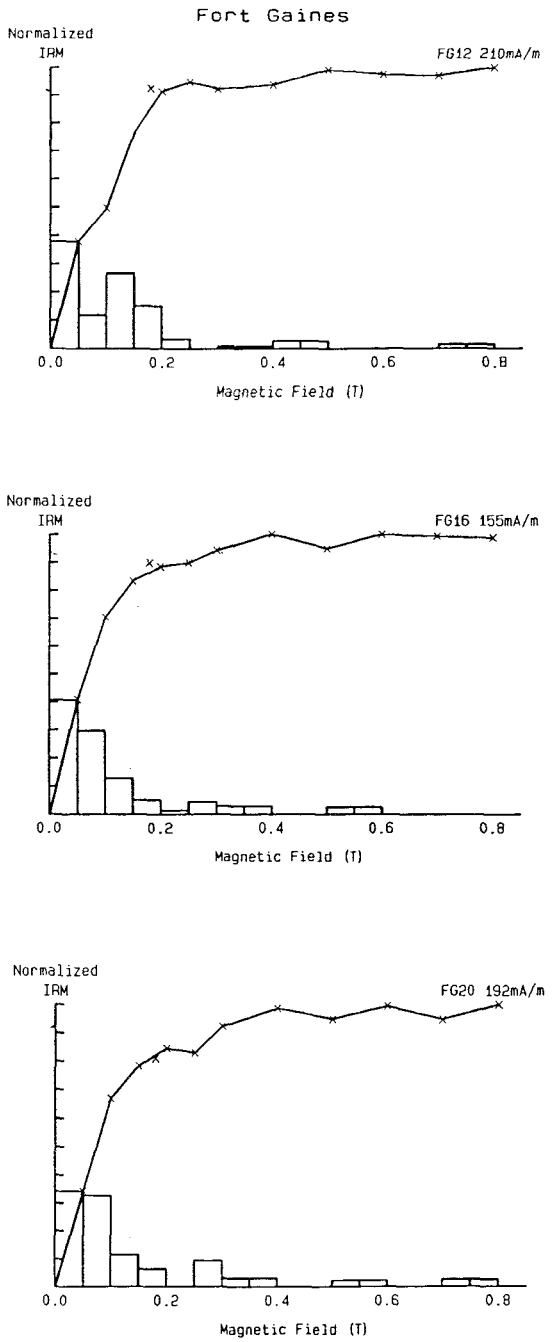

Figure 8-2 *IRM curves for sediments located at 6.3m, 7.7m and 8.7m within the measured section at Fort Gaines.*

Thermal demagnetisation was usually stopped at 350°C when the intensity of samples approached that of the sensitivity of the magnetometer. During successive temperature increments the susceptibility of most of the heated samples usually remained fairly constant to temperatures of 350°C; a small number of specimens however indicated a mineralogical phase transition at temperatures greater than 250°C (Fig.8-3).

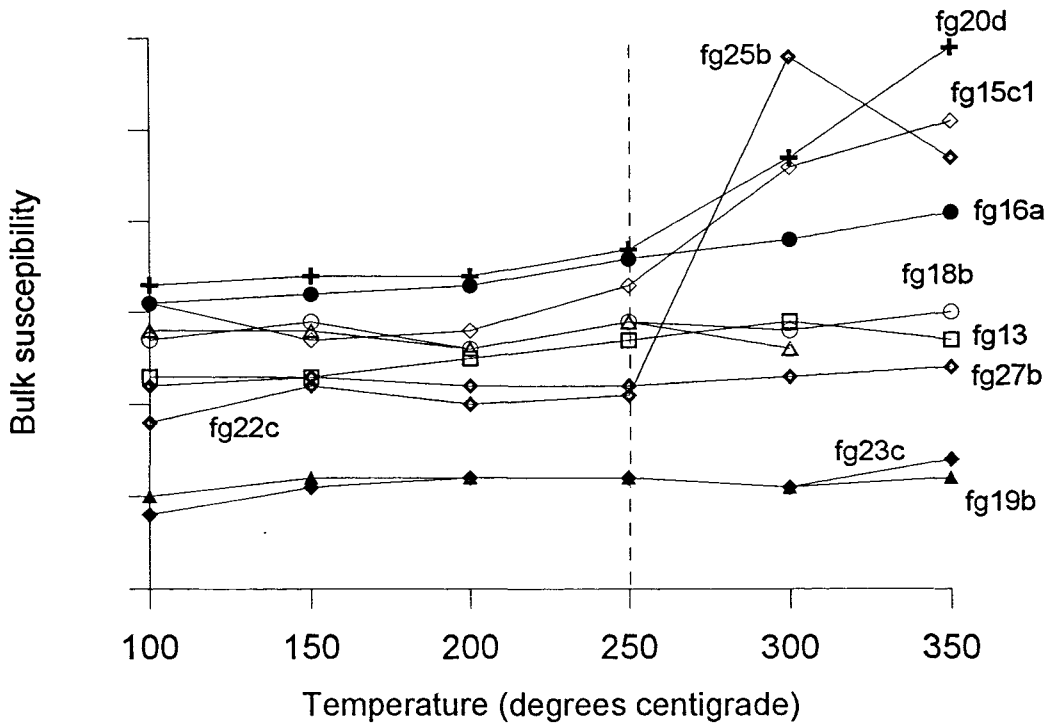

Figure 8-3 *Bulk susceptibility variations during thermal demagnetisation.*

Polarity analysis

The polarity determined for sub-samples from the same block was not always consistent and 36% of all samples yielded a demagnetisation behaviour from which no reliable polarity determination could be made. These findings were similar to previous palaeomagnetic investigations at this locality carried out in the Southampton laboratory (1990).

Figure 8-4 illustrates a polarity sequence based on the most confident trends and SEP data from each site. The position of *question marks* within the sequence highlights those horizons where some doubt still remains on the polarity assignment. Examples of some of the demagnetisation characteristics are given in figures 8-5 to 8-7.

If the uppermost (a) and lowermost (d) normal magnetozones are ignored (each defined by only one site) the remainder of the section consists of a reverse polarity interval interrupted by two well defined normal zones (b) and (c). Due to a sampling interval of 1.5-2m at the top of (b) and base of (c) the polarity boundary is not well resolved and hence the normal zones could be significantly shorter (or longer) than those indicated in figure 8-4.

Magnetostratigraphy of the Fort Gaines locality

The well-defined normal polarity intervals (b) and (c) are divided by a reverse polarity interval that spans the boundary between the Tuscahoma and the Nanafalia Formations at about 10.5m up the section. The upper normal (identified predominantly by trending data) situated within the lower part of the Tuscahoma Formation could represent sediments from Chron C25n; however the weathered condition of the Tuscahoma sands at this location significantly increase the likelihood that this may be an overprint.

The lower normal (c) observed within the Nanafalia Formation between about 5m and 8m may correlate to Chron C26n of the GPTS. Chron C26n has been attributed to the planktonic nannofossil zone of NP6 which should be present in the lower-most Nanafalia Formation at this locality. The normal polarity seen here, however, appears more extensive than expected.

In general, the palaeomagnetic data is not of sufficient reliability to confidently correlate this section with the GPTS. The completeness of the sedimentary record may have some effect on the polarity sequence recorded, however, longer periods of a reverse polarity would be expected here. The data is therefore excluded from the summary diagram of confident magnetostratigraphy from high quality intervals or sections investigated during this study.

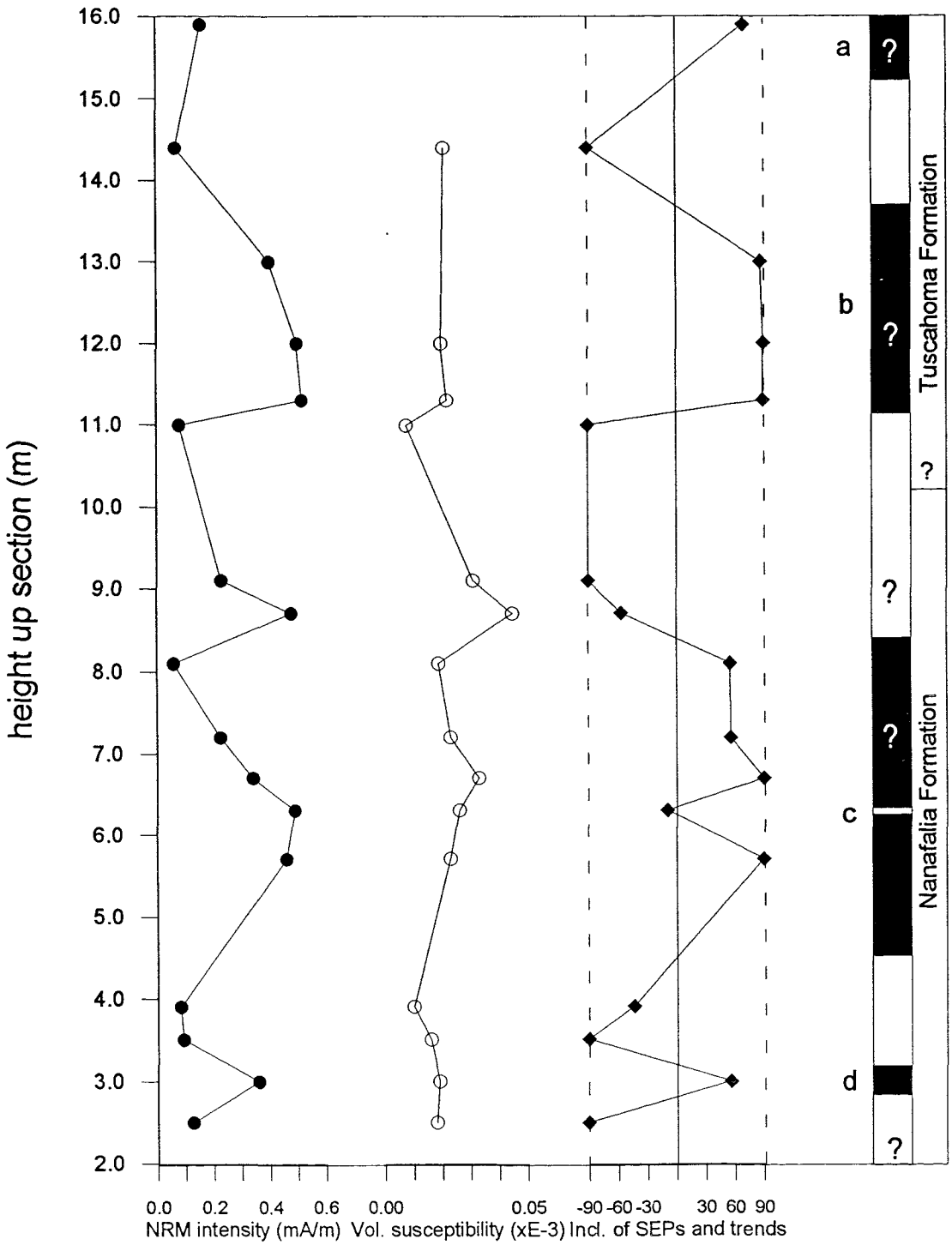

Figure 8-4 *NRM intensity, susceptibility and a polarity sequence defined by reliable inclination values plotted against the sample height in the section.*

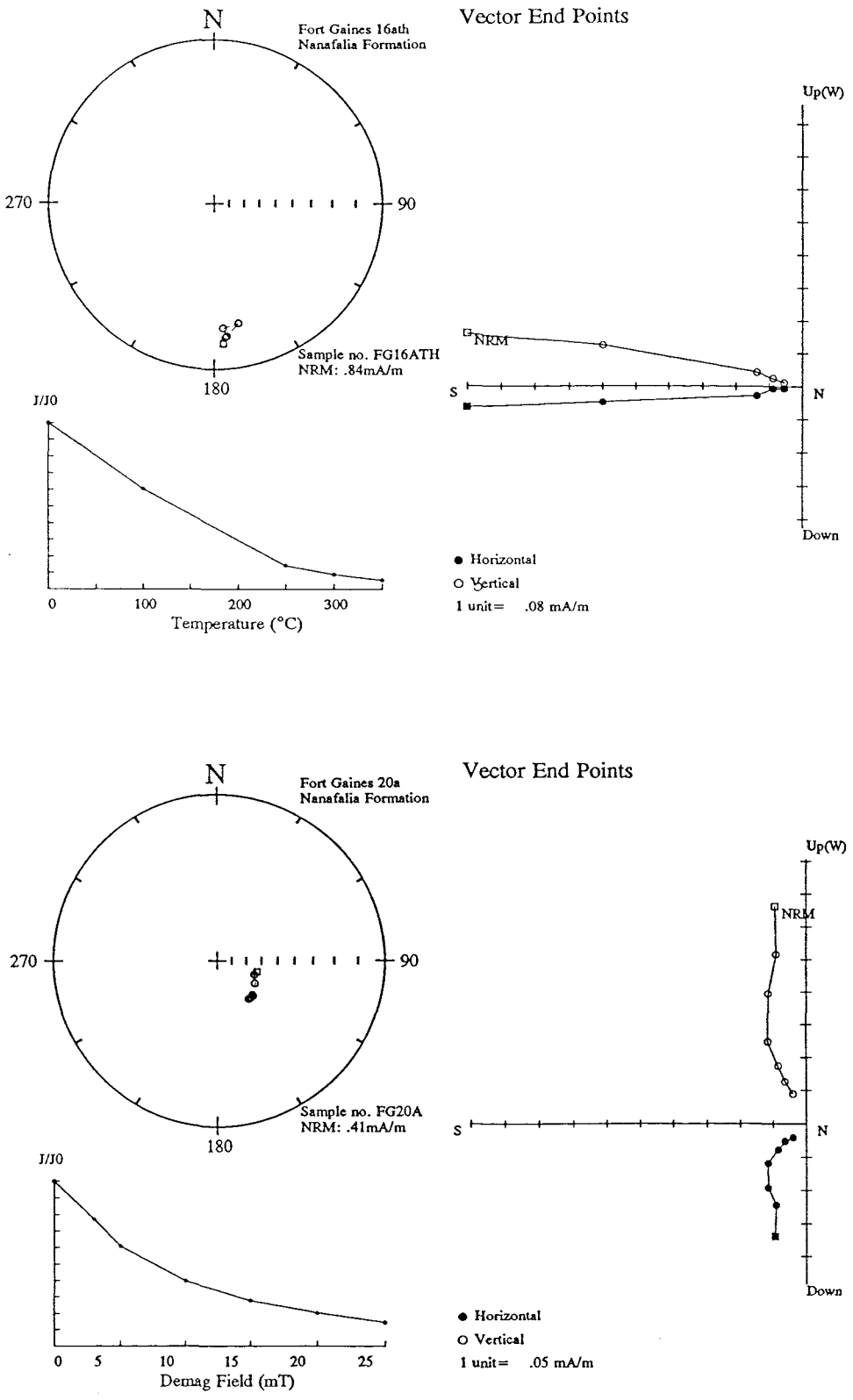

Figure 8-5 *Reverse polarity SEPs from thermal and A.F. demagnetisation.*

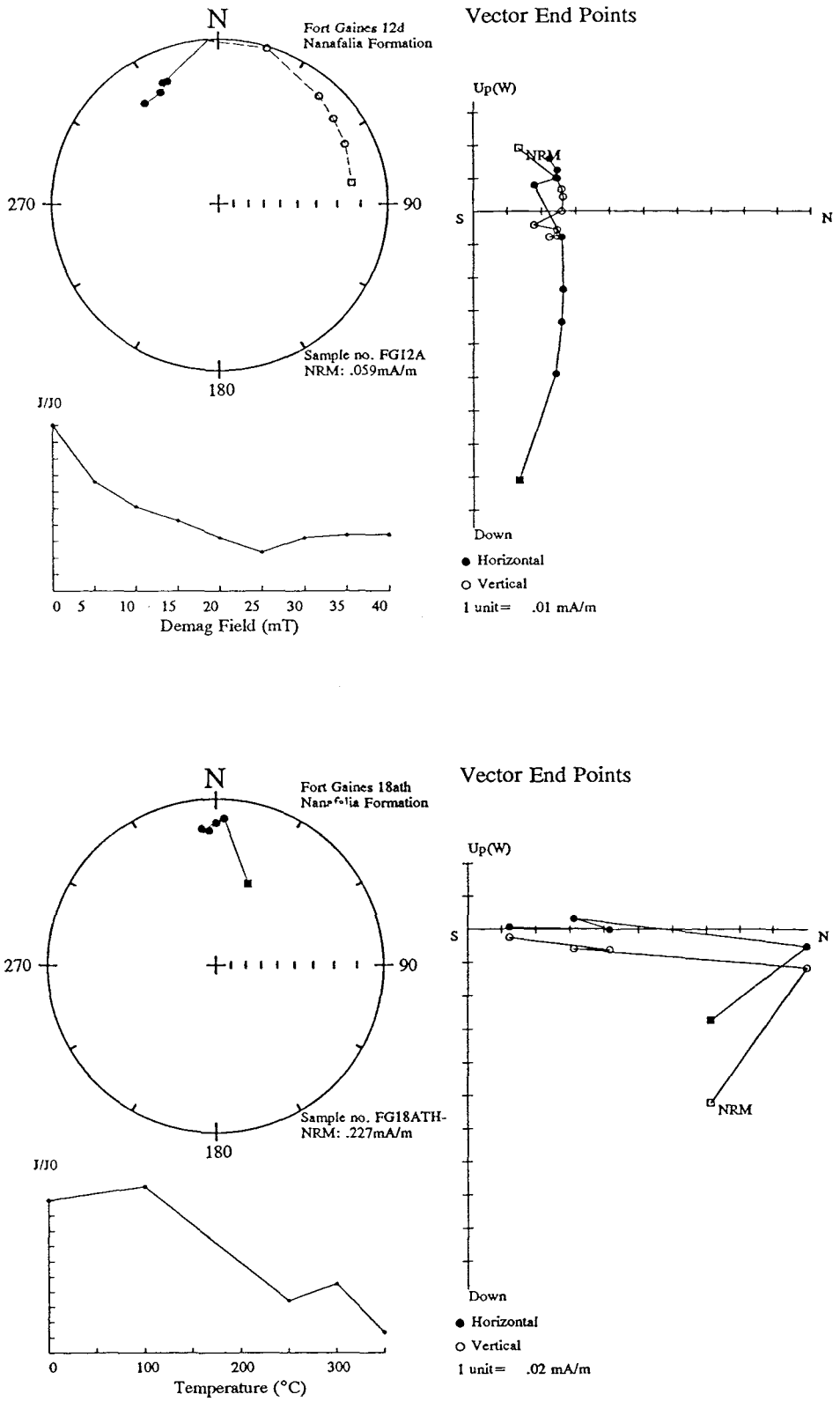

Figure 8-6 *Normal polarity SEPs from thermal and A.F. demagnetisation.*

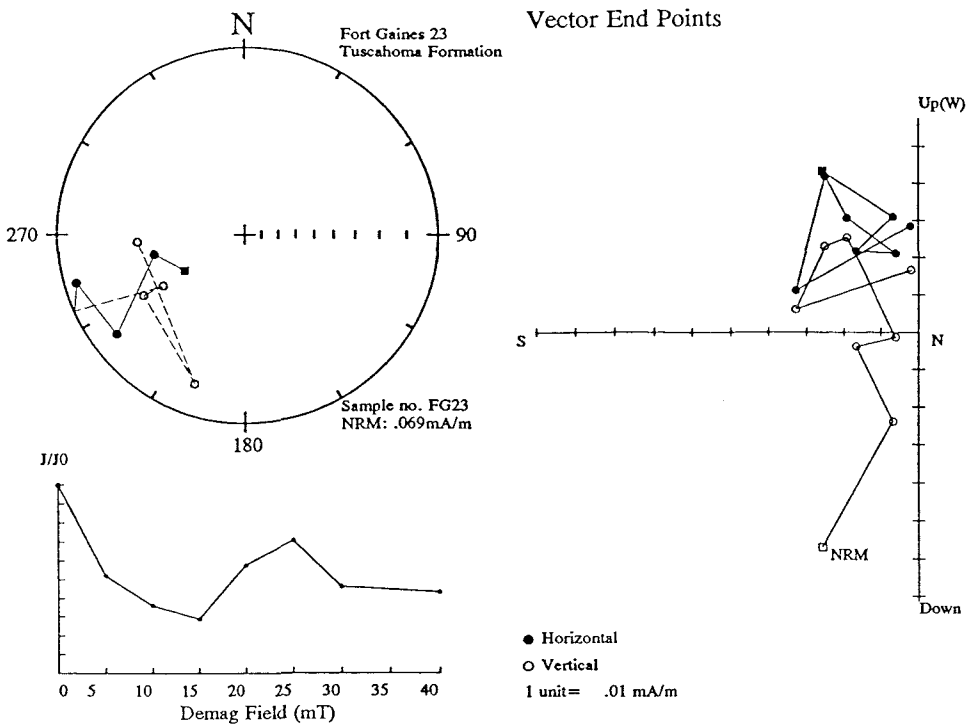

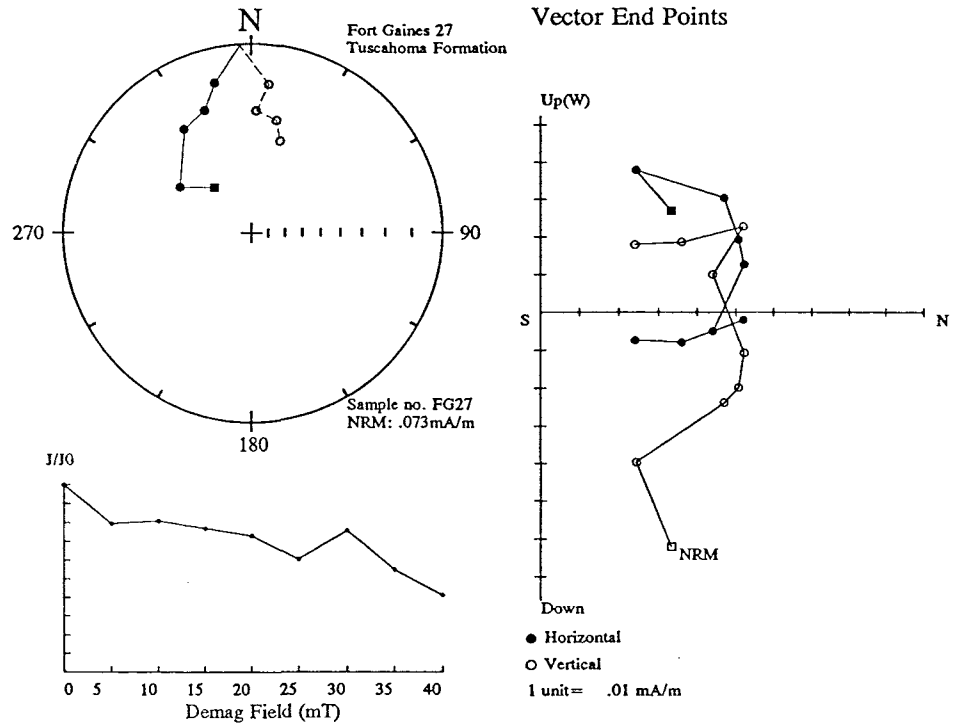

Figure 8-7 *Examples of reverse polarity trends from the Fort Gaines locality.*

8.1.2 McCrea Creek locality

At the McCrea Creek locality the clayey sands of the Grampian Hills Member of the upper Nanafalia Formation are exposed along a stream section (Fig. 8-8). Below the Tuscahoma Formation contact at the top of the logged section, 8 sites were sampled over an interval of approximately 7m.

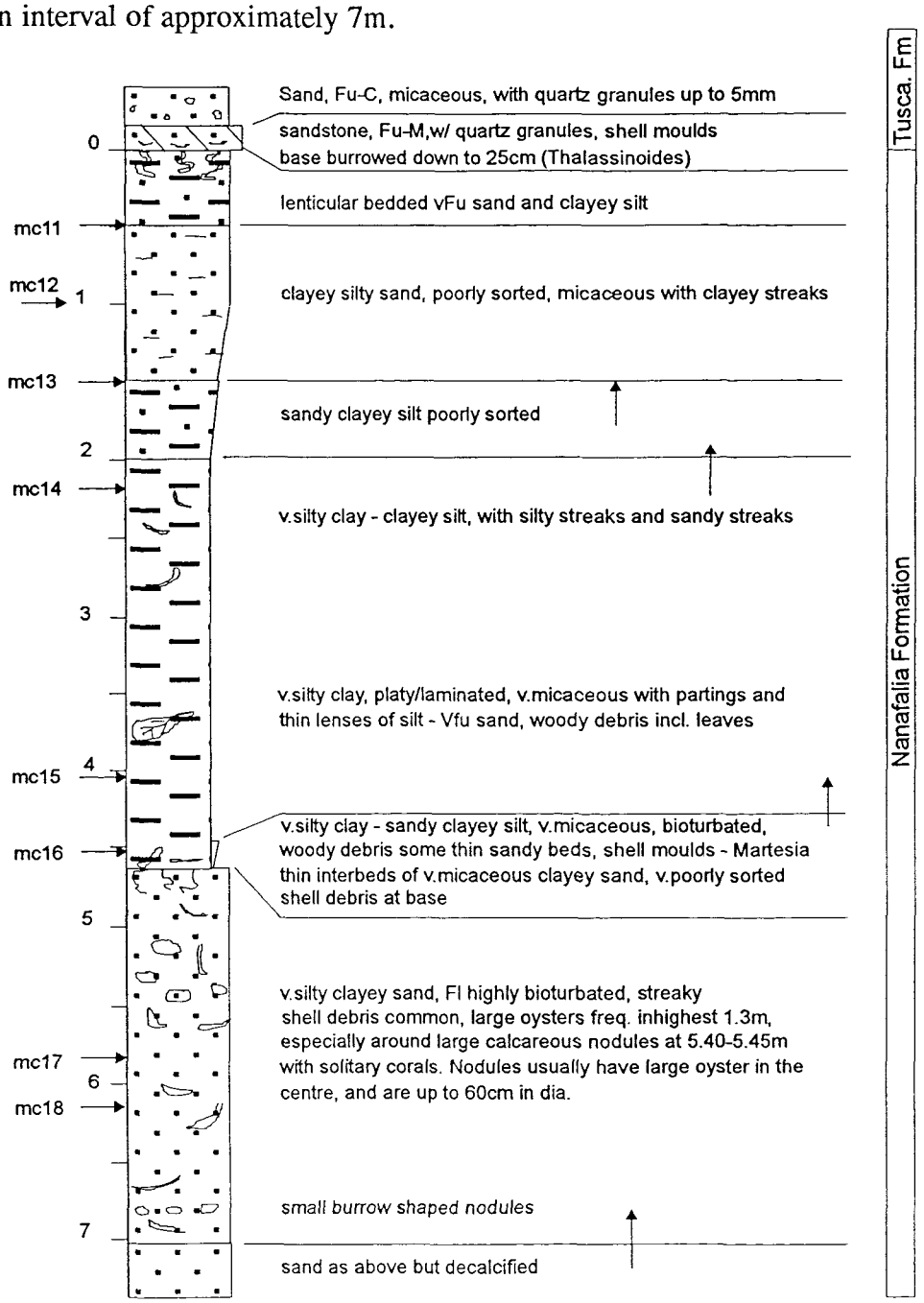

Figure 8-8 *Logged section at McCrea Creek with sampling sites.*

The blocks at each site were split into 2 sub-specimens which were typically demagnetised by thermal and A.F. demagnetisation. IRM acquisition characteristics of two sites (mc11 and mc16) illustrated a relatively early saturation of the magnetic minerals suggesting a probable magnetite composition (Fig. 8-9).

Polarity analysis

The demagnetisation of samples indicate a complex pattern of magnetic overprints at this locality. More than 50% of sub-samples have unreliable polarity assignments. Of the remaining sub-samples there is rarely any consistency between those from the same site or from those demagnetised by thermal and A.F. techniques (see appendix 7).

Sample site 15 (at 4.1m below the Tuscahoma contact) is, however, considered reliable. At this height in the section SEPs from both thermal and A.F. demagnetisation indicate a clear reverse polarity interval (Fig. 8-10).

The upper 2m of the section have a predominance of samples showing trends to a normal polarity or anomalous plots with steep positive inclinations and southerly declinations which may indicate Chron C25n. The quality of data, however, is too poor to make any confident correlations with the GPTS at this location.

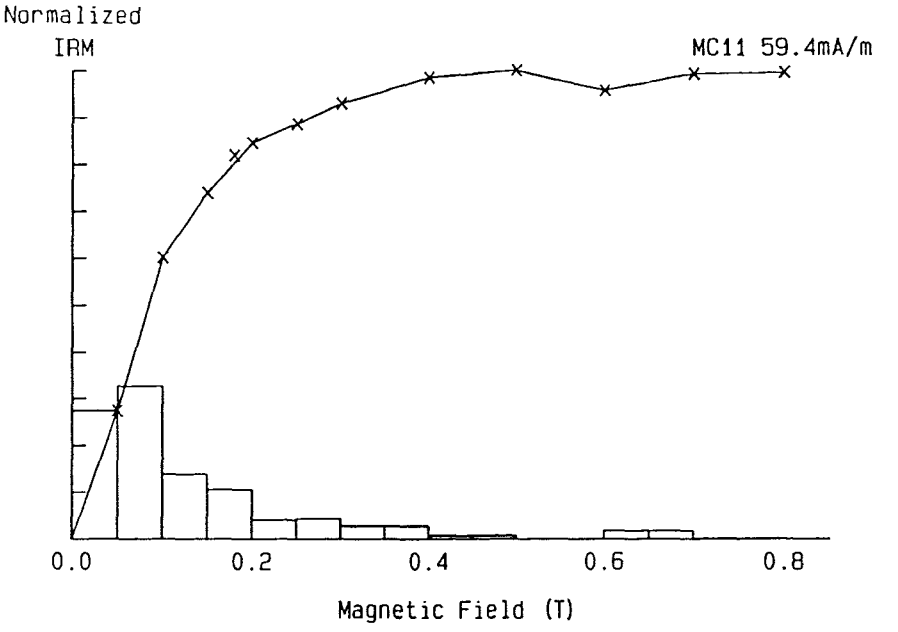

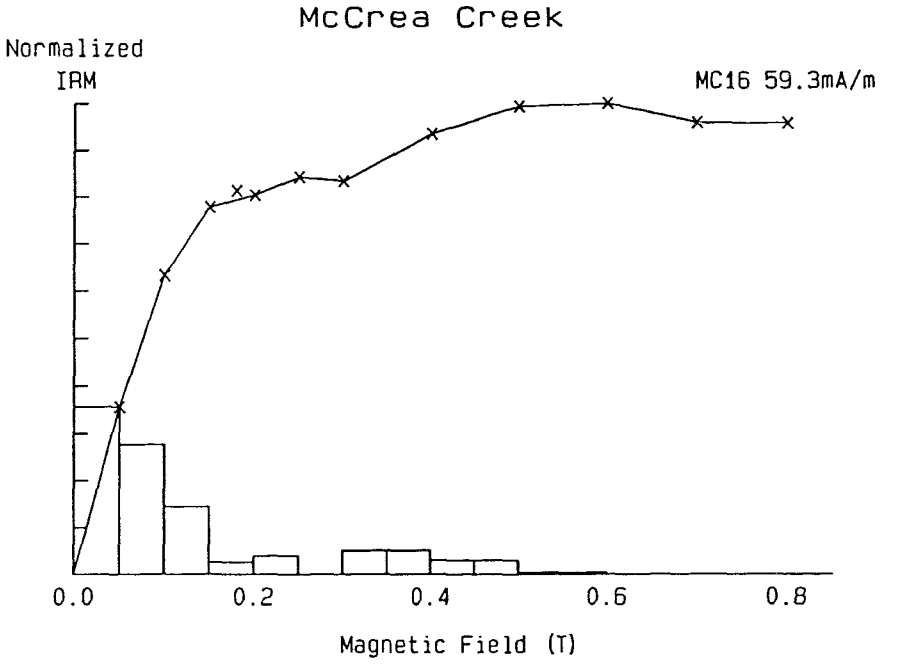

Figure 8-9 *IRM acquisition curves for 2 samples from Miller McCrea Creek.*

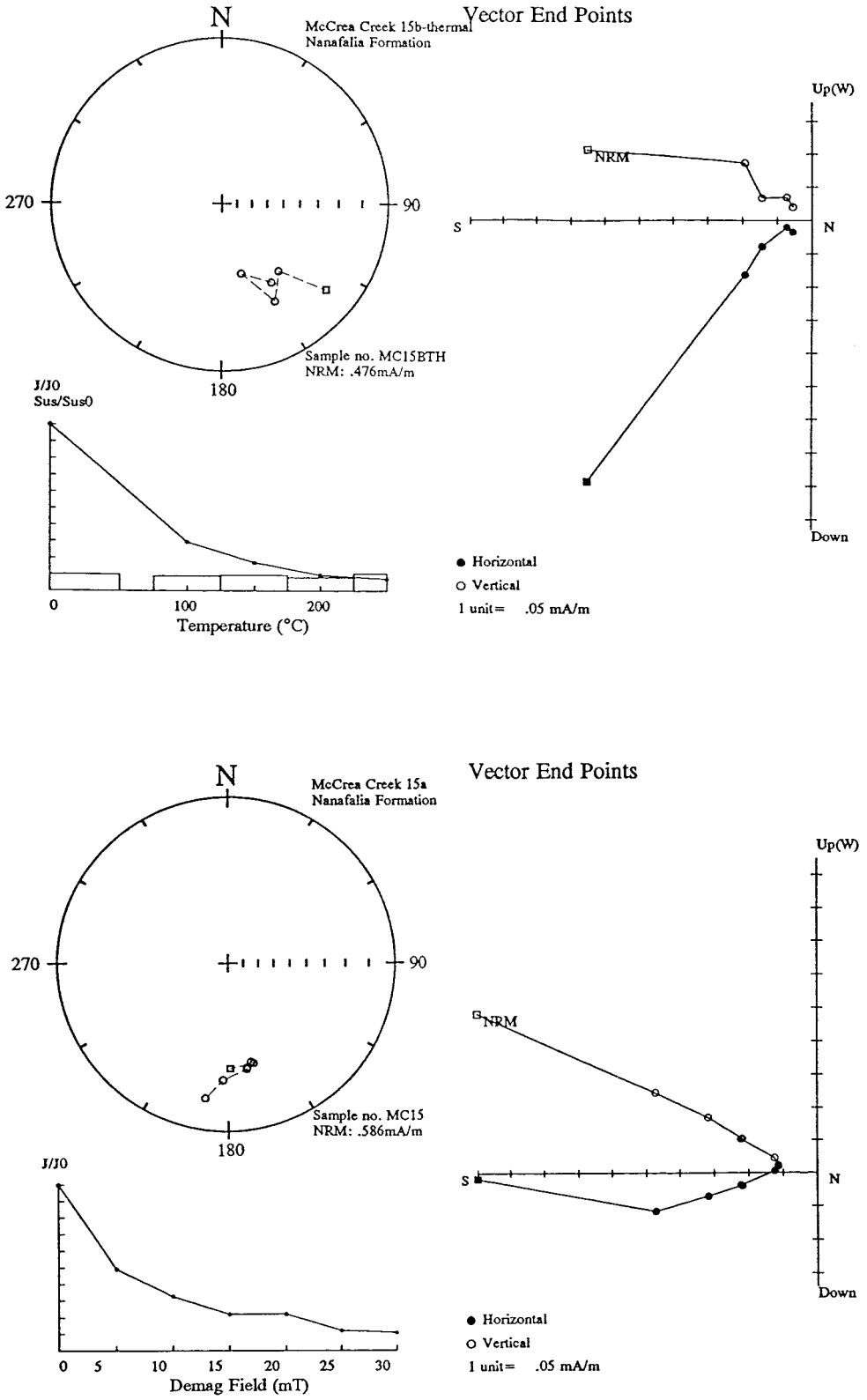

Figure 8-10 *Example of a confident reverse polarity site at -4.1m in the McCrea Creek exposure.*

8.1.3 Camden locality

Location: The Grampian Hills member and *Ostrea thirsae* beds of the Nanafalia Formation are exposed along the roadside of Highway 41 and in a quarry close by, 7 miles south of Camden, Wilcox County, Alabama.

The calcareous concretions within the *Ostrea thirsae* beds were sampled with a rock drill during the 1990 field work and the results from this work are presented here (further work has not been done on this section due to the absence of a drill on this last field trip).

8.1.3a Camden Road locality - Grampian Hills member

The Grampian Hills Member conformably overlies the *Ostrea thirsae* beds and consists of predominantly blue/black silty clays and sands. Mollusc moulds, glauconite and woody debris are seen at some intervals (Fig. 8-11).

The polarities at 9 sites were investigated predominantly using the A.F. demagnetisation techniques. IRM analysis at 2 of these sites (1.5m and 6m) showed the early saturation of a magnetite component (Fig. 8-12).

Polarity analysis

70% of all samples analysed show demagnetisation behaviour which gives reliable normal polarity SEPs (Fig. 8-13). The remaining 30% yield less reliable normal polarities and anomalous positive inclinations with a southerly declination (Appendix 8).

Magnetostratigraphy of the Camden road locality

The 10m of uppermost Nanafalia Formation sampled is considered a reliable normal polarity interval and correlates with the base of Chron C25n.

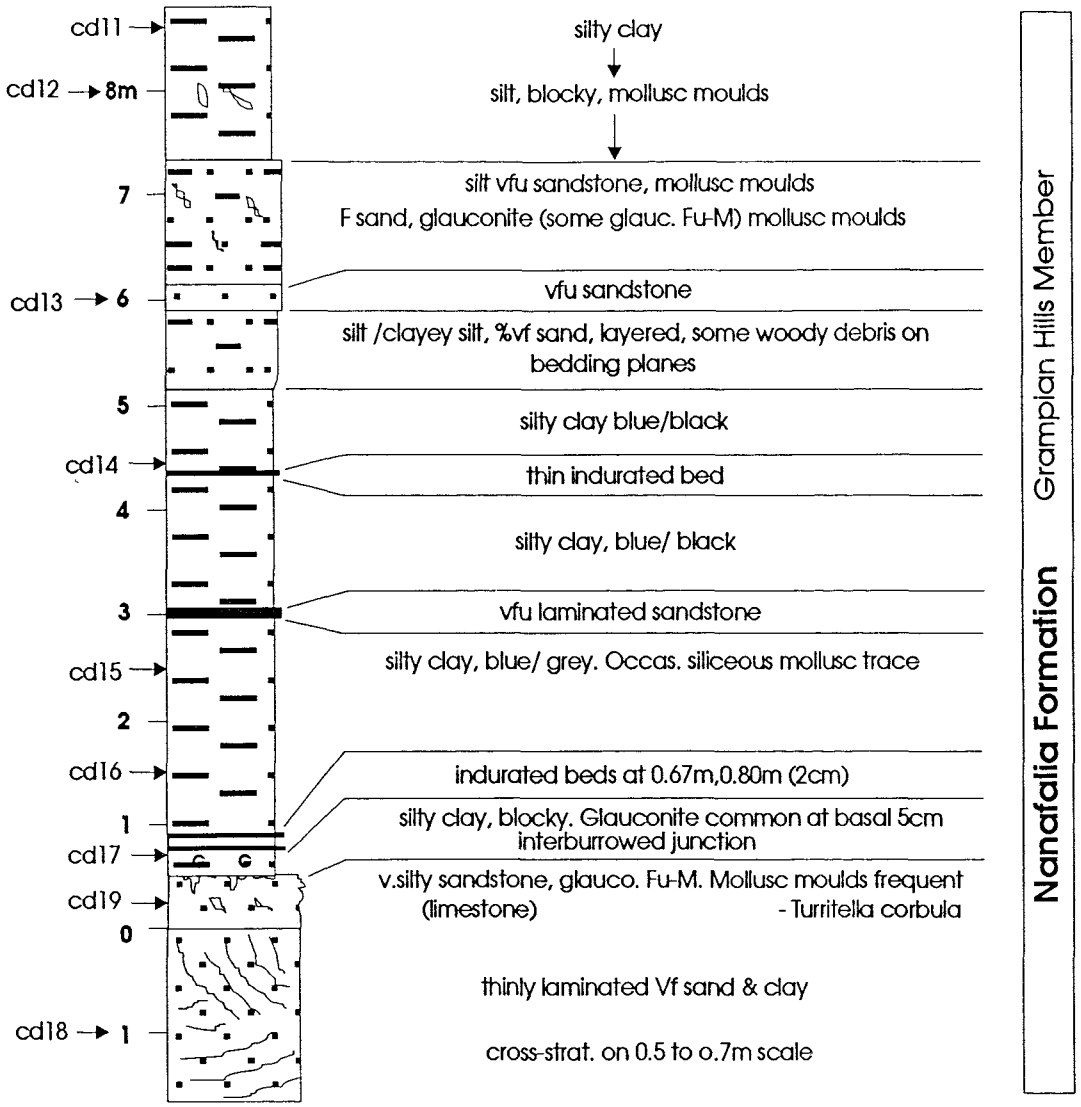

Figure 8-11 *Stratigraphic log and sampling sites at the Camden road cutting.*

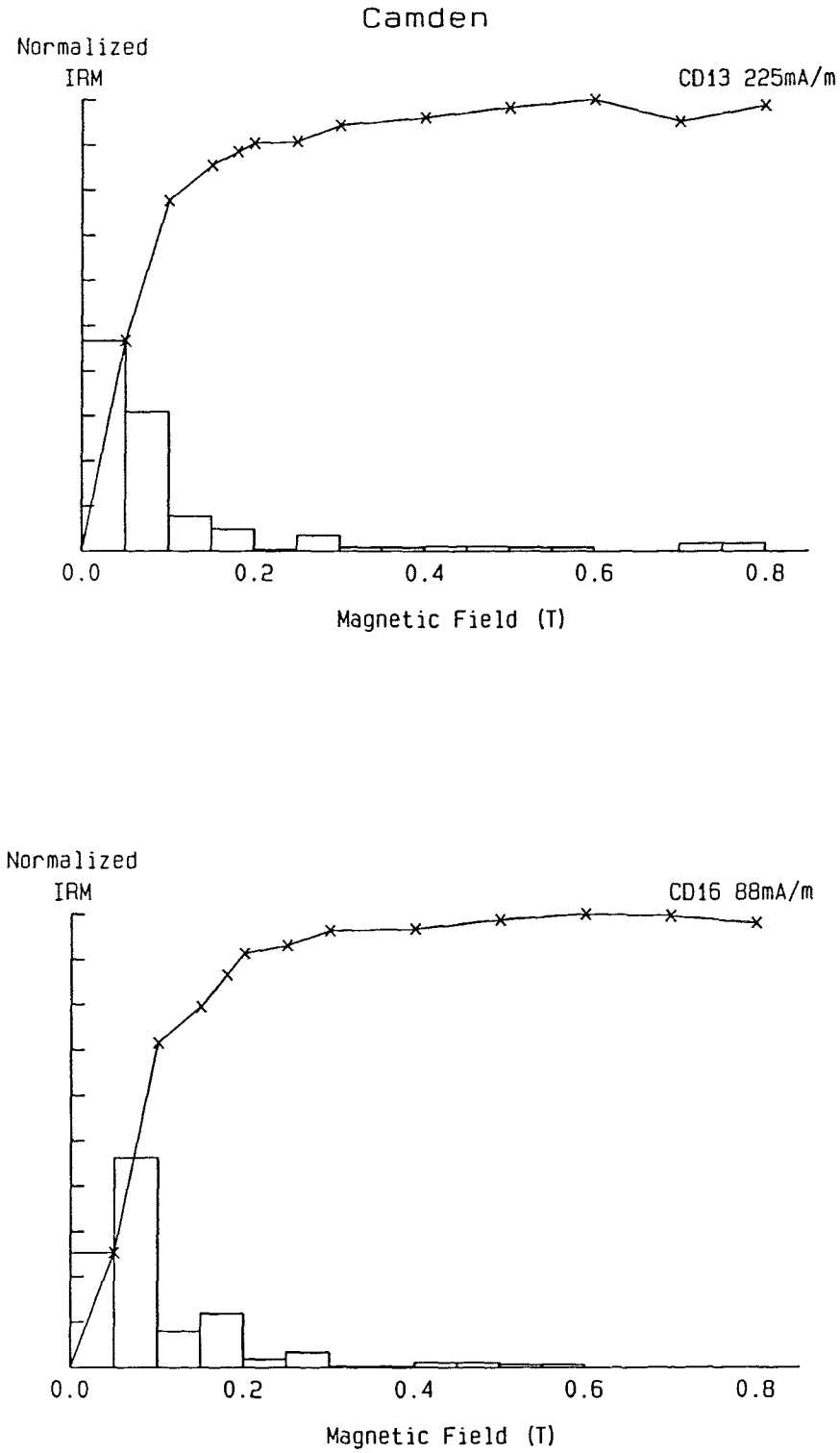

Figure 8-12 *IRM acquisition curves of material from the Grampian Hills Member.*

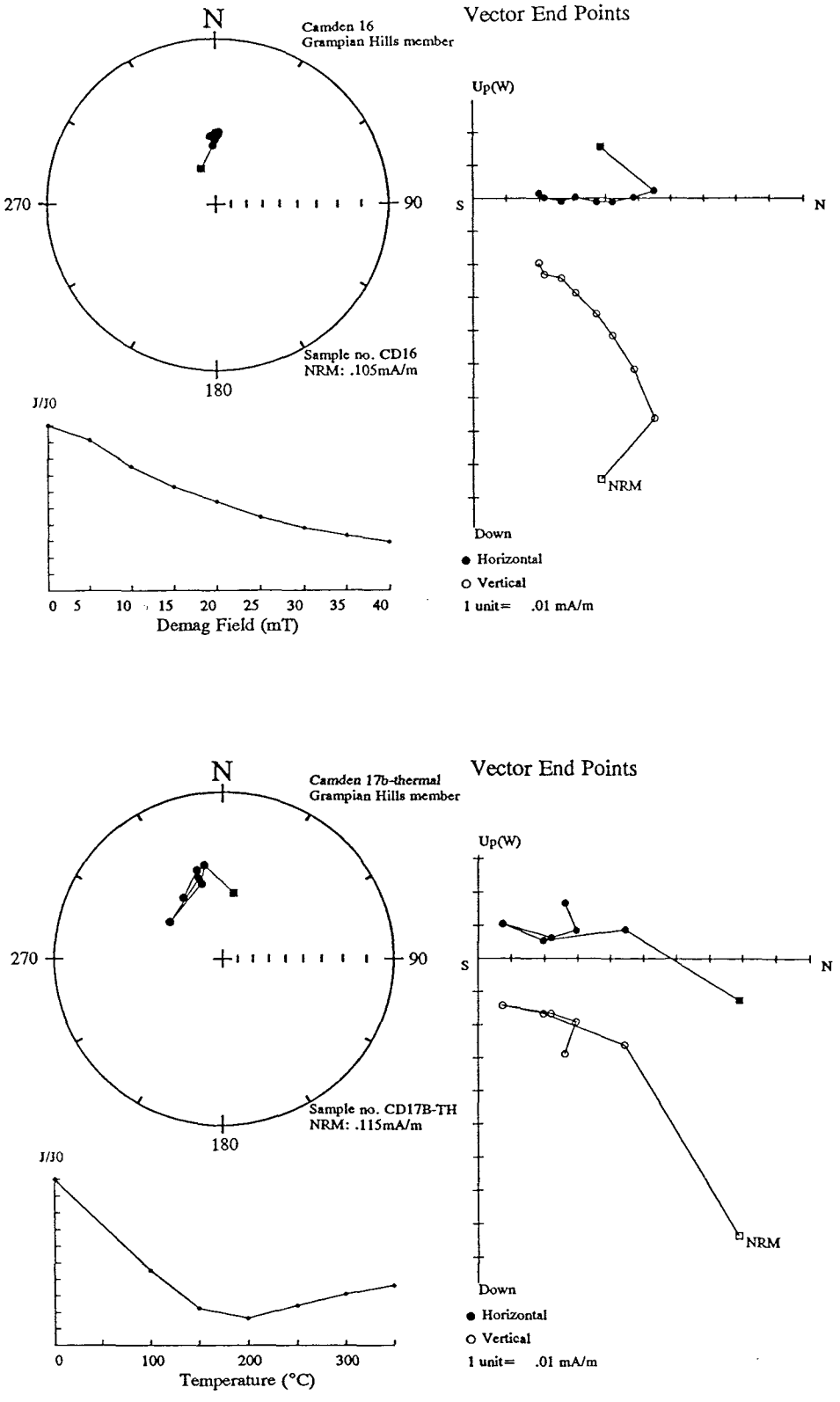

Figure 8-13 *Examples of normal polarity SEPs from both A.F. and thermal demagnetisation techniques at the Camden locality.*

8.1.3b Camden quarry locality - Ostrea thirsae beds and Gravel Creek member

The Gravel Creek Sand Member consists of white micaceous, unconsolidated, cross-bedded, medium to coarse grained sand. The *Ostrea thirsae* beds discomformably overlie the Gravel Creek Member and consist of weathered clayey sands with abundant glauconite and oyster shells with intermittent calcareous concretions occurring at between 1-3m intervals (Fig. 8-14).

Sites were restricted to 4 levels of calcareous nodules which were sampled using a rock drill. The cores were then split into 3-4 sub-samples each of which was A.F. demagnetised up to a maximum of 45mT.

Polarity analysis

Samples from Camden quarry showed a range of poor quality demagnetisation characteristics which were generally categorised as trends to reverse with varying degrees of reliability. The consistency between sub-samples from the same stratigraphic height was often poor. However a probable reverse polarity component of primary magnetism was tentatively identified at each site. Figures 8-15 and 8-16 illustrate the quality of much of the data.

Magnetostratigraphy of Camden quarry locality

The reverse polarity at this locality suggests a polarity correlation with Chron C25r.

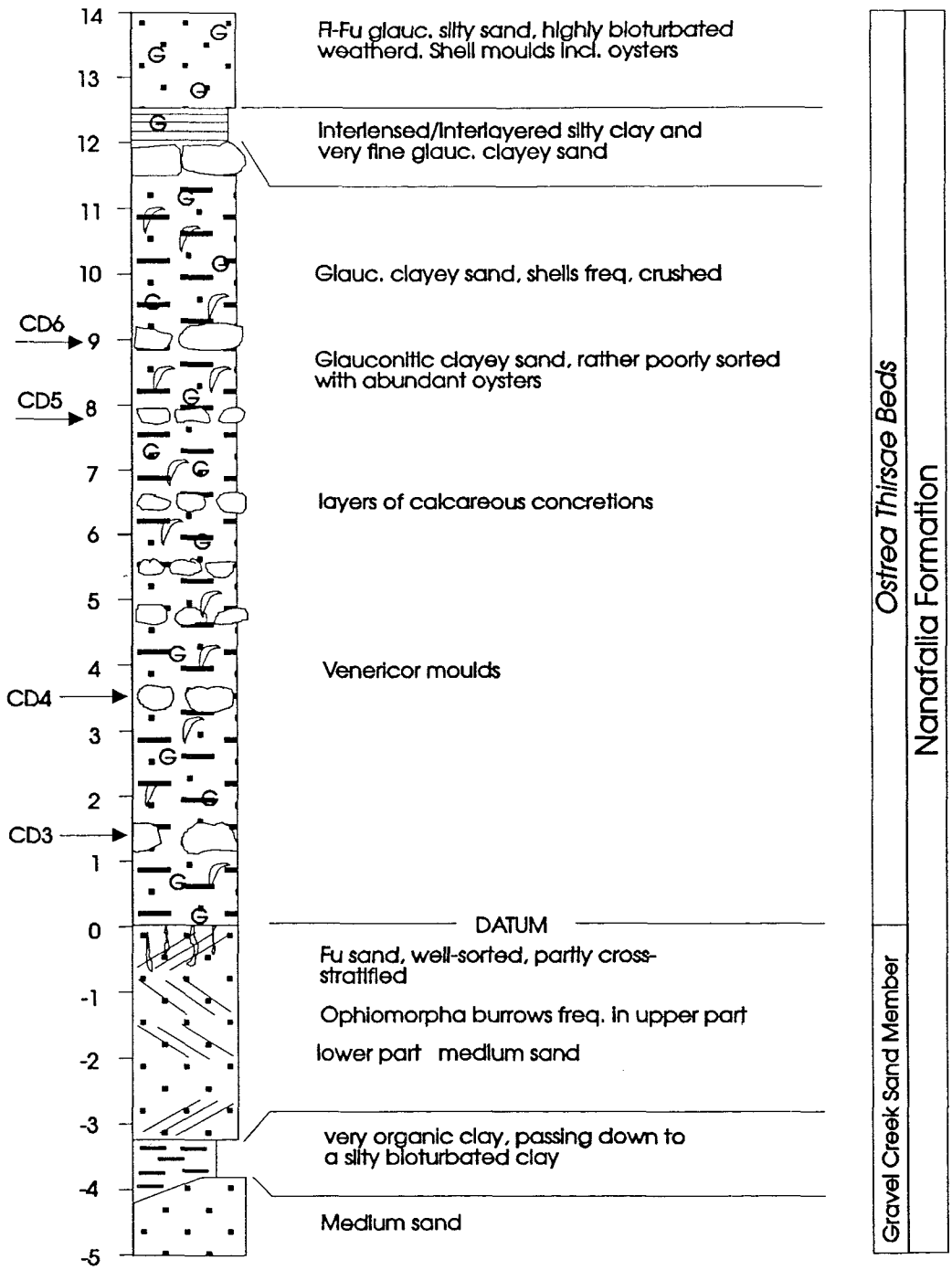

Figure 8-14 *Stratigraphic log and sample sites at Camden quarry locality.*

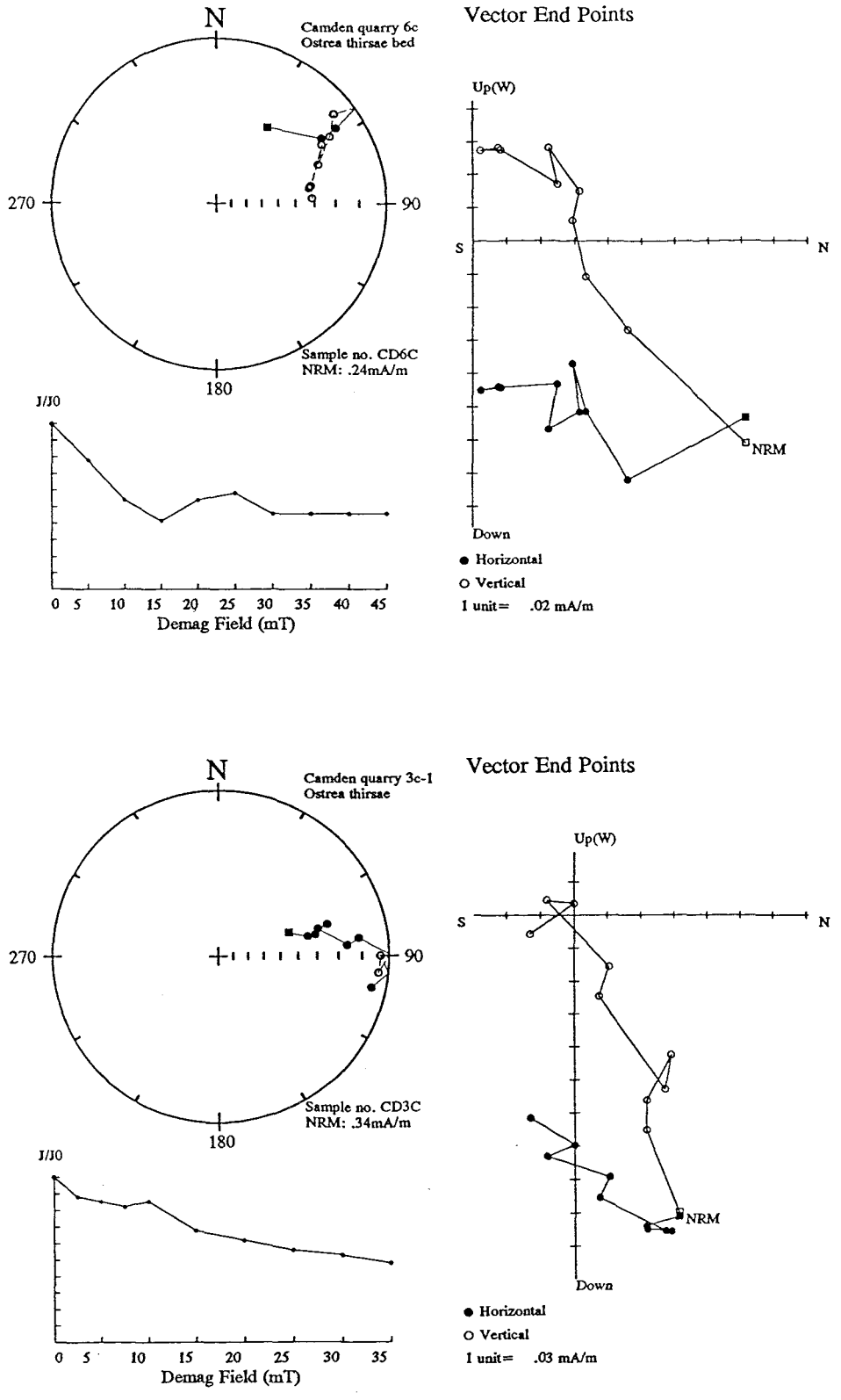

Figure 8-15 *Examples of confident trends to a reverse polarity at Camden quarry.*

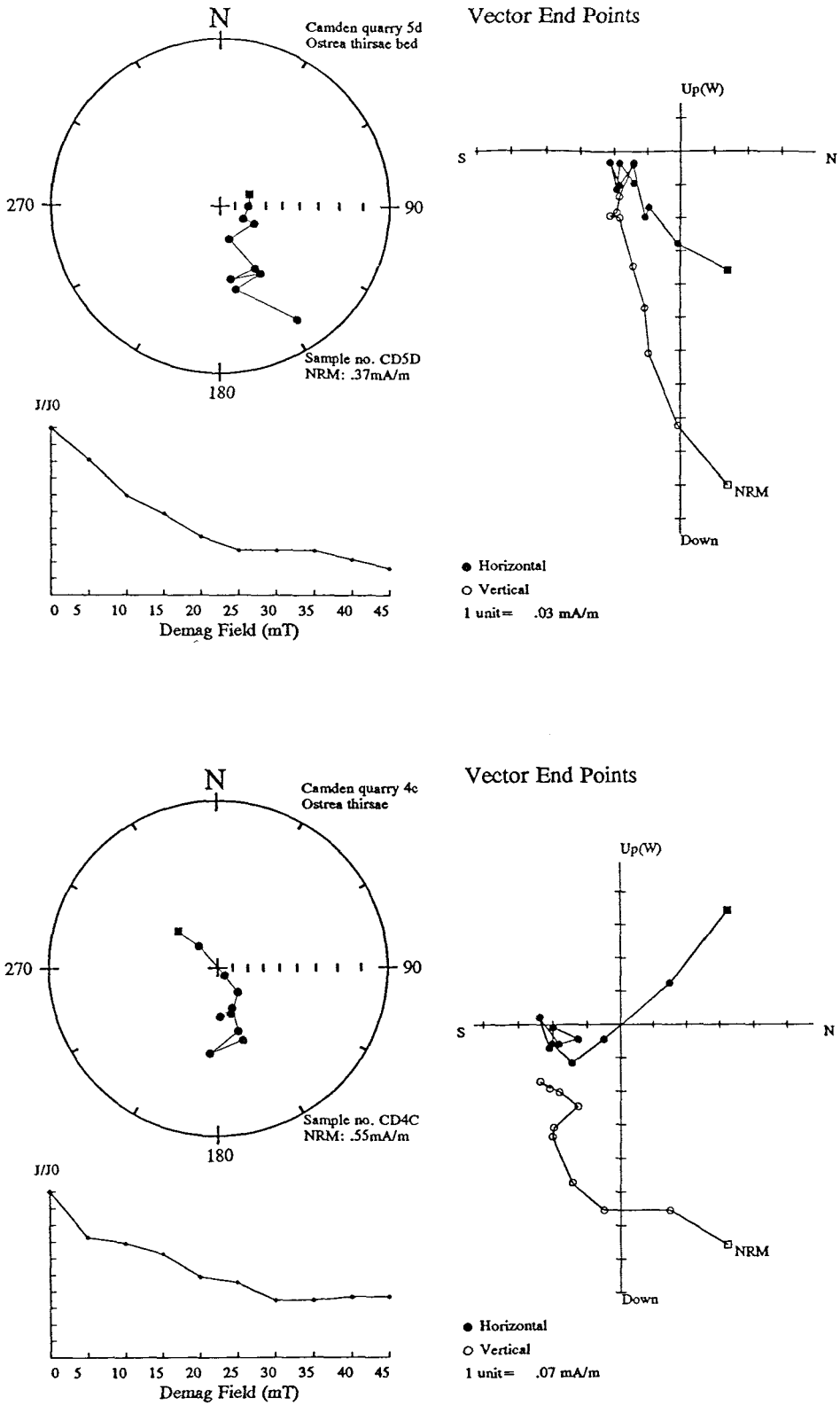

Figure 8-16 *Examples of questionable trends to a reverse polarity at Camden quarry.*

8.1.4 Camden Radio Mast locality

The road section at this locality exposes sediments of the Grampian Hills Member of the Nanafalia which should correlate with the main Camden section nearby. Six sites were sampled from consolidated clayey silts which were lithified and fractured and appeared to show some degree of weathering

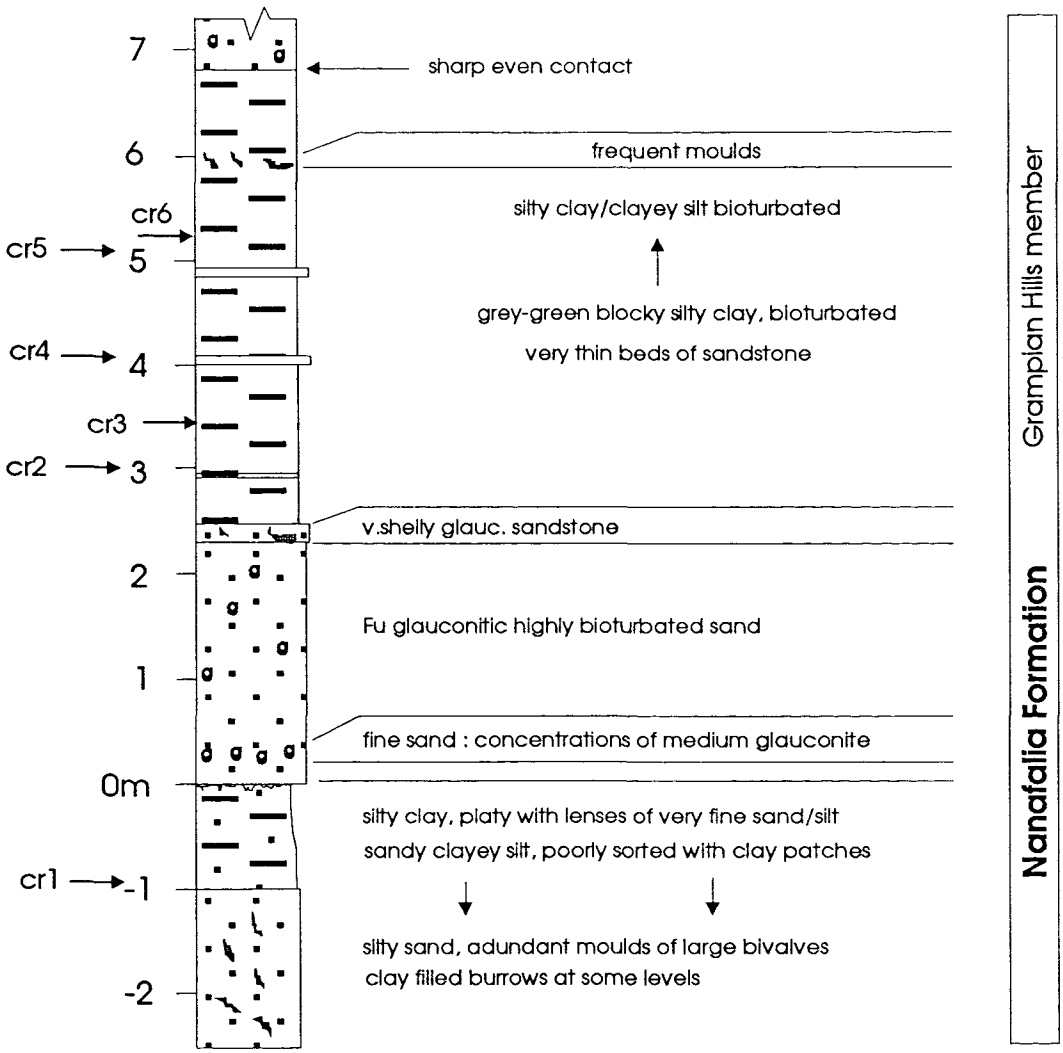

Figure 8-17 *Stratigraphic log and sample sites at Camden radio mast locality.*

IRM investigations were consistent with characteristics observed from sediments at the main Camden section (Fig. 8-18) although the first sample site at -1m in the logged

section indicated a slower saturation of magnetic material. This would suggest either that a hematite component is present or that the coercivity spectrum of the magnetite contains a higher proportion of lower coercivity grains. If hematite, this could be a reflection of the weathering seen at the surface of the sediments in outcrop.

Polarity analysis

Five of the six sites show reliable SEPs from both A.F. and thermal demagnetisation which are entirely consistent with the good normal polarities seen at the main Camden section (Figs. 8-19). Interestingly, the sample at site 1 which shows the lower IRM ratio (figure 8-18) gives an anomalous demagnetisation plot with steep positive inclination and a southerly declination.

Magnetostratigraphy of Camden Radio Mast locality

A normal polarity here suggests a polarity correlation with the base of Chron C25n.

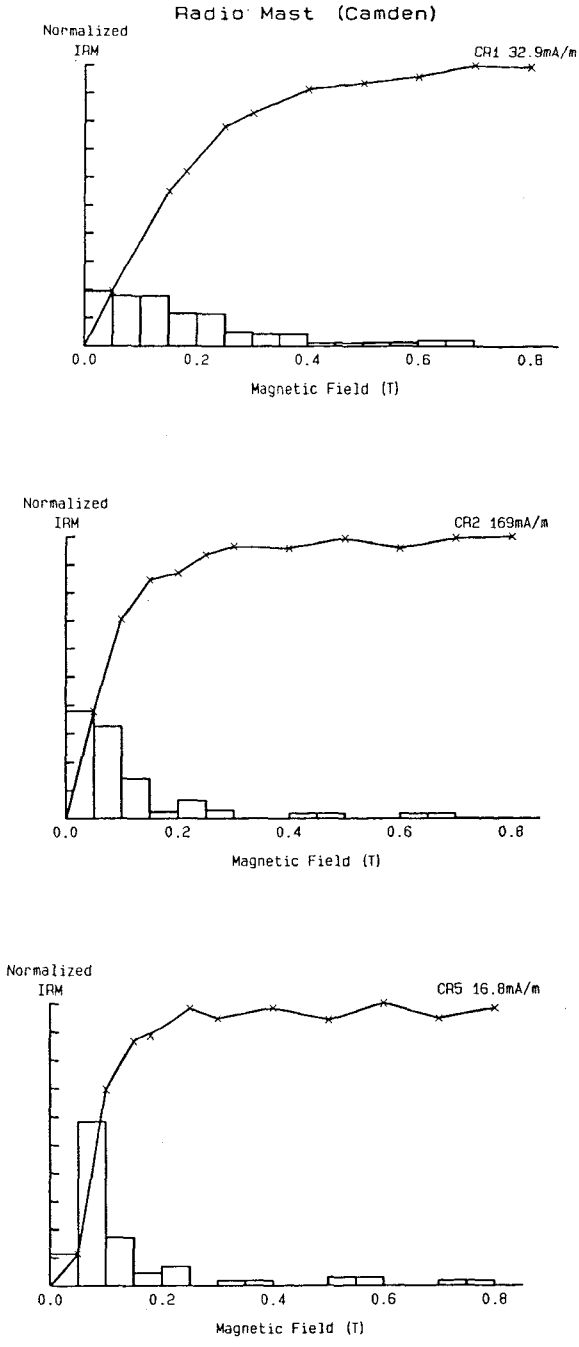

Figure 8-18 *IRM acquisition curves for sediments at Camden radio mast locality*

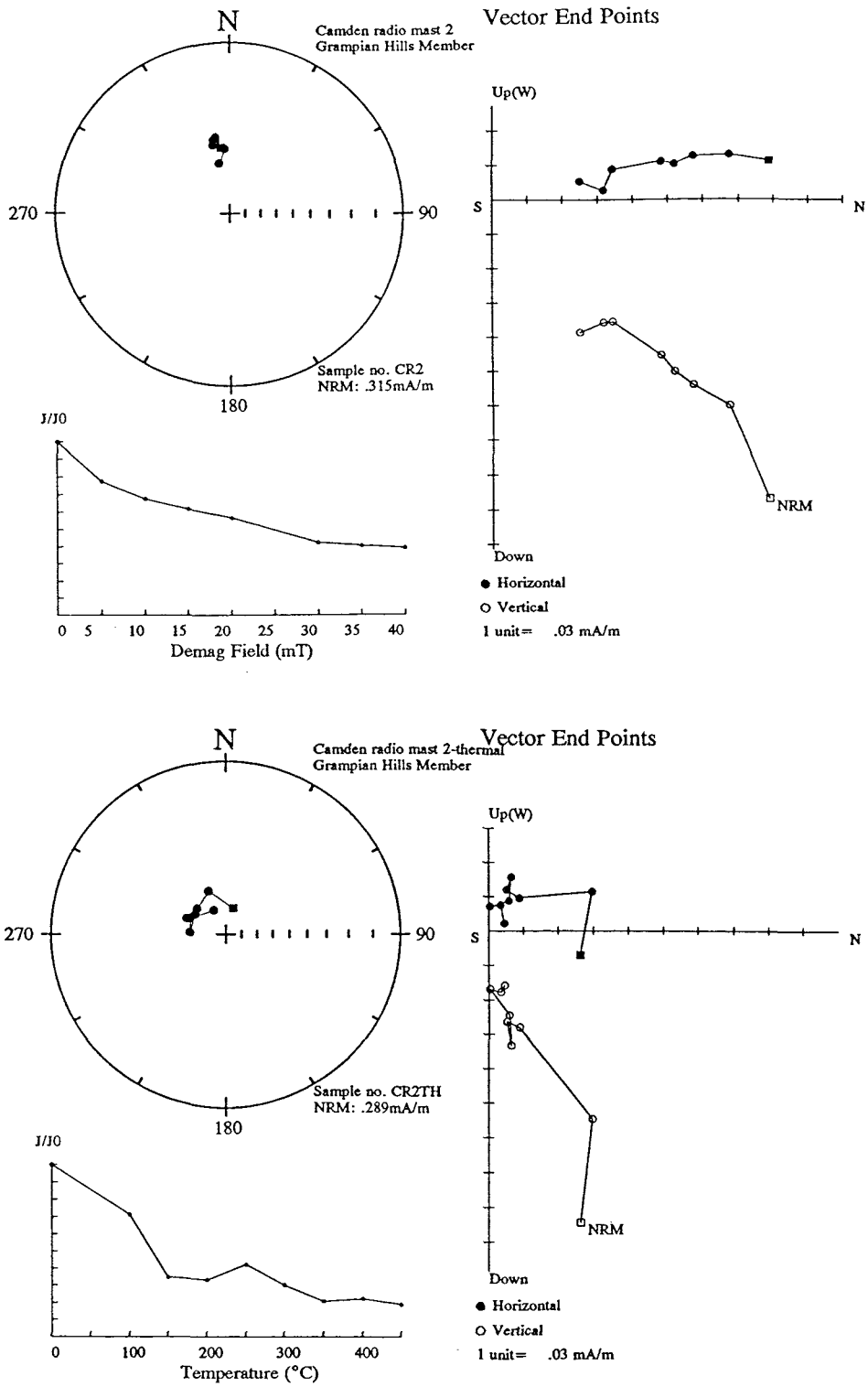

Figure 8-19 *Examples of normal polarity demagnetisation plots from sites at the Camden radio mast locality.*

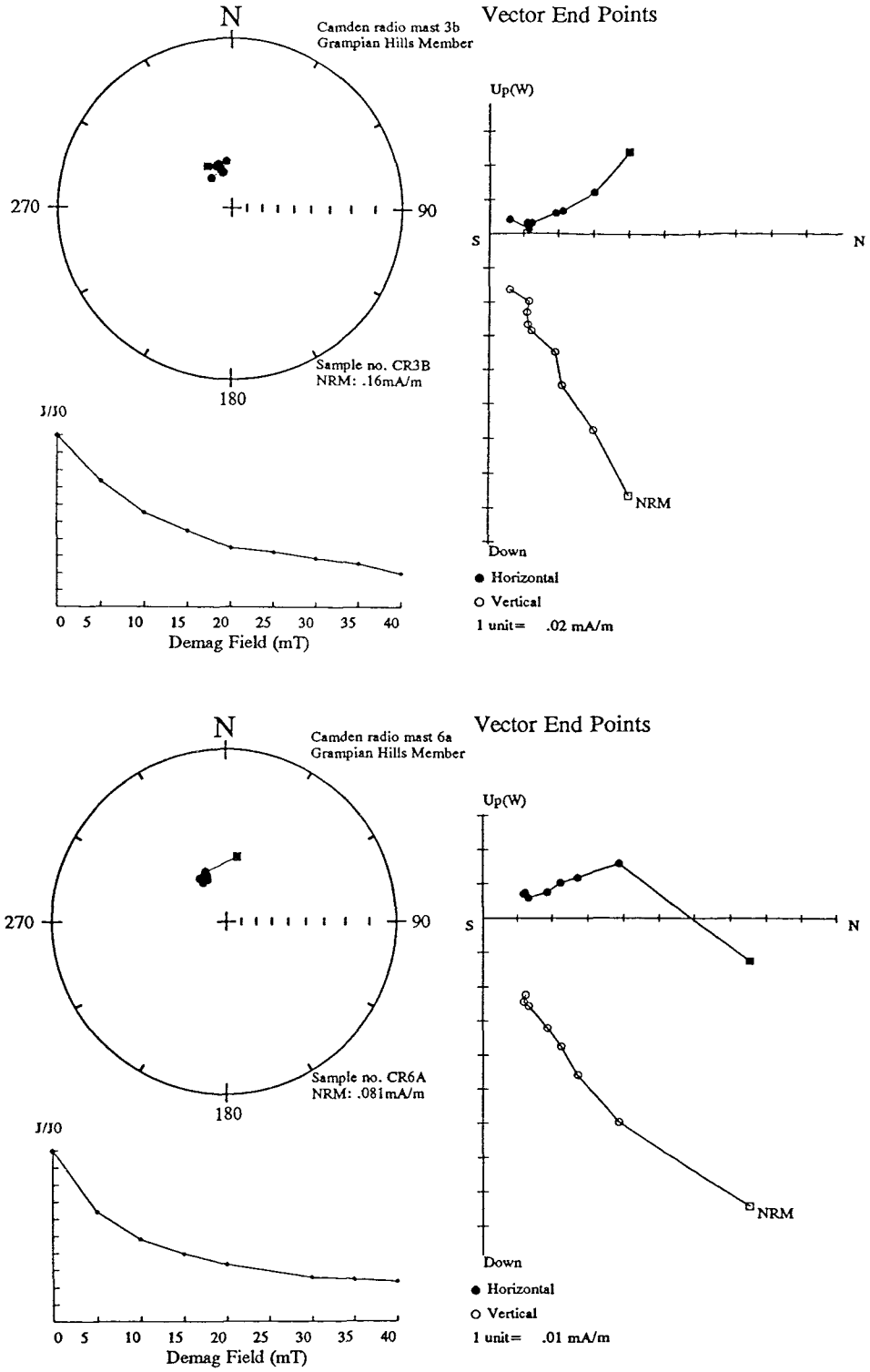

Figure 8-19 - continued *Examples of normal polarity demagnetisation plots from sites at the Camden radio mast locality.*

8.1.5 Salt Mountain locality

Location: The Salt Mountain limestone is exposed only in the vicinity of the type locality, Salt Mountain, 10km south of Jackson in Clarke County, Alabama.

The limestone was brought to the surface on the upthrown side of the Jackson fault and is approximately 25m in thickness (Toulmin, 1941). Foraminifera indicate that the Salt Mountain limestone belongs to the lower part of the Wilcox Group, having the same age as the Nanafalia Formation.

The palaeomagnetic group at Southampton University drilled samples from 6 sites and A.F. demagnetised 2 sub-samples from each horizon. Thermal investigations were also carried out on some specimens (1990).

Polarity analysis

The samples exhibited a predominance of good reverse SEPs and clear trends to a reverse polarity (Fig. 8-20). There was some uncertainty about the bedding at this location and therefore results were not corrected for tilt (Ali, pers. comm.). Ali (pers. comm.) has suggested that the consistent easterly shift in SEP directions may be due to effects of the Jackson fault.

Magnetostratigraphy of the Salt Mountain limestone

The good reverse interval observed in the Salt Mountain limestone correlates with Chron C25r of the GPTS.

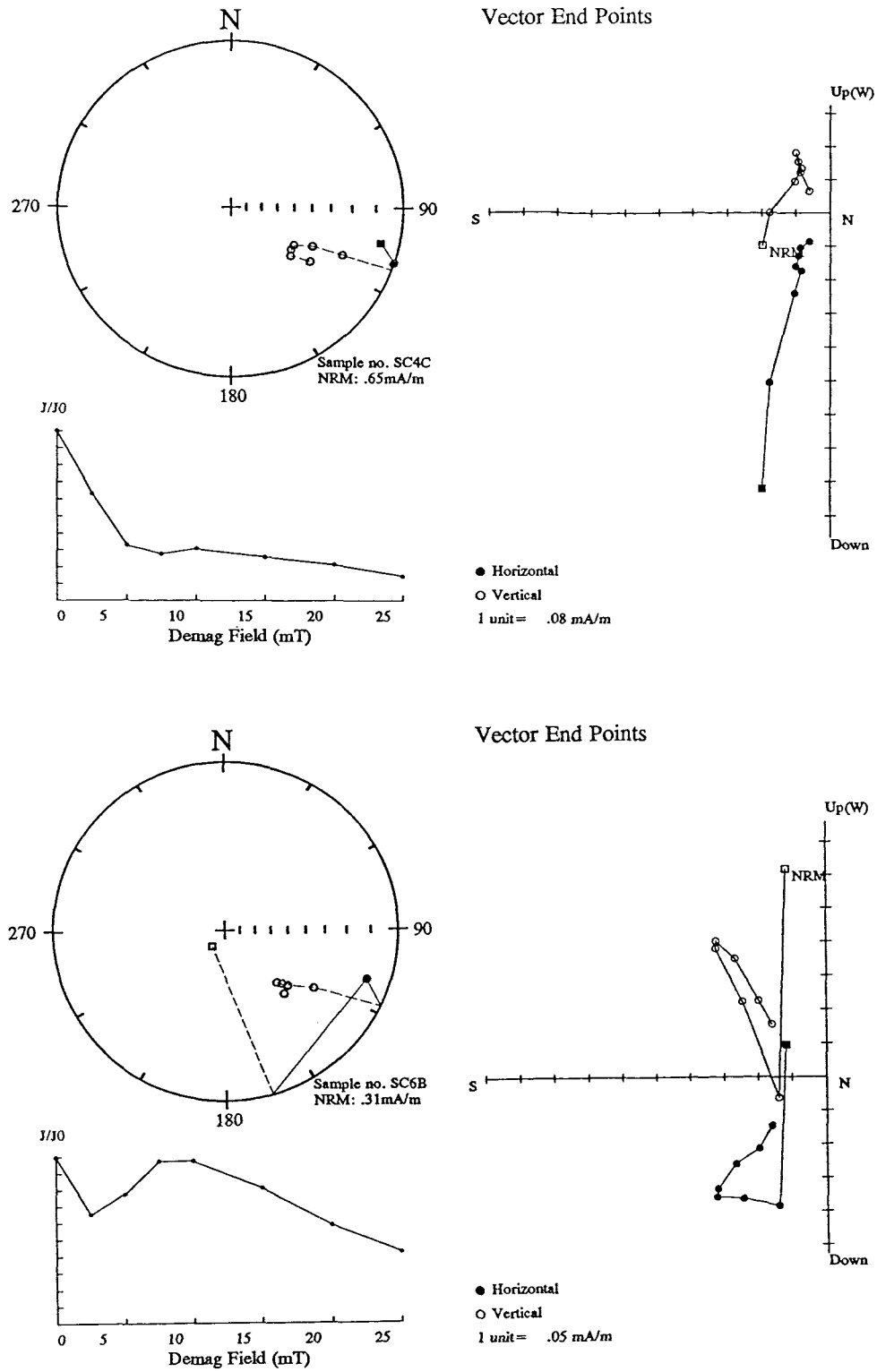

Figure 8-20 *Reverse polarity SEPs at the Salt Mountain locality.*

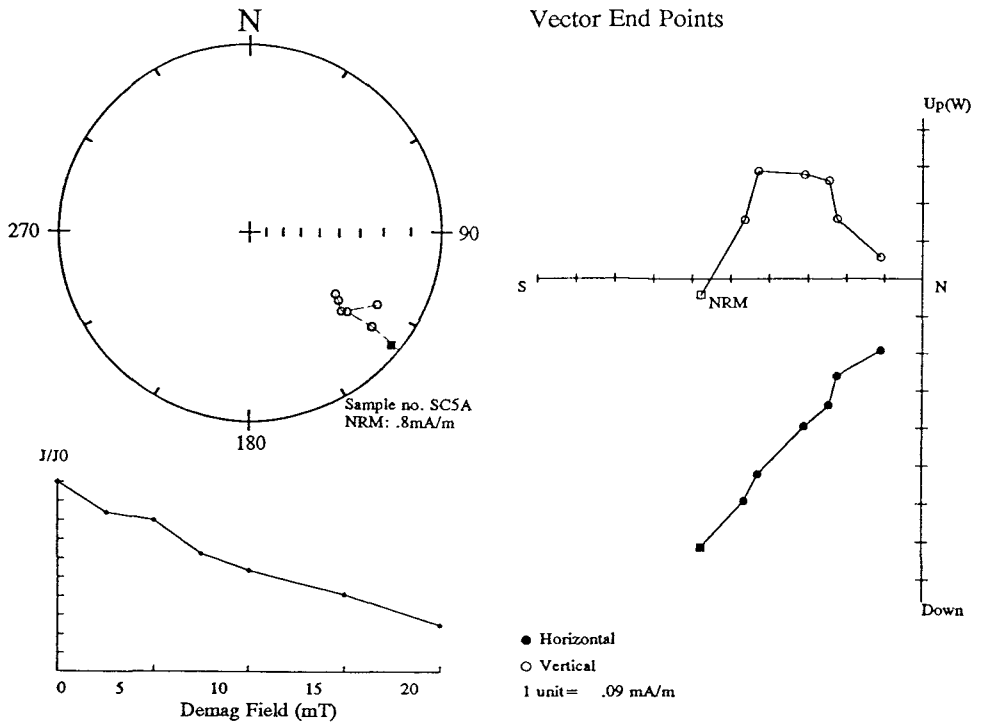

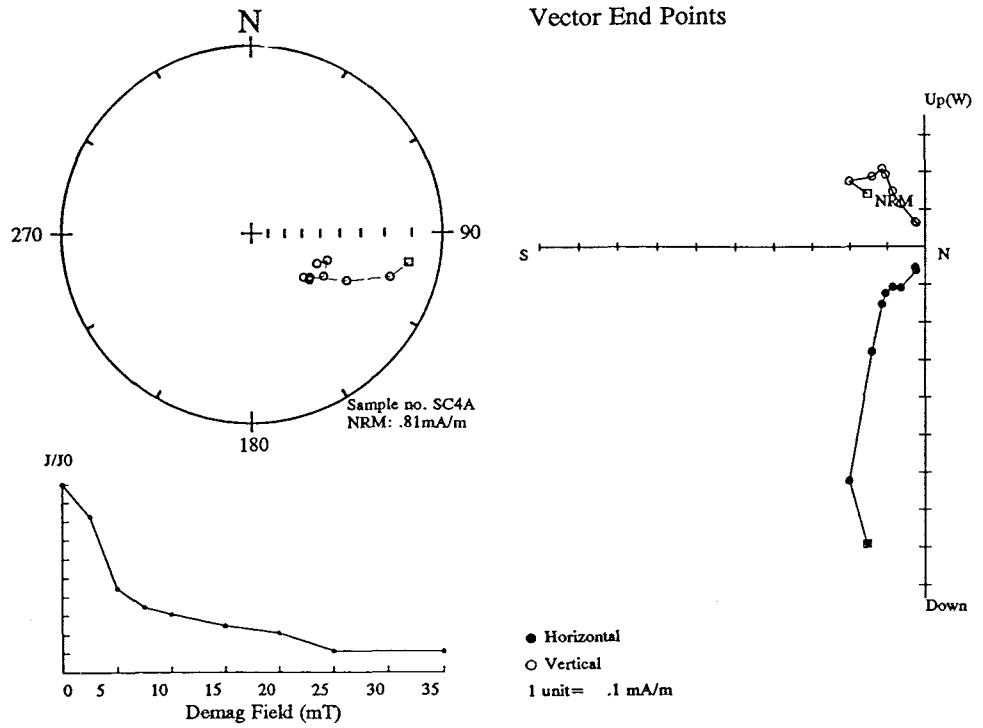

Figure 8-20 - continued *Reverse polarity SEPs at the Salt Mountain locality.*

8.2 Tuscahoma Formation outcrops

8.2.1a Bear Creek locality

Location: Bear Creek is located 12.9km south of Sunny South, Wilcox County, Alabama and includes a stream-cut along Bear Creek which continues up a gully to the south (section 8.2.1a) and a road-cut along Wilcox County Highway 1 (section 8.2.1b).

Plate 8-2 *Bear Creek locality.*

The geologic section at this location extends through the Tuscahoma Sand and includes three marls (Fig. 8-21). The lower marl unit, which was formally referred to as the 'Bear Creek Marl' is about 0.3m thick and consists of fossiliferous, glauconitic sand. The middle unit which is about 0.9m thick is the Gregg's Landing Marl Member and

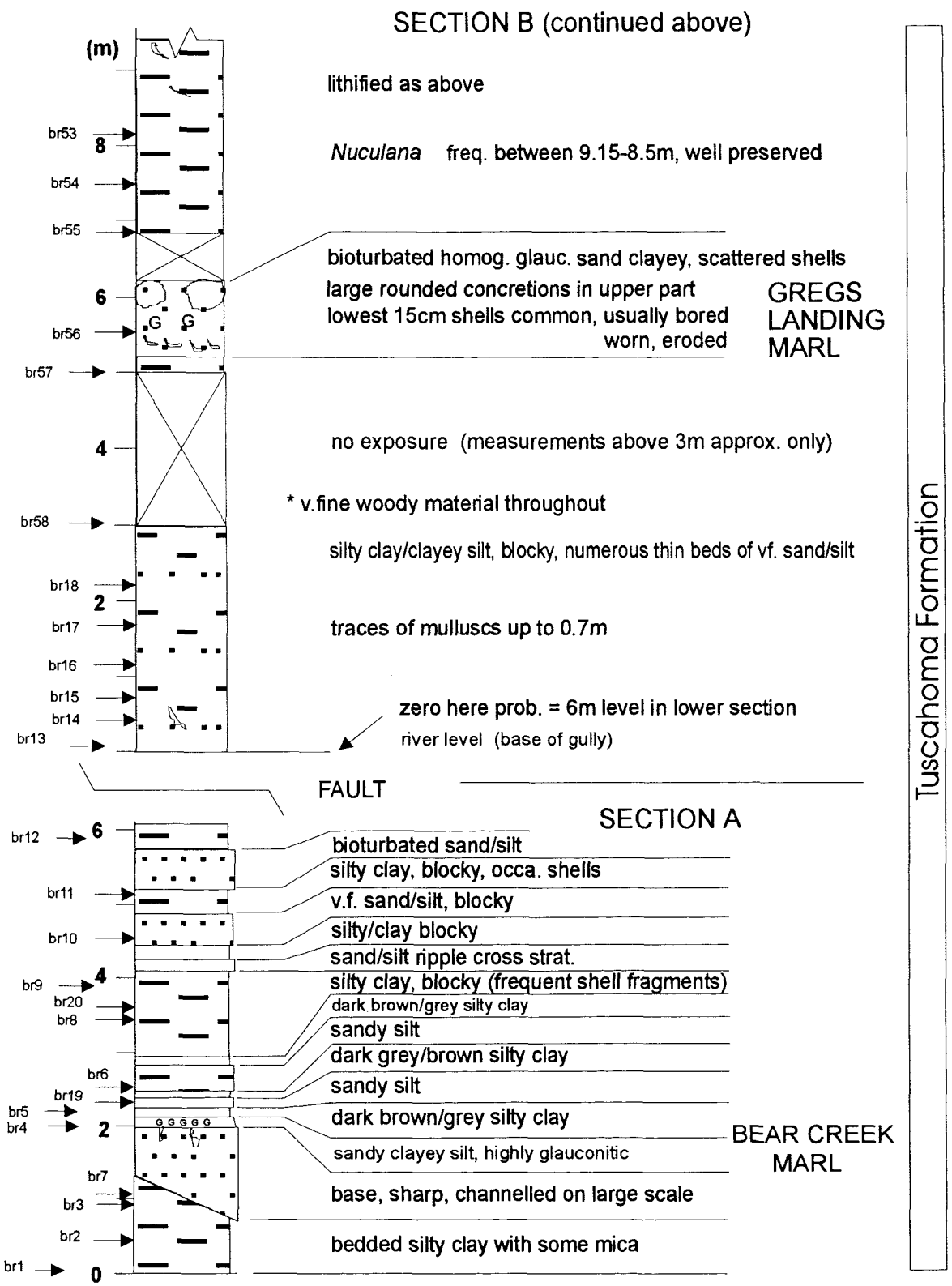

Figure 8-21 *Stratigraphic log and sample sites at Bear Creek.*

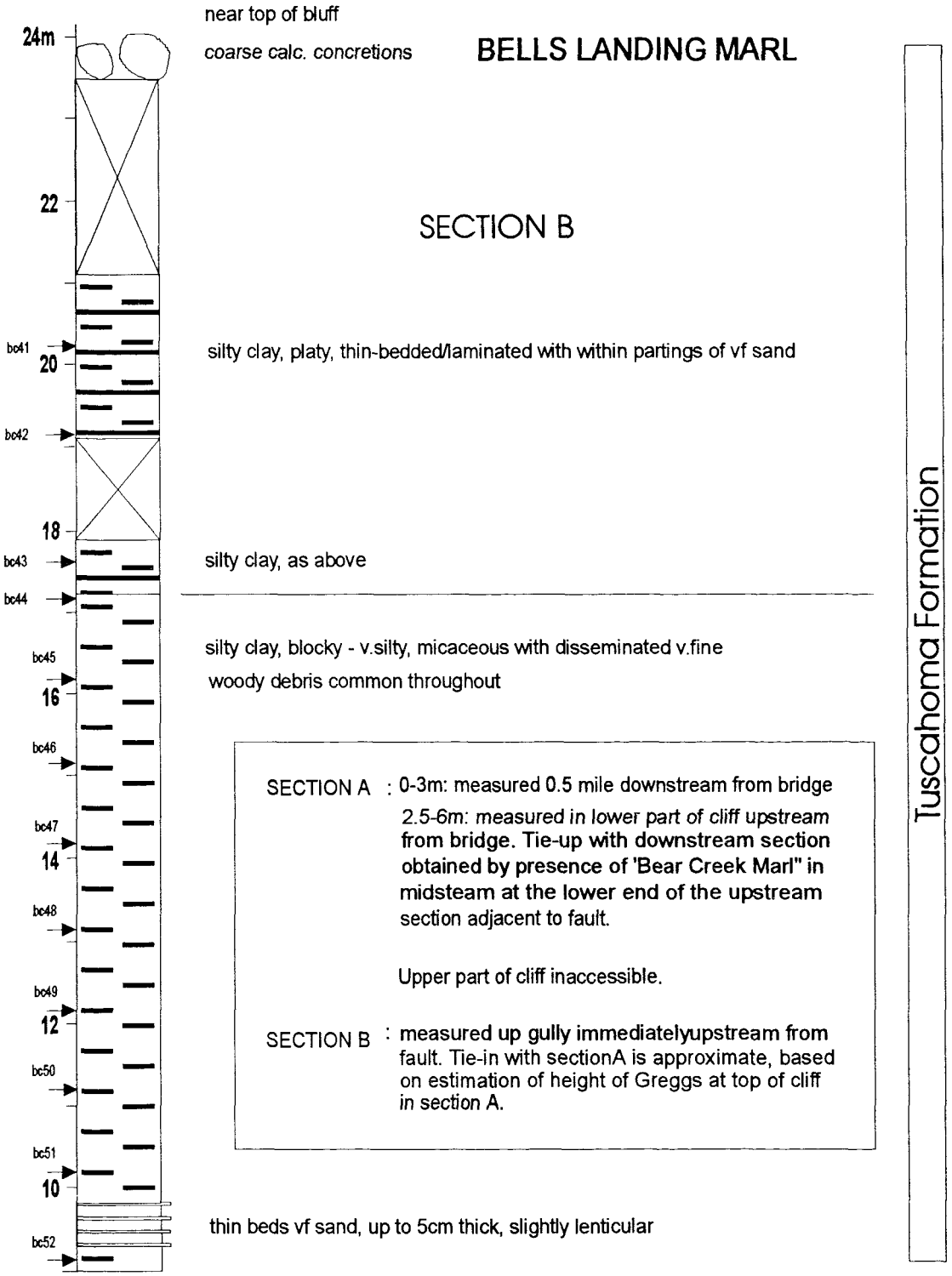

Figure 8-21 - contined *Stratigraphic log and sample sites at Bear Creek.*

consists of a clayey, fossiliferous, carbonaceous, glauconitic sand (Mancini, 1991). The upper unit, identified by King at this locality at approximately 26m up section, is the Bell's Landing Marl Member which consists of coarse calcareous concretions. The remainder of the Tuscahoma Sand at this locality consists of fresh interbedded sand, silt and clay. Mancini and Oliver (1981) have used planktonic foraminifers to place the 'Bear Creek Marl' almost at the base of the formation and the Bells Landing Marl Member at a stratigraphic height approximately near the middle of the Tuscahoma Formation.

A number of extensional faults with throws of approximately 2m are observed in the outcrop of the lower section. The upper Bear Creek section, upstream under the bridge of Highway 1 appears to be less faulted except for a single fault with a throw of about 5m. To the west of this fault a bivalve bed, approximately 0.7m in thickness, contains *Nucleana dentanium* which is a marine mollusc (King, pers. comm.). A high sedimentation rate occurred during this period with 15-20m of clays, silts and sands between the Bear Creek marl and the Gregg's Landing Marl Member.

Sampling

Hand samples were taken from 38 sites over a section interval of 26m where sites were restricted to predominantly homogeneous fresh clays and silts which exhibited IRM ratios typically >0.9 (Fig. 8-22).

The finer-grained fresh sediments at this location contrasted with the coarser and frequently weathered material of the Nanafalia Formation below. The increased NRM intensities (average 1.63mA/m compared to 0.38mA/m for the Nanafalia) and the consolidated nature of the sediments from the Tuscahoma Formation considerably aided sampling and sub-sampling and enabled smaller more convenient samples ($16cm^3$) to be demagnetised in the laboratory. All sites responded well to A.F. demagnetisation which was confirmed by the comparable behaviour of thermally demagnetised sub-samples from the same stratigraphic horizon. Temperature steps during thermal demagnetisation however, were kept below a threshold of 450°C at which point susceptibility measurements showed a systematic mineralogical change (Fig. 8-23).

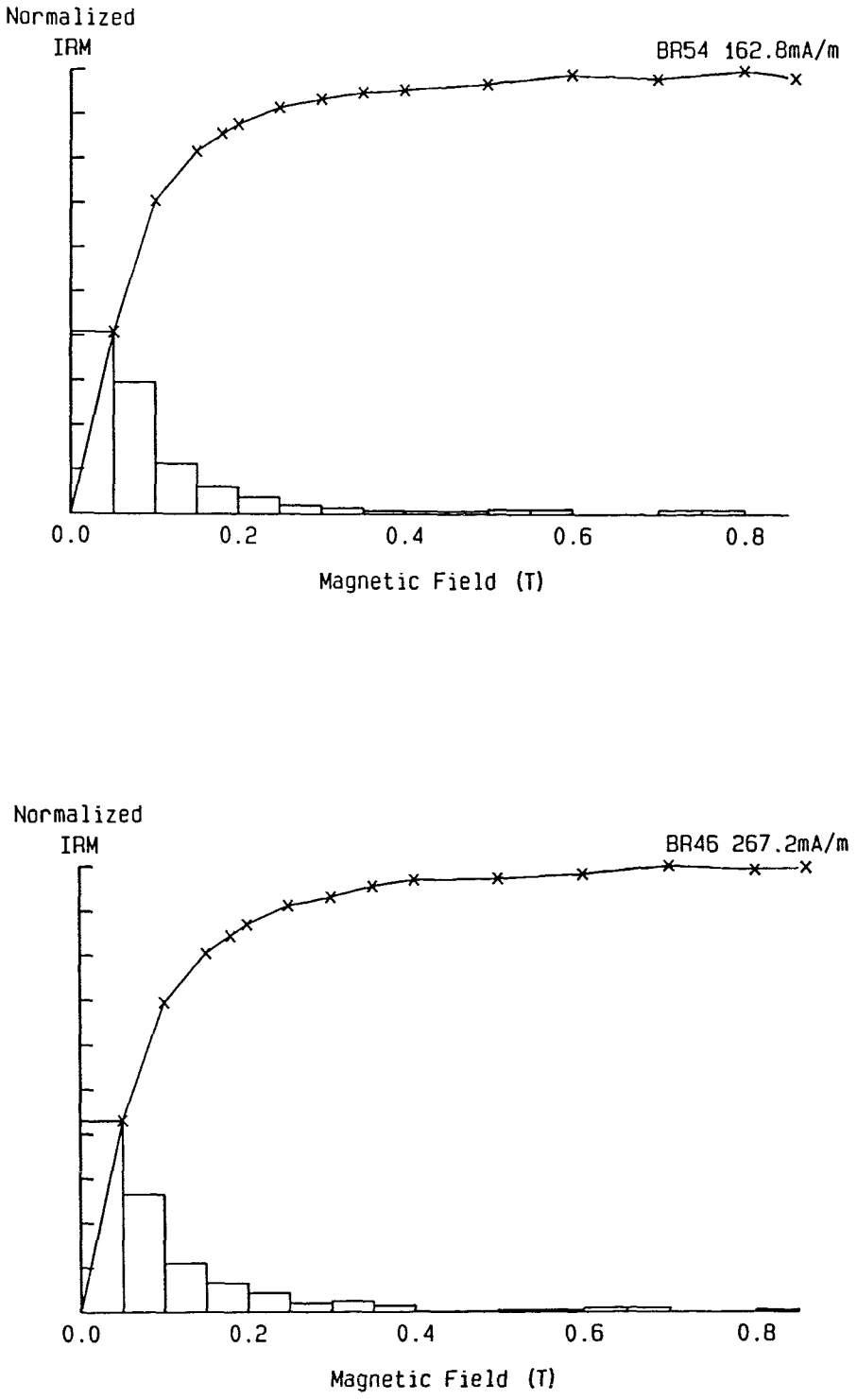

Figure 8-22 *Typical IRM acquisition curve for specimens from the Tuscahoma Formation at Bear Creek.*

Polarity analysis

Sediments at Bear's Creek exhibited clear reverse polarity behaviour where most samples gave reliable 'S1-category' SEP demagnetisation plots (for example: figures 8-24; appendix 12). The small number of samples that showed an affinity to a normal polarity (<5%) were confined to horizons that appeared to have a higher degree of weathering.

Figure 8-25 presents a palaeomagnetic summary for samples from the Bear Creek locality. The magnetic properties of the 38 sites analysed do not differ significantly. The combined data points of all SEP (S1 and S2 category) directions give a declination of 162.9° and inclination of -26.4° (95 = 7°, k = 10.5).

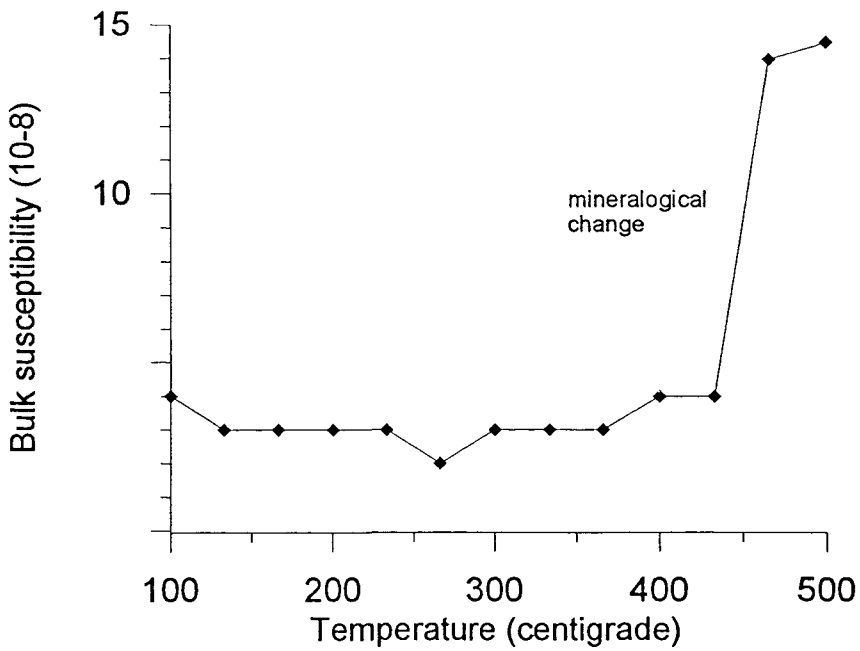

Figure 8-23 *Susceptibility behaviour seen during the heating of material from the Tuscahoma Formation at Bear Creek.*

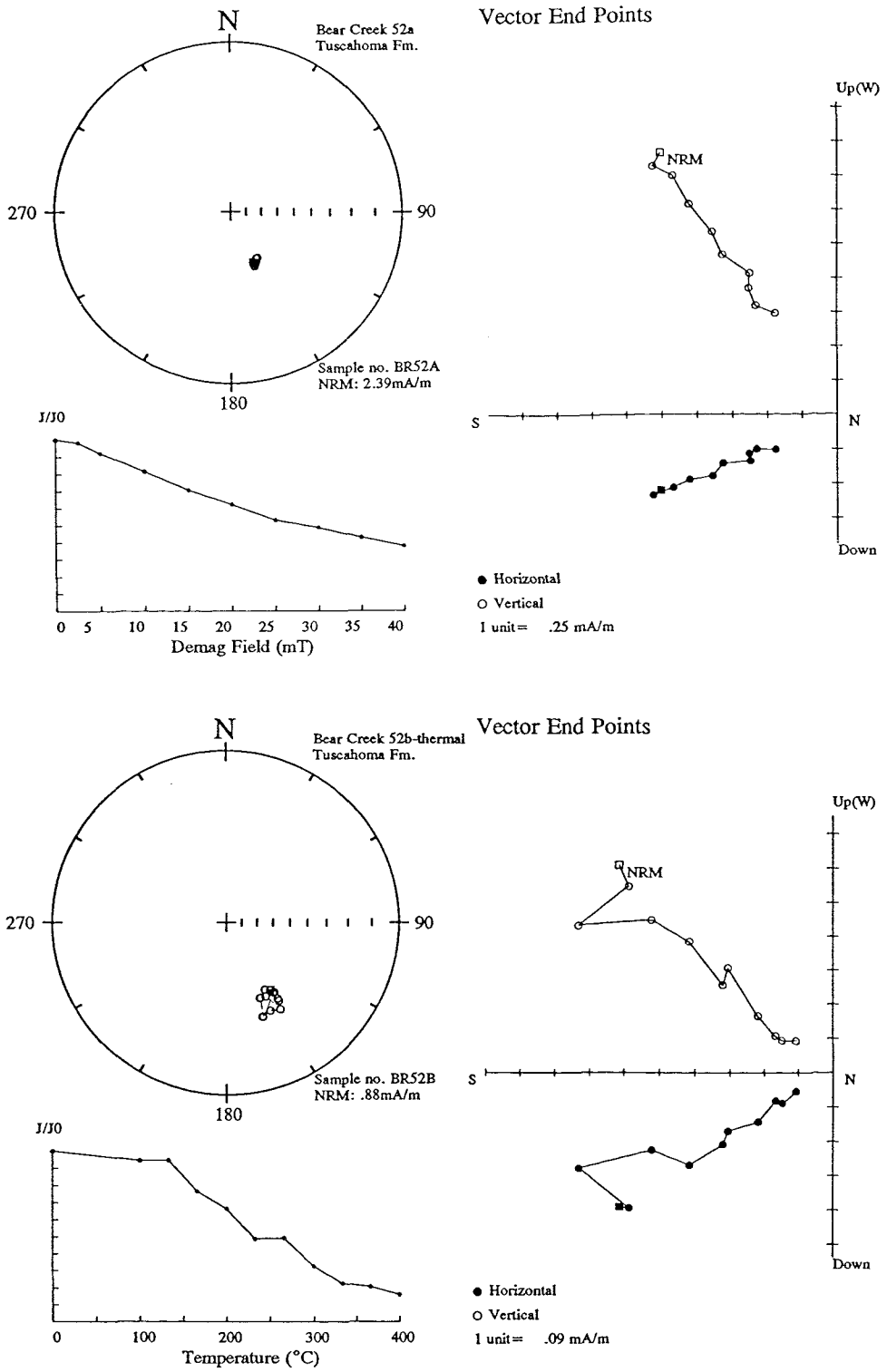

Figure 8-24 *A.F. and thermal demagnetisation behaviour of sediments from the Bear Creek locality.*

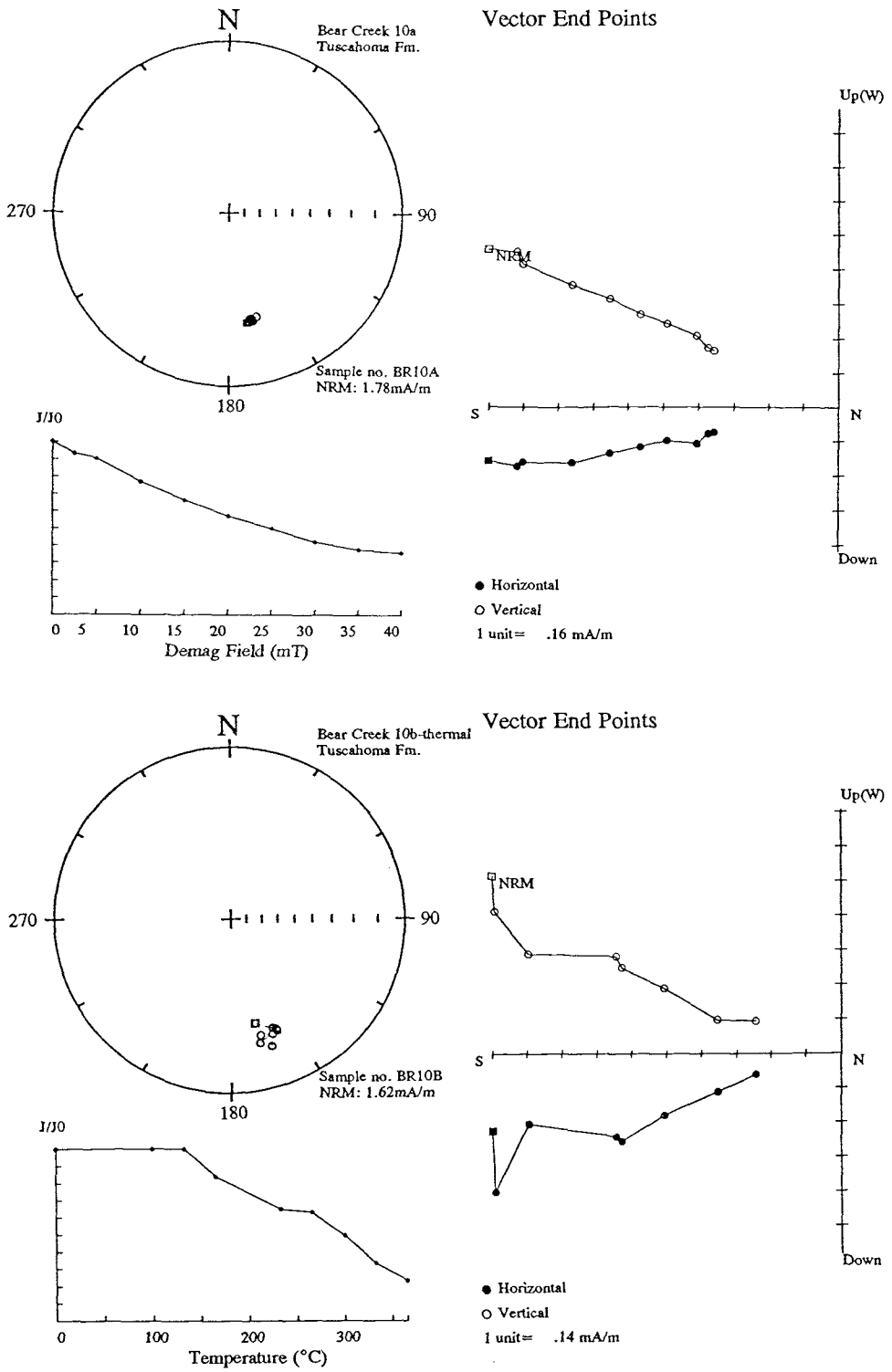

Figure 8-24 - *continued* *A.F. and thermal demagnetisation behaviour of sediments from the Bear Creek locality.*

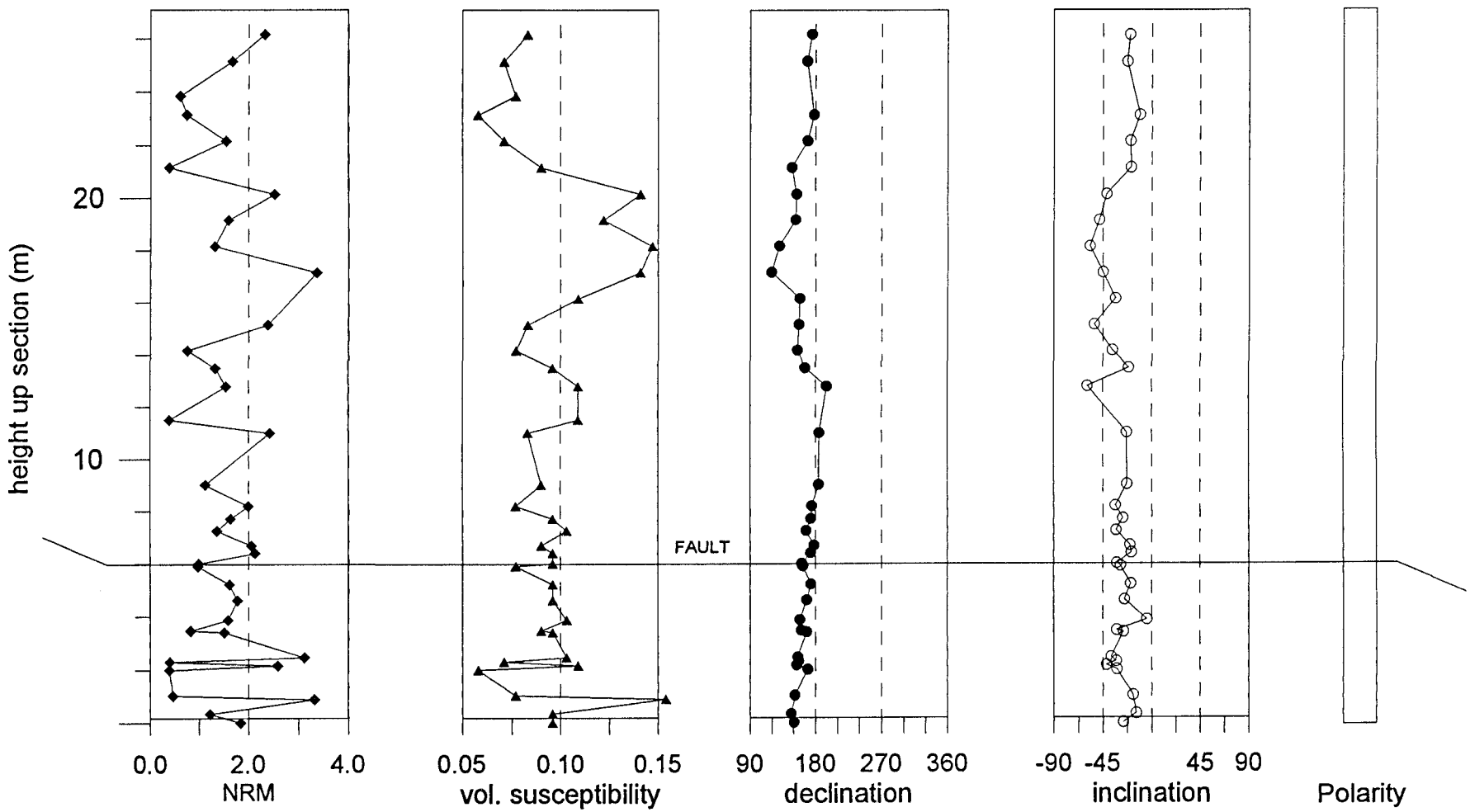

Figure 8-25 *Graphical summary of palaeomagnetic properties of samples from Bear Creek.*

8.2.1b Bear Creek road cutting

The sediments exposed in the road cutting 0.5km south of Bear Creek are probably located above the Bell's Landing Marl, illustrated at the top of the Bear Creek stratigraphic log (Fig. 8-21). The lithologies are very similar, with thinly bedded clay and silt laminated material (Fig. 8-26).

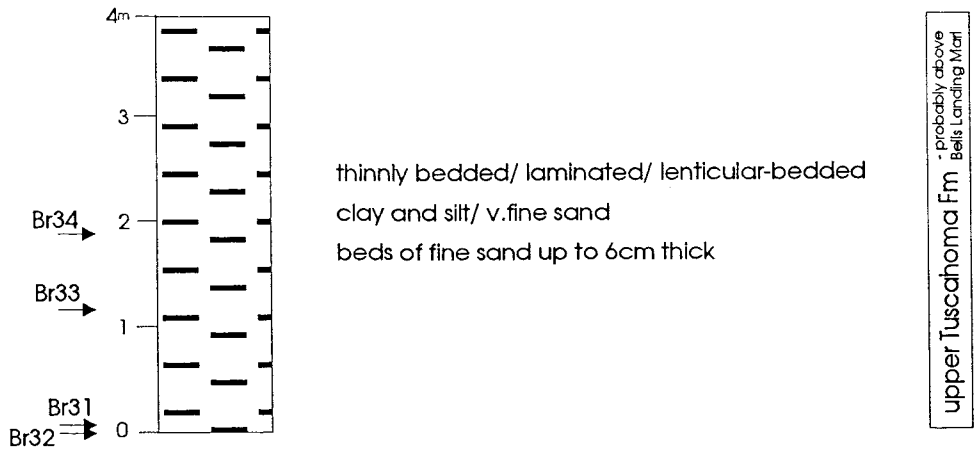

Figure 8-26 *Stratigraphic log of the sample sites at the Bear Creek road cut locality.*

Four samples were A.F.demagnetised and yielded reliable reverse polarity plots (Fig. 8-27; appendix 13).

Magnetostratigraphy of the Bear Creek localities

The reliable reverse polarity identified in these samples correlates with lower Chron C24r.

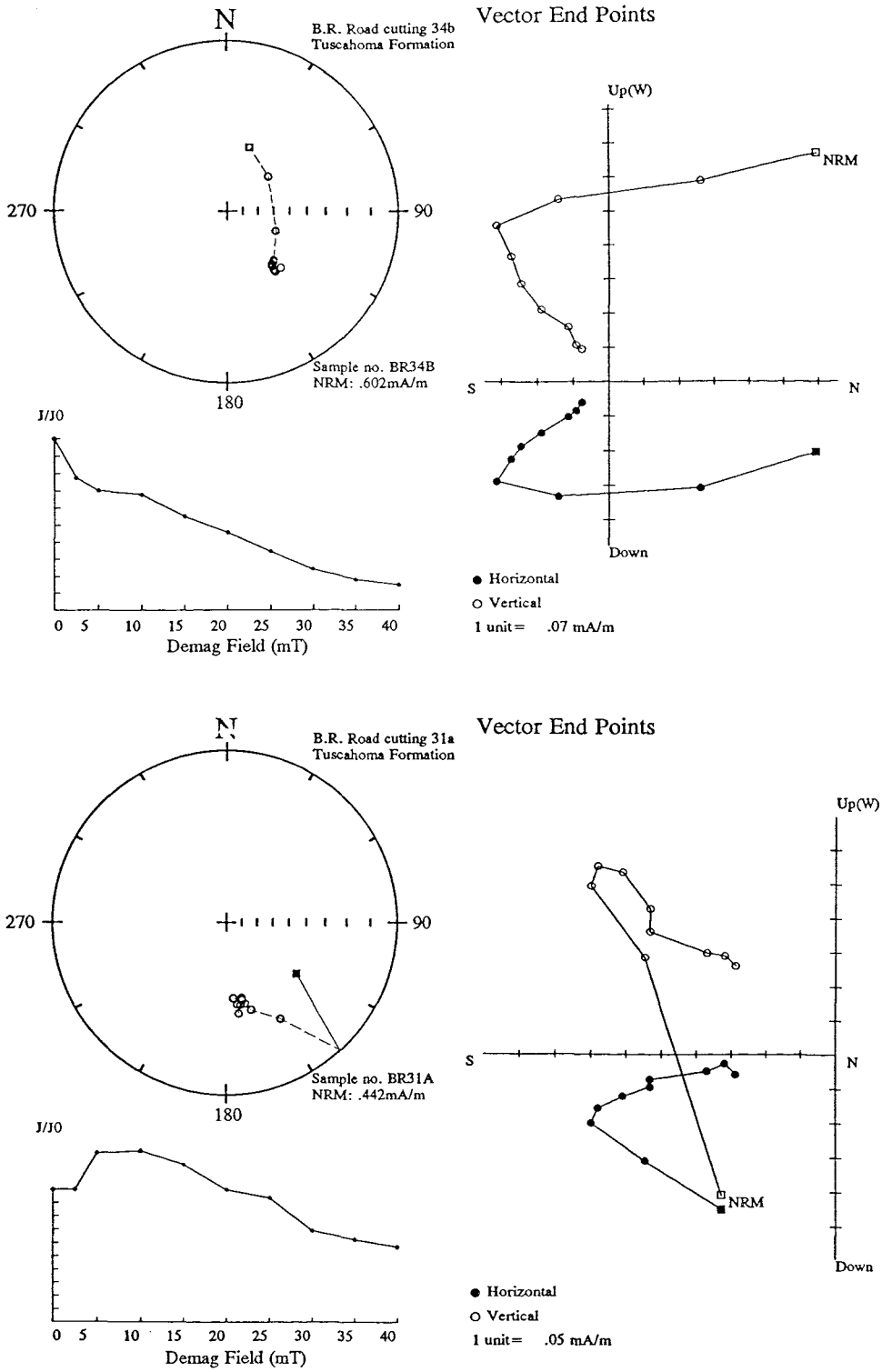

Figure 8-27 *A.F. demagnetisation behaviour of samples at Bear Creek road-cutting.*

8.2.2 Tuscahoma Landing locality

Location: Tuscahoma landing, Tombigbee River, Choctaw County, Alabama.

This is the type section of the Tuscahoma Formation (Smith et al, 1894). It consists of interlaminated silty clay, silt, fine-grained sand and marl. Eight sites were sampled over a 6m interval at the slipway itself (Fig. 8-28); the remainder of the section to the south along the Tombigbee River is only accessible by boat and was not sampled.

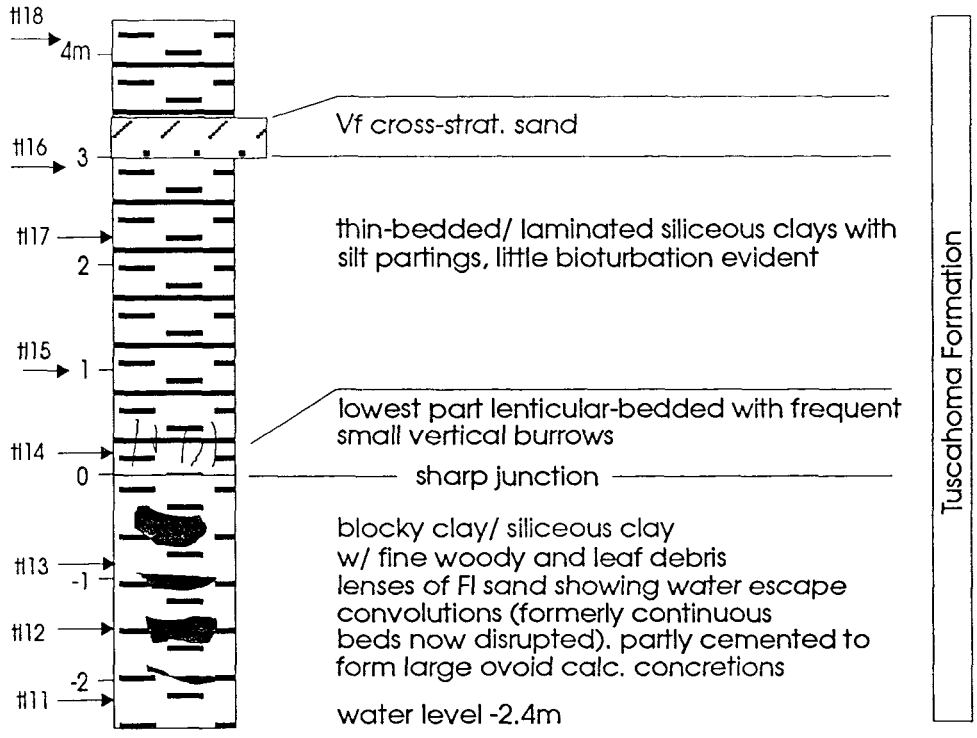

Figure 8-28 *Stratigraphic log and sample site positions at Tuscahoma Landing.*

Polarity analysis

IRM curves indicate magnetite-type saturation characteristics (Fig. 8-29). Thermal and A.F demagnetisation produced high quality data, with reverse polarity SEPs,

which were consistent with the declination and inclination observed in samples from Bear Creek (Fig. 8-30; appendix 14).

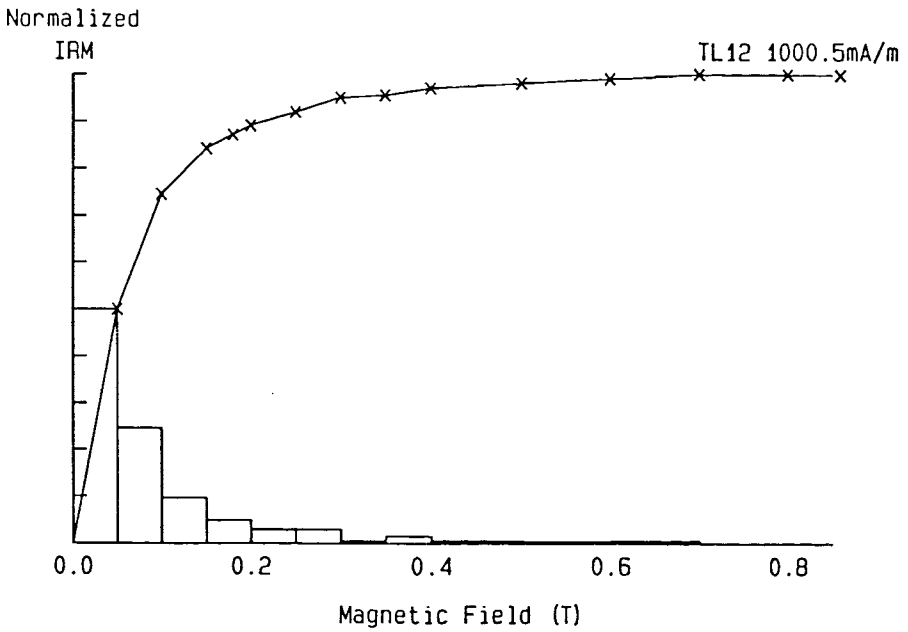

Figure 8-29 *Typical IRM curve from a sample from the Tuscahoma Landing locality.*

Magnetostratigraphy of the Tuscahoma Landing locality

The reliable reverse polarity identified in these samples correlates with Chron C24r.

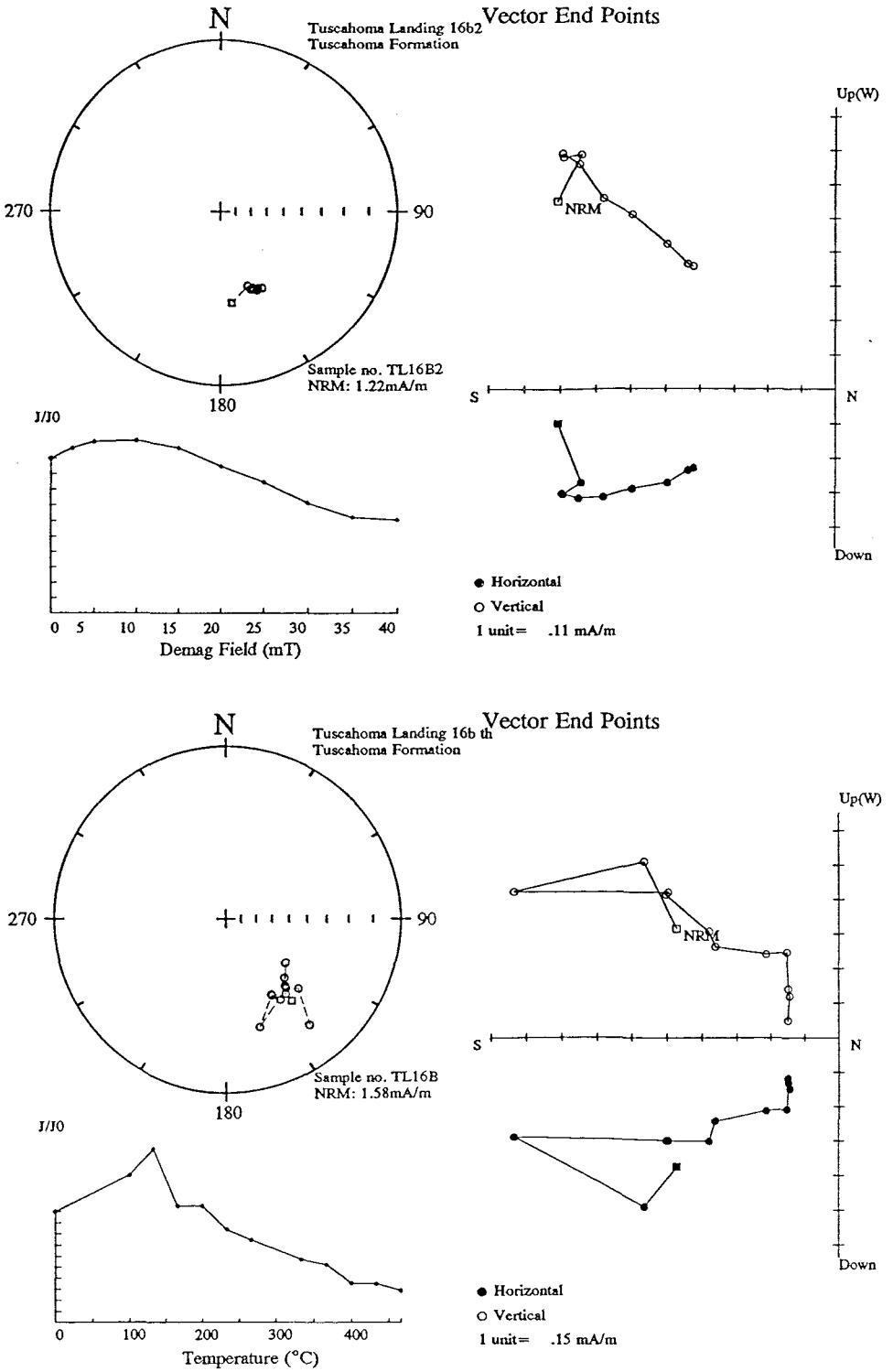

Figure 8-30 *Examples of the demagnetisation behaviour of samples from Tuscahoma Landing.*

8.2.3 Roaring Creek and Kolomokei Creek localities

Location: 8-9km south of Fort Gaines, State Route 39 crosses both Roaring Branch Creek and Kolomokei Creek, Clay County, Georgia.

Roaring Creek and Kolomokei Creek flow east-west into the Chattahoochee River exposing the silty clays and fine sands of the Tuscahoma Formation (Fig. 8-31 & 8-32).

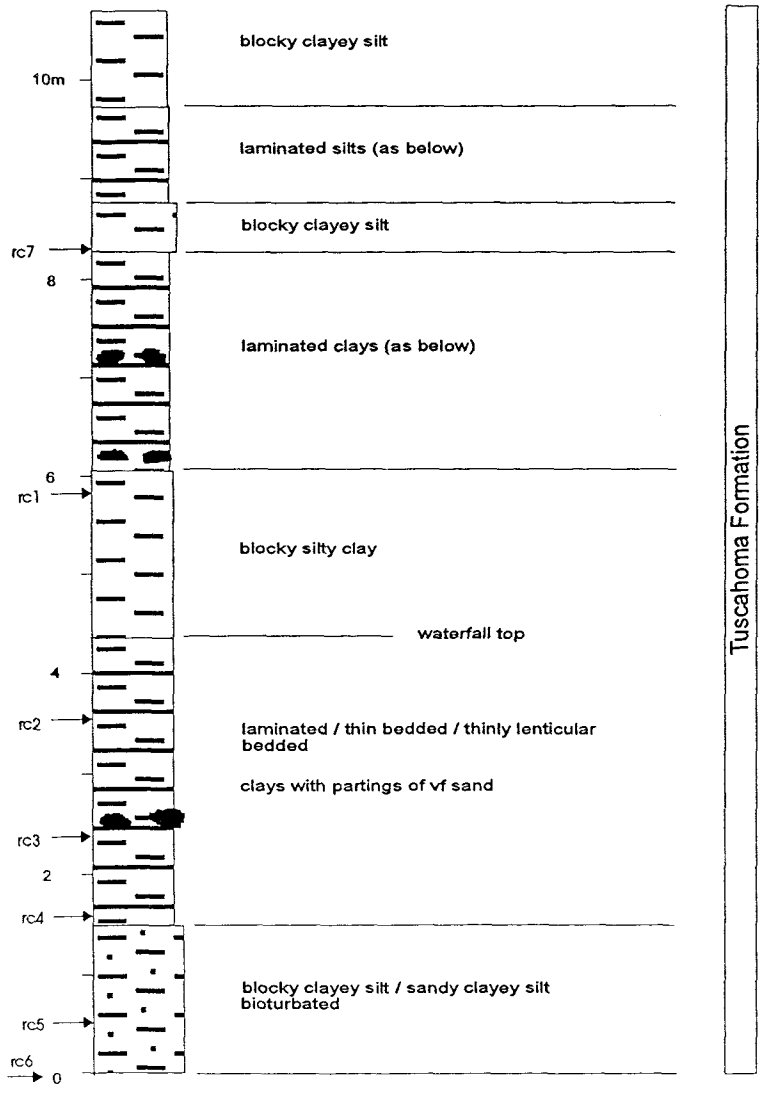

Figure 8-31 *Stratigraphic log and sample sites at the Roaring Creek locality.*

The medium to dark grey sand, silt and clay contained abundant carbonaceous debris, seen as fine woody fragments throughout the sampled intervals. Distinct calcareous concretions, large and regular in shape are present as prominent features along the length of the creek.

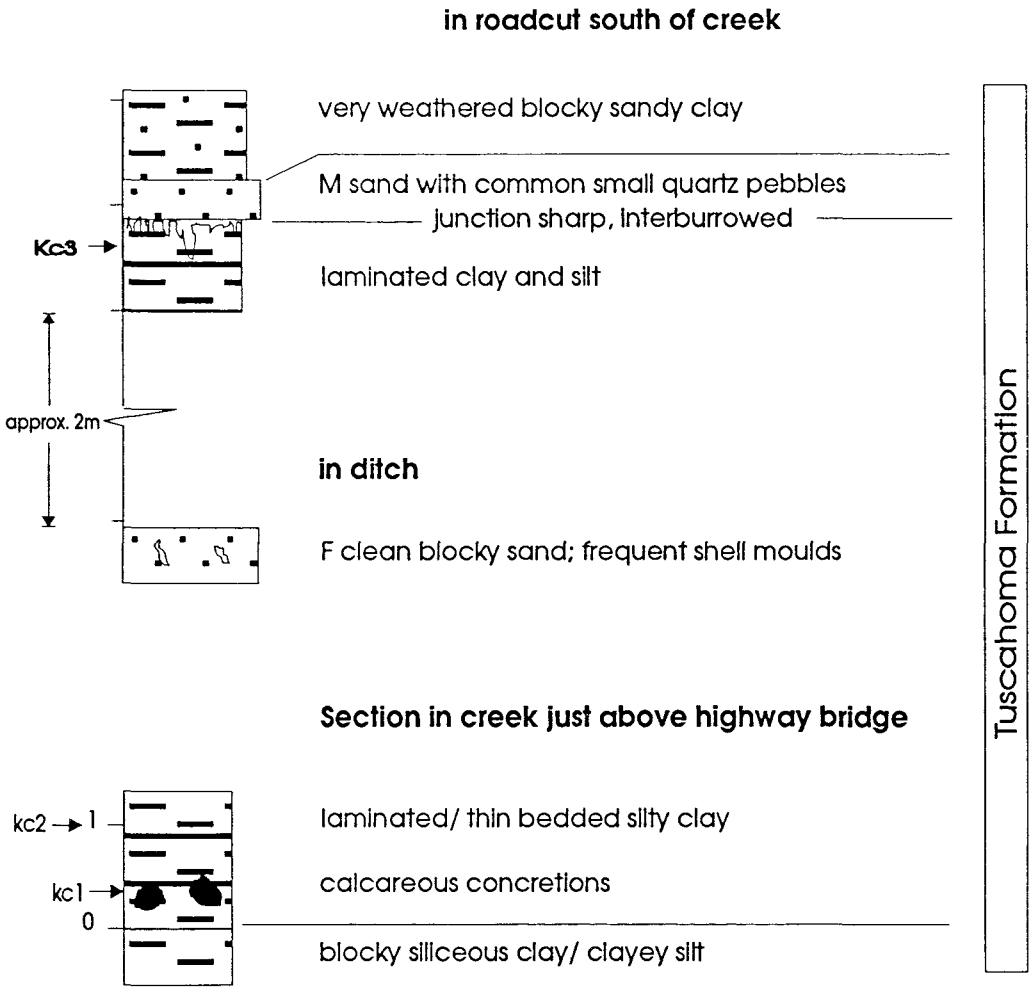

Figure 8-32 *Stratigraphic log and sample sites at the Kolomokei Creek locality.*

IRM analysis was consistent with material from Tuscahoma Landing and Bear Creek, showing early saturation of the magnetic minerals and indicating a dominance of magnetite (Fig. 8-33).

Polarity analysis

Thermal and A.F. demagnetisation of samples from Roaring Creek and Kolomokei Creek show the typical reverse polarity directions of the Tuscahoma Formation (Fig. 8-34 and 8-35; appendices 15 and 16).

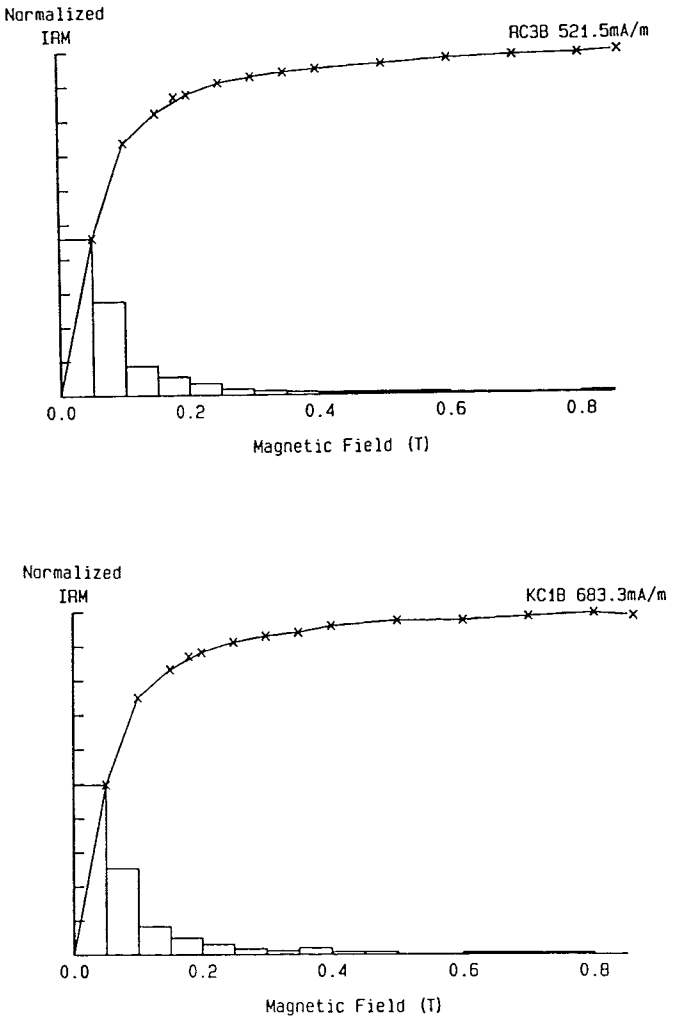

Figure 8-33 *IRM acquisition curves of sample from Roaring Creek (RC3b) and Kolomokei Creek (KC1b).*

Magnetostratigraphy of Roaring Creek and Kolomokei Creek

The reliable reverse polarities seen at these locations correlate with Chron C25r.

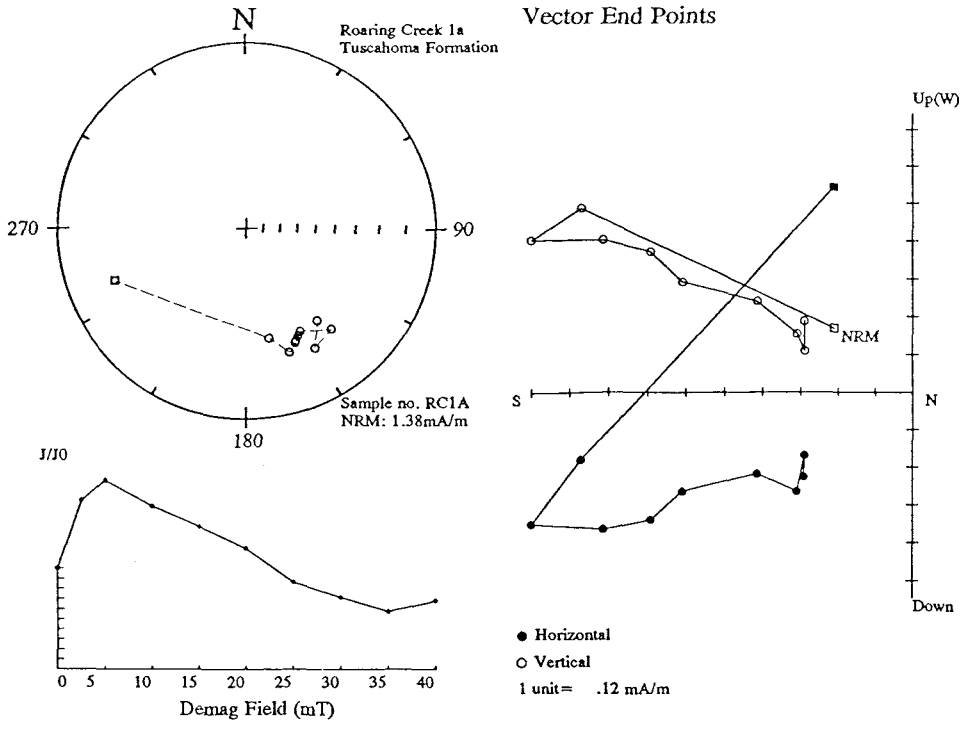

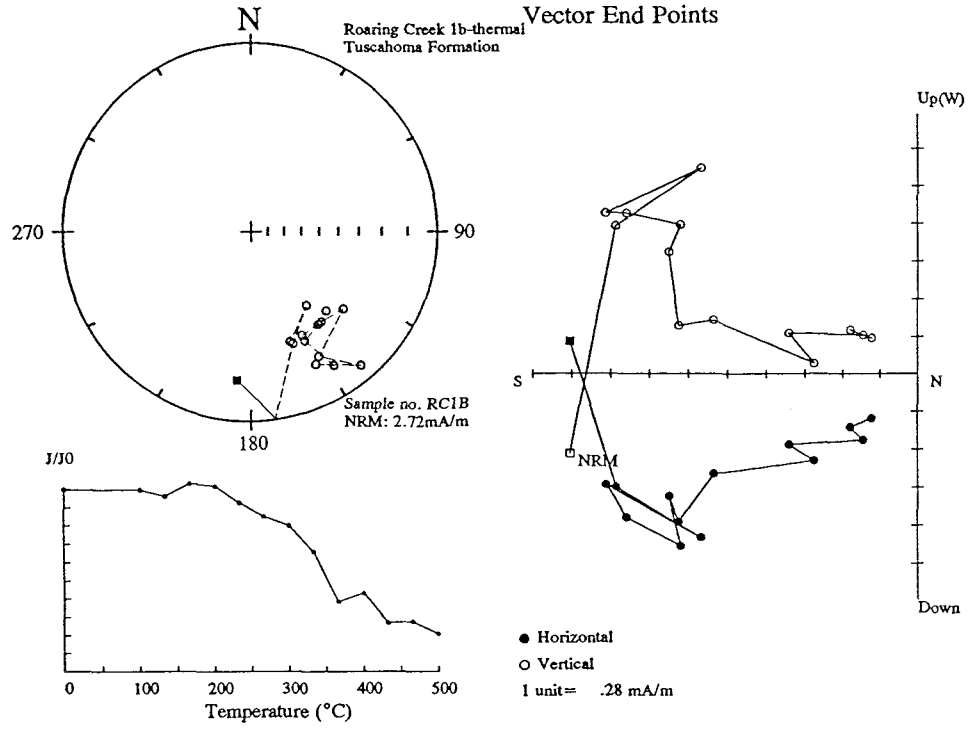

Figure 8-34 *Reverse polarity demagnetisation behaviour of samples from Roaring Creek.*

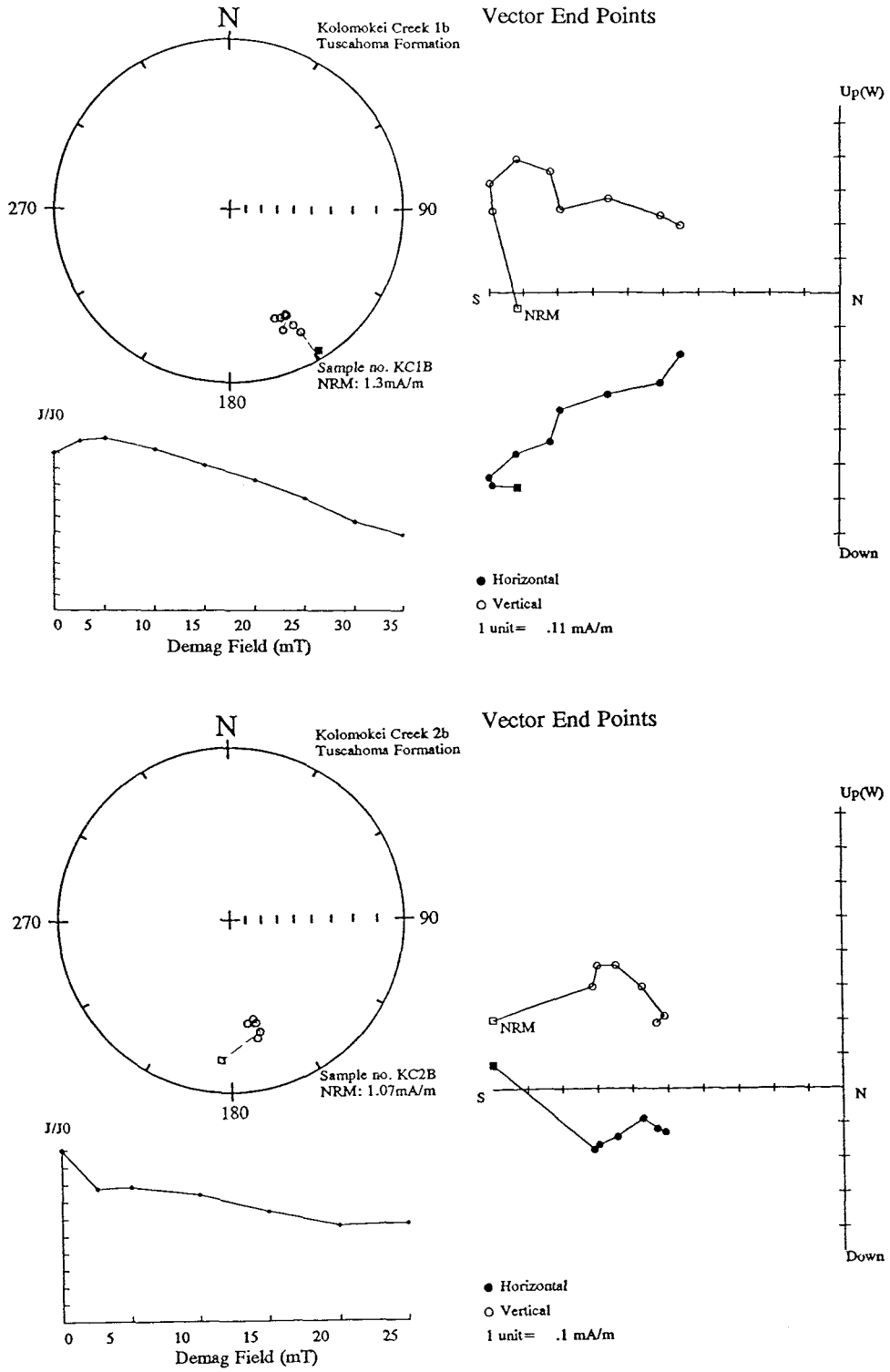

Figure 8-35 *Reverse polarity demagnetisation behaviour of samples from Kolomokei Creek.*

8.2.4 Bennett's Creek locality

Location: 2km north of Hayes, Henry County, Alabama.

Bennett's Creek is a short section of thin bedded clays and silts with abundant fine woody debris (Fig. 8-36). Three layers of large ovoid calcareous concretions up to 80x30cm are present which probably correlate across the Chattahoochee River 5km to the east with the similar sections at Roaring Creek and Kolomokei Creek.

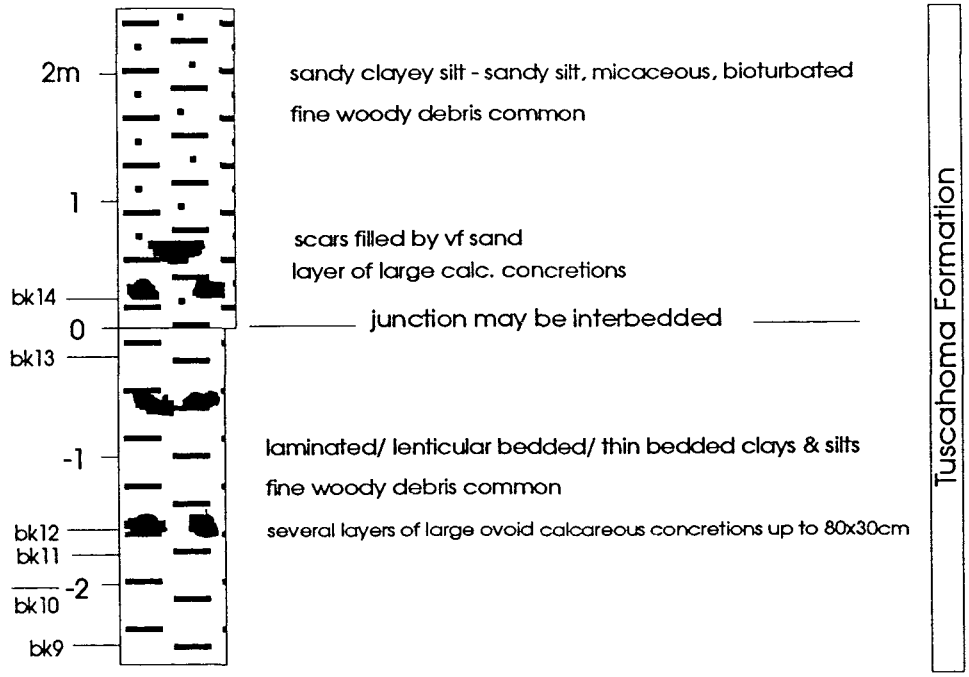

Figure 8-36 *Stratigraphic log and sample sites at Bennett's Creek.*

The palaeomagnetic characteristics of samples at Bennett's Creek that have been investigated using A.F. and thermal demagnetisation are entirely consistent with other Tuscahoma material (Fig. 8-37). Reliable SEPs show a primary component of reverse magnetisation which correlates with Chron C25r (appendix 17).

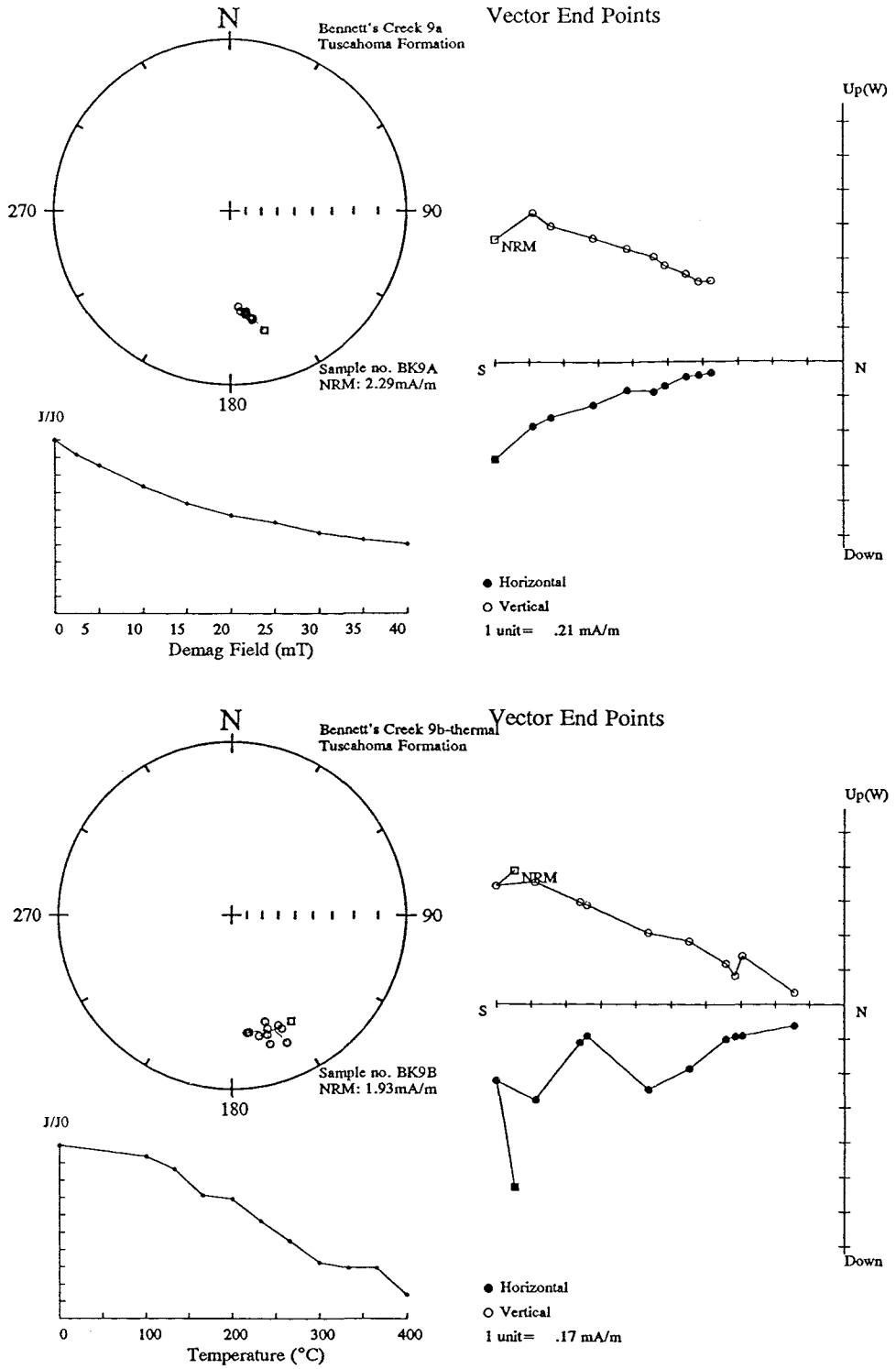

Figure 8-37 A.F. and thermal demagnetisation behaviour of a sample from Bennett's Creek.

8.2.5 Peach Tree locality

Location: Peach Tree Landing, west of Peach Tree Village, Alabama River

At Peach Tree Landing, the Bell's Landing Marl disconformably overlies the Tuscahoma silts and clays (Fig. 8-38). The Bell's Landing Marl is exposed here as a highly fossiliferous decalcified fine-grained sand containing large ovoid-flattened calcareous concretions. The clays and silts below are typical Tuscahoma sediments of thin-bedded clays occasionally blocky with fine woody debris common.

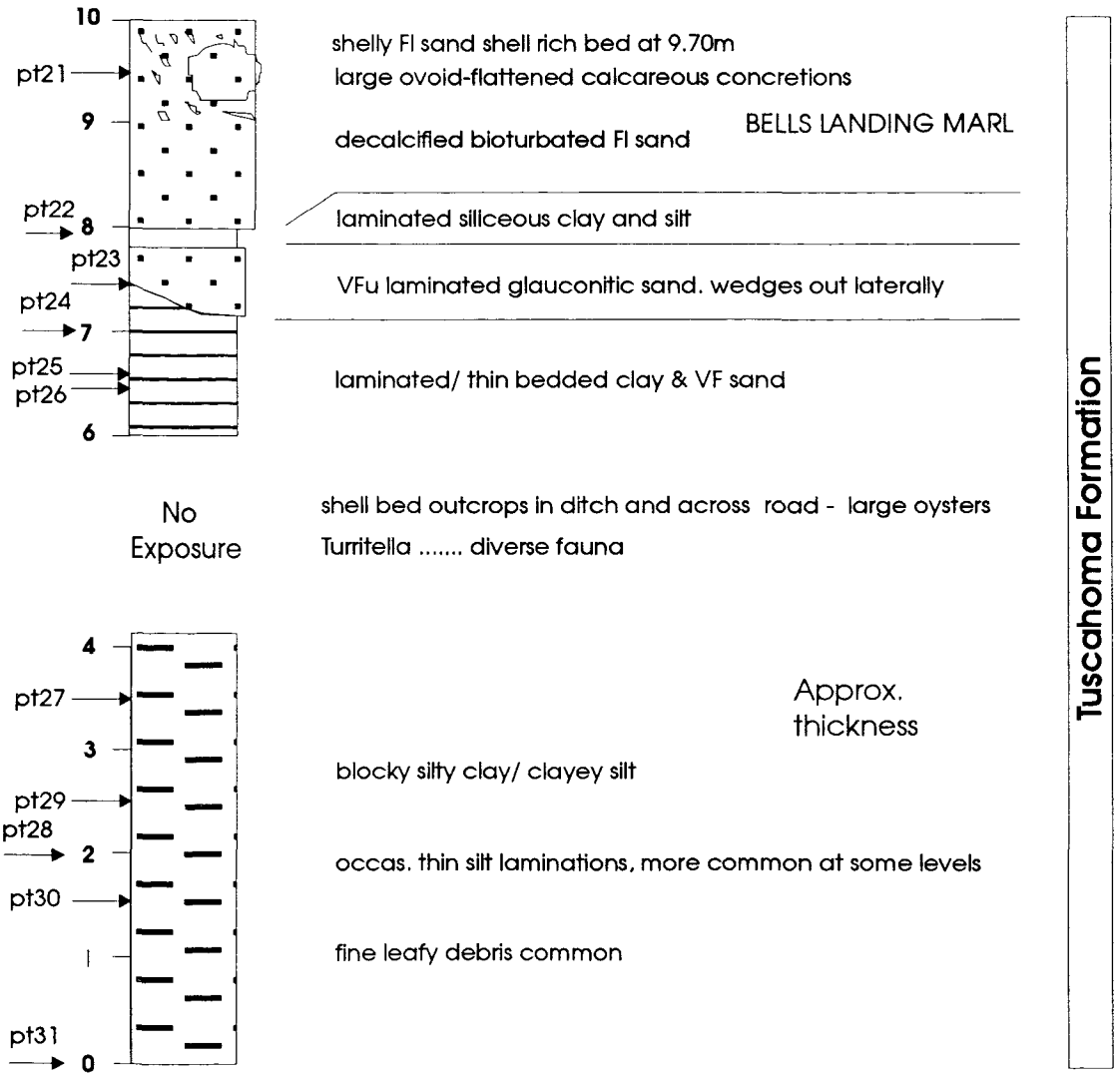

Figure 8-38 *Stratigraphic log and sample sites at Peach Tree landing.*

Samples were taken from both the Bell's Landing Marl and the clay intervals beneath and demagnetised by thermal and A.F. demagnetisation techniques

Polarity analysis

The demagnetisation behaviour of the clay material gave reliable SEPs with a reverse polarity that was consistent with other Tuscahoma outcrops (Fig. 8-39). The Bell's Landing Marl samples also exhibited a reverse polarity but the negative component of primary magnetisation was not as well preserved as that found in the clays and was only identified by the trending behaviour during successive demagnetisation steps (Fig. 8-40).

Magnetostratigraphy of Peach Tree Landing

The reverse primary magnetisation this section corresponds to Chron C25r.

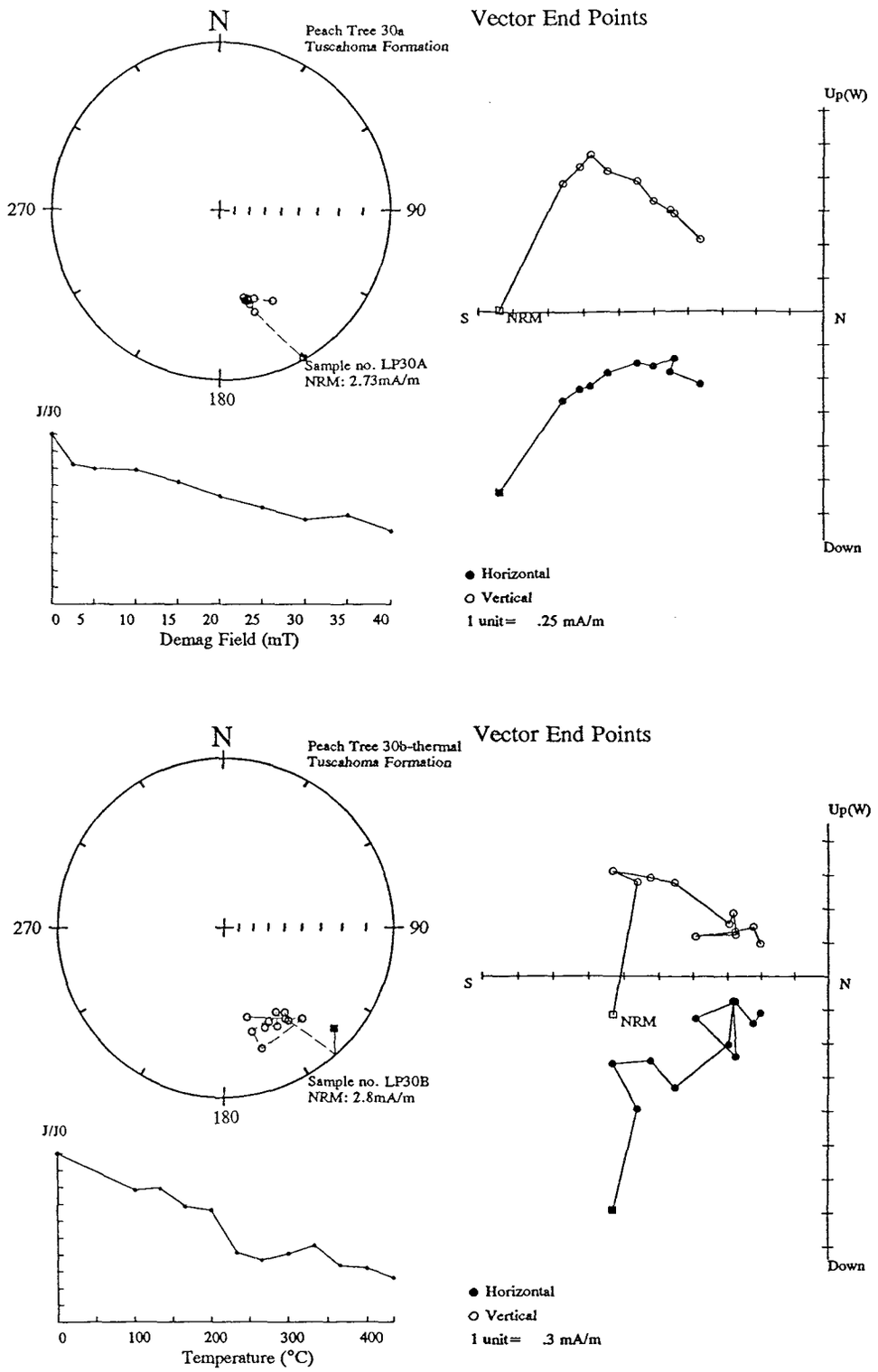

Figure 8-39 *A.F. and thermal demagnetisation behaviour of clay sediments from Peach Tree Landing.*

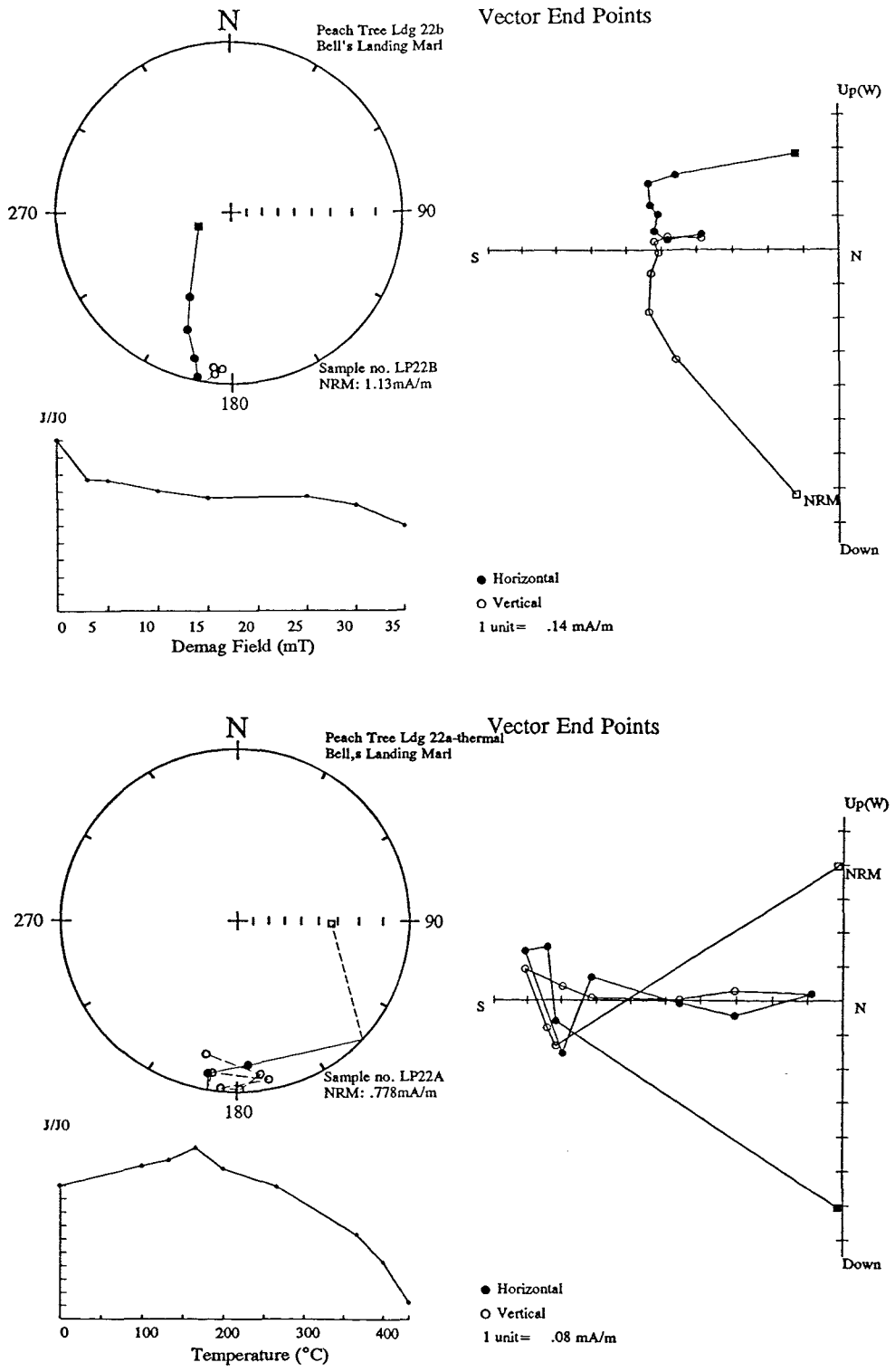

Figure 8-40 *A.F. and thermal reverse polarity trends of samples from the Bell's Landing Marl member at Peach Tree Landing.*

Chapter 9 Magnetostratigraphy of early Eocene field sections of Alabama

9.1 Hatchetigbee Formation outcrops

9.1.1 Tunnel Springs locality

Location: Railway cutting at the north-western entrance to the tunnel 4km north of Tunnel Springs, Monroe County, Alabama.

The Tunnel Springs section exposures 9m of Hatchetigbee sediments, the Tallahatta /Hatchetigbee contact and approximately 6m of Tallahatta material (Fig. 9-1). The lowest 3m of section contains a shelly interval which includes calcareous nannofossil species of lower NP10 (Gibson, 1981). Above this interval the sediments are decalcified and no biostratigraphic control is available. If the section is characteristic of the typical relationship between the two formations, however, a considerable hiatus at their contact may exclude some, if not all of material of NP11 age from the sedimentary record.

Block samples were taken from 12 sites over the first 11m of the section; these were typically split into 2-3 sub-samples and demagnetised by A.F. and thermal demagnetisation methods. IRM analysis was carried on samples from 3.7m, 4.7m, 5.3m, 6.9m and 10m, all of which yielded curves that exhibited fast initial rates of saturation suggesting that magnetite was the dominant magnetic mineral present (Fig. 9-2).

Polarity analysis

The quality of demagnetisation data was generally poor which was probably a function of the weak intensities and the altered state of much of the largely unconsolidated sediments from this outcrop. The average NRM intensity was 0.09mA/m although between 5m and 12m in the section it was reduced to 0.049mA/m; these values rarely decreased below 50% of their initial value during demagnetisation.

The demagnetisation behaviour from 66% of the samples showed low-confidence polarity determinations which were classified as categories T3 and S3 (Appendix 9-1).

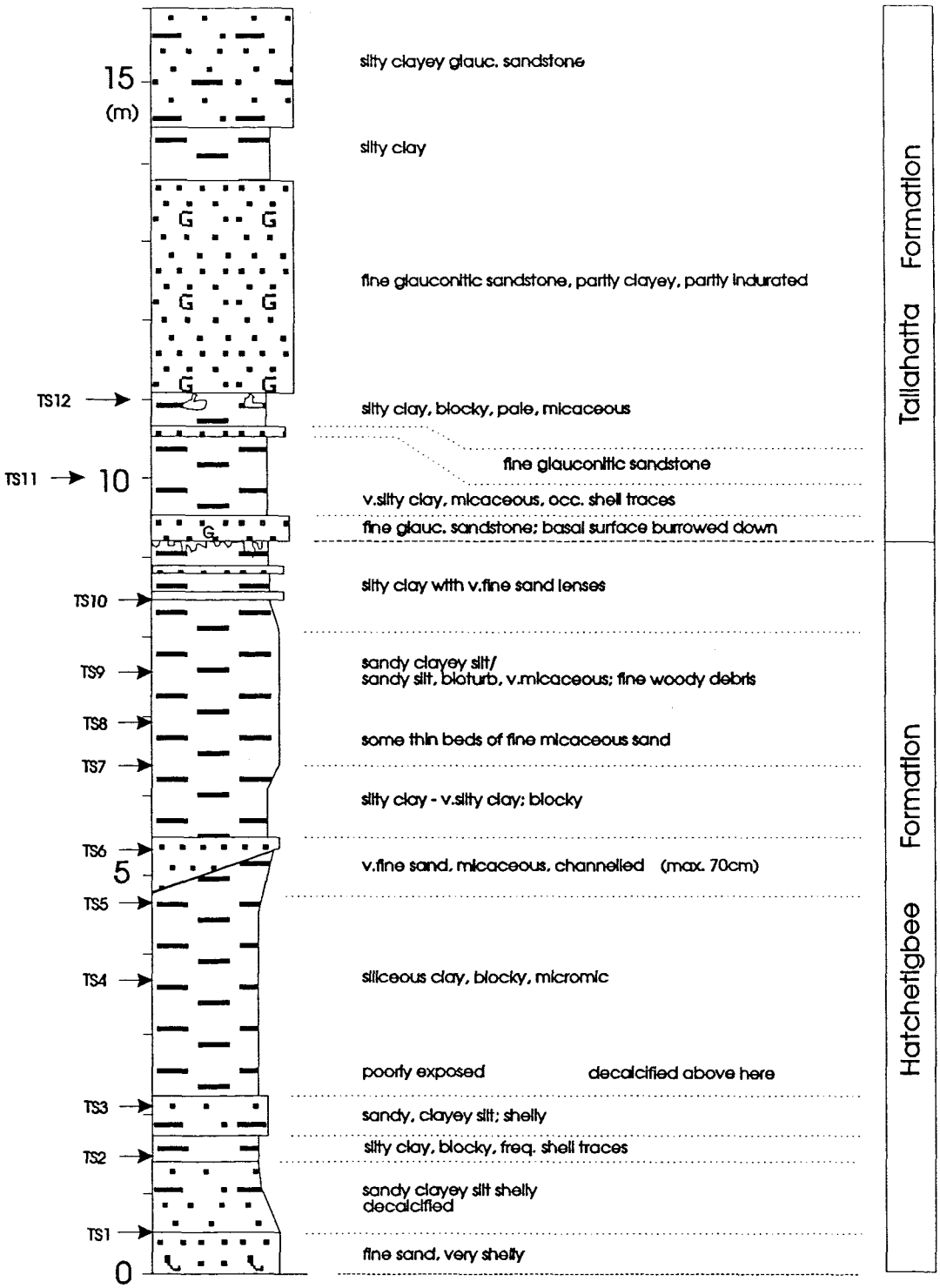

Figure 9-1 *Stratigraphic log and location of sample sites at the Tunnel Springs locality.*

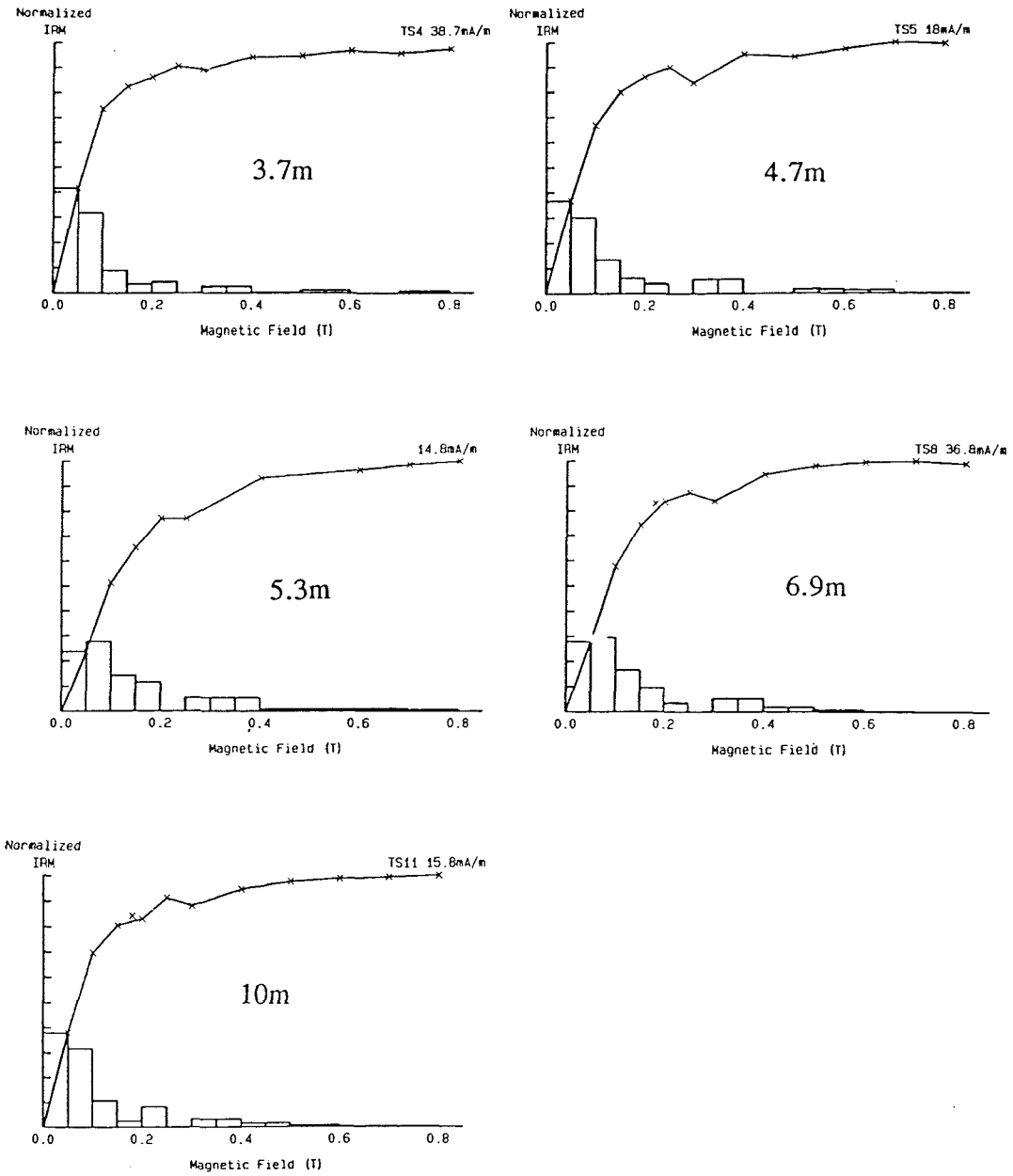

Figure 9-2 *IRM acquisition curves for 5 sites at Tunnel Springs.*

A further 14% exhibited anomalous normal polarities with a southerly declination. However, 57% of the total number of samples showed some affinity to a reverse polarity which was particularly emphasised by the consistency in the response of thermally treated sub-samples at each site.

Figures 9-2, 9-3 and 9-4 for instance, illustrate the behavioural difference between responses of the samples to the A.F. and thermal techniques from sub-samples at 2.1m, 6.3m and 10m in the section. Although the polarity determination may be questionable, there is a clear correlation of negative inclination values from thermal samples and an agreement of positive inclinations from A.F. samples (which may show possible trends to reverse or not). The differences between NRM directions between thermal and A.F. demagnetised sub-samples is attributed to the different storage conditions of the samples prior to measurement.

Magnetostratigraphy of the Tunnel Springs locality

Due to the poor quality of palaeomagnetic data a confident polarity assessment of each sampling site is not possible. Assuming that A.F. demagnetisation is unsuccessful at isolating the reverse polarity, throughout the section there is a predominance of reverse polarities.

A hiatus that has excluded NP11 material from this location (proposed by Gibson, 1981) is tentatively confirmed by the data in this study as there is no significant evidence for Chron C24n being present in the upper Hatchetigbee Formation at Tunnel Springs. If this is correct then the reverse polarities identified here indicate that this section should be correlated, at least at the base, with Chron C24r where NP10 zone is identified.

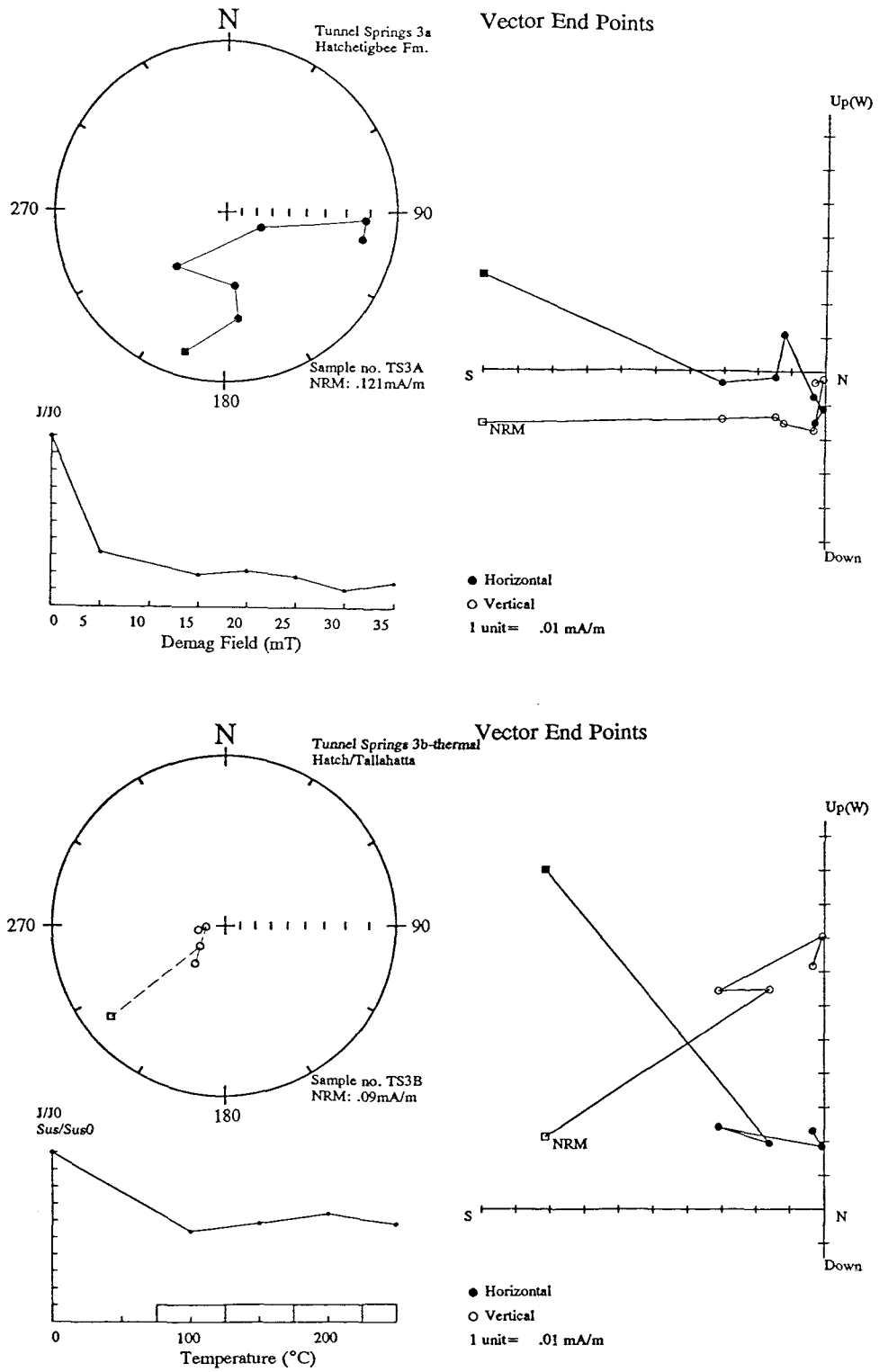

Figure 9-3 *A.F. and thermal demagnetisation behaviour of sub-samples at 2.1m.*

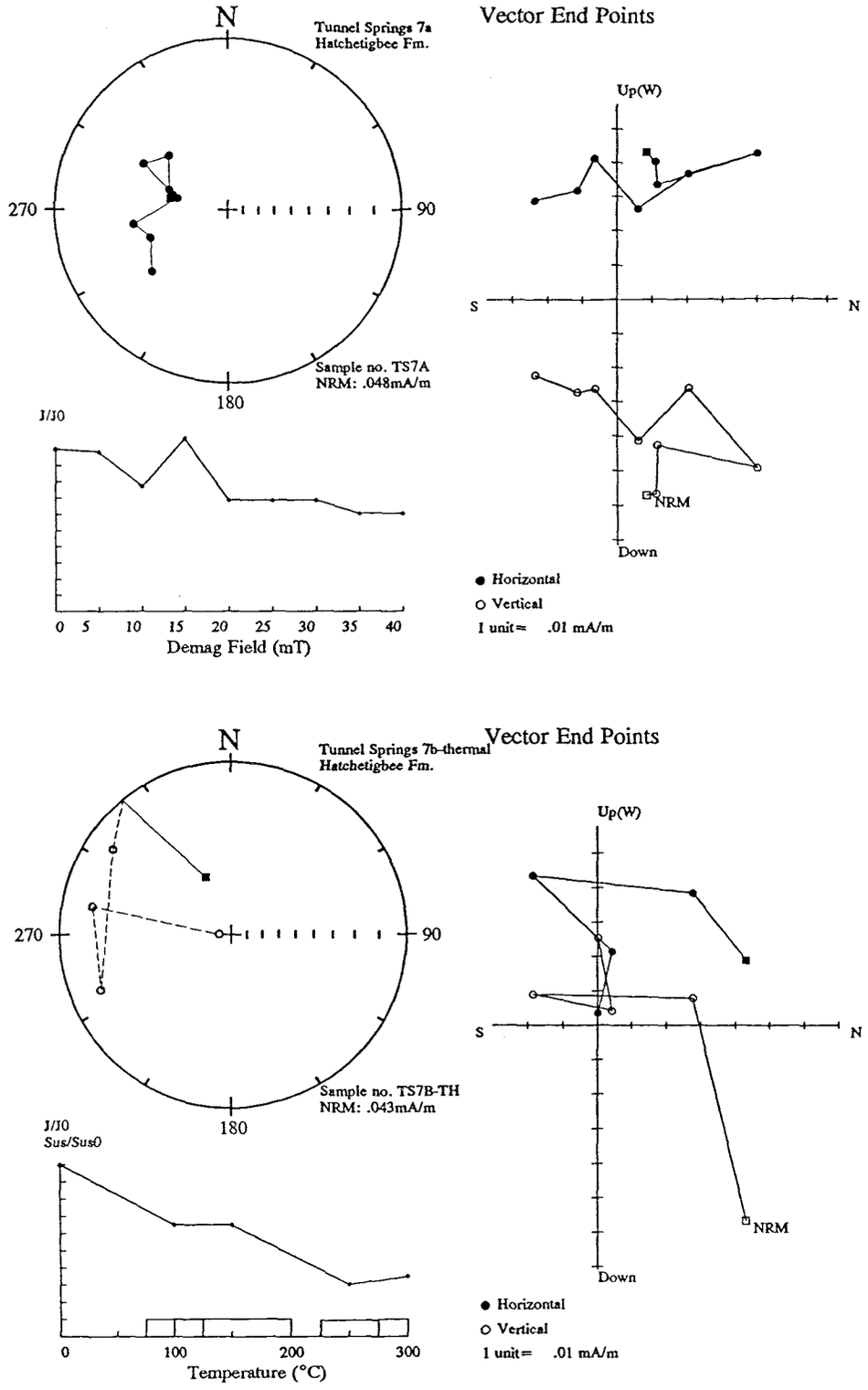

Figure 9-4 *A.F. and thermal demagnetisation behaviour of sub-samples at 6.3m.*

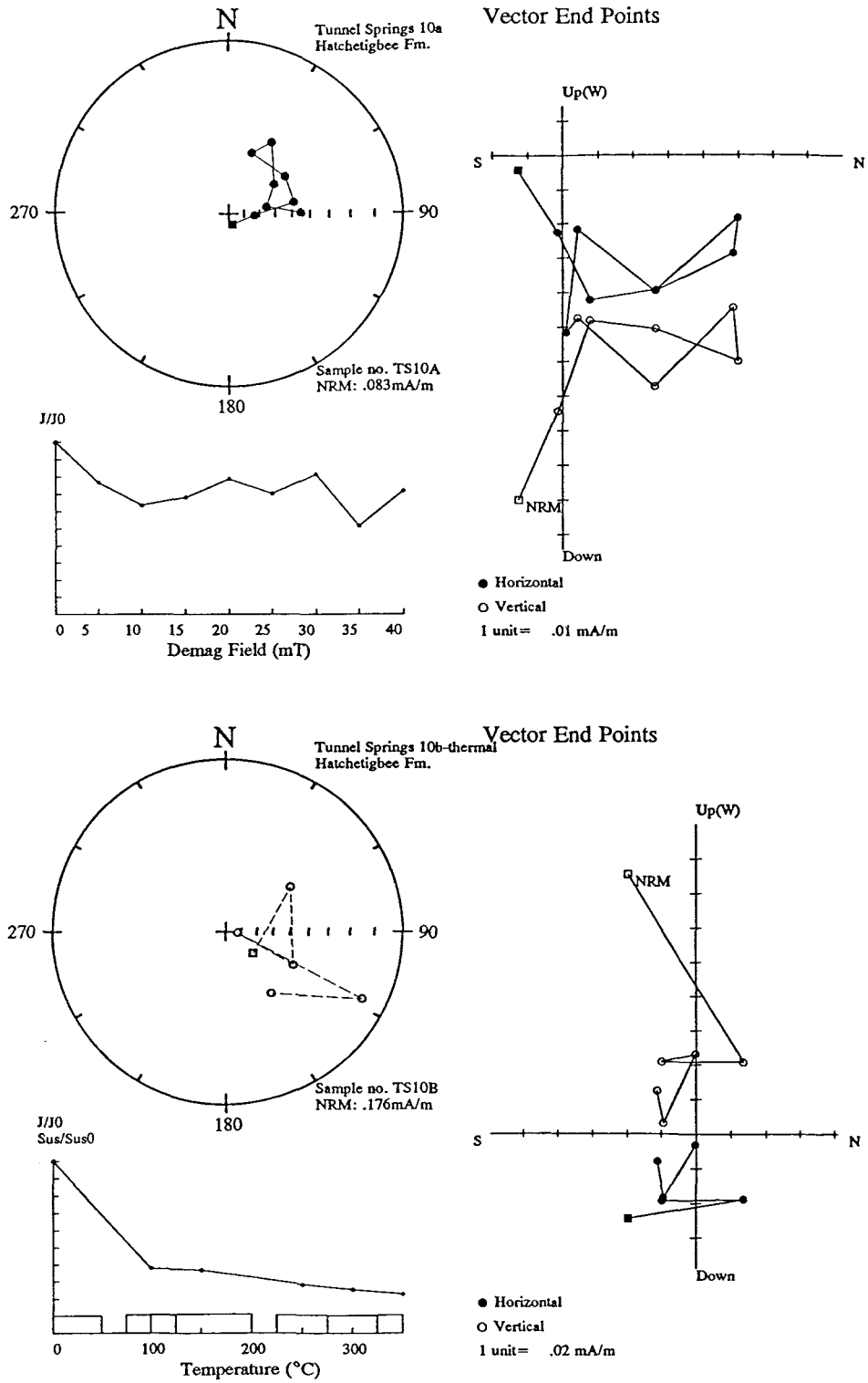

Figure 9-5 *A.F. and thermal demagnetisation behaviour of sub-samples at 10m.*

9.1.2 Hatchetigbee Bluff locality

Location: On the west bank of the Tombigbee River, 5.5km east of Frankville, Washington County, Alabama.

The geological section at this locality, which is the type section for the Hatchetigbee Formation, includes the upper part of the upper unnamed member of the Hatchetigbee.

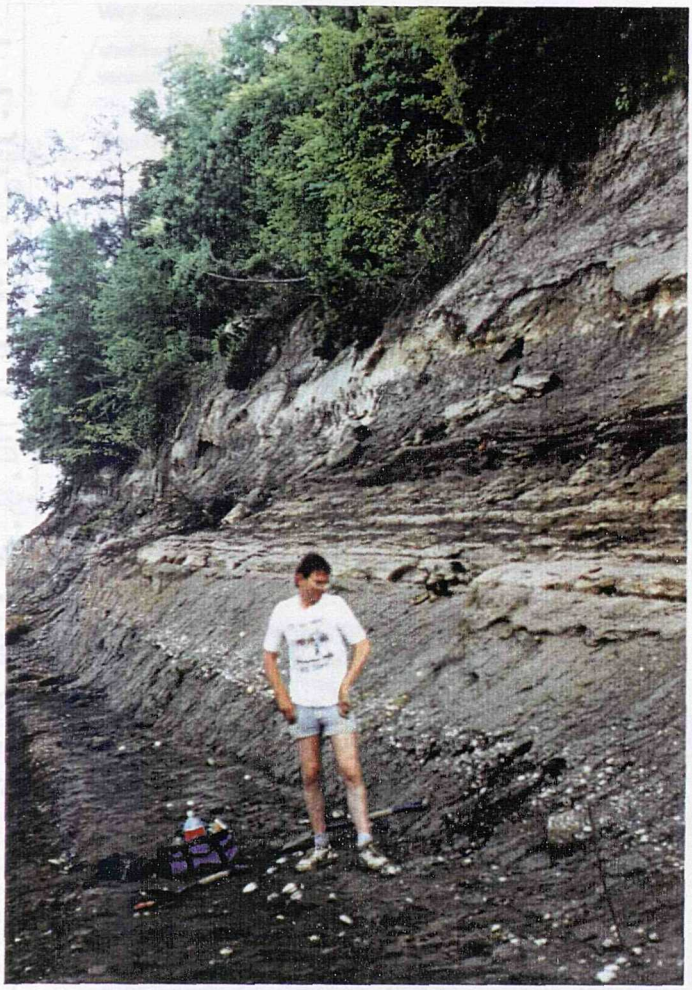

Plate 9-1 Hatchetigbee Bluff

The Hatchetigbee anticline brings the unit to the surface a considerable distance downdip from most outcrops of the formation. Behind the main bluff away from the river the weathered and slumped lower part of the overlying Tallahatta Formation is exposed.

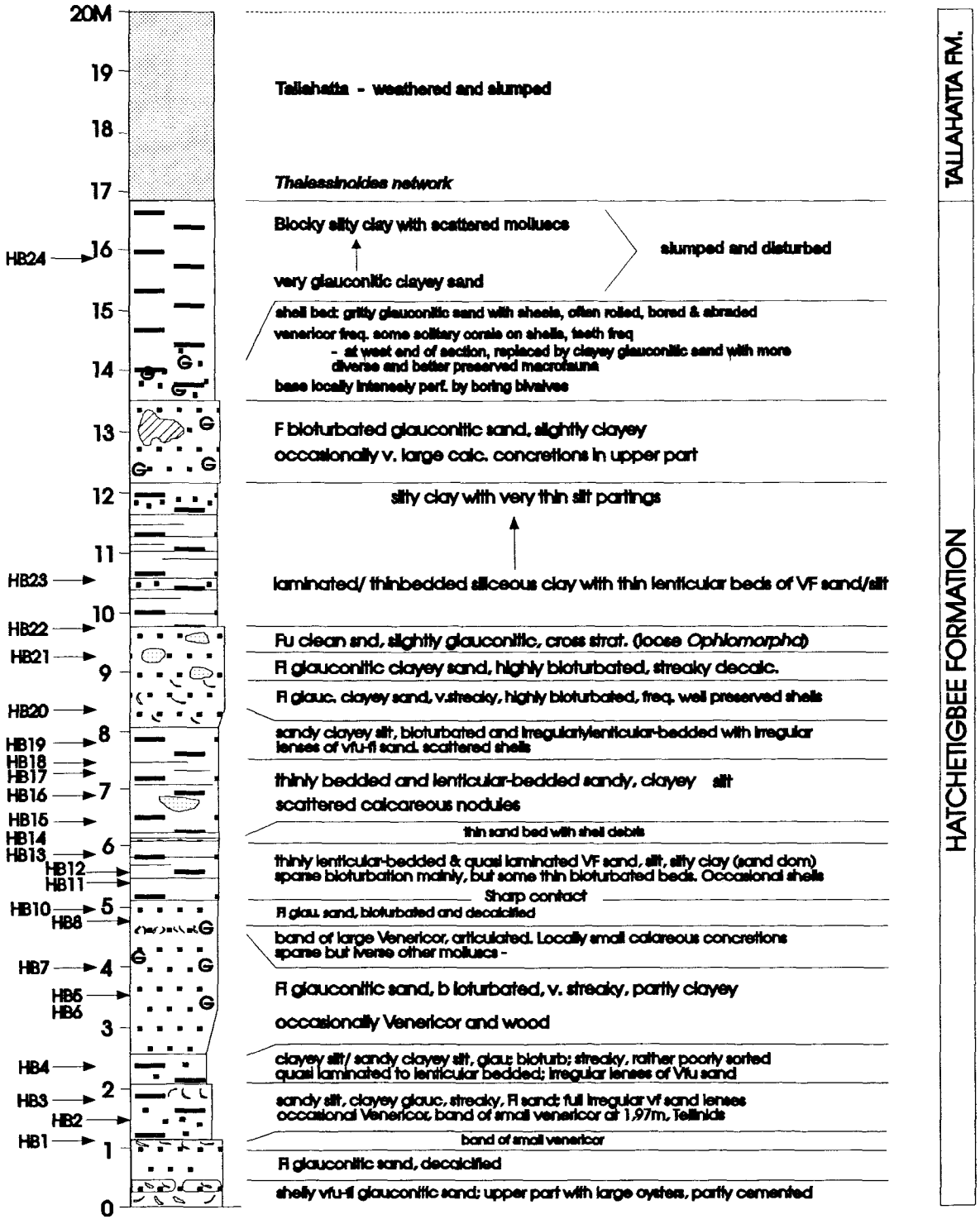

Figure 9-6 *Stratigraphic log and sample site location at the Hatchetigbee Bluff locality.*

Two prominent marine zones in the Hatchetigbee are exposed at this locality (Mancini, 1991). The lowermost has several visible beds which are characterised by an abundant bivalve *Venericardia hatcheplata*, the majority of which are articulated. This species is restricted to the Hatchetigbee Formation. The upper marl unit contains a large number of moderately well-preserved shells of numerous mollusc species; it has been placed in the planktonic foraminifera zone P6 by Mancini (1991).

Sampling

Due to the weathering and slumping of some of the uppermost beds of the Hatchetigbee sediments, samples were largely restricted to below 11m (Fig. 9-6). Only one large sample at each site was recovered at this locality; these were A.F. demagnetised in fields up to 40mT.

Polarity analysis

The sediments at Hatchetigbee Bluff have relatively high NRM intensities (average 0.36mA/m). The demagnetisation behaviour of the vast majority of samples analysed here however, resulted in spurious plots from which no reliable polarity sequence could be determined.

The directions of most SEPs plotted on an equal area stereogram illustrate steep positive inclination values with a variety of declinations which can not be adequately explained as representing primary components (Fig. 9-7).

The demagnetisation plots can be split into 4 broad categories:

i) 32% of samples showed anomalous SEPs that had positive inclinations and southerly declinations and frequently exhibited intensities which only decreased to 50-60% of the NRM value during A.F. demagnetisation to 40mT (Fig. 9-8).

ii) 25% of samples showed SEPs that had positive inclinations and northerly declinations representing what might be considered normal polarities (Fig. 9-9). However, the average inclination value was 74.5° which is considerably steeper

than that expected at this latitude (I=51°). Inclination shallowing is commonly seen in sediments but discrepancies that show inclination steepening are difficult to explain. These apparent normal polarities are therefore also considered to be the result of overprints.

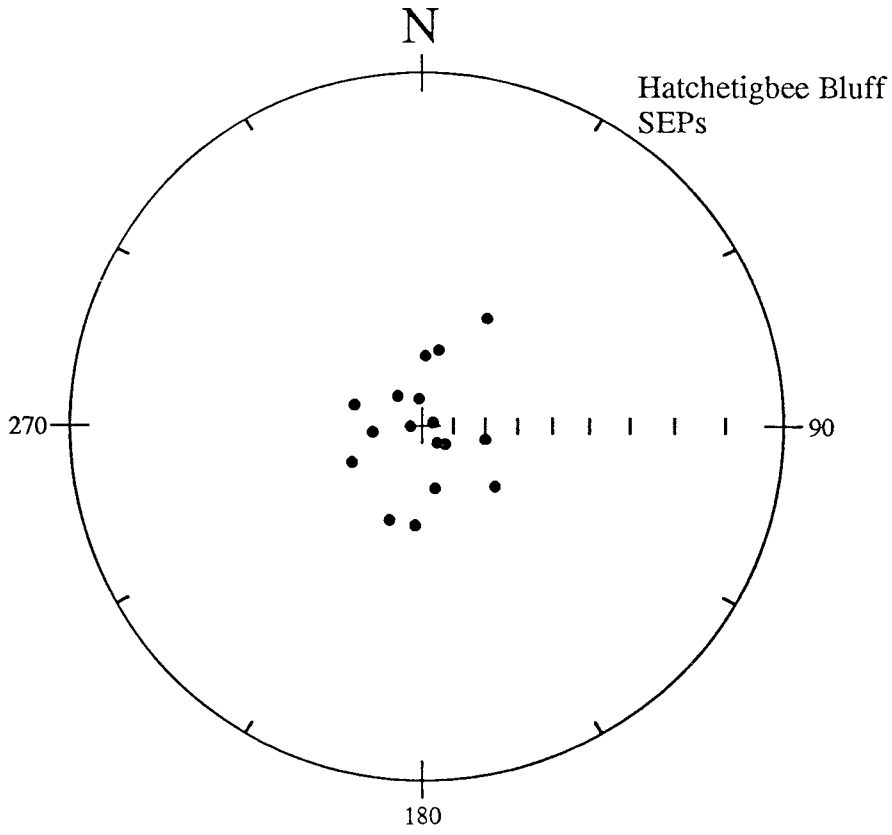

Figure 9-7 *Equal area stereogram illustrating the SEPs from samples at Hatchetigbee Bluff.*

iii) 22% of samples show trending behaviour that commonly displays 'aborted' trends to reverse or questionable reverse polarities (Fig. 9-10). This category of samples has consistent declination values which have affinities with those seen in SEP data from reverse polarity samples from sections of similar age.

iv) Those samples that do not fall into the above 3 categories and which mainly represent poor quality trending data which show no consistent direction of trend and from which no reliable polarity determination can be inferred.

There appears to be a general correlation between sample lithology and demagnetisation behaviour. Those samples from *category iii* are normally associated with more coarser silts and sands whilst those from *categories ii and iv*, showing SEP with steep positive inclinations, are restricted to finer silts and clays.

The inability to apply a tilt/fold test to these data exemplifies the problem of readily identifying overprints in these sediments. However the declination and inclination values of SEPs are not consistent with those expected or observed in samples from other outcrops. The samples from coarser silts and sands may still show some evidence of a primary component but the quality of data is too poor to reach any reliable conclusions.

Magnetostratigraphy of the Hatchetigbee Formation

It was not possible to determine confident polarities for samples at the Hatchetigbee Bluff locality.

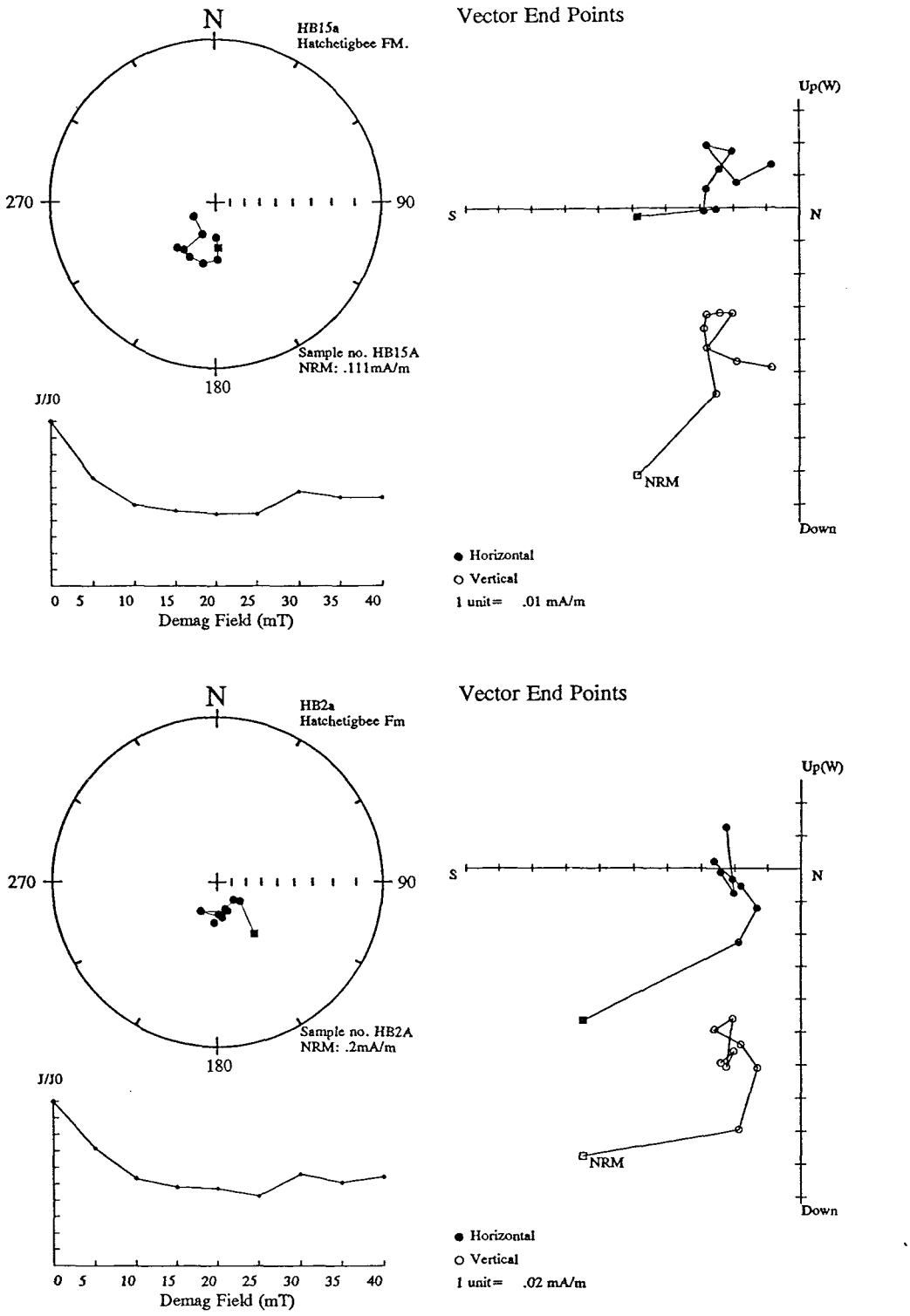

Figure 9-8 *Examples of anomalous SEP demagnetisation plots with southerly declinations.*

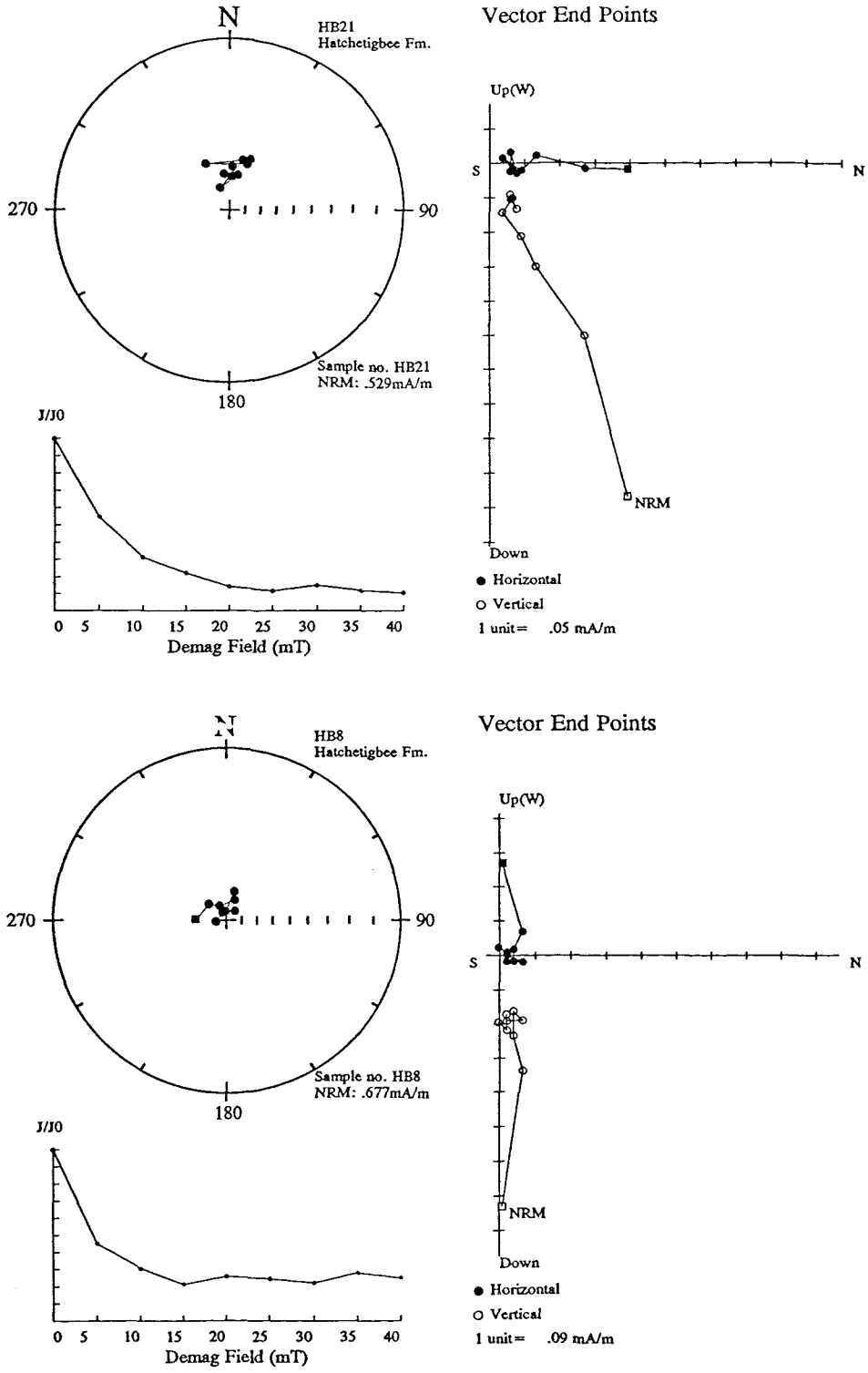

Figure 9-9 *Examples of SEP demagnetisation behaviour which exhibit steep 'normal' polarities.*

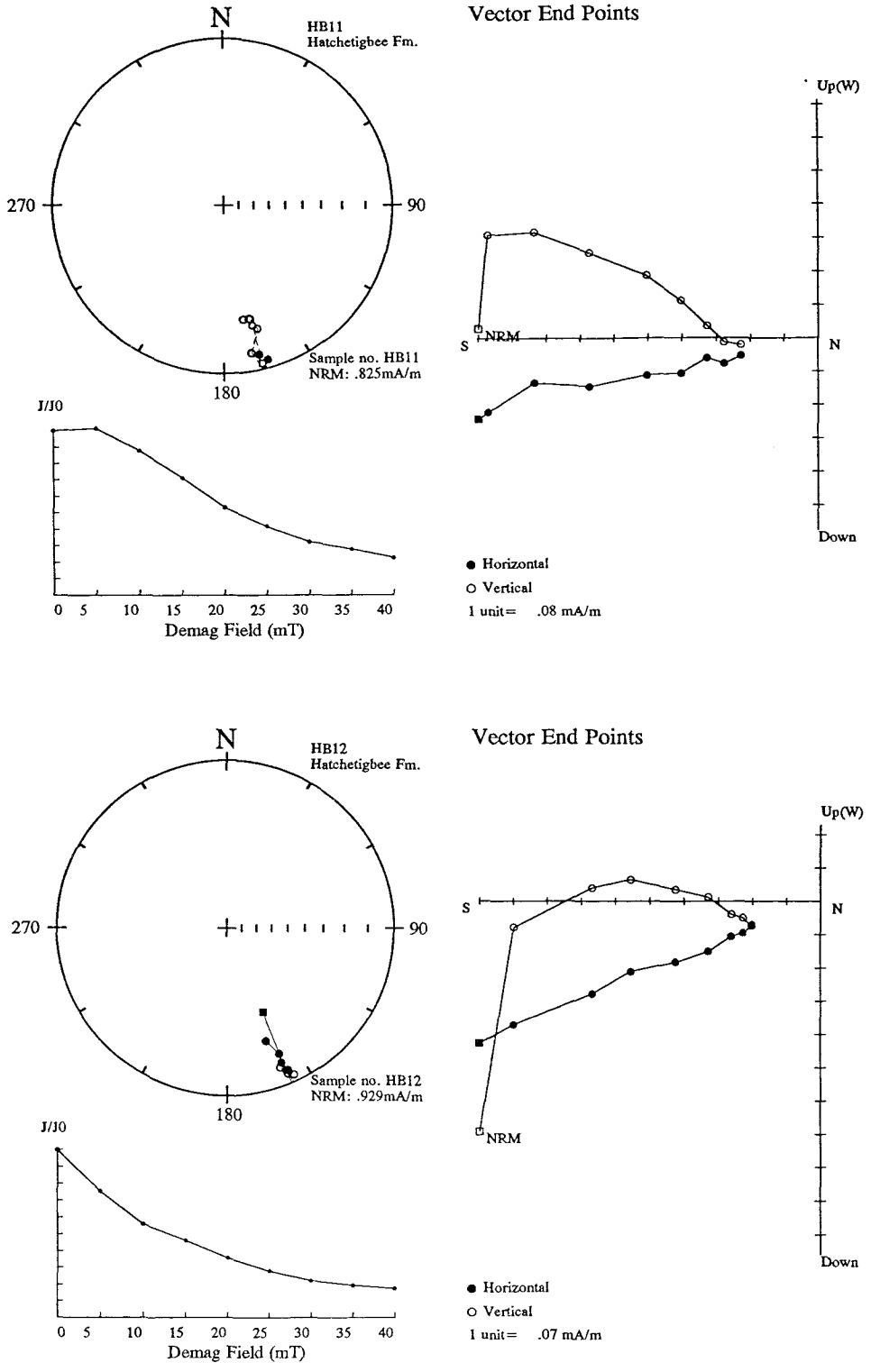

Figure 9-10 *Examples of trends that display 'aborted' trends to reverse or questionable reverse polarities with common declination directions.*

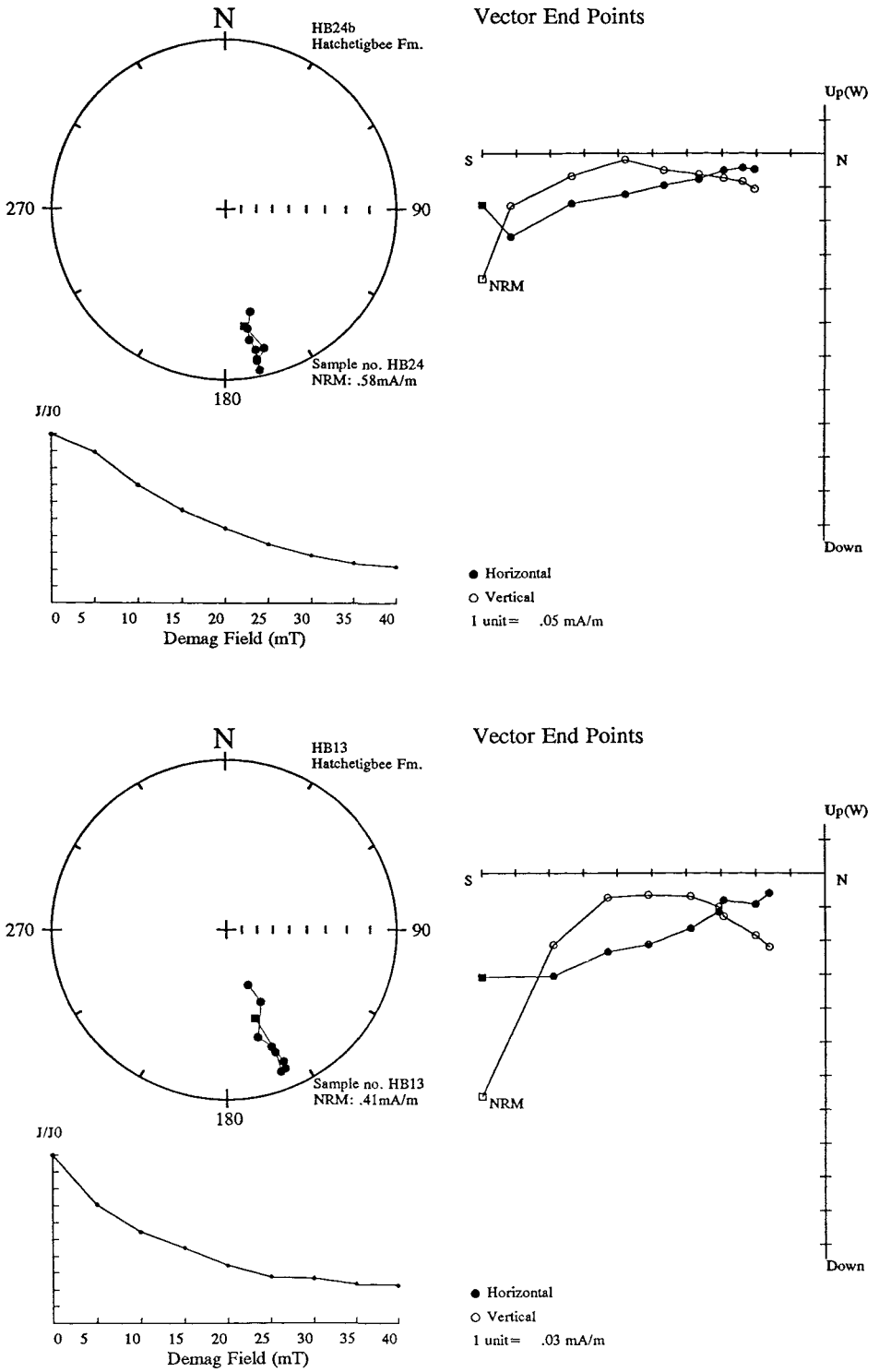

Figure 9-10 - continued *Examples of trends that display 'aborted' trends to reverse or questionable reverse polarities with common declination directions.*

9.1.3 Lower Peach Tree locality

Location: Road section 6 miles west of Lower Peach Tree, Wilcox County.

The road cutting exposes the Tuscahoma, Hatchetigbee and Tallahatta Formations including the Meridian Sand Member. The condition of the section is generally poor with many weathered intervals.

Sampling

Sampling was restricted to the Hatchetigbee and Tallahatta Formations which covered a stratigraphic height of approximately 14m. The Meridian Sand Member at the base of the Tallahatta Formation was not sampled due to its coarse sandy nature; however it was used as a marker horizon for logging purposes and measurements of sample sites were made from its upper and lower contact (Fig. 9-11). The uppermost site, lp25, was located at about 2m below the Tallahatta/Lisbon Formation contact and the lowermost site, lp36, within the Hatchetigbee formation, above the Bashi Marl Member. The sampling interval was approximately 1m, although due to the lack of suitable lithologies between 3.2m-5.7m of the Tallahatta and between -3.7m and -6.9m of the Hatchetigbee, the resolution was reduced here. Block samples from each site were then divided into 2-3 sub-samples and demagnetised using thermal and A.F. demagnetisation techniques.

IRM acquisition analysis was carried out on 2 specimens: one specimen at 3.2m, taken from the Tallahatta Formation and one at -6.9m from the Hatchetigbee Formation. Both specimens were considered to be broadly representative of samples from each formation (Fig. 9-12).

In each case magnetic saturation was reached in applied fields of approximately 0.5 Tesla, indicating that the dominant magnetic mineral present is titanomagnetite. This was reaffirmed by susceptibility measurements during thermal demagnetisation which indicated no mineralogical phase transitions up to a maximum temperature of 500°C (pyrrhotite has been reported as producing similar IRM saturation curves to titanomagnetite but thermochemical reactions typically occur between 300°C and 350°C (for example: Schwarz and Vaughan, 1972; Menyeh and O'Reilly, 1991)).

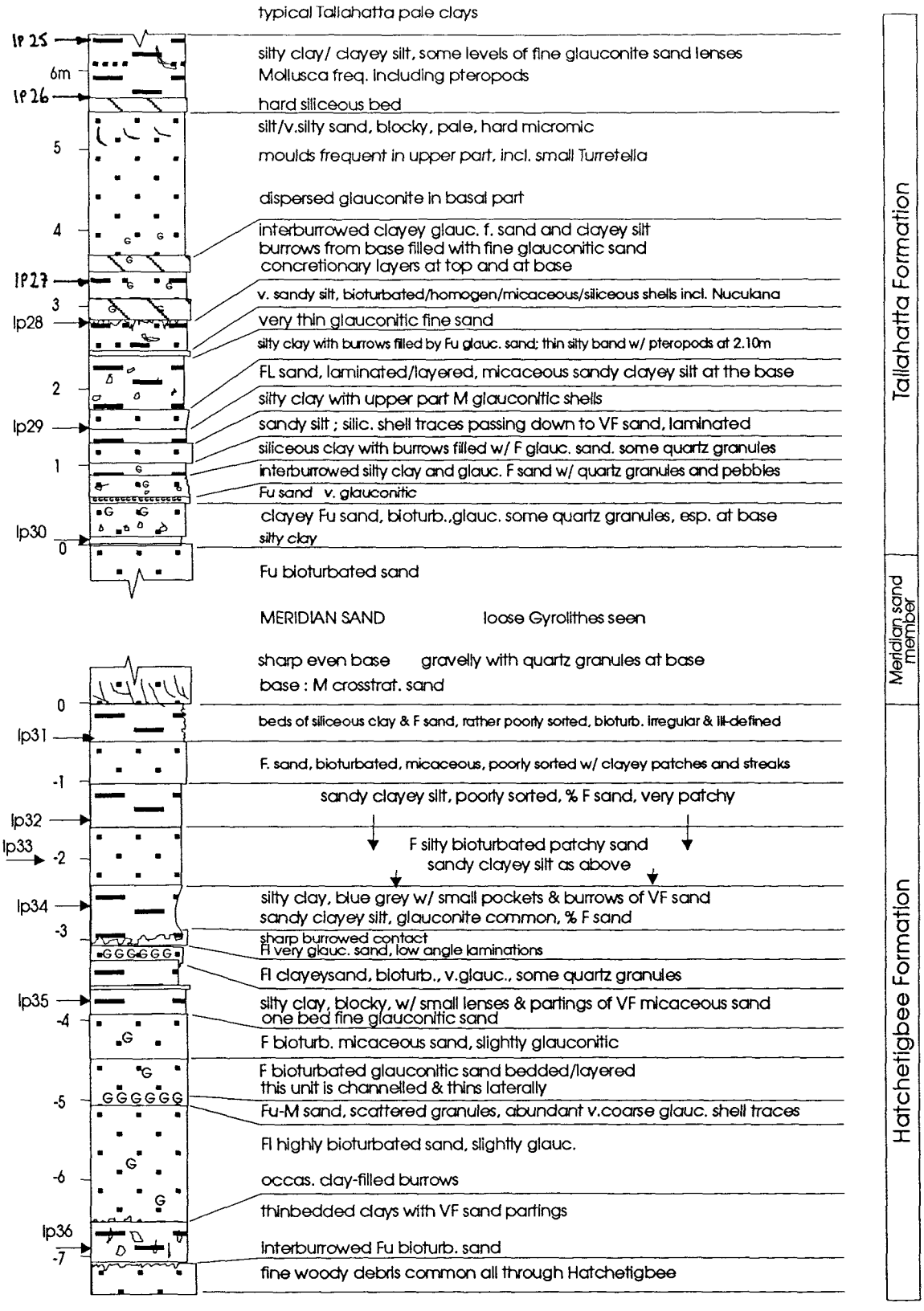

Figure 9-11 *Stratigraphic log and sample sites at the Lower Peach Tree locality.*

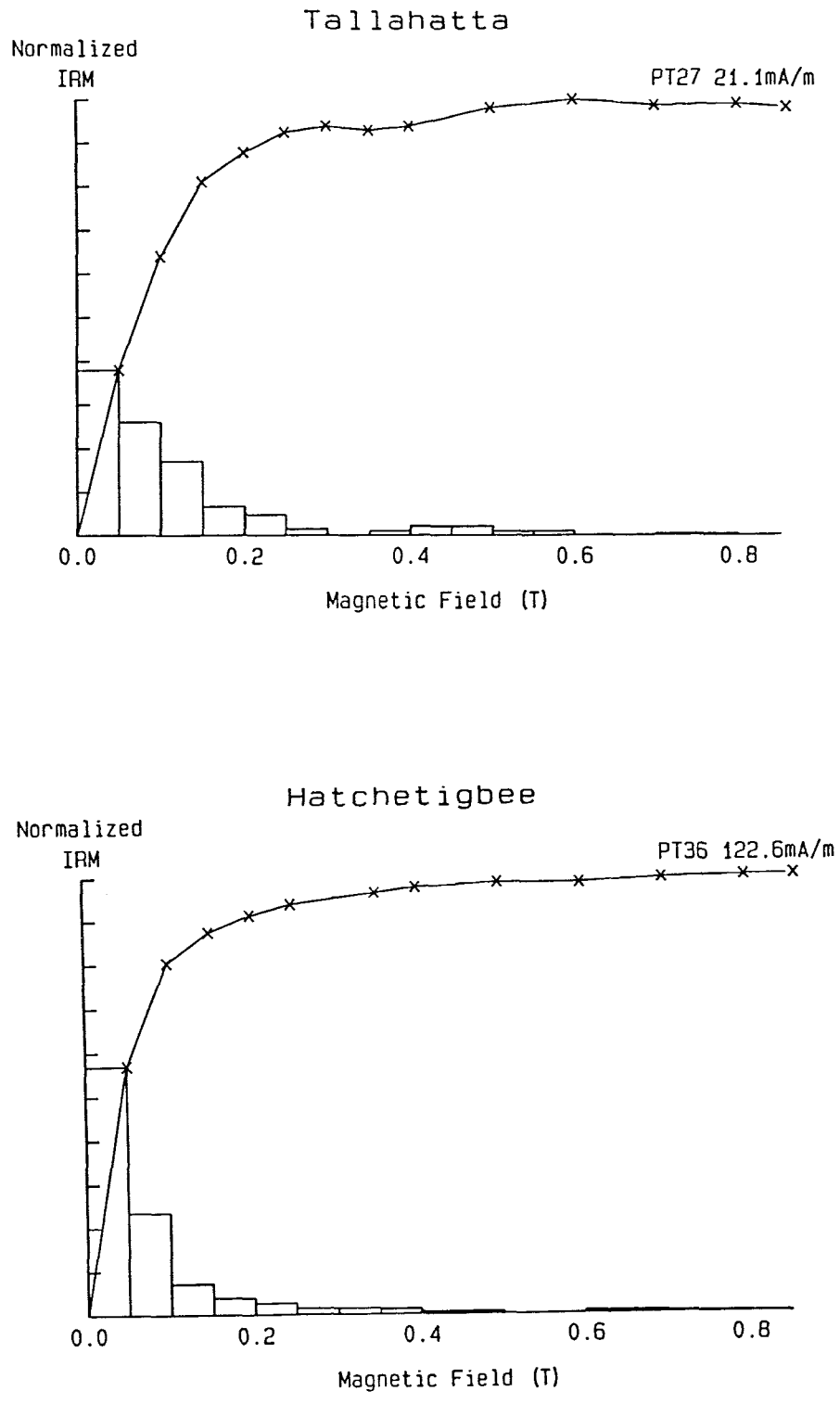

Figure 9-12 *IRM acquisition curves for samples from the Lower Peach Tree locality.*

Polarity analysis

The polarity determinations from A.F. demagnetised sub-samples from each site are broadly consistent and suggest a normal polarity interval throughout the Tallahatta and Hatchetigbee section at this location (Appendix 21). The quality of data is generally good with most demagnetisation plots being assigned an S2-type category, the SEPs being located in approximately the same area on a stereogram (Fig. 9-13).

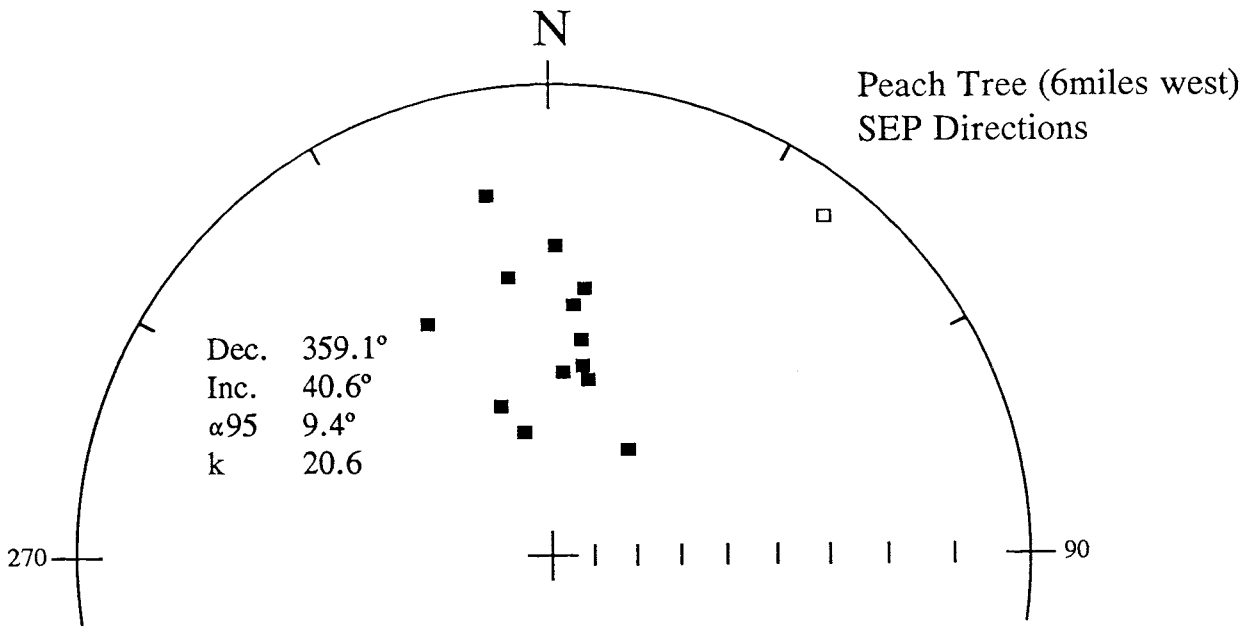

Figure 9-13 *Equal area stereograph of SEPs from A.F. demagnetised samples at the Lower Peach Tree locality.*

In most cases thermally demagnetised sub-samples are remarkably consistent with A.F. demagnetised material from the same site (for example: Figs. 9-14, 9-15 and 9-16).

In other cases however, the thermal demagnetisation behaviour of some specimens suggests a possible trend to a reverse polarity (Figs. 9-17, 9-18 and 9-19). This apparent inconsistency is graphically summarised in figure 9-20 where the polarity sequence defined by A.F. and thermally demagnetised sub-samples are illustrated in separate columns.

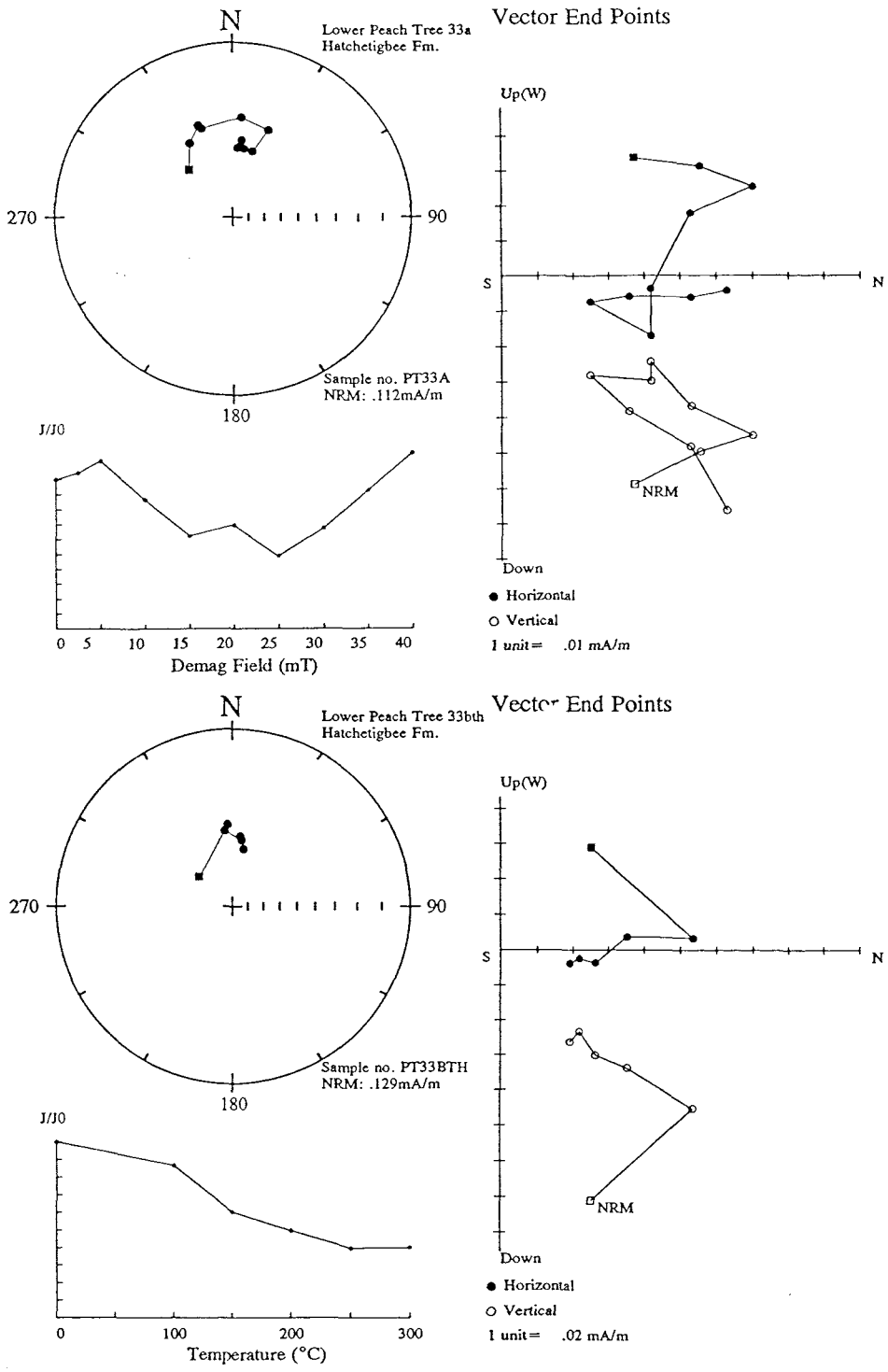

Figure 9-14 *Sub-samples 33a and b illustrating the consistency of A.F. and thermal demagnetisation behaviour from a site at 2m below the Meridian Sand Member.*

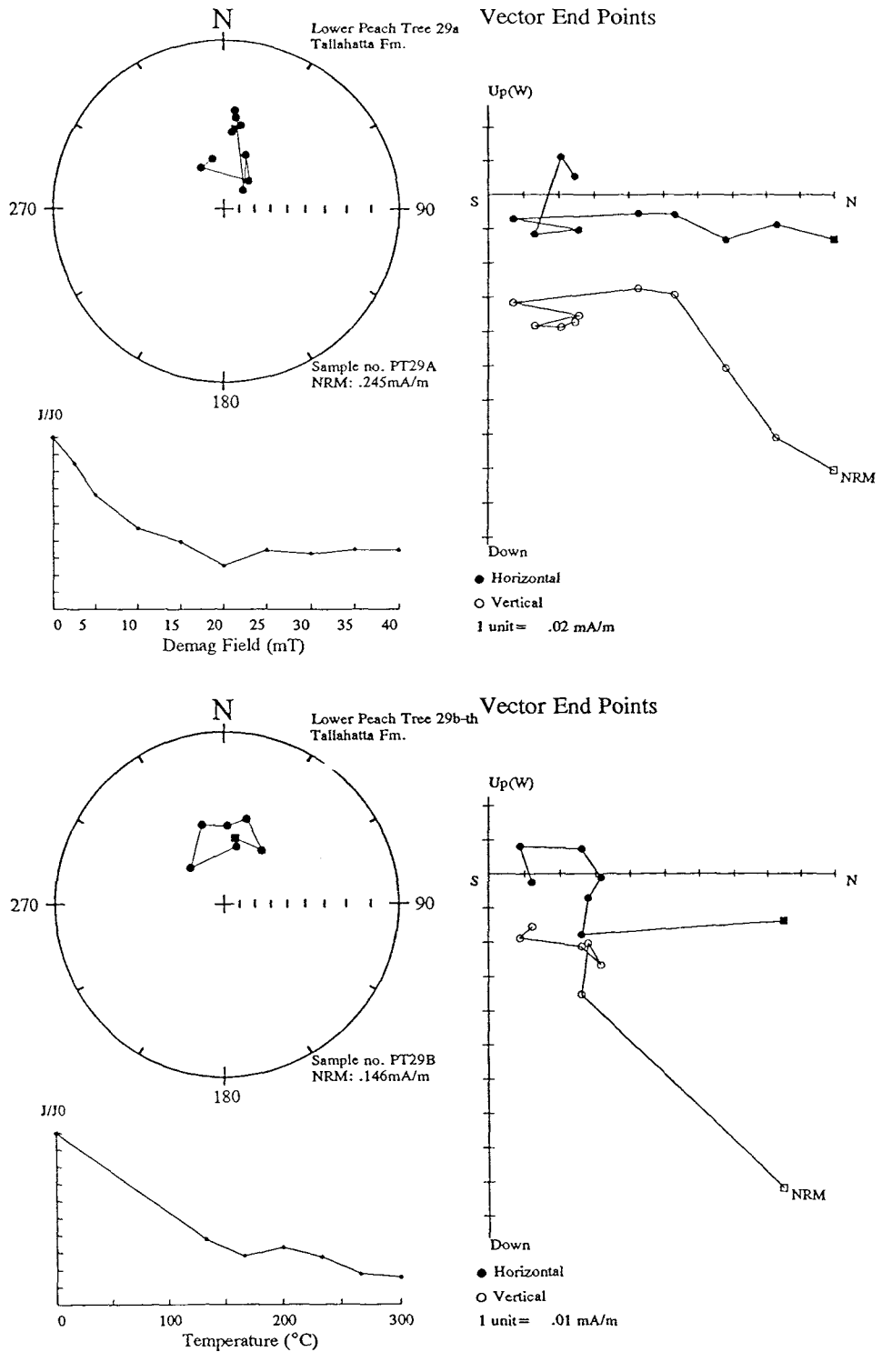

Figure 9-15 *Sub-samples 29a and b illustrating the consistency of AF. and thermal demagnetisation behaviour from a site at 1.5m above the Meridian Sand Member.*

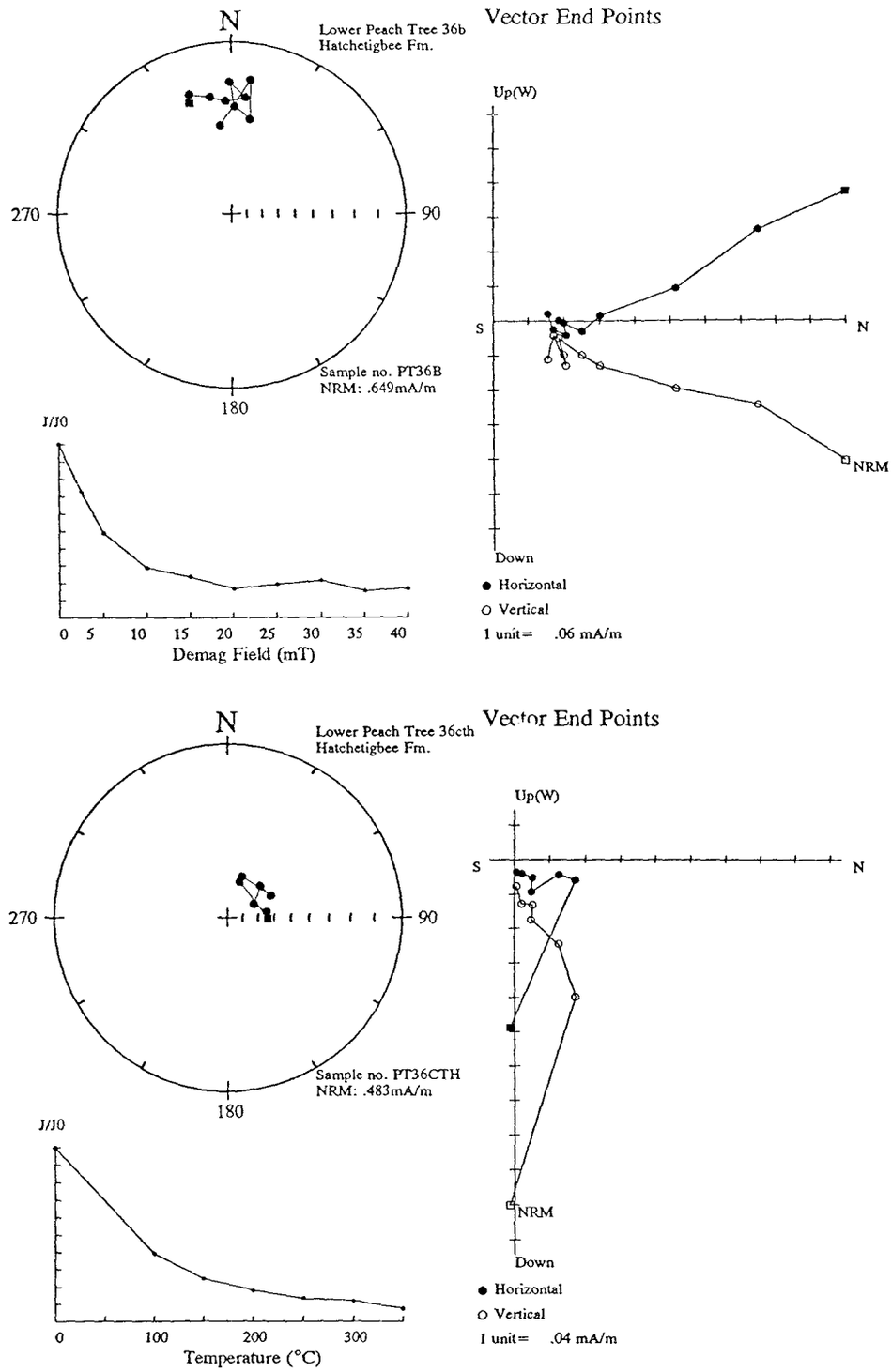

Figure 9-16 *Sub-samples 36b and b illustrating the consistency of A.F. and thermal demagnetisation behaviour from a site at 6.9m below the Meridian Sand Member.*

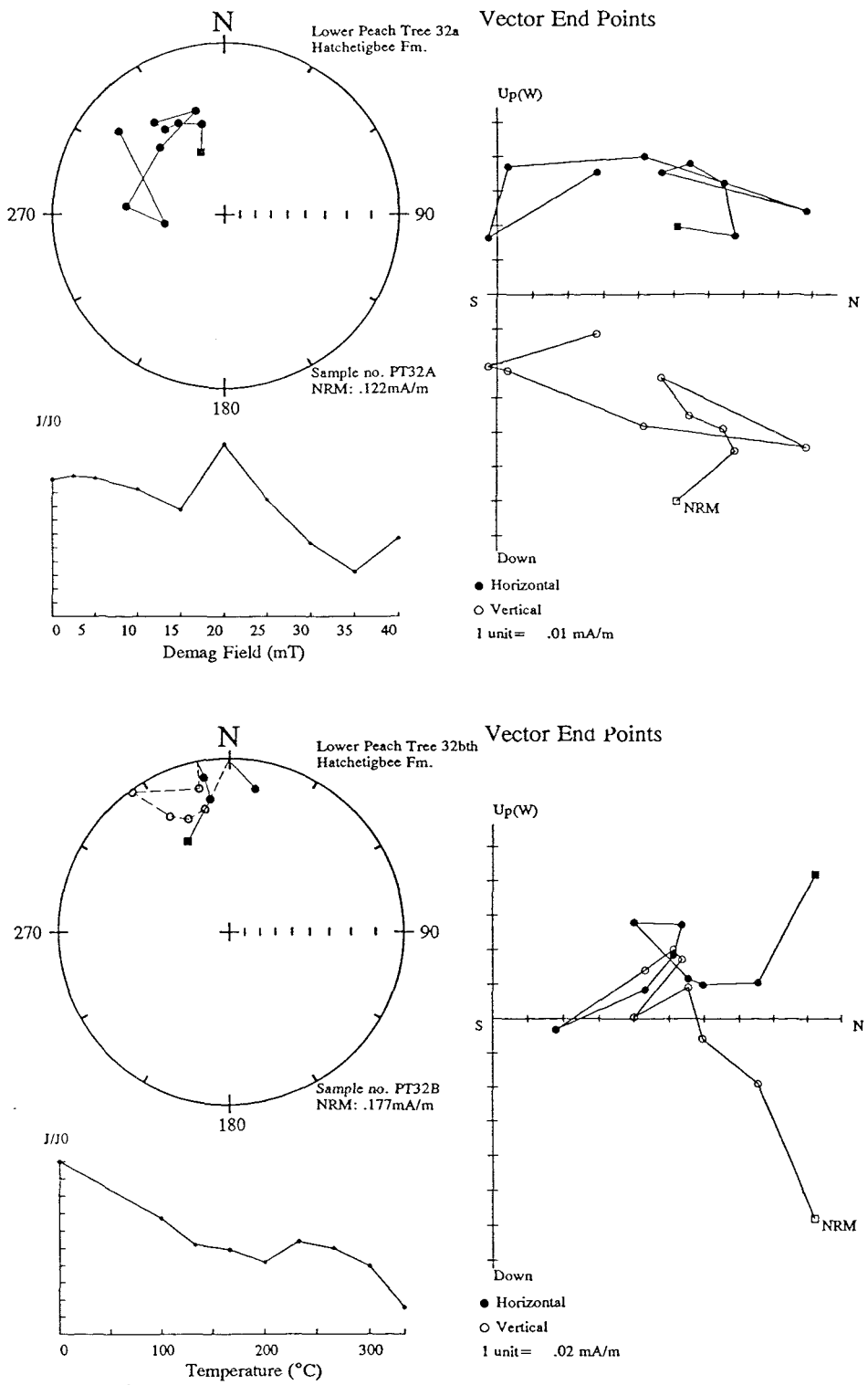

Figure 9-17 *Sub-samples 32a and b illustrating the inconsistency of A.F. and thermal demagnetisation behaviour from a site at 1.3m below the Meridian Sand Member.*

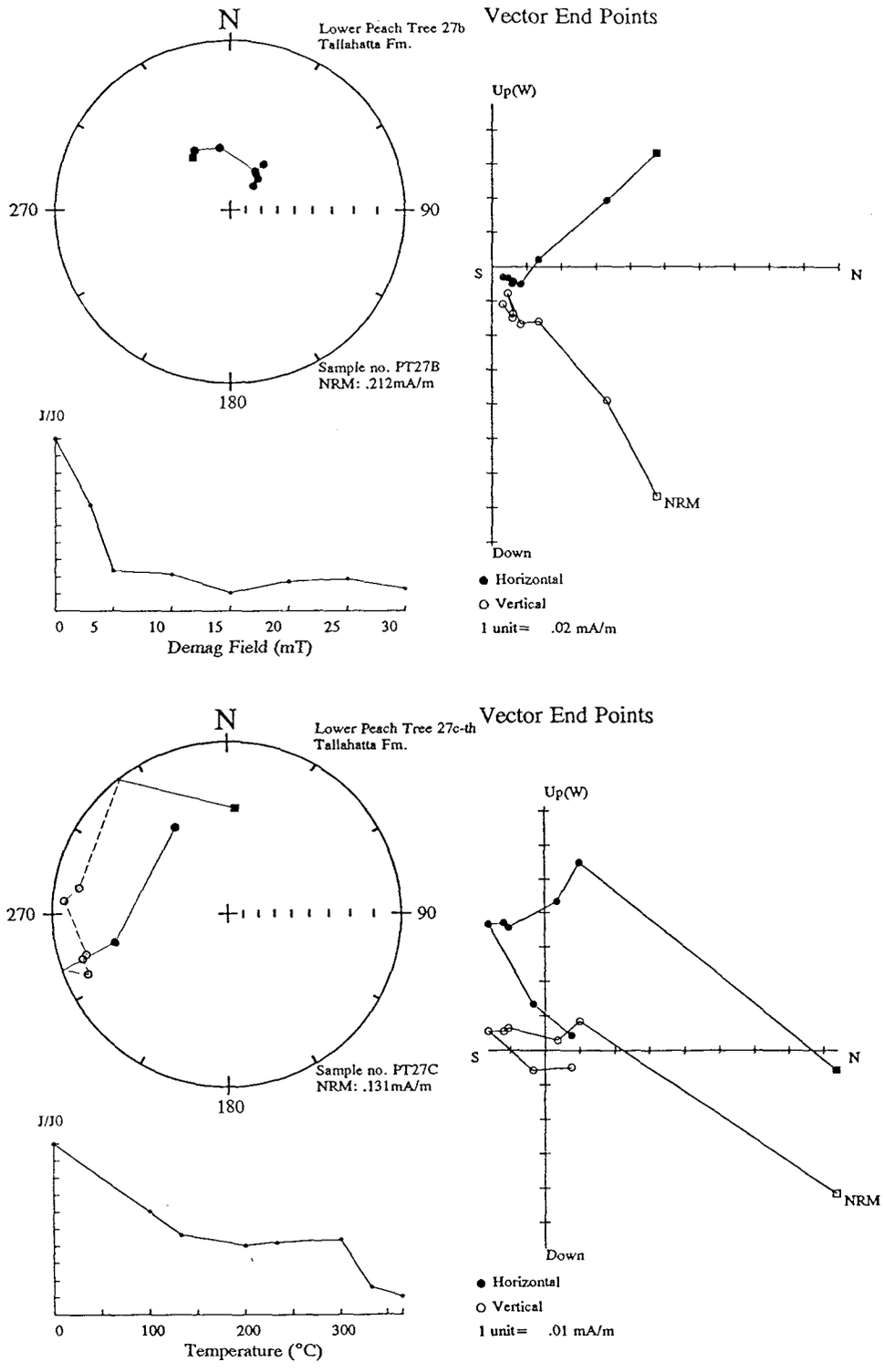

Figure 9-18 *Sub-samples 27b and c illustrating the inconsistency of A.F. and thermal demagnetisation behaviour from a site at 3.2m above the Meridian Sand Member.*

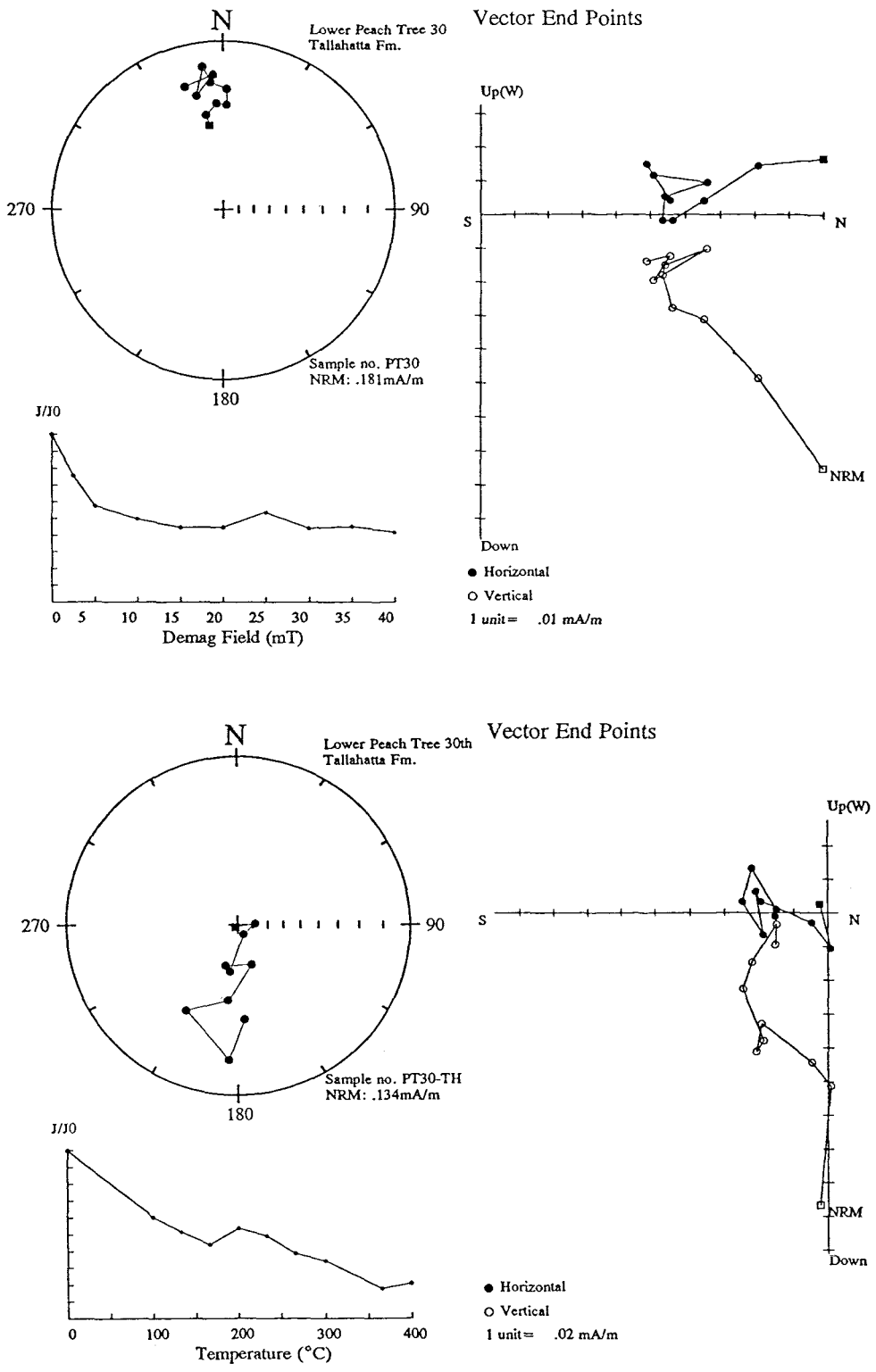

Figure 9-19 *Sub-sample at 0.1m above the Meridian Sand illustrating the inconsistency of A.F. and thermal demagnetisation behaviour.*

Magnetostratigraphy

A normal polarity zone for the entire interval of Tallahatta and Hatchetigbee material exposed at this section which is suggested by the A.F. demagnetisation data seems unlikely. Additional evidence from nearby outcrops (e.g. Tunnel Springs), the Peterman Core and the polarity sequence predicted by the GPTS for sediments of this approximate age suggests that some of the normal polarity samples here are overprints. Furthermore, the SEPs at this section have typical positions where D=359.1°, I=40.6° (Fig. 9-13). All specimens that are considered to have genuine primary components from other sections in Alabama and Virginia exhibit an anticlockwise shift in declination of 10-12°.

A polarity sequence suggested by thermally demagnetised material introduces 3 reverse polarity magnetozones however the poor quality of thermal demagnetisation trends (categories T3 and T2) and the small number of specimens defining these possible reverse polarity intervals limits the confidence of any correlations with the GPTS. In addition, there still remain some questions regarding the sedimentary record at this location, where the vertical height of the Tallahatta material for instance, is approximately 10m compared to 50m of Tallahatta strata sampled by the Peterman core. The lack of biostratigraphical control creates some doubt about the extent of the hiatus at the Tallahatta/Hatchetigbee contact. However, a normal interval has been determined within the Hatchetigbee Formation which is confirmed from SEP data from both thermal and A.F. demagnetised samples (specimens analysed from earlier field work in 1990 also yield good SEPs for this interval when much of the other data is extremely poor). If the normal polarity represented here is a genuine primary component then it would correlate with Chron C24n indicating that sediments of NP11 in age exist below the hiatus at the top of the Hatchetigbee Formation. This is in contrast to the findings within the Hatchetigbee Formation exposed at the Tunnel Springs, the Peterman core and tentatively at the Bell's Crossing locality where a predominance of reverse polarities are identified from thermal and A.F. demagnetisation of samples below the upper formation contact down to a level which has been positively identified as NP10.

In summary, the overall magnetostratigraphy remains questionable and due to the difficulties in adequately correlating this section with other outcrops and the GPTS it has not been included in the summary magnetostratigraphy for the Gulf Coast.

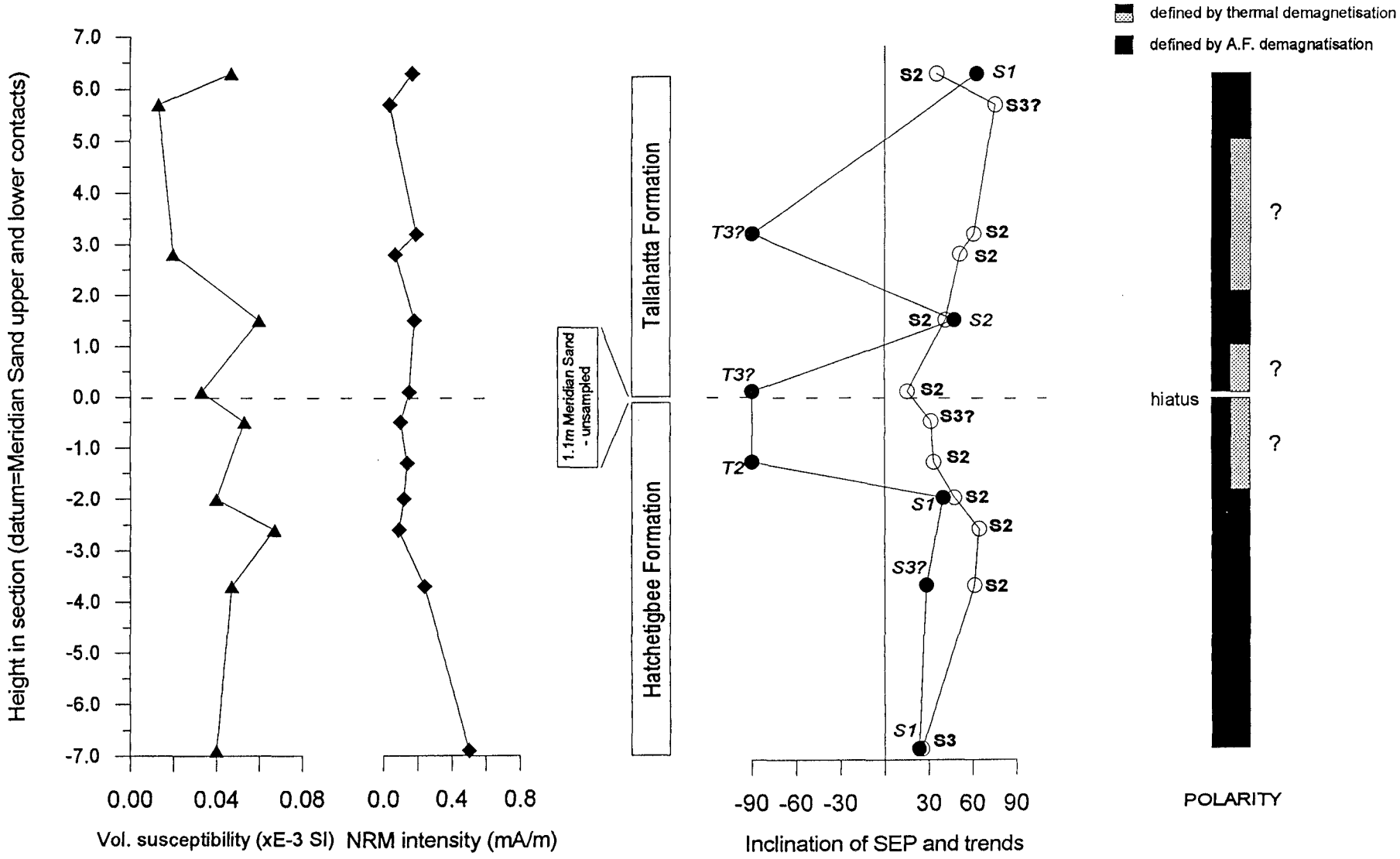

Figure 9-20 *Susceptibility, NRM intensities and inclination values of SEPs and trends for A.F. and thermally demagnetised samples plotted against height in the Lower Peach Tree section.*

9.1.4 Bell's Crossing locality

Location: Road-cut on both sides of the road, 1km north of Bell's Crossroads, Dale County, Alabama.

The section here is reported by Gibson (1982), to show the complete Hatchetigbee Formation with contacts above with the Tallahatta and below with the underlying Tuscahoma Formation.

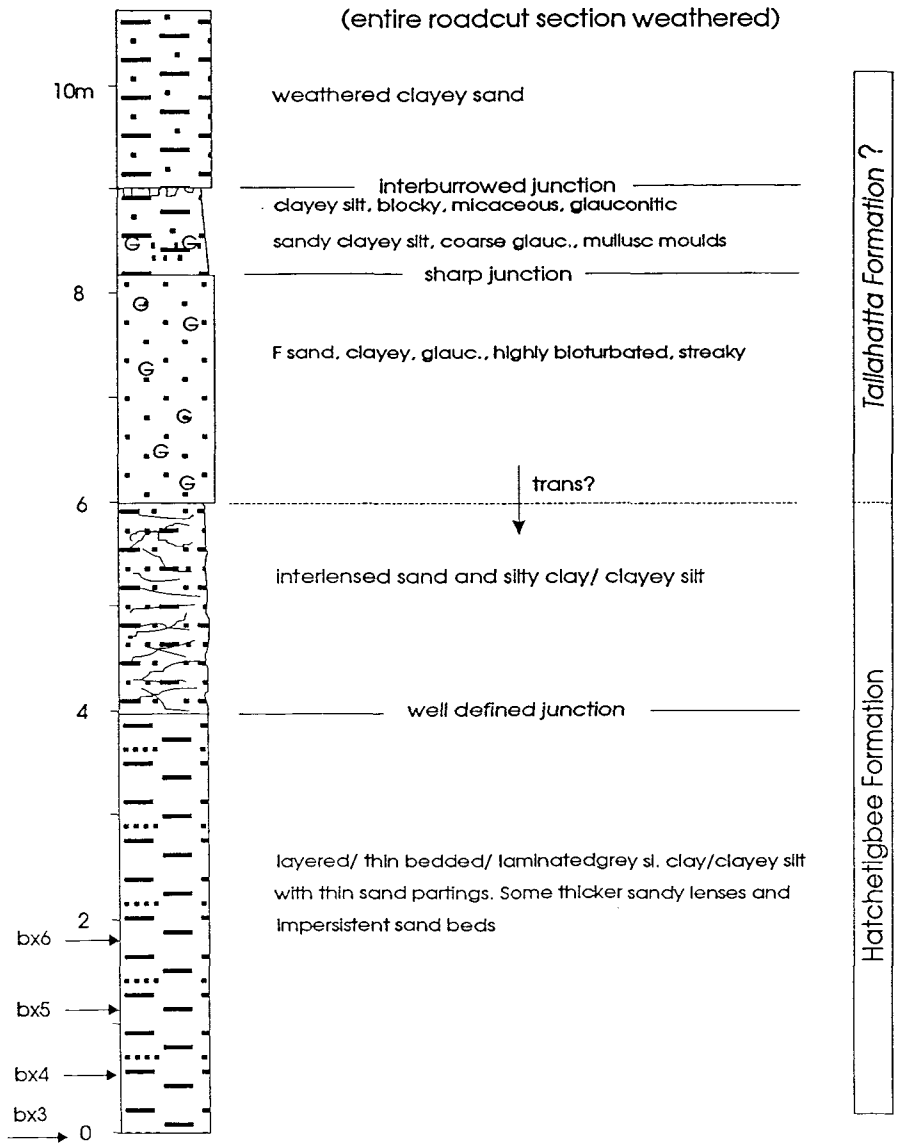

Figure 9-21 *Stratigraphic log and sample sites at the Bell's Crossing locality.*

The beds have since weathered and slumped and therefore requiring a significant amount of material to be removed in order to access *in situ* beds, particularly at the base where the lower formation contact is no longer exposed (Fig. 9-21).

Due to the general condition of the outcrop, blocks from only 4 sites were recovered. No parallel biostratigraphic control exists for these sites but they were located within the Hatchetigbee Formation between 4-6m below what was regarded as the upper Tallahatta Formation contact by King (pers. comm.). Although no direct biostratigraphy is available, Gibson considers the 'upper unnamed member' of the Hatchetigbee Formation as being a time-equivalent of the more downdip facies of the Bashi Marl Member which is well dated as being within the lower calcareous nannoplankton zone NP10 and middle planktonic foraminiferal zone P6 (Gibson and Bybell, 1981).

Two sub-samples were prepared from at least one each site, at least one of which was A.F. demagnetised up to a maximum field of 40mT. A sub-sample from both the upper and lower sites was in addition, thermally demagnetised (Appendix 22).

Polarity analysis

Three sub-samples exhibited what was considered reliable polarity information (for example: Fig. 9-22); the remainder showed inconsistent behaviour of questionable trends and SEPs of an anomalous nature (Fig. 9-23). An IRM acquisition investigation of *sample bx3* indicated a magnetite-type saturation curve.

Magnetostratigraphy of Bell's Crossing locality

A small number of palaeomagnetic samples, taken over a restricted stratigraphic range without parallel biostratigraphic investigations are of little use magnetostratigraphically. The questionable polarity determinations of some sites within this section further reduces the significance of this locality. A predominance of reverse polarity sites however, confined within NP10 (as suggested by Gibson and Bybell, 1982) indicates a correlation with Chron C24r.

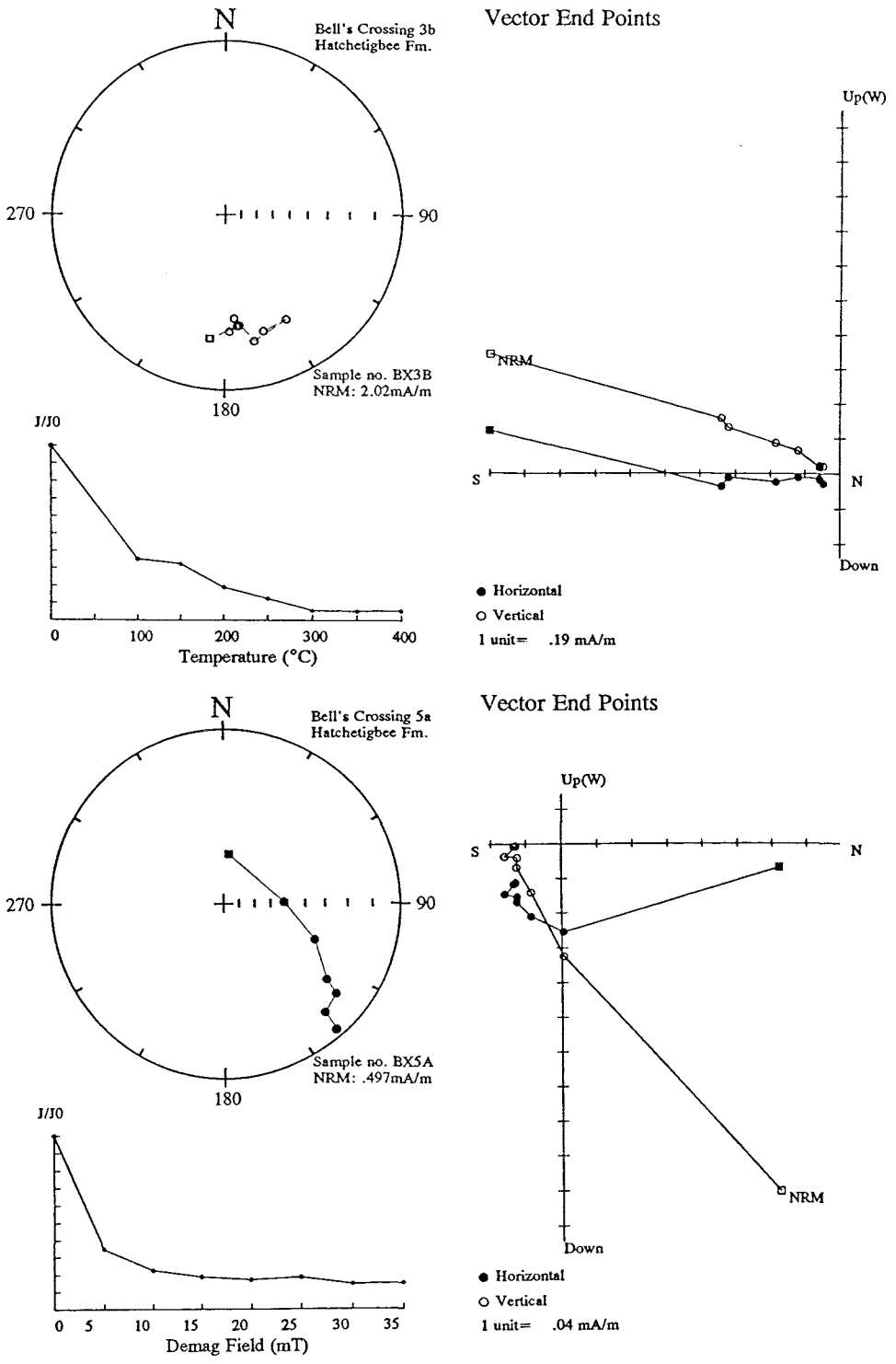

Figure 9-22 *Demagnetisation behaviour at the Bell's Crossing locality.* ***Top.*** *Thermally demagnetised sample illustrating an SEP reverse polarity plot.* ***Bottom.*** *A.F. demagnetised sample illustrating a trend to a reverse polarity.*

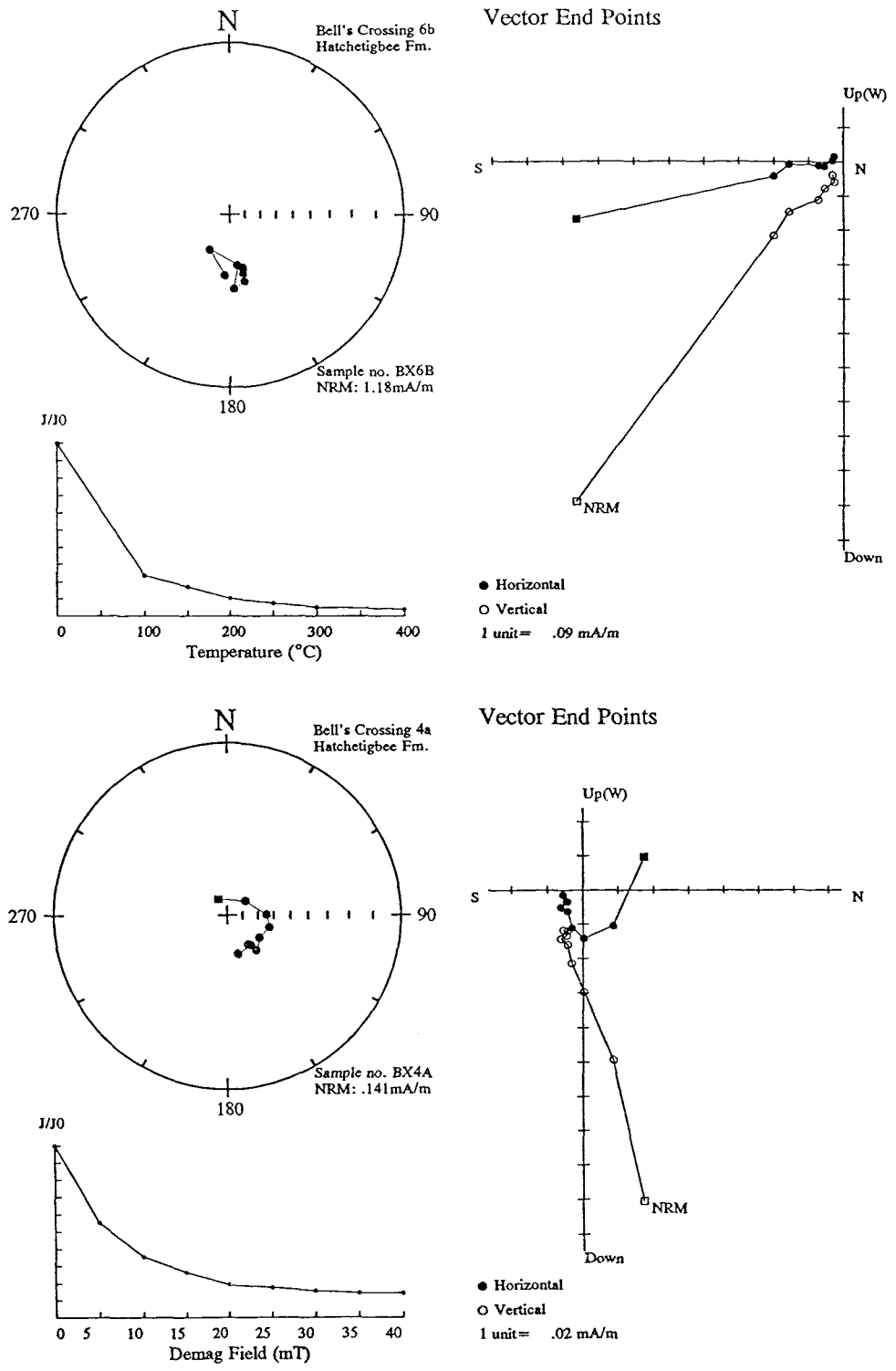

Figure 9-23 *Anomalous demagnetisation behaviour showing positive inclinations with southerly declinations at the Bell's Crossing locality.*

9.2 Tallahatta Formation core and outcrops

9.2.1 Peterman Core (supplied by the U.S. Geological Survey)

Location: Corehole C178A - north bank of Walker's Creek, 2.2 miles south of Peterman, Monroe County, Alabama.

Lithology and condition of core

The 2.75" (4.5cm) core penetrates the Tallahatta and upper Hatchetigbee Formation and is generally in good condition, consisting of siliceous clays, silts and glauconitic sands (Fig. 9-24). Core recovery of 93% reflects 3m of core loss between 37ft (11.3m) and 50ft (15.2m). The Tallahatta core interval appeared dark blue and very fresh at drilling but the siliceous silts and clays alter to a hard white material after several months (Gibson, pers. comm.). The Hatchetigbee interval is characterised by finely laminated organic sediments which are quite friable at certain points along the core. The intervening Meridian Sand Member, which appears in various thicknesses at the base of the Tallahatta Formation in outcrop is not present in the Peterman core (possibly due to lack of recovery during drilling).

Biostratigraphy

Based on calcareous nannofossils, the Tallahatta Formation of the Peterman core has been placed in zones NP12-14 although a barren interval of approximately 14m within the upper section of the core has excluded the positive assignment of NP13 (Fig. 9-25). The top of the core is below the Lisbon/Tallahatta junction.

Several species of nannofossils have their FAD's (*first appearance datum*) and LAD's (*last appearance datum*) within Zone NP14; these can be used to finely divide this zone. In the Peterman core the basal NP14 age sediments are presumed missing because the lowest fossiliferous NP14 sediments encountered in this section contain *R. inflata, C. acanthodes* and *Discolithina wechesensis* which are considered to represent mid- to upper NP14 (Bybell and Gibson, 1985).

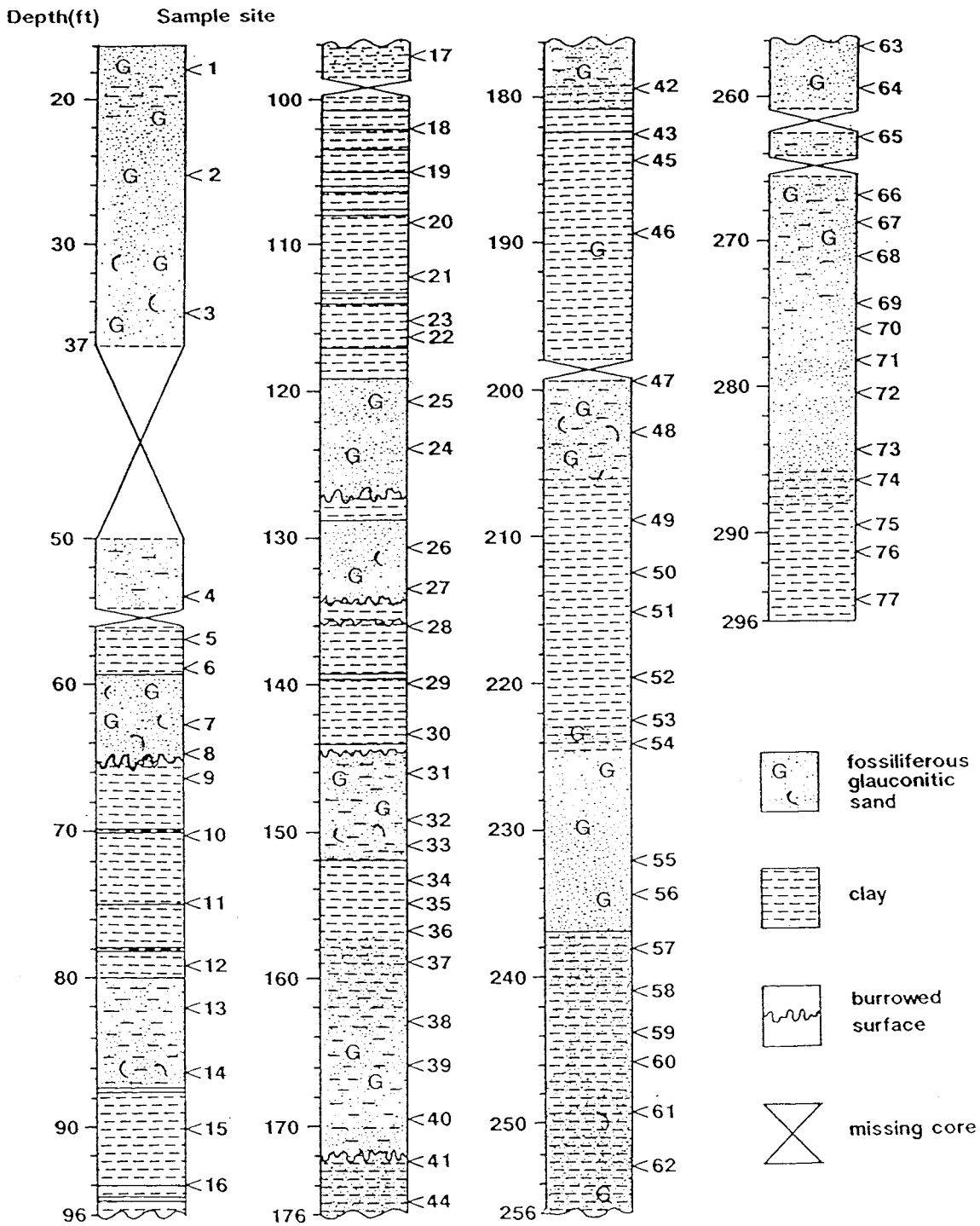

Figure 9-24 *Stratigraphic log and sampling sites along the Peterman core (based on original logs of King, pers. comm.).*

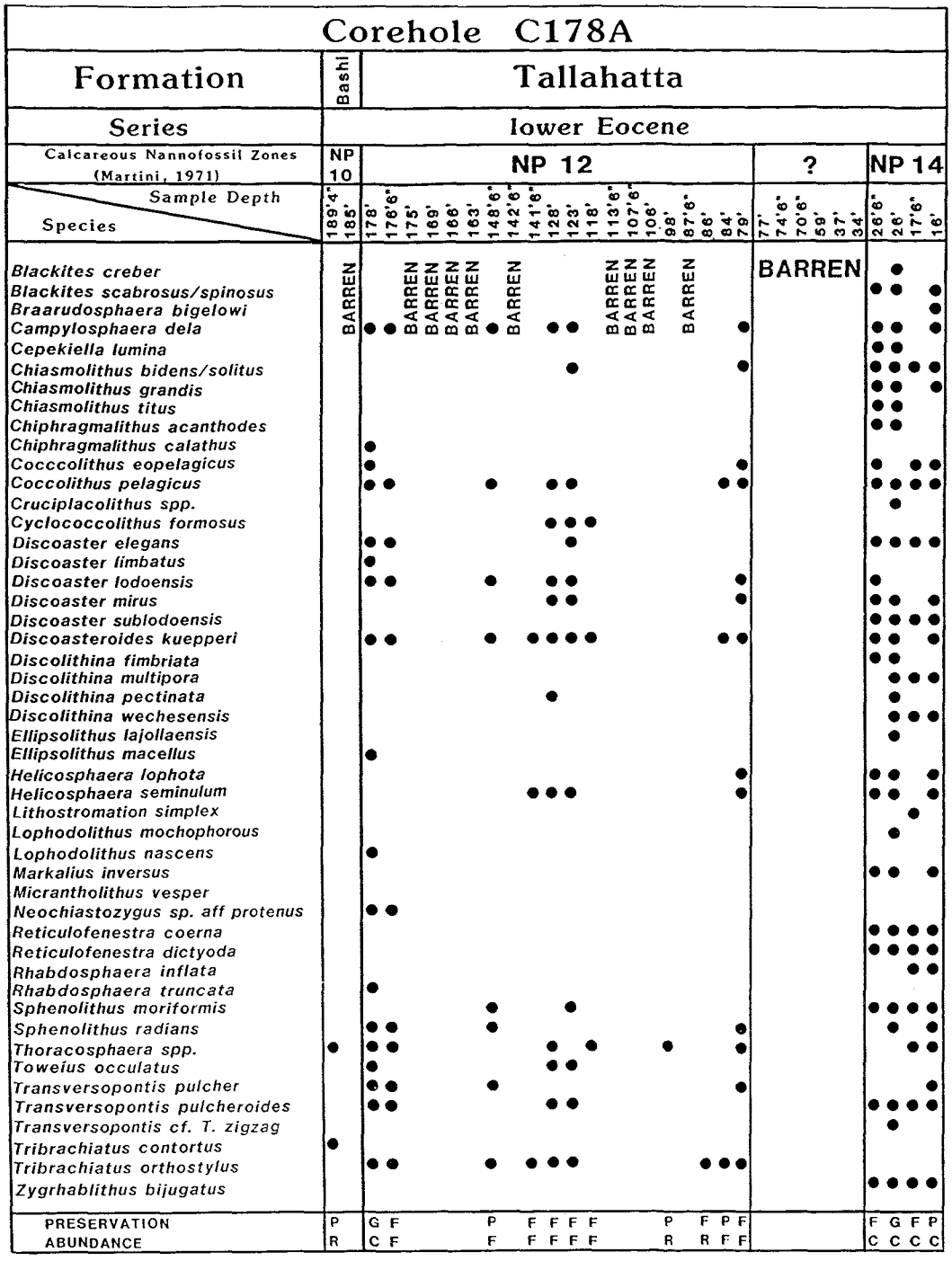

* metre equivalents for depth are available in appendix 23.

Figure 9-25 *Occurrence of calcareous nannofossils in the Tallahatta of the Peterman corehole. Samples are listed by the number of feet below ground level (from: Bybell and Gibson, 1985).*

The lowest Tallahatta clayey sand represents the downdip (south) equivalent of the Meridian Sand Member. These beds are placed in Zone NP12 on the basis of the presence of both *Discoaster lodoensis* (FAD marks the base of NP12) and *T. orthostylus* (LAD marks the base of Zone NP13).

The Hatchetigbee section of the core, below a depth of about 55m (180ft) has had less biostratigraphic work carried out on it. However, according to Bybell and Gibson (1985) the nannofossil zone NP11 is totally missing due to a hiatus at the Tallahatta/Hatchetigbee Formation contact which represents an interval of approximately 1 m.y. The remainder of the core should be entirely NP10 although samples taken below 61m were barren of calcareous nannofossils.

Palaeomagnetic sampling

Palaeomagnetic samples were taken at an average interval of 1.11m along the core from a depth of 16ft(4.9m) to 296ft (90.2m) although the interval was reduced where core material had deteriorated, especially within friable sand units (Fig. 9-24).

At each site a short length of the complete core, typically 5-7cm was removed for A.F. demagnetisation analysis. Permission from the U.S.G.S. was only granted for thermal demagnetisation on a selected number of samples over one problematical interval.

Polarity analysis

NRM intensities ranged from 0.02-5mA/m with 55% of the samples lying in the interval 0.1 -1mA/m (Appendix 23). The Tallahatta section of the core possessed the weakest material with almost 50% of the samples having NRM intensities <0.1mA/m. There was, however, a pronounced increase in values downcore, which was also evident from the susceptibility and maximum IRM (acquired at 0.86T) plots (Fig. 9-26)

A polarity sequence based predominantly on inclination values from A.F. demagnetisation was determined; it was then correlated with the GPTS using the nannofossil zonation scheme of Bybell and Gibson (1985) (Fig. 9-27).

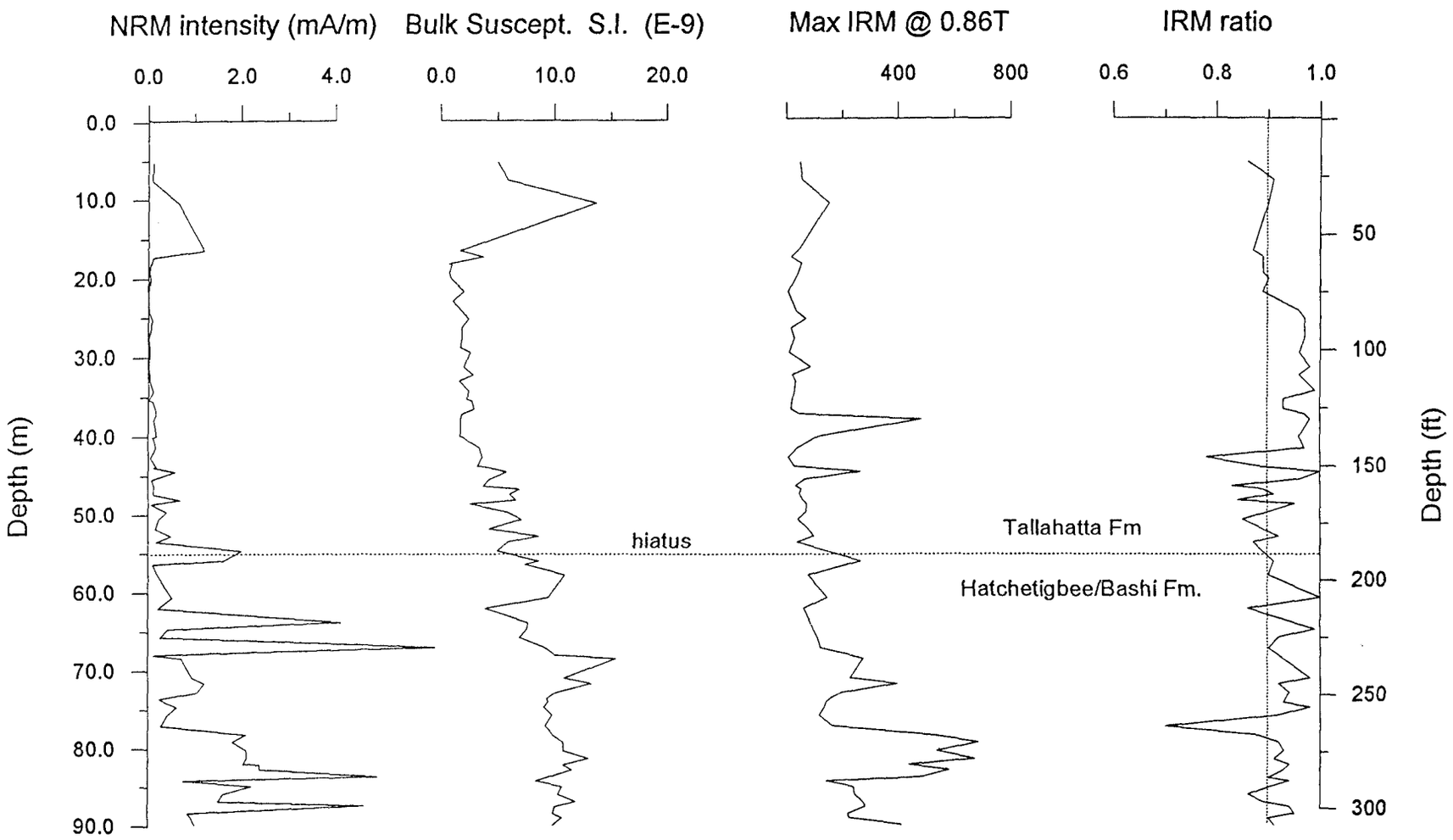

Figure 9-26 *The magnetic properties of the Peterman core.*

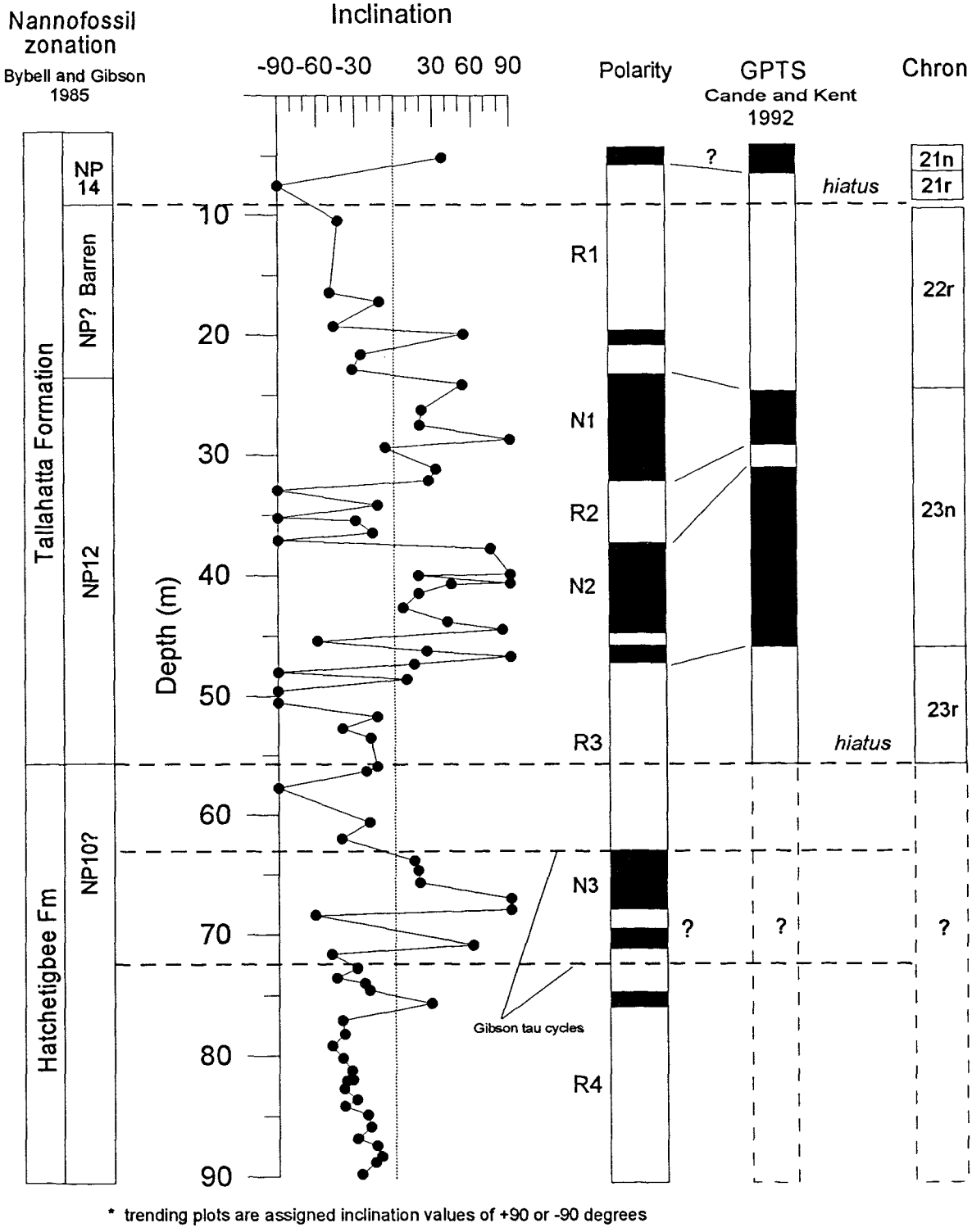

Figure 9-27 *The magnetostratigraphy determined for the Peterman core.*

Each polarity zone identified within the core was investigated using IRM analysis from which the principle magnetic carrying mineral was magnetite. (Figs. 9-28a and b).

Discussion of the polarity zones identified by 5 or more samples (typically representing sediment intervals >5m) are outlined below:

- *Reverse polarity zone R1*

The reverse polarity interval from 6m to 23.5m spans the upper core section which is barren of calcareous nannofossils. The quality of palaeomagnetic data defining this polarity zone is based on intermediate quality trends and SEPs (Fig. 9-29). IRM analyses of 3 samples from this interval are illustrated in figure 9-28a (labelled 'R1'), the early saturation of the magnetic minerals is characteristic of magnetite.

Sediments from the top 2m contain nannofossils which are representative of mid to upper NP14 and the base of the polarity zone rests on NP12 material. Lower NP14 and possibly upper NP13 are expected to span Chron C22n (Hardenbol, 1994); the absence of any significant normal polarity within this reverse interval would suggest that a break in sedimentation occurred during this period or a phase of erosion has removed sediments of this age from the sedimentary record. A hiatus might be present at a depth of approximately 20m where a burrowed surface exists; alternatively, the lost core between 11.3 -15.2m may show evidence of a period of non-deposition or stripping of sediment. Assuming the biostratigraphy to be correct, this hiatus is apparently not extensive in the eastern Gulf Coast since basal NP14 and NP13 sediments are observed in other coreholes within Alabama (for example at Prestwood Bridge, Covington County, 100km to the east - Bybell and Gibson, 1985).

- *Normal polarity zone N1*

Sediments within upper NP12, from a depth of approximately 24-33m, have a normal polarity based on intermediate quality palaeomagnetic data (S2/S3 categories)(Fig. 9-30).

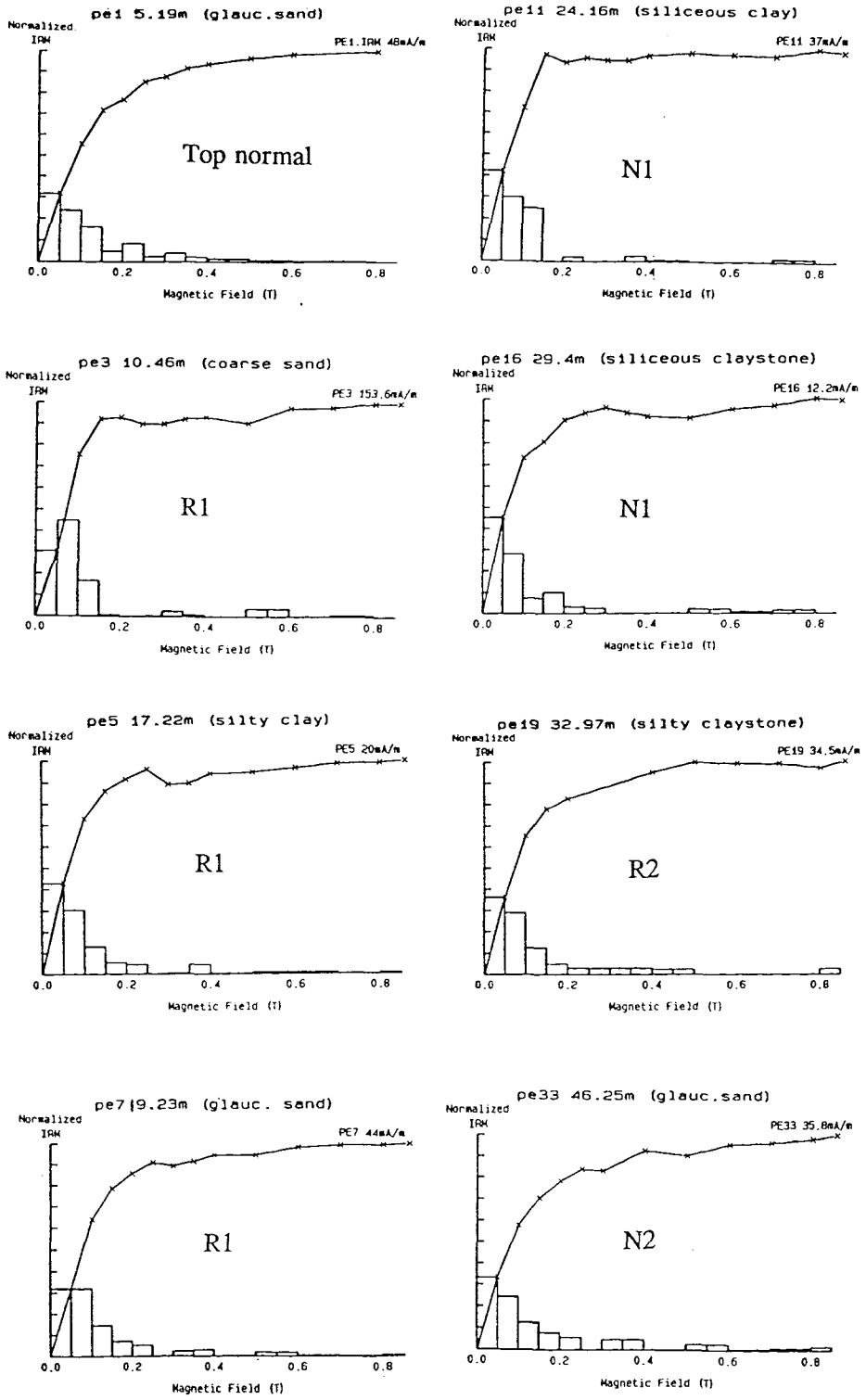

Figure 9-28a *IRM acquisition curves for samples from the Peterman core. The code of each graph (e.g. R1) refers to the magnetozone from which the sample has been taken (* Fig. 9-27).

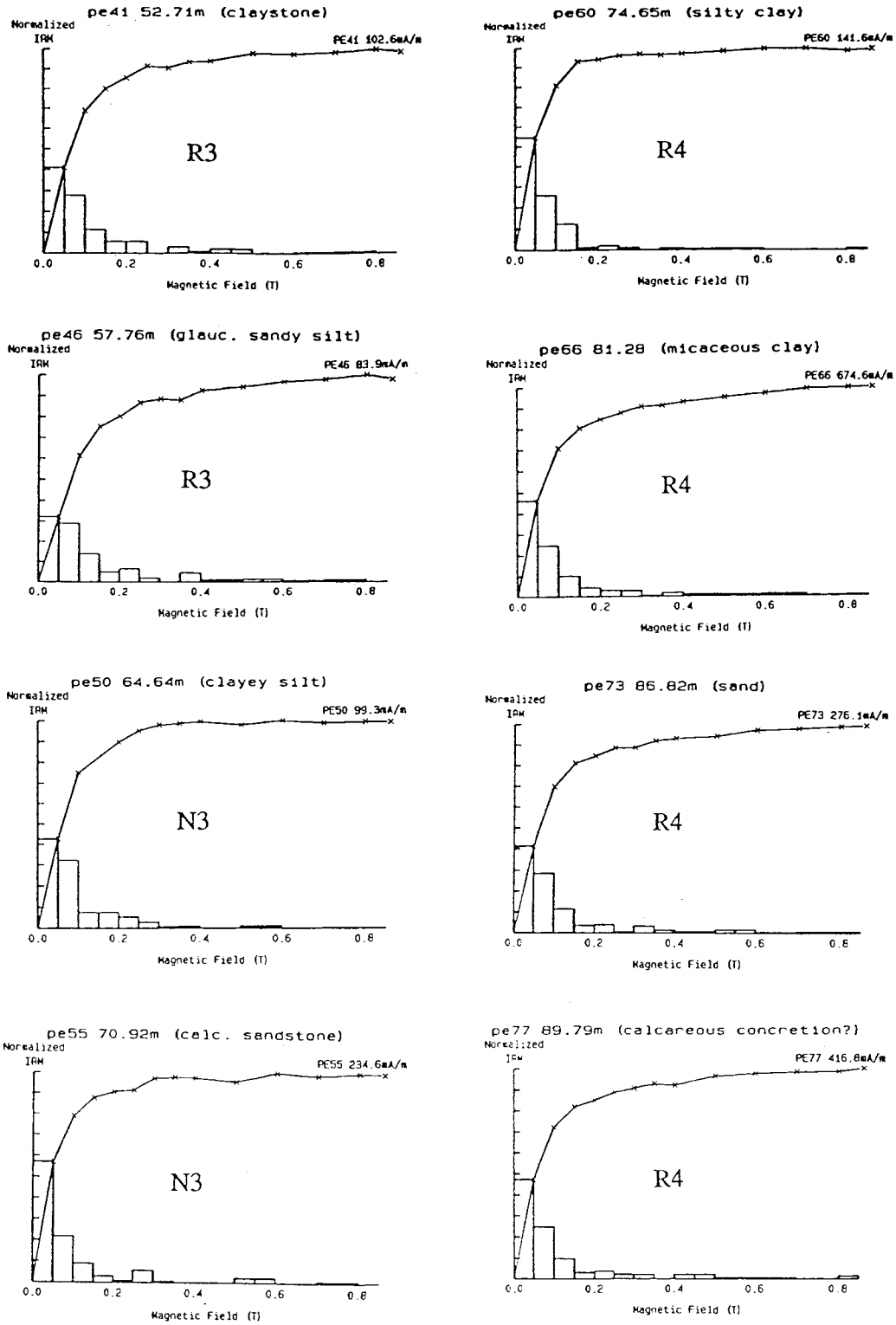

Figure 9-28b - *continued.*

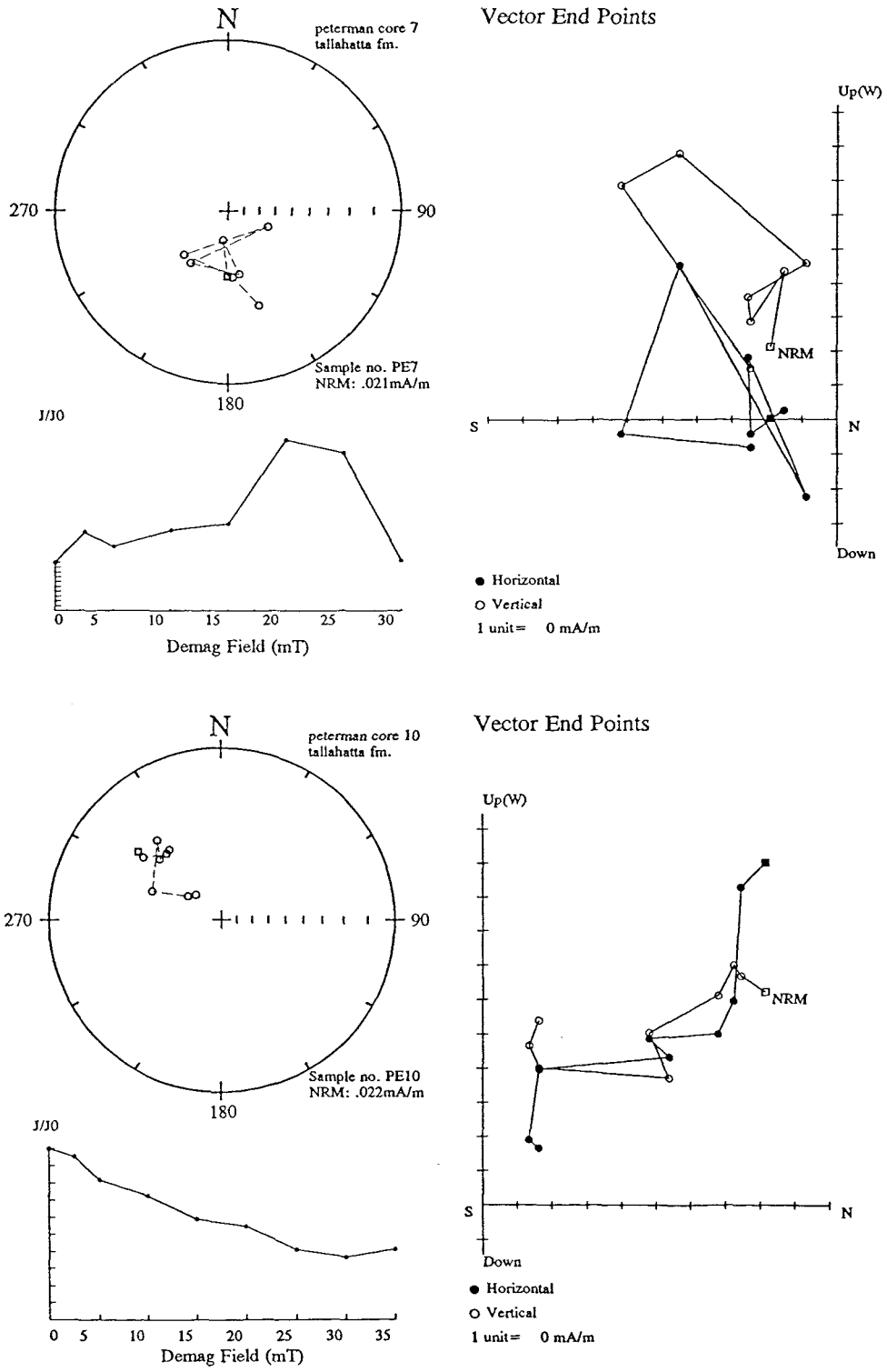

Figure 9-29 *SEP (category S2)* demagnetisation of samples from the upper reverse polarity zone (R1).

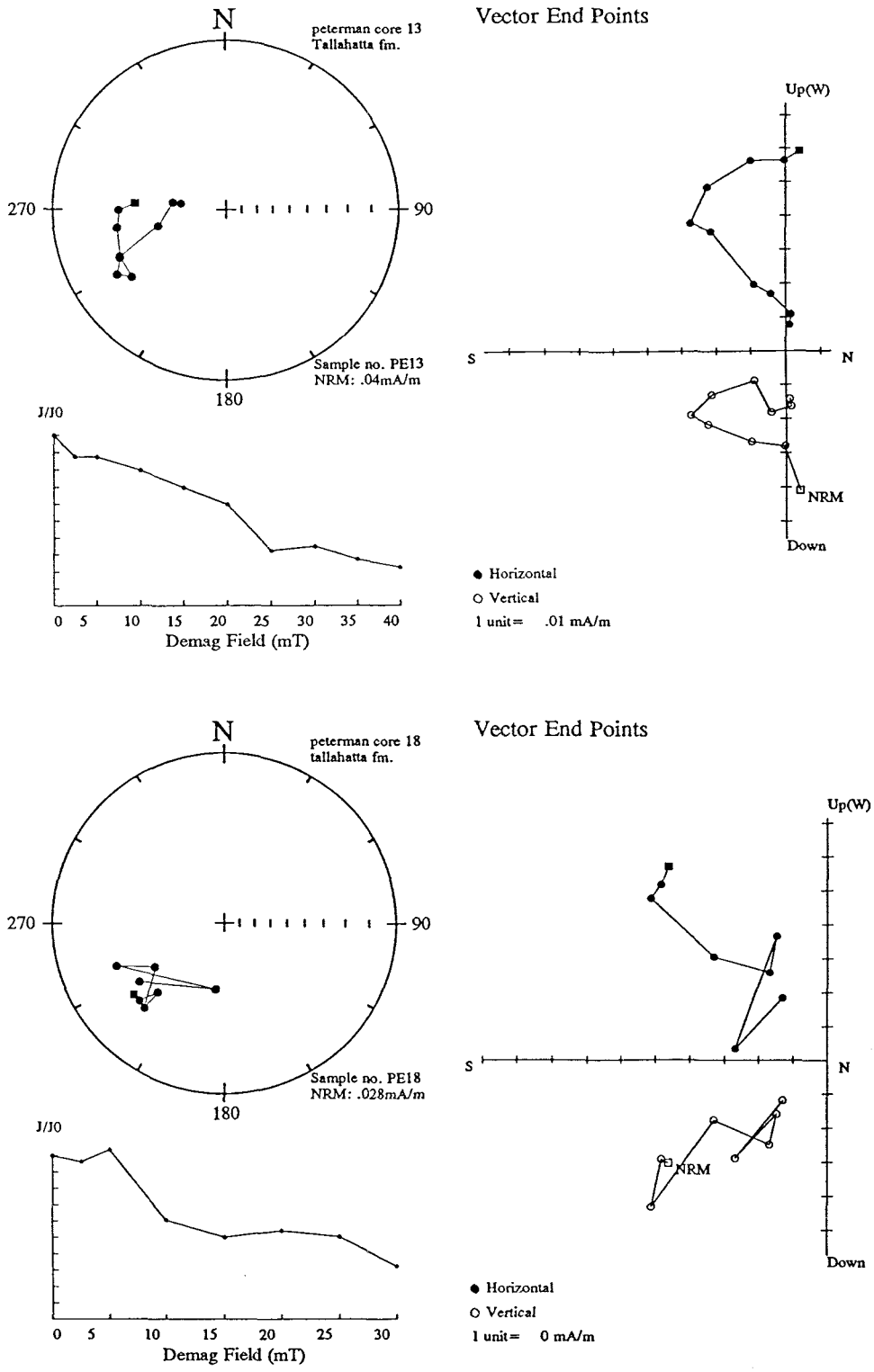

Figure 9-30 *SEP (category S2)* demagnetisation of samples from the upper normal polarity zone (N1).

IRM analyses on 2 samples from this zone indicate that magnetite is the predominant magnetic carrier (Fig. 9-28a). The normal zone here correlates with at least the upper portion of Chron C22n of the GPTS (Fig. 9-27).

- *Reverse polarity zone R2*

A reverse polarity zone interrupts the normal polarity interval within NP12. Examples of the quality of palaeomagnetic data are given in figure 9-31 which show reliable trends to a reverse polarity and reasonable reverse polarity SEPs in other samples. The IRM acquisition of a sample at the upper limit of the reversed zone (a depth of 33m) illustrates slower saturation rates of the magnetic minerals than seen in sediments above; however by 0.5T maximum saturation has occurred suggesting that magnetite is still the predominant magnetic mineral.

The position of the reverse polarity zone R2, is consistent with the position of Chron C23n.1r of the GPTS.

- *Normal polarity zone N2*

The polarity zone N2, which is well defined by 12 samples over 10m, correlates with the lower portion of Chron C23n (Fig. 9-27). Examples of the demagnetisation behaviour of the samples in this interval are illustrated in figure 9-32.

- *Reverse polarity zone R3*

The reverse polarity interval R3, covers a depth interval of 15m which includes the hiatus at the base of NP12 (proposed by Gibson, 1985). The quality of data from demagnetisation investigations (Fig. 9-33) and IRM analysis (Fig. 9-28b) is considered reliable but due to the poor biostratigraphic constraints below the hiatus, only the upper portion of the reverse polarity can be confidently matched with the GPTS (Chron C23r).

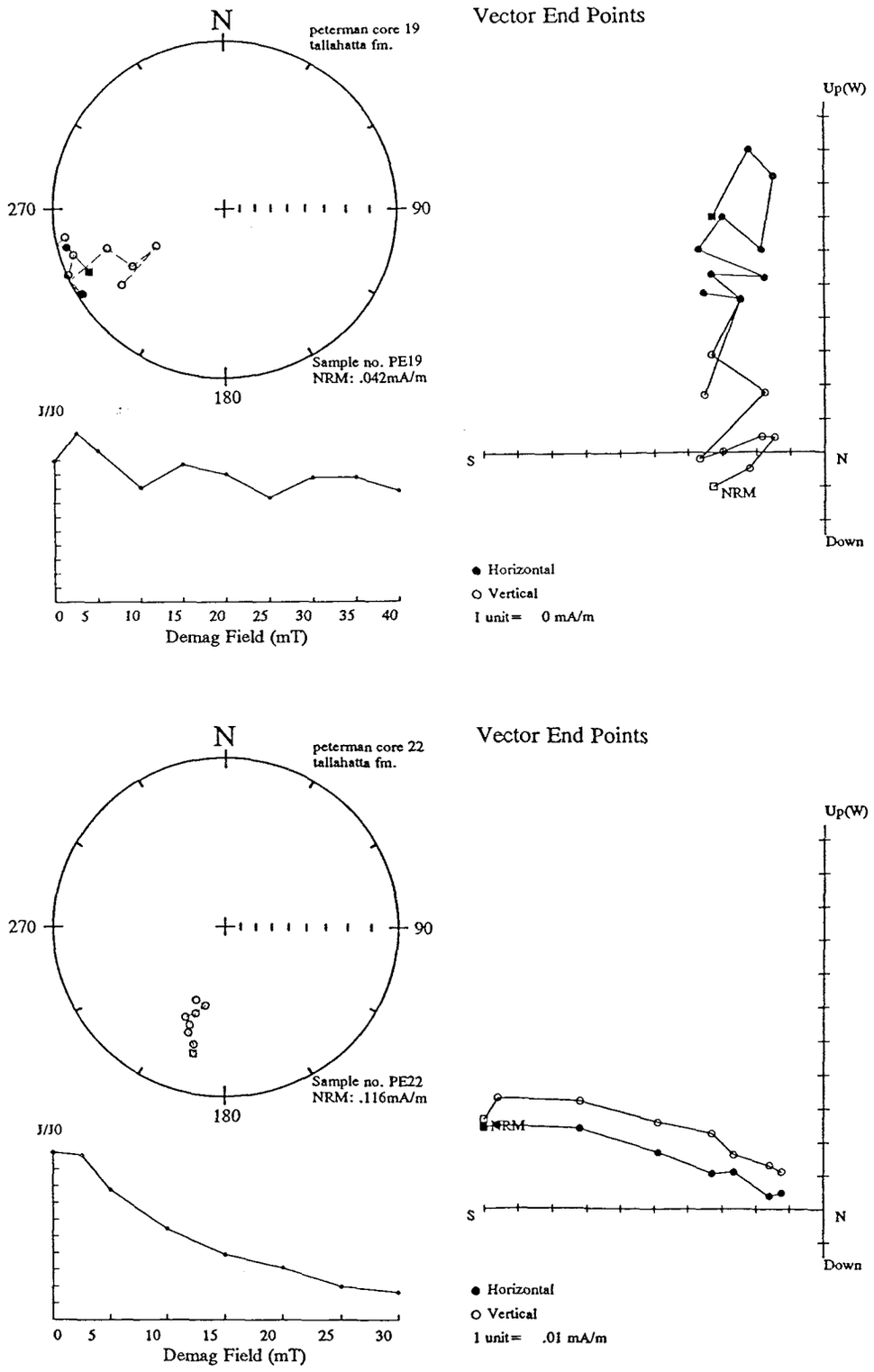

Figure 9-31 Demagnetisation behaviour of samples from the reverse polarity zone, R2.

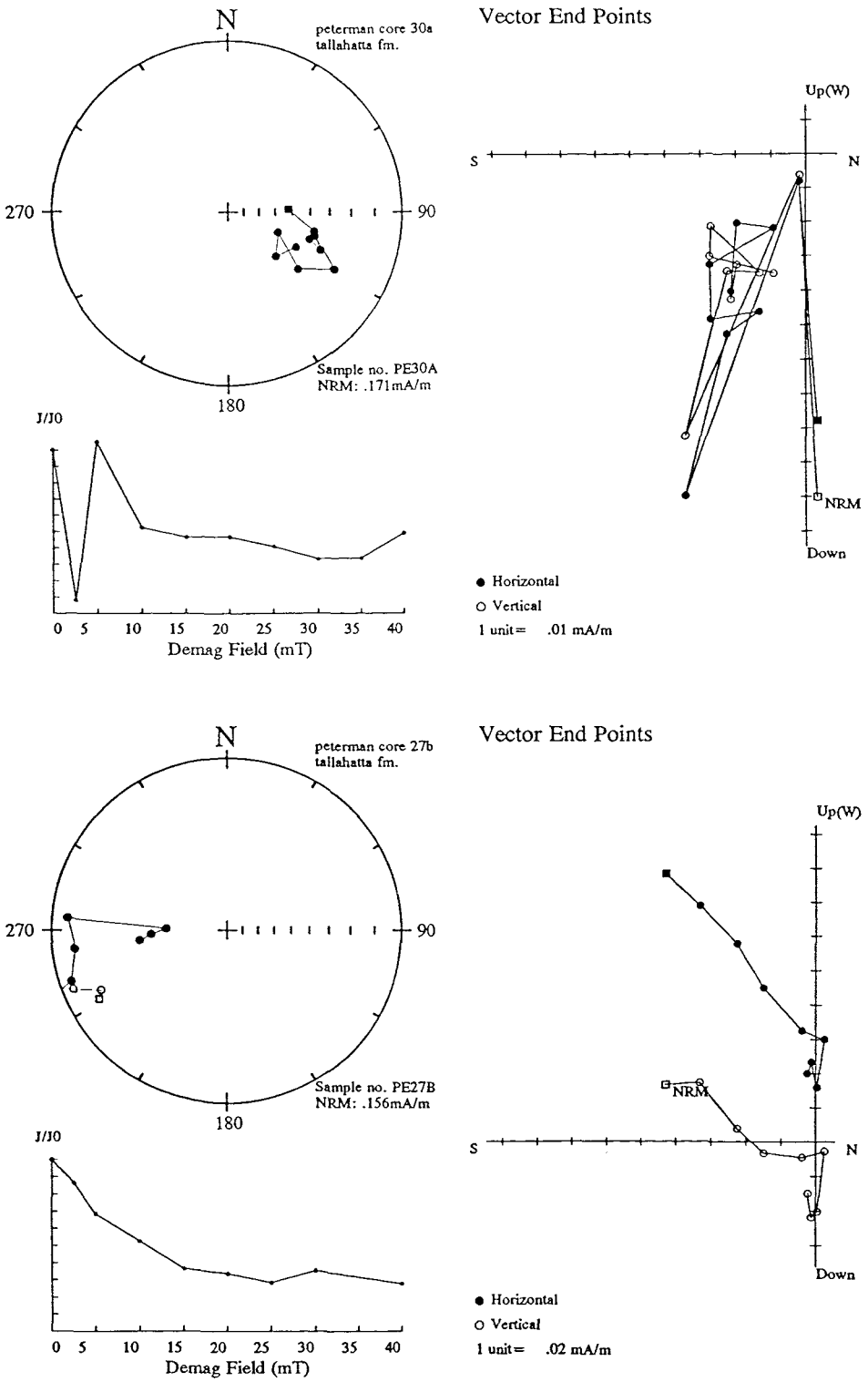

Figure 9-32 *Demagnetisation behaviour of samples from the normal polarity zone, N2.*

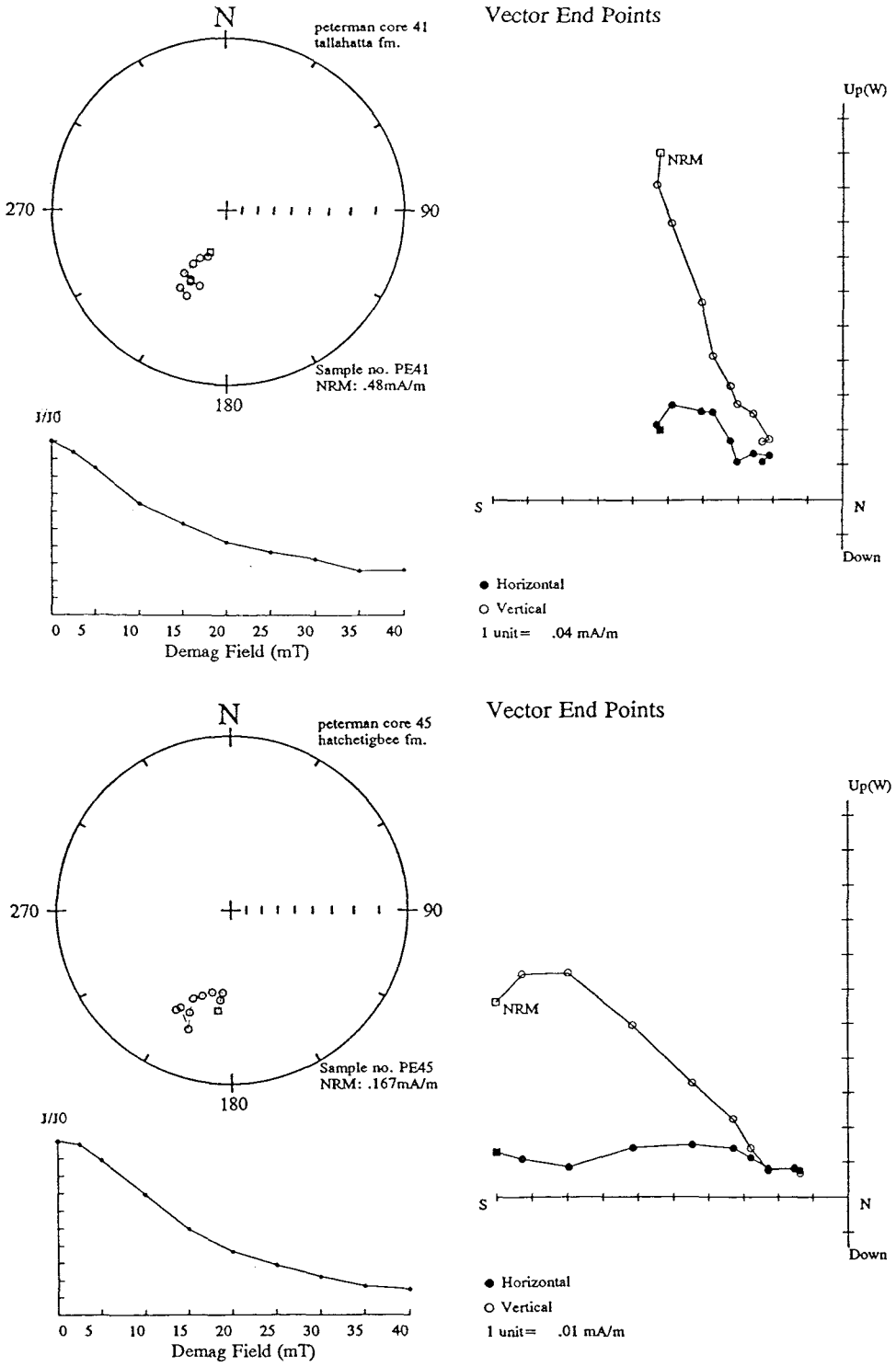

Figure 9-33 *Demagnetisation behaviour of samples from the reverse polarity zone, R3. The upper example is from the Tallahatta Formation and that below from the Hatchetigbee Formation, the two sites being separated by the major unconformity suggested from the nannofossil record.*

- *Normal polarity zone N3*

Assuming the biostratigraphy to be correct, the basal sediments of NP12 lie directly on top of NP10 material, therefore excluding NP11 (and presumably Chron C24n) from the sedimentary record. If this is the case, the entire Hatchetigbee/Bashi section of the core is NP10.

The normal polarity zone N3 is defined by intermediate quality palaeomagnetic data typically represented by SEPs and trends of reliability category S2 and T2. Thermal demagnetisation of 9 sites across the anomalous interval confirmed the existence of the normal polarity zone (Fig. 9-34a and b). In addition, the IRM curves for samples from both glauconitic sand and silty clay lithologies within this apparent normal interval saturate by 0.3T.

The presence of this N3 normal interval is problematical. It may be explained in 3 ways:

i) The biostratigraphy is incorrect and the hiatus at the Hatchetigbee/Tallahatta contact does not represent the duration of time proposed by Bybell and Gibson (1985). In this case sediment representing part of NP11 and thus recording Chron C24n may be present.

ii) N3 represents a severe magnetic overprint. However, there is no substantial evidence from IRM work, thermal or A.F. demagnetisation analyses suggest that this is the case.

iii) The samples from N3 are recording a previously unidentified event in the geomagnetic record. This is highly unlikely due to the vertical extent of the anomaly downcore (representing at least 4m) although the lack of biostratigraphic control does not rule out a period of rapid deposition during a magnetic crypto-Chron, especially considering that the Hatchetigbee Formation represents deposition in estuarine, tidal flat and shallow inner neritic environment.

The presence of a spurious normal interval within sediments of the same age in the Oak Grove core (Virginia) may be significant. (See Chapter 10).

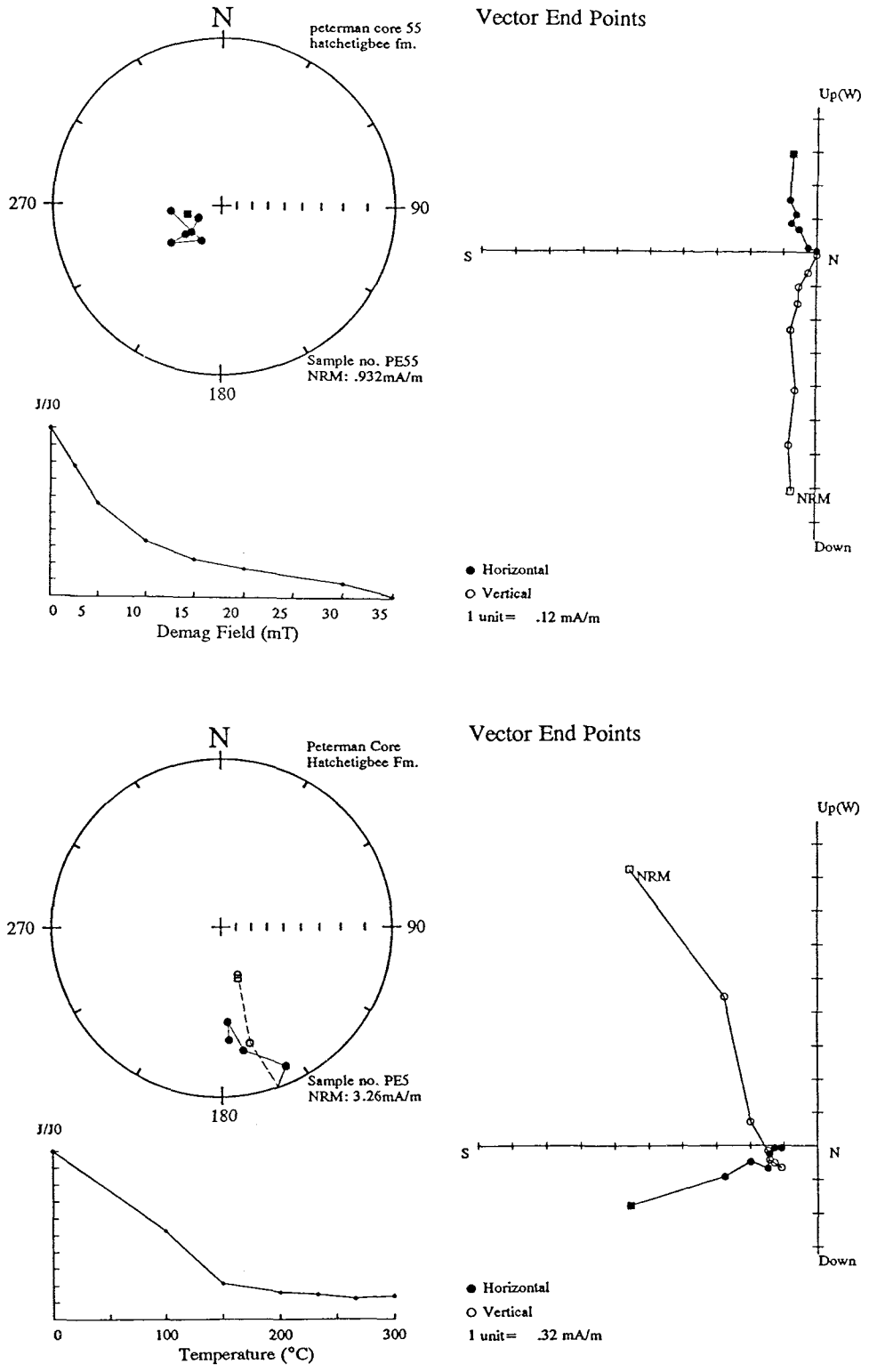

Figure 9-34*a* *Demagnetisation behaviour of samples from polarity zone N3.*

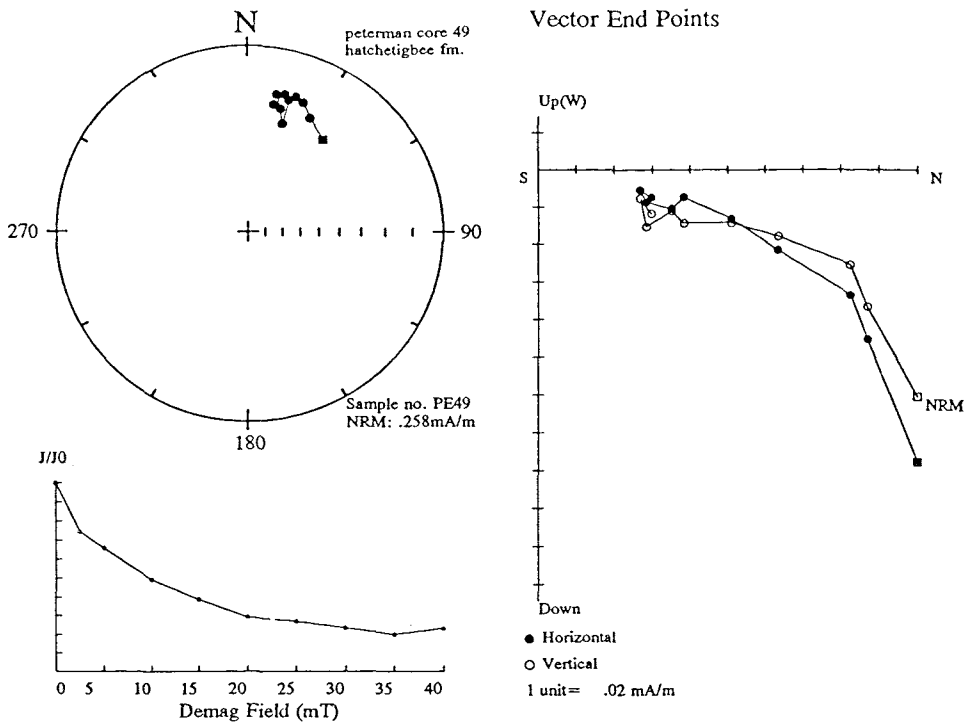

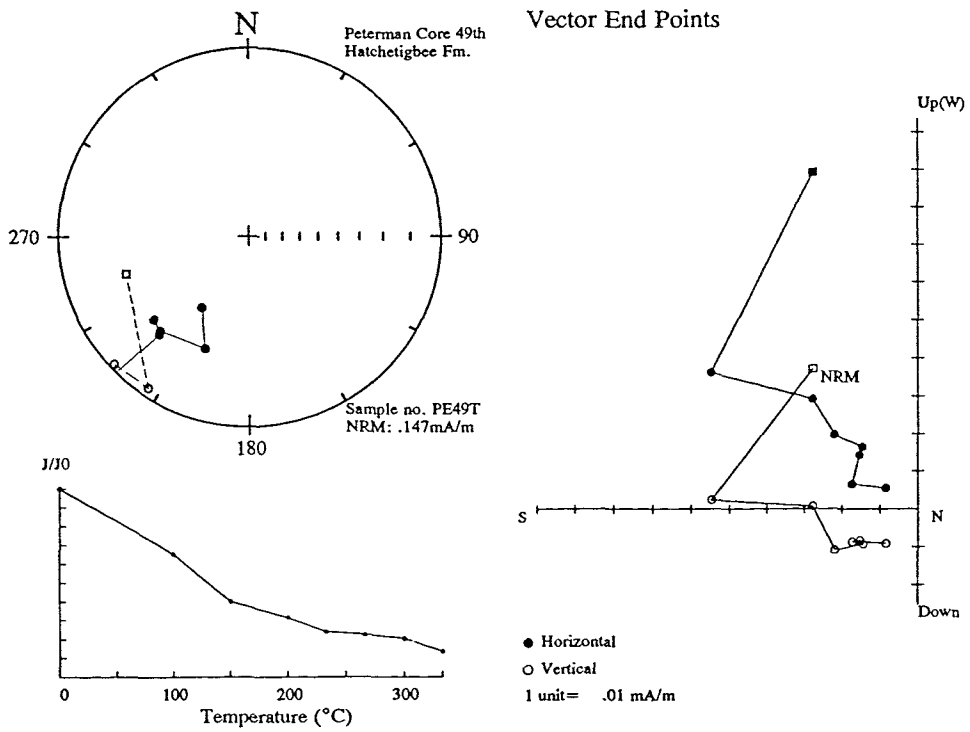

Figure 9-34*b* *Demagnetisation behaviour of samples from polarity zone N3.*

- *Reverse polarity zone R4*

Within the lowest 22m of core only one sample has a normal polarity SEP (Fig. 9-27); the remaining 23 samples show high quality reverse polarity plots where SEPs are categorised as type-S1 (Fig. 9-35). IRM analyses of 4 samples from the R4 interval show magnetite-type saturation curves (Fig. 9-28b). The reverse polarity zone here can be confidently correlated with Chron C24r.

NRM intensities, demagnetisation behaviour and SEP vector positions of samples from the bottom 15m of the core have characteristics that are very similar to the consistent reverse polarity material found throughout the Tuscahoma Formation. It is possible that the core has in fact penetrated the Tuscahoma Formation at this point; however, due to the absence of calcareous nannofossils, there is no biostratigraphic evidence to confirm this. Outcrop sections indicate that the Hatchetigbee/Bashi Formations should have a thickness of 50-60m in the Peterman core which suggests that the 35m of sediments penetrated are indeed confined to the Hatchetigbee/Bashi Formations (Gibson, pers. comm.).

Summary of the magnetostratigraphy of the Peterman core

Chron C23n is confidently identified in NP12, possibly incorporating sub-Chron C23.1r. This has Chron C23r at the base and at least a portion of Chron C22r at the top, although the interval was barren of nannofossils. Separated by a probable hiatus at the top of the core, in sediments of mid NP14 age, a single sample indicates a confident polarity that may represent the base of Chron C21n. The suspected hiatus is possibly responsible for the absence of Chron C22n. At the Tallahatta/Hatchetigbee Formation boundary biostratigraphic evidence indicates a hiatus that excludes Chron C24n from the sedimentary record although a normal interval is evident at about 65m (see Chapter 10). Below this normal interval sediments of Chron C24r are preserved.

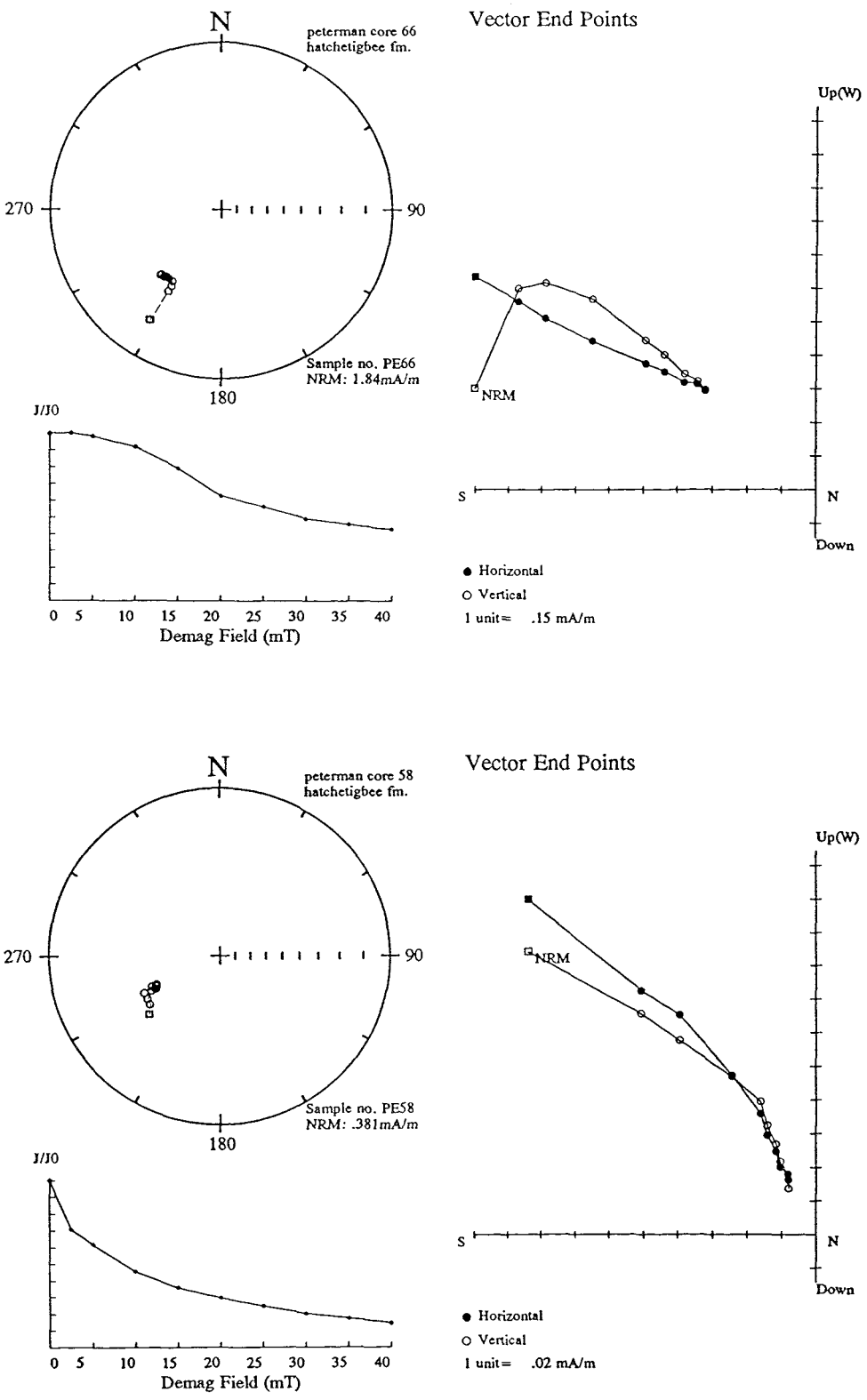

Figure 9-35 *SEP demagnetisation behaviour of samples from polarity zone R4.*

9.2.2 Campbell locality

Location: Roadcuts along the east and west sides of Alabama Highway 69, approximately 3km south of and 1.6km north of Campbell, Alabama.

Within the roadcut section along Highway 69, the lower and upper contacts of the Tallahatta Formation are exposed. The formation covers a stratigraphic height of approximately 20m although some intervals are poorly exposed (Fig. 9-36 and 9-37). At the top of the section the lower beds of middle Eocene Lisbon Formation are visible but highly weathered and at the bottom the Meridian Sand Member is present as a white, micaceous, bioturbated, fine-grained sand. It has a discomformable contact with the Hatchetigbee Formation at the base and a sharp but highly burrowed upper contact with the Lisbon sediments above.

Sampling

Large hand samples were taken from 15 sites. These were split into 2-3 sub-samples and demagnetised using predominantly an alternating field (only 12% of sub-samples were thermally demagnetised). The sampling technique used restricted sites to soft sediments which increased the sampling interval over some lithified units. The Meridian Sand Member was not sampled.

Polarity analysis

The quality of demagnetisation data is generally poor, partly due to the weak average NRM intensities of samples from the Tallahatta Formation (0.046mA/m). Repeat measurements ensured that all the data points have alpha 95 values $< 10°$, however sample demagnetisation categories are at best intermediate quality SEPs and trends (S2/T2) with 60% of specimens falling in this group. Of the remaining specimens, 18% show questionable trends (T3), 3% questionable SEPs (S3) and 18% show anomalous positive inclination values with southerly declinations.

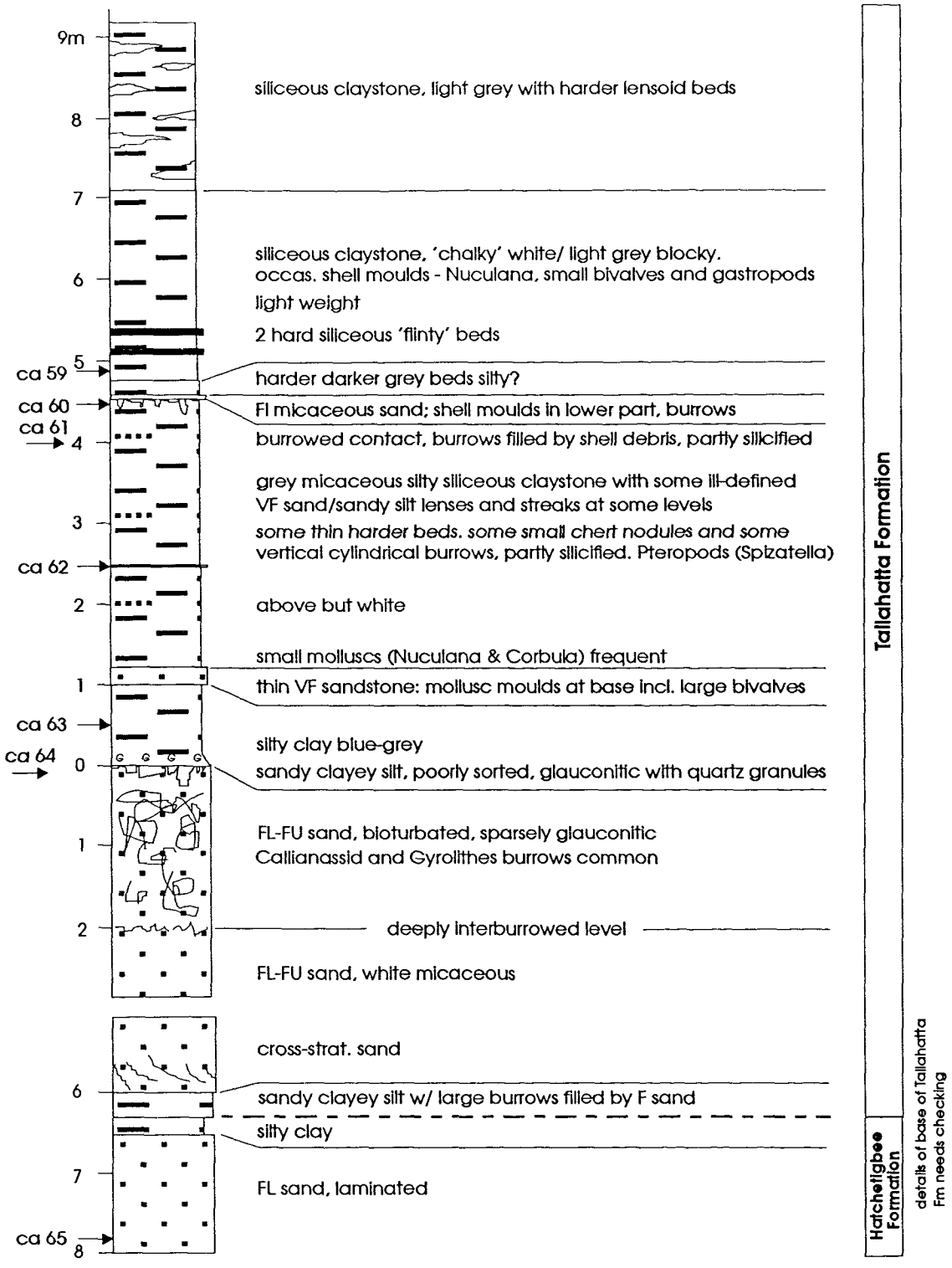

Figure 9-36 *Stratigraphic log and sample sites in the lower beds of the Tallahatta Formation at the Campbell locality.*

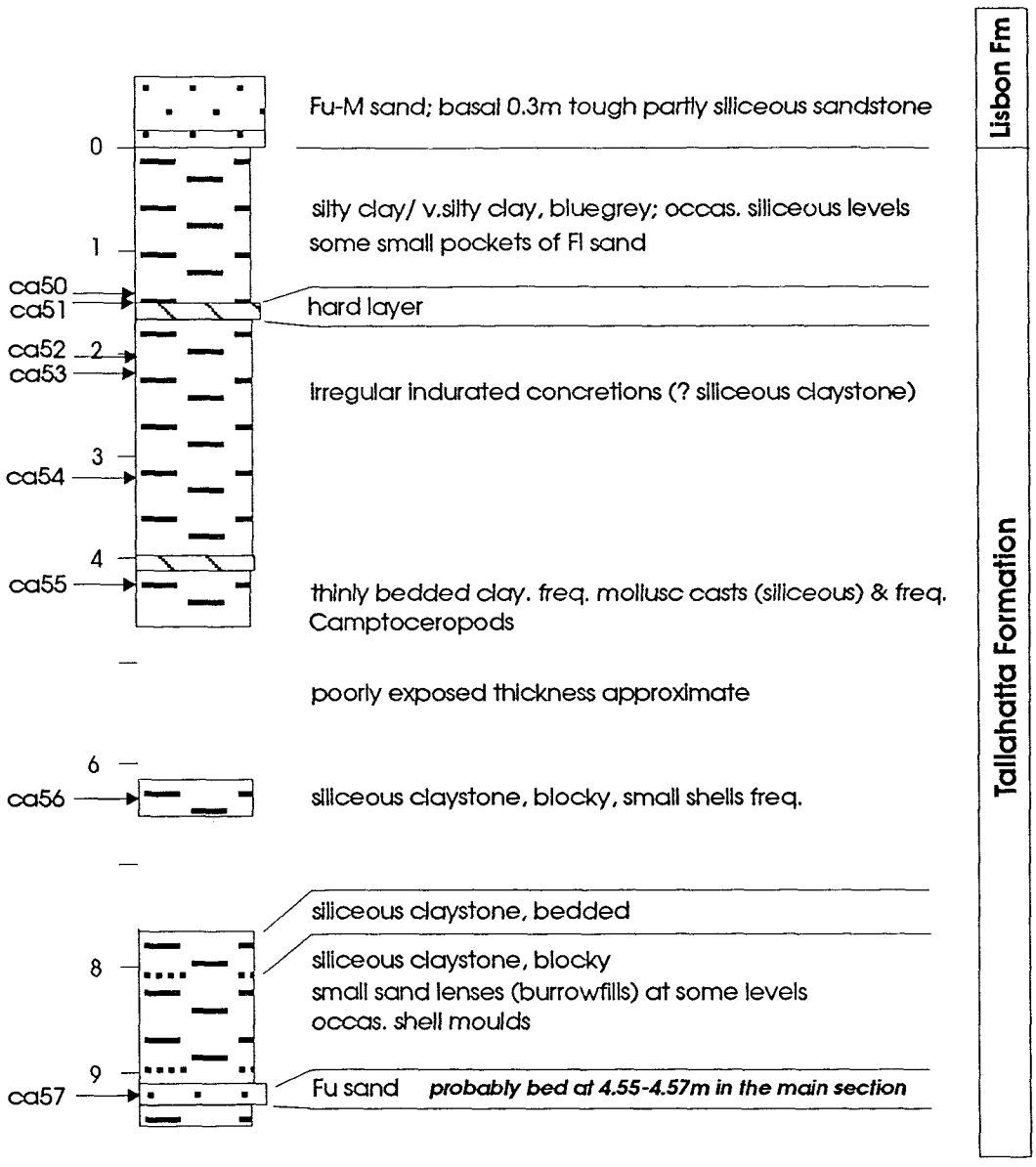

Figure 9-37 *Stratigraphic log and sample sites of the upper beds of the Tallahatta Formation at the Campbell locality.*

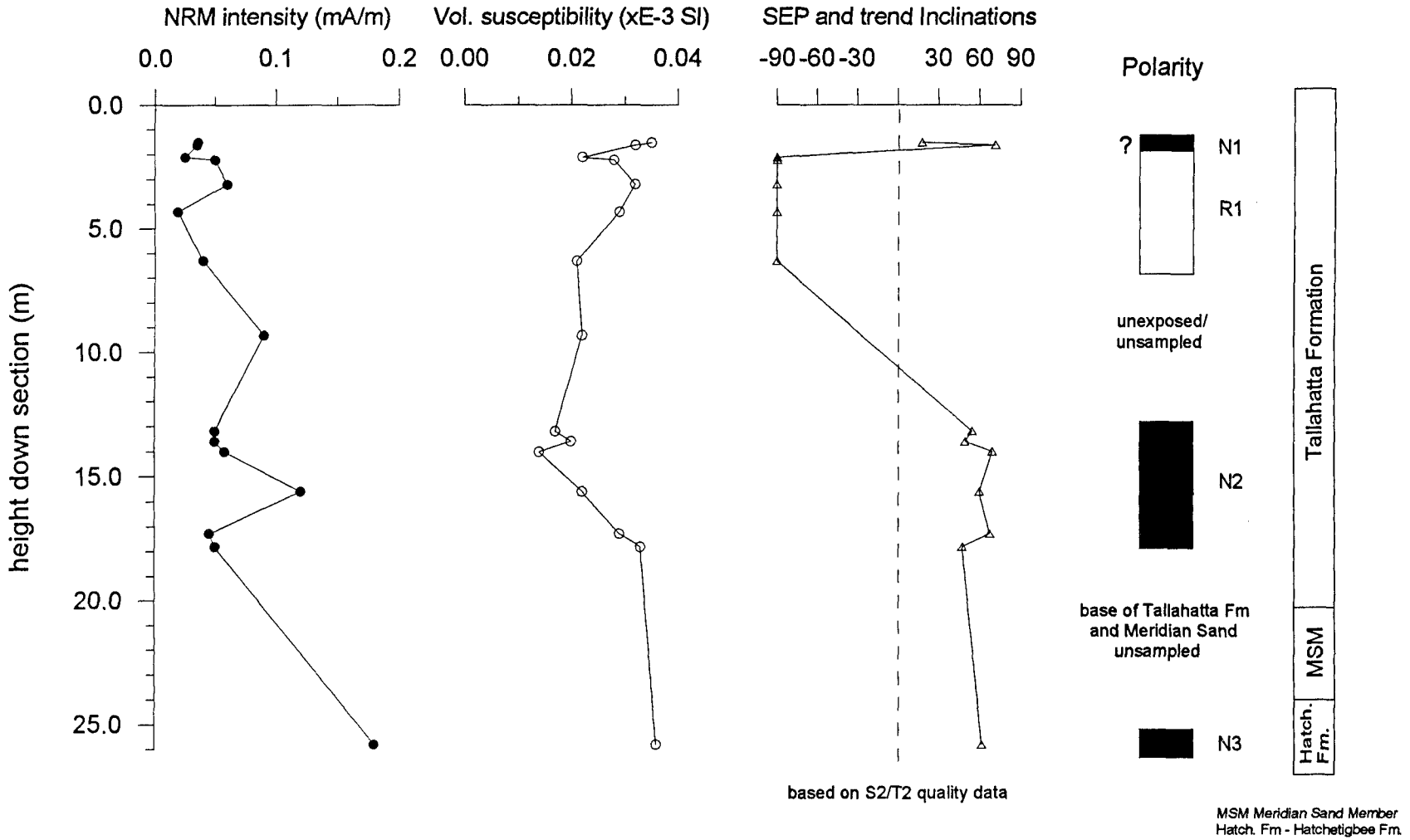

Figure 9-38 *Graphical summary of the NRM intensities, susceptibility and polarity determination of samples from the Campbell locality.*

In the section sampled, 4 distinct polarity zones have been identified (labelled N1, R1, N2 and N3 in figure 9-38).

The uppermost normal polarity zone (N1) is based on only 2 sites which exhibit poor quality SEPs and which therefore remains questionable (Fig. 9-39). An interval of reverse polarity is then recorded by confident trends in at least 4m of sediment below the apparent normal polarity at the top of the section. Within this interval there is a good consistency between hand samples from the 1991 field trip (Fig. 9-40) and those drilled at this section in 1990 (Fig. 9-41).

A normal polarity interval between 13.2-17.8m (Fig. 9-38, 'N2') is defined by samples from 6 sites which show good internal consistency of sub-samples from the same stratigraphic height (Fig. 9-42; appendix 24). At approximately 1.5m below the base of the Meridian Sand Member, within a sandy unit of the upper Hatchetigbee, one sample shows a normal polarity which is confirmed from A.F. and thermal demagnetisation of separate sub-samples (Fig. 9-43).

IRM investigations at 2 sites (from the upper reverse polarity interval, R1, and lower normal polarity interval, N2) yield saturation curves that indicate magnetite as the main magnetic mineral; this is supported by thermal demagnetisation behaviour during which no thermochemical reactions involving magnetic minerals are evident.

Magnetostratigraphy

A significant proportion of the samples (45%) have been assigned questionable polarities, which clearly affect the resolution of those polarity intervals identified.

There is some doubt about polarity correlations with the GPTS due to the exposure problems which severely restrict continuous sampling and to some extent the lack of nannofossil zonation for this particular section. Various sections and 5 coreholes spanning the Tallahatta Formation (including the Peterman core, section 9.21) studied by Bybell and Gibson (1985) have shown that the formation spans NP12, NP13 and NP14 although sediments expected to be of NP13 age appear to be barren of nannofossils in western Alabama.

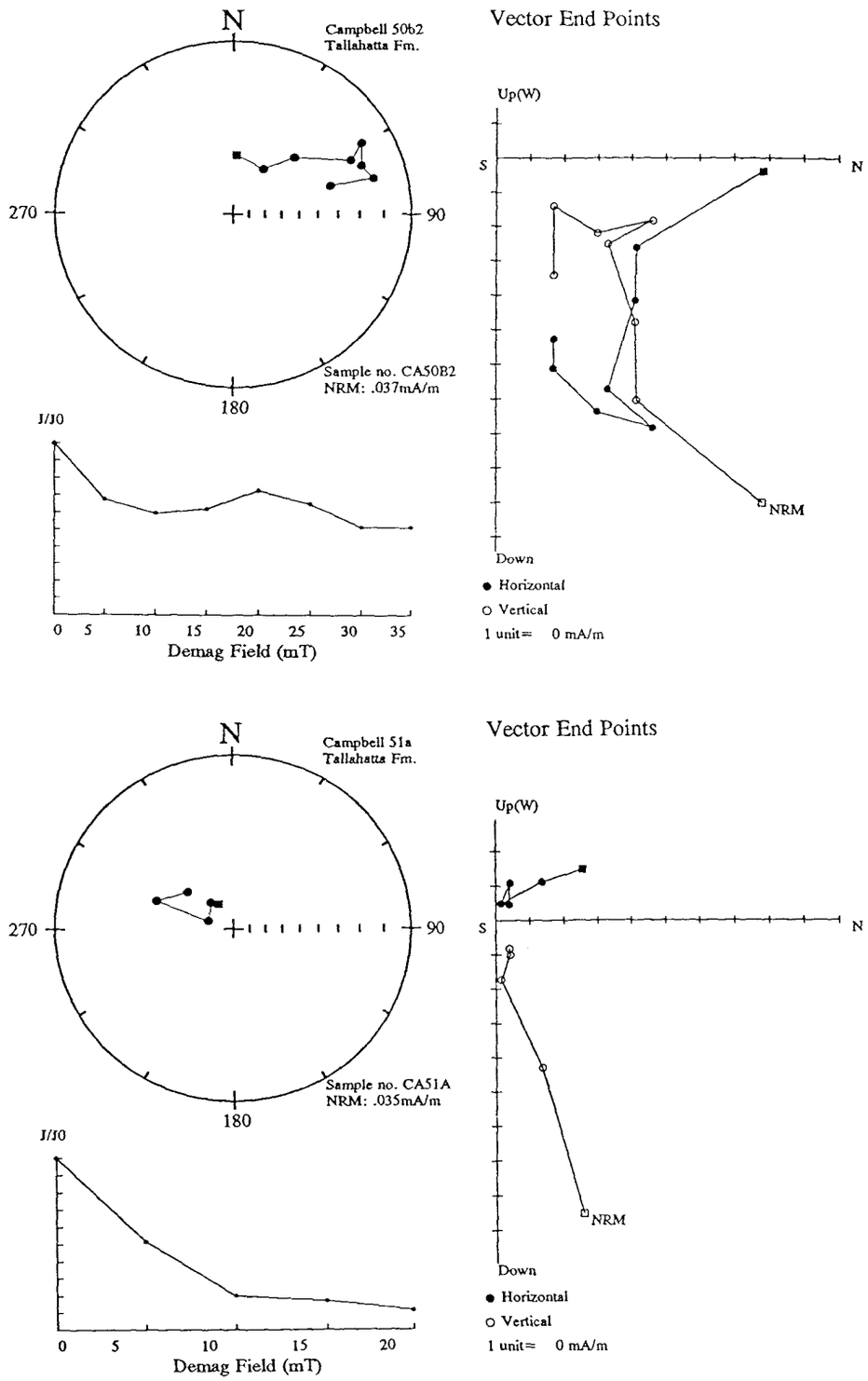

Figure 9-39 *Demagnetisation behaviour of sites from the top of the Tallahatta Formation section immediately below the Lisbon Formation contact (position N1).*

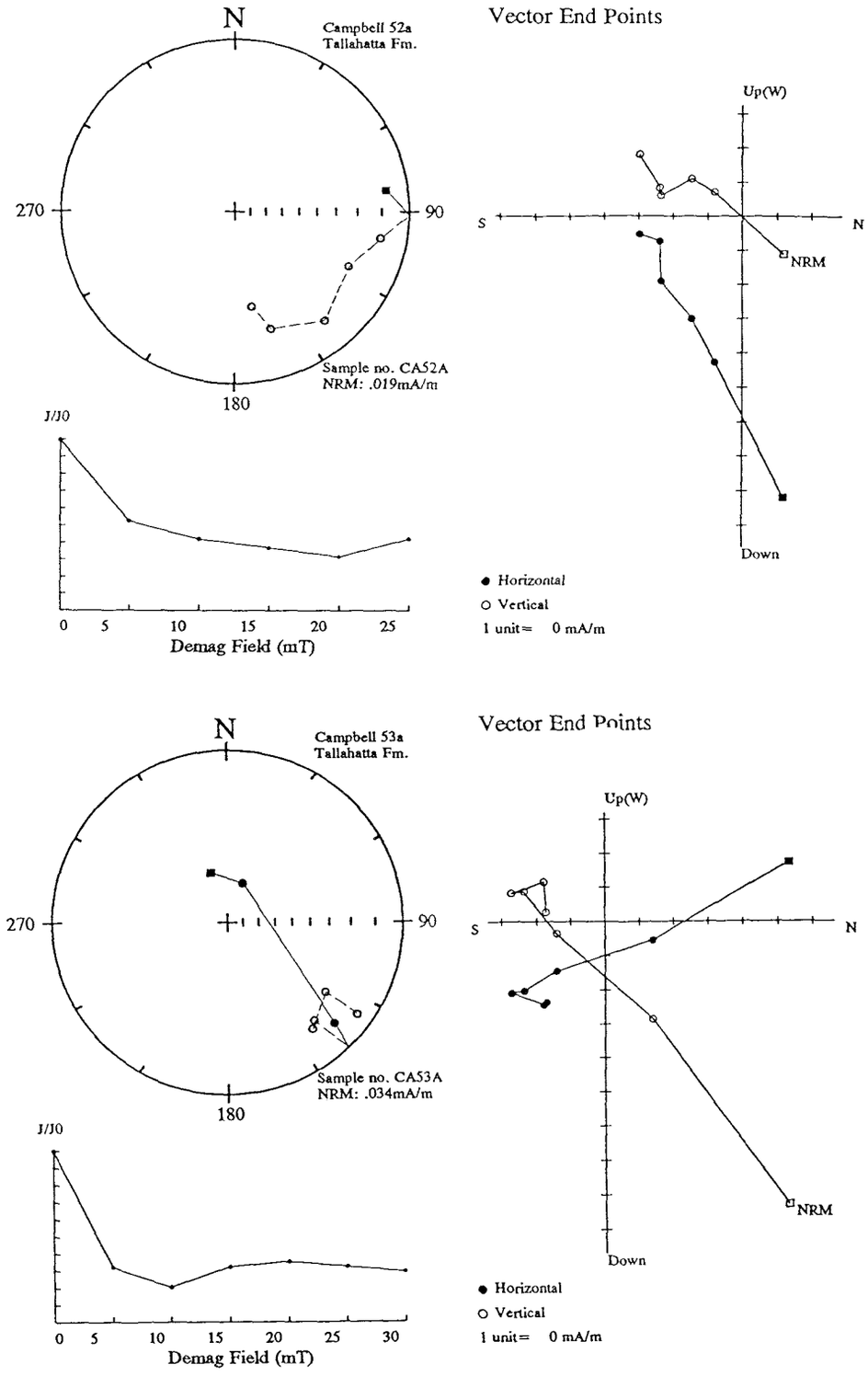

Figure 9-40 *Examples of reverse polarity trends from hand samples from interval 'R1' (Fig. 9-38).*

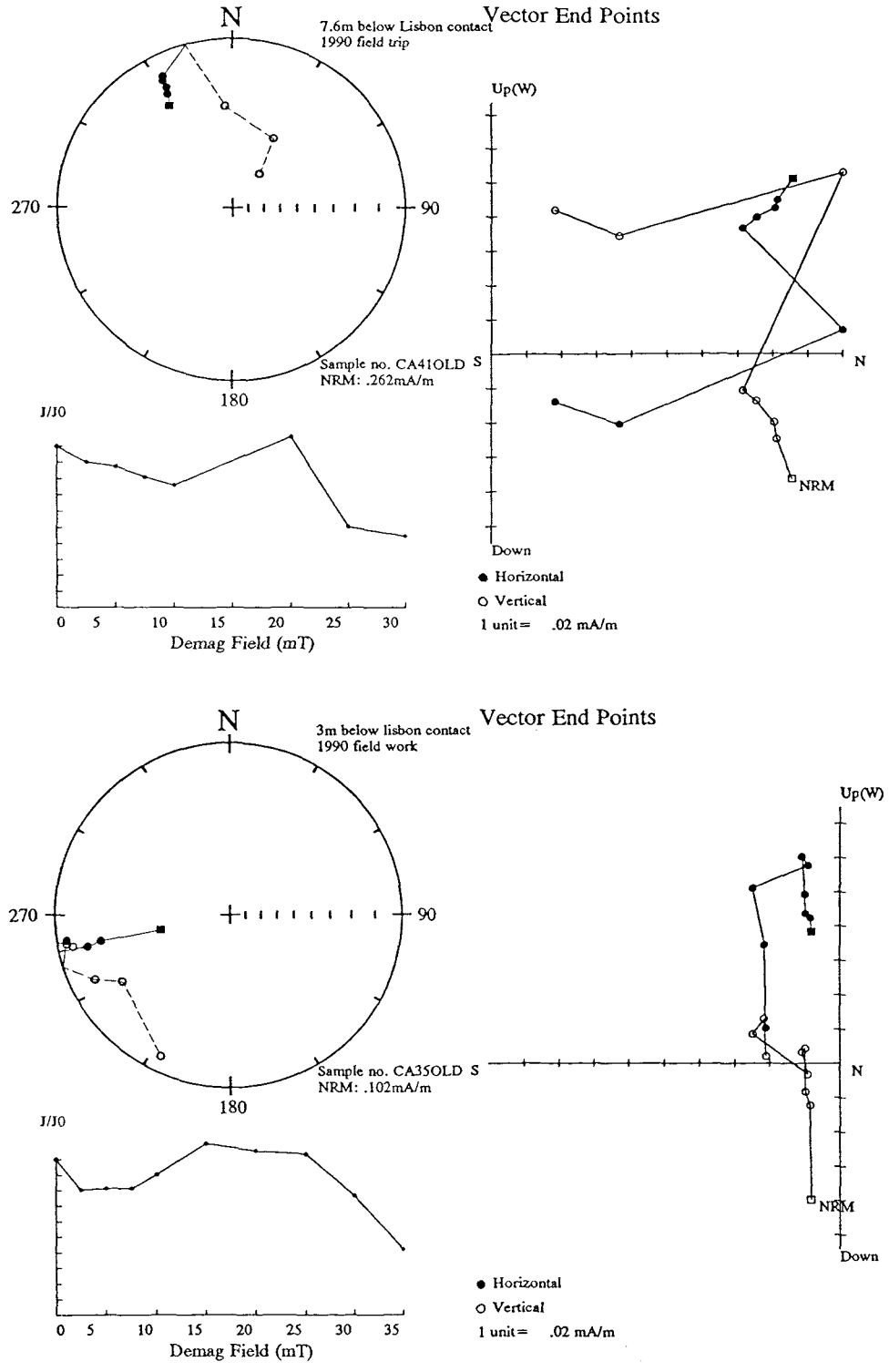

Figure 9-41 *Examples of reverse polarity trends from lithified units drilled in 1990 from interval 'R1' (Fig. 9-38).*

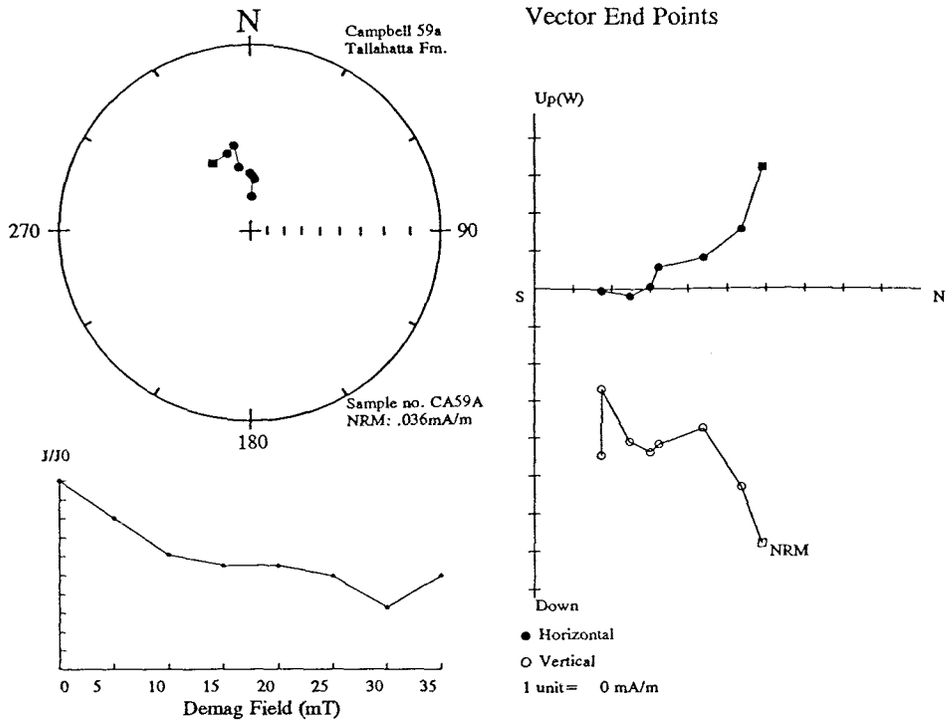

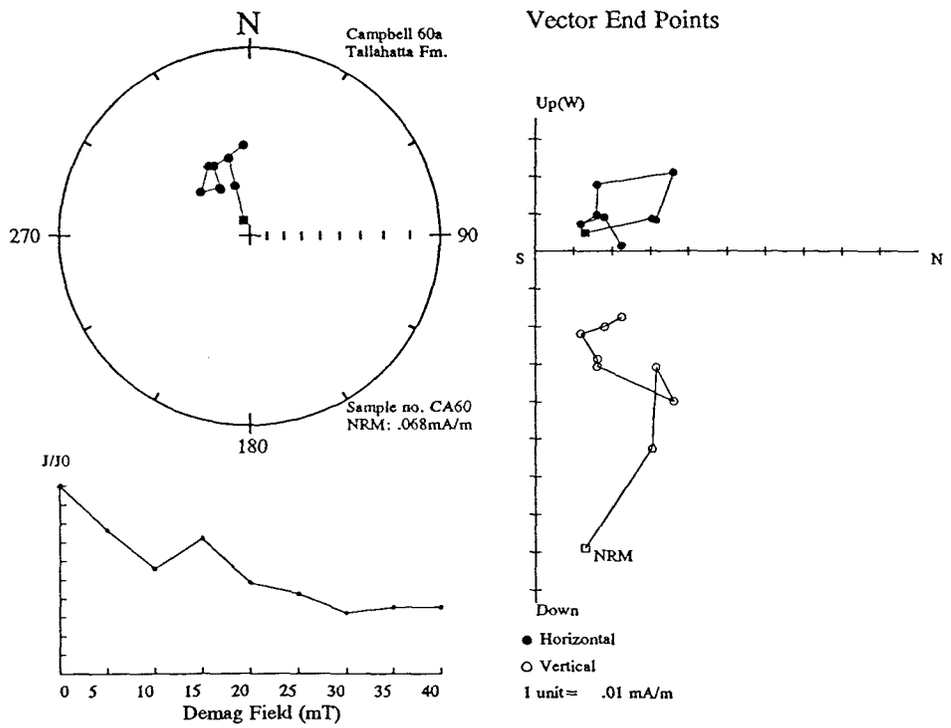

Figure 9-42 *Examples of normal polarity SEPs from interval 'N2' (Fig. 9-38).*

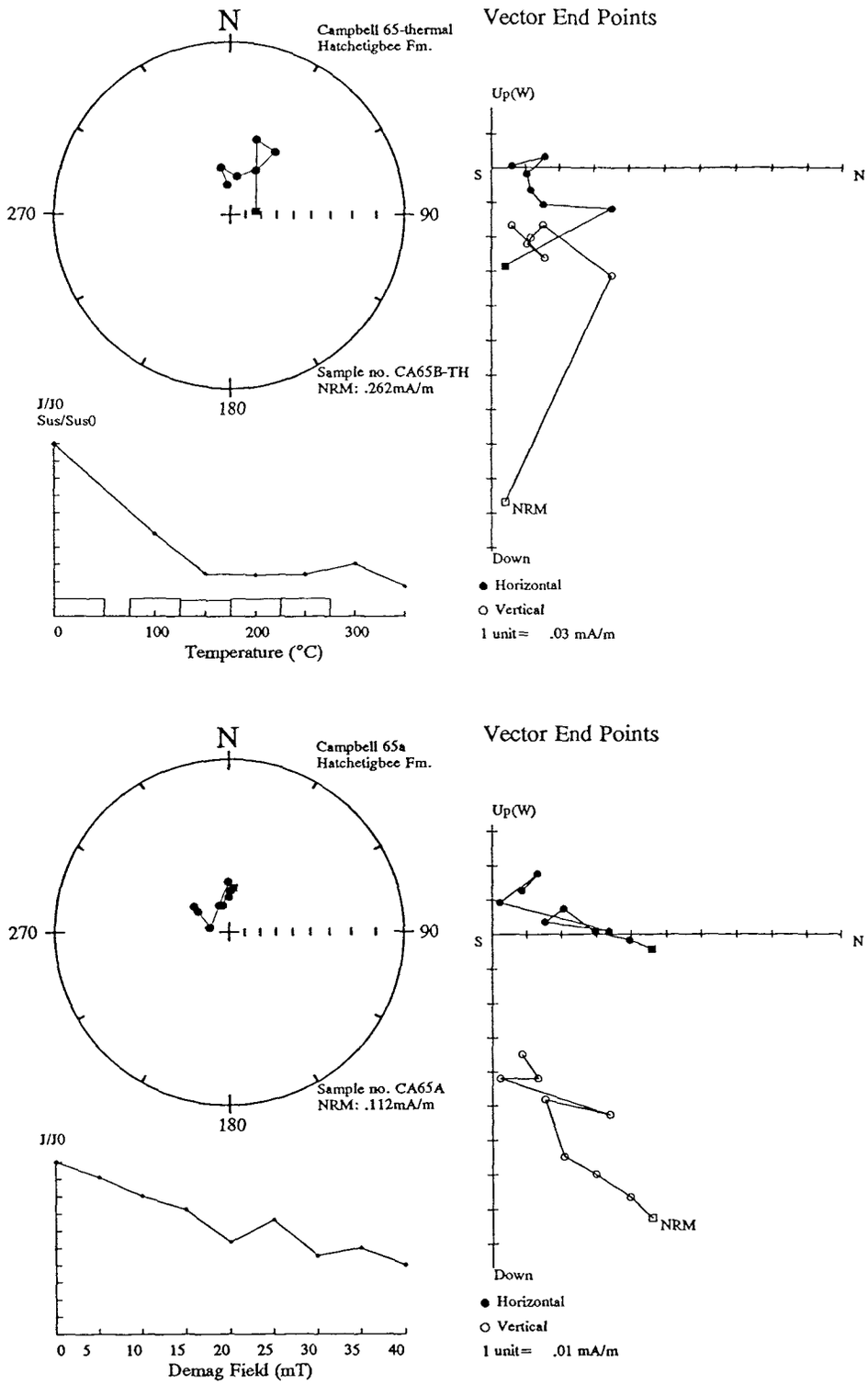

Figure 9-43 *Normal polarity site 'N3', within the upper Hatchetigbee Formation determined from Thermal (top) and A.F. demagnetisation (bottom) techniques.*

The relative position of the camptoceratops bed when compared to that at Little Stave Creek is considered by C.King (pers. comm.) to indicate that the upper beds of the Tallahatta at the Campbell locality (and Butler) have been removed. Based on this assumption the following correlations of the polarity zones identified (N1-N3) are suggested:

N1 Probably represents the base of Chron C22n which is expected within upper NP13 and lower NP14 sediments.

R1 The reverse polarity zone defined by consistent trends correlates with Chron C22r.

N2 The normal polarity zone here correlates with Chron C23n and can be linked to the Butler and Midway sections by the position of a glauconite rich interval.

N3 There is some doubt about the precise location of the formation contact (King, pers. comm.) and since only one sample defines the normal polarity zone a correlation with the GPTS has not been made.

9.2.3 Butler locality

Location: The section is exposed in a roadcutting a route 17, 6km south of Butler, Choctaw County, Alabama.

The Tallahatta Formation at this locality outcrops in an upper section, where the contact with the Lisbon formation is visible; in a middle section in a ditch of severely weathered claystone and in a lower section along a stream which exposed the lower Tallahatta contact with the Meridian Sand Member (Fig. 9-44). Two datums have been used to measure the section; the top 12 sites were measured relative to the upper formation contact and the lower 11 sites are measured above the Meridian Sand Member.

Forty six specimens were analysed from 23 sites over an estimated stratigraphic height of 20m. These were predominantly A.F. demagnetised to a maximum field of 40mT with specimens from 5 sites being thermally demagnetised (Appendix 25). Maximum temperatures during thermal demagnetisation were typically 350°C by which time the intensities of the samples had dropped to a level where $\alpha 95$ values for repeat measurements reached unacceptable levels. A sample at the top of the section (site 31) however, was heated to 500°C by which point no significant susceptibility increases had occurred (Fig. 9-45). In addition, IRM analyses were carried out on samples from 2 sites which indicated a magnetite dominated curve(Fig. 9-46).

Polarity analysis

The quality of demagnetisation behaviour was poor and polarity assignments were generally even more difficult than at the Campbell section. Appendix 25 illustrates the extent of the problem: 24% of samples were categorised as anomalous from which no polarity assignment was possible and a further 35% exhibited category 3 demagnetisation behaviour (T3/S3) which provided questionable polarities. Throughout the section therefore, 59% of the specimens were potentially unreliable.

Graphical representation of only the intermediate quality data (S2/T2) identifies a possible polarity sequence where polarity intervals are generally poorly defined by a small number of samples (Fig. 9-47). Two of these intervals however are considered

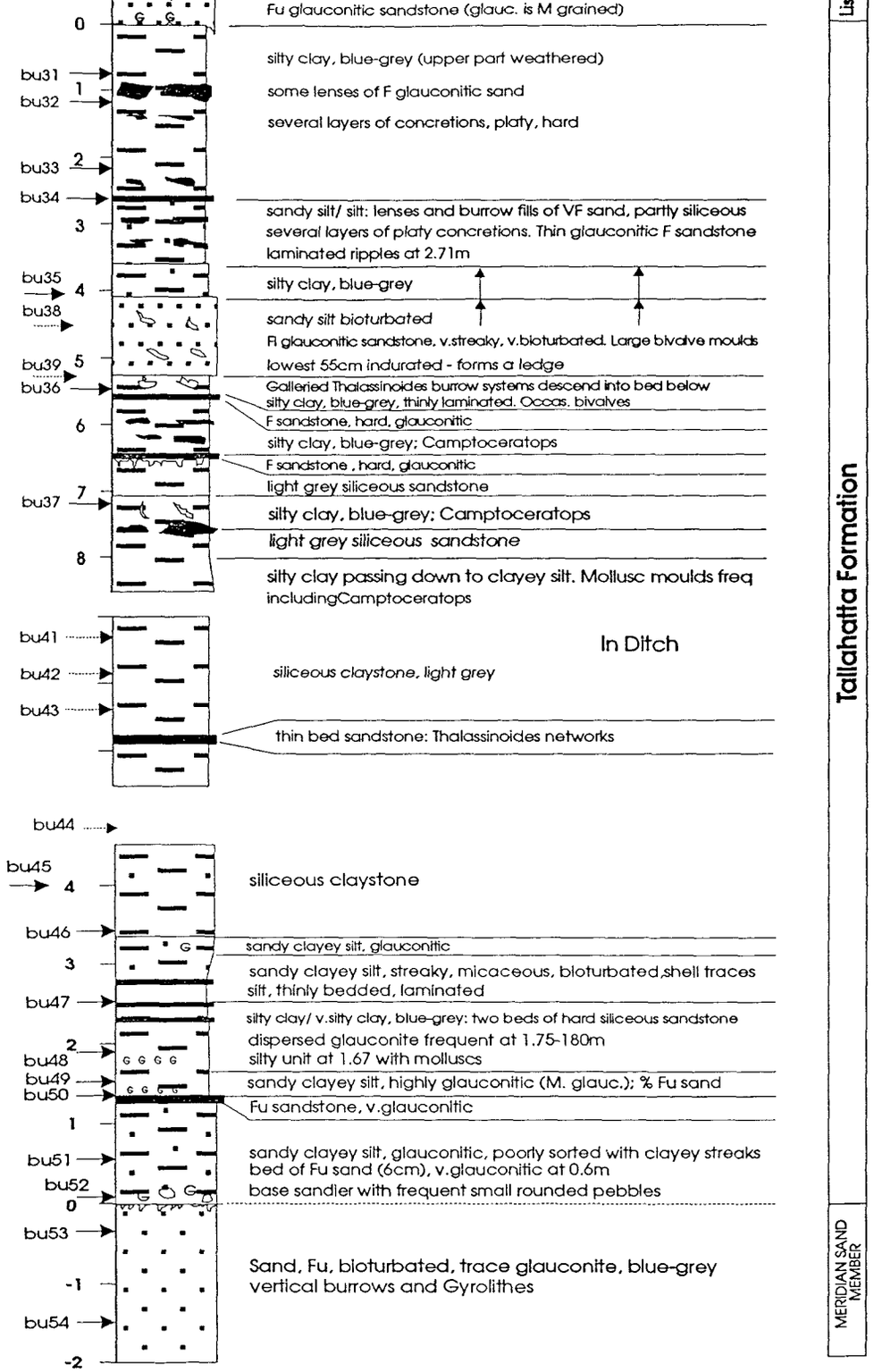

Figure 9-44 *Stratigraphic log and sample sites at the Butler locality.*

reliable: at least the lower 3m (sites bu52-48; interval polarity 'R2') of the Tallahatta section, above the Meridian Sand Member carries a reverse polarity (Fig. 9-48) and samples from a 2m interval within the upper section (sites bu31-33; interval 'N1') have a normal polarity, based on type S2 and S3 demagnetisation data (Fig. 9-49). Below the upper normal zone, several sites show affinities to a reverse polarity (sites bu34-38; interval 'R1'; fig. 9-50) and S2/T2 samples from the majority of sites from the central portion of the section (bu39-46; interval 'N2/N3') suggest a predominantly normal interval (Fig. 9-51) although the sampling interval and exposures are poor.

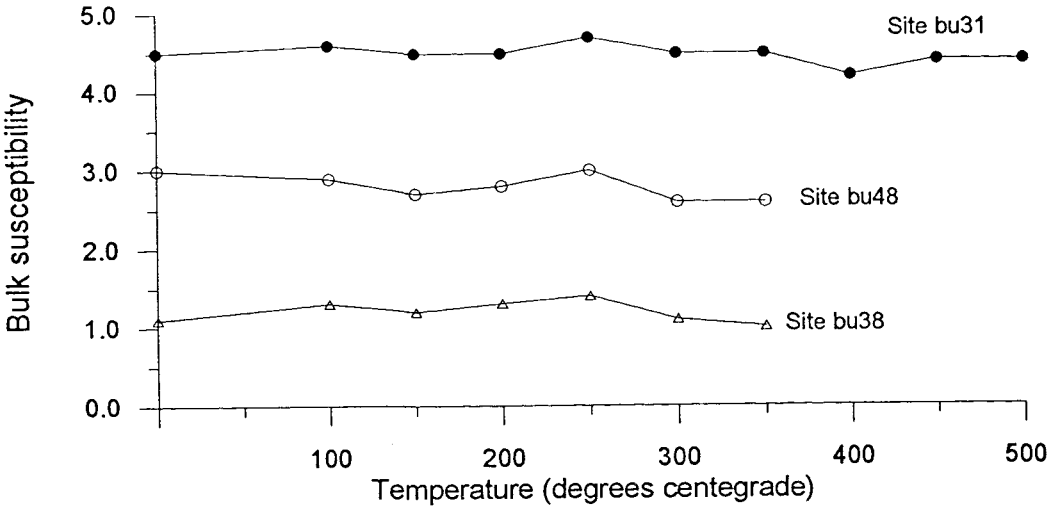

Figure 9-45 *Variations in susceptibility during thermal demagnetisation.*

Magnetostratigraphy

The degree of confidence of the magnetostratigraphy determined during this study was based on several criteria (see section 3.6). The quality and consistency of palaeomagnetic results from the Butler section combined with the poor exposure and lack of biostratigraphic control result in few of these criteria being satisfied and therefore there is considerable doubt when attempting magnetostratigraphic correlations for most of this section. However, within the uppermost and lowermost

parts of the section there is some consistency between neighbouring sites that define polarity zones which can be tentatively linked with other Tallahatta sections. The upper normal zone (N1), directly below the Lisbon Formation contact is considered by C.King (pers. comm.) to represent Chron C22n (and hence the reverse zone (R1), Chron C22r). The lower reverse polarity interval (R2), directly above the Hatchetigbee/Tallahatta contact may correlate with Chron C23r and the 2 normal polarity samples above with Chron C23n.

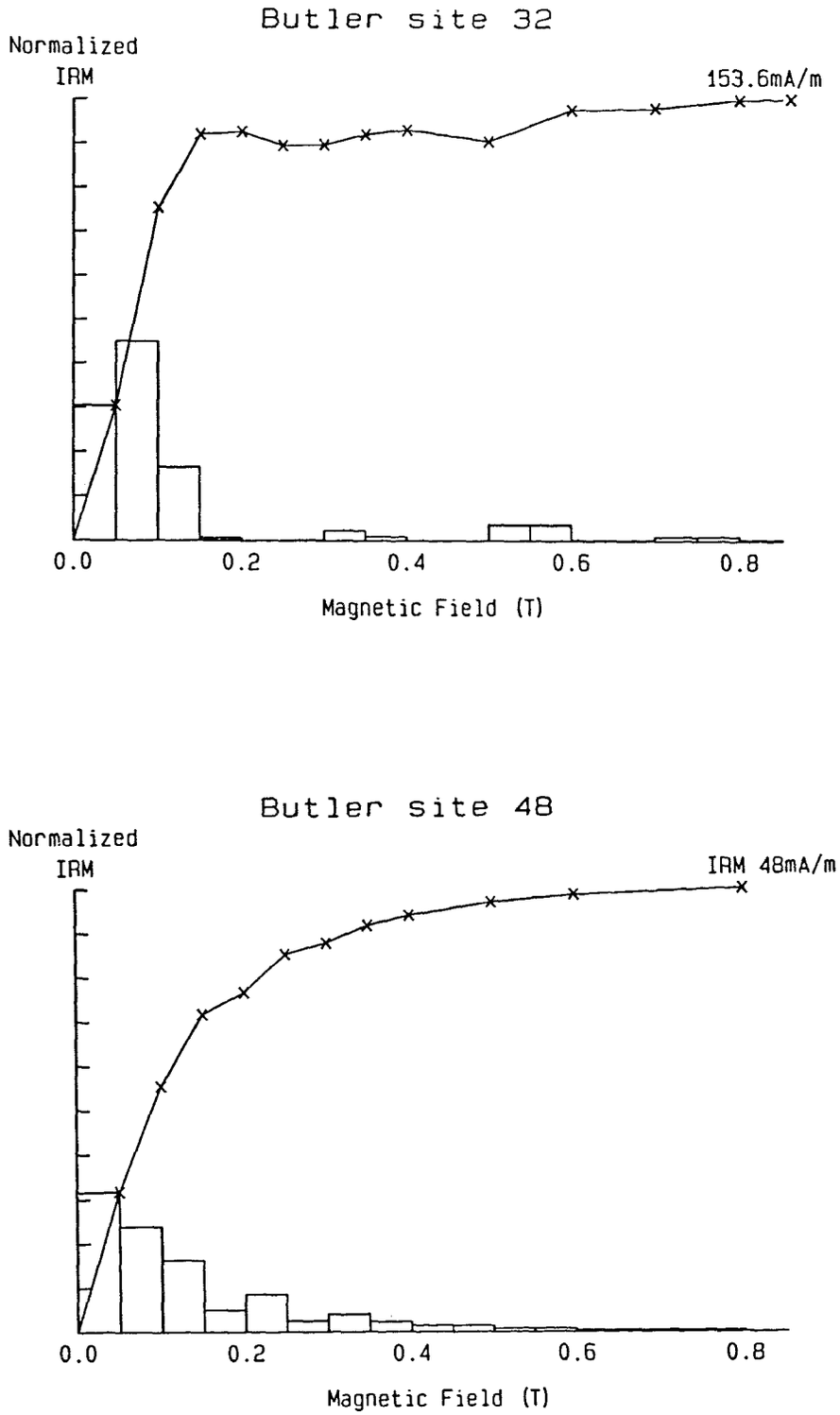

Figure 9-46 *IRM acquisition curves for samples at 1.2m and 17.1m.*

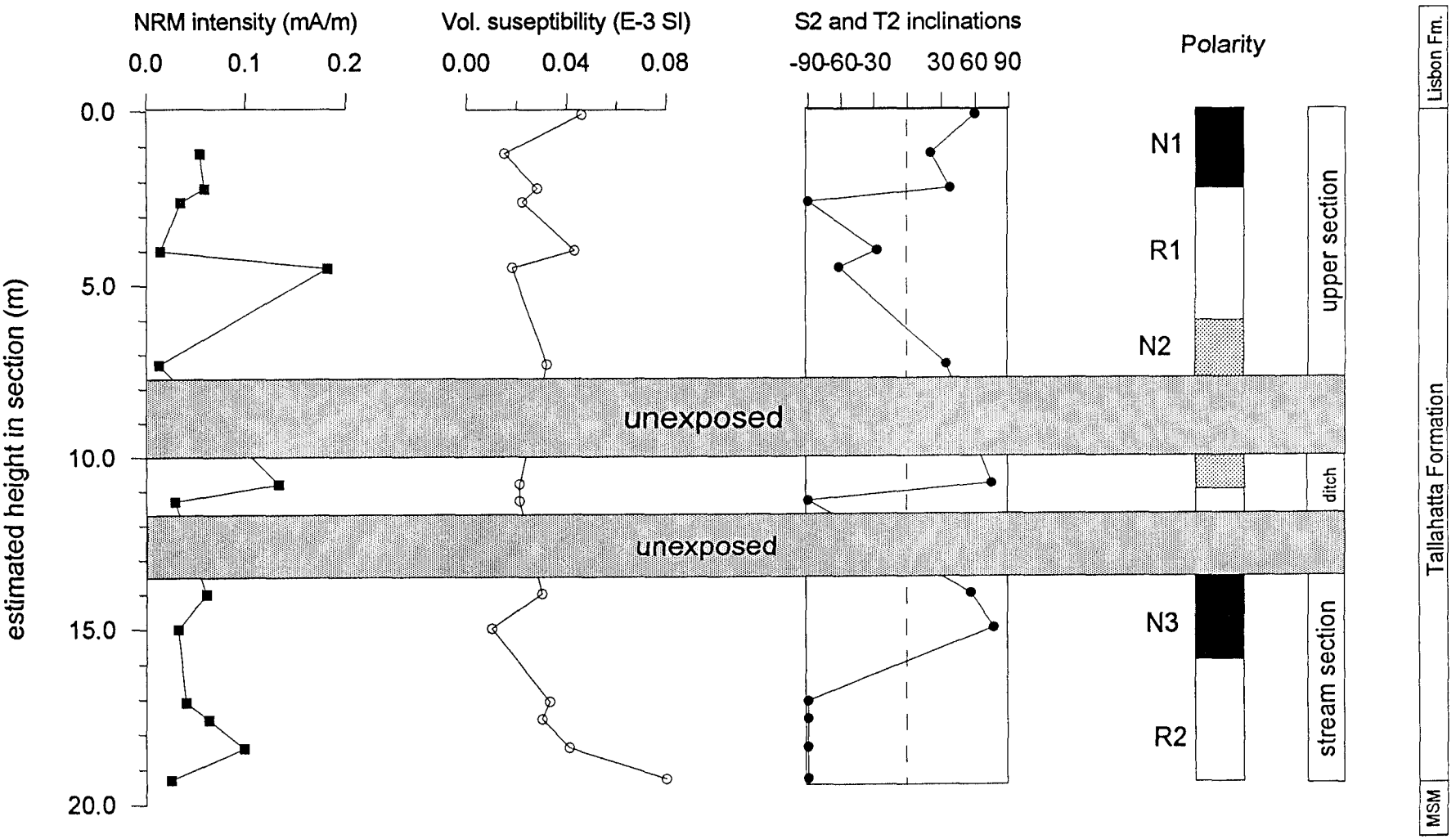

Figure 9-47 *NRM, susceptibility and inclination values of S2 and T2 samples from the Butler section.*

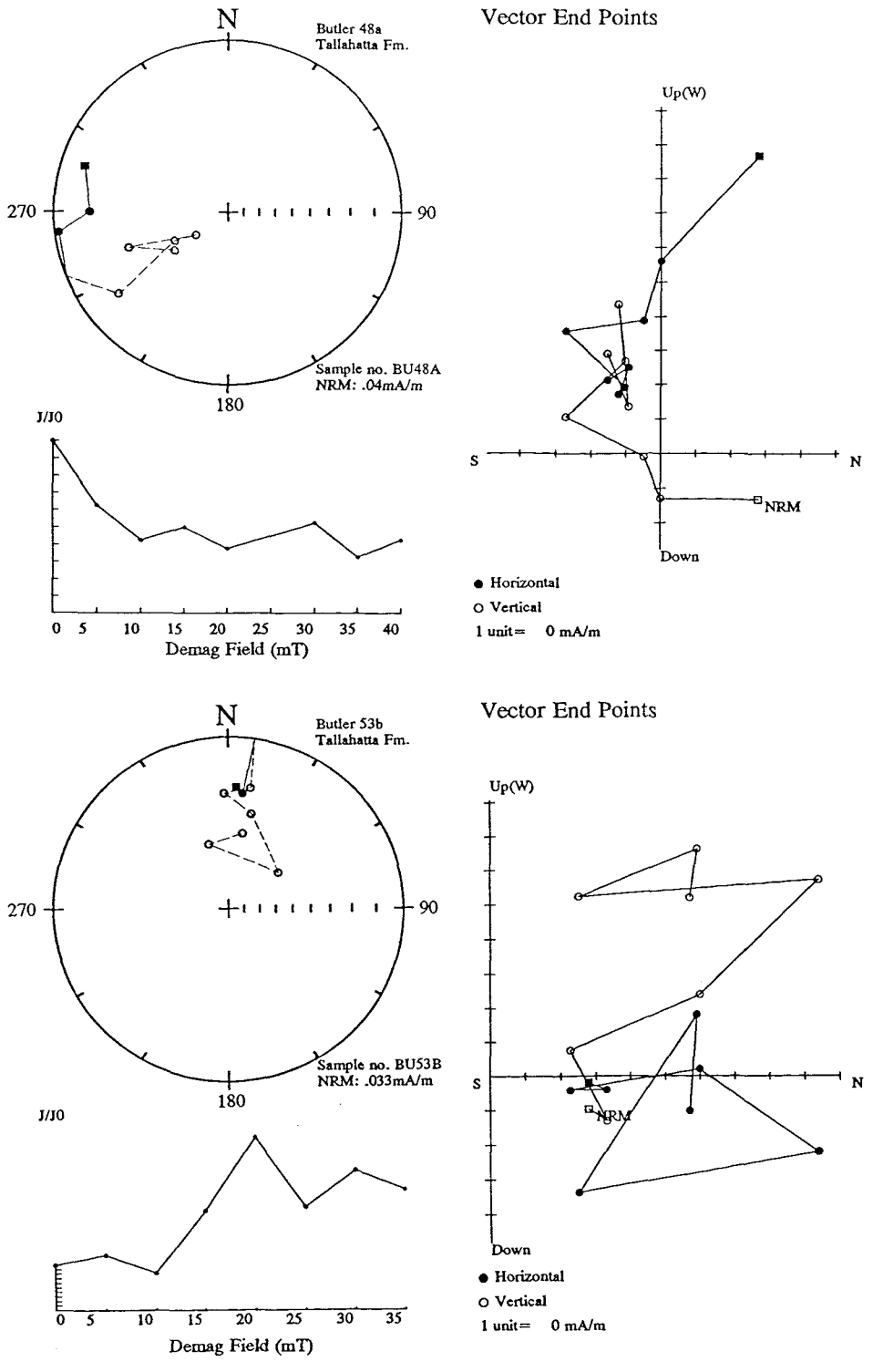

Figure 9-48 *Examples of reverse polarity trends from the lowermost beds above the Tallahatta Formation / Meridian Sand Member contact (Fig. 9-47, interval R2).*

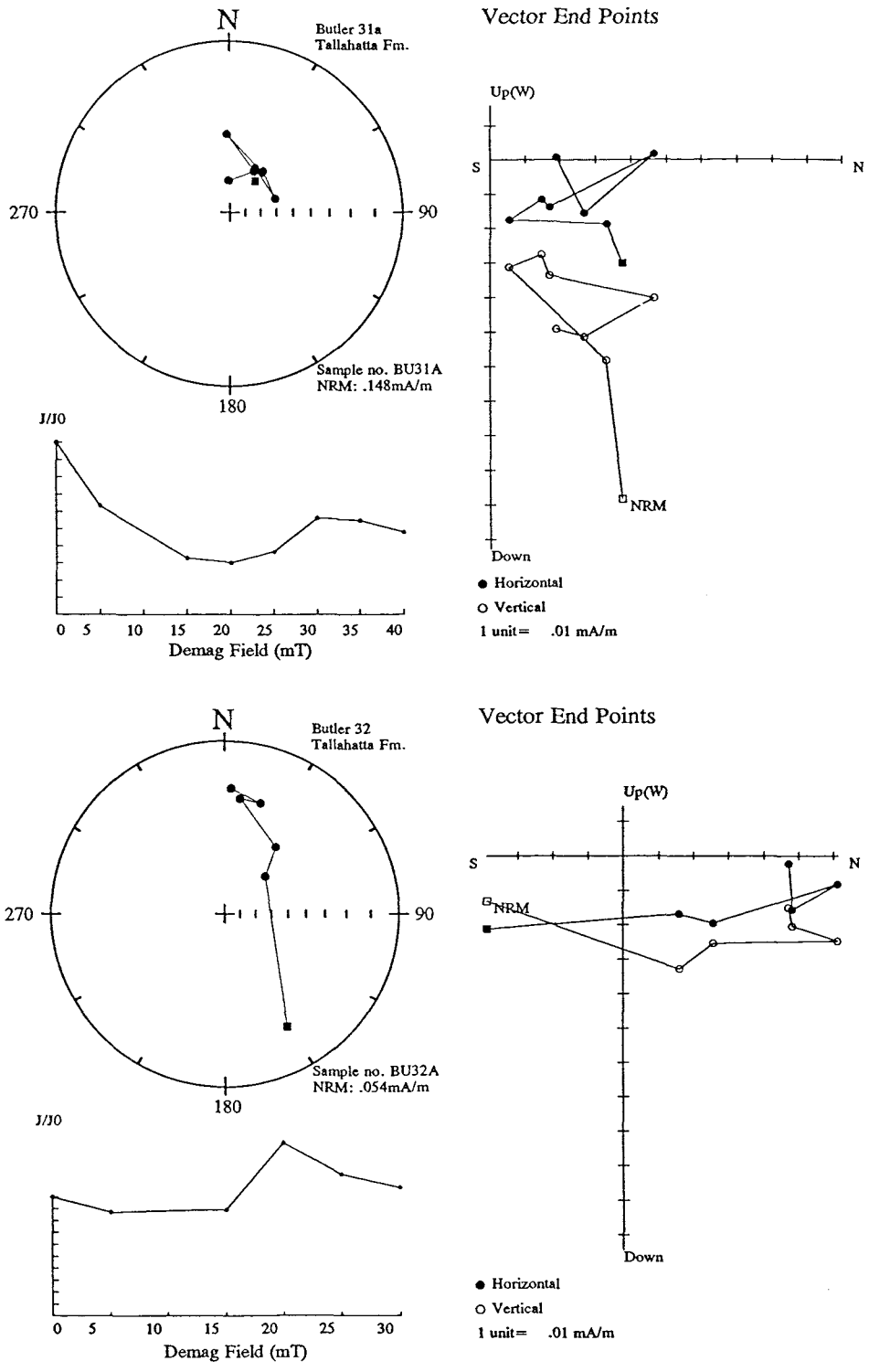

Figure 9-49 *Examples of normal polarity samples from the top of the section (Fig. 9-47 interval 'N1').*

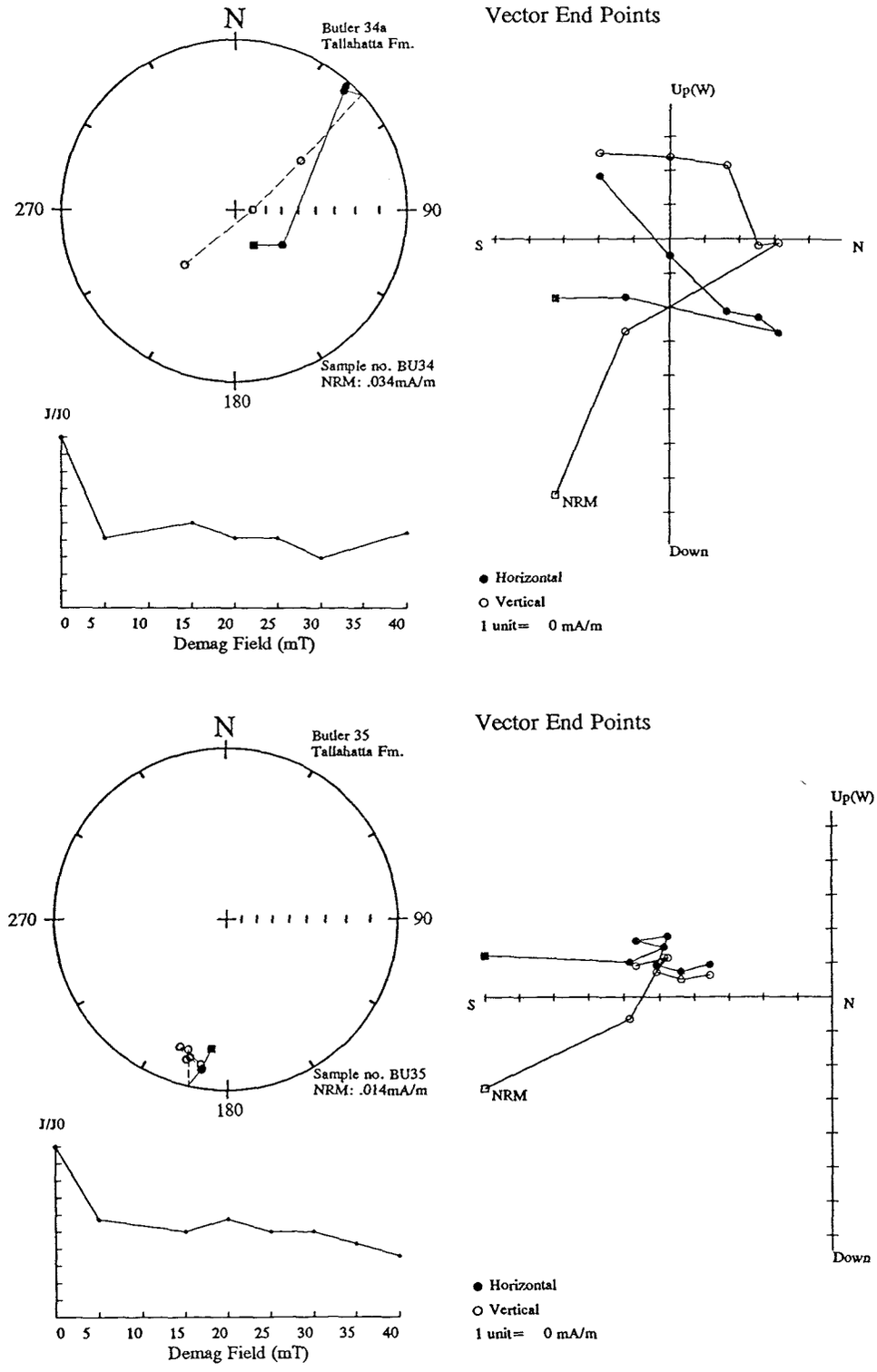

Figure 9-50 *Examples of reverse polarity samples from interval 'R1' of figure 9-47.*

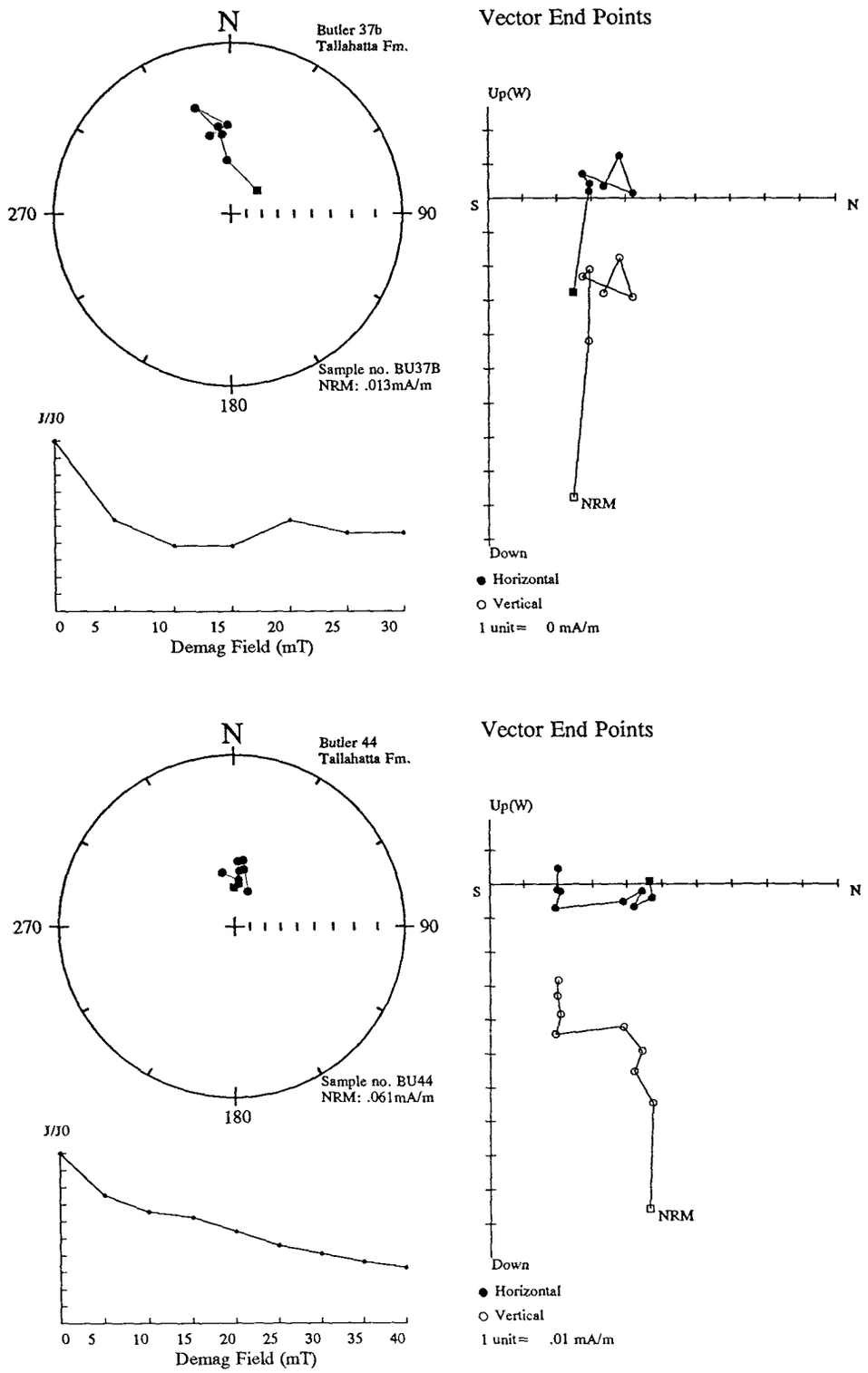

Figure 9-51 *Examples of normal polarity samples from interval 'N2/N3" of figure 9-47.*

9.2.4 Little Stave Creek locality

Location - 5.6 km north of Jackson, Clarke County, Alabama.

The strata exposed along Little Stave Creek include a near complete section of the Claiborne Group (Tallahatta, Lisbon and Gosport Formations) which outcrop on the east of the Jackson fault that intersects Little Stave Creek. The fault truncates the lower beds of the Tallahatta Formation, exposing Oligocene beds downstream, to the west of the fault plane. Although the area is within the coastal province where the regional dip is mostly to the south, the strata in fact dip gently to the east at about 1.5-2°. The deviation of the dip is attributed to the influence of the Hatchetigbee anticline, located 12km to the north east (Bandy, 1948).

Biostratigraphy

Based on 13 samples (Fig. 9-52), the upper 9.4m of the Tallahatta Formation is assigned to nannofossil zone NP14, although there is some dispute whether NP15 is present at the very top of the section (Bybell, 1975; Bybell and Gibson, 1985). Below this, the sediments are barren of calcareous nannofossils. Judging by the difference between the thickness of the Tallahatta Formation seen in other outcrops and that of the Peterman core (50km to the east) a considerable portion of material may be absent as a consequence of the Jackson Fault (possibly all NP12 material). The upper sandier beds of the Tallahatta seen here and within the Peterman core however, are not present at the Campbell and Butler localities and therefore C. King (pers. comm.) positions these upper beds above those at Butler and Campbell.

Sampling

Thirty seven samples from 18 sites were obtained from unlithified units exposed along the stream section. Within the lower Tallahatta however, an interval of approximately 6m was not sampled due to the lithified nature of the outcrop (Fig. 9-53).

The majority of samples were demagnetised using an alternating field with only 14% being thermally demagnetised. Of the samples treated thermally a typical increase in the susceptibility of the material was observed between 350-400°C although one sample at 13.1m showed no such increase after heating up to 500°C (Fig. 9-54).

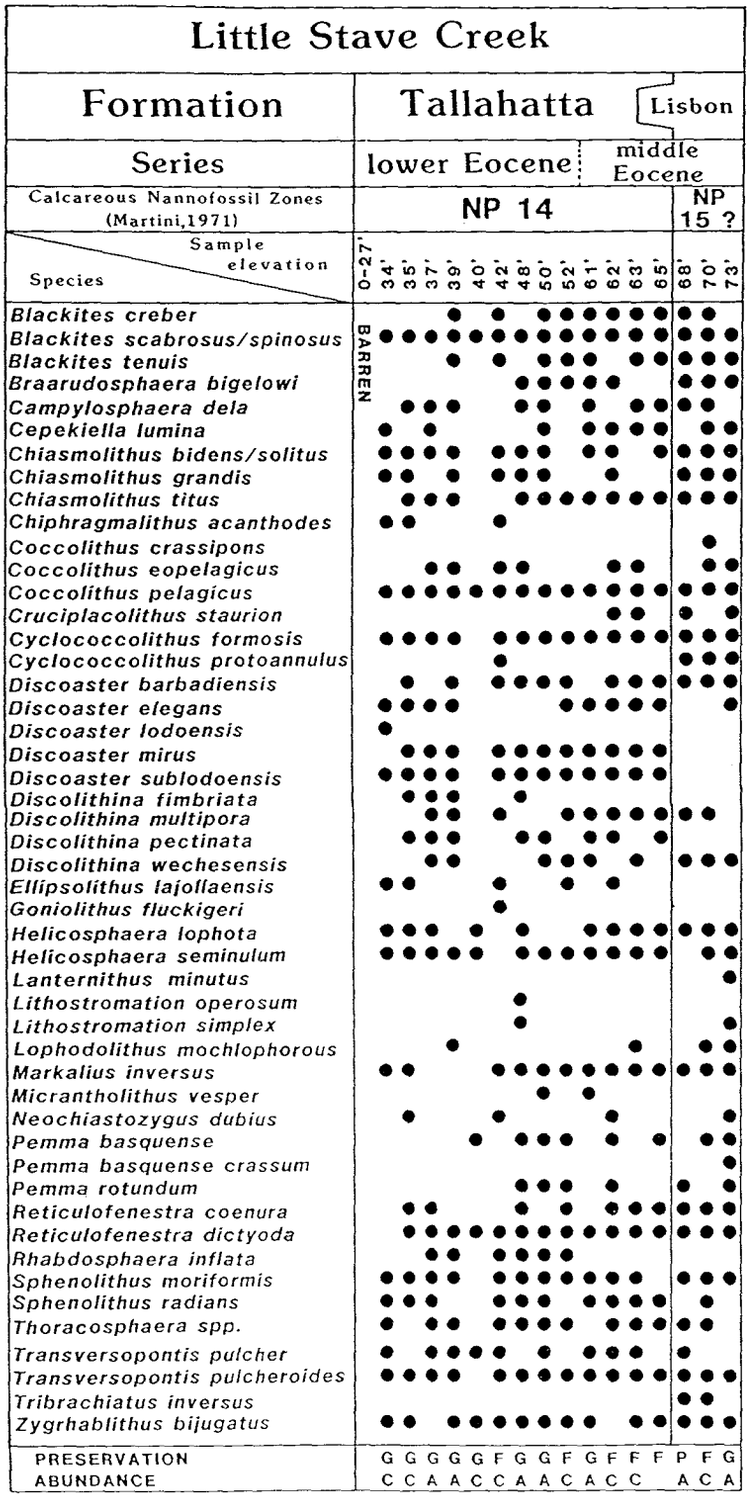

Figure 9-52 *Nannofossil zonation of the Tallahatta Formation at Little Stave Creek (from Bybell and Gibson, 1985).*

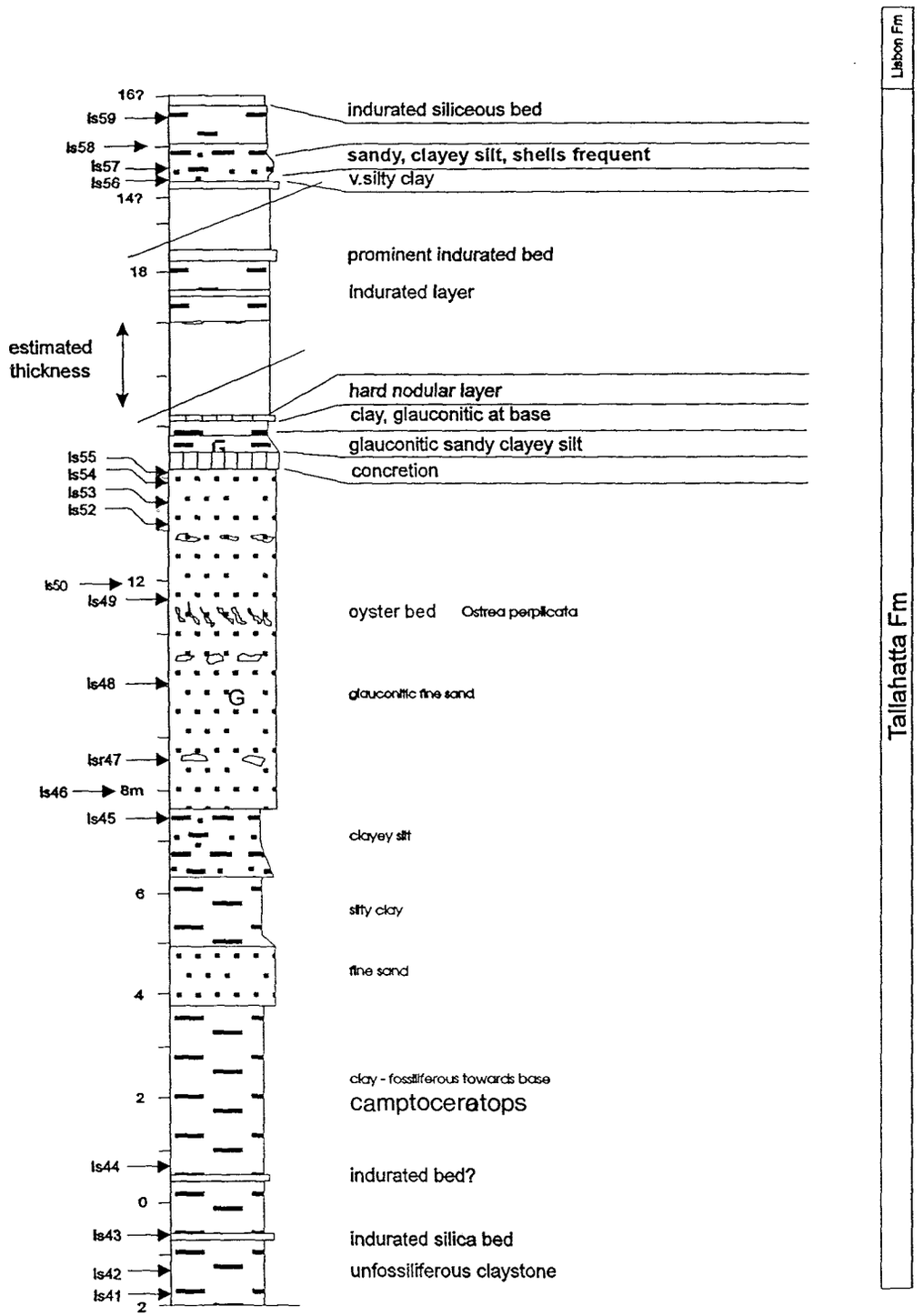

Figure 9-53 *Stratigraphic log and sampling site location at the Little Stave Creek locality.*

Polarity analysis

The NRM intensities at this location are typical of Tallahatta sediments (0.095±.092mA/m); however, the comparison of data between sub-samples at the same sites and that between thermal and A.F. demagnetised samples generally shows better consistency than for other outcrops of similar age. This is attributed to the freshness of the material in outcrop (although questionable polarity assignments still account for about 35% of the samples in this section).

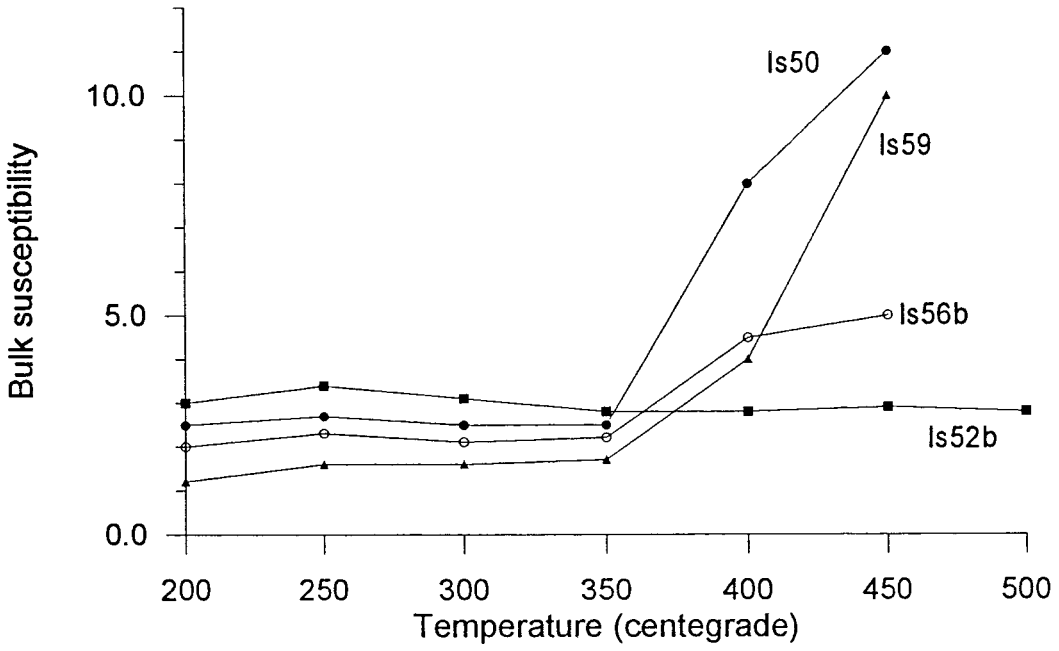

Figure 9-54 *Bulk susceptibility fluctuations during thermal demagnetisation of samples from 4 sites at the Little Stave Creek locality.*

Inclination values from reliable SEPs and trends (quality ≥S2/T2) have been used to define a simple polarity sequence of 4 intervals (Fig. 9-55).

N1 Well defined 3m normal interval based on 5 sites that exhibit good normal polarity SEPs which are consistent between sub-samples (for example: figs. 9-56a and b). It is positioned within upper NP14 possibly lowermost NP15.

R1 Defined by one site with demagnetisation behaviour from thermal and A.F. procedure that indicate a reverse polarity (Fig. 9-57).

N2 Normal polarity interval identified by two type S2 SEP samples (Fig. 9-58). Other sites within this interval exhibit plots from which a reliable polarity can not determined. Positioned in lower NP14.

R2 Reverse polarity interval near the base of the section defined by 2 specimens that show type-T2 trends to a reverse polarity (Fig. 9-59).

In addition, a single site carries a confident normal polarity at the base of the measured section.

Magnetostratigraphy

A confident correlation of the entire polarity sequence with the GPTS is not possible with such a restricted set of dispersed data points and a lack of biostratigraphic control towards the base. Considering these limitations a tentative placement of the identified polarity intervals has been attempted.

The upper normal polarity interval (N1) has good biostratigraphic control and being defined by 6 confident SEPs is likely to represents Chron C21n. The poorly defined reverse polarity interval below, positioned within the middle of the nannofossil zone NP14 represents Chron C21r. The normal interval 'N2' in lower NP14 may represent some of Chron C22n however the extent of this polarity zone in not known due to the unsampled lithified units. Interval 'R2' has no nannofossil control but could be Chron C22r with the top of Chron C23n visible at the base. Due to the uncertainties however, only the upper par tof this section is included within the integrated magnetostratigraphic summary of outcrops and core material in the following chapter.

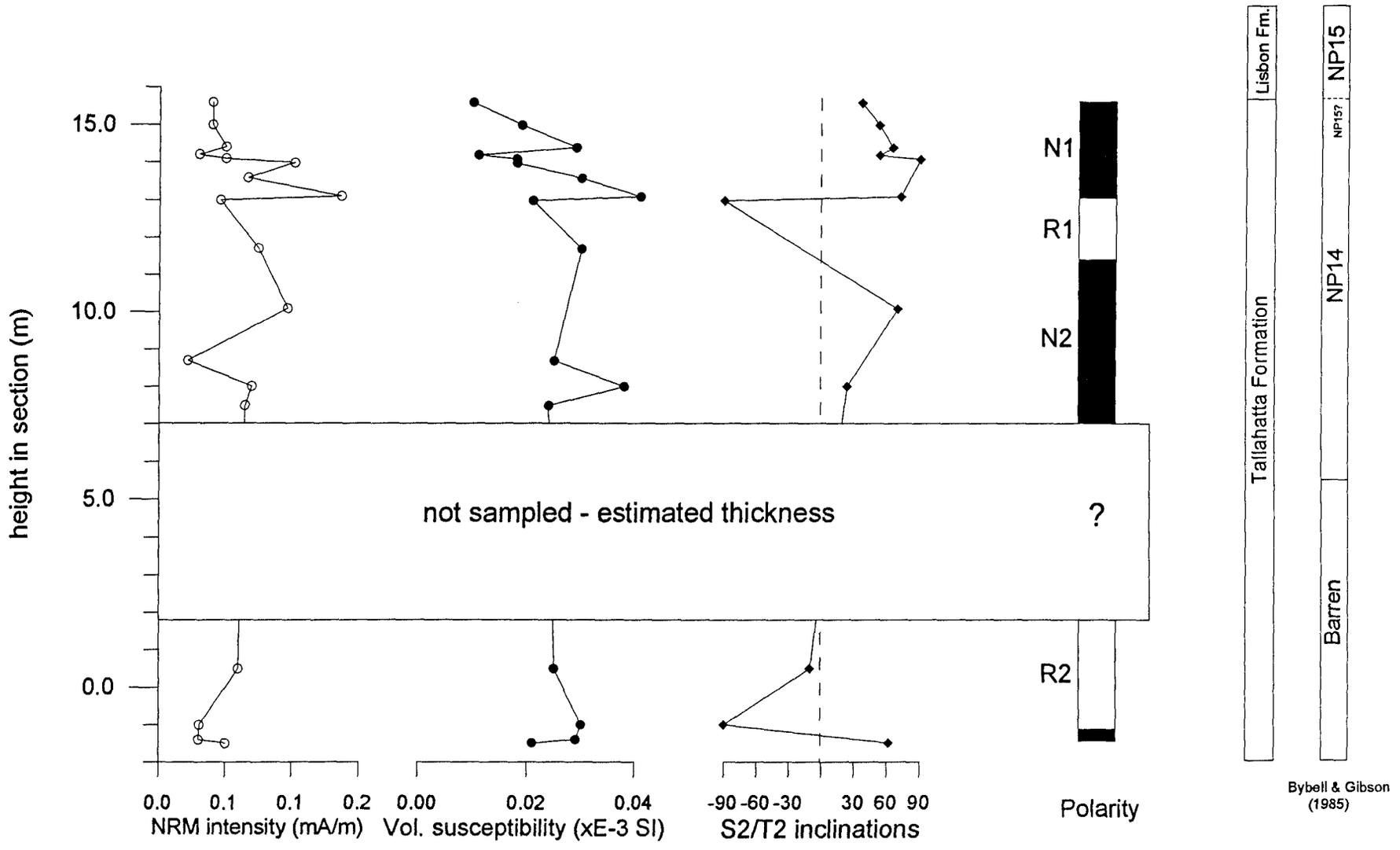

Figure 9-55 *NRM intensity, susceptibility and inclination values of intermediate categories S2 and T2 demagnetisation data. The log of inclinations was used to define the polarity sequence.*

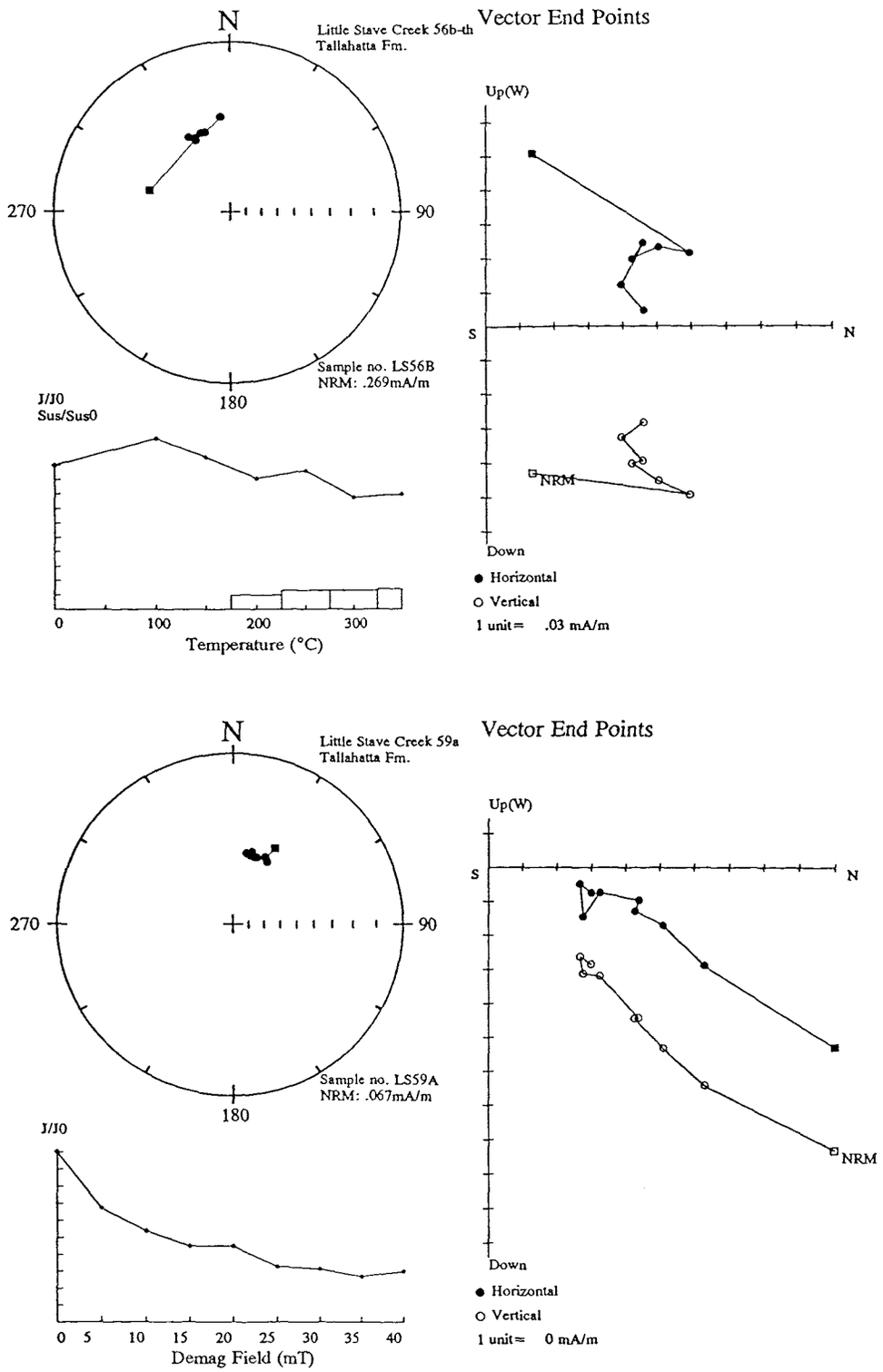

Figure 9-56a *Thermal and A.F. demagnetisation behaviour of samples from the upper normal interval 'N1'.*

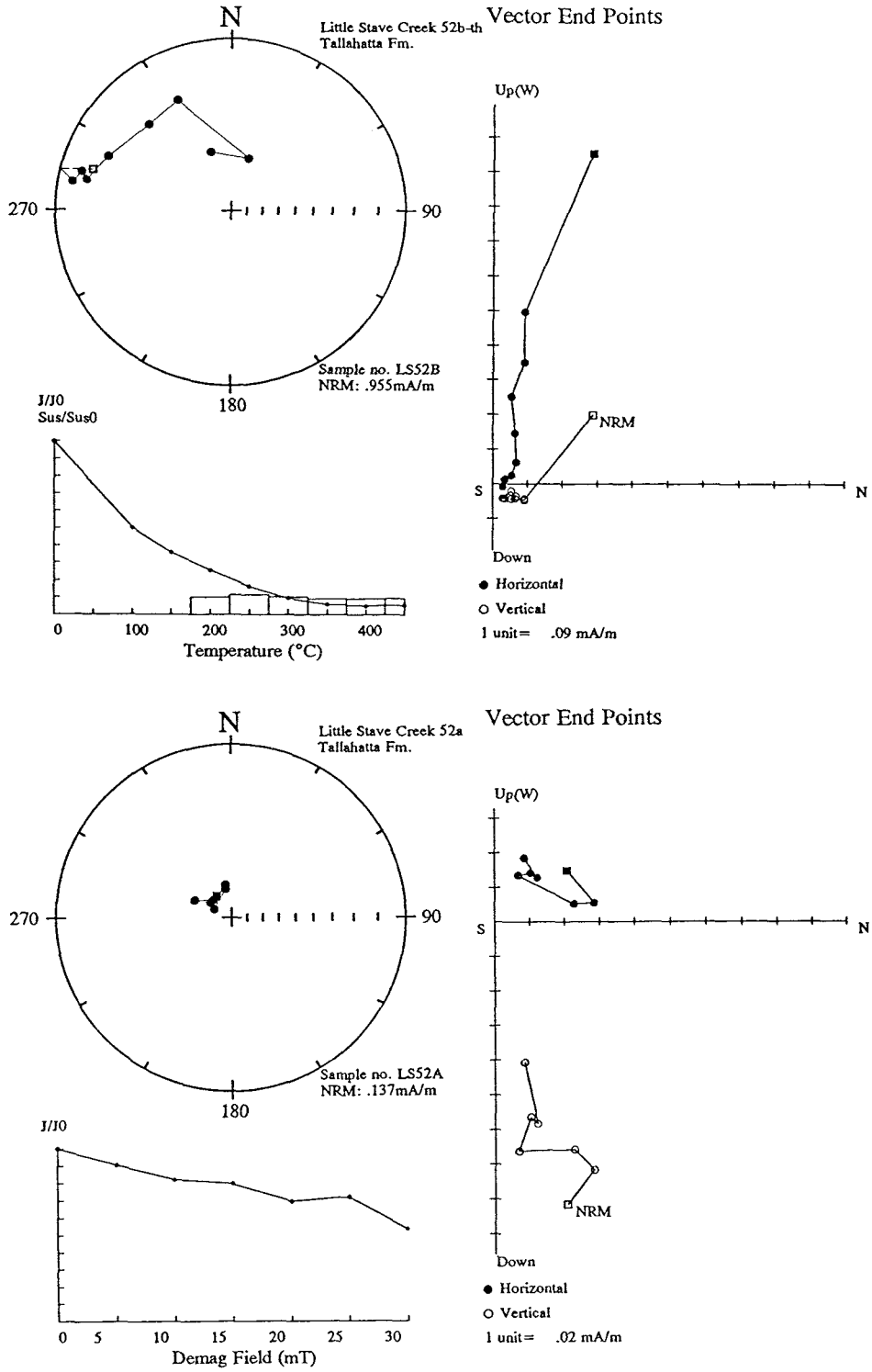

Figure 9-56b *Thermal and A.F. demagnetisation behaviour of samples from the upper normal interval 'N1'.*

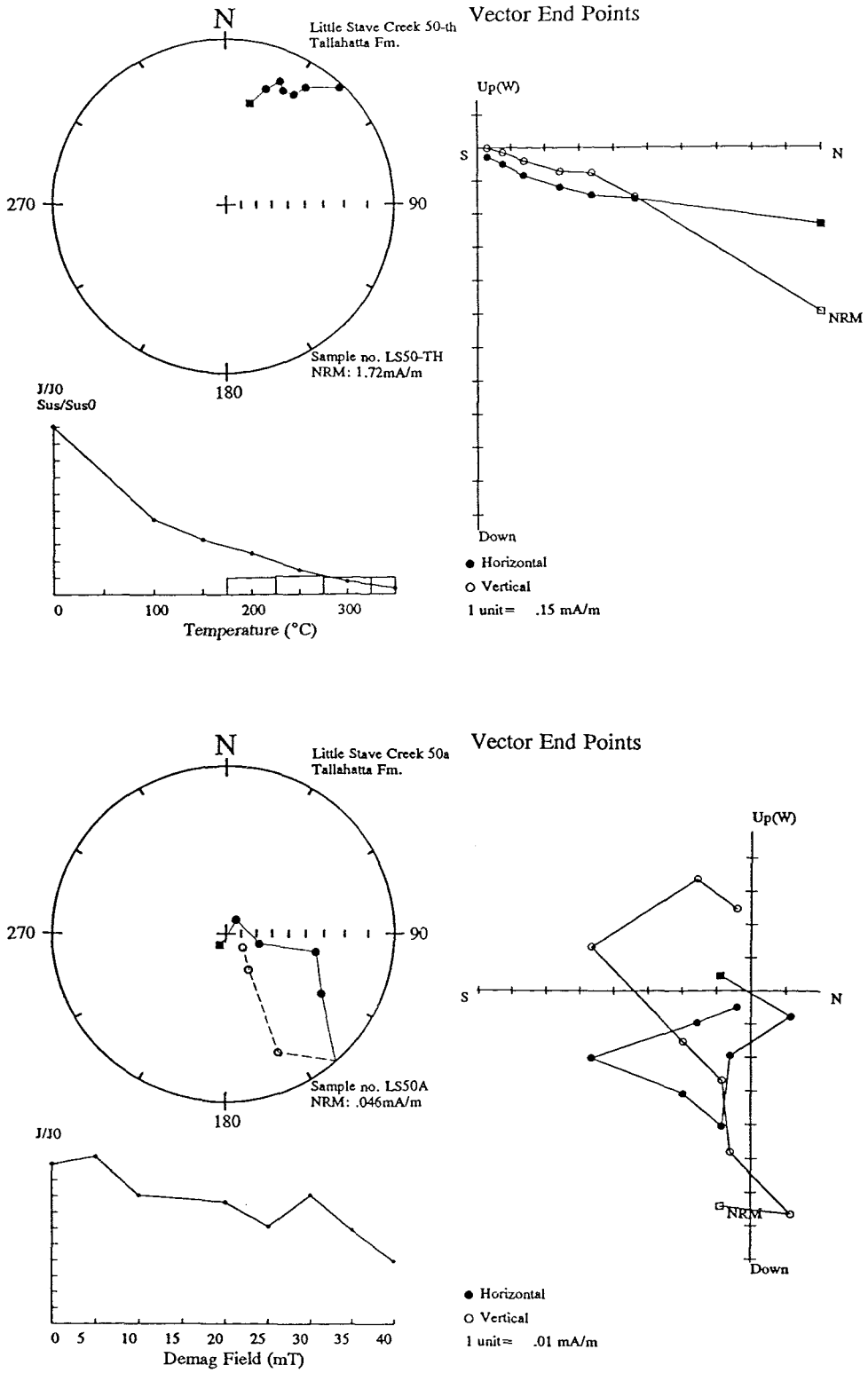

Figure 9-57 *Examples of the demagnetisation behaviour from interval 'R1'.*

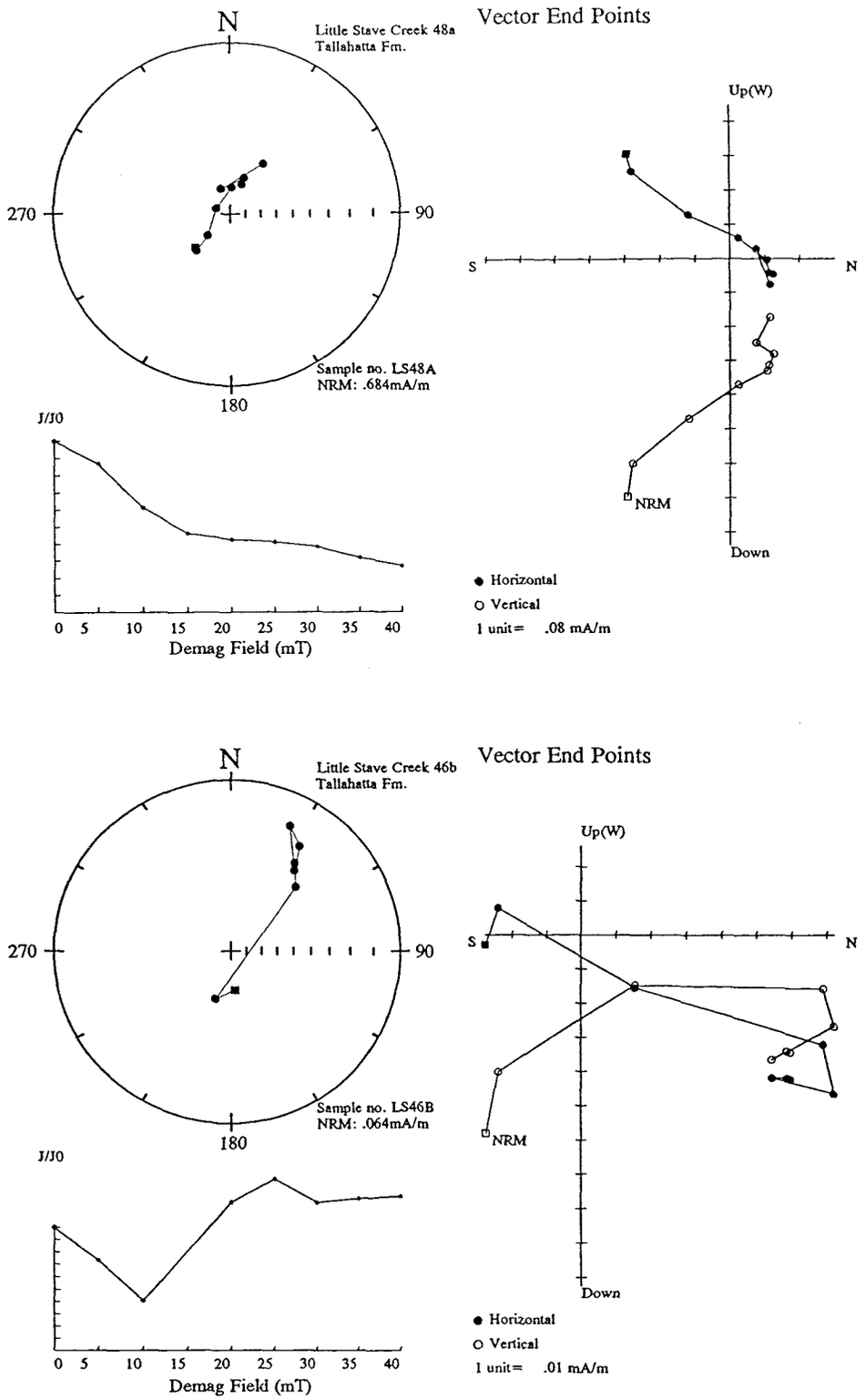

Figure 9-58 *Examples of demagnetisation behaviour from interval 'N2'.*

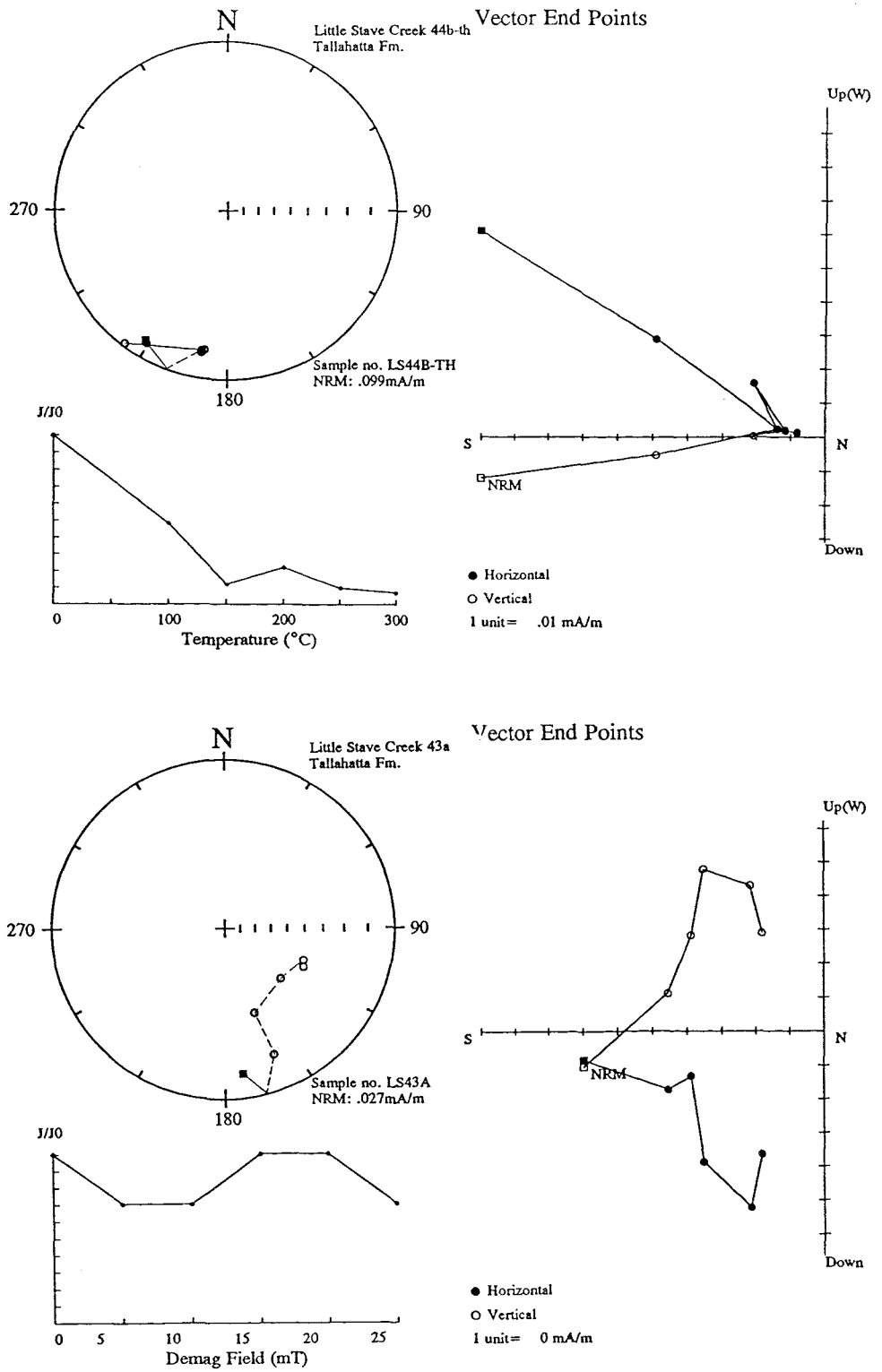

Figure 9-59 *Examples of demagnetisation behaviour from interval 'R2'.*

9.2.5 Midway locality

Location: Highway 47, 3km west of Midway, Monroe County, Alabama.

The Midway HW47 roadcut exposes approximately 10m of the lower Tallahatta Formation (including 2m of the Meridian Sand Member) and the underlying Hatchetigbee (Fig. 9-60; Plate 9-2).

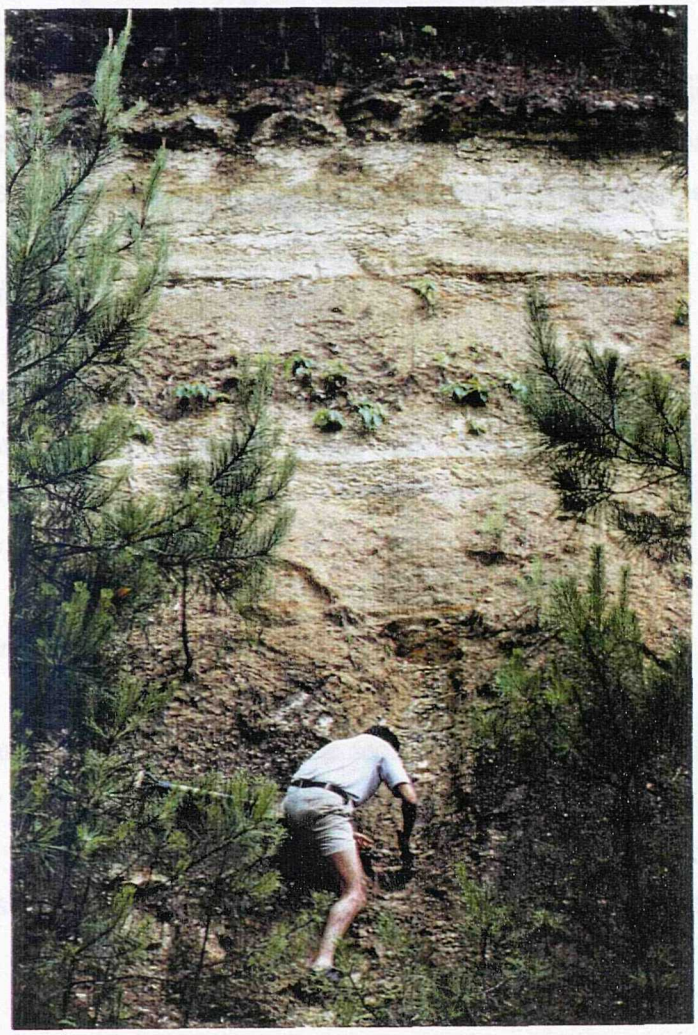

Plate 9-2 *Midway road cutting.*

The siliceous intervals observed in the Tallahatta Formation here may correspond with silica events in the London Clay and cherts of the North Sea (King, pers. comm.). There

are also several glauconite horizons and sharp burrowed contacts which probably correspond to 4th order cycles at this location.

Sampling

The conditions of the sediments are variable: the Hatchetigbee is not well exposed due to the collapse of higher beds and to reach relatively fresh material in the Tallahatta some effort was required to dig back into the outcrop at most sites. Sites were concentrated above the Meridian Sand Member up to a height of approximately 7m although some attempt was made to integrate samples from the previous 1990 field trip higher up the section. Most sites were subjected to A.F. and thermal demagnetisation and 5 had IRM analysis carried out which gave magnetite dominated curves (Fig. 9-61).

Polarity analysis

Five metres of sediments directly above the Meridian carry a good normal polarity which is observed from good SEPs from both A.F. and thermal demagnetisation (Figs. 9-62; 9-63a and b). Above the normal interval, trending plots indicate a reverse polarity over the remainder of the sampled interval (Fig. 9-64).

Magnetostratigraphy

The normal polarity zone at the base of the section probably represents Chron C23n. The reverse polarity above a glauconite horizon at about 5.6m possibly corresponds to the base of Chron C22r although further biostratigraphic control across this glauconite interval is necessary to place the magnetozones in a rigid time framework.

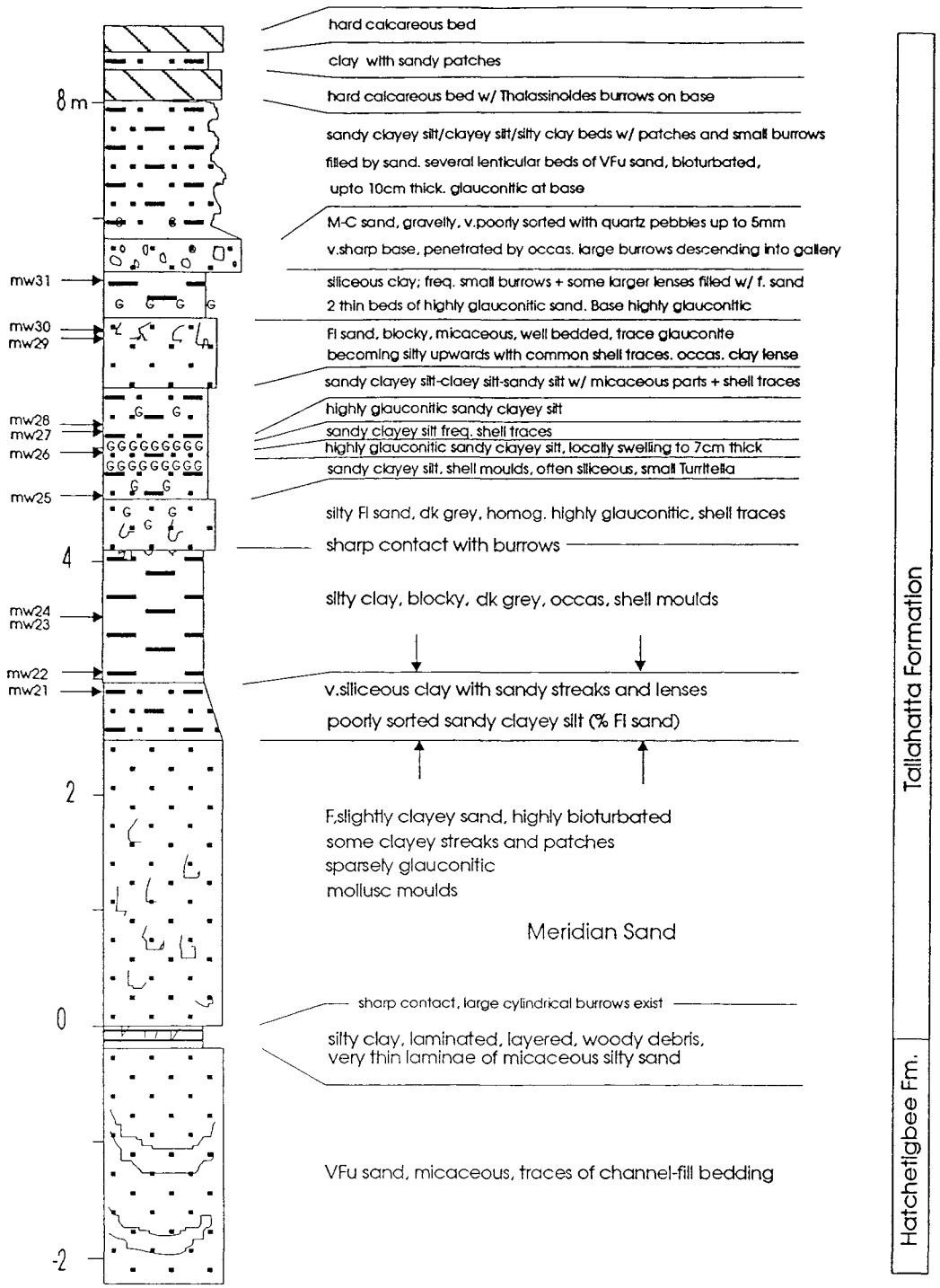

Figure 9-60 *Stratigraphic log and sampling site positions at the Midway locality.*

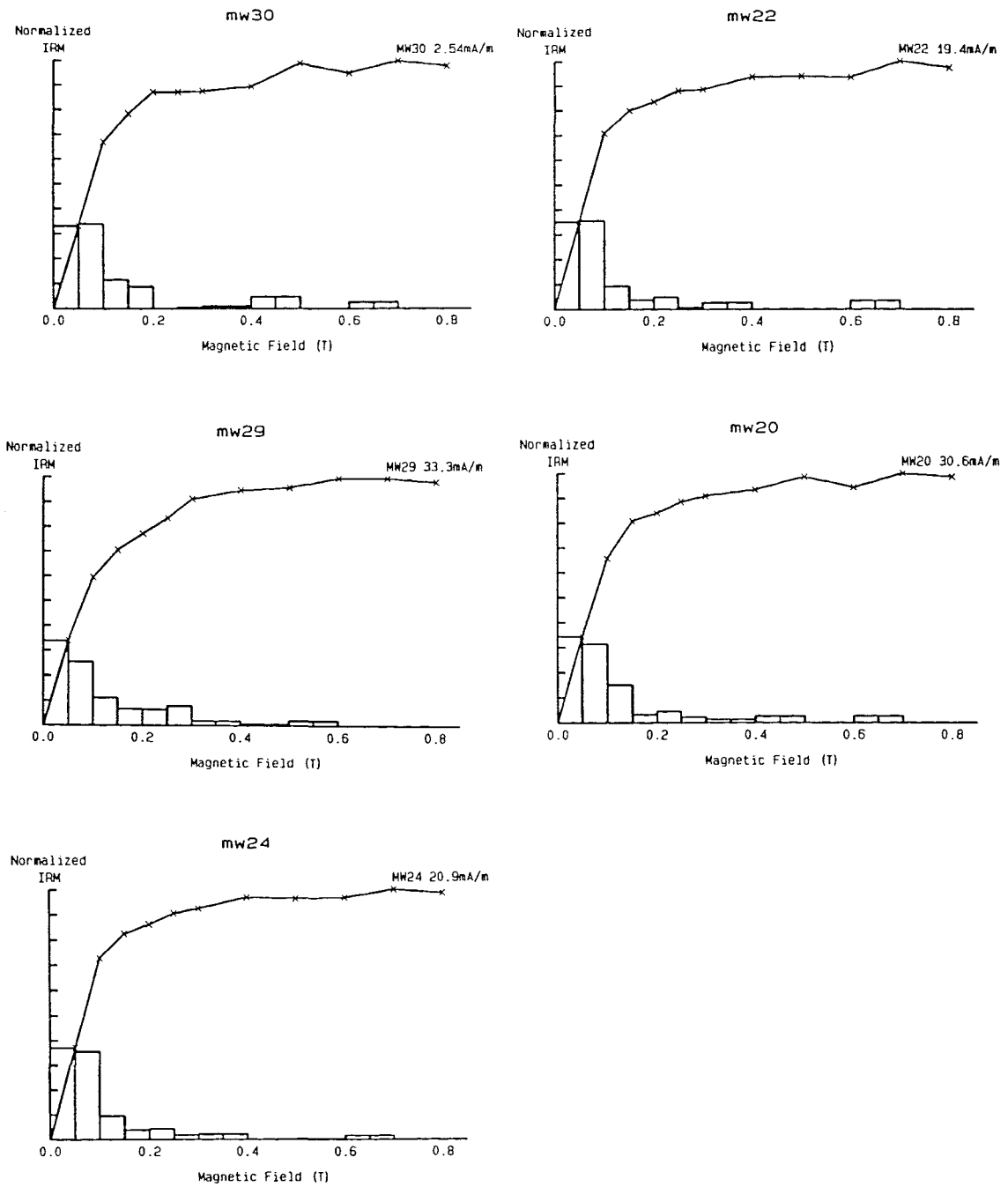

Figure 9-61 *IRM acquisition curves for samples from 5 sites at the Midway locality.*

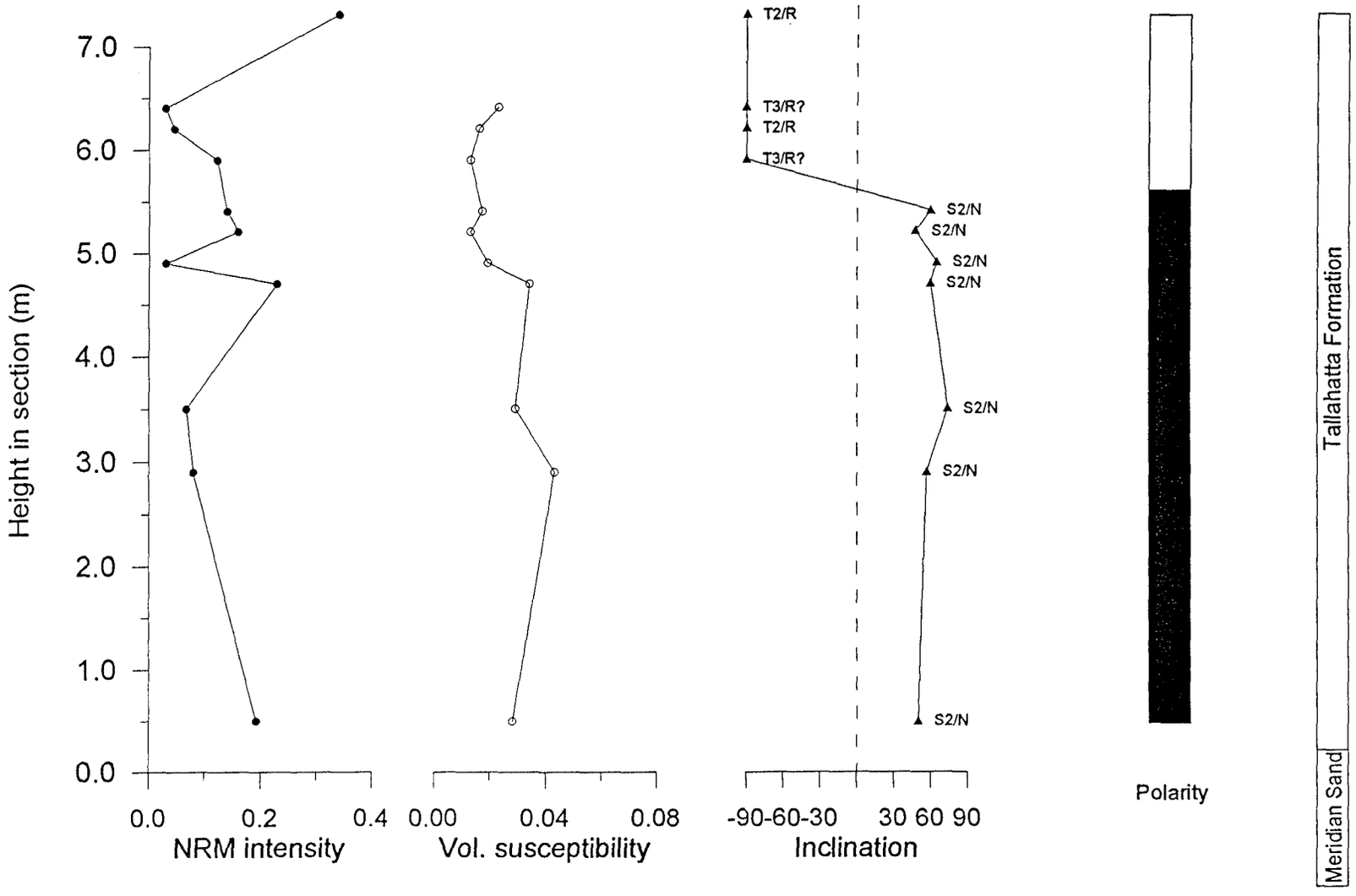

Figure 9-62 *NRM intensities, susceptibility and inclination of reliable SEPs and trends.*

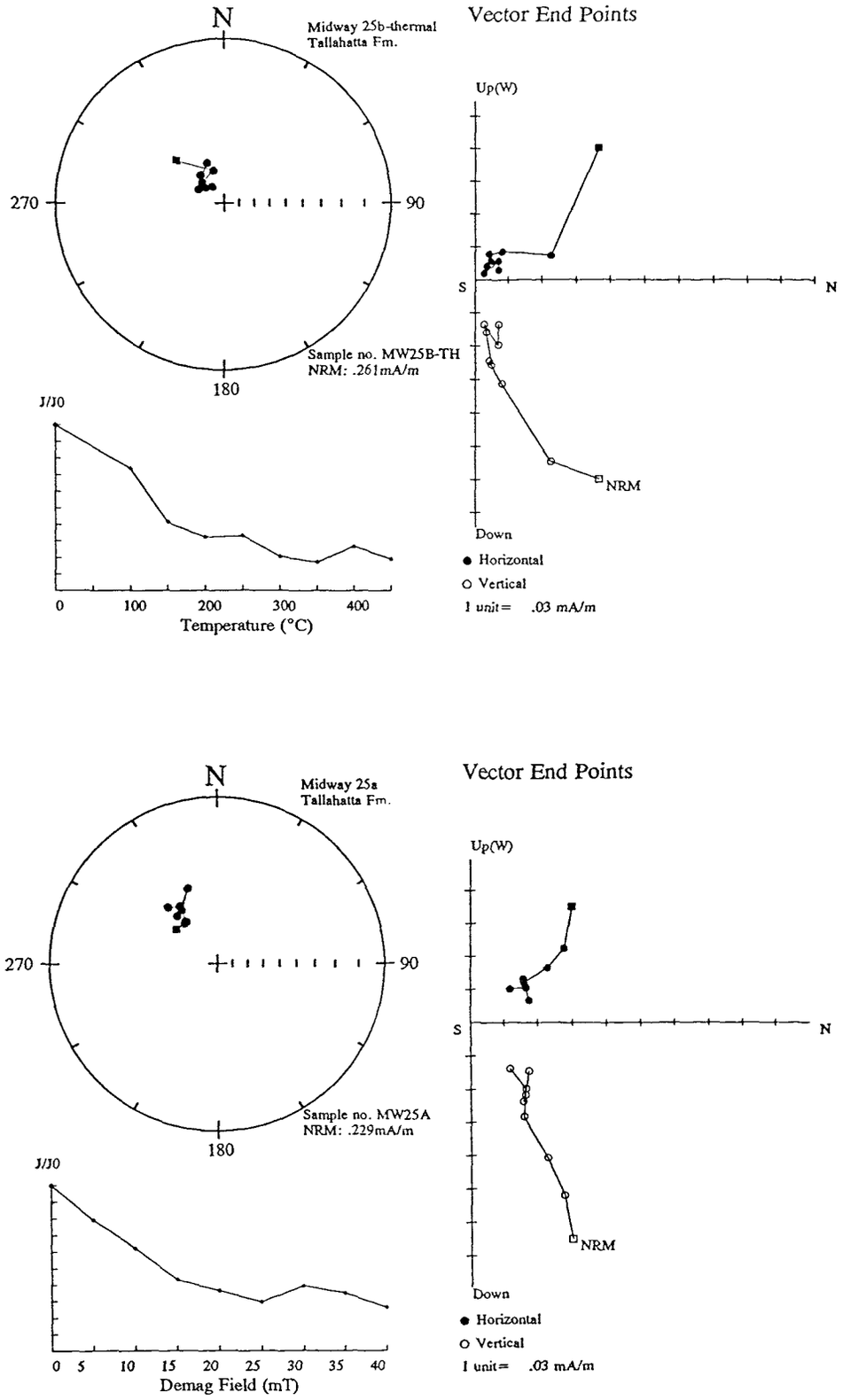

Figure 9-63a *Examples of SEPs from the lower normal polarity interval.*

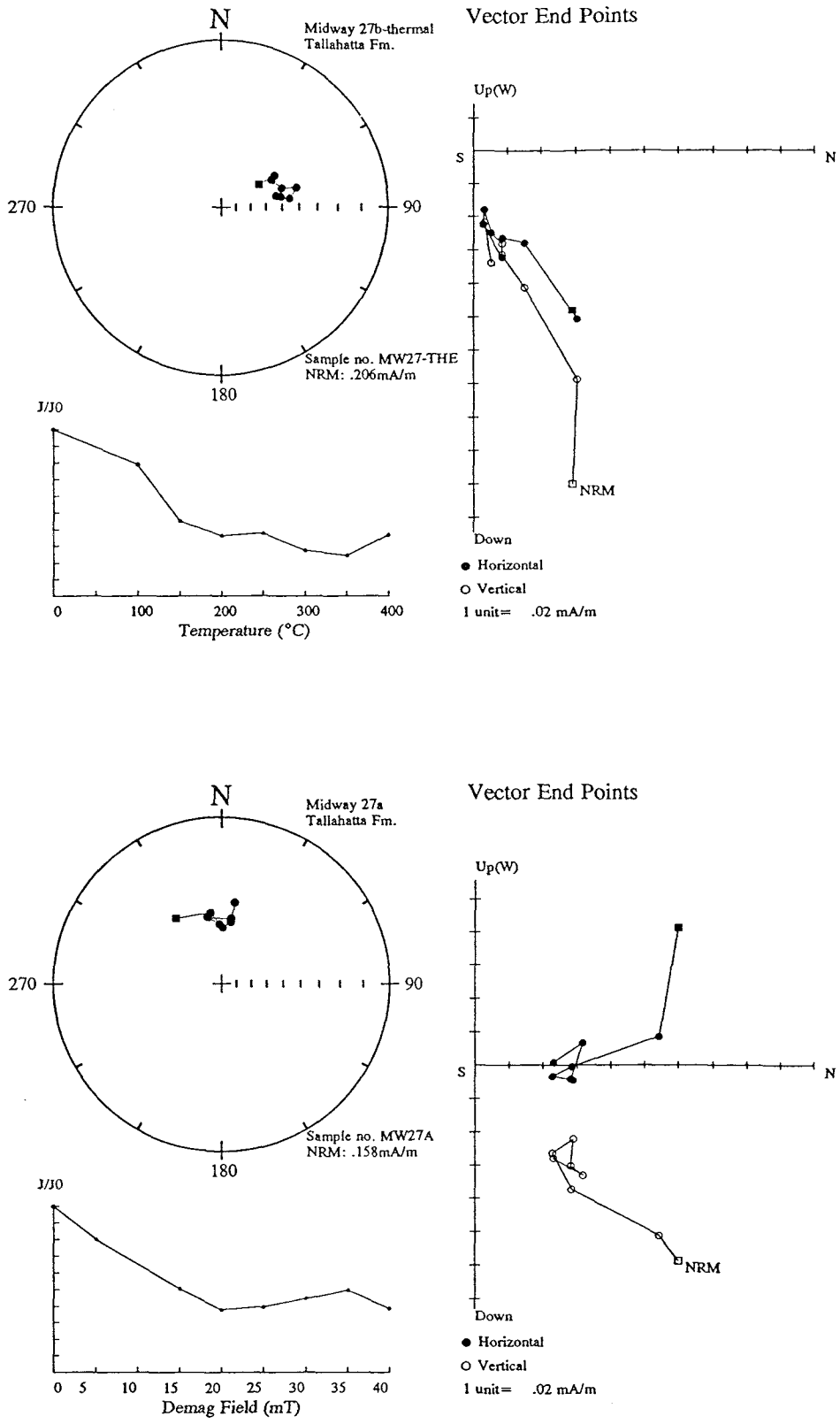

Figure 9-63b *Examples of SEPs from the lower normal polarity interval.*

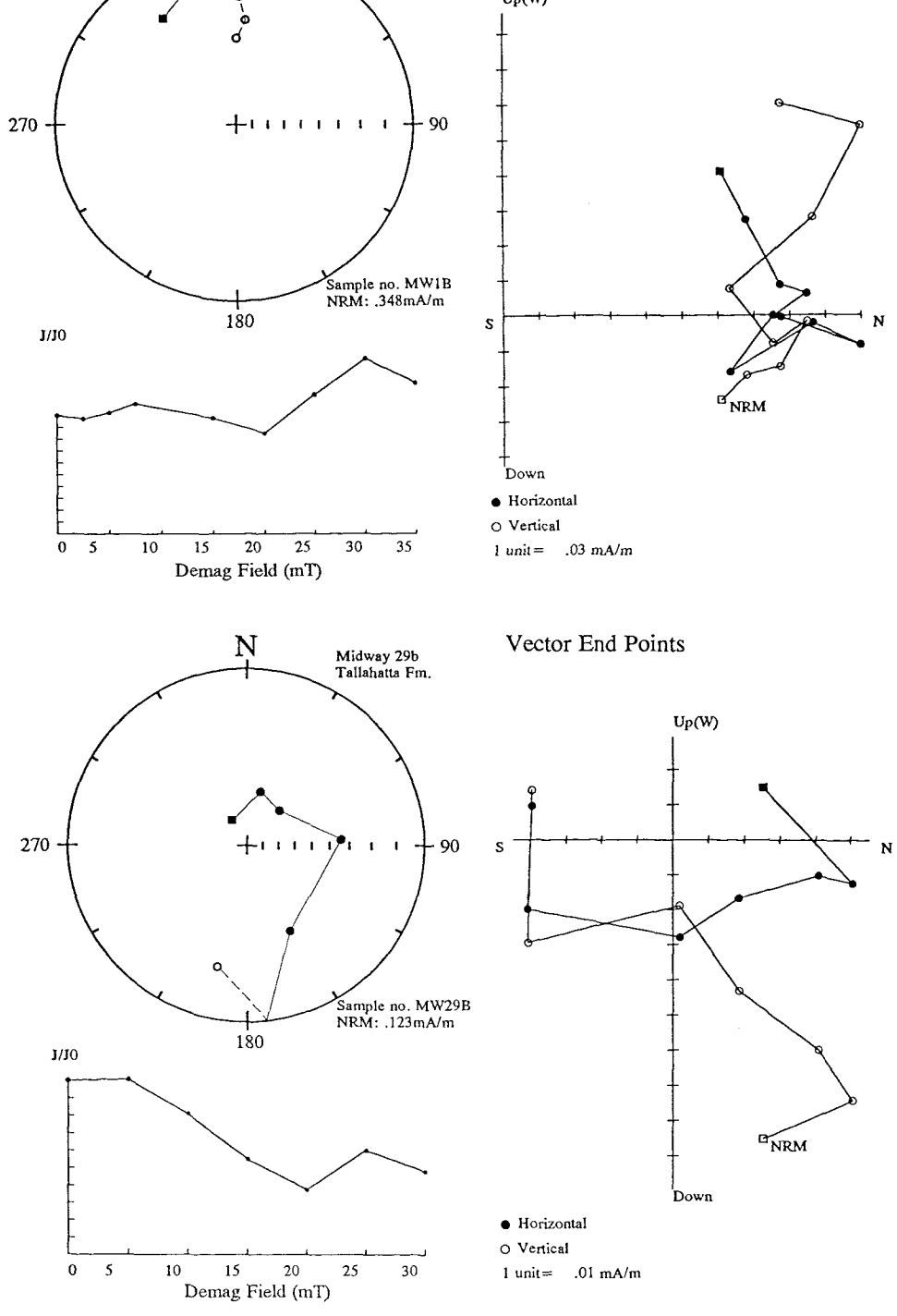

Figure 9-64 *Examples of possible trends to a reverse polarity seen within the upper beds of the Midway section.*

SECTION D

Magnetostratigraphic correlation of sediments across the Atlantic. Implications for dating depositional sequences and the eustatic sea. level curve using magnetostratigraphy. Palaeomagnetic pole position for the early Paleogene.

Chapter 10 Conclusions

10.1 Summary of the magnetostratigraphy of US sequences and correlation with those of NW Europe.

The summary magnetostratigraphy of late Paleocene and early Eocene outcrop sections and cores investigated during this study is shown in figure 10-1. Those sections or portions of sections that are considered to carry magnetic overprints and which do not provide confident polarity assignments (based on the criteria in section 3.6) have been excluded.

The following discussion focuses on the correlation of magnetochrons between sections in the Gulf and Atlantic Coastal Plains with those identified in northwestern European sequences (Ali & Hailwood, in press). The distribution of Paleogene deposits, the location of sections and cores investigated and the summary of the magnetostratigraphy for the northwestern European early Tertiary sediments are shown in figures 10-2 and 10-3. The geomagnetic polarity timescale of Berggren et al (1994), based on Cande and Kent (in press), has been used to age-calibrate the magnetochron boundaries. Martini's (1971) nannofossil zonation scheme has been positioned against this scale using the fossil zone-magnetochron correlations of Berggren et al (1985) and Berggren et al (1994).

Chron C26n (57.55-57.91Ma)

U.S. Atlantic and Gulf Coastal Plains

In the Atlantic Coastal Plain sediments, the upper and lower boundaries of Chron C26n have been placed within the Aquia Formation of the Oak Grove core at depths of 117.1m and 122.5m respectively. In the Gulf Coast, poor palaeomagnetic results from the lower Nanafalia Formation prohibit a confident identification of Chron C26n.

NW Europe

At Hales and Ormesby, Norfolk, the upper and lower boundaries of Chron C26n have been identified within the Ormesby Clay Formation (Ali and Hailwood, in press). In all other sections between Halesworth (Suffolk) and Kent (Fig. 10-2), the

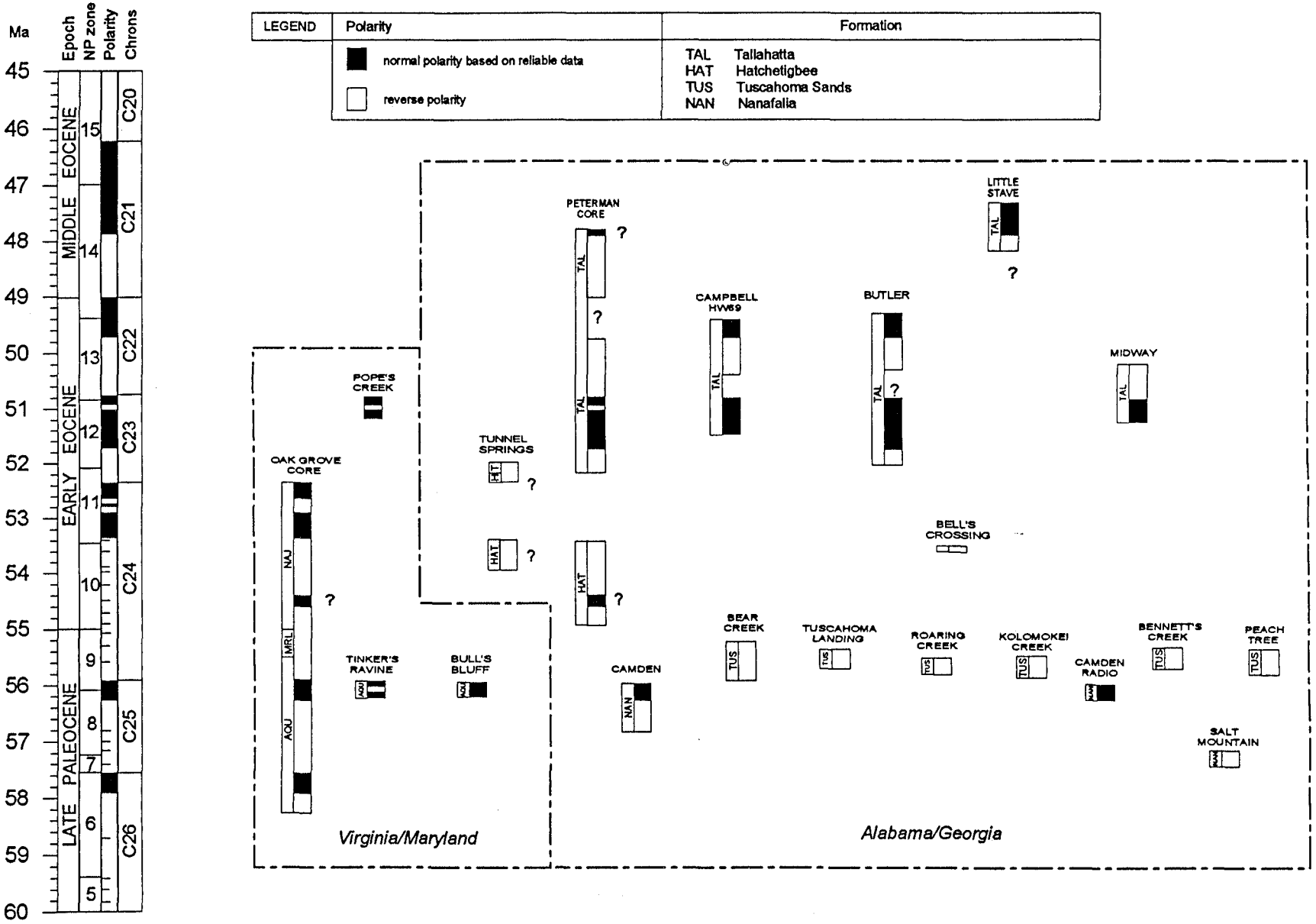

Figure 10-1 *Magnetostratigraphic summary for lower Paleogene deposits from the Gulf and Atlantic Coastal Plains investigated during this study.*

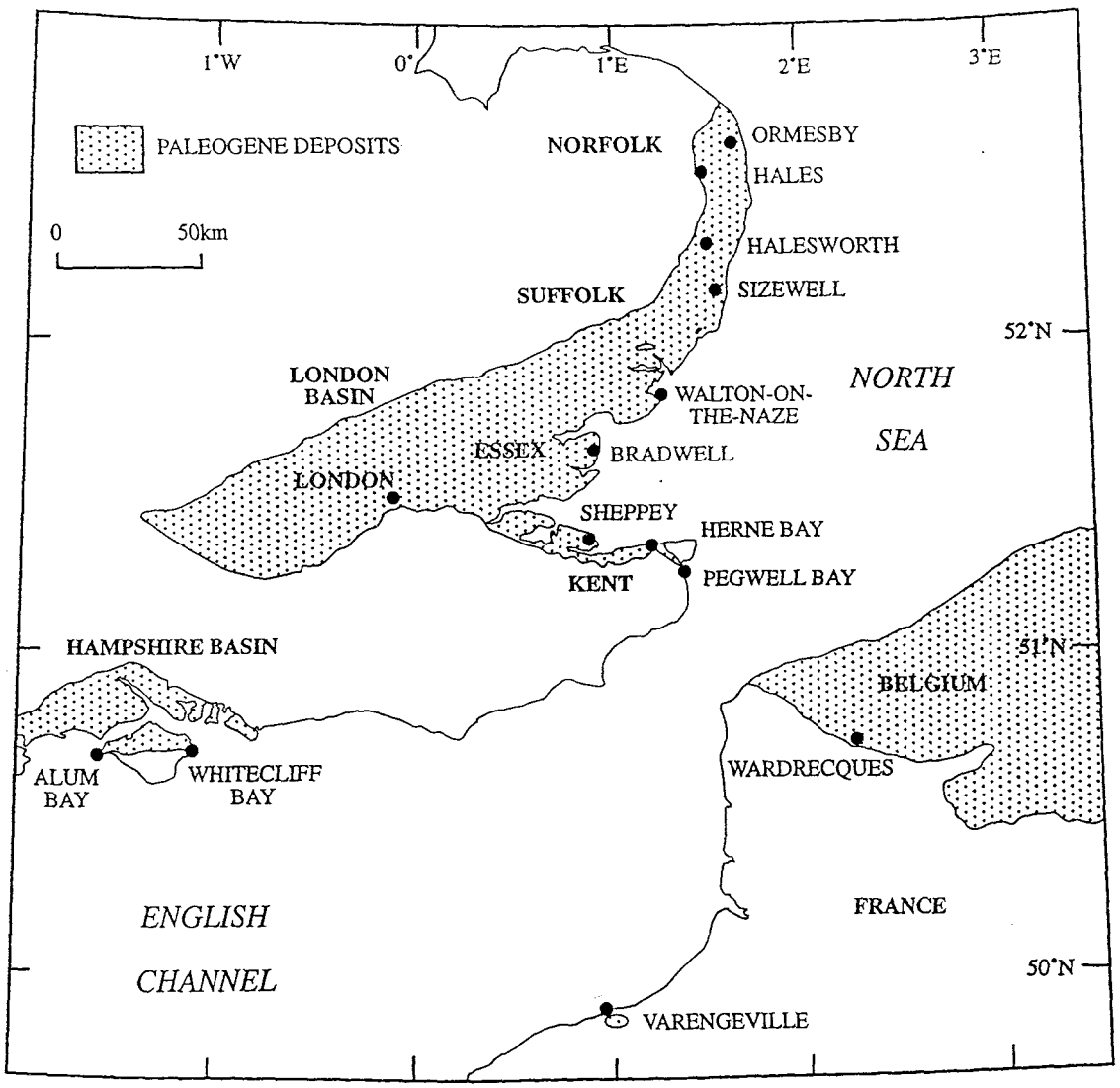

Figure 10-2 *Map showing the lower Paleogene deposits of southeast England, northern France and western Belgium and the location of boreholes and outcrops which have been magnetostratigraphically correlated (from Ali and Hailwood, in press).*

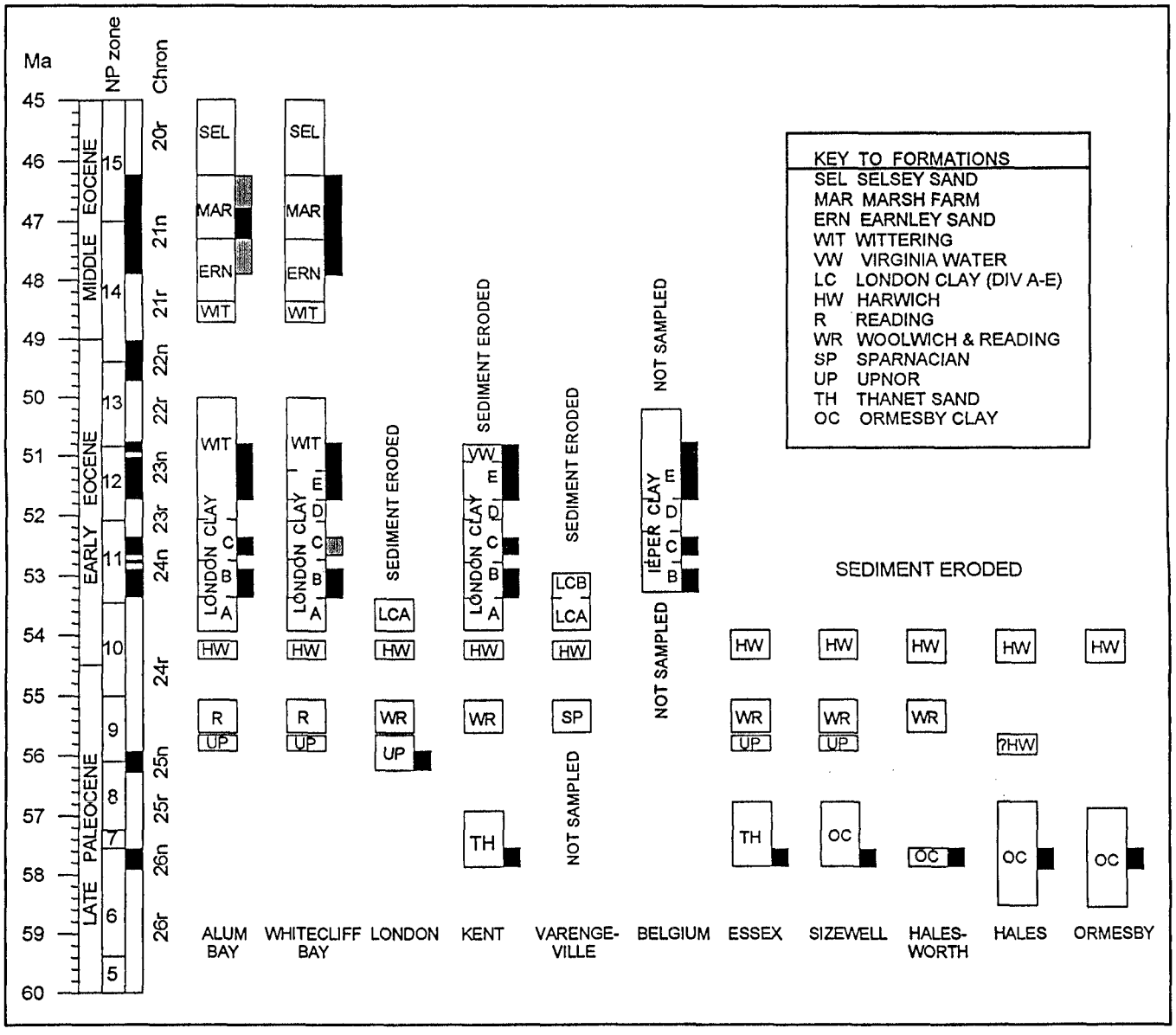

Figure 10-3 *Magnetostratigraphic correlation of the upper Paleocene through lower middle Eocene of southeast England, northern France and Belgium (from Ali and Hailwood, in press).*

basal Tertiary sediments carry a normal polarity magnetisation. Nannoplankton evidence at thebase of the Thanet Formation at Bradwell (Knox et al, 1994) indicate an NP6 age for these levels, indicating that the normal polarities represent a record of Chron C26n.

Chron C25r (56.39-57.55Ma)

U.S. Atlantic and Gulf Coastal Plains

Chron C25r is identified within the Aquia Formation of the Oak Grove core in Virginia; however there were no suitable outcrops of this age exposed along the Potomac River. In the Gulf Coastal Plain sediments, calcareous nodules sampled from within the *Ostrea thirsae* beds of the Nanafalia Formation at Camden preserve Chron C25r. The Salt Mountain limestone, dated NP7 (Siesser, 1983), also carries a record of Chron C25r.

NW Europe

In southern England the upper beds of the Thanet Sand and Ormesby Clay Formations record Chron C25r.

Chron C25n (55.90-56.39Ma)

U.S. Atlantic and Gulf Coastal Plains

Chron C25n is associated with the upper part of nannofossil zone NP8 and the lower part of NP9 (Berggren et al, 1985). It is preserved in approximately 7m of Aquia Formation in the Oak Grove core, at Tinker's Ravine and probably at Bull's Bluff on the Atlantic Coast. Along the Gulf Coast, in Alabama, the Grampian Hills Member of the upper Nanafalia Formation carries a record of Chron C25n at Camden and Camden Radio localities. There is no evidence for Chron C25n being preserved in the Tuscahoma Formation.

NW Europe

Aubry et al (1986) report that Chron C25n was not preserved in Southern England; the lack of such a record resulting from non-deposition or an erosional event which removed Chron C25n age material. The non-sequence/erosional event was located at the unconformity which separates the Thanet Sand Formation from the Lambeth

Group of the Upnor Formation.

Recent studies by Ellison et al (in press) and Ali and Jolly (in press) report a record of Chron C25n in the lower part of the Upnor Formation in central London. It appears to extend only over a few square kilometres and has been interpreted as representing isolated sediments preserved beneath material of Chron C24r age which was deposited during the main Upnor Formation transgression (Ali and Jolly, in press).

Chron C24r (53.35-55.90Ma) and associated cryptochrons

U.S. Atlantic and Gulf Coastal Plains

The relatively long reversed interval of Chron C24r spans the upper Aquia, Marlboro Clay and lower Nanjemoy Formations in Virginia and Maryland and the Hatchetigbee/Bashi and Tuscahoma Formations in Alabama and Georgia (Fig. 10-1). In the Oak Grove core, of the Atlantic Coast, Chron C24r covers an interval of 24m of sediments assigned to calcareous nannofossil zones NP9, NP10 and NP11. Within NP10, short term normal polarity events are identified in the lower Nanjemoy Formation (Oak Grove core, section 6-2). Interestingly, the Peterman core of Alabama records a similar normal polarity event in NP10 age sediments of the Hatchetigbee Formation. These sites exhibiting short normal polarity intervals may have an important stratigraphic significance as short normal polarity intervals have also been reported in sediments of NP10 age within the Bighorn Basin of Wyoming (Tauxe et al, 1994) and possibly in the Harwich Formation of the London Basin (Aubry et al, 1986). Based on the stacking of a number of anomaly profiles for this interval, Cande and Kent (1992) noted several short wavelength features, termed 'cryptochrons' between anomalies 24 and 25. Tauxe et al (1994) speculate that the normal polarity identified in the Willwood Formation of the Bighorn Basin correlates with the single point normal polarity zone defined at DSDP site 550, the Oldhaven magnetozone in the Harwich Formation and cryptochron C24r.6. Within the early Eocene Atlantic and Gulf Coast sediments investigated in the present study, it is plausible that the particularly well-defined normal polarity events in nannofossil zone NP10 (at depths of 65m in the Peterman core, Alabama and 96m in the Oak Grove core, Virginia) are also correlatable with C24r.6. Unfortunately the resolution of these palaeomagnetic features are beyond biostratigraphic capabilities.

The outcrops of Hatchetigbee sediments at the type section of Hatchetigbee Bluff and at lower Peach Tree in Alabama yielded poor palaeomagnetic results and further thermal work is necessary to obtain a reliable magnetostratigraphy for these sections. At Bell's Crossing, however, a reverse polarity preserves a record of Chron C24r. The Tuscahoma Sands which correlate with the Marlboro Clay and upper Aquia Formations in Virginia were closely sampled at 6 sections, over a distance of 300km, from eastern Georgia to southwestern Alabama. Sites spanned the stratigraphic interval from the Bear Creek Marl, identified at Bear Creek which is considered by Mancini and Tew (1991) to represent the lowest beds of the formation to above the Bell's Landing Marl. Palaeomagnetically, the polarity determinations were homogenous, giving a confident reverse polarity signal throughout the entire interval, correlating with Chron C24r. In Virginia, only two short outcrop sections within sediments of NP9 and NP10 age were sampled: at Fairview Beach within the lower Nanjemoy Formation (assigned to zone NP10 by Gibson, 1991) and at the Yacht Club locality (assigned to upper zone NP9 by Gibson, 1991) neither of which yielded a confident polarity determination.

NW Europe

The Woolwich, Reading and Harwich Formations and the lowest beds of the London Clay Formation were all deposited during Chron C24r (Ali and Hailwood, in press). The Upnor Formation at Alum Bay, Whitecliff Bay and at the top of the Upnor Formation in the London Basin are reversely magnetised (early Chron C24r). Ali and Jolly (in press) position the Paleocene/Eocene boundary in southeast England just below the base of the Harwich Formation, at the unconformity which separates this formation from the Lambeth Group.

Chron C24n (52.36-53.35Ma)

US Atlantic and Gulf Coastal Plains

A record of magnetochron C24n was detected within an interval of 13m of the Nanjemoy Formation strata within the uppermost part of the Oak Grove core, Virginia. The top 7m of predominantly normal polarity is considered to represent sub-Chron C24n.1n, the middle reverse polarity interval of about 3.7m, possibly sub-Chron C24n.1r and C24n.2r combined and the bottom 2.7m sub-Chron C24n.3n. The sub-Chron C24n.2n of Cande and Kent (1992) was not identified. In the Gulf

Coast, the nannofossil zone NP11 appears to be partially or totally absent (Gibson and Bybell, 1981; Gibson et al, 1982) which, based on the fossil zone-magnetochron correlations of Berggren (1985), would suggest that Chron C24n is also either lacking or only partially preserved in these sediments. This appears to be confirmed by the more recent planktonic nannofossil data (Bybell and Gibson, 1985) and palynomorph data of Edwards (pers. comm.) from samples from Tunnel Springs and the Peterman core. Within the Peterman core, samples which carry a reliable reverse polarity are located above the proposed hiatus in material of zone NP12 and below it in sediments of NP10 age. These are considered to represent parts of Chron C23r and Chron C24r respectively. At Tunnel Springs those samples below the Tallahatta/Hatchetigbee contact which yield nannofossils are characteristic of Zone NP10. This is supported by the palaeomagnetic results from thermal demagnetisation of specimens from this study which indicate a reverse polarity interval (correlated with Chron C24r). Unfortunately the crucial intervals where the Hatchetigbee is exposed at Hatchetigbee Bluff and Lower Peach Tree yielded poor results and further thermal demagnetisation investigations are necessary for samples from these localities.

NW Europe

Chron C24n.1n and Chron C24n.3n have been identified within the Hampshire Basin, at Sheppey, Kent and in Belgium (Ali and Hailwood, in press). Chron C24n.2n is not clearly identified, although, two normal polarity sites at about 30m below datum in the Warden Bay borehole at Sheppey suggest that it is may be present here (Ali et al, 1993, figure 6). At Sheppey, Kent, the base of Chron C24n.1n is positioned at 8m above the base of the London Clay Formation Division C1 (of King, 1981) and its top is placed 8m below the C/D junction (Fig. 10-3). In Belgium, Chron C24n.1n extends from the lower part of Division C1 to the upper part of Division C2. In the Hampshire basin, the record of Chron C24n.3n is considered unreliable at Whitecliff Bay but is well defined in Division C of the London Clay Formation at Alum Bay (Ali and Hailwood, in press). The base of Chron C24n.3n coincides with the base of the London Clay Formation Division B and terminates within this division at Alum Bay, Whitecliff Bay (Aubry et al, 1986) and Sheppey (Ali et al, 1993). In Belgium, Chron C24n.3n is preserved within the type section of the Ieper Clay Formation Wardrecques Member which is equivalent to Division B of the London Clay Formation, although the base is not identified here (King, 1990).

Chron C23r (51.74-52.36Ma)

US Atlantic and Gulf Coastal Plains

A record of Chron C23r was not identified in sediments from the Atlantic Coast due to the lack of sections and core material spanning this interval. On the Gulf Coast, however, the record of upper Chron C23r and its contact with Chron C24n above is well defined in the lower Tallahatta Formation of the Peterman core and at the Butler locality.

NW Europe

Spanning the NP11/NP12 nannofossil boundary, Chron C23r coincides with Division D and the upper part of Division C of the London Clay Formation (King, 1981). These sediments are exposed at Whitecliff Bay and Alum Bay on the Isle of Wight, in the London and Kent sections and in time-equivalent beds in the Ieper Clay of Belgium.

Chron C23n (50.78-51.74Ma)

US Atlantic and Gulf Coastal Plains

Chron C23n is recorded in sediments from both the Atlantic and Gulf Coasts. Within the Nanjemoy Formation at Pope's Creek, biostratigraphic control positions the section in upper nannofossil zone NP12 (possibly extending into NP13) where a normal polarity interval is interrupted by a period of reversed polarity, probably representing sub-Chron C23n.1r. The advent of sub-Chron C23n.1r occurs at about 2m above the beach level. In sediments of the Gulf Coast, Chron C23n has been identified within the NP12 nannofossil zone of the Tallahatta Formation in the Peterman core and also at a number of outcrops. In the Peterman core the upper and lower boundaries of Chron C23n occur at depths of about 24m and 47m respectively; furthermore, sub-Chron C23n.1r is clearly defined within this interval by 6 sites from 33-37m below datum.

In outcrop, biostratigraphic control was limited and therefore magnetozones were positioned relative to the Lisbon Formation contact above, the Hatchetigbee Formation below and using three clear stratigraphic markers: the Meridian Sand

Member (MSM), a glauconite horizon and a *Camptoceratops* bed observed at Little Stave Creek, Butler and Campbell (C King, pers. comm., 1995). Normal polarity sites which are considered to represent a record of Chron C23n occur above the MSM at Campbell, Butler and Midway and coincide with an interval of sediment rich in glauconite. At the Midway locality, the polarity boundary marking the contact with Chron C23r above is also clearly identified.

NW Europe

In the UK, the upper and lower boundaries of Chron C23n have been identified within the Wittering Formation at Bracklesham Bay, Whitecliff Bay and Alum Bay in the Hampshire Basin (Townsend and Hailwood, 1985) and the base of Chron C23n is positioned just below the London Clay Formation Division D/E boundary at Sheppey, Kent (Ali et al, 1993). Ali et al (1993) repositioned the base of the magnetozone at Whitecliff Bay at 3.5m below the base of the Wittering Formation close to the Division D/E junction of the London Clay (Fig. 10-3). In Belgium, the start of Chron C23n is recorded 1.4m above the base of the Aalbeke Clay Member and the record of this chron terminates in the lower part of the Egem Sand Member (Ali et al, 1993). Chron C23n.1r was not resolved in NW European sediments by Ali and Hailwood (in press).

Chron C22r (49.71-50.78Ma)

US Atlantic and Gulf Coastal Plains

The Atlantic Coast early Eocene outcrops sampled during this study did not appear to extend into Chron C22r. In Alabama, however, at least 10m of the Peterman core record Chron C22r although its upper limit is not defined due either to a hiatus at approximately 9m below datum or the relatively wide sampling intervals and/or poor core recovery over this interval. In corresponding outcrops at Little Stave Creek, Butler and at Campbell a reversed polarity interval containing *Camptoceratops* was considered to represent a record of Chron C22r though palaeomagnetic data was often poor due to the weak magnetic intensity of samples. At the top of the Midway section, a record of lowermost Chron C22r is reliably identified.

NW Europe

Chron C22r is recorded by sediments which carry a reverse polarity signature in the

Wittering Formation at Alum Bay and Whitecliff Bay on the Isle of Wight. In Belgium, Chron C22r is identified in the upper part of the Ieper Formation.

Chron C22n (49.04-49.71Ma)

Gulf Coastal Plain

Chron C22n is not identified in material from the Peterman core which suggests that a hiatus (proposed by Hazel et al, 1984) excludes Chron C22n from the magnetic record here; however, the expected position of Chron C22n, based on the available biostratigraphy, falls within an interval where core recovery was extremely poor.

C.King (pers. comm. 1995) has proposed that the upper part of the Tallahatta Formation is missing from Butler and Campbell sections. The normal polarity interval recorded in sediments at the top of these sections would then represent Chron C22n. Equivalent-age sediments in Virginia and Maryland were not sampled.

NW Europe

Magnetostratigraphic data for this interval of time is available only from the Hampshire Basin since all Tertiary sediments younger than about 50 Ma (Chron C22r) have been eroded from the London Basin and sediments from Belgium and northern France are yet to be investigated (Ali and Hailwood, in press). In the Hampshire Basin, Aubry et al (1986) suggested that a record of Chron C22n was missing. They proposed an hiatus of duration >0.66 my at the level of the Whitecliff Bay (lignite) Bed in the upper Wittering Formation to explain this phenomenon. Reinvestigation by Ali et al (1993) confirmed the absence of Chron C22n but suggested that the hiatus could be positioned at two alternative levels: the first at the top of Plint's Unit WB6 (Plint, 1983) and the second between the Wittering and Earnley Sand Formations.

Chron C21r (47.90-49.04Ma)

Gulf Coastal Plain

Chron C21r is identified in sediments of NP14 age in the upper part of the Peterman core and at Little Stave Creek.

NW Europe

On the Isle of Wight at Whitecliff Bay and Alum Bay, sediments recording Chron C21r are seen in the upper Wittering beds and within the lower part of the Earnley Sand.

Chron C21n (46.26-47.91Ma)

Gulf Coastal Plain

The base of Chron C21n is well defined in the upper Tallahatta Formation (upper NP14 age) at Little Stave Creek. A single site at the top of the Peterman core (also NP14) may represent the lower part of this polarity interval. These sediments are the youngest sampled during this investigation in Alabama. Strata of this age are not present along the Potomac River of the Atlantic Coastal Plain.

NW Europe

A record of Chron C21n has been identified within the early Tertiary deposits of Alum Bay and Whitecliff Bay on the Isle of Wight. Although the extent of the magnetochron is debateable at Alum Bay (where C21N appears to be restricted to the lower Marsh Farm Formation), at Whitecliff Bay the normal polarity interval starts in the Earnley Sand and continues to the top of the Marsh Farm Formation (Fig. 10-3).

10.2 Implications for dating and testing the early Paleogene eustatic sea level curve using magnetostratigraphy

The thicknesses of sedimentary units in the Central Atlantic Coastal Plain are considerably less than those of the corresponding strata on the Gulf Coast. Gibson (in press) considers that portions of Paleogene sedimentary sequences of the Atlantic Coastal Plain have been removed and consequently the sedimentary record of this region represents only fragmented sections of transgressive-regressive cycles. Magnetostratigraphic results from this study suggest that all magnetozones expected within the interval of time investigated are in fact encountered (see Oak Grove core and Pope's Creek magnetostratigraphy, figure 10-1). This implies that large intervals of time, of duration comparable to that of complete magnetozones, are not entirely missing from the sedimentary record.

In order to investigate the effect of eustasy on sediment deposition, a relatively complete sedimentary record within the study areas is required (see section 1.1). Therefore, in view of the thicker sedimentary sequences in the Gulf Coastal Plain and the focused cycle work of Baum and Vail (1988) and Mancini and Tew (1991) in this region, the main emphasis here is placed on sediments from the Gulf Coastal Plain, with further evidence from the Atlantic Coastal region included where applicable.

The magnetostratigraphies for the Paleogene of the US Atlantic and Gulf Coastal Plains determined during this study and for NW Europe defined by Ali and Hailwood (in press) are correlated in figure 10-4. In this compilation, magnetozones with well defined polarity boundaries have been used to link the composite sections from either side of the Atlantic. In addition, sea level curves identified from the patterns of cyclic sedimentation for this interval of time on each margin, have been integrated into the magnetostratigraphic framework. The curve for NW Europe is taken from Neal et al (1994) and is based on well log, seismic and biostratigraphic data from the Central North Sea (CNS) combined with outcrop information, including formations and sequences from the Isle of Wight and London-Hampshire basins. The more generalised sea level curve for the US Gulf Coast has been developed from the data of Baum & Vail (1988) by Mancini and Tew (1991) and is based entirely on sequence stratigraphy derived from outcrop and core data from Alabama.

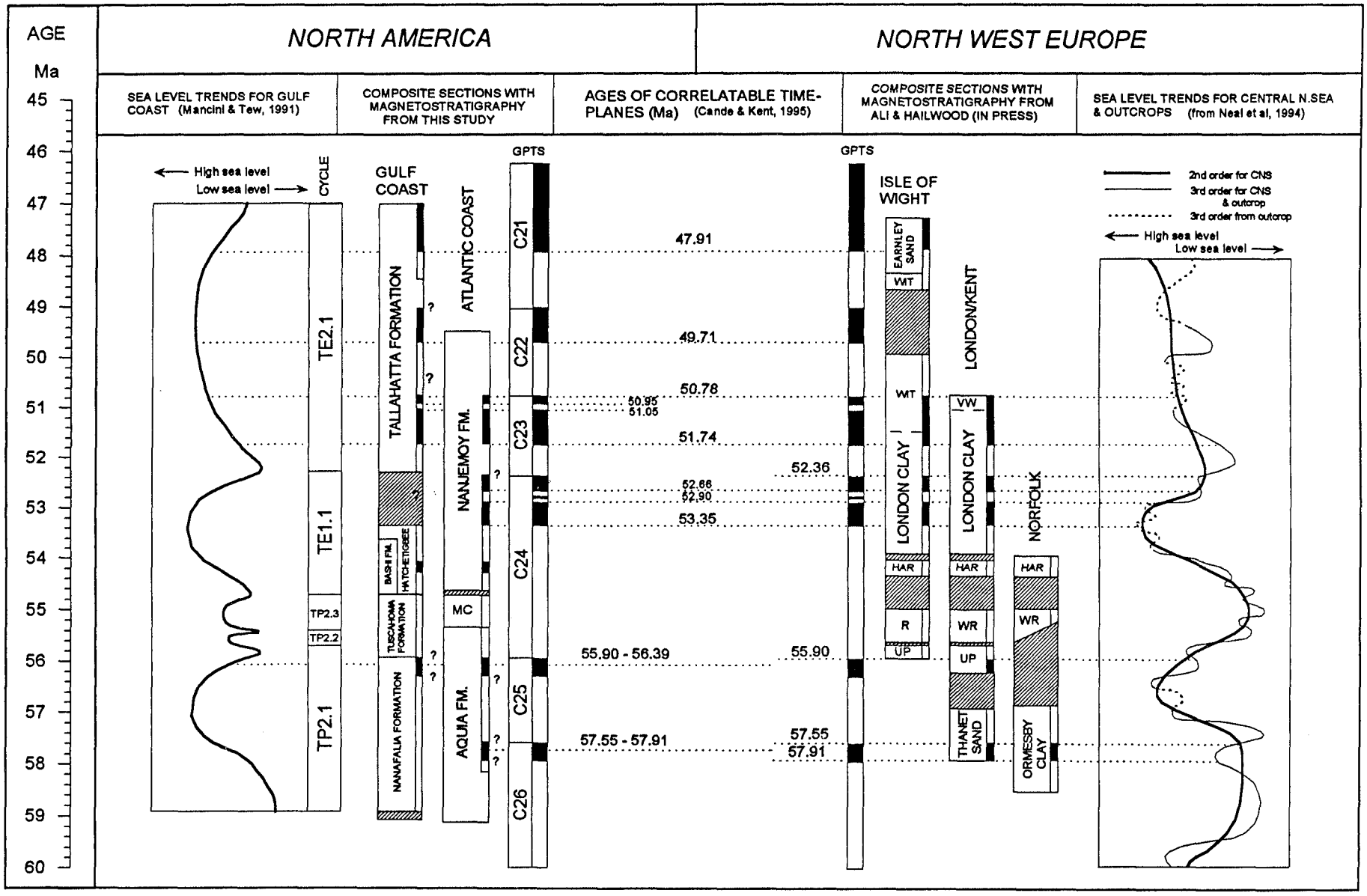

Figure 10-4 *Magnetostratigraphic correlation of Paleogene polarity zone boundaries in NW Europe and North America, linked to corresponding sea level curves defined from depositional sequences.*

10.2.1 Correlation of sea level cycles identified from 2nd and 3rd order depositional sequences

For the interval of time under investigation in the present study, Mancini and Tew (1991) identified 5 depositional cycles in Alabama (see section 7.3). The oldest cycle, TP2.1, is reported to span sediments from the base of the Nanafalia Formation through to the lower Tuscahoma Sands (including the Bear Creek Marl, which itself represents a cycle of higher order). Sediments that carry a record of Chron C25n are seen in the Grampian Hills Member of the Nanafalia Formation (which represents a highstand deposit) although the actual polarity boundaries have not been identified. In NW Europe, only the Upnor Formation of central London carries a record of Chron C25n (Ali & Jolly, in press); elsewhere this chron is not preserved which suggests either complete erosion of the corresponding sedimentary unit or the presence of a non-sequence (Aubry et al, 1986). The recording of Chron C25n in both US Atlantic and Gulf Coastal sections suggests that its absence in the NW European sections reflects a regional tectonic event.

The broad sea level change representing cycle TP2.1 appears to correlate with the late Paleocene 2nd order cycle defined for NW Europe (Fig. 10-4). In broad terms therefore, a general agreement between the two curves occurs for this interval, although the higher frequency fluctuations that are superimposed on the curve for NW Europe have not been defined on the Alabama curve.

Cycles TP2.2 and TP2.3 of Mancini and Tew (1991) include sediments of the Middle Tuscahoma (including the Gregg's Landing Marl) and the Upper Tuscahoma Formation (including the Bell's Landing Marl) respectively. Unfortunately, both of these cycles occur within a period of reversed polarity (Chron C24r) and therefore do not contain polarity boundaries that can be utilised for magnetostratigraphic correlation. They appear, however, to coincide with the basic frequency of 3rd order cycles seen in NW Europe for this period of time. Furthermore, the TP2.3/TE1.1 cycle boundary of Alabama coincides with a relative lowstand in Virginia identified by the erosional surface at the top of the Marlboro Clay. The increasing water depth within the lower part of TE1.1 of Alabama corresponds with the increase in water depth suggested by the rising *tau* values of Gibson (in press) at the base of the Nanjemoy Formation. This lowstand is similarly reflected in NW Europe by a hiatus between the Woolwich/Reading and

Harwich Formations and by the 2nd order curve of Neal et al (1994) which indicates a low sea level for the Paleogene of the Central North Sea during this time (Fig. 10-4).

The TE1.1 cycle of Mancini and Tew (1991) spans the Hatchetigbee Formation including the Bashi Marl Member. In this instance the Bashi Marl Member of the Hatchetigbee Formation is considered a single marine transgressive unit that is overlain by a single regressive complex of shallow-marine to marginal-marine beds (termed the unnamed upper member) of the Hatchetigbee Formation (Gibson, in press). In contrast, Baum and Vail (1988) placed the Bashi and Hatchetigbee strata into two separate sequences, but provided no justification for this subdivision; furthermore, the age of the younger of their two sequences does not agree with published biostratigraphic data of Gibson et al (1982) and Bybell and Gibson (1985) and hence the scheme of Mancini and Tew (1991) is preferred here.

The lack of adequate magnetostratigraphic data for this interval in Alabama limits any sequence correlations between NW Europe and the US Gulf Coast. However, on the US Atlantic Coast, reliable palaeomagnetic results from the Oak Grove core enables correlation of some of the 6 lower-order cycles reported in the Nanjemoy Formation by Gibson (in press - see figure 5-4) with the corresponding cycles identified in the London Clay by King, 1981. The relationships between these depositional sequences are discussed in the following section (Section 10.2.2).

The Tallahatta Formation, including the basal Meridian Sand member, has been identified by Baum and Vail (1988) and Mancini and Tew (1991) as representing a complete depositional cycle (TE 2.1, figures 7-3 and 10-4). The lower boundary of Chron C23n.2n (dated 51.74 by Cande & Kent, 1995) is positioned in the lower part of the formation, above the Meridian Sand Member and can be directly correlated with the base of Division E within the London Clay Formation in NW Europe. These lower Tallahatta beds, located below the Chron C23n.2n lower boundary are commonly rich in glauconite (observed in the Peterman core and at the Butler, Campbell and Midway outcrop localities) suggesting a shallow marine environment which is consistent with the base of cycle TE2.1 and the low sea level indicated in NW Europe at approximately 52Ma (Fig. 10-4).

The sea level curve proposed by Mancini and Tew (1991) for the Tallahatta sequence is particularly simplistic considering the duration of time that the formation spans (approximately 5my). Within the Tallahatta Formation, *time planes* at 50.78Ma and 47.91Ma could potentially be correlated with higher order sequences associated with the Wittering and Earnley Sand Formations, if further more detailed sequence investigations were done.

10.2.2 Implications for higher frequency sea level correlations (3rd and 4th order)

There is a potential to accurately correlate higher frequency sea level fluctuations when they span a number of well defined polarity zone boundaries. The positions of the polarity boundaries relative to the sequence boundaries, however, are critical. If a polarity boundary is positioned precisely at a depositional cycle boundary it may not represent a true record of the time of the geomagnetic reversal due to the removal of material by erosion or by a period of non-deposition associated with the sequence boundary which would effectively offset the correct position. The polarity boundary should be close to the sequence boundary or two polarity zone boundaries should be situated either side of the sequence boundary, so that the age of the latter can be determined by interpolation over a relatively short interval.

In sediments of NP11 age sampled from the Oak Grove core in Virginia, for instance, Chron C24n is clearly recorded and can be used to accurately correlate cycle 4 and to some extent cycle 5 and 6 of Gibson (in press, see figure 5-4) with division B and C determined within the London Clay and Ieper Clay of NW Europe (King, 1981). Chron C24n.3 is observed to lie entirely within cycle 4 (Figs. 6-10 and 10-5) where the base of the magnetozone is positioned 2.7m above the start of the cycle and the top of the magnetozone lies 2.4m below the end of the cycle. This coincides approximately with division B of the London Clay although the lower boundary of Chron C24n.3 occurs at the division A-B boundary. The *tau* values from the base of cycle 4 indicate a significant initial rise in sea level when compared to other cycles identified for this interval (Fig. 5-4) which may represent the flooding event seen at the base of division B of the London Clay (King, 1981).

The short normal polarity interval represented by Chron C24n.2 was not identified in the

Nanjemoy Formation of the Oak Grove core, nor within the London Clay Formation.

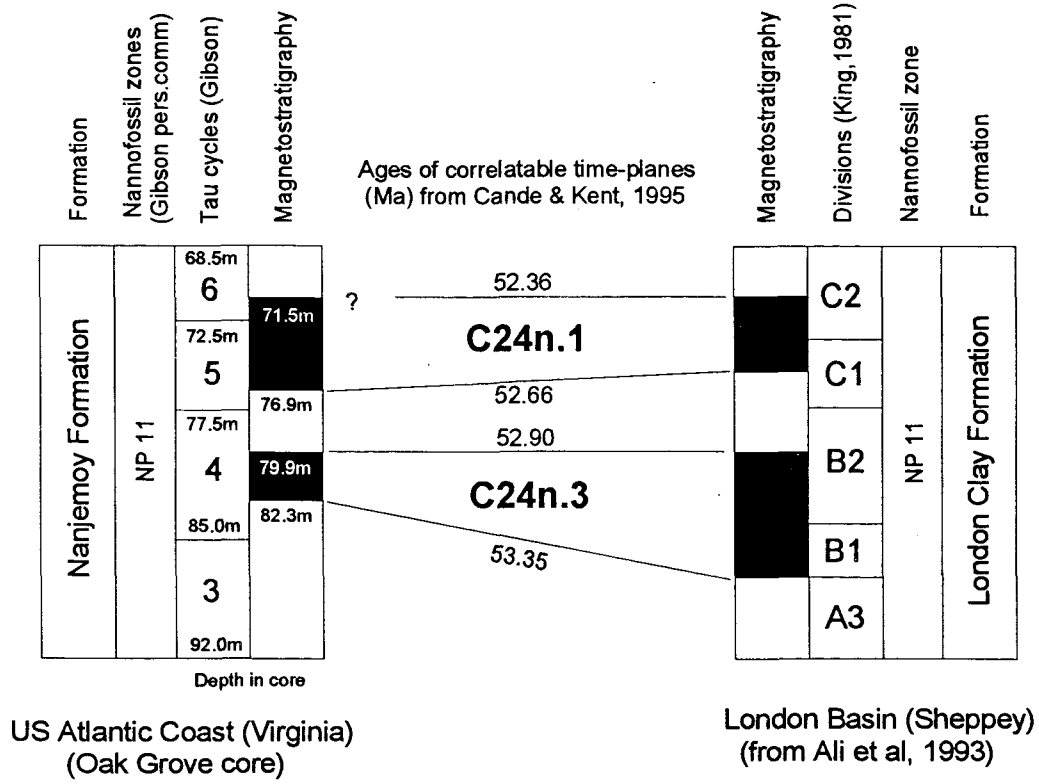

Figure 10-5 *Correlation of depositional cycles in the Nanjemoy Formation of the US Atlantic Coast with those in the London Clay of NW Europe.*

The interval of time between the end of Chron C24n.3 and the start of Chron C24n.1 according to Cande & Kent is 240,000 years. Within this interval, the boundaries of both Gibson's *tau* cycles 4/5 and King's divisions B/C occur (Fig. 10-5).

In younger sediments of the Oak Grove core, Chron C24n.1 has a lower boundary which is positioned 0.6m above the base of cycle 5. The upper limit of Chron C24n.1 is not so clear but probably lies within the lower part of cycle 6. In the London Basin at Sheppey, Chron C24n.1 is recorded in the lower part of division C of the London Clay; thus the onset of the depositional cycle mirrors that of cycle 6 on the North

American margin.

Using magnetostratigraphy, it is evident that during the interval of time under investigation here, depositional sequences which are considered to represent 3rd or 4th order cycles have a similar frequency on both sides of the Atlantic. Furthermore, the age of the sequence boundaries, as defined by the magnetozone boundaries appears to be synchronous across the Atlantic, thus supporting the Vail/Haq eustatic model.

A more detailed sequence stratigraphic investigation of Gulf Coast sediments, with a resolution compatible with existing schemes for NW Europe would enable the timing of sequence boundaries and associated sea level curves to be investigated more fully. This study illustrates, however, the vital role that magnetostragraphy can play in dating sea level curves worldwide and examining their synchronous or diachronous nature.

An important step to expand this work further would be to incorporate additional data from passive margins on other continents into this study. A set of fine scale depositional sequences from several margins, fixed in a magnetostratigraphic framework would provide an accurate global comparison of high order sea level fluctuations.

10.3 Palaeomagnetic pole for the late Paleocene and early Eocene

The primary magnetic vectors recorded by sediments can be used to determine the position of the corresponding palaeomagnetic pole, on the geocentric axial dipole model (Tarling, 1983). Any sediment magnetised at the same time on the same tectonic plate should have the same palaeomagnetic pole position. Successive poles through time, for any one stable block, will define an apparent polar wandering path (APWP).

Age	λ	ϕ	$\alpha 95$	Radiometric or Stratigraphic Age	Rock Unit
47	79	146	10	45-50	Rattlesnake Hills, Wyoming (Sheriff and Shive, 1980)
47	83	177	10	45-49 K/Ar	Absaroka Basalts, Wyoming (Shive and Pruss, 1977)
50	82	170	3	47-54	Montana Intrusives (Diehl et al, 1983)
60	76	148	3	TPA	Nacimiento Formation, New Mexico (Butler and Taylor, 1978)

Table 10-1 *Palaeomagnetic poles for the Paleocene and Eocene of stable cratonic USA (from Besse and Courtillot, 1991).*

An APWP for North America over the last 200 my has been proposed by Besse and Courtillot (1991) based on 51 published palaeomagnetic poles positions from independent studies which fulfill the following criteria:

i) the results are based on at least 6 separate sampling sites per pole and 6 independantly oriented samples per site

ii) 95% confidence interval for the overall mean direction of magnetisation of $< 15°$

iii) evidence of successful application of A.F. / thermal demagnetisation procedures

iv) a maximum dating uncertainty of ± 15 Ma.

Within the interval of time under investigation for the present research (47-58 Ma) four palaeomagnetic poles for North America were used to construct the APWP (Table 10-1).

The palaeomagnetic pole position calculated from data generated in this study

The stable end-point directions identified from samples at each outcrop are displayed on equal area stereographic projections in figures 10-6 to 10-10. The mean directions for each formation show a counter-clockwise declination swing of approximately 10° away from the north (Fig. 10-11). At the Salt Mountain section (Fig. 10-7) the greater counter-clockwise declination swing is probably associated with local movement related to the Jackson fault.

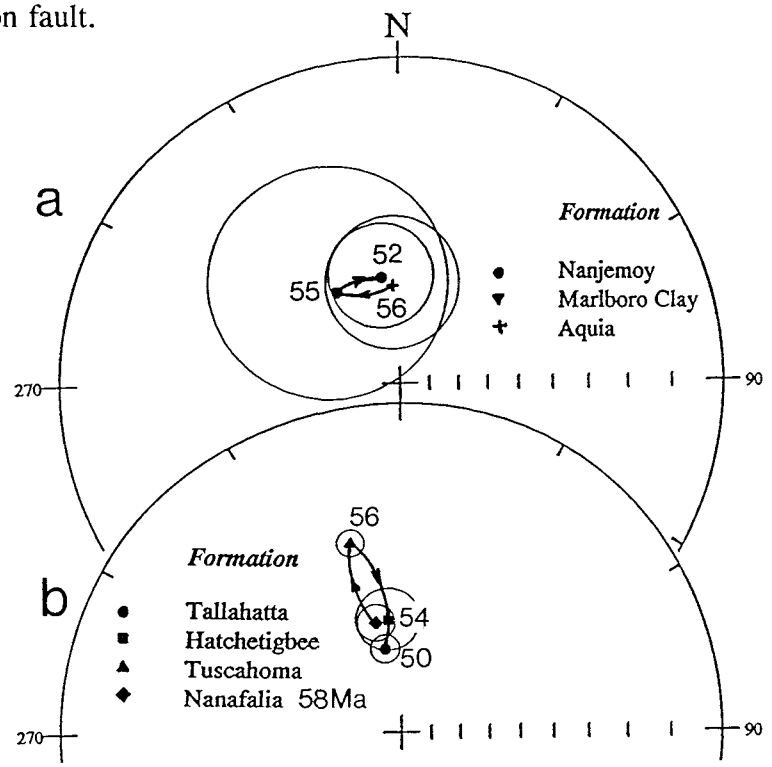

Approximate ages of the formations are indicated units (Ma).

Figure 10-11 **a.** *mean direction of palaeomagnetic vectors for each formation from the Atlantic Coastal Plain.* **b.** *mean direction of palaeomagnetic vectors for each formation from the Gulf Coastal Plain.*

In figure 10-11a and b the stable end-points from all outcrops within a formation are combined to produce a single palaeomagnetic direction for each stratigraphic unit

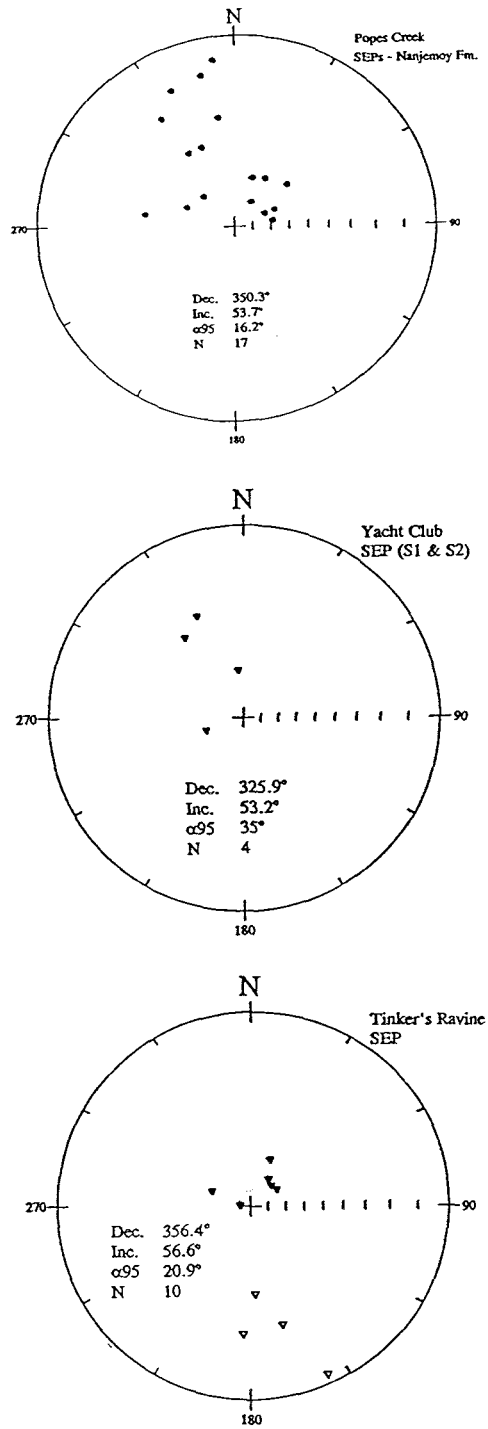

Figure 10-6 *Stereographic projection of stable end point directions from the Virginia and Maryland region.* Top. *Pope's Creek locality (Nanjemoy Fm.).* Middle. *Yacht Club locality (Marlboro Clay/Aquia Fm.).* Bottom. *Tinker's Ravine locality (Aquia Fm.). Solid and open symbols represent positive and negative inclinations respectively.*

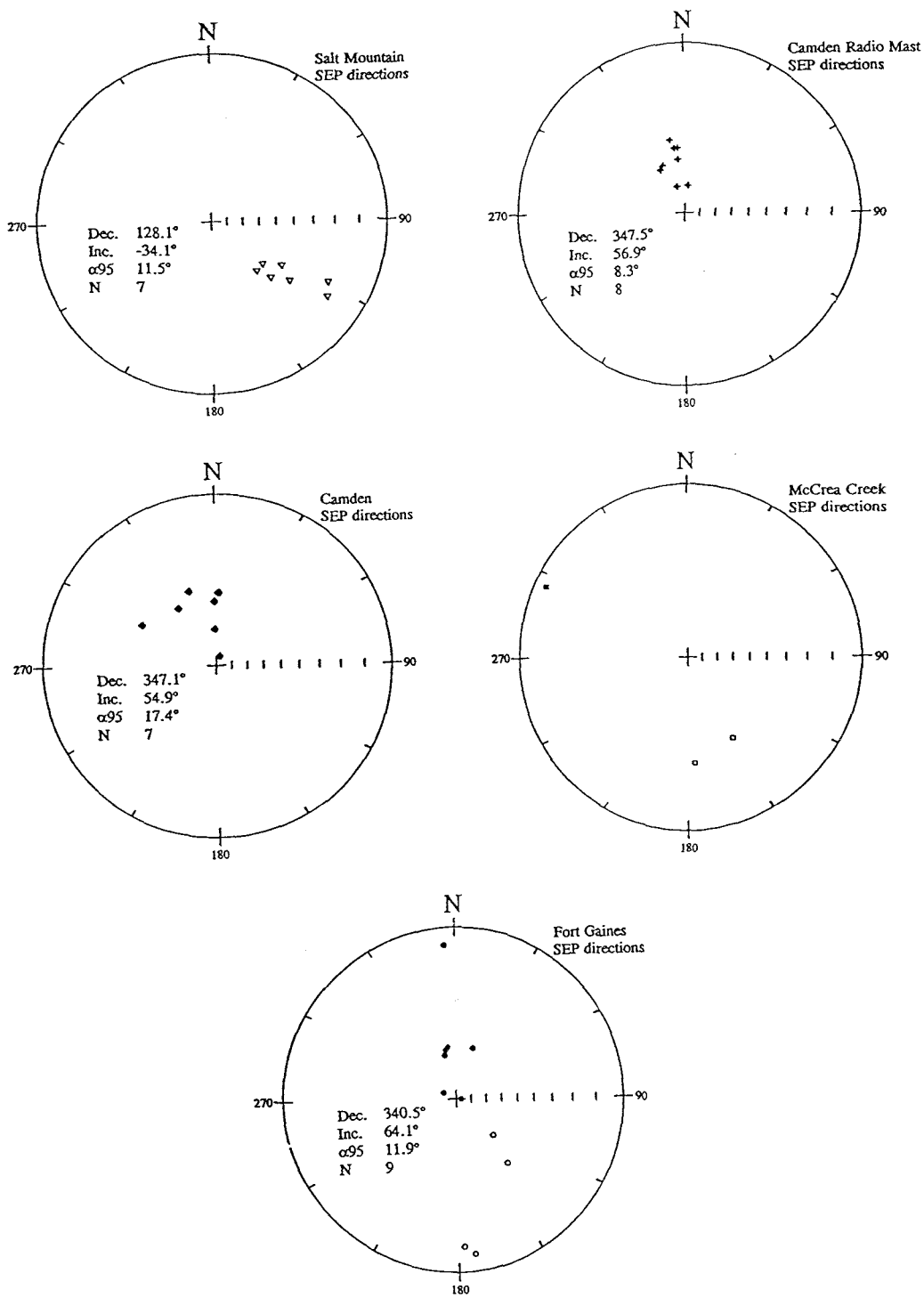

Figure 10-7 *Stereographic projection of stable end point directions from outcrop sections of the Nanafalia Formation, Gulf Coastal Plain.*

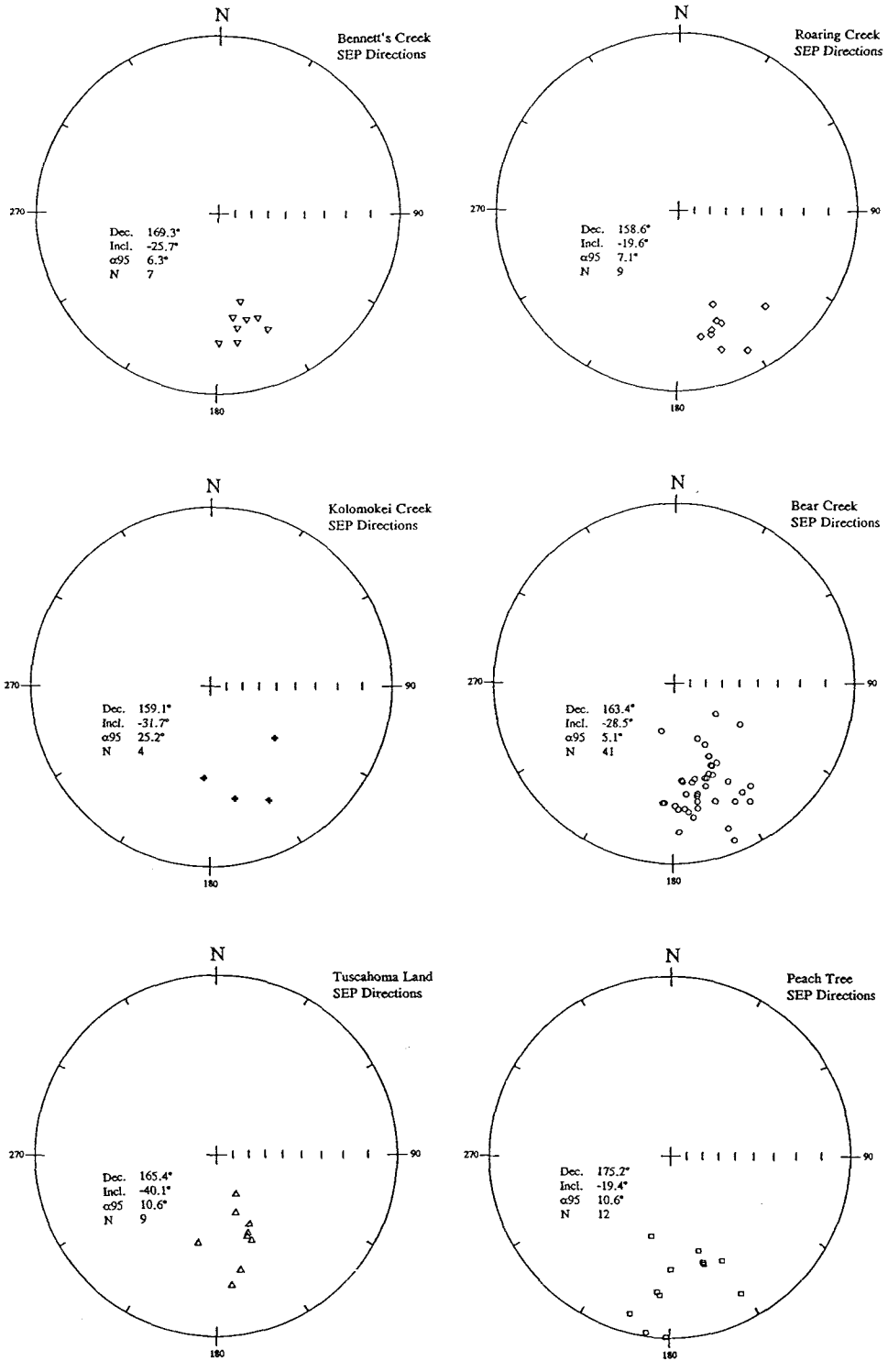

Figure 10-8 *Stereographic projection of stable end point directions from outcrop sections of the Tuscahoma Formation, Gulf Coastal Plain.*

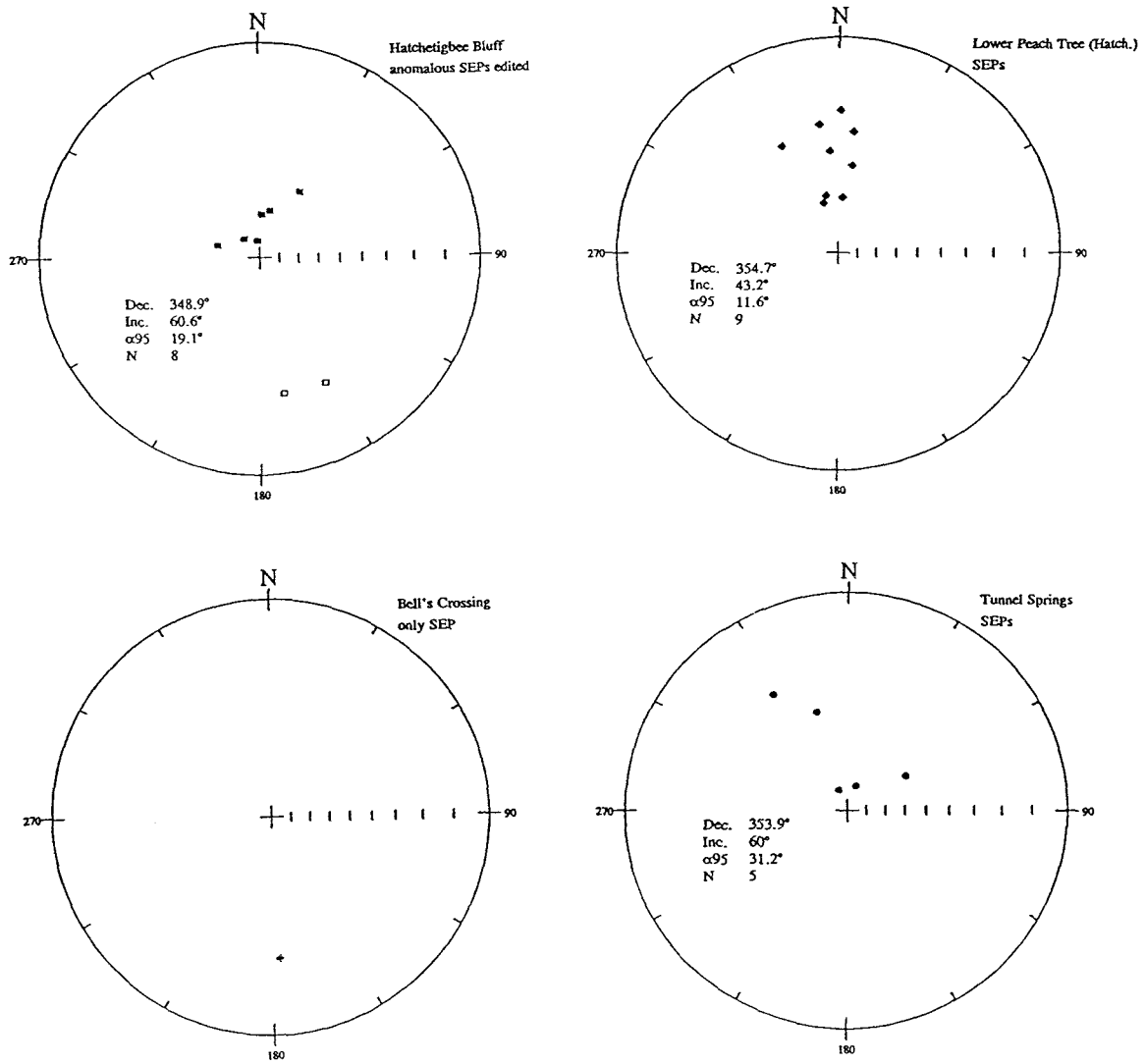

Figure 10-9 *Stereographic projection of stable end point directions from outcrop sections of the Hatchetigbee Formation, Gulf Coastal Plain.*

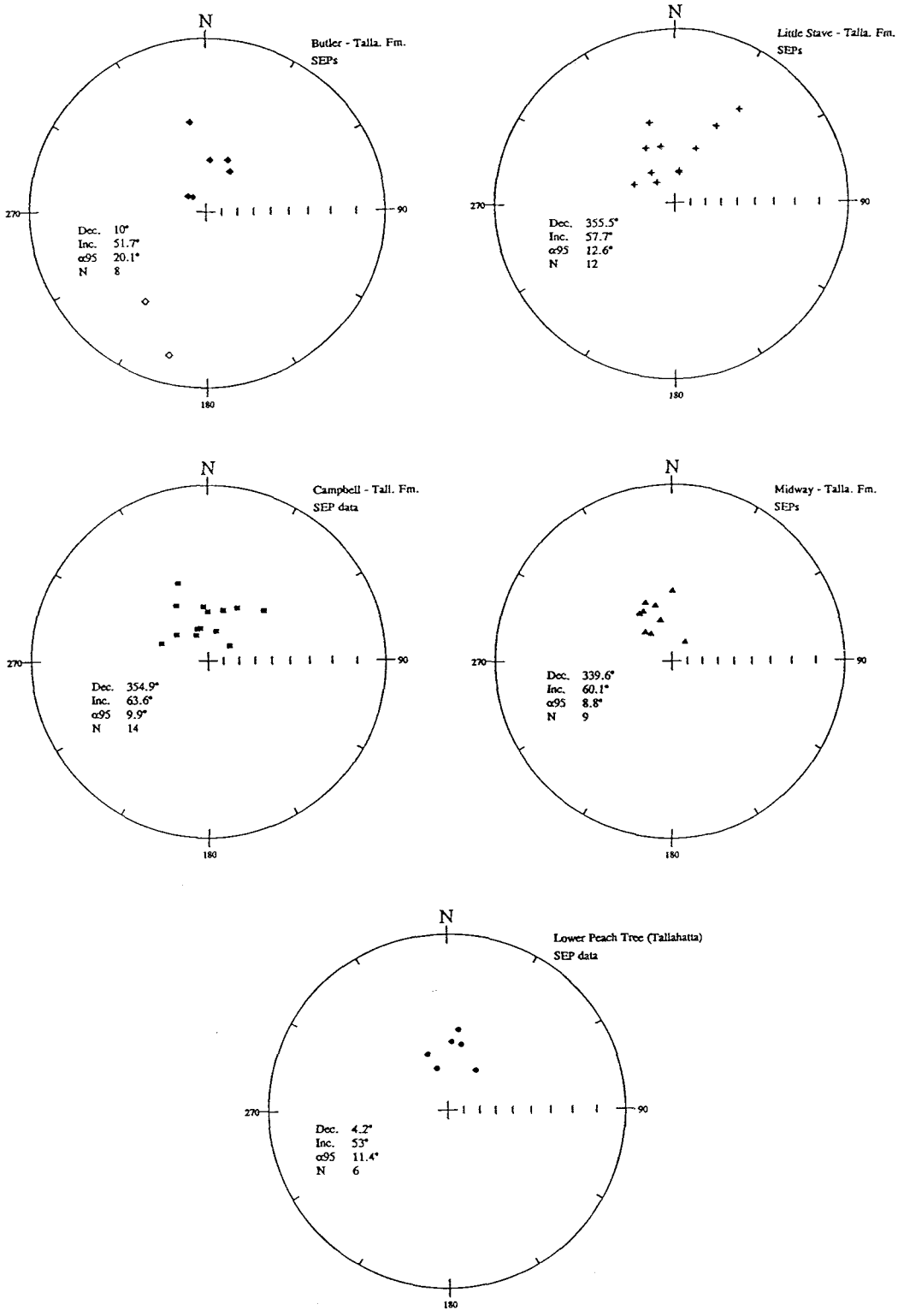

Figure 10-10 *Stereographic projection of stable end point directions from outcrop sections of the Tallahatta Formation, Gulf Coastal Plain.*

sampled on the Atlantic and Gulf Coastal Plains respectively. Although the overall mean directions for formations in the two regions are broadly similar, the $\alpha 95$ values for the Atlantic Coast formations are considerably larger than those for the Gulf Coast formations, reflecting the poorer quality of palaeomagnetic data and the relatively small number of SEPs observed for the latter region.

There is no clear systematic change of the mean formation directions with age and therefore, in calculating a palaeomagnetic pole position for this interval of time, the SEP directions from all four formations were combined. The data from the Atlantic Coastal Plain were not included in the calculation because of the greater uncertainty associated with the formation directions.

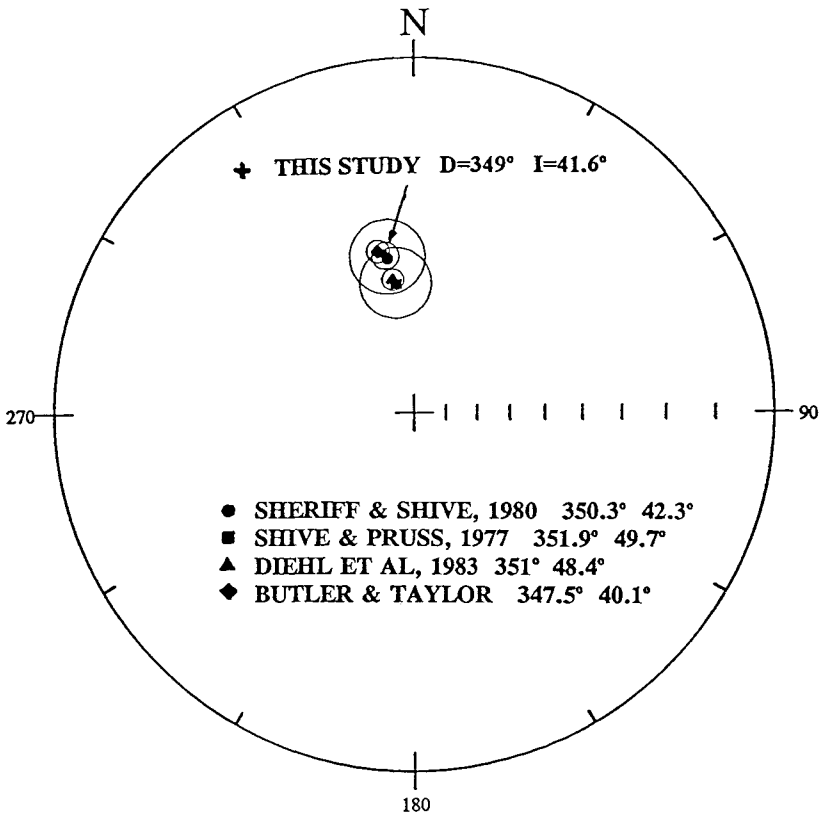

Figure 10-12 *The predicted direction of the geomagnetic field for central Alabama during the late Paleocene and early Eocene (calculated using the palaeomagnetic poles listed in Table 10-1 and a site latitude of 31.5°N and longitude of 87°W) compared to the mean direction derived from the present study.*

The mean direction of magnetisation for the Tuscahoma Formation is distinct from that of the other three Gulf Coast formations which have similar declination values but steeper inclinations. This may be due to inclination shallowing in the Tuscahoma Formation due to compaction or alternatively to this formation having recorded a geomagnetic 'excursion'. The quality of the Tusahoma data based on both thermal and A.F. demagnetisation analysis was particularly high. Consequently, no justification could be found for excluding this data from the overall mean direction used for calculating the palaeomagnetic pole position.

Figure 10-12 shows the predicted directions of the palaeomagnetic vector for the central Alabama region derived from the published palaeomagnetic poles (Table 10-1). The declination values agree well with those observed in the present study (350.3°, 351.9°, 351° and 347.5° compared to 349° for this study). The inclinations calculated from the published poles of Sheriff and Shive (1980) and Butler & Taylor (1978) have values close to 40° while those based on the poles of Shive & Pruss (1977) and Diehl et al (1983) are steeper, having values closer to 50°. The overall mean inclination of the palaeomagnetic vector from the present study is 41.6°, showing a closer agreement with the data of Sheriff and Shive (1980) and Butler & Taylor (1978).

The palaeomagnetic pole position used by Besse and Courtillot (1991) for the construction of the Apparent Polar Wander Path for North America during the age window 40-60Ma is:

$$\text{Age}=51\text{Ma} \quad \text{Lat } (\lambda)=80°\text{N} \qquad \text{Long } (\phi)=203°\text{E} \qquad \alpha 95=5°$$

The corresponding pole position calculated for the four formations from Alabama in this study is:

$$\text{Approx. mean age} = 55\text{Ma} \quad \lambda=78.2°\text{N} \qquad \phi=214°\text{E} \qquad \alpha 95=3.6°$$

Figure 10-13 compares the pole position of Besse & Courtillot (*solid circle*) with that calculated from the present study (*cross*). There is a considerable overlap of the 95% confidence circles for the two mean poles which indicates a good agreement between the two results. The small discrepancy between the two pole positions may reflect the ~4my

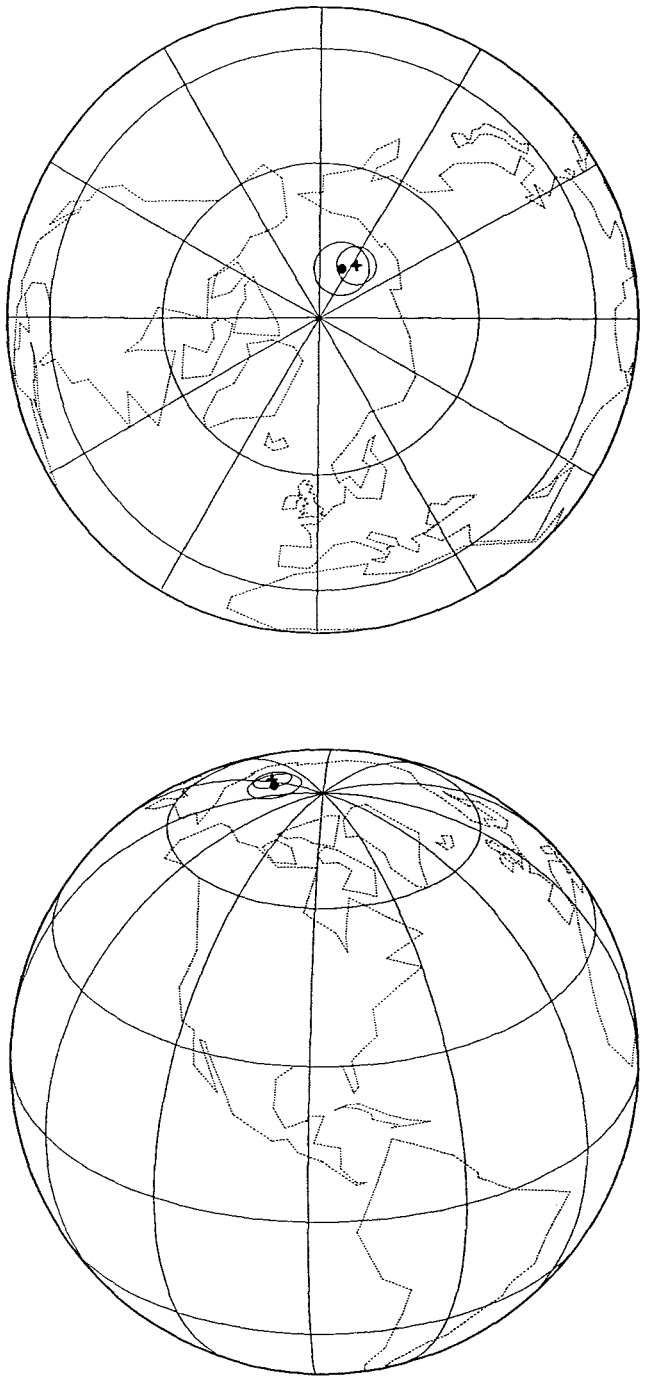

Figure 10-13 *Palaeomagnetic pole positions for the North American continent during the late Paleocene and early Eocene. Cross symbol shows the palaeomagnetic pole calculated from this study and the solid circle indicates that of Besse & Courtillot (1991).* ***Top.*** *plan projection over the north pole.* ***Bottom.*** *Side elevation centred on the state of Alabama.*

difference in mean ages, however the smaller error associated with the present data set indicates that the palaeomagnetic pole calculated here may represent a more accurate position. The pole position from this study suggests that the North American Continent has rotated clockwise through 11.8° since the early Eocene and late Paleocene which is 1.8° greater than that proposed by Besse & Courtillot (1991).

The best overall palaeomagnetic pole position for this interval of time may be achieved by combining the poles of Besse & Courtillot (1991) and that of this study:

Approx. age=53Ma Lat=79.6° Long=207.5° Angular Sep.=4.5°

References

Ali, J.R. 1989. *Magnetostratigraphy of early Palaeogene sediments from NW Europe.* Unpublished PhD thesis, University of Southampton, pp 277.

- King, C & Hailwood, E.A. 1993. Magnetostratographic calibration of early Eocene depositional sequences in the southern North Sea Basin. In: Hailwood, E.A. & Kidd, R (Eds), High Resolution Stratigraphy, *Geological Society Special Publication,***70**, 99-125.

- & Hailwood, E.A. (in press). Magnetostratigraphy of the upper Paleocene through lower middle Eocene of NW Europe. In: Berggren, W.A., Kent D.V. & Hardenbol, J. (eds) *Geochronology, timescales and stratigraphic correlation: framework for a historical geology*. Soc. Econ. Paleont. Min. Spec. Pub.

Anson, G.L. & Kodama, K.P. 1987. Compaction-induced inclination shallowing of the post-depositional remanent magnetization in a synthetic sediment. *Geophys. J. R. astr. Soc.*, 88, 673-692.

Arason, P. & Levi, S. 1990. Models of inclination shallowing during sediment compaction. *J. Geophys. Res.*, **95**. 4481-4499.

Aubry, M-P. 1985. Northwestern European Paleogene magnetostratigraphy, biostratigraphy and paleogeography: calcareous nannofossil evidence. *Geology.* 198-202.

- Hailwood, E.A. & Townsend, H.A. 1986. Magnetic and calcareous-nannfossil stratigraphy of the lower Palaeogene formations of the Hampshire and London Basins: *Journal of the Geological Society London*, **143**, 729-35.

Bandy, O.L. 1948. Eocene and Oligocene foraminifera from Little Stave Creek, Clarke County, Alabama. *Bulls. Am. Paleont.*, **32**, 425-32.

Barton, C.E., McElhinny, M.W. & Edwards, D.J. 1980. Laboratory studies of depositional DRM. *Geophys. T. R. astr. Soc.*, 61, 355-377.

Baum, G.R. 1986. The recognition of allothemic (unconformity bounded) units in Paleogene outcrops, Gulf and Atlantic Tertiary basins. Soc. Econ. Paleont. Mineral. third Ann. Midyear Meeting, Raleigh, North Carolina, Abstracts, **3**, 6.7.

- & Vail, P.R. 1988. Sequence stratigraphic concepts applied to Paleogene outcrops, Gulf and Atlantic basins. Sea-Level Changes - An Integrated

Approach, SEPM Special Publication No. 42.

Beauchamp, R.G. 1984. Stratigraphy and depositional environments of the Brightseat and Aquia Formations of Maryland and Virginia. In: Frederiksen, N.O & Krafft, K., eds., Cretaceous and Tertiary stratigraphy, palaeontology and structure, SW Maryland and NE Virginia. *Am. Ass. of Strat. Palynologists field trip Volume and Guidebook*: 78-111

Berggren, W.A., Kent, D.V. & Flynn, J.J. 1985. Cenozoic geochronology. *Geol. Soc. Am. Bull.*, **96**: 1407-1418.

- 1994. In defense of the Selandian Age/Stage. *Geol. Soc. of Sweden (GFF)*, **116**, 44-46.

- Kent, D.V., Swisher, C.C., III & Aubry, M-P. 1994. A revised Cenozoicgeochronology and chronostratigraphy. *Soc. Econ. Paleont. and Min. Spec. Vol.* (in press.

Besse, J & Courtillot, V. 1991. Revised and Synthetic Apparent Polar Wander Paths of the African, Eurasian, North American and Indian Plates, and True Polar Wander Since 200 Ma. *Journal of Geophysical Research*, **96**, 4029-4050.

Bolli, H.M. 1957. The genera Globigerina and Globorotalia in the Paleocene- lower Eocene Lizard Springs Formation of Trindad, BWI. *US Nat. Mus. Bull.*, **215**, 51-81.

- 1966. Zonation of Cretaceous to Pliocene marine sediments based on Planktonic Foraminifera. *Bol. Inform. Asoc. Venez. Geol. Miner. Petroleo.*, **9**,3-32.

Bond, G. 1978. Speculations on real sea-level changes and vertical motions of continents at selected times in the Cretaceous and Tertiary Periods. *Geology*, **6**. 247-250.

Brunhes, B. 1906. Recherches sur la direction d'aimantation des roches volcaniques. *J. Phys.*, **5**, 705-724.

Bukry, D. 1973. Low latitude coccolith biostratigraphic zonation. In: Edgar, N.T. & others, *Initial reports of the Deep Sea Drilling Project*, **15**, 685-703.

- 1978. Biostratigraphy of Cenozoic marine sediments by calcareous nannofossils. *Micropaleontology*, **24**,44-60.

Butler, R.B. & Taylor, L.H. 1978. A middle Paleocene paleomagnetic pole from the Nacimiento Formation, San Juan Basin, New Mexico. *Geology*, **6**, 495-498

Bybell, L.M. 1980. Paleogene calcareous nannofossils. In: Frey, R.W. (ed); *Excursions in southeastern geology*, **II**, 416-422.

- & Gibson, T.G. 1991. Calcareous nannofossils and foraminifera from the Paleocene and Eocene strata of Maryland and Virginia. In: *Paleocene Eocene boundary sedimentation in the Potomac River Valley, Virginia and Maryland - field trip guidebook.*

- & Gibson, T.G. 1985. The Eocene Tallahatta formation of Alabama and Georgia: Its lithostratigraphy, biostratigraphy and bearing on the age of the Claibornian stage. *US. Geol. Survey Bull.* 1615., 1-20.

Cande, S.C. & Kent, D.V. 1992. A new geomagnetic polarity time scale for the late Cretaceous and Cenozoic. *Journal of Geophysical Research*, **97**, 13,917-13,951

Cande, S.C. & Kent, D.V. (in press).

Childress, S.C. 1973. Mississippi geologic names: *Mississippi Geological Survey. Bull.* **118**, 172.

Christie-Blick, N. 1990. Onlap, offlap and the origin of un-conformity-bounded depositional sequences. *Marine Geology*, **97**, 35-56.

- Mountain, G.S. & Miller, K.G. 1988. Sea level history. *Science*, **241**, 596.

Clark, W.B. & Martin, G.C. 1901. The Eocene deposits of Maryland. *Maryland Geological Survey Eocene Volume 1*, 19-92.

Clement, B.M., Kent, D.V. & Opdyke, N.D. 1982. Brunhes-Matuyana polarity transition in three deep sea sediment cores. *Phil. Trans. R. Soc., London,* **A306**, 113-119.

Cloetingh, S. 1988. Intraplate stresses: a tectonic cause for third-order cycles in apparent sea level? Sea-Level Changes - An Integrated Approach, SEPM Special Publication No. 42.

Cushing, E.M., Boswell, E.H. & Hosman, R.L. 1964. General geology of the Mississippi Embayment. US Geological Survey Professional Paper 448-B.

Deamer, G.A. & Kodama, K.P. 1990. Compaction induced inclination shallowing in synthetic and natural clay-rich sediments. *J. Geophys. Res.*, **95**,4511-4529.

Diehl, J.F., Beck, M.E., Beske-Diehl, S., Jacobson, D. & Hearn, B.C. 1983.

Paleomagnetism of the late Cretaceous-early Tertiary north-central Montana alkalic province. *J. Geophys. Res.*, **88**, 10593-10609.

Dodson, R., Dunn, J.R., Fuller, M., Williams, I., Ito, H., Schmidt, V.A. & Wu Yu, M. 1978. Palaeomagnetic record of the late Tertiary field reversal. *Geophys. J.*, **53**.

Edwards, L.E, Goodman, D.K. & Witmer, R.T. 1984. Lower Tertiary (Pamunkey Group) biostratigraphy of the Potomac area, Virginia and Maryland. In: Frederiksen, N.O. & Krafft, K., eds., Cretaceous and Tertiary stratigraphy, palaeontology and structure, SW Maryland and NE Virginia. *Am. Ass. of Stratigraphy, Palynologists field trip Volume and Guidebook.* 78-111.

Fisher, W.L. 1961. Stratigraphic names of the Midway and Wilcox Groups of the Gulf *Coastal Plain. Gulf Coast Assn. Geol. Soc. Trans.*, **11**, 263-295.

Fluegeman, R.H., Berggren, W.A. & Briskin, M. 1990. Paleocene benthonic foraminiferal biostratigraphy of the eastern Gulf Coastal Plain. *Micropaleontology*, **36**, 56-64.

Frankel, R.B., Blakemore, R.P. & Wolfe, R.S. 1979. Magnetite in fresh water magnetotactic bacteria. *Science*, **203**, 369-372.

Frederiksen, N.O., Gibson, T.G. & Bybell, L.M. 1982. Paleocene-Eocene boundary in the eastern Gulf Coast. *Trans. Gulf Coast Ass. of Geol. Soc*, **32.**, 289-294.

Gibson, T.G. 1988. Assemblage characteristics of modern benthic foraminifera and application to environmental interpretation of Cenozoic deposits of eastern North America. *Rev. Paleobiol. Spec. Pub.* **2**, 777-787.

- 1980. Facies changes of lower Paleogene strata. In: Reinhardt, J. & Gibson, T.G. Upper Cretaceous and Lower Tertiary geology of the Chattahoochee River Valley, western Georgia and eastern Alabama. In: Fret, R.W. (ed. Excursions insoutheastern geology, 2. Geol. Soc. Am. Annual Meeting, Atlanta 1980, Fieldtrip guidebooks, 402-411.

- 1982a. New stratigraphic unit in the Wilcox Group in Alabama and Georgia. *US Geological Survey Bull.*

- 1982b. Revision of the Hatchetigbee and Bashi Formations in the eastern Gulf Coastal Plain. *US Geological Survey Bull.*

- & Bybell, L.M. In press. Sedimentary patterns across the Paleocene-Eocene boundary in the Atlantic and Gulf Coastal Plains of the US.

- 1981. Facies changes in the Hatchetigbee Formation in the Alabama- Georgia and the Wilcox-Claiborne Group unconformity. Gulf Coast Association og Geological Societies Transactions, **31**, 301-306.

- Mancini, E.A. & Bybell L.M. 1982. Paleocene to middle Eocene stratigraphy of Alabama. *Trans. Gulf Coast Ass. of Geol. Soc.* **32.**, 449-457.

- Andrews, G.W., Bybell, L.M., Frederiksen, N.O.,Hansen, Thor, Hazel, J.E., McLean, D.S. 1980. Biostratigraphy of Tertiary strata of the core: *In Geol. of the Oak Grove Core, Part 2, Virginia Division of Mineral Resources.* Publication **20**, 14-30.

- Bybell, L.M. & Govoni, D.L. 1991. Paleocene and eocene strata of the Central Atlantic Coastal Plain. In: Paleocene-Eocene boundary sedimentation in the Potomac River Valley, Virginia and Maryland field trip guidebook.

Gilbert, W. 1600. *De Magnete.*

Glazer, J.D. 1971. Geology and mineral resources of southern Maryland: *Maryland Geological Survey Report of Investigations*, **15**, pp 84.

Govoni, D.L. 1991. Gastropod molluscs from the Brightseat Formation of Maryland. Unpublished MS Thesis, George Washington University, USA.

Hailwood, E.A 1989. *Magnetostratigraphy.* Geological Society Special report No.19.

Hailwood, E.A., Grothier, C., Ting, F. & Riddy, P.J. 1992. Magnetostratigraphic resolution using the 2G whole-core magnetometer: an experimental study. Annales Geophysicae. Atmosphere, Hydrospheres and Space Sciences. Part 1, Solid Earth Geophysics and Natural Hazards. Supplement 1-10, C23. European Geophysical Society, Springer International.

Hansen, H.J. 1978. Upper Cretaceous (Senonian) and Paleocene (Danian) pinchouts on the south flank of the Salisbury Embayment, Maryland and their relationship to antecedent basement structures. *Maryland Geol. Survey. Report of investigations* **29**, pp 36.

Haq, B.U., Hardenbol, J. & Vail, P.R. 1987. Chronology of fluctuating sea levels since the Triassic. *Science*, **235**, 1156-1167.

Hardenbol, J. 1994. Sequence stratigraphic calibration of the Paleocene and Lower Eocene continental margin deposits in NW Europe and the US Gulf Coast with the oceanic chronostratigraphic record. *Geol. Soc. of Sweden (GFF)*, **116**. 49-50.

Hay, W.W., Mohler, H.P., Roth, P.H., Schmidt, R.R. & Boudreaux, J.E. 1967. Calcareous nannoplankton zonation of the Cenozoic of theGulf Coast and Caribbean-Antillean area and trans-oceanic correlation. *Trans. Gulf Coast assn. Geol. Soc.*, **17**, 428-480.

Hazel, J.E., 1968. Ostracods from the Brightseat Formation of Maryland. *J. of Paleont.*, **42**, 100-142.

Hazel, J.E., Edwards, L. & Bybell, L.B. 1984. Significant unconformities and the hiatuses represented by them in the Palaeogene of the Atlantic and Gulf Coastal Province.

Heirtzler, J.R., Dickson, G.O., Herron, E.M., Pitman, W.C., III & Le Pichon, X. 1968. Marine magnetic anomalies, geomagnetic field reversals and motions of the sea floor and continents. *J. geophys. Res.*, **73**, 2119-2136.

Henshaw, P.C. & Merril, R.T. 1980. Magnetic and Chemical changes in marine sediments. *Revs. Geophys. Space Phys.*, **18**, 483-504.

Irving, E. 1964. *Palaeomagnetism and its application to geological and geophysical problems.* Wiley, New York.

- & Major, A. 1964. Post-depositional detrital remanent magnetisation in a synthetic sediment. *Sedimentology*, **3**, 135-43.

Jacobs, J.A. 1984. *Reversals of the earth's magnetic field.* Published by Adam Hilger Ltd.

Kendall, C.G.St.C & Lerche, I. 1988. The rise and fall of eustacy. Sea level changes: an integrated approach. *Soc. Econ. Paleontol. Mineral. Spec. Publ.*, **42**, 1-17.

Kent, D.V. 1973. Palaeomagnetism of some Neogene sedimentary rocks on Oga Peninsula, Japan. *J. Geomag. Geoelect*, **25**, 87-103

Kerr, R.A. 1987. Refining and defending the Vail sea level curve. *Science*, **235**, 1141-1142.

Kirchvink, J.L. 1980) The least squares line and plane analysis of palaeomagnetic data. *Geophys. J.R. astr. Soc.*, **62**, 699-718.

King, C. 1981. The stratigraphy of the London Clay and associated deposits. *Tertiary Research Special Paper*, **6**, 158.

- 1990. Eocene stratigraphy of the Knokke borehole (Belgium. *Toelicht, Verhand,*

Geologische en Mijnkaarten van Belgie, **29**, 67-102.

King, R.F. 1955. Depositional remanent magnetisation in sediments. *Mon. Not. R. Astron. Soc. Geophys. Suppl.*, **7**, 115-134.

Knox, R.W. O'B., Hine, N.M. & Ali, J.R. 1994. New information on the age and sequence stratigraphy of the type Thanetian of Southeast England. *Newsletters on Stratigraphy*, **30**, 45-60.

Koci, A. 1985. Variations in the geomagnetic field at the time of reversals. *Stud. Geophys. Geod.*, **29**, 280-289.

LaMoreaux, P.E. & Toulmin, L.D. 1959. Geology and groundwater resources of Wilcox County, Alabama. Alabama Geological Survey, County Report. **4**. p280.

Lowerie, W. & Alvarez, W. 1981. One hundred million years of geomagnetic polarity. *Geology*, **9**, 392-397.

- & Heller, F. 1982. Magnetic properties of marine limestone. *Rev. Geophys. Space Phys.*, **20**, 170-192.

Mancini, E.A. 1981. Lithostratigraphy and biostratigraphy of Paleocene subsurface strata in southwestern Alabama. *Gulf Coast Assoc. Geol. Socs. Transactions*, **31**, 359-367.

- 1984. Biostratigraphy of Paleocene strata in southwestern Alabama. *Micropaleontology*, **30**, 268-291.

- & Tew, B.H. 1988. Paleocene sequence stratigraphy of southwestern Alabama. *Trans. Gulf Coast Assoc. Geol. Socs.* **38**, 453-60.

- & Tew, B.H. 1991. Relationships of Paleogene stage and planktonic foraminiferal zone boundaries to lithostratigraphic contacts in the eastern Gulf Coastal Plain. *Journal of Foraminiferal Research*, **21**, 48-66.

- & Tew, B.H. 1991. Tertiary sequence stratigraphy and biostratigraphy of southwestern Alabama. Alabama Gulf Coastal Plain Fieldtrip Guidebook.

Martini, E. 1971. Standard Tertiary and Quaternary calcareous nannoplankton zonation. Planktonic Conference, 2nd, Rome, 1969, Proceedings. pp739-785.

Matuyama, M. 1929. On the direction of magnetisation of basalt in Japan, Tyosen and Manchuria. *Japan. Acad. Proc.*, **5**, 203-205.

Menyeh, A. & O'Reilly, W. 1991. The magnetization process in monoclinic pyrrhotite (Fe_7S_8) particles containing few domains. *Geophys. J. Int.*, **104**, 387-399.

Miall, A.D. 1992. Exxon global cycle chart: An event for every occasion. *Geology*, **20**, 787-790.

Miller, K.G., Aubry, M-P., Khan, M.J., Melillo, A.J., Kent, D.V. & Berggren, W.A. 1985. Oligocene to Miocene biostratigraphy, magnetostratigraphy and isotopic stratigraphy of the Western North Atlantic. *Geology*, 13, 257-261.

Mixon, R.B & Powars, D.S. 1984. Folds and Faults in the inner coastal plain of Virginia and Maryland: their effect on distribution and thickness of Tertiary rock units and local geomorphic history. In: Frederiksen, N.O. & Krafft, K. (eds.) Cretaceous and Tertiary stratigraphy, palaeontology and structure, SW Maryland and NE Virginia. *Am. Ass. of Stratigraphy, Palynologists field trip Volume and Guidebook*, 112-122.

Montgomery, P. 1995. PhD thesis. Magnetostratigraphy of the Cretaceous chalk of southern EnglandUniversity of Southampton.

Morgan, G.E. & Smith, P.P.K. 1981. Transmission electon microscopic and rock magnetic investigation of remanence carriers in a PreCambrian metadolerite. *Earth Planet Sci. Lett.*, **53**, 226-230.

Neal, J.E., Stein, J.A. & Gamber, J.H. 1994. Graphic correlation and sequence stratigraphy in the Paleogene of NW Europe. *J. Micropalaeontol.*, **13**, 55-80.

Nogan, D.S. 1964. oraminifera, stratigraphy and paleoecology of the Aquia Formation of Maryland and Virginia. *Cushman Foundation for Foraminiferal research.* Special publication **7**, 50.

Okada, H. & Bukry, D. 1980. Supplimentary modification and introduction of code numbers to the low latitude coccolith biostratigraphic zone. *Marine Micropaleontology*, **5**, 321-325.

Olsson, R.K., Gibson, T.G., Hamsen, H.J. & Owens, J.P. 1988. Geology of the Northern Atlantic Coastal Plain: Long Island to Virginia. *The Geol. of N. Am*, **1-2**.

Opdyke, N.D. & Henry, K.W. 1969. A test of the dipole hypothesis. *Earth Planet Sci. Letters*, **6**, 315-15.

Payton, C.E. 1977. Editor. Seismic Stratigraphy - applications to hydrocarbon exploration. *Am. Assoc. of Pet. Geol.* Mem., 26.

Piper, J.D.A. 1987. Palaeomagnetism and the continental crust. Published by the Open University Press.

Plint, A.G. 1983. Facies environments and sedimentary cycles in the middle Eocene Bracklesham Formation of the Hampshire Basin: evidence for sea-level changes? *Sedimentology*, **30**, 624-653.

Rees, A.I. 1961. The effect of water currents on the magnetic remanence and anisotropy of susceptibility of some sediments. *Geophys. J. R. astron. Soc*, **5**, 235-251.

Reinhardt, J., NMewell, W.L. & Mixon, R.B. 1980. Tertiary lithostratigraphy of the core. In: *Geol. of the Oak Grove Core, Virginia Division of Mineral Resources* Publication **20**, Part 1, 1-13.

Richards, H.G. 1948. Studies on the sub-surface geology and palaeontology of the Atlantic Coastal Plain. *Philadelphia Academy of Natural Science Proceedings.* **100**, 39-76.

Robinson, S.G. 1992. Lithostratigraphic applications for magnetic susceptibility logging of deep-sea sediment cores: examples from ODP Leg 115. In: Hailwood, E.A. & Kidd, R.B. (eds), High Resolution Stratigraphy. *Geol. Soc. Spec. Pub*, **70**, 65-98.

Schuchert, C. 1955. Atlas of Paleogeographic Maps of North America. Chapman & Hall, London.

Schwarz, E.J. 1974. Magnetic fabric in massive sulphide deposits. *Can. J. Earth Sci.*, **11**, 1669-1675.

- & Vaughan, D.J. 1972. Magnetic phase relations of pyrrhotite. *J. Geomag. Geoelect.*, **24**, 441-458.

Sheriff, S.D. & Shive, P.N. 1980. The Rattlesnake Hills of central Wyoming revisited: further palaeomagnetic results. *Geophys. Res. Let.* **8**, 589-592.

Shive, P.N. & Pruss, E.F. 1977. A palaeomagnetic study of basalt flows from the Absaroka Mountains, Wyoming. J. Geophys. Res., **82**, 3039-3048.

Siesser, W.G. 1983. Paleogene calcareous nannoplankton biostratigraphy. Mississippi, Alabama and Tennessee: Mississippi Department Natural Resources. *Bureau of Geology Bull.*, **125**, p61.

Sloss, L.L. 1988. Forty years of sequence stratigraphy. *Geological Society of American Bull*, **100**, 1661-1665.

Smith, E.A., Johnson, L.C. & Langdon, D.W., Jr. 1894. Report on the coastal plain of Alabama, with contributions to its paleontolgy by T.H. Aldrich & K.M. Cunningham. *Alabama Geol. Survey Spec. Rept.*, **6.**

Smith, C.C. & Mancini, E.A. 1983. Calcareous nannofossil and planktonic foraminiferal biostratigraphy, in Russell, E.E., Keady, D.M., Mancini, E.A. and Smith, C.C. Upper Cretaceous lithostratigraphy and biostratigraphy in northeast Mississippi, southwest Tennesse and northwest Alabama, shelf chalks and coastal clastics. Soc. Econ. Paleont. Min. Guidebook for Spring Field Trip. pp16-23.

Smith, P.P.K. 1979. The identification of single domain titanomagnetite particles by means of transmission electron microscopy. *Can. J. Earth Sci.*, **16**, 375-379.

Smith, A.G., Hurley, A.M. & Briden, J.C. 1980. Phanerozoic palaeocontinental world maps. Cambridge University press.

Stacy, F.D. 1963. The physical theory of rock magnetism. *Adv. Phys.*, **12**,46-133.

Stainforth, R.M., Lamb, J.L., Luterbacher, H., Beard, J.H. & Jeffords, R.M. (1975. Cenozoic planktonic foraminifera zonation and characteristic index forms. *Univ. Kans. Paleont, Contri. Art.*, 62, 1-465.

Tarling, D.H. 1983. Palaemagnetism. Chapman and Hall, London.

Ting, F. 1991. *Magnetostratigraphiy of Lower Cretaceous and Oligocene Formations in the U.K. and Northwest Belgium.* Unpublished PhD thesis, University of Southampton, England.

Toulmin, L.D. 1940. Eocene brachiopods from the Salt Mountain Limestone of Alabama. *J. Paleontology*, **14**, 227-233.

- 1944. General features of the Tertiary formations in Alabama: Southeastern Geological Soc. guidebook, 5-15

- LaMoreaux, P.E. & Lanphere, C.R. 1951. Geology and groundwater resources of Choctaw County, Alabama. *Alabama Geological Survey County Report*, **2.**

- & LaMoreaux, P.E. 1963. Stratigraphy along the Chattahoochee River, connecting link between Atlantic and Gulf Coastal Plains: *Am. Assoc. Petroleum Geologists* Bull, **47**, 385-404.

- 1977. Stratigraphic distribution of Paleocene and Eocene fossils in the eastern Gulf Coast region: Alabama Geol. Survey Monograph, **13**, p602.

Townsend, H.A. & Hailwood, E.A. 1985. Magnetostratigraphic correlation of the Palaeogene sediments in the Hampshire and London basins, southern U.K. *J. Geol. Soc. London*, **142**, 1-27.

Turner, P. 1975. Depositional magnetisation of Carboniferous limestones from Craven basin of northern England. *Sedimentology*, **22**, 543-581.

Vail, P.R., Mitchum, R.M., Jr., Todd, R.G., Widmier, J.M., Thompson, S., III., Sangree, J.B., Bubb, J.N. & Hatlelid, W.G. 1977. Seismic stratigraphy and global changes of sea level. In: C.E. Payton (Editor), Seismic Stratigraphy - applications tohydrocarbon exploration. *Am. Assoc. of Pet. Geol.* Mem., **26**, 47-212.

Van Wagoner, J.C., Posamentier, H.W., Mitchum, R.M., Jr., Vail, P.R., Sarg, J.F., Loutit, T.S. & Hardenbol, J. 1988. An overview of the fundamentals of sequence stratigraphy and key definitions. *In:* C.K. Wilgus, B.S. Hastings, C.G.St.C. Kendall, H.W. Posamentier, C.A. Ross & J.C. Van Wagoner (Eds.) Sea level changes: an integrated approach. *Soc. Econ. Paleontol. Mineral. Spec. Publ.*, **42**, 39-45.

Ward, L.W. & Strickland, G.L. 1985. Outline of Tertiary stratigraphy and depositional history of the US Atlantic Coastal Plain. In: *Geological Evolution of the US Atlantic Margin*, Poag, C.W., (ed.), Van Nostrand Reinhold Co., New York. pp 87-123.

Watts, A.B. 1982. Tectonic subsidence, flexure and global changes of sea level. *Nature*, **297**, 467-473.

Weems, R.E. 1984. Vertebrate biozones of the Pamunkey Group (Paleocene and Eocene, Maryland and Virginia. *In:* Ward, L.W. and Krafft, K. (eds. Stratigraphy and paleontology of the outcropping Tertiary beds of the Pamunkey River Region, central Virginia Coastal Plain, 198-204.

- 1988. Paleocene turtles from the Aquia and Brightseat Formations with a discussion of their bearing on sea turtle evolution and phylogeny. *Proceedings of the Biological Society of Washington*, **101**, 109-145.

Wind, F.H. 1974. Calcareous nannoplankton of Salt Mountain Limestone (Jackson, Alabama): *Trans Gulf Coast Assn. Geol. Soc.*, **24**, 327-335.

Sample number	Depth (m)	Depth (ft)	NRM (mA/m	Susc. Bulk (x10-3)	Low Coerc. Com. Range	Dec	Inc	a95/Rc	High Coerc. Com. Range	Dec	Inc	a95/Rc	Typ	Bio-strat.	Pol.
49A	70.49	231.25	5.07	3.215					20 - 40	67.4	32.9	a1.22	S		N
49B(1)			0.506						0 - 40	121.6	26.9	a1.32	S		N
49B(2)			0.232										S		N
48(1)	71.2	233.58	0.245	2.756					0 - 40	143.3	-66.7	a2.56	S		R
48th			2.69						350-500	166.3	-39.4	a5.64	S		R
48(2)			3.09		0 - 15	112.9	2.3	0.83/0.61	15 - 40	107.3	-52	0.91/0.91	S		R
47(1)-1	71.88	235.83	0.566	2.243					0 - 40	234	40.7	a1.67	S		N
47(1)-2			0.1						0-40	233.2	39.8	a1.72	S		N
47(2)			6.2						2.5 - 40	340.3	35.6	a1.36	S		N
46B(1)	74.07	243	0.125	0.867	0 - 15	80.1	-6.9	0.78/0.64	20 - 40	180.3	31.4	a10.5	E		N
46B(2)			0.085									mixed pol.	E		R
45A(1)	75.64	248.17	0.096	0.714	0 - 10	4	32	0.61/0.98	20 - 35	173	24.7	a5.90	S		N
45A(2)			0.276						0 - 40	165.8	1.1	a4.66	S		I
45B			0.057		0 - 15	321.1	27.3	0.91/0.98					T	NP11	R?
45C			0.073		4 - 12	322	33.1	0.99/0.95	20	309.1	54.6	n/a	T?		N
44A(1)	76.2	250	0.088	0.967	0 - 20	168	70.5	a5.7	20	160.1	73.9	n/a	?		N
44B(1)			0.149		0 - 10	156.1	6.6	0.93/0.94	15 - 40	147.9	7.2	0.96/0.68	E		N?
44A(2)			0.07		0 - 15	145.4	21.5	0.98/1.0	40	201.6	32.4	n/a	T		N
44B(2)			0.088		2.5 - 25	282.6	50.5	0.89/0.69					T		N?
43A(1)	76.95	252.47	0.075	0.967	0 - 5	182.4	48	0.41/0.99	5 - 15	320.2	76.8	0.98/0.97	E/T		N
43B(1)			0.175		0 - 20	209.3	18.1	a3.42	25	190.5	23.6	n/a	S		N
43A(2)			0.067		5 - 25	327.7	-68.9	a10.7	40	28.7	-63	n/a	S		R
43B(2)			0.074						40	247.1	-26	a5.6	E		R?
42A	77.98	255.83	0.093	1.019	0 - 10	223.6	25.9	1.00/0.96	20 - 40	225.3	-4.9	0.99/0.28	T		R?
42B			0.055						15	261.5	-0.29		T		R
41A	78.69	258.16	0.08	2.089	0 - 15	63.7	-9.7	a5.8	20	78.1	-8.9	a7.2	S?		R
41B(1)			1.2												?
41B(2)			0.054						20	228.1	-75	n/a	T		R
40(1)	79.65	261.33	0.027	1.529					25	229.8	-33	n/a	T		R
40(2)			0.102		0 - 10	222.8	26.5	0.98/0.80	10 - 30	208.8	-14.4	0.88/0.81	T		?
39(1)	80.21	263.17	0.03	1.427					2.5-25			weak	S		R?
39(2)			0.082		0 - 15	164.5	-51.8	0.90/0.99	40	104.2	-42	n/a	E		R
38(1)	81.05	265.92	0.12	3.16	0 - 15	316.9	30.5	0.91/0.98	15 - 35	233.5	17.8	a5.74	T		N
38(2)			0.116		0 - 5	251.1	-32	0.99/0.99	35	49.8	30	weak	T?		N??
37A(1)	82.4	270.33	0.055	1.733	5 - 15	66.2	26.2	a7.89	40	113.6	54.8	n/a	S		N
37A(2)			0.027												
37B			0.105		0 - 10	37.7	25	0.99/0.94	25 - 35	55.7	53	0.93/0.84	S		N
36A	82.81	271.67	0.064	1.631	0 - 20	53	24	0.97/0.89	30	103.9	23.6	N/A	T?		N?
36B			0.05												
35A	83.84	275.08	0.034	2.089											
35B			0.043		0 - 10	141.4	-30.3	a6.45	25	249.4	-34.5	@5.70	T		R
34A	83.97	275.5	0.067	1.478	0 - 10	3.8	32.3	0.38/0.99	35	255	-30.5	@6.2	T		R
34B			0.09		0 - 15	287.2	27.5	0.92/0.73	35	1.4	-35	@19.1	E	NP11	R
33A	84.99	278.83	0.012	0.816											
33B			0.069		0 - 15	127.1	18.6	0.96\0.71	25	112.8	-58.6	@9.6	E		R?
32(1)	85.29	279.83	0.059	0.867	0 - 10	114.1	56.7	0.64/0.80	40	325.6	17.2	n/a	T		R
32(2)									10 - 40	50.9	-13	a5	E		R
31A	85.8	281.5	0.048	1.376	0 - 15	132.1	14.5	1.0/0.92				weak	T		R?
31B			0.047						20 - 35	163.2	-30.6	a7.81	T		R
30(1)	86.94	285.25	0.04	1.478	0 - 15	209.6	3.2	a9.79				weak			?
30(2)			0.064		0 - 10	67.3	-9.4	0.96/0.99	10	104.4	119.3	12.4	T?		R?
29(1)	87.96	288.58	0.04	1.478									E		N
29(2)			0.045												
28(1)	88.72	291.08	0.04	1.325								weak	T		R?
28(2)			0.037												
27A(1)	89.28	292.92	0.101	1.631					0 - 40	63.4	-32.4	a5.82	S		R
27A(2)			0.085						15 - 40	171.9	-45.9	a7.7	S		R
27B(1)			0.078		0 - 10	186.1	41.3	a5.03	30	292.4	-7.5	N/A	T?		R
27B(2)			0.094										E		N?
26A	90.45	296.75	0.118	1.121	0 - 10	120.2	5.1	0.92/0.52				mixed pol.	E		N
26B			0.081						0 - 30	330.3	-16.8	a6.28	E		R
25(1)	90.93	298.83	0.098	0.969	0 - 10	41.7	22.5	0.99/1.0	30	111.8	2.6	0.045	T		R?
25(2)			0.044											NP11	?
24(1)	91.36	299.75	0.201	0.765	0 - 5	211.8	5.2	1.0/0.98	5 - 35	217.3	22.2	0.96/0.97	S		N
24(2)			0.149		0 - 5	169.8	-1.9	0.94/0.63	5 - 30	226.9	59	0.88/0.97	E		N
23(1)	92.23	302.58	0.133	0.714	0 - 10	159.5	24.4	0.99/0.98					T		?
23(2)			0.112		2.5 - 15	143.8	19.7	0.94	25 - 40	102	1.75	a7.44	T		R
22(1)	93.14	305.58	0.18	0.714	0 - 5	160.7	23.7	0.93/1.0	40	310.1	30.6	@7.8	T		R??
22(2)			0.119	0		317.4	-9.9	N/A	5 - 40	318.3	9.5	0.97/0.74	T		R

Appendix 1 *Oak Grove core palaeomagnetic data summary sheet*

21A(1)	93.78	307.67	0.062	1.07					25 - 15	277	25.8	a7.01	E		N	?
21A(2)			0.063		2.5 - 10	197.4	34.1	0.91/0.99	5 - 0	225	27.1	0.98/0.97	T		R?	
21B(1)			0.213						40	63.9	4	N/A	T		R?	
21B(2)			0.136												?	
20(1)	94.51	310.08	0.111	1.223	0 - 10	257.8	-1.4	0.96/0.8	35	160.2	0.4	N/A	T		R?	
20(2)			0.135						0 - 35	73	21.3	a6.75	E	NP10	N	?
19A	95.1	312	0.242	1.172	0 - 10	342.4	14.6	1.0/1.0	20 - 40	327.6	9.5	0.93/0.50	S/T		I	
19B			0.16		0 - 10	209.7	20.6	0.92/0.98	15 - 30	272.1	-9.2	a6.4	T		R	
18A	95.94	314.75	0.163	0.918	0 - 10	164.7	-5.4	0.85/0.80	25 - 40	239.3	31	0.99/0.92	T		N	
18B(1)			0.249										T		N	
17(1)	96.72	317.33	0.245	0.561	0 - 10	204.4	-6.5	0.99/0.76	40	110.9	48.8	N/A	T		N	
17(2)			0.445		0 - 15	99.6	-5	0.91/0.91	40	94	34.9	N/A	T		N?	
16(1)	97.61	320.25	0.23	0.918	0 - 25	227.7	7.4	0.97/0.95	40	285.9	18.5	@9.2	T		?	?
16(2)			0.137		0 - 15	115	13.4	0.94/0.96	20 - 0	29.4	-20.8	1.0/0.99	T		R	
15	98.53	323.25	0.134	0.816					0 - 40	111.9	15.8	a2.89	S		N	
14(1)	98.83	324.25	21.4	1.376					0 - 40	236	-13.6	a1.53	S	NP9	R	
14th			19.1		0	247.1	-22.4	n/a	150-500	232.2	-28.9	a4.3	S		R	
14(2)			65.1		3 - 15	10.3	-34.2	0.61/0.89	25 - 0	163.6	-26.6	1.0/1.0	S		R	
13A(1)	99.69	327.08	22.6	2.956	0 - 10	352.2	6.8	0.69/0.89	20 - 40	289.1	-29.6	1.0/0.99	T		R	
13A(2)			13.7		0 - 5	199.1	10.5	0.99/0.95	10 - 40	118.1	-26.4	0.92/0.92	T		R	
13B(1)			19.1		0 - 15	301.1	-0.3	0.98/0.04	20 - 40	235.6	-33.9	1.0/1.0	S		R	
13B(2)			15						25 - 40	273.2	-42.4	0.98/0.99	S		R	
12(1)	100.4	329.25	22.46	2.549	0 - 15	223.2	-0.7	0.92/0.26	20 - 40	184.4	-23.8	0.57/0.69	T		R	
12(2)			19.6		0 - 5	207.2	3.8	0.98/0.47	25 - 35	141.3	-37.2	1.0/0.99	T		R	
11A(1)	101.2	331.92	53.23	3.058	0 - 10	225.5	-18.1	0.98/0.95	20 - 40	327.8	-43.4	1.0/1.0	T		R	
11A(2)			34.3						25 - 40	161.3	-6.7	0.99/0.99	E	NP9	R	
11B(1)			59.7		0 - 10	338.2	-28.9	0.94/0.96	20 - 40	75.1	-42.3	1.0/1.0	S		R	
10A	102.2	335.33	86.7	4.078	0 - 10	164.5	-31.8	0.78/1.0	20 - 40	292	-41.7	0.99/1.0	S		R	
10B(2)			79.66		2.5 - 10	211.6	-9.9	0.98/0.98	20 - 40	329.3	-43.2	0.99/1.0	S		R	
9	103	338	27.03	6.066	0 - 10	174.9	-6.4	0.95/0.99	25 - 40	114.2	-17.1	1.0/1.0	T		R	
8	104.6	343.08	4.806	1.631					0 - 40	174.4	-14.2	a16.0	S?		R	
7	110	360.83	0.39	2.039	0 - 20	219	-12.7	0.98/0.93	10 - 40	240.2	14.8	a7.14	S		N	
6A	111	364.08	0.376	2.294	0 - 15	164.6	17	0.99/0.99	35	177.8	6.9	N/A			N/I	
6B			0.269						5 - 20	74.7	18.3	0.99/0.94	S?		N	
5A	112	367.33	1.336	2.498	2.5 - 20	230.2	26.4	0.98/0.97	25 - 40	267.2	4.8	a4.82	S		N	
5B			0.717		2.5	43.5	12.3	N/A	2.5 - 40	39.8	12.5	a2.60	S	NP8	N	
4A	116.5	382.33	0.064	2.243	0 - 15	193.9	20.8	0.97/0.99	40	302.1	-17.9	@6.7	T		R	
4B			0.302		0 - 20	204.3	-5.3	1.0/0.55	40	157.1	-6	@4.2	T		R/I	
3A	117.6	385.75	9.719	4.791					15 - 40	79.5	13	a1.69	S	NP	N	
3B			18.42		10 - 30	164.7	4.6	0.99/0.71	30 - 40	98.1	32.3	0.91/0.99	S?	6/7	N	
2(1)	122.4	401.47	3.817	2.759	NRM	199.6	6	N/A	5 - 40	259.2	11.6	a4.34	S		N	
2(2)			8.77						15 - 40	53.2	20.9	a1.21	S	NP5	N	
1(1)	122.6	402.25	5.018	1.937					15 - 40	353.9	-13.2	a3.13	S		R	
1(2)			22.3		0 - 10	343.4	-2.76	a5.19					E		R/I	

Pope's Creek data summary sheet

Sample code	Depth (m)	Suscept. xE-3 SI	Max temp./ AF field	NRM (mA/m)	Demag (C/mT)	'Low Tb/Hc components Dec	Inc	MAD/alpha 95	Demag (C/mT)	High Tb/Hc components Dec	Inc	MAD/alpha 95	reliability category	Polarity	Mean NRM (mA/m)	General site pol.
PC1A-TH	0.1	1.46	300	0.101	0	16.8	6.8		100-300	353	7.3	6.8à	S3	N?	0.112	N
1B			35	0.115					0-35	31.1	57.5	8.7à	S2	N		
1			40	0.121					0-40	327	22.1	9.1à	S2	N		
1C			40	0.111					0-40	338	42.3	4.2à	S2	N		
PC2A	0.9	1.63	40	0.184	0-10	156.1	-19	6.8µ			90		T2	N	0.206	N?
2B-TH			250	0.33	0	195.1	-3.96		100-250-o	185.5	1.2	8.8µ	T3	?		
2C			300	0.242					0-origin	181.5	6.1	9.3µ	T3	?		
2			25	0.185	0-25	183.1	-11.2	7.5µ	10-25	336	13.9	7.6à	S3	N?		
2F			40	0.088					0-40	352	30	6.3à	S3	N?		
PC3A	1.35	1.29	40	0.24					10-40	50.3	53	12.4à	S2	N	0.246	N
3B			40	0.109	0-10	117.7	17.8	6.1µ	10-40	329.6	41.7	9.7à	S2	N		
3C			40	0.153					5-40	32.4	73	15.2à	S2	N		
3D-TH			300	0.302	0-150	174	28.2	5µ			90		T2	N		
3			40	0.22	2.5-15	129.2	45.215	5.6µ					T3	?		
3F			40	0.45					15-40	189.5	8.4	11.9à	S3	?		
PC4A	1.85	1.63	40	0.13	0	27.2	70.9		2.5-40	315.4	64.7	4.9à	S2	N	0.117	N
4B			40	0.117	0-5	184.3	-1.5	4.7µ	25-40	65.9	66	10.1à	S2	N		
4C-TH			350	0.104									0			
PC5A	2.96	1.89	40	0.116	0	222.4	63.4				-90		T3	R?	0.162	R
5B			40	0.34							-90		T2	R		
5C-TH			300	0.066	0	235.2	23.6		200-300	175	-18		T2	R		
5			40	0.126									0			
PC6A	4.41		40	0.056	0-10	241.4	54.5	4.6µ	20-40	284	-49.4	30.3à	T2	R	0.054	R
6C			40	0.039									0			
6			40	0.047	0	249.7	-19.2		0-40	264.2	-17.2	9.6à	S3	R?		
6			35	0.074	2.5-10	173.8	-62.6	5µ	35	205	-31.1		T2	R		
PC7A	4.56	2.06	35	0.126	0-5	63.7	15.7	4.6µ	5-35	67.1	-8	9à	S3/A	?	0.079	
7C			40	0.038	0	355.2	84.1				-90		T2	R		?
7			40	0.073					0-40	293.2	61.3	5.3à	S2	N		
PC8A	5.16	1.89	40	0.026	0-5	221.2	2	8.3µ			-90		T2	R	0.38	R
8B			40	0.05	0	15.5	-75.6		0-40	29.3	-79	6.7à	S2/A	?		
PC9A-TH	5.91	1.71	350	0.101	0	239.4	62.3						T3	?	0.109	
9B			40	0.045	0-30	274.7	38.5	11à			-90		T2	R		
9C			40	0.129	0	352.2	11.5		2.5-40	348.2	12.2	9.2à	S2	N		?
9			40	0.174	0-15	239.6	53.4	2.8à					T3	?		
9			40	0.094	0-15	170.8	-19.4	11.5µ					T3	?		
PC10A	6.13	1.46	40	0.081	0	306.2	7.8				-90		T1	R	0.067	R
10B			40	0.053	0	269	-3.2						T3	?		
PC11A-TH	7.31	1.63	350	0.203					0-origin	19.1	60.4	9.6µ	S1	N	0.172	N
11B			40	0.16	0-10	40.3	64.7	13.6à	10-40	80.7	68.7	6.7à	S2	N		
11C			40	0.154	0-5	283.1	33.8	8.9à					T3	?		
PC12A-TH	8.31	1.37	350	0.18									T2	?	0.156	
12B			40	0.164	0-5	108.5	52.3	5.9à	20-40	65.4	71.6	16.5à	S2	N		N?
12C			40	0.125									T3	?		
PC13A-TH	9.21	1.53	350	0.015	0	221.6	35.8						T3	?	0.059	N
13B			40	0.103					0-40	278	41.3	2.6à	S2	N		

Appendix 2 *Pope's Creek palaeomagnetic data summary sheet*

Sample code	Depth (m)	Max temp./ AF field	NRM (mA/m)	Demag (C/mT)	'Low Tb/Hc components			Demag (C/mT)	High Tb/Hc components			reliability category	Polarity	Mean NRM (mA/m)	General site pol.
					Dec	Inc	MAD/alpha 95		Dec	Inc	MAD/alpha 95				
YC5A	2	40	0.21	0-10	44.6	47.1	2.9µ	15-origin	191.4	86.3	8.4µ	S1	A?	0.189	?
5B-TH		400	0.168									T3	?		
YC6B	2.4	40	0.15	0-5	33.5	57	5.2µ			-90		T2	R?	0.185	
6A		40	0.184	0-5	341.4	63.2	3.8µ	10-25	188.9	78.7	6.7µ	T2	R?		R
6C-TH		400	0.221	0	62.8	67.2				-90		T1	R		
YC4C-TH	1.9	400	0.262	0	257	66.9				-90		T1	R	0.195	
4A		40	0.156	0-5	296	40.5	4.9µ	5-origin	250.1	67.8	4.2µ	S1	N		?
4C-2		40	0.166	0	205.1	59.8		0-origin	203.1	61.5	5.6µ	S1	A?		
YCE	1.8	35	0.194	2.5-10	170.1	61.9	8.8µ			-90		T2	R	0.194	R
YC3A	1.6	40	0.113					0-40	336.5	30	15.2à	S3	N?	0.312	?
3-TH		400	0.51	0	342.9	18.1				-90		T3	R?		
YCD	1.5	35	0.217	0	106.7	17.9				-90		T3	R?	0.217	R?
YC2D-1-TH	0.92	400	0.221									T3	R?	0.262	
2A		40	0.215	0-5	327.2	-18.8	9.7µ	10-orig	324.7	36.1	3.6µ	S1	N		N
2B		40	0.266	2.5-30	220.2	58.8	6.2µ	25-40	354	61.8	7.3à	S2	N		
2C		40	0.36	0-5	358.3	46.3	6.6µ	5-40	113.6	82.8	9.6à	S2	N		
YCC	0.8	35	0.665	195.8	43.9			2.5-35	208.2	76.2	7.6à	S3	A?	0.665	?
YCB	0.6	35	0.629	0	172.7	30.4		20-35	87.5	-1	4.9µ	T1	R	0.629	R
YC1A	0.5	35	0.21	0	244	-26.9	.2µ			90		T1	N	0.35	
1B		35	0.3					0-35	223.7	34.2	4.9à	S2	A?		N?
1C		35	0.43	0	216.9	14.5		2.5-origin	213.3	11.1	10.µ	T2	N?		
YCA1	0.21	35	0.39	0-15	192.8	65.2	4.8à			-90		T2	R?	0.53	
A2		35	0.772	0-15	261.2	79.3	4.3à			90		T2	N		?
A3		35	0.409	0	3.3	73.4				-90		T3	R?		

Appendix 3 *Yacht Club palaeomagnetic data summary sheet*

Sample code	Depth (m)	Max temp./ AF field	NRM (mA/m)	Demag (C/mT)	'Low Tb/Hc components Dec	Inc	MAD/alpha 95	Demag (C/mT)	High Tb/Hc components Dec	Inc	MAD/alpha 95	reliability category	Polarity	Mean NRM (mA/m)	General site pol.
TR21A	5.2	40	0.51	NRM-5	150.1	58.1	10.2µ	5-origin	56.4	71.9	6.7µ	S1	N	0.361	N
21B-TH		350	0.238									S3	A		
21C		40	0.334	NRM-5	186.2	26.7	.8µ	5-40	129.8	64.4	6.5µ	T1	N		
TR22A	4.6	40	0.574	NRM-5	121.5	72.6	3.6µ	5-origin	33.3	71.5	6.6µ	S1	N	0.453	N
22-TH		350	0.167									T2	A		
22B		40	0.619					2.5-40	44	73	8.8µ	S1	N		
TR23A	4.2	40	0.446	NRM-5	148.1	33.3	2.8µ	10-30+	159.3	60.3	8.9µ	S1	A	0.473	
TR23B		40	0.576					5-origin	22.7	60.9	5µ	S1	N		N?
TR23-TH		350	0.453									S3	A		
TR24A	3.7	40	0.371					0-origin	156.1	-2.6	9.6µ	S2	I	0.268	
TR24B		40	0.227	NRM-5	158.8	18.8	3.3µ	2.5-40	183	-22.7	7.4à	S2	R		R?
TR24C		40	0.205									T3	A		
TR25A	2.6	40	0.219					5-40	176.7	-40.9	9.4à	S2	R	0.465	
TR25B		40	0.437	0-20	218.7	17.3	6.1µ					T2	?		R?
TR25C		40	0.74									T1	N?		
TR26A	1.1	40	0.732					5-40	165.4	-25	11.3à	S2	R	0.472	
TR26B		40	0.483	0-5	206.2	60	9.2µ	5-origin	349.5	57.3	5.8µ	S1	N		N?
TR26-TH		350	0.328									A	A		
TR26C-2	0.5	40	0.27	0-5	169.9	32.8	2.4µ	5-40	102.8	39.1	6.1à	S2	A		
TR27A		40	0.328	0	256.3	60.7		2.5-40	292.1	65.7	5.2à	S1	N	0.41	
TR27-TH		350	0.413									T2	R		N?
TR27B		40	0.575	0-10	287.4	0.4	4.8µ	35-origin	298.8	11.2	8.3µ	T2	N		
TR28A	0	40	0.408	0	198.7	72.8		5-25	273.8	84.9	4à	S2	N	0.498	
TR28-TH		350	0.386									T3	R?		N?
TR28C		40	0.689	0	255	61.1		2.5-origin	264.5	61	5.3µ	T2	A		

Appendix 4 *Tinker's Ravine palaeomagnetic data summary sheet*

Sample code	Depth (m)	Max temp./ AF field	NRM (mA/m)	Demag (C/mT)	'Low Tb/Hc components			Demag (C/mT)	High Tb/Hc components			reliability category	Polarity
					Dec	Inc	MAD/alpha 95		Dec	Inc	MAD/alpha 95		
BB1/3	0.6	35	0.19	0	122.6	42.2		35	68.6	24		T2	N
1-TH	0.8	350	0.16	0	80.8	58.6		150-350	178.9	28	24.8à	A	A
1B		40	0.5	2.5-20	150.9	8.4	6.1µ	30-40	277	69.1	12.5à	T1	N
1C		35	0.56					0-origin	184.5	20.7	6.6à	A	A
1		35	0.34	0	176.3	29.6				90		T3	N
BB3/2	1	35	0.4	0	187.5	61.5		2.5-20	45.6	86.8	11.9à	T3	N
BB4/1	1.2	35	0.41	0	209.6	77.6				-90		T1	R
4/3		40	0.17	0	54	42.4	.1µ			-90		T2	R
BB2A	1.4	40	0.39					0-40	192.9	54.2	2.6à	S1	A
2B		40	0.45	0-5	203.7	-4.1	5.4µ			90		T3	N
2C		40	0.2	0_1	141.2	31		2.5-40	141	58.6	5.4à	A	A
2		40	0.16	0-10	210.4	6.8	6.2µ			90		T2	N
BB3	1.6	40	0.36	0	150	32		2.5-40	145.9	29	11.9µ	T2	N
BB4B-2	1.9	40	0.31							90		T3	N

Appendix 5 *Bull's Bluff palaeomagnetic data summary sheet*

Sample code	Depth (m)	Suscept. xE-3 SI	Max temp/ A.F. field	NRM (mA/m)	Demag (C/mT)	Low Tb/Hc components Dec	Inc.	MAD/alpha 95	Demag. (C/mT)	High Tb/Hc components Dec	Inc.	MAD/alpha 95	IRM ratio	reliability category	Polarity	Mean NRM (mA/m)	General site pol.
FG28A	15.9		40	0.222	0-10	236.4	67.1	7.7µ	10-origin	345.1	60.3	9.9µ		S2	N	0.159	N
28B			40	0.096	5-20	92.3	59.5	6.9µ	15-25	292.1	79.7	8.3à		S3	N		
27A	14.4	0.021	40	0.073	0	320.8	55.3				-90			T2	R	0.067	R
27B-TH			350	0.06										?	?		
26	13		40	0.398	0-10	138.4	-17.8	5.9µ	15-30	84.3	87	17.6à		S3	N	0.398	N
25B-TH		0.02	350	0.472	0	287.9	-47							?	?	0.472	?
24A	11.3	0.022	40	0.866	0-10	231.3	2.8	4.9µ	10-40	204.2	51.7	6.4à		A	?	0.525	N?
24B			40	0.183										T2	N?		
23	11	0.008	40	0.069										T1	R	0.083	
23B			40	0.09	0-5	14.2	31.7	6.3à	20-35	348	57.3	14.7à		S3	N?		R?
23C-TH			350	0.09	0	339.1	-17.8							?	?		
22A	9.05	0.031	40	0.353	0	160.9	-0.1		5-40	151.2	-6.3	7.6à		T2	N	0.23	
22B			40	0.22					0-origin	153.4	21.4	6.6µ		T3	N?		R?
22C-TH			350	0.118										T2	R		
20	8.7	0.045	40	0.615	0	150.4	12.3		0-origin	148.5	8.7	7.5µ		T2	N	0.479	
20A			40	0.41	0-10	82.6	-60.8	4.3µ	10-origin	135.4	-56.2	2.3µ	0.92	S1	R		R
20C2			40	0.254	0-15	123.9	33.7	2.9µ						T2	R		
20D-TH			350	0.637	0	178.7	-3.6		0-250	174.1	-5.7	6.9à		S2	R		
19B	8.05	0.019	40	0.083	0-5	341	58.1	6.4µ	0-origin	19.1	55.3	11.7à		S2	N	0.054	
19B-TH			350	0.056	0	9.9	-15.9		350	266.5	11.3			T3	N?		N
19C			40	0.027	0	141	0.43							?	?		
18	7.15	0.023	40	0.256	0-20	187.7	15.1	5.5µ	25-35	341.1	67.7	12à		T2	N	0.255	
18A2			40	0.198	0-15	151.3	72.7	2.1µ	30-40	142	-38.8	5.9à		S2	R		
18A3			40	0.25	0-10	151.4	-71.8							T1	N		N
18B-TH			350	0.227	0	201.9	34.4		100-350	356	5.7	2.9µ		S1	N		
18C			40	0.345	0-15	172.2	19	1.9µ	15-origin	155	55.9	6.6µ		T3	N?		
17B	6.67	0.033	40	0.335	0-5	233.2	58.1	2.3µ	10-40	181.8	-5.1	5.5µ		T1	N	0.335	N
16A-TH	6.26	0.026	350	0.84	0	176.4	-9.1		0-350	176.6	-8.9	1.9µ		S1	R	0.489	
16B			40	0.643	0	167.1	3.9		0-origin	166.4	0.8	4.9µ	0.93	T2	N		N?
16C			40	0.223	0	237.3	60.3		0-35	232.7	48.3	8.9µ		T2	N		
16C2			40	0.25	5	194.4	45.4							T3	R?		
15A	5.7	0.023	40	0.482	0-5	184.6	-9.4	2.4µ	10-35	167.1	-24.5	8.2µ		T3	N?	0.462	
15B			40	0.334	0-15	266.8	-15.5	9.2µ	35-40	65.8	49.3			T1	N		N
15C1-TH			350	0.607										T2	N		
15C2			40	0.428										T2	N		
14A	3.9	0.009	40	0.039	0	357.9	-63.6							T3	R?	0.075	
14B1			40	0.094	0	91.8	19.9		35	232.5	-43.7			T1	R		R
14B2			40	0.108	0	91.3	37.5							T3	R		
14C			40	0.058	0	355.6	14.9							T3	R?		
13A	3.5	0.016	40	0.034	0	185.1	3.2		0-350	183.9	3.5	3.9µ		I	I	0.089	
13B			40	0.037										T2	R		R
13C			40	0.197	0-10	239.5	50.5	7.9à	25	280.2	65.9			A	?		
12A	3	0.019	40	0.25	0-20	183.7	1.7	8.8µ						T3	N?	0.3	
12B			40	0.216	2.5-10	236.2	-4.8	8.7µ						T2	N		
12B2			40	0.564	0-20	152.2	72.9	4.5µ						S3	N		N
12B3			40	0.547	0-25	64.3	48.7	4.4µ	25-40	350.7	56.1	9.3à	0.91	S2	N		
12C			40	0.164	2.5-10	232.7	18.4	3.8µ						T2	N		
12			40	0.059	0-20	100.2	-14.2	4.7µ	25-40	332.8	13.9	7à		T1	N		
11A	2.45	0.018	40	0.151	0-10	183.6	16.8	5.7µ	15-35	184.3	35.8	9.9µ		A	?	0.125	R
11B			40	0.098	0-25	130.1	-20.9	9.4µ						T3	R?		

Appendix 6 *Fort Gaines palaeomagnetic data summary sheet*

Camden road data summary sheet

Sample code	Depth (m)	Suscept. xE-3 SI	Max temp/ A.F. field	NRM (mA/m)	Demag (C/mT)	Low Tb/Hc components			Demag. (C/mT)	High Tb/Hc components			IRM ratio	reliability category	Pol.	Mean NRM (mA/m)	General site pol.
						Dec	Inc.	MAD/a95		Dec	Inc.	MAD/a95					
CD11	8.6	0.049	40	0.21	0	241.9	15.9		0-origin	231.5	35.4	9.9µ		A	N?	0.049	N?
CD12	8	0.053	40	0.233	0-20	194.1	30	3.7µ	25-40	19.2	83.6	8.9à		S2	N	0.053	N
CD13	6	0.043	40	0.36	0	283.9	40.2		5-40	299.7	38.8	8.3µ	0.94	S2	N	0.043	N
CD15	2.5	0.033	40	0.132	0	4.9	55.4		5-origin	2.9	43.8	4.5µ		S1	N	0.033	N
CD16	1.5	0.035	40	0.105	0	338.2	63.8		5-origin	359	49.3	5.9µ	0.95	S1	N	0.035	N
CD17	0.8	0.046	40	0.11	0	338.3	58.1		5-30	2.3	43.8	10.3à		S1	N	0.046	N
17-TH			350	0.115	0	9	46.2		0-350	341.1	40.6	12à		S2	N		
CD18	-1	0.078	40	0.68	0	168.2	49.7		0-origin	169.1	49.2	6.2µ		A	N?	0.078	N
CD19	0.3	0.061	40	0.21	0	25.8	87.1		5-40	359.7	68.7	4.7à		S1	N	0.061	N
19-TH			350	0.2	0	13.9	73.2		0-500	298.4	82.4	11.6à		A	N		

Appendix 8 *Camden Road palaeomagnetic data summary sheet*

Sample code	Depth (m)	Suscept. xE-3 SI	Max temp/ A.F. field	NRM (mA/m)	Demag (C/mT)	Low Tb/Hc components			Demag. (C/mT)	High Tb/Hc components			IRM ratio	reliability category	Pol.	Mean NRM (mA/m)	General site pol.
						Dec	Inc.	MAD/alpha 9		Dec	Inc.	MAD/alpha 95					
MC11A	-0.5	0.033	40	0.038	0	95.7	-9.4		15-30	110.5	35.6	8.2à	0.92	T3	N?	0.12	N??
11B			40	0.203	0-15	126	57.8							A	?		
MC12A	-1	0.026	40	0.09	0	327.1	13.1		5-30	296	3.9	13.2µ		S3	N?	0.119	N??
12B-TH			300	0.148	0	164.9	18		100-300	191.1	38.8	16.8à		A	?		
MC13	-1.5	0.039	40	0.226	0-15	164.5	-21.8	5.3à	35	295	66.7			T3	N?	0.226	N?
MC14A	-2.2	0.016	40	0.065	0	186.6	83.6		35	325.5	-8.9			T3	R?	0.063	N?
14B			40	0.06	0	170.6	21.1		35	96	59			T2	N		
MC15A	-4.05	0.032	40	0.586	0	179	-25.6		0-35	176.3	-27	9.3µ		S2	R	0.528	R
15B-TH			300	0.476	0	129.6	-11.8		100-250	150.7	-33.4	13.3µ		S2	R		
MC16A	-4.55	0.027	40	0.17	0	167.8	-30.1		35	205.9	62.5		0.83	T2	N	0.17	N
MC17A	-5.8		40	0.414	0	312.5	80.3		5-35	197.8	73	10à		A	?	0.349	?
17B-TH			300	0.284	0	101.7	38.3		100-250	103.5	33.4	4.8µ		A	?		
MC18A	-6.15	0.012	40	0.139	0	153.9	10.2		20	47.8	41.9			T2	N?	0.2	N?
18B-TH			300	0.261	0	72.7	47.6							E	?		

Appendix 7 *McCrea Creek palaeomagnetic data summary sheet*

Camden quarry data summary sheet

Sample code	Depth (m)	Max temp/ A.F. field	NRM (mA/m)	Demag (C/mT)	Low Tb/Hc components Dec	Inc.	MAD/a95	Demag. (C/mT)	High Tb/Hc components Dec	Inc.	MAD/a95	reliability category	Pol.	Mean NRM (mA/m)	General site pol.
CD3A	1.6	40	0.361	0-7.5	13.3	51.7	2.1à			-90		T3	R?	0.28	R
3B		40	0.306					0-35	327.5	46.6	5.7à	S2	N		
3C-1		40	0.34							-90		T2	R		
3C-2		40	0.104							-90		T2	R		
CD4A	3.47	40	0.442					0-45	230.5	69.7	6.9à	A	?	0.41	R
4B		40	0.224							-90		T2	R		
4C		40	0.55							-90		T2	R		
CD5A	7.75	40	0.423	0-15	295.9	56.5	5.3à			-90		T3	R?	0.38	R
5D		40	0.368							-90		T2	R		
5E		40	0.342	0-20	335.8	32.7	7.1à					T3	R??		
CD6A	9.25	40	0.34							-90		T2	R?	0.31	R
6B		40	0.324							-90		S3	R?		
6C		40	0.24							-90		T1	R		
6		40	0.329					0-35	118.1	69.2	6.8à	A	?		

Appendix 9 *Camden Quarry palaeomagnetic data summary sheet*

Salt Mountain data summary sheet

Sample code	Max temp/ A.F. field	NRM (mA/m)	Demag (C/mT)	Low Tb/Hc components			Demag. (C/mT)	High Tb/Hc components			reliability category	Pol.	Mean NRM (mA/m)	General site pol.
				Dec	Inc.	MAD/a95		Dec	Inc.	MAD/a95				
SC1A	35	0.08	0	23	-0.9				-90		T2	R	0.34	R
1C	35	0.603	0-7.5	350.4	21.4	6.1M	7.5-20	139.3	-48	9.4A	S2	R		
SC2A	35	0.5	0	0.2	4.8		15-40	61.3	60	7.2A	S2	N	1.8	?
2B	35	3.1	2.5-15	326.7	-0.2	2M					T3	R		
SC3A	35	0.35	0	22.5	43						T3	R?	0.31	R
3C	35	0.26	0	63.2	54		5-25	119.2	-16	9.8A	S2	R		
SC4A	35	0.81	0	101	-10.2		7.5-ORIG.	131.3	-48	7M	S1	R	0.73	R
4C	35	0.65	0-5	103.6	6.6		7.5-25	123.7	-40	6.5A	S1	R		
SC5A	35	0.8	0	128.5	53.5	3.3M	7.5-ORIG.	128.6	-32	8.6M	S1	R	0.52	R
5C	35	0.24	0	100	6.8		5-20	127.8	-13	10.9A	S2	R		
SC6A	35	0.33	0-5	45.6	57.3	9.6M	5-ORIG.	139	-48	5M	S1	R	0.31	R
6B	35	0.31	2.5-7.5	8.8	67.4	1.7M	10-25	135.3	-40	4.1A	S1	R		

Appendix 11 *Salt Mountain palaeomagnetic data summary sheet*

Sample code	Depth (m)	Suscept. xE-3 SI	Max temp/ A.F. field	NRM (mA/m)	Demag (C/mT)	Low Tb/Hc components			Demag. (C/mT)	High Tb/Hc components			IRM ratio	reliability category	Pol.	Mean NRM (mA/m)	General site pol.
						Dec	Inc.	MAD/a95		Dec	Inc.	MAD/a95					
CR6A	5.2	0.037	40	0.081	0	9.5	47.7		5-origin	335.4	56.2	3.2µ	0.94	S1	N	0.09	N
6B			40	0.1	0-10	45.4	34.6	12.6µ	10-origin	343.4	71.8	6.7µ		S1	N		
5A	5.08	0.032	40	0.063	0	27.1	42.3		5-30	354.1	48.3	5.2à		S2	N	0.063	N
4A	4.1	0.027	40	0.049	0	330.7	31.9		5-origin	351.2	47.6	7.2µ		S1	N	0.076	N
4B			40	0.103	0	311.2	38.5		5-40	352.6	55.3	6.2à		S1	N		
3A	3.38	0.025	40	0.071					0-40	7.1	71.6	8.1à		S2	N	0.116	N
3B			40	0.16					0-origin	330.8	58.4	6.2µ	0.93	S1	N		
2	2.98	0.026	40	0.315	0	351.9	47.6		5-origin	348.8	43.4	5.7µ		S1	N	0.315	N
1	-0.97	0.025	40	0.107	0	108.4	74.7		0-40	171	81.6	9.7à	0.83	A	N?	0.107	N?

Appendix 10 *Camden Radio Mast palaeomagnetic data summary sheet*

Bear Creek data summary sheet

Sample code	Depth (m)	Suscept. xE-3 SI	Max temp/ A.F. field	NRM (mA/m)	Demag (C/mT)	Low Tb/Hc components Dec	Inc.	MAD/a95	Demag. (C/mT)	High Tb/Hc components Dec	Inc.	MAD/a95	IRM ratio	reliability category	Pol.	Mean NRM	General site pol.
BR1A-1	0	0.096	40	1.84	0	164.3	-23.6		5-origin	150.6	-26.2	1.9µ		S1	R	1.84	R
BR2	0.34	0.096	40	1.23	0-5	209.7	-17.3	6.2µ	5-origin	146.8	-14	2.93µ		S1	R	1.23	R
BR3A-1	0.89	0.154	40	3.32	0-15	237.2	-0.8	4.9µ	15-origin	148.6	25	8.5µ		T2	N	3.32	N
BR7A	1.02	0.077	40	0.47	0-5	148.8	-25	8.5µ	5-origin	152.2	-17.1	4.48µ		S2	R	0.47	R
BR4A	2	0.058	40	0.39	0-10	271.6	1.2	2.1µ	10-origin	169.3	-31.7	7.03µ		S2	R	0.39	R
BR5A	2.15	0.109	40	2.59	0-10	241.7	-11.1	9.5µ	10-origin	153.9	-41.7	5.39µ		S1	R	2.59	R
BR19A	2.3	0.071	40	0.41	0-10	101.1	-34.2	13.5µ	10-origin	156.9	-32.2	3.99µ		S1	R	0.41	R
BR6A	2.45	0.103	40	3.12	0-10	172.7	-14.8	2.6µ	10-origin	155.6	-37.1	3.85µ		S1	R	3.12	R
BR8A	3.39	0.096	40	1.51	0	163.6	-27.7		0-origin	167.6	-25.8	3.45µ		S1	R	1.4	R
BR8B-TH	3.39	0.096	500	1.37	0	155.9	-5.7		133-origin	159.1	-8.6	11.4µ		S2	R		
BR20A	3.47	0.09	40	0.83	0	152.5	-40.7		5-origin	160.5	-31.7	3.62µ		S1	R	0.83	R
BR9A	3.87	0.103	40	1.59	0-5	156.6	-4.9	2.6à	5-origin	158.4	-3.9	2.8µ		S1	R	1.59	R
BR10A	4.6	0.096	40	1.78	0	171.1	-24.3		5-origin	168.1	-24.9	2.7µ		S1	R	1.7	R
BR10B-TH	4.6	0.096	500	1.62	0	167.3	-26.7		133-origin	160.2	-20.5	8µ		S1	R		
BR11B-1	5.2	0.096	40	1.06	0-5	173	-4.9	2.6à	5-origin	142.8	-19	2.7µ		S1	R	1.06	R
BR12A-1	5.9	0.077	40	0.98	0	163.4	-29.1		2.5-origin	162.4	-28.3	2.54µ		S1	R	0.98	R
BR13A	6	0.096	40	0.99	0	161.3	-34.6		2.5-origin	161.6	-32.1	5.63µ		S1	R	0.99	R
BR14A	6.4	0.096	40	2.13					0-origin	173.4	-18.6	3.17µ		S1	R	2.13	R
BR15A	6.67	0.09	40	2.06	0	178.4	-22.9		2.5-origin	177.9	-20	1.84µ		S1	R	2.06	R
BR16A	7.23	0.103	40	1.36	0	166.4	-32.7		2.5-origin	167.5	-33	1.64µ		S1	R	1.36	R
BR17A	7.7	0.096	40	1.64	0	171.9	-25.6		2.5-origin	173.5	-26.5	2.88µ		S1	R	1.64	R
BR17B-TH	7.7	0.096	500	1.19					100-origin	174.7	-32.5	9.4µ		S1	R	1.19	R
BR18A	8.18	0.077	40	8.18	0	179.4	-30.5		2.5-origin	175.3	-33.2	5.18µ		S2	R	8.18	R
BR58A	9	0.09	40	1.13	0	181.3	-18.3		5-origin	184.4	-22.8	2.97µ		S2	R	1.13	R
BR57A	11	0.083	40	2.43					0-origin	185.2	-22.6	2.75µ		S1	R	2.43	R
BR56A	11.5	0.109	40	0.39										E	R?	0.39	R?
BR55A	12.8	0.109	40	1.55	0	130.4	-72.2		5-40	194.8	-59.4	3.31à		S2	R	1.55	R
BR54A	13.5	0.096	40	1.33	0-5	163.3	-20.8	2.7à	5-origin	179.3	-21.6	4.4µ	0.96	S1	R	1.33	R
BR53A	14.95	0.077	40	0.76	0-5	166.4	-82.6	7.3µ	5-origin	155.1	-36.3	3.93µ		S1	R	0.76	R
BR52A	15.15	0.083	40	2.39					0-origin	156.8	-53.2	3.29µ		S1	R	1.65	R
BR52B-TH	15.15	0.083	500	0.88					0-origin	151.4	-36.9	9.6µ		S1	R		

Appendix 12 *Bear Creek palaeomagnetic data summary sheet*

Bear Creek data summary sheet

BR51A	16.15	0.109	40	3.37					0-origin	158.8	-33.5	3.45µ		S1		R	3.37	R
BR50A	17.15	0.141	40	1.32	0-5	175.6	-31.4	5.2µ	50-40	121.5	-43.2	5à		S2		R	1.32	R
BR49A	18.15	0.147	40	1.36	0-5	137.4	-53.7	8.9à	10-origin	126.3	-58.1	6.4µ		S1		R	1.24	R
BR49-3TH	18.15	0.147	500	1.08					10-40	171.5	-16.1	7.4à		S3		R		
BR48A	19.15	0.122	40	1.6	0	156.7	-21.9		2.5-origin	152.9	-48.3	7.27µ		S2		R	1.6	R
BR47A	20.15	0.141	40	2.52	0	152.4	-31.1		2.5-origin	154.4	-41.7	7.07µ		S2		R	2.52	R
BR46A	21.15	0.09	40	0.38					0-40	40.8	56.9	6.32à	0.95	E		N?	0.29	?
BR46B-TH	21.15	0.09	500	0.21					133-266	147.4	-18.9	11.9à		E		R?		
BR45A	22.15	0.071	40	1.54	0	170.2	-23.5		2.5-origin	168.9	-19.5	2.63µ		S1		R	1.54	R
BR44A	23.15	0.058	40	0.74	0-5	169.6	46.2	9.7µ	5-origin	177.8	-10.9	11.7µ		S3		R	0.74	R
BR43A	23.85	0.077	40	0.61	0-10	73	59.7	8.2µ	10-origin	177.3	3.8	9.9µ		T3		R	0.61	R
BR42A	25.15	0.071	40	1.67	0	169.3	-17.4		2.5-origin	168.5	-22.4	3.22µ		S1		R	1.67	R
BR41A	26.15	0.083	40	2.32	0	174.4	-17.1		2.5-origin	174.9	-20	4.91µ		S2		R	2.32	R

Road cutting south of Bear Creek data summary sheet

Sample code	Depth (m)	Suscept. xE-3 SI	Max temp/ A.F. field	NRM (mA/m)	Demag (C/mT)	Low Tb/Hc components Dec	Inc.	MAD/a95	Demag. (C/mT)	High Tb/Hc components Dec	Inc.	MAD/a95	reliability category	Pol.	Mean NRM	General site pol.
BR32A		0.058	40	0.328	NRM-5	70.5	18.7	6.3µ	10-origin	161.4	-39.7	8.49µ	S2	R	0.328	R
BR31A	0.1	0.071	40	0.442	0-5	33.9	64.9	4.6µ	5-origin	167.7	-37.9	6.55µ	S2	R	0.442	R
BR33A	1.2	0.058	40	0.71	0-10	38.9	-9.8	5.7µ	10-origin	148.1	-31.7	5.11µ	T1	R	0.71	R
BR34B	1.9	0.058	40	0.603	0-10	354.5	-12.1	5.7µ	10-origin	139	-46.6	4.55µ	S1	R	0.603	R

Appendix 13 *Bear Creek road cutting palaeomagnetic data summary sheet*

Tuscahoma Landing

Sample code	Depth (m)	Suscept. xE-3 SI	Max temp/ A.F. field	NRM (mA/m)	Demag (C/mT)	Low Tb/Hc components Dec	Inc.	MAD/a95	Demag. (C/mT)	High Tb/Hc components Dec	Inc.	MAD/a95	reliability category	Pol.	Mean NRM	General site pol.
TL18B	4.15	0.12	40	0.82	0-5	276.2	64.6	3.1µ	10-origin	154.9	-44.3	12.29µ	S2	R	0.82	R
TL17B	2.9	0.11	40	2	0	172.9	-61.1		10-origin	154.1	-63.1	10.4µ	S2	R	2	R
TL16B-TH	2.25	0.13	500	1.58					133-466	162	-53.2	8.3à	S2	R	1.36	R
TL16B2	2.25	0.13	40	1.22	0	173	-33.9		5-origin	159.5	-38.8	5.42µ	S2			
TL15B1	1	0.075	40	1.24	0	160.7	-28.2		10-origin	157.8	-36.1	3.98µ	S1	R	1.24	R
TL14À1	0.25	0.088	40	0.48	0-15	94.3	76.9	6.8µ	15-origin	168.4	-24.2	6.56µ	S2	R	0.48	R
TL13B	-0.8	0.13	40	1.44	0-10	190.5	-0.4	2.3µ	5-30	191.9	-37.6	12.4µ	T2	R	1.44	R
TL12À2-TH	-1.5	0.14	500	1.76					166-origin	152.3	26.2	11.8µ	S2	R	2.13	R
TL12À1	-1.5	0.16	40	2.49	0-5	198.4	25.2	4.6µ	10-origin	173.3	-18.2	4.8µ	S1			
TL11À	-2.2	0.17	40	1.52	0	161.1	-15.9		10-35	158.3	-40.3	2.6à	S2	R	1.52	R

Appendix 14 *Tuscahoma Landing palaeomagnetic data summary sheet*

Roaring Branch Creek and Kolomokei Creekdata summary sheet

Sample code	Depth (m)	Suscept. xE-3 SI	Max temp/ A.F. field	NRM (mA/m)	Demag (C/mT)	Low Tb/Hc components Dec	Inc.	MAD/a95	Demag. (C/mT)	High Tb/Hc components Dec	Inc.	MAD/a95	IRM Ratio	reliability category	Pol.	Mean NRM	General site pol.
RC6A		0.119		1.13	2.5-15	161.8	61.3	10.3µ	15-40	169.2	-19	7µ		T2	R	1.13	R
RC5A	0.5	0.094		2.07	0-5	186.5	27.5	6.8µ	5-origin	162	-12	4.01µ		S1	R	2.07	R
RC4	1.6	0.119		2.86	0	140.9	-30.5		2.5-origin	164.5	-18.9	8.41µ		S3	R	2.93	R
RC4-TH	1.6	0.119	500	3.1					133-400	159.1	-31.6	13.5µ		S3	R		
RC3A	2.3	0.081	40	1.89	0	154.9	-13.2		2.5-origin	160.3	-23.9	3.82µ		S1	R	2.03	R
RC3B-TH	2.3	0.081	500	2.17					266-400	137.1	-18.2	10.21µ	0.95	S2	R		
RC2A	3.5	0.081	40	1.9	0-5	134.3	16.7	7.8µ	5-origin	163.8	-20.7	3.08µ		S1	R	1.9	R
RC1A	5.8	0.444	40	1.38	0-5	311.7	13.3	6µ	5-origin	158.4	-22.2	6.7µ		S2	R	2.05	R
RC1B-TH	5.8	0.444	500	2.72					300-500	152.8	-7.9	12.3µ		S3	R		
RC7A	8.5	0.456	40	14.5	0-5	151.1	15.6	1µ	5-origin	158.8	-12.4	3.16µ		S1	R	14.5	R
KC3B	10	0.094	40	1.82	0	182	35.1		2.5-origin	184	-35.9	9.87µ		S1	R	1.82	R
KC2B	1	0.118	40	1.07	0	166.1	-22.2		2.5-25	167.8	-24.9	4.02à		S2	R	1.07	R
KC2A	1	0.118	40	0.32	0	78.3	10.5		5-20	129	-41	9à		S3	R	0.32	R
KC1B	0.3	0.113	40	1.3	0-5	15.7	76.1	3.2µ	10-origin	152.9	-19.2	8.3µ	0.97	S2	R	1.3	R

Appendix 15 *Roaring Branch Creek palaeomagnetic data summary sheet*

Appendix 16 *Kolomokei Creek palaeomagnetic data summary sheet*

Bennett's Creek data summary sheet

Sample code	Depth (m)	Suscept. xE-3 SI	Max temp/ A.F. field	NRM (mA/m)	Demag (C/mT)	Low Tb/Hc components Dec	Inc.	MAD/a95	Demag. (C/mT)	High Tb/Hc components Dec	Inc.	MAD/a95	reliability category	Pol.	Mean NRM	General site pol.
BK14B	0.25	0.3	40	2.24	0	224.5	-2.2		5-origin	159.5	-26.2	9.44μ	S2	R	2.51	R
BK14A-TH	0.25	0.3	400	2.71	0	206.9	-9.2		100-466	166.1	-36	17.8μ	S3	R		
BK13B	-0.25	0.1	40	2.16	0	179.3	-19.5		2.5-origin	170.5	-24.1	2.5μ	S1	R	2.16	R
BK12A	-1.5	0.075	40	1.81	0	160.9	-23.1		2.5-origin	165.2	-27	2.39μ	S1	R	1.81	R
BK11A	-1.75	0.08	40	2.19	0	176.4	-11.9		2.5-origin	171.3	-18	4.26μ	S1	R	2.19	R
BK10A	-2	0.075	40	2.13	0	185.1	-17.5		2.5-origin	179.2	-18.3	3.61μ	S2	R	2.13	R
BK9A	-2.5	0.09	40	2.29	0	164.5	-19		2.5-origin	172	-29.2	4.02μ	S1	R	2.13	R
BK9B-TH	-2.5	0.09	400	1.93	0	150.9	-19.7		233-400	156.9	-19.9	4.54μ	S2	R		

Appendix 17 *Bennett's Creek palaeomagnetic data summary sheet*

Peach Tree Ferry road-cutting data summary sheet

Sample code	Depth (m)	Suscept. xE-3 SI	Max temp/ A.F. field	NRM (mA/m)	Demag (C/mT)	Low Tb/Hc components Dec	Inc.	MAD/a95	Demag. (C/mT)	High Tb/Hc components Dec	Inc.	MAD/a95	reliability category	Pol.	Mean NRM	General site pol.
PT21A		0.138	40	1.27	0-10	15.1	47.6	1.8µ			-90		T2	R	1.27	R
PT22B	7.9	0.106	40	1.13	0-5	348.5	51.1	2.3µ	30-40	188	-1.1	9.3à	T2	R	0.98	R
PT22A-TH	7.9	0.106	450	0.78	0	91.5	-33.2		100-433	181.2	-0.2	5.8à	S3	I		
PT23A	7.4	0.119	40	1.8	0	198	-11.1		5-origin	179.8	-26.1	7.12µ	S2	R	1.8	R
PT24A	7	0.088	40	2.64	0-5	213.7	31.9	3.3µ	2.5-origin	194.6	-6.2	3.61µ	S1	R	2.64	R
PT25A-TH	6.65	0.113	450	3.19	0	184.8	-18.1	3.19µ	100-origin	185.5	-16.2	12.4µ	S2	R	3.19	R
PT25B	6.65	0.113	40	3.89	0-5	213.9	32.2	6.1µ	5-origin	184.3	-15	4.96µ	S1	R		
PT26A	6.52	0.088	40	3.97					2.5-origin	193.5	-41.1	1.12µ	S1	R	3.97	R
PT27B	3.5	0.063	40	0.79	0-5	345.4	58	10µ			-90		T2	R	0.79	R
PT27A-TH	3.5	0.063	450								-90		T1	R		
PT28A-1	2.5	0.125	40	1.57	0-10	249.1	84.6	2.4µ	15-origin	162.8	-27.1	4.79µ	S2	R	1.57	R
PT29A	2	0.131	40	1.54	0	170.4	-2.4		10-origin	162.5	-26.1	4.51µ	S1	R	1.54	R
PT30A	1.5	0.15	40	2.73	0-10	127.6	48.6	3.1µ	10-origin	163.2	-33	4.21µ	S2	R	2.75	R
PT30B-TH	1.5	0.15	450	2.8	0	132.4	6.97		100-433	153.2	-24.7	5.8à	S2	R		
PT31A		0.09	40	2.11	0	154.2	3.5		5-origin	152.1	-9	3.35µ	S1	R	2.11	R

Appendix 18 *Peach Tree palaeomagnetic data summary sheet*

Tunnel Springs data summary sheet

Sample code	Depth (m)	Suscept. xE-3 SI	Max temp/ A.F. field	NRM (mA/m)	Demag (C/mT)	Low Tb/Hc components Dec	Inc.	MAD/a95	Demag. (C/mT)	High Tb/Hc components Dec	Inc.	MAD/a95	IRM ratio	reliability category	Pol.	Mean NRM (mA/m)	General site pol.
TS1A	0.6	0.019	40	0.122	0	176.9	-7.2							T3	R?	0.122	R?
TS1B-TH			350		0	205.9	17.9							T3	R?		
TS2A	1.4	0.04	40	0.25	0	219.8	75.2		5-25	18.5	76.2	12.1à		S2	N	0.25	N
TS3A	2.1	0.047	40	0.121	0	195.9	8.6							T3	R?	0.121	R
TS3B-TH			350		0	230.9	-9.3		100-250	238.7	-70.3	13à		S2	R		
TS4A	3.7	0.033	40	0.19	0	280.3	85.6						0.89	T3	R?	0.19	R?
TS4E-TH			350		0	214.2	79.7		0-300	139.1	83.4	13à		A	?		
TS5A	4.7	0.034	40	0.07	0	246.7	70.6		15-35	169.6	71.2	10à	0.9	A	?	0.07	N?
TS5B			40		0	345.6	40.9		0-30	342.5	39.3	6.7à		S2	N		
TS5E-TH			350		0	323.1	41.5							T3	R?		
TS6	5.3	0.021	40	0.054	0	321	58.1		10-40	229.9	45.6	9.8à	0.81	A	?	0.054	R?
TS6B-TH			350		0	227.2	-1.7							T3	R?		
TS7A	6.3	0.026	40	0.048	0-25	293.1	48.2	10.6à						T3	R??	0.048	R
TS7B-TH			350		0	336.4	50.2							T2	R		
TS8	6.9	0.039	40	0.053	0	223.8	51.4		15-25	327.1	25.3	10.7à	0.84	T3	N?	0.053	N?
TS9A	7.6	0.028	40	0.047	0-15	278.3	63.1	7.6µ						T3	R?	0.047	R?
TS9E-TH			350		0	158.7	12.5							T3	R?		
TS10A	8.6	0.033	40	0.083	0	161.8	82.4		5-40	59.6	55.2	13.8à		S3	N?	0.083	?
TS10E-TH			350		0	128.8	-67.5							S3	R?		
TS11A	10	0.027	40	0.021	0	292.8	63.8						0.9	T2	R?	0.021	R?
TS12	11	0.064	40	0.012	0	36.5	63.2		0-30	337.3	78.3	13.6à		S3	N?	0.012	N?

Appendix 19 *Tunnel Springs palaeomagnetic data summary sheet*

Hatchetigbee Bluff data summary sheet

Sample code	Depth (m)	Max temp/ A.F. field	NRM (mA/m)	Demag (C/mT)	Low Tb/Hc components			Demag. (C/mT)	High Tb/Hc components			reliability category	Pol.	Mean NRM (mA/m)	General site pol.
					Dec	Inc.	MAD/a95		Dec	Inc.	MAD/a95				
HB1	1.1	40	0.259	0-20	9.2	72.5	9.6µ	15-40	126.5	54.6	15à	T?/A	?	0.241	R
1B		40	0.224	5-25	43.8	41.4	10à					T3	R		
HB2	1.43	40	0.494	0	283.2	69.1		0-30	320.1	77.2	5.5à	S2	N	0.36	N
2A		40	0.2	0	144.5	47.6		5-40	168.8	69.7	6.6à	S2/A	?		
HB3	1.72	40	0.148	0-15	324.4	54.4	8.4µ	15-40	243	64.5	7.4à	S2/A	?	0.148	?
HB4	2.37	40	0.276	0	130.7	35.7		15-40	101.9	69.7	6.3à	S1/A	?	0.276	?
HB5	3.54	40	0.669	0-15	64.2	79.7	2.7µ	15-40	30.6	50.9	4.1à	S1	N	0.669	N
HB6	3.54	40	0.359	0	32.4	66.3		15-30	68.2	86.5	5.2à	S2	N	0.359	N
HB7	4	40	0.426	0-15	47.1	21.54	3.9µ	15-40	130	60.3	8.4à	S2/A	?	0.426	?
HB8	4.8	40	0.677	0	271.9	69.7		5-40	352	81	6à	S2	N	0.677	N
HB10A	4.8	40	0.188	0	116.4	26.6		10-40	184.3	58.6	11à	S2	?	0.257	N
10B		40	0.326	0-10	129.2	-54.6		15-40	287.4	66.8	13.6à	S2	N		
HB11	5.42	40	0.825	0	166.5	-1.6		10-origin	170.4	-25.1	-25.1µ	S2	R?	0.825	R?
HB12	5.64	40	0.929	5-15	155.4	21.4	4.1µ	20-40	153.1	-24	5.2µ	T2	?	0.929	?
HB13	5.87	40	0.41	5-15	160.8	28.4	9.3µ	15-40	156.6	-23.1	10.4µ	T2	N?	0.41	N?
HB14	5.87	40	0.427	0-15	161.9	-7.5	8.1µ	20-40	165.2	-30.9	7.5µ	T2	N?	0.427	N?
HB15A	6.42	40	0.111	0	176.9	59.1		0-40	199.8	58.6	8.8à	S2/A	?	0.121	?
15		40	0.131	0-15	69.1	51.9	5.2µ	15-40	139.2	82.9	11.3à	S3/A	?		
HB16	6.93	40	0.197	5-25	163.5	82.7	5.9µ	25-40	128.8	80.8	11.6à	S2/A	?	0.197	?
HB18	7.33	40	0.406	0	160.9	71.5		5-40	268.6	86	10à	S2/A	?	0.406	?
HB20	8.23	40	0.304	0-10	165.6	-47.6	3.8µ	10-35	60.8	15.9	7.6à	T2	N	0.304	N
20B		40	0.32	0-15	168.3	-33	6.5µ	15-40	11.7	65.1	11.5à	S2	N		
HB21	9.44	40	0.529	0	2.4	67.9		0-40	2	67.4	5.5µ	S1	N	0.529	N
HB22	9.74	40	0.046	0-15	44.3	32.6	5.5µ	20-40	263.5	73.6	12.4à	S2	N?	0.046	N?
HB23	10.64	40	0.032	5-15	16.4	-0.3	9.9µ	25-35	115.5	-46.5	1.8µ	T3	N?	0.063	N?
23A		40	0.096	0-15	258.2	41.3	5.8µ	20-35	152.1	-47.9	8.5µ	T2	N?		
HB24	15	40	0.58	5-15	151.9	-3.2	.7µ	15-40	152.8	-15.2	2.1µ	T2	N?	0.57	N
24A		40	0.56	0-15	172.5	38.5	17µ	15-40	167.7	-11.3	3µ	T2	N		

Appendix 20 *Hatchetigbee Bluff palaeomagnetic data summary sheet*

Lower Peach Tree (6 miles west) data summary sheet

Sample code	Depth (m)	Max temp/ A.F. field	Suscept. xE-3	NRM (mA/m)	Demag (C/mT)	Low Tb/Hc components Dec	Inc.	MAD/a95	Demag. (C/mT)	High Tb/Hc components Dec	Inc.	MAD/a95	reliability category	Pol.	Mean NRM (mA/m)	General site pol.
LP25A	6.25	40	0.047	0.19	0	9.6	18.8		2.5-25	4.9	33.8	12.6à	S2	N?	0.156	N
LP25B-TH	6.25	350		0.123	0	349.3	65		0-origin	346.4	62.6	8µ	S1	N		
LP26A	5.7	40	0.013	0.06	0	35.2	14.9						E	?	0.046	
LP26B	5.7	40		0.032	0-10	300.3	66.2	6.6à	0-25	311.1	73.7	12.8à	S3	N?		N?
LP27B	3.2	40		0.212	0-5	317.8	47.7	3.4µ	5-25	34.9	59.3	4.95à	S2	N	0.172	N
LP27C-TH	3.2	350		0.131	0	3.9	26.4						T3	R?		
LP28A	2.8	40	0.02	0.67	0	2.2	57.8		0-20	341.2	529	11.61à	S2	N	0.67	
LP29C	1.47	40	0.06	0.11	0	12.4	49.5		0-origin	11.3	48.4	8.1µ	S2	N	0.17	N
LP29A	1.47	40		0.25	0	7.5	38.6		0-15-orig.	7.5	40.4	6.4µ	S2	N		
LP29B-TH	1.47	350	0.06	0.15	0	9.3	46.9		0-300	3.3	47.4	13.4à	S2	N		
LP30	0.05	40	0.033	0.18	0-5	336.5	46.9	6.58µ	15-40	350	14.4	6.32µ	S2	N?	0.15	?
LP30-TH	0.05	350		0.13	0	350.5	36.6						T3	R?		
LP31A	-0.5	40	0.053	0.1	0-15	358.2	32.8	3.8à	0-40	7	30.6	11.1à	S3	N?	0.1	N?
LP31C	-0.5	40		0.11	0-5	318.8	66.7	10.5µ	20-35	38.4	-5.2	14.1µ	T3	N?		
LP31B-TH	-0.5	350		0.08	0	172.9	57.7						E	?		
LP32A	-1.3	40		0.122	0	339	47.6		0-30	332.2	31.7	9.6à	S2	N	0.15	?
LP32B-TH	-1.3	350		0.177	0	335.8	29.8		133-300	341.3	-9.5	12.3à	T2	R		
LP33A	-2	40	0.04	0.112	0-5	193.9	22.4	5.1µ	25-40	8.95	45.6	5.02µ	S2	N	0.121	N
LP33B-TH	-2	350		0.129	0	311.1	61.7		100-origin	354.9	39.7	10.6µ	S1	N		
LP34A	-2.6	40	0.067	0.08	0	161.9	49.7						T3	R?	0.09	N?
LP34B	-2.6	40		0.102	0	253	67.8		0-40	343.4	63.1	4.3à	S2	N		
LP35C	-3.7	40	0.047	0.28	0	57	67		5-40	347.3	59.8	8.2à	S2	N	0.23	N?
LP35A	-3.7	40		0.18	0-10	199.6	60.7	5.3µ					T3	R?		
LP35B-TH	-3.7	350		0.23	0	331.8	30.7		0-40	351.3	28.3	14.2à	S3	N?		
LP36A-TH	-6.9	350	0.04	0.48	0	91.5	64		100-350	4.2	61.5	11µ	S1	N	0.57	
LP36B	-6.9	40		0.65	0-15	331.5	18.4	4.4µ	10-40	0.8	23.3	7à	S3	N		N

Appendix 21 *Lower Peach Tree palaeomagnetic data summary sheet*

Bells Crossing data summary sheet

Sample code	Depth (m)	Max temp/ A.F. field	NRM (mA/m)	Demag (C/mT)	Low Tb/Hc components Dec	Inc.	MAD/a95	Demag. (C/mT)	High Tb/Hc components Dec	Inc.	MAD/a95	reliability category	Pol.	Mean NRM (mA/m)	General site pol.
BX6A	1.8	40	0.239	0	28.2	60.7						T?	?	0.701	?
6B-TH		400	1.18	0	167.6	51.6		100-origin	172.4	42.1	12.7µ	S1/A?	?		
5A	1.2	40	0.497	0	6.3	58				-90		T2	R	0.438	R
5B		40	0.379	0	6.8	70.1				-90		T2	R		
4A	0.5	40	0.215	0-10	348.3	56		10-origin	4	5.6	5.6µ	S2/A	?	0.178	?
4B		40	0.141	0-10	303.5	64		15-40	136.8	65	7.5à	?	?		
3A		40	0.374	0	18.2	60.5		20-40	123.2	27	4.9à	S2/A	?	1.19	R
3B-TH		400	2.02	0	187.7	-18.9		100-origin	177.4	-24	5µ	S1	R		

Appendix 22 *Bell's Crossing palaeomagnetic data summary sheet*

Sample number	Depth (m)	(ft)	NRM mA/m	Vol Suscept. xE-3 (S.I)	MaxIRM @.86T mA/m	IRM ratio	Low coer. Range	Dec.	Inc.	95/Rc	High coer. Range	Dec.	com. Inc.	95/Rc	Plot Cat.	Inc.	Bio-strat.	Pol.
Pe 1	5.19	17.47	0.11	0.063	49.1	0.86	15-30	143.8	37.1	(12.62)					T3	37.1	NP14	N
2	7.52	24.67	0.09	0.088	56.2	0.91	0-5	169.7	71.5	0.97/1.0					T3	-90		R
3	10.46	34.33	0.65	0.226	153.6	0.9					0-40	131.7	-43.8	1.91	S2	-43.8		R
4	16.41	53.83	1.2	0.025	43.5	0.87	0-5	168.2	-49.4	4.81	5-ogn	169.4	-49.9	0.98/0.98	S2	-49.9		R
5	17.22	56.5	0.1	0.05	20	0.89					0-40	69.7	-11.5	(10.4)	S2	-11.5		R
6a	18.04	59.33	0.073	0.01	54.9	0.89											Barren	E
6b	18.12		0.053	0.013													NP?	E
7	19.23	63.08	0.03	0.01	44	0.89	0-10	176	-46.7	4.21					S2	-46.7		R
8	19.91	65.33	0.05	0.013	34.2	0.9	8-15	332	53.3	9.29					S3	53.3		R
9	21.62	70.92	0.02	0.025	8	0.89	0-15	212.3	-25.7	3.49	10-30	166.8	-56.5	0.92/0.99	T/S?	-25.7		N
10	22.88	75.08	0.02	0.013			0-20	316.1	-32.2	6.08					S2	-32.2		R
11	24.16	79.25	0.02	0.025	36.5	0.96	0-25	5.5	11.3	0.78/0.65	25-40	241.4	52.9	(22.2)	S3	52.9		N
12	25.12	82.47	0.08	0.038	71.4	0.97									T			N?
13	26.29	86.25	0.07	0.025	19.9	0.97	3-15	327.2	15.9	0.9/0.98	15-ogn	234.9	20.8	0.98/0.99	S2	20.8		N
14	27.56	90.47	0.02	0.025	31	0.97	0-15	229.3	14.8	1.0/1.0	20-40	57.5	19.6	6.99	S3	19.6	NP12	N
15	28.78	94.47	0.04	0.025											T3	90		N?
16	29.4	96.5	0.04	0.038	12.2	0.96					0-25	321.7	-7	5.69	S2	-7		I/R
17	31.24	102.5	0.017	0.025	89.8	0.98	0-20	36.85	31.94	10.75					S3	31.9		N
18	32.18	105.58	0.04	0.038	23.6	0.96					0-30	232.4	26.2	8.03	S2	26.2	Barren	N
19	32.97	108.17	0.04	0.025	34.5										T2	-90	Barren	R
20	34.21	112.25	0.1	0.025	29.9	0.99					0-40	234.2	-13	5.45	S2	-13	Barren	R
21	35.26	115.67	0.02	0.038	22.4	0.93									T3	-90		R
23	35.48	116.47	0.11	0.038			2.5-15	192.9	-9.6	0.94/0.96	5-25	198.4	-30.2	6.23	T2	-30.2		R
22	36.52	119.83	0.16	0.038	20.3	0.93	0-5	144.6	1.87	8.83	15-25	128.8	-16.9	10.9	S2	-16.9		R
25	37.11	121.75	0.18	0.025	46.9	0.97					0-40	299.5	-17	0.97/0.86	T3	-90		R?
24	37.82	124.08	0.12	0.025	484.4	0.98	0-8	176.5	27	4.29	25-40	239.5	74.4	9.3	S2	74.4		N
26a	39.94	131.17	0.185	0.025	117.4	0.96	5-15	215.3	-54.6	0.97/1.0					T1	90		N
26b	40.02		0.108	0.025			2.5-15	157.6	23.8	0.97/0.99	20-40	133.6	18.6	12.6	S3	18.6		N?
27a	40.64	133.47	0.141	0.038			2.5-15	219.4	-18.7	6.65					T2	90		N
27b	40.7		0.156	0.038			2.5-10	231.9	-35.7	0.99/0.99	25-40	266.9	43.6	10.26	S2	43.6	NP12	N
28	41.48	136.08	0.16	0.05	42.7	0.97					20-40	95.9	18.5	5.42	S3	18.5		N?

Appendix 23 *Peterman core palaeomagnetic data summary sheet*

29	42.65	139.92	0.05	0.05	9.6	0.78					10-40	326.3	6.07	3.59	S2	6.07		N
30a	43.8	143.83	0.171	0.05	31.2	0.88					0-40	115.3	40.9	8.93	S3	40.9		N
30b	43.88		0.113	0.05			0-10	239.8	50.2	0.96/0.98					T3			?
31	44.48	145.92	0.59	0.088	270	1					0-ogn	258.9	83.7	5.21	S1	83.7		N
32	45.42	149	0.08	0.063	68.5	0.96					2.5-ogn	44.9	-59.6	0.98/1.0	S1	-59.6		R
33	46.25	151.75	0.13	0.05	35.8	0.83	2.5-15	304.2	-38.2	0.96/0.98	20-35	53.5	24.7	(18.5)	S3	24.7		N?
34	46.71	153.25	0.12	0.113	54.9	0.89	0-5	160.7	41.3	0.95/0.99	10-40	151.5	-19.5	0.93/0.87	T3	90		N?
35	47.34	155.33	0.12	0.08	49.7	0.91					2.5-30	93.6	14.9	5.7	S3	14.9	NP12	N?
36	48.03	157.58	0.69	0.101	61.7	0.84	0-5	175.5	50.8	0.92/0.98					T2	-90		R
37	48.56	159.33	0.07	0.038	74.8	0.95	0-5	235.5	64	0.96/0.96	10-35	194.9	8.87	6.65	S3	8.87		N?
38	49.58	162.67	0.4	0.088	73.9	0.9	5-20	11.9	22.2	0.99/1.0					T1	-90	Barren	R
39	50.52	165.75	0.23	0.101	44	0.85	2.5-20	337.2	60.1	0.91/0.99					T3	-90	Barren	R?
40	51.74	169.75	0.16	0.063	79		0-20	68	-13.7	3.99					S2	-13.7	Barren	R
41	52.71	172.92	0.49	0.126	101.4	0.92					20-ogn	204.4	-41	0.93/0.98	S2	-41	Barren	R
44	53.52	175.58	0.17	0.088	39.3	0.87					2.5-ogn	109	-19.3	0.99/0.99	S3	-19.3	Barren	R?
42	54.64	179.25	2	0.063							10-ogn	247.9	42.3	0.91/0.81	S2	42.3		N
43	55.96	183.58	1.6	0.113	271.6	0.91	2.5-10	124.3	34.8	1.0/0.92	30-ogn	148.3	-13.9	0.99/0.96	S2	-13.9		R
45	56.34	184.83	0.1	0.101			0-5	191.9	19.2	1.0/0.8	25-ogn	200.8	-22.5	0.95/0.94	S2	-22.5	NP10	R
46	57.76	189.5	0.21	0.138	82	0.9	0-5	204	39.8	0.98					T2	-90		R
47	60.63	198.92	0.52	0.113	149	1					25-ogn	254.4	-19.8	0.97/0.98	S2	-19.8	?	R
48	61.97	203.33	0.22	0.05	64.6	0.86	0-15	224.6	-41.7	10.6					S3/2	-41.7		R
49	63.83	209.42	4.1	0.101			0-5	68.4	35.9	1.0/1.0	5-ogn	22	14.4	0.96/0.94	S2	14.4		N
50	64.64	212.08	0.43	0.101	98.6	0.99	0-5	118.5	28.8	1.0/1.0	40	79.8	17.2	-	S2	17.2		N
51	65.68	215.5	0.27	0.08	114.3	0.92					30-40	37.8	18.9	6.48	S2	18.9		N
52	67.03	219.92	6.1	0.126	125.5	0.9	0-5	19.7	-44	0.88/0.99	10-ogn	21.4	-15.1	1.0/0.95	T3	90		N?
53	67.97	223	0.13	0.126			2.5-10	238.5	-25.6	0.99/1.0	15-30	1	-33.8	0.64/0.86	T1	90	?	N
54	68.43	224.5	0.72	0.201	281		0-10	197.4	-22.9	0.98/1.0	10-ogn	218.4	-62.4	0.94/0.90	S2	-62.1		R
55	70.92	232.67	0.95	0.113	233	0.98					10-ogn	230.6	60.3	0.97/0.97	S1	60.3		N
56	71.65	235.08	1.2	0.176	401.7	0.92	0-5	337.1	78.3	0.98/0.98	25-40	267.5	-49.3	4.56	S2	-49.3		R
57	72.8	238.83	1.04	0.126	201.7	0.94					2.5-40	251.8	-29.8	0.99/0.98	S2	-29.8		R
58	73.61	241.5	0.25	0.126	160.1		0-5	218.5	-24.9	1.0/1.0	15-ogn	245.2	-45.6	1.0/0.99	S1	-45.6		R
59	74.07	243	0.38	0.126	145.3	0.93					5-ogn	124.2	-24	1.0/1.0	S1	-24	?	R
60	74.65	244.92	0.62	0.126	141	0.98	0-5	162.9	-21.4	0.96/1.0	20-ogn	193.7	-20.4	0.98/0.99	S1	-20.4		R
61	75.74	248.5	0.41	0.126	121.2	0.92					0-30	100.8	27.2	2.8	S2	27.2		N

62	77.09	252.92	0.28	0.126	168.7	0.7	0-5	44.6	23	0.96/0.90	15-40	92.5	-41.3	1.71	S1	-41.3		R
63	78.23	256.67	2.1	0.126	532	0.88	0-5	113.3	-51.2	0.99/1.0	10-ogn	66.6	-39.5	1.0/0.99	S1	-39.5		R
64	79.17	259.75	1.8	0.138	689	0.92	2.5-10	322.5	-11.8	1.0/1.0	20-40	317.5	-49.1	0.99/1.0	S2	-49.1		R
65	80.21	263.17	2.1	0.138	541.8	0.93					10-ogn	37.2	-41.3	0.99/0.99	S1	-41.3	?	R
66	81.28	266.67	2.1	0.163	674.6	0.91					10-ogn	211.6	-34.1	0.97/0.99	S1/2	-34.1		R
67a	82	269.17	2.03	0.138	441.9	0.94					10-ogn	255.3	-33	0.99/0.99	S1	-33		R
67b	82.08		2.37	0.138							10-ogn	276.3	-37.9	0.97/0.97	S1	-37.9		R
68	82.75	271.5	2.4	0.151	586.7	0.93					5-ogn	356	-39.9	0.75/0.98	S1/2	-39.9		R
69	83.64	274.42	4.88	0.126	479.8	0.9					5-ogn	285	-30.3	1.0/0.99	S1	-30.3		R
70	84.18	276.17	0.76	0.113	145.8	0.94	0-5	2.86	-28	4.06	10-ogn	1.7	-39.7	0.91/0.98	S1	-39.7	?	R
71	84.91	278.58	2.2	0.126	244.8	0.9					10-40	250.8	-21.9	1.0/0.99	S2	-21.9		R
72	85.9	281.83	1.6	0.126	247.7	0.86	0-5	65	-22.6	0.99/1.0	15-0	94.1	-19.7	0.81/0.86	S1/2	-19.7		R
73	86.82	284.83	1.5	0.151	276.1	0.89	0-5	235.9	7.3	0.98/0.97	15-0	339.9	-29.8	1.0/1.0	S1	-29.8		R
74	87.45	286.92	4.6	0.138	288.1	0.94					20-ogn	229	-14.7	1.0/0.97	S1	-14.7		R
75	88.32	289.75	0.86	0.126	225.1	0.95	0-7.5	78.8	49.2	0.71/0.9	20-ogn	83.2	-11	0.93/0.97	S1	-11		R
76	88.85	291.5	0.92	0.138	228.6	0.9	0-15	178.4	12.5	0.63/0.84	20-ogn	176.1	-16	0.94/0.99	S1	-16	?	R
77	89.79	294.58	1	0.126	416.8	0.91	0-10	210.2	74.5	0.57/0.82	15-ogn	227.1	-26.6	1.0/0.99	S1	-26.6		R

Sample code	Depth (m)	Suscept. xe-3	Max temp/ A.F. field	NRM (mA/m)	Demag (C/mT)	Low Tb/Hc components Dec	Inc.	MAD/a95	Demag. (C/mT)	High Tb/Hc components Dec	Inc.	MAD/a95	reliability category	Pol.	Mean NRM (mA/m)	General site pol.
CA50B1	1.45	0.035	35	0.036	0	336.1	80.2						T3	?	0.037	N??
50B2			35	0.037	5-15	281.9	46.9	5.3µ	15-35	67.6	17.9	9.6à	S3	N??		
CA51A	1.53	0.032	35	0.035	0	329.9	70.9		0-orig.	334.9	71.8	3.7µ	S2	N	0.035	N?
51C			35	0.034	0	203.5	77.7	0-4µ	0-40	193.3	82.6	7à	S2/A	?		
51-TH			350	0.04	0	9.8	59.3						T3	?		
CA52A	2.1	0.022	35	0.019	0	81.7	7.7						T2	R	0.026	R
52B			35	0.034	0	124.2	44.5		0-30	122.4	40.7	7.4à	S2/A	?		
CA53A	2.2	0.028	35	0.034	0-15	334.5	46.7	2.8µ	15-30	133.8	-14.1	12.2à	T2	R	0.051	R
53-TH			350	0.068	0	189.3	55.2						T2	?		
CA54A	3.2	0.032	35	0.048	0	160	15.1						T2	R	0.06	R
54B			35	0.072	0-20	144.2	59.9	7µ	25-35	196.5	56.8	11.8à	S3/A	?		
CA55A	4.25	0.029	35	0.013	0	316.1	17.8		10-30	279.3	-37.7	3.8à	S2/A	?	0.018	?
55B			35	0.024	0	217.2	15.3						T3	?		
CA56A	6.25	0.021	35	0.036	0	38.2	67		5-15	354.7	55.5	2.1µ	S2	N?	0.04	N?
56-TH			350	0.044	0	352.4	77.9		0-250	49.6	84.6	12.2à	?	?		
CA57A	9.25	0.022	35	0.126	0	281	-34.2		0-orig.	280	-32.8	10µ	S2/A	?	0.126	?
CA58A			35	0.051	0	194.9	16.9		0-30	200.7	13	8.µ	T2	N?	0.075	N?
58B			35	0.099	0-15	193.4	26.2	2.7µ	10-30	226.2	15.4	10.2µ	T2	N?		
CA59A	4.84	0.017	35	0.036	0-10	301.7	46.6	7.5µ	15-35	358.8	58.5	6.7à	S2	N	0.045	N
59B			35	0.053	0-10	352.5	48.5	3.2µ	0-35	339	38.3	10.8à	S2	N		
59C			35	0.053	0-20	4.4	29.6	8.4µ	15-35	346.2	68.3	3.4à	S2	N		
CA60A	4.4	0.02	35	0.068	0-10	169.2	67.5	8.8µ	10-35	330	50.1	7.9à	S2	N	0.06	N
CA61		0.014	35	0.058	5-15	278.8	56.9	5.2µ	10-40	15.6	70.1	9.8à	S2	N	0.058	
CA62A	2.44	0.022	35	0.091	0	153.3	53.2		0-40	177.7	46.6	10.9à	S2/A	?	0.136	N
62B			35	0.168	0	83.3	86.9		0-40	54.6	73	8.9à	S2	N		
CA63A	0.65	0.029	35	0.033	0-10	321.1	12	11.2µ	25-40	268.9	78.1	6à	S2	N	0.04	N
63B2			35	0.046	0	244.1	58.8		5-40	290.7	58.5	8.8à	S2	N		
63B1			35	0.046	0	229.5	72.8		5-40	310	64.1	4.5à	S2	N		
CA64A	0.2	0.033	35	0.032	0-10	82.4	76.6	10.4µ	5-25	47.9	44.9	9.8à	S2	N	0.05	N
CA64C			35	0.076	0-15	105.4	35.1	301µ	10-40	28.5	52.2	7.5à	S2	N		
64B			35	0.041	0	142.3	69.5						T3	?		
CA65A	-7.8	0.036	35	0.112	0-15	23.8	32.4		0-40	340.7	68.5	8.2à	S2	N	0.189	N
65B-TH			350	0.262	0	81.8	73.4		100-350	15.9	56.6	13.3à	S2	N		

Appendix 24 *Campbell palaeomagnetic data summary sheet*

Sample code	Depth (m)	Suscept. xe-3	Max te A.F. fie	NRM (mA/m)	Demag (C/mT)	Low Tb/Hc components Dec	Inc.	MAD/a9	Demag. (C/mT)	High Tb/Hc compone Dec	Inc.	MAD/a	irm ratio	reliability category	Pol.	Mean (mA/m)	Gener site p
BU31A	0.079	0.046	40	1.48	0-20	27.3	64.4	11.4µ	10-40	29.7	59.8	10.3à		S2	N	0.99	N
31B-TH			350	0.49	0	266.8	71.9		0-500	145.6	84	8.3à		S2/A	?		
BU32A	1.2	0.015	35	0.054	0-20	173.3	-7.2	9.4µ	20-30	9.3	20.6	11.7à	0.92	T2	N	0.054	N
BU33A	2.15	0.028	40	0.067	0-15	229.6	49.4	5.4µ	15-25	304.2	37.2	7.5µ		S3	N??	0.05	N
33B			40	0.059	0	2.3	64.2		10-25	347	38.3	9.4à		S3	N?		
33C			40	0.04	0	21.7	59.7		0-35	43.9	45.4	12à		S3	N??		
BU34A	2.64	0.022	40	0.034	0-15	189.1	48.8	11.3µ						T2	R	0.041	R?
34B			40	0.047	0-15	133	65.9	4µ						S3	N?		
BU35	3.97	0.043	40	0.014	0	187	14.9		15-40	194.8	-9.9	4à		S2	R	0.015	R
35B			40	0.007	0	178.8	54.7		0-30	187.5	60.1	9à		S2/A	?		
35B1			40	0.024	0-10	17.8	33	5.1µ	15-40	214.4	-26.8	8.7à		S2	R		
BU38A	4.5	0.018	40	0.183	0	336.7	64.7		10-40	268.6	64.7	9.5à		S2	?	0.262	R
38B-TH			350	0.34	0	84.9	-63		0-350	90.6	-61.6	9.9à		S2	R		
BU39A	5.1		40	0.267	0	129	-7.1							T2	N	0.381	?
39C			40	0.75	0	149	16							T3	N?		
39-TH			350	0.125	0	183.7	33.2							?	?		
BU36A	5.45	0.036	40	0.02	0	17.4	82.6							T3	R??	0.22	R?
36C			40	0.018	0-15	79.9	52.3	7.9µ						T3	?		
36B			40	0.03	5-20	355.3	34.1	13.3µ	15-30	176.5	58.5	8à		S2/A	?		
BU37B	7.3	0.032	40	0.013	0-10	98.3	62.4	5.8µ	10-30	350.1	34.5	8à		S2	N	0.013	N
BU41	10.2	0.018	40	0.421	0-20	89.7	62.8	2.8µ	20-40	188.1	67.5	5.2à		S1/A	?	0.421	?
BU42A	10.8		40	0.174	5-20	154.8	49.4	6.4µ	5-40	115.3	70.4	8.1à		S2/A	?	0.174	N
42B		0.021	40	0.134	0-10	238.2	62.6	4.6µ	10-35	311.5	74.5	4.9à		S2	N		
BU43	11.3	0.021	40	0.029	0-15	284.3	31.5	6.7µ						T2	R?	0.029	R?
BU44	(14)5	0.03	40	0.061	0	359	64		0-40	4.3	56.3	5.2à		S1	N	0.059	N
44B			40	0.057	0	39.9	67		5-40	22.2	54	2.9à		S2	N		
BU45A	(15)4	0.01	40	0.047	0	164.5	35.1		5-orig.	107.3	66.8	7.5µ		S2/A	?	0.42	
45B			40	0.037	0	265.5	81.4		0-40	318.2	77.2	5.2à		S2	N		N
BU46	(15.6)3.4	0.02	40	0.056	0-15	258.7	64.6	5.9µ						T2	?	0.056	?
BU47A	(16.4)2.6	0.02	40	0.117	0	165.5	36.7		0-orig.	164.3	36.7	15µ		S2	?	0.295	?
47-TH			350	0.475	0	260	3.3							?	?		
BU48A	(17.1)1.9	0.033	40	0.04	0	287.9	8.3						0.83	T2	R	0.037	R
48C			40	0.031	5-20	178.3	68.2	10.7µ						T2	R		
48-TH			350	0.035	0	182.5	-27.8		100-350	240.2	35.2	10.5à		S2/A	?		
BU49	(17.5)1.5	0.041	40	0.065	0	201.5	54.3		5-40	214.9	59.6	9.7à		S2/A	?	0.061	N??
49B			40	0.057	0-15	302.7	46.7	7.1µ	10-40	69.6	72.8	10.2à		S3	N?		
BU50A	(17.6)1.4	0.03	40	0.063	0	226.4	69.7							S2	R	0.069	R
50B			40	0.074	0	181.6	72.8		0-35	202.2	67.7	10à		S2/A	?		
BU51A	(18.4)0.6	0.041	40	0.099	0	212.2	26.5							T2	R	0.098	R
51B			40	0.096	0	166.6	61							T3	?		
BU52A	(18.9)0.1	0.034	40	0.036	0	271.5	47.5							T3	R?	0.052	R
52B			40	0.063	5-15	254.1	-13.2							T3	?		
BU53A	(19.3)-0.3	0.08	40	0.025	0	149	-76.3							T3	N??	0.03	R?
53B			40	0.033	0	3.7	19.2							T2	R		
BU54	(20.5)-1.5	0.007	40	0.047	0	253.2	36							TS	R??	0.092	R/
54B			40	0.128	5-20	192.9	3.6	12µ						T3	R?		

Appendix 25 *Butler palaeomagnetic data summary sheet*

Sample code	Depth (m)	Suscept. xe-3	Max temp/ A.F. field	NRM (mA/m)	Demag (C/mT)	Low Tb/Hc components Dec	Inc.	MAD/a95	Demag. (C/mT)	High Tb/Hc components Dec	Inc.	MAD/a95	reliability category	Pol.	Mean NRM (mA/m)	General site pol.
LS41	-1.5	0.021	40	0.052	0	9.4	35.3		10-35	334.4	38.5	9.5à	S3	N?	0.051	N
41B			40	0.049	0	325	60		0-35	295.2	62.1	8.8à	S2	N		
LS42	-1.4	0.029	40	0.042	0-10	251.8	73.4	6.8µ					T3	N?	0.031	N?
42B			40	0.019	0-10	8.5	48.4	12.8µ	10-40	159.3	-9.7	13.5µ	T3	?		
LS43B	-1	0.03	40	0.036	0	79.6	-14.8						T3	?	0.032	R
43A			40	0.027	0	174.3	11						T2	R		
LS44A	0.5	0.025	40	0.019	0	179	42.6		0-35	174.3	36.1	7.4à	S2/A	?	0.059	R
LS45A	7.5	0.024	40	0.033	0	3.9	3.18						T3	N?	0.066	N?
45B			40	0.099	0	357	-26.1	10-4µ	10-40	104.1	28.3	7.3à	S2/A	?		
LS46A	8	0.038	40	0.08	0	179.7	6.5						?	?	0.072	N
46B			40	0.064	0	174.1	64.1		25-40	35.3	23.9	5.6à	S2	N		
LS47B	8.69	0.025	40	0.022	0	131.9	53.6		30-40	123.2	30.7	6.6à	?	?	0.022	?
LS48A	10.1		40	0.097	5-20	213	30.6	3.1µ	20-35	7.2	70.2	8.5à	S2	N	0.097	N
LS49A	11.7	0.03	40	0.061	0	21.7	63.9		0-40	6.8	69	9.3à	S3	N?	0.079	N?
49B			40	0.097	0-10	338.4	49.3	2.8µ	30-40	132.6	72.1	1.3à	S3	N?		
LS50A	12.97	0.021	40	0.046	0	206.6	81.3						T3	R?	0.883	R
50-TH			40	1.72	0-150	7.7	32.1	.5µ	150-orig.	22.7	13.5	4.4µ	T2	R?		
LS52A	13.07	0.041	40	0.137	0	324.7	72.7		0-30	319.5	72.4	6.3à	S2	N	0.546	N
52B-TH			500	0.955					150-300	273.8	2.2	6.2µ	T2	N		
LS53B	13.55	0.03	40	0.067	0	299.7	54.9		0-40	295.5	65.4	8.9à	?	?	0.082	N??
53B2			40	0.058	5	280	14.3		5-40	292.1	19.2	12.4à	S3	N?		
53A			40	0.121	0	234.6	66.6		0-20	256	77.7	10à	S2/A	?		
LS54A	13.97	0.018	40	0.102	0-10	198.8	26	7.3µ					T2/?	?	0.102	?
LS55A	14.1	0.018	40	0.059	0	215.9	32.7		10-20	255.9	19.8	2.µ	T2	N?	0.052	N?
55B			40	0.046					5-30	258	51.1	11.7à	S3/A	?		
LS56A	14.2	0.011	40	0.319	5-20	41.5	2.7	4.3µ	15-40	21	53.4	7.8à	S2	N	0.205	N
56B			40	0.027	0	116.5	71.4		0-40	128.2	67.8	7.4à	S3	N?		
56B-TH			350	0.269	0	285	39.2		100-300	342.9	38.3	2.4à	S2	N		
LS57A	14.4	0.029	40	0.068	0	241.7	47.5		5-30	322.7	65.3	11.1à	S2	N?	0.054	N
57B			40	0.04	0	333.3	49		0-40	333	50.8	4.8à	S3	N?		
LS58A	15	0.019	40	0.039	0	341	48		0-35	346.1	53	6.1à	S2	N	0.038	N
58B			40	0.04	0	300	47		0-40	312.2	50.1	7à	S2	N?		
58B2			40	0.038					0-35	346.1	53	6.1à	S2	N		
LS59A	15.61	0.01	40	0.067	0	27.9	36.3		0-40	28.8	36.9	9µ	S1	N	0.139	N
59-TH			350	0.353	0	194.8	54.8		0-300	164	44.2	4.8à	S1/A	?		
59C			40	0.027	0	42.7	51.9		5-40	34.3	44	2.4à	S2	N?		
59C2			40	0.039	0	257.5	79.4		10-30	290.9	68.5	6.5à	S2	N		

Appendix 26 *Little Stave Creek palaeomagnetic data summary sheet*

Midway data summary sheet

Sample code	Depth (m)	Suscept. xe-3	Max temp/ A.F. field	NRM (mA/m)	Demag (C/mT)	Low Tb/Hc components Dec	Inc.	Demag. (C/mT)	High Tb/Hc components Dec	Inc.	MAD/a95	IRM RATIO	reliability category	Pol.	Mean NRM (mA/m)	General site pol.
19901B	7.3		40	0.348	nrm	76	18.4						T2	R		R
MW31A	6.42	0.023	40	0.01	nrm	211.8	26.6						T3	R?		R?
31B			40	0.027	nrm	199.2	41.8	5-30	142.1	72.1	8à		S2/A	?		
30	6.17	0.016	40	0.045	nrm	220	47.9					0.84	T2	R		R
29A	5.9	0.013	40	0.197	nrm	304.8	45.7	5-35	354.6	32.4	17.3à		S3	N??		R?
29B-TH			200	0.123	nrm	329.5	70.9					0.9	T2	R?		
28A	5.23	0.017	40	0.14	nrm	262.7	69.7	5-30	343.3	53.4	10.4à		S2	N		N
27A	5.15	0.013	40	0.158	nrm	325.5	38.8	5-40	0.5	46.5	5.9à		S2	N		N
27B-TH			300	0.206	nrm	58.7	60.7	100-300	73.1	50.3	9à		S2	N		
26	4.9	0.019	40	0.03	nrm	298.9	49.7	5-40	318.1	64.9	11.7à		S2	N		N
25A	4.65	0.034	40	0.229	nrm	310.6	54.7	5-40	326.8	53.9	5.8à		S2	N		N
25B-TH			450	0.261	nrm	312.5	47.8	100-450	322.5	68.2	6.4à		S2	N		
24	3.55	0.039	40	0.037	nrm	159.6	61.3	5-20	127.3	80.1	5.2à	0.91	S2/A	?		?
23	3.5	0.029	40	0.066	nrm	72.8	79.1	0-35	35.2	74.5	7.1à		S2	N		N
22	3.1	0.03	40	0.052	nrm	7.6	41.3					0.88	T2	?		?
21A	2.9	0.043	40	0.069	nrm	327.4	81.6	0-35	345.2	62.6	13.7à		S2	N		N
21B-TH			40	0.111	nrm	320.7	43	0-25	330.1	53.4	9.2à		S2	N		
20	0.5	0.028	40	0.192	nrm	330.3	48.2	0-40	335.6	49.4	2.6à	0.9	S2	N		N

Appendix 27 *Midway palaeomagnetic data summary sheet*